Design, Synthesis, and Properties of Novel Bio-Based and Ethylene-Based Copolymers

Philip Benjamin Vincent Scholten

April 2019

Thesis accepted for the title Doctor of Sciences

Academic Year 2018-2019

Supervisors:

Dr. Christophe Detrembleur

Université de Liège, Belgique

Prof. Dr. Michael A. R. Meier

Karlsruher Institut für Technologie, Deutschland

European Commission | Horizon 2020 European Union funding for Research & Innovation

Design, Synthesis, and Properties of Novel Bio-Based and Ethylene-Based Copolymers

Zur Erlangung des akademischen Grades eines

DOKTORS DER NATURWISSENSCHAFTEN

(Dr. rer. nat.)

von der KIT-Fakultät für Chemie und Biowissenschaften
des Karlsruher Instituts für Technologie (KIT)
genehmigte

DISSERTATION
von

Philip Benjamin Vincent Scholten
aus Kiel

Dekan: Prof. Dr. Reinhard Fischer
Vorsitzende der Prüfungskommission: Prof. Dr. Anne-Sophie Duwez
Referent: Prof. Dr. Michael A.R. Meier
Referent: Dr. Christophe Detrembleur
Koreferent: Prof. Dr. Franck D'Agosto
Koreferent: Prof. Dr. Michael Shaver
Koreferent: Dr. Serge Bettonville
Tag der mündlichen Prüfung: Dienstag 9. April 2019

The work presented in this dissertation was performed under the supervision of Dr. Christophe Detrembleur at the Université de Liège (ULiège) in Belgium, and Prof. Dr. Michael A. R. Meier at the Karlsruher Institut für Technologie (KIT) in Germany from January 2016 to Febuary 2019 as part of the European Union Horizon 2020 Marie Skłodowska Curie EJD FunMat program (Project ID 641640). A three week internship in November 2018 at INEOS Polymers & Olefins Europe in Brussels (Belgium) supervised by Dr. Serge Bettonville was also carried out.

Eidesstattliche Versicherung gemäß § 13 Absatz 2 Ziffer 3 der Promotionsordnung des Karlsruher Instituts für Technologie für die KIT-Fakultät für Chemie und Biowissenschaften:

Bei der eingereichten Dissertation zu dem Thema „*Design, synthesis, and properties of novel bio-based and ethylene-based copolymers*" handelt es sich um meine eigenständig erbrachte Leistung. Ich habe nur die angegebenen Quellen und Hilfsmittel benutzt und mich keiner unzulässigen Hilfe Dritter bedient. Insbesondere habe ich wörtlich oder sinngemäß aus anderen Werken übernommene Inhalte als solche kenntlich gemacht. Die Arbeit oder Teile davon habe ich bislang nicht an einer Hochschule des In- oder Auslands als Bestandteil einer Prüfungs- oder Qualifikationsleistung vorgelegt.

Die Richtigkeit der vorstehenden Erklärungen bestätige ich. Die Bedeutung der eidesstattlichen Versicherung und die strafrechtlichen Folgen einer unrichtigen oder unvollständigen eidesstattlichen Versicherung sind mir bekannt. Ich versichere an Eides statt, dass ich nach bestem Wissen die reine Wahrheit erklärt und nichts verschwiegen habe.

_____ _____

Ort und Datum Unterschrift

Acknowledgements

The journey that I have taken over the last three years has been enriched by many individuals and I would like to thank every single one for helping shape who I am today.

I would like to acknowledge the European Union for their funding as part of the H2020 Marie Curie Actions. Without this fantastic program I would not have been able to perform my research and attend many of the interesting workshops and conferences.

I would like to thank my supervisors Christophe Detrembleur and Michael Meier for their guidance, support and patience throughout my thesis. Chris, merci beaucoup pour le temps que tu as dédié a nos discussions et la correction de mes présentations et articles. C'était un plaisir d'avoir travaillé avec toi et d'avoir partagé des chouettes moments à des conférences ou en courant. Mike, vielen Dank für das Vertrauen in meine Fähigkeiten und den Freiraum, den Du mir während meines Aufenthaltes am KIT gegeben hast. Des Weiteren möchte ich mich bei Dir für die vielen anregenden Gespräche, besonders zu den Themen Wissenschaft und Zukunft, bedanken.

Most of my time I spent at CERM in Liège and I would like to thank all of the current and past members that crossed my path. Particulièrement, je veux remercier Jérémy pour son aide au début de ma thèse mais aussi pour les discussions sur le PE et la CMRP. Merci Daniela de m'avoir cherché un appartement quand je n'étais pas encore à Liège et pour tous les bons moments passés ensemble au labo ou en dehors, que ce soit en courant, mangeant ou en faisant la fête. Pierre et Jérémie, sans vous je n'aurais jamais gouté à la vraie vie estudiantine de Liège, ni passé un aussi bon moment à Liège ces dernier temps, merci beaucoup. Merci aussi, à mes « mamans belges », Valérie et Martine, pour leur aide au labo mais surtout pour les moments de bonheur en dehors du travail. Greg, sans qui rien ne marche au labo, c'était un plaisir de travailler avec toi. J'apprécie énormément les analyses (chiantes) et manips que tu as fait pour moi. Merci Jean-Michel pour ton expertise dans les compatibilisants et les analyses thermiques des polymères, mais également pour toutes les parties des différents jeux auquel on a joué ensemble. Bruno, merci pour ton aide pour la synthèse et l'extraction par le CO_2 et aussi pour les nombreuses discussions. Merci Antoine, pour les discussions scientifiques et non-scientifiques qu'on a eu et de m'avoir aidé avec la correction des mes articles. Sophie, merci pour ton aide avec les démarches administratives et d'être toujours aussi souriante et chaleureuse. Merci Christine pour les nombreuses activités du labo pendant l'année. Merci à Charlène et Robin pour les chouettes soirées apéro-dinatoire. Rahmet, thank you for the fun times spend together and your Turkish lessons. Un grand merci à Sandro, Pauline, Maxime B., Assala, Kevin, Charlotte, Alvaro, Zeynep, Stephan, Maxime H.,

Clement, Fabiana, Satya, Thomas, Walid, Muhammad, Enza, Abdel, Raphaël, Farid et Alice pour les agréables moments au labo.

Although the time spent in KIT was shorter, lots of fond memories were made in Karlsruhe and on numerous trips. Audrey, merci de m'avoir pris par la main les premiers jours en arrivant au KIT, et pour toute ton expertise et les discussions scientifiques. Sans toi j'aurais certainement moins joué au tennis et sûrement jamais gouté le Patxaran. Katharina, vielen Dank für das Korrigieren meiner « deutschen » Manuskripte, die Gespräche über Belgien und seine Eigenheiten, sowie das Beherbergen von Lena und mir. Danke auch an Patrick für das Korrekturlesen, die IT-Expertise und die schönen Tage in Warwick. Bapti, grâce à toi j'étais pas le seul au labo avec un accent bizzare en français ; merci pour les chouettes moments passés ensemble. Rebekka und Nico, euch einen großen Dank für die Möglichkeit, in eurer coolen Wohnung zu übernachten. Kenny and Zafer, the two cellulose kings, thank you for the discussions, fun excursions and meals we shared. Becci, dir einen großen Dank für das Messen meiner Proben und das Fahren einiger meiner Versuche. Charlotte, vielen Dank für deine Expertise in der „Grünen Chemie" und Lignocellulose. Thank you Dafni for the corrections of my manuscript and the enriching insights into PostDoc life and academia in general. Danke Dir Pinar für das Organisieren der (komplizierteren) Verträge und die Hilfe bei administrativen Dingen. Ein großes Dankeschön geht auch an Yasmin, Hatice, Marc, Susanne, Julian, Eren, Stefan & Wiebke, Ben, Andreas, Barbara, Maike, Gregor, Bohni, Roman, Michi, Maxi, Luca und Kevin.

Merci beaucoup à INEOS Polymers & Olefins Europe de m'avoir donné la possibilité de découvrir la recherche industrielle. Je remercie particulièrement Serge et Raphael pour l'organisation de mon stage ainsi que de m'avoir montré tous les aspects du travail chez INEOS. Merci aussi à Xavier, Dominique et Alain ainsi que le reste de l'équipe, c'était un plaisir de faire votre connaissance.

I would also like to thank the EJD-FunMat organising committee for the smooth organisation of numerous workshops and meetings. Fellow EJD-PhDs thank you for the great times spend together in France, Portugal and Luxemburg.

A thank you to my non-chemist friends who allowed me to forget my science problems and supported me during this time.

Lena, die letzten drei Jahre waren nicht immer ganz leicht mit mir, danke, dass du mich trotzdem unterstützt hast und immer für mich da warst und es weiterhin bist.

Ein immenser Dank geht an meine Eltern, meine Schwester und die restliche Familie, die immer für mich da sind und mir meinen bisherigen Lebensweg ermöglicht haben.

Abstract

Renewable monomers have the potential to replace petroleum-derived monomers for reversible deactivation radical polymerisations (RDRP) for a variety of applications, such as adhesives and coatings. Yet, challenges in the polymerisation of non-activated and often internal double bonds found in natural molecules still remain. Moreover, functionalisation pathways attaching renewably-sourced double bonds to natural molecules are rare and sustainable strategies using catalytic or enzymatic reactions are sought after.

This thesis aims to introduce a set of renewable monomers for reversible deactivation radical polymerisation (RDRP), namely organometallic-mediated radical polymerisation (OMRP) using a cobalt complex, in the quest for renewable and functional (co)polymers. This particular type of OMRP was chosen because it controls the polymerisation of a large range of non-activated monomers with excellent control over the chain growth process under mild experimental conditions. The monomers prepared in this thesis were obtained from plant oils and/or CO_2 *via* catalytic reactions and contain ester and carbonate functionalities of interest for post-polymerisation modifications. Successful copolymerisations with monomers bearing non-activated double bonds, namely vinyl acetate and ethylene, were performed using OMRP under mild conditions and the comonomer content was tuned *via* the initial polymerisation feed or the ethylene working pressure. The introduction of carbonate moieties into vinyl acetate copolymers allowed for the synthesis of three discrete functional poly(vinyl alcohol) copolymers. Moreover, the ability to incorporate such carbonate functionalities into polyethylene copolymers by OMRP was shown for the first time. Highly linear ethylene copolymers over a broad range of carbonate content were obtained with significantly altered properties compared to homo-polyethylene. Particularly the ability to finely tune the molecular copolymer parameters, such as molecular weight and copolymer architecture, allows a systematic study of their influence on the compatibilisation capability of such copolymers. The potential of polyethylene copolymers bearing functional groups as compatibilisers was highlighted for poly(ethylene-*co*-vinyl acetate) copolymers. Finally, a fully renewable compatibiliser, based on starch and high oleic sunflower oil, obtained by non-radical means was applied to cellulose/LDPE composites. An improved cellulose dispersion within the matrix was observed by rheology, while the mechanical properties, notably Young's modulus, was increased.

This work aims to highlight the unexplored potential of renewable resources for the synthesis of functional polymers for their application in polyolefin composites.

Résumé

Les monomères provenant de ressources renouvelables peuvent constituer des alternatives « vertes » aux monomères pétro-sourcés. En utilisant des techniques de polymérisation radicalaire par désactivation réversible (RDRP), de nouveaux copolymères fonctionnels aux potentiels d'applications variés dans divers secteurs (adhésifs, revêtements, etc.) pourraient voir le jour. Néanmoins, la polymérisation de doubles liaisons non-activées et souvent internes qui sont présentes dans les molécules naturelles reste un défi. De plus, les voies de fonctionnalisation de ces molécules, introduisant des doubles liaisons issues de ressources renouvelables, sont rares et des stratégies durables, utilisant des réactions catalytiques ou enzymatiques sont activement recherchées.

Cette thèse a pour but de préparer une gamme de monomères renouvelables porteurs d'une double liaison non conjuguée et d'en investiguer la polymérisation radicalaire contrôlée, *via* l'utilisation de complexes de cobalt (la technique OMRP). Le but est de proposer une stratégie permettant d'avoir accès à de nouveaux (co)polymers fonctionnels (partiellement) renouvelables. Cette technique OMRP a été choisie en raison de sa capacité à contrôler la polymérisation d'une large gamme des monomères non-activés et ce, dans des conditions réactionnelles douces. Ces monomères, porteurs de fonctions esters ou carbonates, ont été obtenus à partir d'huiles végétales et/ou de CO_2 *via* diverses réactions catalytiques. Ces groupements fonctionnels, introduits dans les polymères après OMRP, peuvent ensuite être exploités pour l'introduction d'autres fonctions chimiques. La copolymérisation de ces monomères avec l'acétate de vinyle ou l'éthylène a été réalisée avec succès dans des conditions douces. La teneur en comonomères dans le copolymère a pu être ajustée soit en modifiant la composition du mélange initial lorsque l'acétate de vinyle était utilisé comme comonomère, soit en variant la pression d'éthylène lorsque ce dernier faisait office de comonomère. L'introduction de groupements carbonates cycliques dans des chaînes de poly(acétate de vinyle) a permis de synthétiser trois nouveaux copolymères fonctionnels à base d'alcool polyvinylique. Des copolymères à base d'éthylène et de monomères porteurs d'une fonction carbonate cyclique ont également été préparés pour la première fois et ce, sur une large gamme de composition. La modulation des paramètres macromoléculaires du copolymère (masse molaire, composition, architecture) permet d'ajuster ses propriétés. Le potentiel des copolymères à base d'éthylène et d'acétate de vinyle en tant que compatibilisant de mélanges de polyéthylène et de cellulose est également illustré dans ce travail. Enfin, un compatibilisant entièrement renouvelable, à base d'amidon et d'huile de tournesol, obtenu par des voies non-radicalaires, a été utilisé pour compatibiliser des matériaux composites de

cellulose et de polyéthylène (LDPE). Une amélioration de la dispersion des fibres de cellulose dans la matrice LDPE a été observée, avec un impact positif sur les propriétés de la matrice.

Ce travail permet de souligner le potentiel inexploré des ressources renouvelables pour la synthèse de polymères fonctionnels et leur application pour les matériaux composites à base de polyoléfines.

Zusammenfassung

Erneuerbare Rohstoffe haben das Potenzial Erdöl-basierte Monomere in kontrollierten radikalischen Polymerisationen (RDRP) zu ersetzen. Dies ist wichtig, um eine Vielzahl unterschiedlicher Anwendungen, wie z.B. Klebstoffe oder Beschichtungen, nachhaltig bereit zu stellen. Es bestehen jedoch weiterhin Herausforderungen bei der Polymerisation von nicht-aktivierten und internen Doppelbindungen, wie sie häufig in natürlichen Molekülen vorhanden sind. Darüber hinaus fehlen nachhaltige Funktionalisierungsstrategien die Doppelbindungen an natürlich vorkommende Moleküle anbringen.

Diese Dissertation setzt sich zum Ziel, eine Reihe erneuerbarer Monomere mittels kontrollierte radikalische Polymerisation für die Synthese von erneuerbaren und funktionellen (Co)Polymeren zugänglich zu machen. Die Polymerisationen wurden gezielt mit einem Kobaltkomplex (OMRP) durchgeführt, da diese die Polymerisation von einer Vielzahl nicht-akitivierter Monomere ermöglicht mit exzellenter Kontrolle über das Kettenwachstum unter milden Reaktionsbedingungen. Die jeweiligen Monomere wurden zunächst durch katalytische Reaktionen aus Pflanzenölen und/oder CO_2 hergestellt und enthalten Ester oder Carbonat Gruppen, welche sich besonders für Post-Polymerisationsmodifikationen eignen. Die erfolgreiche kontrollierte radikalische Co-Polymerisation von diesen Monomeren, die nicht-aktivierte Doppelbindungen tragen, mit Vinylacetat und Ethen wurde bei milden Reaktionsbedingungen mit Hilfe eines Kobaltkomplexes (OMRP) durchgeführt. Die Polymerzusammensetzung konnte dabei durch die anfängliche Monomerzusammensetzung oder durch den Druck während der Polymerisation präzise kontrolliert und eingestellt werden. Die Einführung der Carbonatgruppen in Vinylacetat Co-Polymere erlaubte die Synthese von drei unterschiedlichen funktionellen Poly(Vinyl Alkohol) Co-Polymeren. Zudem wurde die kontrolliert radikalische Co-Polymerisation dieser funktionellen Monomere mit Ethen zum ersten Mal durchgeführt. Lineare Ethylen Co-Polymere mit einstellbarem Carbonatgehalt und daher wesentlich veränderten Eigenschaften im Vergleich zu Homopolyethylen konnten erhalten werden. Insbesondere erlaubt die genaue Abstimmung der molekularen Polymerparameter, wie molare Masse und Co-Polymerarchitektur, eine systematische Erforschung der Auswirkungen dieser Parameter auf die Fähigkeit des Co-Polymers als Phasenvermittlungs-Agent zu fungieren. Das Potenzial von Polyethylen Co-Polymeren mit funktionellen Gruppen als Seitenketten als Phasenvermittler wurde für Ethylen/Vinylacetat Co-Polymere veranschaulicht. Zuletzt wurde ein ausschließlich aus nachwachsenden Rohstoffen aufgebautes Polymer, basierend auf Stärke und Sonnenblumenöl mit hohem Ölsäureanteil, als Phasenvermittler zwischen Cellulose und stark verzweigtem Polyethylen

(LDPE) eingesetzt. Eine verbesserte Dispersion der Cellulose in der LDPE-Matrix wurde rheologisch nachgewiesen, wobei sich die mechanischen Eigenschaften, insbesondere das Elastizitätsmodul, verbesserten.

Diese Arbeit möchte somit auch auf die bislang kaum beschriebenen Vorzüge erneuerbarer Rohstoffe in der Synthese von funktionellen Polymeren für Anwendungen in Verbundwerkstoffen aufmerksam machen.

Table of Contents

1 Introduction 4
2 Theoretical Background and State of the Art 5
2.1. Reversible Deactivation Radical Polymerisations 5
2.1.1. Organometallic-Mediated Radical Polymerisation using Cobalt Complexes 10
2.2. Renewable Monomers for Controlled Radical Polymerisations 14
2.2.1. Renewable Molecules Containing Double Bonds 15
2.2.1.1. Terpenes 15
2.2.1.2. Cellulosic Biomass 26
2.2.1.2.1. Itaconates 26
2.2.1.2.2. α-Methylene-γ-butyrolactones 33
2.2.1.2.3. Phenylpropanoids 38
2.2.2. Renewable Molecules Functionalised with Double Bonds 41
2.2.2.1. Sugars and Carbohydrates 41
2.2.2.2. Lignin 42
2.2.2.3. Terpenoids 47
2.2.2.4. Triglycerides 58
2.2.2.4.1. Fatty Acids 60
2.2.2.4.2. Glycerol-Derived Monomers 63
2.2.3. Conclusions 69
2.3. Ethylene (Co)Polymerisations 70
2.4. Nanocomposites of Polyethylene and Cellulose 72
3 Aim of the Thesis 76
4 Synthesis of Plant-Based Non-Activated Olefins: A New Class of Renewable Monomers for Controlled Radical Polymerisation 80
4.1. Abstract 81
4.2. Introduction 82
4.3. Synthesis of Plant Oil-Based Monomers 84
4.4. (Co)Polymerisations of Renewable Monomers 87
4.5. Conclusion 97
5 CO_2-Based Building Blocks as Monomers for the Synthesis of Functional Poly(Vinyl Alcohol) 98
5.1. Abstract 99
5.2. Introduction 100

5.3. Statistical Copolymerisation of VAc and DMMDO by Cobalt-Mediated Radical Polymerisation 103
5.4. Chemo-Selective and Complete Hydrolysis of P(VAc-*co*-DMMDO) 116
5.5. Post-Polymerisation Modification of the Selectively Hydrolysed Copolymer P(VOH-*co*-DMMDO) 120
5.6. Conclusion 123
6 Functional Polyethylene by Reversible Deactivation Radical Copolymerisation of Ethylene with Renewably-Sourced Carbonate Monomers 124
6.1. Abstract 124
6.2. Introduction 125
6.3. Copolymerisations of Ethylene with M1 and DMMDO using Cobalt-Mediated Radical Polymerisation 127
6.4. Conclusion 132
7 Synthesis of Poly(Ethylene-*co*-Vinyl Acetate) Copolymers and Poly(Ethylene-*co*-Vinyl Acetate)-*b*-Poly(Ethylene) Block Copolymers for the Compatibilisation of Cellulose and Polyethylene 134
7.1. Introduction 135
7.2. EVA Copolymer and Block Copolymer Synthesis 137
7.3. Compatibilisation of Cellulose and Polyethylene using EVA as Compatibiliser 143
7.4. Conclusion 146
8 Rheological and Mechanical Properties of Cellulose/LDPE Composites using Sustainable and Fully Renewable Compatibilisers 148
8.1. Abstract 148
8.2. Introduction 149
8.3. Preparation of Cellulose/LDPE Composites 151
8.4. Rheological Properties of the Composites 152
8.5. Scanning Electron Microscopy Analysis of the Composites 156
8.6. Thermal Properties of the Composites 157
8.7. Mechanical Properties of the Composites 158
8.8. Conclusion 160
9 General Conclusions and Perspectives 162
10 Experimental Part 166
10.1. Materials 166
10.2. Characterisation Methods 167

10.3. Experimental Section for Chapter 4 170
10.4. Experimental Section for Chapter 5 213
10.5. Experimental Section for Chapter 6 231
10.6. Experimental Section for Chapter 7 241
10.7. Experimental Section for Chapter 8 243
11 Bibliography 247
12 Appendix 279
12.1. Abbreviations 279
12.2. List of Figures 284
12.3. List of Schemes 296
12.4. List of Tables 299

1 Introduction

Reversible deactivation radical polymerisations (RDRP) have completely changed the landscape of polymers over the last few decades, as the unprecedented control over the growing chains allows for the precision-design of polymers. Whether it is the chain length, the composition, the polymer structure or the selective functionalisation of the chain ends, RDRPs allow to tune and dictate these parameters and a few high-value applications can already be found industrially.[1,2] Classically monomers used for RDRP are based on petroleum as they are easily obtained as side streams from the cracking of crude oil. The development of Green Chemistry[3] over the last 20 years and the recent increasing focus of governments and media on aspects like sustainability and renewability,[4] the application of these two aspects to monomers for RDRP seems evident. However the extraction or synthesis of renewably-sourced monomers is not trivial, as not many natural molecules contain polymerisable double bonds and hardly any sustainable functionalisation pathways exist for the attachment of renewably sourced double bonds to natural molecules. Furthermore, the non-activated nature of many naturally occurring double bonds and the functionalities present in renewably-sourced molecules still pose challenges for most polymerisation techniques.

Similarly, fossil fuel-based α–olefins, and more precisely ethylene, are also extremely difficult to polymerise in a controlled fashion by radical pathways as the radical species is non-stabilised and highly reactive. Only recently have strategies been developed to allow for the controlled growth of these radical species and thus the synthesis of well-defined ethylene polymers by radical means.[5,6] The copolymerisation of ethylene with polar, functional monomers is further complicated by the difference in the reactivity of the ethylene and the comonomer double bond. Up to date only reversible-addition fragmentation (RAFT) polymerisation and organometallic mediated radical polymerisations (OMRP) have mastered this challenge for a few non-activated monomers.[5,7–9] Yet ethylene copolymers containing functional groups are extremely attractive for a variety of applications, such as coatings and compatibilisers, and gain even more interest if the polar groups allow for degradability or are renewably-sourced.

2 Theoretical Background and State of the Art

2.1. Reversible Deactivation Radical Polymerisations

The first discoveries relating to the reversible deactivation of radicals in polymer chemistry were reported in the late 70s and early 80s by Tatemoto *et al.* and Otsu *et al.*,[10,11] and since then the field of controlled radical polymerisations has become one of the most important methods for macromolecular engineering. Through the reversible deactivation of the radical species during the propagation step of the polymerisation using a controlling agent (Figure 1), a precise control over molecular weights, polymer composition and microstructure is possible.

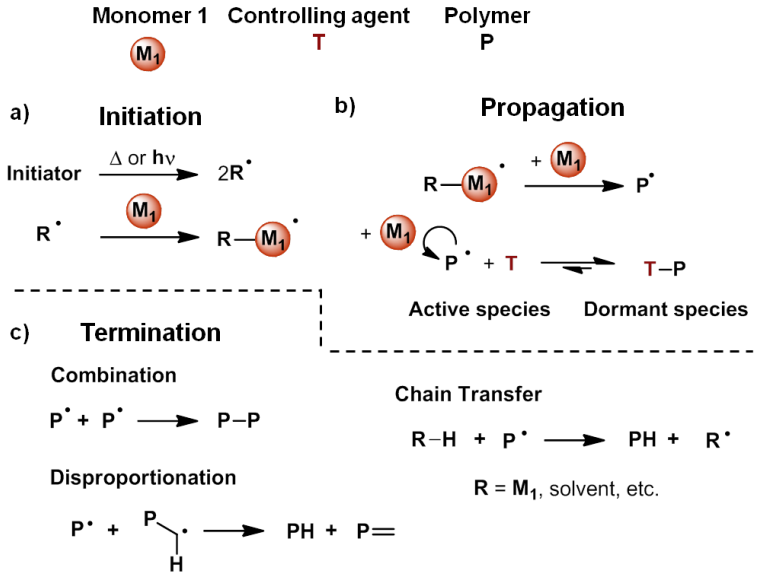

Figure 1. The different steps of reversible deactivation radical polymerisations: a) initiation, and b) propagation, while the different termination modes which are suppressed during RDRP through the controlling agent are shown in c).

The key to this control lies in the equilibrium between active and dormant radical species (Figure 1b), as the controlling agent allows to shift this equilibrium towards the dormant side and reduce the instantaneous concentration of radicals in the polymerisation medium. As a result of this low radical concentration, termination or side reactions common in free radical polymerisations (FRP), such as combination, disproportionation, or chain transfer (Figure 1c), are almost completely suppressed. Such polymerisations are characterised by a linear increase in molecular weight, a pseudo-first order kinetic plot and by the fact that at the end of the polymerisation the controlling agent is still attached to the ω-chain end, allowing for the reactivation of this dormant species and the synthesis of block copolymers (Figure 2). Equally, depending on the choice of initiator, complex architectures and homofunctional or

telechelic polymer chains – containing functionalities at one or both chain ends – can be synthesised (Figure 2).

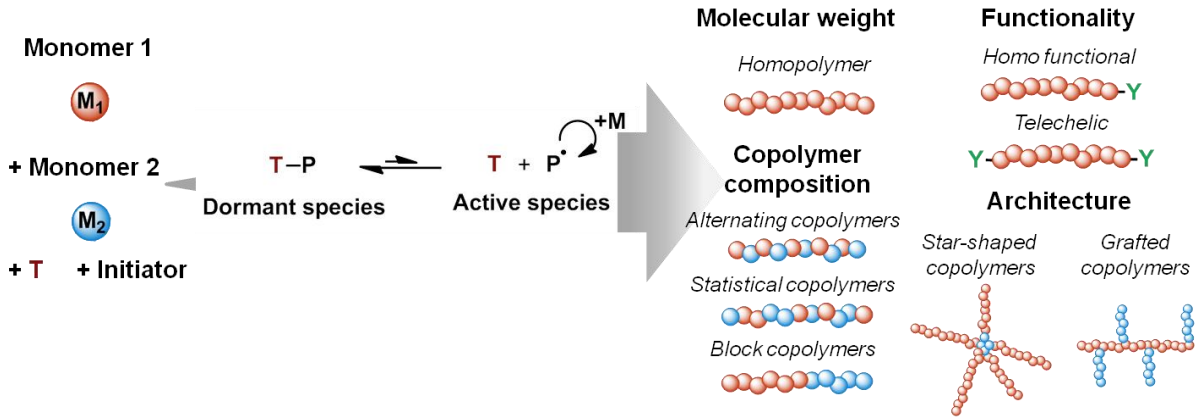

Figure 2. RDRP allows to control the molecular weight, functionality, and architecture of the polymers as well as the copolymer composition.

Several techniques exist for such reversible-deactivation radical polymerisation (RDRP), all creating a dormant radical species *via* the reversible bond formation between a controlling agent and the carbon-centred radical. The most popular methods include atom transfer radical polymerisation (ATRP; Scheme 1a)[12], reversible addition fragmentation chain transfer (RAFT) polymerisation, also known as macromolecular design by interchange of xanthate (MADIX; Scheme 1b),[13] nitroxide-mediated radical polymerisation (NMP; Scheme 1c),[14,15] organometallic-mediated radical polymerisation (OMRP; Scheme 1d),[16–19] and organotellurium-, organostibine-, and organobismuthine-mediated radical polymerisation (Scheme 1e).[20] The detailed mechanism of these systems is outside of the scope of this thesis and has been described elsewhere.[12–18,20,21] However, as the radical polymerisations in this thesis are primarily performed by OMRP using a cobalt complex, also called cobalt-mediated radical polymerisation (CMRP), the exact mechanism for this specific RDRP technique will be detailed below (Chapter 2.1.1).

a) **Atom Transfer Radical Polymerisation (ATRP)**

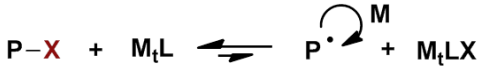

X = Cl, Br M_t = Cu, Ru, ... L= Ligand

b) **Reversible Addition Fragmentation Chain Transfer (RAFT)**

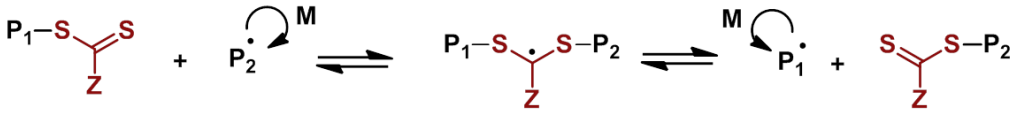

P_1 and P_2 = polymer chains

c) **Nitroxide-Mediated Polymerisation (NMP)**

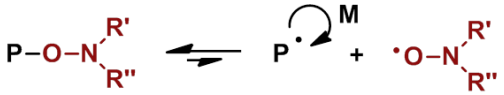

d) **Organometallic-Mediated Radical Polymerisation (OMRP)**

Reversible Termination Mechnism

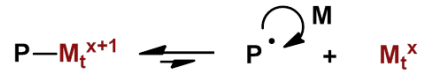

M_t = Co, Fe, ... x = initial oxidation state

Degenerative Transfer Mechnism

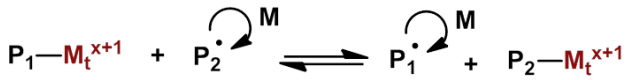

e) **Organotellurium-, Organostibine-, and Organobismuthine-Mediated Radical Polymerisation**

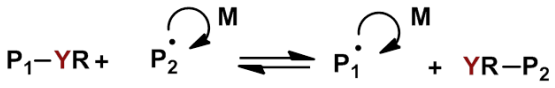

Y = Bi, Te, Sb...

Scheme 1. Different RDRP methods and their equilibrium between dormant and active species: a) atom transfer polymerisation (ATRP), b) reversible addition fragmentation (RAFT) polymerisation or macromolecular design by interchange of xanthate (MADIX), c) nitroxide-mediated radical polymerisation (NMP), d) organometallic-mediated radical polymerisation (OMRP), and e) organotellurium-, organostibine-, and organobismuthine-mediated radical polymerisation.

Since the discovery of each of these systems, intense research for the optimisation of the control over the polymerisation process and the improvement of the monomer and solvent scope, as well as the ability to incorporate complex and functional monomers has been performed. Major advances in these fields, particularly for more-activated monomers (MAMs), such as acrylates and stryrenics (Scheme 2a), have allowed for the synthesis of self-

assembling, functional and responsive polymers with applications ranging from drug delivery to 3D-printing.[22] Nonetheless, several RDRP techniques, namely NMP and ATRP, still struggle with non-conjugated, less-activated monomers (LAMs), such as vinyl esters, vinyl amides, α-olefins, *etc*. (Scheme 2b). The underlying difficulty lies in the highly reactive, non-stabilised propagating radical which is formed during the polymerisation (Scheme 2c). While the deactivation of such radicals is most often unproblematic, the reactivation or regeneration of the poorly stabilised radical chains from the dormant species is often slow or impossible. Additionally misinsertions of such less-activated monomers, *i.e.* head-to-head (HH) additions instead of head-to-tail (HT) additions (Scheme 2d),[23,24] occur more frequently as a result of the absence of any stabilisation of the formed radical for either form of addition. The HH additions leads to the formation of a primary radical which is less stable compared to the secondary radical formed *via* HT additions. As a result, the equilibrium between the dormant and active species for a HH addition is pushed towards the dormant side resulting in their accumulation and a loss of control over the polymerisation.

Over the last 10 years, intense research on the control of such reactive radical species has allowed to develop controlling agents capable of polymerising some less-activated monomers in a controlled manner, namely for RAFT,[5,9,25,26] OMRP.[17] Yet, many other LAMs, *e.g.* olefinic and allylic monomers, remain extremely challenging to homo- or copolymerise using reversible deactivation radical polymerisations.

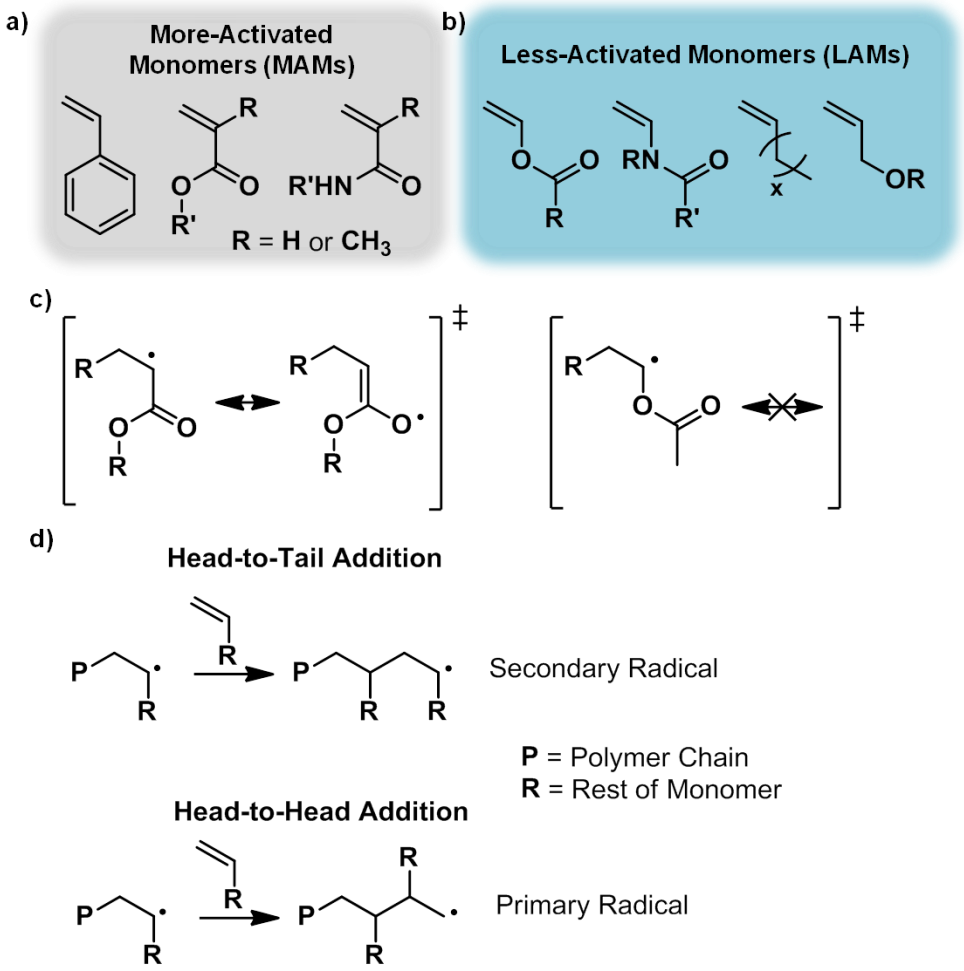

Scheme 2. Examples of a) more activated monomers (MAMs), b) less activated monomers (LAMs),[17,27] and c) the resonance stabilisation of the formed radical species as observed for MAMs while for LAMs no stabilisation is possible. d) Displays the two types of additions which can take place during radical polymerisations, Head-to-Tail and Head-to-Head.

2.1.1. Organometallic-Mediated Radical Polymerisation using Cobalt Complexes

Organometallic-mediated radical polymerisation (OMRP) is a reversible deactivation radical polymerisation method based on the temporary deactivation of the growing radical chains by a metal transition complex. The first example of OMRP was reported by Wayland *et al.* in 1994 for the controlled polymerisation of acrylates using organocobalt porphyrin complexes.[28] Since then, cobalt salen, cobalt oxime, vitamin B12, and cobalt *bis*(acetylacetonato) complexes, as well as complexes based on other metals, have been considered as controlling agents.[16,18] The type of monomers polymerised in a controlled manner by this RDRP technique extends from activated double bonds, such as acrylates, to non-activated double bonds, such as vinyl acetate (VAc) or ethylene. The ability of OMRP to mediate the polymerisation of such a large variety of monomers originates from the possible tuning of the metal-carbon bond strength through ligand adjustment. For example, the bond dissociation energy (BDE) of the cobalt-carbon (Co-C) bonds involved in this process is generally between 84 and 188 kJ/mol depending on the ligand.[29] The type of ligands coordinating to the cobalt and the type of carbon-centred radical (*i.e.* the type of monomer) play an important role in the strength of the Co-C bond and have a strong effect on the ability to control the chain growth of a particular monomer.

From a mechanistic point of view, organometallic-mediated radical polymerisation using a cobalt complex can undergo two pathways, reversible termination (RT) and degenerative chain transfer (DT). In the former, the growing radical chains are reversibly capped by the cobalt(II) complex leading to the formation of an alkylcobalt(III) dormant species. The cobalt-carbon bond of the latter can be cleaved upon thermal or photolytic treatment. This RT mechanism is illustrated in Scheme 3b for the OMRP of VAc using a $Co(acac)_2$ complex as controlling agent. Such a polymerisation can be initiated by a preformed organocobalt complex of *bis*(acetylacetonato) (R-$Co(acac)_2$) consisting of a short poly(vinyl acetate) chain (4 monomer units on average) bearing a V-70 radical initiator fragment and is end-capped by $Co(acac)_2$ (Scheme 3a).[30] Most polymerisations in this thesis were performed in the RT mode, which often offers the best level of control of the polymerisation, and were initiated using the above-mentioned R-$Co(acac)_2$ species. The RT mechanism can also occur when the polymerisation is initiated from V-70/$Co(acac)_2$ provided that a stoichiometric amount of radicals are generated form the initiator compared to the cobalt complex. In contrast, when the amount of radicals released in the medium exceeds the amount of metal, this cobalt-mediated radical polymerisation proceeds *via* a DT mechanism (Scheme 3c). In this case, the cobalt

complex exchanges one radical chain for another in a concerted manner. Interestingly, the addition of coordinating molecules can also prevent the DT mechanism from occurring by blocking the vacant coordination site of the alkylcoblat(III) species necessary for the degenerative transfer.

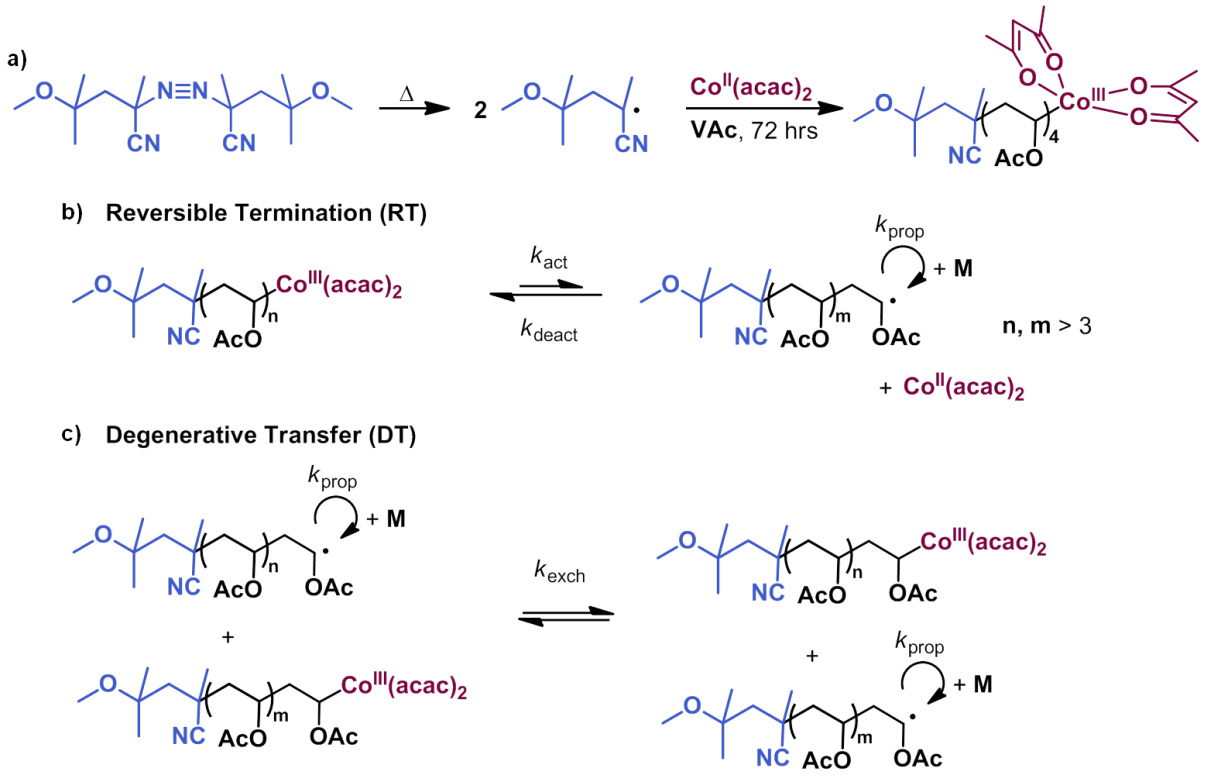

Scheme 3. a) Preparation of the alkylcobalt complex R-Co(acac)$_2$ used in the experiments performed in this thesis, with b) reversible termination (RT) and c) degenerative transfer mechanisms that can occur for this complex.

Another particularity of the OMRP was observed for the Co(acac)$_2$-mediated polymerisation of vinyl esters[24] and vinyl amides,[31] in that an intramolecular chelation of the oxygen or nitrogen atoms of the last monomer unit of the polymer chain to the metal centre takes place.[24,31] This phenomenon stabilises the dormant species as the additional ligation provides a favourable octahedral coordination sphere around the cobalt metal (Scheme 4). This extra-stabilisation generally improves the control over the chain growth process. It is particularly true for the OMRP of VAc which also undergoes head-to-head (HH) additions (Scheme 4).[23,24] In general, when applied to VAc, most other RDRP suffer from difficulties to reactivate the more stable HH-dormant species. For example in the case of RAFT, the rate of polymerisation is greatly reduced leading to polymers with broader molar mass distribution[25] while organotellurium-mediated radical polymerisations of VAc are completely inhibited.[32] This problem is not observed in the OMRP of VAc.[30] In this case, the H-H misinsertions form

a stronger C-Co σ-bond compared to the H-T addition (Scheme 4) but the stabilisation resulting from the intramolecular chelation phenomenon is more efficient for the regular H-T compound (five-membered ring) compared to the H-H dormant species (six-membered ring). All in all, quite similar global BDE were predicted by density functional theory (DFT) calculations for both dormant species resulting in comparable reactivation rates for both H-H and H-T dormant species and a better control over the chain growth process was observed compared to other RDRP techniques.

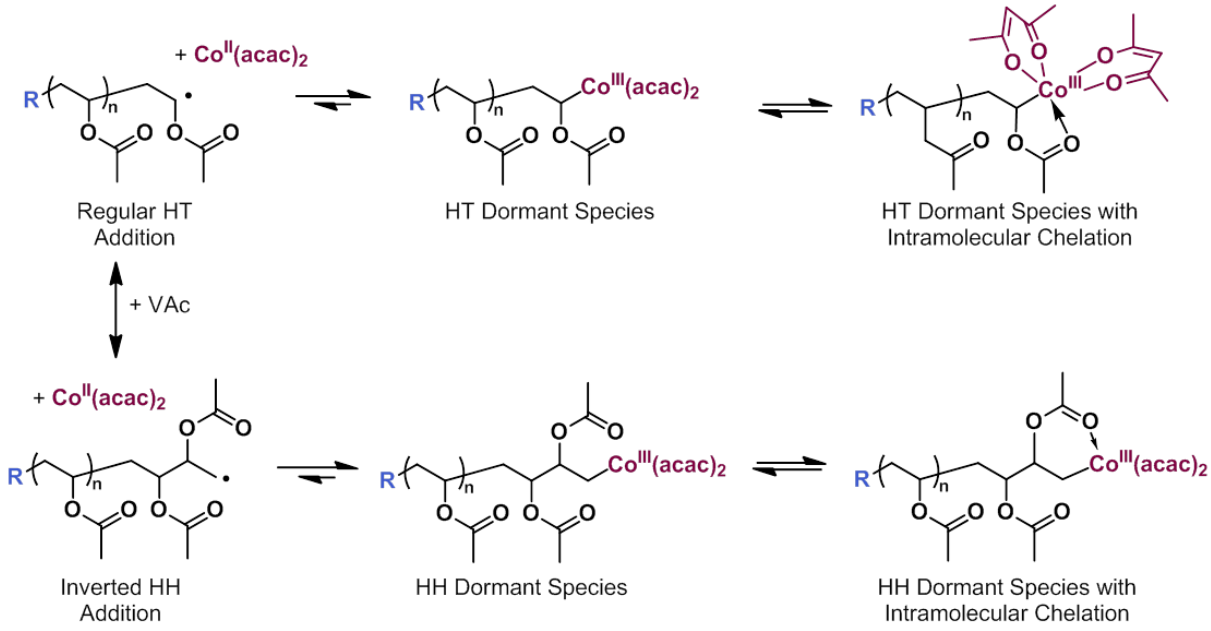

Scheme 4. Active/dormant equilibria for the head-to-head (HH) and head-to-tail addition (HT) of vinyl acetate to a growing polymer chain using $Co(acac)_2$ as the controlling agent. The intramolecular chelation observed for the HT and HH dormant species stabilising these species is also shown.

Another point to consider in OMRP is the effect of solvents or additives on the polymerisation as these can act as ligands to the metal. This was clearly demonstrated for the $Co(acac)_2$–mediated radical polymerisation.[30] Indeed, coordinating molecules, like pyridine, water, and DMF, stabilise the dormant species by saturating the coordination sphere of the metal but also enter into competition with the intramolecular chelation described above. Overall, upon coordination of the deactivating cobalt(II) complex, these molecules displace the active/dormant equilibrium towards the active species which increases the polymerisation kinetics (right hand side in Scheme 5). As a result a high concentration of coordinating molecules or the use of strongly binding ligands shift the equilibrium further towards the active species. A careful selection of these parameters is necessary in order to speed up the polymerisations while preserving their controlled character.

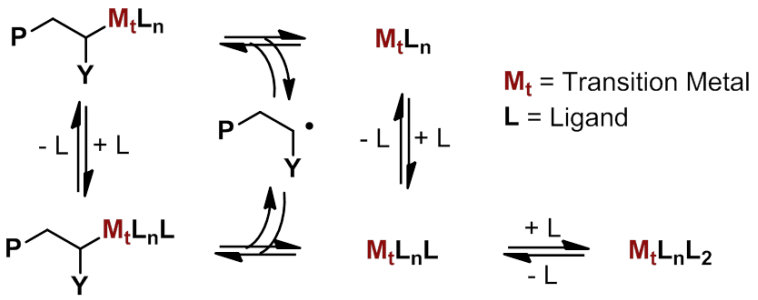

Scheme 5. Active/dormant species equilibria for OMRP in the presence of ligands such as water, dimethyl sulfoxide (DMSO), and dimethylformamide (DMF).

2.2. Renewable Monomers for Controlled Radical Polymerisations

Renewable resources are ubiquitous in our everyday life and have been used since the beginning of mankind whether it be in medicine, perfume or as materials. In contrast to fossil fuel resources, which were formed over millions of years, bio-sourced raw materials can be produced every year by well established agricultural processes. Starting from CO_2, water, light and a few minerals, a multitude of different chemicals and materials, *e.g.* sugars, oils, and fibres, are produced by plants, which at their end of life decompose back into the starting materials. This natural closed loop of raw materials serves as the blueprint for a circular economy, first proposed by Stahel in 1981,[33] and is based on reuse, repair, upcycling and recycling. In light of global warming and the pollution caused by single-use plastics, this idea has been recently put back into the focus of politicians, the media and governments, as exemplified by the proposed action plan for a circular economy in the European Union.[4] The renewability of resources and the sustainable use of them are at the heart of such an economic model. In 2017 less than 1 % of the worldwide polymer production, around 2 Mt, was bio-based.[34] This low amount of renewable polymers available industrially stems from multiple reasons such as higher cost, lower mechanical properties, availability and uniformity of the resources from one year of production to the next. Another issue is the use of raw materials which can also be used as food for the preparation of chemicals and materials. Especially in light of the hunger and poverty which still prevails around the world, the renewable feedstock should be non-food based or use resources which otherwise go to waste, *e.g.* lignin. Whereas this is certainly true, one must also consider that food and feed renewable feedstocks may have different sources in the future, as for instance algal oils for fatty acids or cellulose instead of starch as fermentation feedstock. In the end, a balance needs to be established that allows the use of renewable feedstocks for all applications, including food, without competition, which should be possible considering that our planet produces ~10^{11} tons of biomass annually.[35,36]

In terms of renewable monomers for radical polymerisations, few examples of completely renewably-sourced monomers exist, as not many natural molecules contain polymerisable double bonds[37–39] and hardly any sustainable functionalisation pathways exist for the attachment of renewably sourced double bonds to natural molecules.[40] Furthermore, the non-activated nature of many naturally occurring double bonds and the functionalities present in renewably-sourced molecules still pose many challenges for most controlled radical polymerisation techniques, see LAMs discussion above. Herein recent efforts in the synthesis

of renewable monomers and their controlled radical polymerisation are highlighted. Other types of polymerisations or free radical polymerisations of renewable resources are outside of the scope of this review and have already been described in detail elsewhere.[37,38,41–44]

This chapter deals with monomers from renewable resources in two sections. The first section considers natural molecules which already contain double bonds suitable for polymerisation and derivatives of these molecules in terms of their structure are also discussed. These monomers are entirely bio-based, as no derivatisation is necessary, and are often available on a multi-ton scale *via* established industrial processes, *e.g.* extraction or distillation. The second section deals with natural molecules which cannot be directly polymerised and need to be functionalised with double bonds in order to be used as renewable monomers for CRP. In most cases, such monomers are only partly bio-based as they are functionalised with acrylates or other polymerisable functions stemming from petroleum-sources. In addition, their synthesis is performed on a lab scale and their industrial implementation is far from practical. Yet, recent developments, especially in the enzymatic functionalisation of natural molecules, have provided promising advances into the direction of green and sustainable synthesis of renewable monomers. Unless otherwise stated, 2,2′-azobisisobutyronitrile (AIBN) is used as the initiator for the polymerisations reported.

2.2.1. Renewable Molecules Containing Double Bonds

Natural molecules are often multifunctional bearing many heteroatoms such as oxygen or nitrogen. Unsaturated bonds are often internal, conjugated or non-activated thus still pose great challenges for their controlled radical polymerisation, as the radical formed during polymerisation is not stabilised and thus highly reactive. Examples are the homopolymerisation of allylic or internal double bonds, such as those found in eugenol, pimaric acid, or triglycerides, while several successful examples of CRP of a variety of activated and non-activated double bonds from renewable resources have been reported and are listed below.

2.2.1.1. Terpenes

Terpenes or terpenoids are a major class of compounds extracted industrially on a kiloton scale from coniferous trees and plants.[41] Over 25,000 different terpenes are known,[45] which have historically been used as solvents (turpentine) or as essential oils and fragrances. They consist of a hydrocarbon structure with a low, if any, oxygen content, which sets them apart from most other natural molecules. The most important terpenes in terms of their availability

include α- and β- pinene, menthol, and limonene which vary in their composition in carbon, hydrogen and oxygen (Scheme 6). Radical polymerisation of these molecules is rather challenging, as the internal (in α-pinene, limonene, and carvone) and sterically hindered double bonds (in β-pinene) are prone to termination and transfer reactions.[46,47] Additionally, polyterpenes are poorly soluble in common organic solvents, *e.g.* tetrahydrofuran, chloroform, and require the use of non polar solvents during polymerisation which are not suitable for some RDRP techniques, such as ATRP.[12] As a result, mainly copolymerisations with more soluble comonomers were performed and the different terpene monomers investigated for RDRP are summarised below.

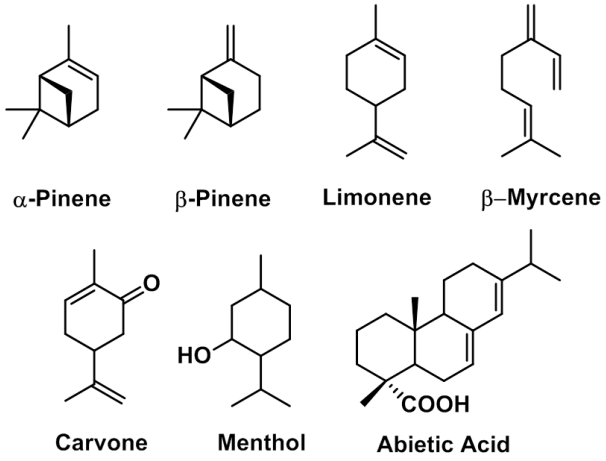

Scheme 6. A selection of naturally occurring terpenoids with different degrees of unsaturation and number of oxygen atoms.

Two different isomers of pinene exist: α-pinene, bearing an internal double bond, and β-pinene, containing a terminal double bond (Scheme 6). While α-pinene has not been successfully copolymerised so far, several examples of β-pinene copolymers with monomers bearing activated or conjugated double bonds, successfully homopolymerised using RDRP in the past, are reported in the literature. Akin to cationic polymerisations the radical moves into its most stable position on the β-pinene molecule which is the tertiary isopropyl carbon (Figure 3a). The first reports in 2016 described the copolymerisation of β-pinene with acrylonitrile and methyl acrylate (Figure 3b) using reversible addition fragmentation (RAFT) polymerisations.[48,49] A variety of different RAFT agents, dithiobenzoates (2-cyano-2-propyl dithiobenzoate (CPDB), 2-cyanoethyl dithiobenzoate (CED), cumyl dithiobenzoate (CDB) and 1-(methoxycarbonyl)ethyl dithiobenzoate (MEDB)) and a xanthate (1-(methoxycarbonyl)ethyl phenyl dithioacetate (MEPD); Figure 3c) were tested at 70 °C in the bulk and a decrease in polymerisation rate compared to free radical polymerisation was

noted. A possible explanation for the low polymerisation rate of acrylonitrile/β-pinene copolymerisations was provided by ^{1}H NMR spectroscopy analysis of the copolymer ω-chain ends. These revealed that the majority of chain-ends carrying the RAFT agent contained a β-pinene unit which suggested that the fragmentation rate for this repeat unit is low. After 40 hours, 33% conversion were reached for acrylonitrile/β-pinene copolymerisations after which a deviation from first-order kinetics and a stagnation of molecular weights (Figure 3d) were observed which indicate a loss over the chain growth process. A similar lack of control was observed for methyl acrylate/β-pinene copolymerisations from 40% conversion onwards and was attributed to the degradative chain transfer of the radical to the allylic hydrogens of β-pinene leading to the termination of the polymerisation (Figure 3e) and is a well known phenomenon for monomers bearing allylic hydrogens.[50] Nonetheless, the copolymers obtained below 40% conversion, displayed low dispersities, below 1.49, and a pinene content of up to 18 and 9 mol% for acrylonitrile and methyl acrylate copolymerisations, respectively. Increasing the β-pinene content in the feed led to a significant drop in conversion for both copolymerisations. The addition of a Lewis acid, Et_2AlCl, to the RAFT polymerisation enabled a higher β-pinene incorporation but reduced the molecular weights while increasing the dispersities.

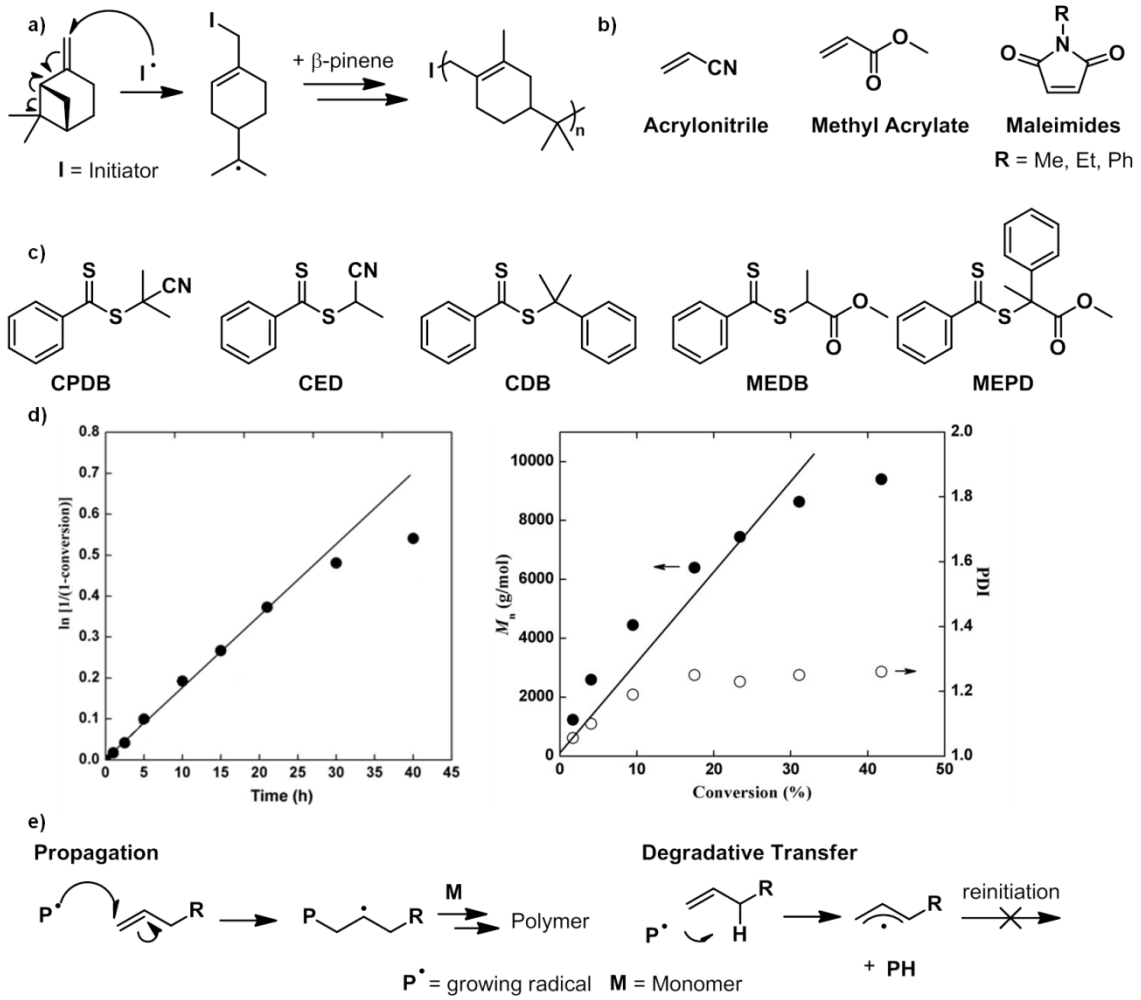

Figure 3. a) Polymerisation mechanism of β-pinene, b) homopolymerisable comonomers bearing activated double bonds used for the copolymerisation of β-pinene, c) various CTA agents tested for the copolymerisation of β-pinene with acrylonitrile and methyl acrylate. d) first-order kinetic plot and d) molecular weights and dispersity versus conversion plot for 10 mol% β-pinene feeds for its copolymerisation with acrylonitrile. e) Degradatative transfer of allylic hydrogen bearing monomers. Adapted with permission from *J. Polym. Sci. Part A Polym. Chem.* **2006**, *44* (8), 2376–2387. © 2006, John Wiley and Sons

Further RAFT copolymerisations of β-pinene using dithiobenzoates and xanthates with monomers bearing activated double bonds, such as *N*-substituted maleimides[51] (Figure 3b) and maleic anhydride[52] (Figure 4a), soon followed. These studies highlighted the importance of the right polymerisation solvent as for example the β-pinene/maleic anhydride copolymerisation was slow in THF (10% conversion after 48 hours), it proceeded much faster in 1,4-dioxane (30 % conversion after 24 hours) but at the cost of a broadening of the molecular weight distributions (M_w/M_n = 1.39). Through the use of a mixed solvent system, 1:9 v/v THF/dioxane, a better control over the chain growth process was obtained leading to similar conversions (22% conversion after 48 hours) as in dioxane but lower dispersities

(M_w/M_n = 1.29). For the same comonomer pair, the control over the polymer chain ends possible using RDRP was exploited for the synthesis of block copolymers with styrene (Figure 4a). These were subsequently hydrolysed to yield amphiphilic poly(β-pinene-*co*-maleic acid-*block*-styrene) copolymers which self-assembled into micelles in water at pH = 6 as observed by scanning electron microscopy (SEM; Figure 4b).

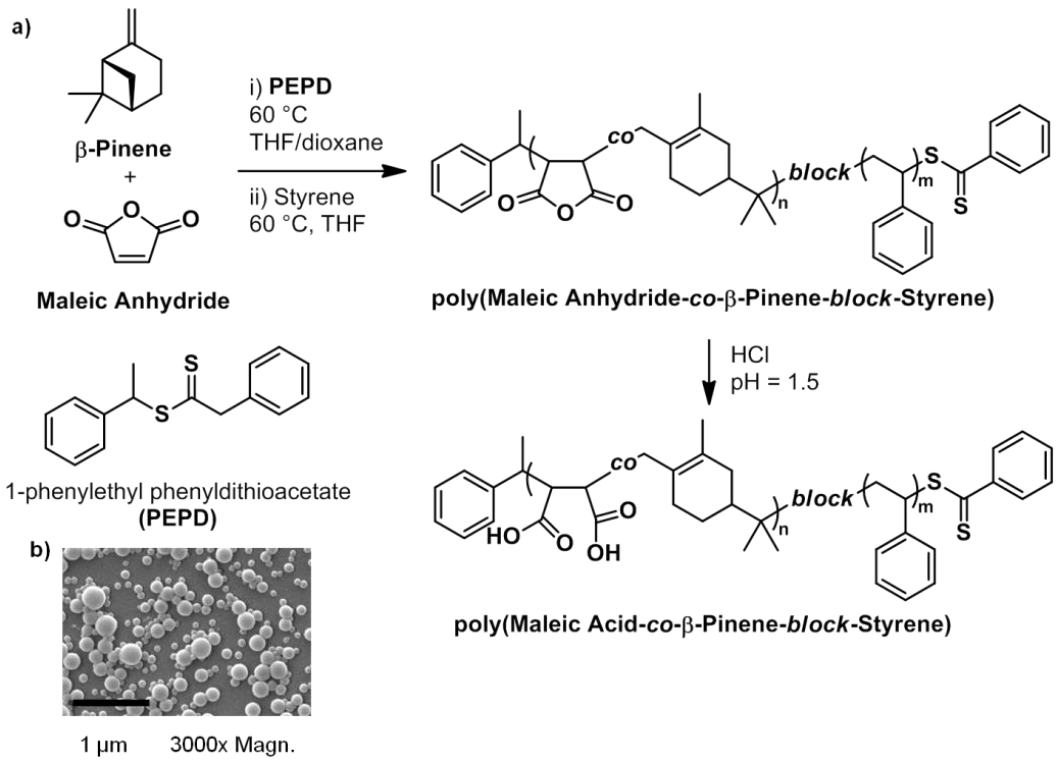

Figure 4. a) Copolymerisation of β-pinene and maleic anhydride into a macroRAFT agent and subsequent chain extension using styrene to form poly(maleic anhydride-*co*-β-pinene-*block*-styrene) copolymers which were b) hydrolysed into poly(maleic acid- *co*-β-pinene-*block*-styrene) copolymers showing self-assembly in aqueous solution. Adapted with permission from *J. Polym. Sci. Part A Polym. Chem.*, **2015**, *53*, 1422-1429. © 2015, John Wiley and Sons

While the copolymerisation of β-pinene resulted in polymers bearing cyclohexene rings in the backbone, the polymers based on limonene would have this group pending from the backbone. Kamigaito *et al.* set out to synthesise a sequence-controlled copolymer based on limonene and derivatives of *N*-maleimide using both free radical and RAFT polymerisations.[53] To achieve this, they first employed free radical polymerisations to determine basic information of the copolymerisation, such as reactivity ratios, copolymer structure and copolymerisation kinetics in different solvents, before applying RAFT polymerisations. RAFT polymerisation was used as it is known to allow polymerisation of

inactive monomers in the presence of a suitable chain transfer agent, which in this case were two trithiocarbonates (*n*-butyl cumyl trithiocarbonate (CBTC) and *n*-butyl 2-cyano-2-propyl trithiocarbonate (CPBTC)). The copolymerisations were performed at 60 °C in a fluorinated alcohol (1,1,1,3,3,3-hexafluoro-2-phenylpropan-2-ol), as this solvent was found to interact via the hydroxyl group with the carbonyls of the maleimide and favour a AAB-sequence of monomer addition independent of the monomer feeds (where A is *N*-phenylmaleimide and B is limonene; Figure 5a). The MALDI-TOF spectrum of a low molecular weight copolymer, not only highlighted the sequence-regulated nature of the copolymer but also that the copolymer was end-capped by the controlling agent (Figure 5b). Yet no evidence, *e.g.* first order kinetic plot, was provided for the controlled chain growth process and rather broad molecular weight distributions (M_w/M_n > 1.48) were obtained for the low molecular weight (M_n < 10,000 g mol^{-1}) copolymers reported. Related sequence-regulated copolymers containing ethyl- and cyclohexyl-substituted maleimides were later reported by the same group using a similar system but again only low molecular weights were reported (M_n < 3,000 g mol^{-1}).[54]

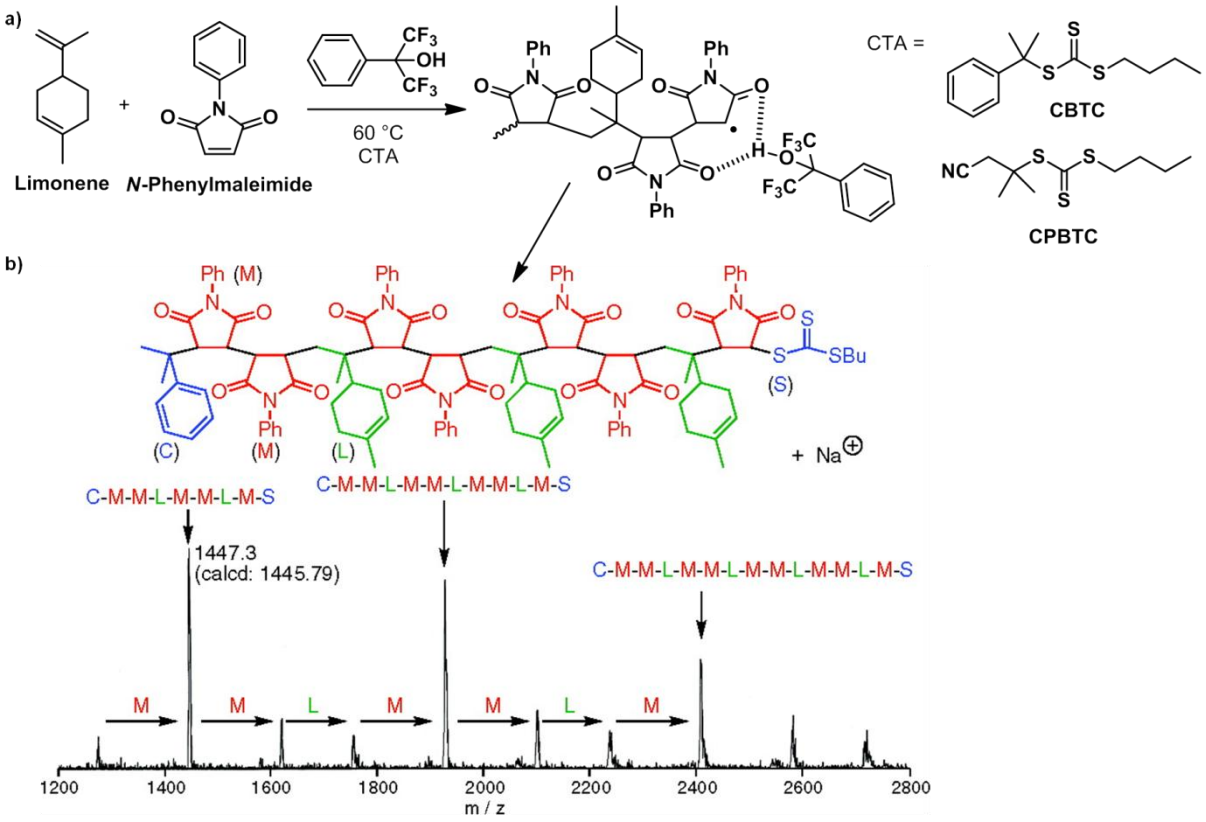

Figure 5. a) Copolymerisation of limonene and maleimide as performed by Satoh *et al.* The presence of a fluoroalcohol favours a sequenced addition of the monomers as verified by b) MALDI-TOF analyses. Adapted with permission from *J. Am. Chem. Soc.*, **2010**, *132*, 10003-10005. © 2010, American Chemical Society

Kali *et al.* were the first to report the homopolymerisation of a terpene, namely myrcene (Figure 6a), using a RDRP technique.[55] RAFT polymerisation with a trithiocarbonate CTA (ethyl 2-[(ethylthio)thiocarbonylthio]propionate (EETP)) was used at 65 °C because of its ability to (co)polymerise non-activated double bonds. Although conversions were limited to below 50%, the linear increase of the molecular weights with conversion (Figure 6b), the low dispersities (Figure 6b), and the linear pseudo first order plot (Figure 6c) evidenced the controlled chain growth process. Analysis of the formed polymyrcene using ^{1}H and ^{13}C NMR spectroscopy, revealed a predominant 1,4-addition of the myrcene unit during the polymerisation in both *cis* and *trans* conformers, while less than 4% of other insertions were identified (Figure 6a), presumably as a result of the steric hindrance. Such a high degree of 1,4-additions was previously not possible to attain using Ziegler-Natta, free radical or anionic polymerisation. Further investigations by the same group complemented these findings and by changing the RAFT agent, radical initiator, and temperature, conversions could be substantially increased to 64%.[56]

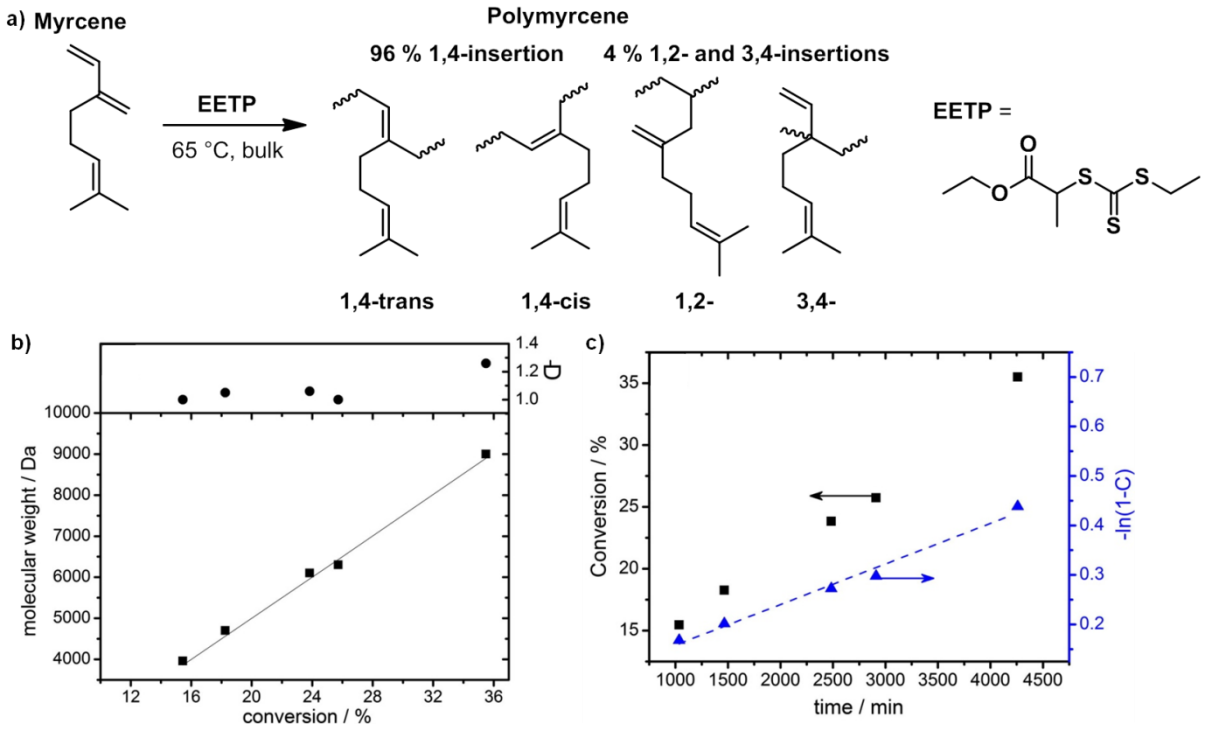

Figure 6. a) Copolymerisation of myrcene into polymyrcene in the bulk with different monomer repeat units identified,[55] b) plot of molecular weight and dispersity versus conversion, and c) plot of conversion and pseudo first order monomer consumption versus time. Reprinted with permission from *Eur. Polym. J.*, **2015**, 73, 363-373. © 2015, Elsevier Ltd.

In 2017, Marić *et al.* demonstrated that the polymerisation of myrcene was also possible using nitroxide-mediated radical polymerisation (NMP).[57] The authors envisaged to synthesise polymyrcene but also statistical and block copolymers with styrene using (2-[*N*-tert-butyl-2,2-(dimethylpropyl)aminooxy]propionic acid, BB; Figure 7a) and a *N*-hydroxy succinimide–functionalised derivative (2-methyl-2-[*N*-tert-butyl-*N*-(1-diethoxyphosphoryl-2,2-dimethylpropyl)-aminoxy]-*N*-propionyloxysuccinimide, NHS-BB; Figure 7a) as the controlling agent in order to obtain (co)polymers with a tunable T_g. The reaction conditions (temperature, solvent, initiator concentration and the addition of excess controlling agent) were screened and the authors found that the NHS-BlocBuilder at 120 °C in bulk without the addition of excess controlling agent gave the best control over the homopolymerisation of myrcene. While polymer microstructure was less regular compared to the above RAFT system, 1,4-addition segments were constant at 80% (compared to 96% for RAFT) with 80% of *cis* content, the NHS-BB system allowed to reach conversions above 80% (cf. 50% for RAFT). Statistical copolymerisations of myrcene and styrene at 110 °C in bulk using NHS-BB, allowed to prepare poly(myrcene-*co*-styrene) statistical copolymers for the whole composition spectrum (*i.e.* 0-100 mol% styrene) which resulted in a T_g tunable from -77 °C to 80 °C (Figure 7b). Furthermore, the chain-end fidelity of the homo- and co-polymers was proven by chain extensions at 110 °C in 50 wt% toluene using styrene (Figure 7c). The mechanical properties of these block copolymers (ultimate tensile strength <1.1 MPa, elongation at break <11%) were however far inferior to poly(isoprene-*b*-styrene) (tensile strength >20 MPa, elongation at break >1000%) and poly(butadiene-*b*-styrene) (tensile strength >20 MPa, elongation at break >700%) copolymers prepared by NMP under comparable conditions.

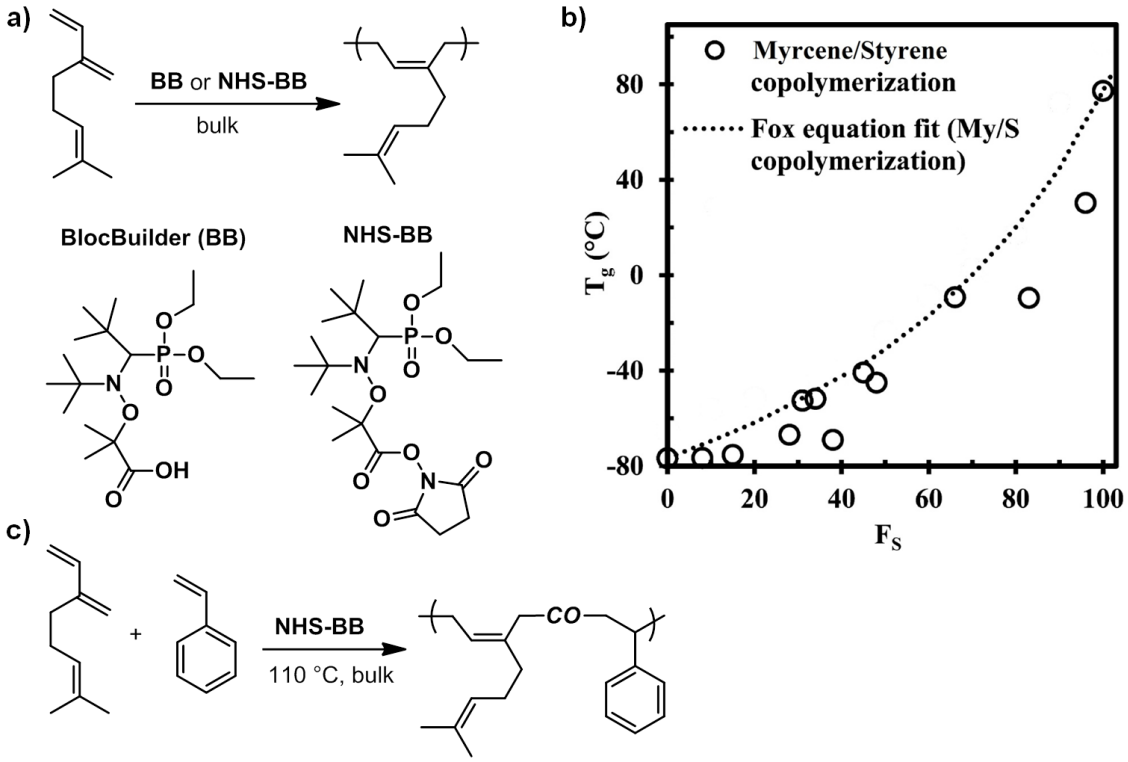

Figure 7. a) Nitroxide-mediated homopolymerisation of myrcene and copolymerisation of myrcene with styrene using BlocBuilder (BB) and NHS-functionalised BlocBuilder and b) a plot of T_g against poly(myrcene-*co*-styrene) composition for copolymers obtained by Marić *et al.*[57] Adapted with permission from *Macromolecules*, **2017**, *50*, 3101-3120. © 2017, American Chemical Society

Apart from myrcene, only Kamigaito *et al.* have reported on the homopolymerisation of a terpene monomer, namely pinocarvone which is obtained from α-pinene via photooxidation (Figure 8a), using RAFT.[58] In an attempt to synthesise bio-based polyketones, CTAs with different activities were tested (dithiobenzoates, trithiocarbonates, dithiocarbamates) and trithiocarbonates displayed the fastest quantitative conversion (50 hours) and displayed the most linear increase in molecular weights with conversions while retaining narrow molecular weight distributions (blue dots/line, Figure 8b). Similar to the copolymerisation of β-pinene discussed above, the polymerisation solvent, or absence of it, strongly affected the polymer structure. For bulk polymerisations, a radical ring-opening polymerisation (rROP) mechanism was in competition with a conventional 1,2-radical polymerisation mechanism which led to a polymer with both a main chain and a pendant 6-membered cyclic ketone in a ratio of 0.32:0.68 as determined by the ^{1}H NMR spectrum (Figure 8c). In a fluorinated alcohol (1,1,1,3,3,3-hexafluoro-2-phenylpropan-2-ol), on the other hand, rROP took place almost exclusively to yield a polymer with 99% of ketone units in the backbone (Figure 8b). These ketone functionalities were shown to be functionalisable using Michael additions, thiol-ene

reactions or reductions, and provided a powerful tool for the synthesis of functional polymers from bio-sources. Investigations into hard-soft block copolymers were performed using a trithiocarbonate-based macroRAFT agent with *n*-butyl acrylate (BA) and methyl acrylate (MA) as the soft segment and pinocarvone as the hard segment. A shift in microphase separation from spherical to lamellae-like was observed in the phase images taken by AFM upon increasing the pinocarvone amount in the block copolymer from 15 to 30 wt% (Figure 8d). This example neatly highlights the potential and versatility that terpene-based polymers hold. Yet they remain challenging to polymerise as only two RDRP techniques (RAFT and NMP) have been able to control the chain growth process for these non-activated hydrocarbon monomers. RAFT appears most promising in terms of monomer scope, control over the microstructure, and its ability to reach high conversions. Yet room for improvements remains especially in light of the slow polymerisation kinetics and the little explored industrial applications of such copolymers, which have been reviewed before.[59]

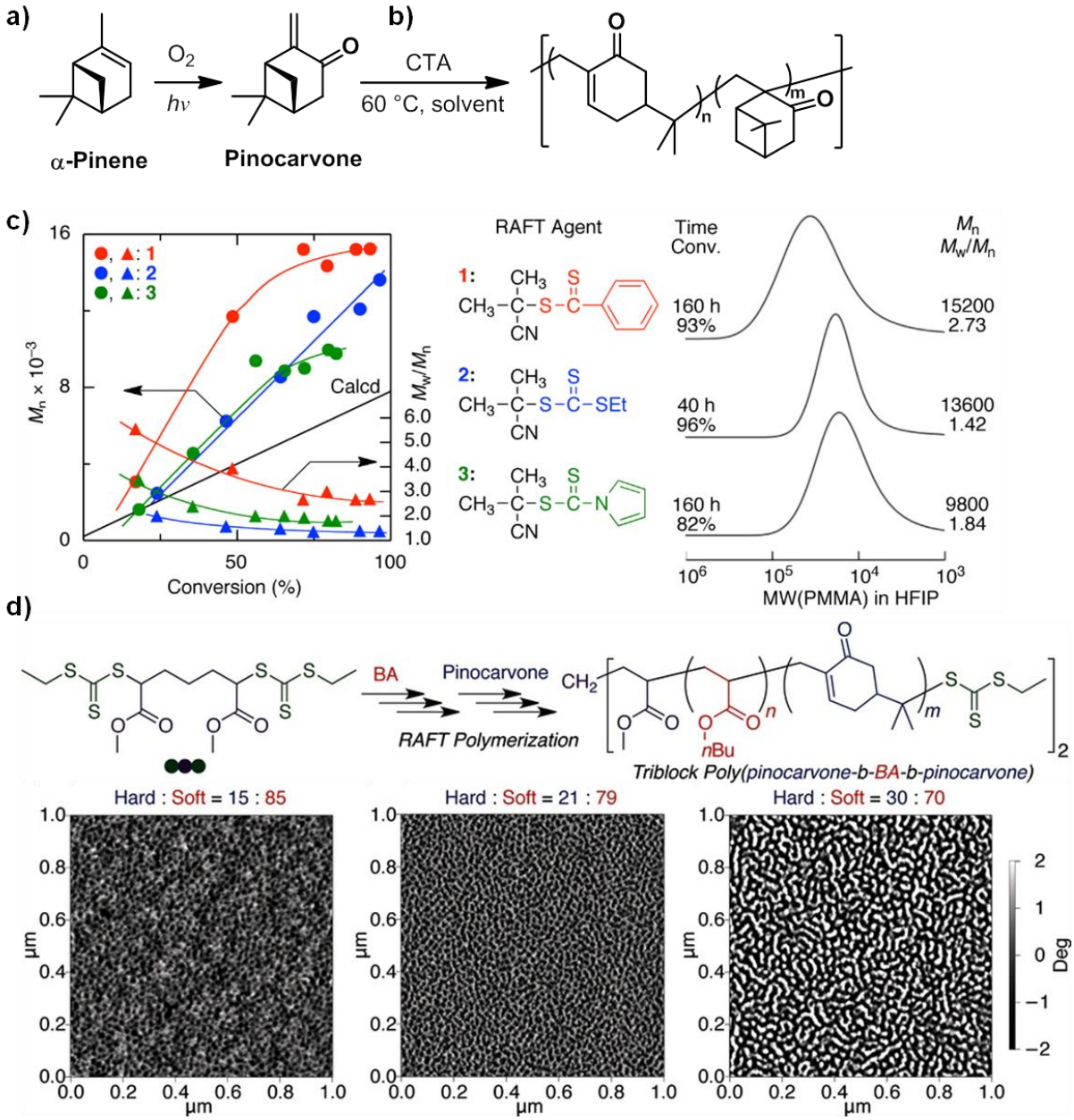

Figure 8. a) Structure of pinocarvone and its synthesis from α-pinene, b) RAFT polymerisation of pinocarvone yielding a polymer with two possible repeating units, c) plot of molecular weight and dispersity versus conversion for different types of CTA tested as well the SEC curves for the obtained polymers, and d) the synthesis of thermoplastic elastomers from butylacrylate and pinocarvone using a difunctional RAFT agent with different phase transitions observed in AFM phase images depending on the block copolymer composition. Reprinted with permission from *Angew. Chemie - Int. Ed.* **2016**, *55* (4), 1372–1376. © 2015, John Wiley and Sons

2.2.1.2. Cellulosic Biomass

Cellulosic biomass constitutes the largest renewable resource available on the planet, with an estimated 10^7 megatons available and a regeneration rate of 3% per year[35] and presents an almost inexhaustible raw material. In comparison, 348 million tons of plastic were produced worldwide in 2017.[60] Apart from its abundance, biomass presents a multitude of different functionalities and structures as a result of its different components, cellulose, hemicelluloses, and lignin. Over the last few years these raw materials have been increasingly studied for their effective transformation into monomers for a variety of different polymerisation processes.[61–63] Especially fermentation has led to promising platform chemicals, such as furfural or lactic acid, but few of these molecules contain a double bond which is polymerisable by radical processes. These examples are summarised below. Molecules derived from biomass which require further transformations to attach a double bond are discussed in Section 2.2.2.

2.2.1.2.1. Itaconates

Itaconic acid, or 2-methylenesuccinic acid, is a dicarboxylic acid (Scheme 2a) industrially produced on the kiloton scale *via* the bacterial fermentation of carbohydrates.[61,62,64,65] As a result of its structural resemblance to acrylates it is sometimes referred to as the natural methacrylic acid analogue (Scheme 7a). The presence of two carboxylic acid functionalities allows for the synthesis of a variety of substituted derivatives (Scheme 7b) and a frequently utilised transformation is that of itaconimides *via* an anhydride derivative (Scheme 7c and d).[66,67] Up to date no direct reversible deactivation radical polymerisations of itaconic acid have been reported.

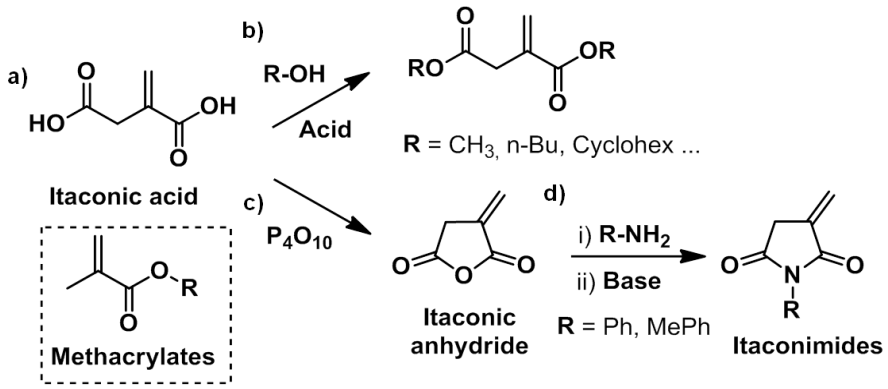

Scheme 7. a) Structure of itaconic acid and its transformation into b) disubstituted itaconates *via* esterifications[68] and c) into itaconic anhydride *via* dehydration[66] and d) subsequent aminolysis leading to itaconimides.[67] e) Structure of iron bromide 1,3-bis(2,6-diisopropylphenyl)imidazol-2-ylidene ($FeBr_3$(IDipp) catalyst for ATRP of phenylitaconimides.[69]

The first studies on the controlled polymerisation of itaconic acid–derived dimethyl itaconate (Scheme 7b) were carried out utilising an unconventional ATRP catalytic system using Cu(I)Cl, *p*-toluene 2-sulfonyl chloride as initiator and 2,2'-bipyridine (bipy) as ligand in the bulk.[70] Nonetheless, some conversion was observed (40%) after which point significant deviations from the linear increase of molecular weight with conversion were observed as a result of elimination and termination reactions. Similar difficulties using an iron-based ATRP catalyst for the copolymerisation of methyl methacrylate and *N*-aryl itaconimides were reported in a later study by Choudhary *et al.*[67] An improvement of the control over the chain growth process for *N*-phenyl itaconimide/methyl methacrylate was only obtained through the use of suitable ATRP initiator and a $CuBr_2$/bipy catalyst (Scheme 8a).[71] Yet, rather large dispersities (M_w/M_n = 1.3-1.56) were obtained and no comment on the comonomer incorporation was made.

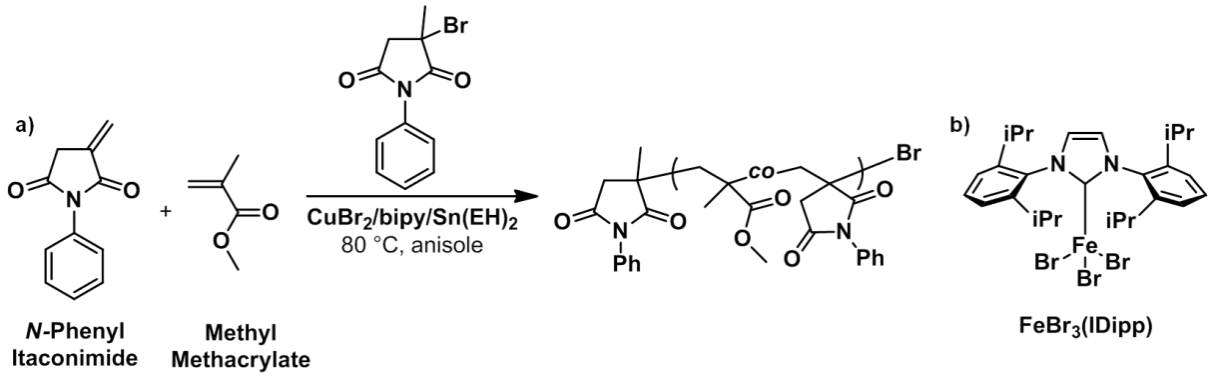

Scheme 8. a) Copolymerisation of *N*-phenyl itaconimide and methyl methacrylate using ATRP as reported by Deoghare *et al.*,[71] and b) a *N*-heterocyclic carbene-based iron catalyst used for the homopolymerisation of *N*-phenyl itaconimide.[69]

The successful homopolymerisation of *N*-phenyl itaconimide using ATRP was reported a year later in 2015 by Matyjaszewski *et al*. using an iron based catalyst (Scheme 8b).[69] Controlled polymerisations were obtained in anisole at 60 °C up to high conversions (70%) but broad molecular weight distributions were obtained (M_w/M_n >1.3). Standard ATRP catalyst systems of CuBr/amine ligands were not suitable for the polymerisation of *N*-phenyl itaconimide as they catalysed the double bond isomerisation forming a deactivated internal double bond which could not be polymerised. Copolymerisations of phenyl itaconimide were also shown to be possible with styrene for *N*-phenyl itaconimide feeds of 22-73 mol% but even broader dispersities were observed (M_w/M_n >1.55).

In an attempt to synthesise completely bio-based thermoplastic elastomers, a combination of ROP of a lysine-derived monomer and ATRP of *N*-phenyl itaconimide catalysed by a CuCl/bipy system was employed.[72] The chain extension of a soft (*i.e.* low T_g) lysine-derived bifunctional ATRP macroinitiator (Figure 9a) in DMF at 100 °C allowed to synthesise triblock copolymers with moderate tensile strength (10-15 MPa) and a high elongation at break with no failure after 800 % of elongation. Comparisons of these mechanical properties with other/commercial thermoplastic elastomers was not provided. A tuning of the *N*-phenyl itaconimide block allowed to tune the tensile strength and elongation at break (Figure 9b). Unfortunately the synthesis of the lysine-derived monomer required the use of phosgene and protecting groups which rendered the synthesis toxic and low yielding (35 %), thus putting into question the sustainability of this monomer and the polymers based on it.

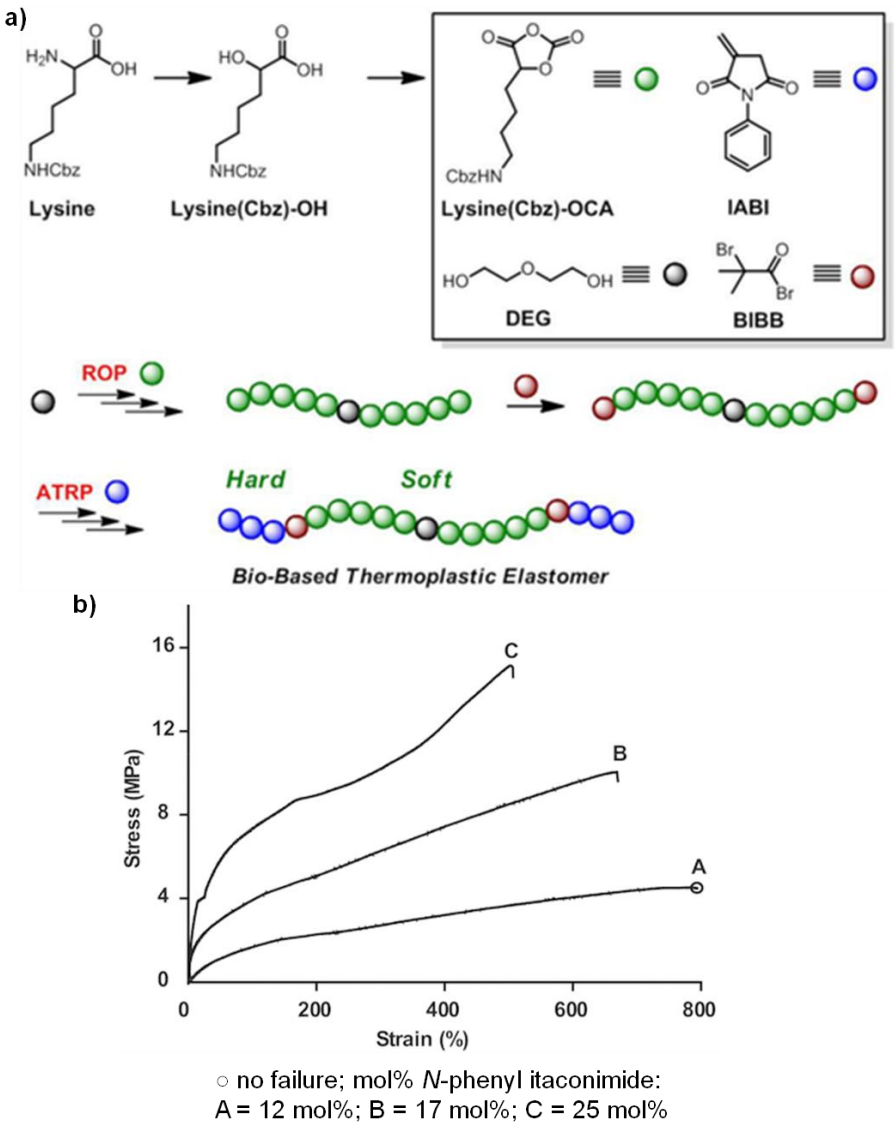

Figure 9. a) Structures of the protected lysine-derived monomer, *N*-phenyl itaconimide, ROP initiator, and acyl halide used to functionalise the lysine block with ATRP initiators, and b) stress-strain curves of triblock copolymers containing different amount of *N*-phenyl itaconimide. Adapted with permission from *J. Polym. Sci. Part A Polym. Chem.* **2016**, *55* (2), 349–355. © 2016, John Wiley and Sons

More successful polymerisations of esterified itaconic acid derivatives were performed by Barner-Kowollik *et al.* using RAFT polymerisation.[73] Dibutyl itaconate and dicyclohexyl itaconate (Scheme 7b) were polymerised using dithiobenzoate, dithioacetate and trithiocarbonate (cumyl dithiobenzoate (CDB), cumyl phenyl dithioacetate (CPDA), and *S*,*S*'-*bis*(α,α'-dimethyl-α''-acetic acid) trithiocarbonate (BDAT)) as CTAs at 65 °C in the bulk (Figure 10a). While the thiobenzaote led to almost no conversion for the butyl functionalised itaconate (3.5% after 12 hours) and the dithioacetate was limited to low conversions for dicyclohexyl itaconate (max. 20% conversion), the trithiocarbonate CTA reached conversions

above 50% and showed a linear increase of molecular weight with conversion for both monomers (Figure 10b). Yet rather large dispersities were observed ($M_w/M_n > 1.5$) which was ascribed to the occurrence of a hybrid polymerisation behaviour between free radical and controlled radical polymerisation. Such systems were characterised by a low initial addition rate constant of the growing radical chain to the RAFT agent (k_{add}) compared to the propagation rate constant (k_p; Figure 10c). A rapid increase of the molecular weights at the beginning of the reaction was observed, followed by the linear increase of molecular weights with conversion, resulting in a semi-controlled polymerisation. Nonetheless, chain extensions with styrene using the trithiocarbonate CTA led to rod-coil block copolymers bearing a stiff itaconate block (rod) and styrene block (coil). The potential of such bio-based copolymers for nanopatterned surfaces was highlighted by Kamigaito *et al.* in 2014.[74] Using dithiobenzoates (CDB, and 4-cyanopentanoic acid dithiobenzoate (CPADB)) and trithiocarbonate (*S*-2-cyano-2-propyl-*S*'-ethyl trithiocarbonate (CPETC)) CTAs, the homopolymerisation of 'soft' dibutyl itaconate and bis(2-ethylhexyl) itaconate at 20 °C in bulk, as well as 'hard' *N*-phenylitaconimide and *N*-(tolyl)itaconimide at 50 °C in 1,4-dioxane were investigated. In both cases, the best control over the polymerisation was obtained using dithiobenzoates, CPADB or its difunctional derivative for the 'soft' monomers (Figure 11a) and CDB for 'hard' monomers (Figure 11b). In both cases molecular weights above 10,000 g mol^{-1} were obtained with excellent dispersities (M_w/M_n <1.4). Block copolymers with very narrow molecular weight distributions (M_w/M_n <1.32) were obtained starting from either a 'soft' or 'hard' macroRAFT agent and again demonstrated the excellent control over the polymerisation. Thermal analysis as well as dynamic mechanical analysis and atomic force microscopy (AFM) revealed a co-continuous lamellae and/or a cylinder-type morphology of the block copolymers (Figure 11c).

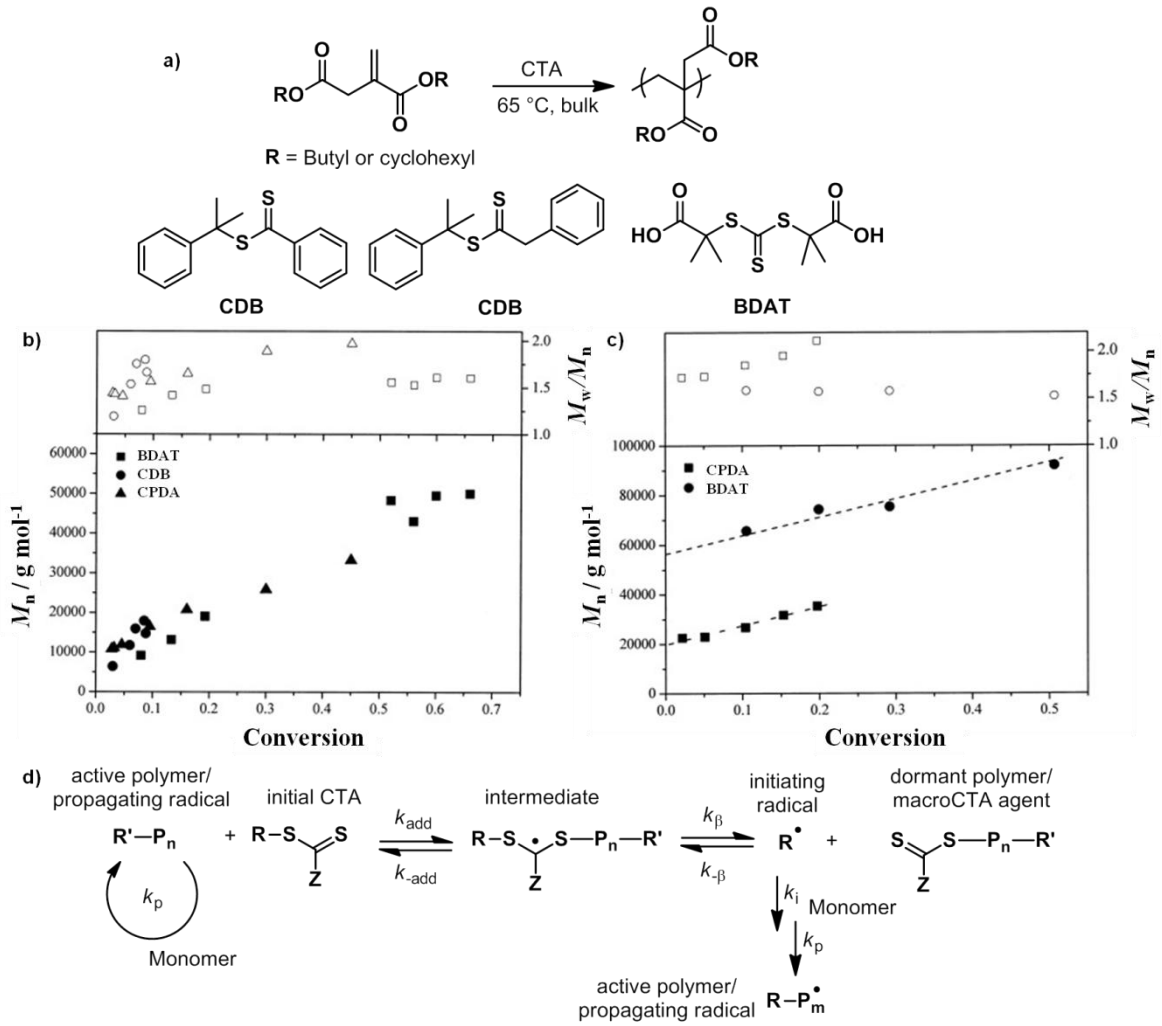

Figure 10. a) Homopolymerisation of dibutyl and diphenyl itaconate using different CTAs and the evolution of molecular weights and dispersities as a function of time for of a) dibutyl itaconate, and b) diphenyl itaconate. Adapted with permission from *J. Polym. Sci. Part A Polym. Chem.* **2004**, *42* (10), 2432–2443. © 2004, John Wiley and Sons. c) Initialisation mechanism for RAFT polymerisations, adapted from Moad.[75]

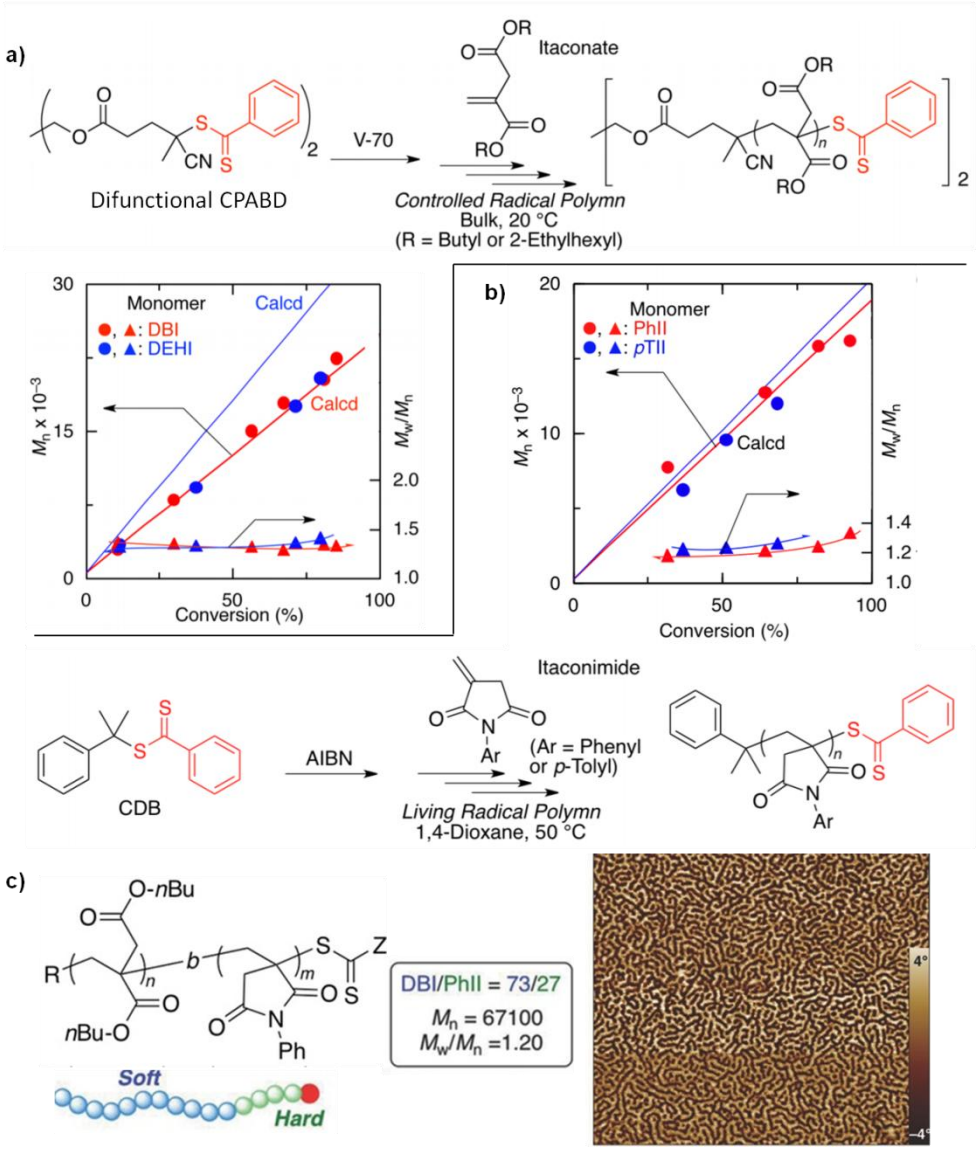

Figure 11. RAFT polymerisations of a) *N*-phenyl and *N*-*p*-tolyl itaconimide at 50 °C in 1,4-dioxane using CDB, and b) dibutyl- and di-2-ethylhexyl itaconate at 20 °C in bulk using a bifunctional CPADB-derivative. c) Block copolymer architectures possible for either CTA and the microphase pattern of the block copolymers as observed by AFM. Adapted with permission from *Macromol. Rapid Commun.* **2014**, *35* (2), 161–167. © 2013, John Wiley and Sons

The dual functionality of itaconic anhydride (Scheme 7) was thoroughly investigated by Hvilsted *et al.* as its copolymer with methoxyethyl acrylate allowed for the synthesis of a multifunctional nanoparticle scaffold using a combination of RAFT copolymerisation and efficient azide-alkyne cycloaddition reactions.[76] Bulk RAFT copolymerisations at 70 °C using CPDB as CTA showed a perfectly linear evolution of molecular weight with conversion along with low dispersities ($M_w/M_n \approx 1.25$) and a linear pseudo-first order kinetic plot, all indicative of a controlled polymerisation. The anhydride moieties in a low molecular weight polymer

(M_n = 4,100 g mol^{-1}) were aminolysed with propargylamine to introduce alkyne functionalities to the copolymer and reduce the dithioester of the CTA (Scheme 9a). The strained ring conformation of the anhydride ensured that side reactions with the acrylate did not take place. Subsequently, the copolymer was attached to gold nanoparticles *via* the thiol chain-end obtained through the reduction of the dithioester RAFT agent. As a proof of concept, these nanoparticles were functionalised with a bulky dendron bearing amino acids segments (Scheme 9b) which can be replaced by other molecules of biological importance and thus be useful for drug delivery and other medical applications.

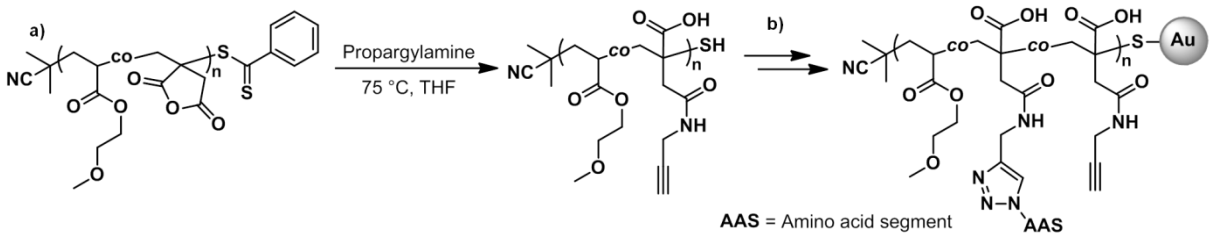

Scheme 9. Structures of a) poly(methoxyethyl acrylate-*co*-itaconic anhydride) prepared by RAFT polymerisation using CPDB and its aminolysed form, and b) the copolymer attached to a gold nanoparticle via its thiol chain end, bearing a protected amino acid residue on some of its itaconic anhydride repeat units. Adapted from Hvilsted *et al.*[76]

The few reports on itaconatic acid-derived monomers that can be found in the literature, demonstrate the versatility of the itaconic building block for different applications. Yet, RAFT polymerisation is the only RDRP technique that has allowed to control the polymerisation of these monomers.

2.2.1.2.2. α-Methylene-γ-butyrolactones

α-Methylene-γ-butyrolactones (MBL) are a class of five-membered lactones with an *exo*-methylene unit (Scheme 10c) and can be extracted from tulips.[77] Although several synthetic pathways to methylene butyrolactones from renewable resources have been reported (*e.g.* Scheme 10a),[78–80] Fors *et al.* were the first to report a one-step procedure for the synthesis of γ,γ-dimethyl-α-methylene-γ-butyrolactone (Me_2MBL) and MBL from itaconic acid, *via* a reduction and a selective addition, respectively (Scheme 10a).[81] The first controlled radical polymerisation of the simplest butyrolactone, α-methylene-γ-butyrolactone (MBL), was reported by Matyjaszewski *et al.* in 2008 using ATRP.[82] At 50 °C in DMF using a CuBr/bipy catalyst complex and 2-bromoproprionitrile as initiator, rapid and controlled polymerisations were observed giving rise to well-defined polymers (M_n = 18,200 g mol^{-1}, M_w/M_n = 1.09).

Chain extension of an MBL macroinitiator was not successful due to the poor solubility of this first block, however diblock copolymers were synthesised starting from butyl acrylate (BA) and MMA macroinitiators.

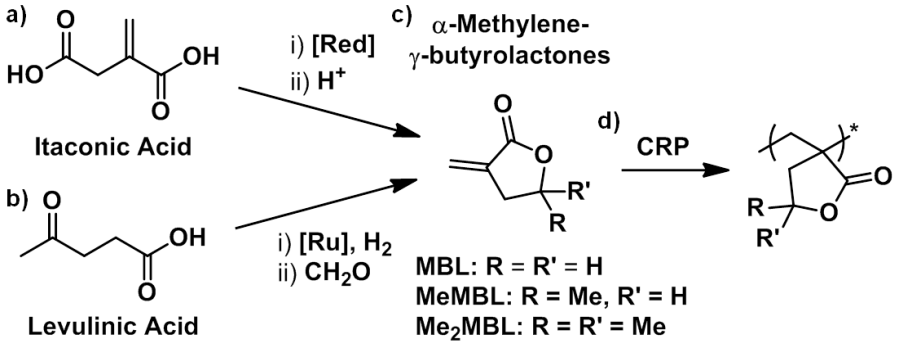

Scheme 10. Transformation of a) itaconic acid and b) levulinic acid into c) methylene butyrolactones, and d) the controlled radical polymerisation of these monomers into poly(α-methylene-γ-butyrolactone)s

Controlled miniemulsion polymerisations in water of γ-methyl-α-methylene-γ-butyrolactone (MeMBL; Scheme 10c) were attempted using RAFT polymerisation in order to prepare heat-resistant polymer latexes.[83,84] Using oil-soluble dithiobenzoate and dithioacetate CTAs in water at 70 °C miniemulsion homopolymerisations of MeMBL led to little success as either latex aggregation or a poor control were observed.[83] Stable polymer colloids and a controlled polymerisation could only be achieved through the addition of a comonomer (styrene). Polymerisations showed some level of control but slower polymerisation rates were observed for the miniemulsion compared to the bulk, which was attributed to a lower initiator efficiency and to a lower concentration of radicals and MeMBL monomers in the dispersed phase. In order to improve the control of the polymerisation, a short poly(acrylic acid)-*b*-PS copolymer was synthesised and subsequently used as both macroRAFT agent and surfactant for the emulsion copolymerisation of styrene and MeMBL.[84] Stable latex particles with narrow dispersities (*ca*. 1.2) and a linear increase in molecular weights with conversion were observed (Figure 12a) and the MeMBL content was varied from 21 to 72 wt%. A strong composition drift was observed during the polymerisation which lead to the formation of gradient copolymers with T_gs above 100 °C and a loss of control at high conversion was observed for feeds of 1:1 styrene:MeMBL (Figure 12b).

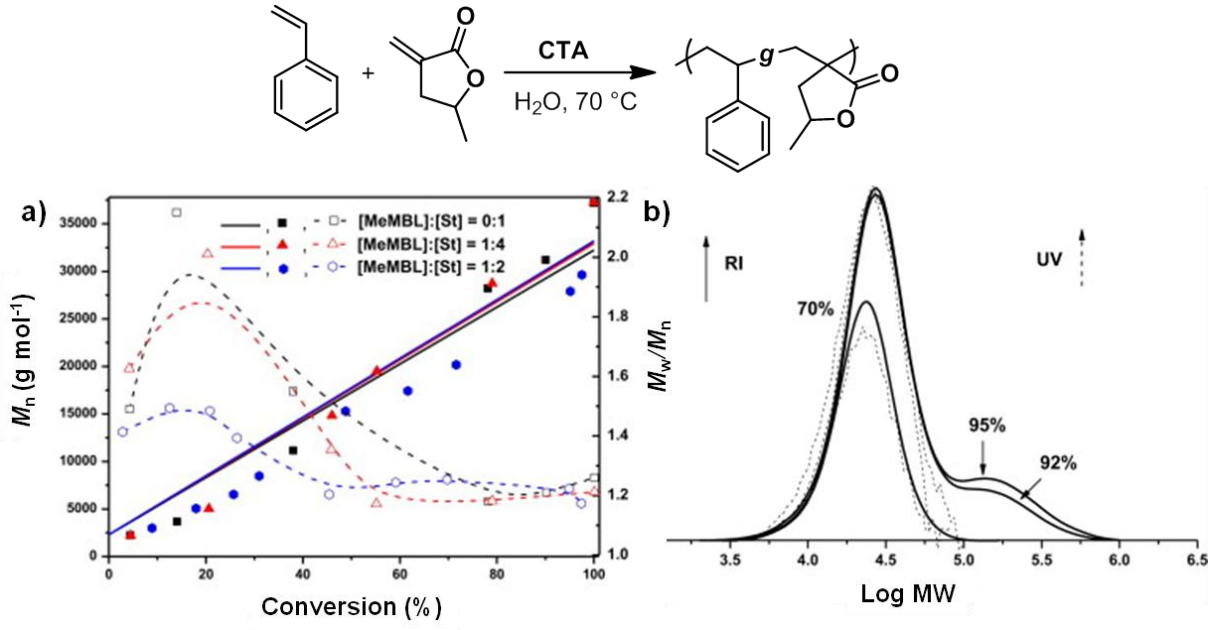

Figure 12. Miniemulsion polymerisation of styrene and MeMBL using a macroCTA agent.[84] a) Plot of molecular weight (M_n) and dispersity versus conversion and b) size exclusion chromatography (SEC) curves of emulsion copolymersiations of styrene and MeMBL at a styrene:MeMBL feed of 1:1. Adapted with permission from *Polym. (United Kingdom)* **2013**, *54* (7), 1779–1785. © 2013 Elsevier Ltd.

In an attempt to attain superior mechanical properties to those of commodity polymers currently used in a range of applications, block copolymers based on MBL were synthesised using a similar ATRP system (Figure 13a).[85] The two blocks were immiscible and depending on the size of the hard block, different phase morphologies were observed by AFM and SAXS which were stable even above the T_g of the MBL block. Yet only slight improvements of the tensile strength and elastic modulus were observed (< 50%, compared to a triblock copolymer made of commercial BA and MMA), while the elongation at break was poor for all samples as a result of the brittle MBL blocks (Figure 13c). Improvements in the stress at break values were achieved for multi-armed P(BA-*b*-MBL) star block copolymers (Figure 13d).[86] Even so the mechanical properties were still comparable to simple diblock copolymers based on BA and MMA (comparison of Figure 13c and Figure 13d) whose synthesis is less cumbersome.

Nonetheless, the groups of Higaki and Takahara showed that bio-based PMBL polymer brushes synthesised on a silicon waver were superior to PMMA brushes synthesised on the same substrate in terms of wear resistance and relative elastic modulus (Figure 13e) which are important for potential scratch-resistant coating applications.[87] PMBL brushes were grown from a silicon wafer functionalised with an ATRP initiator using a CuBr/bipyridine catalyst in DMF at 30 °C to give a homogeneous polymer layer on the substrate. Yet, no comment on the

effect of the surface-bound initiator on the control of the polymerisation, nor the molecular parameters of the copolymers were made.

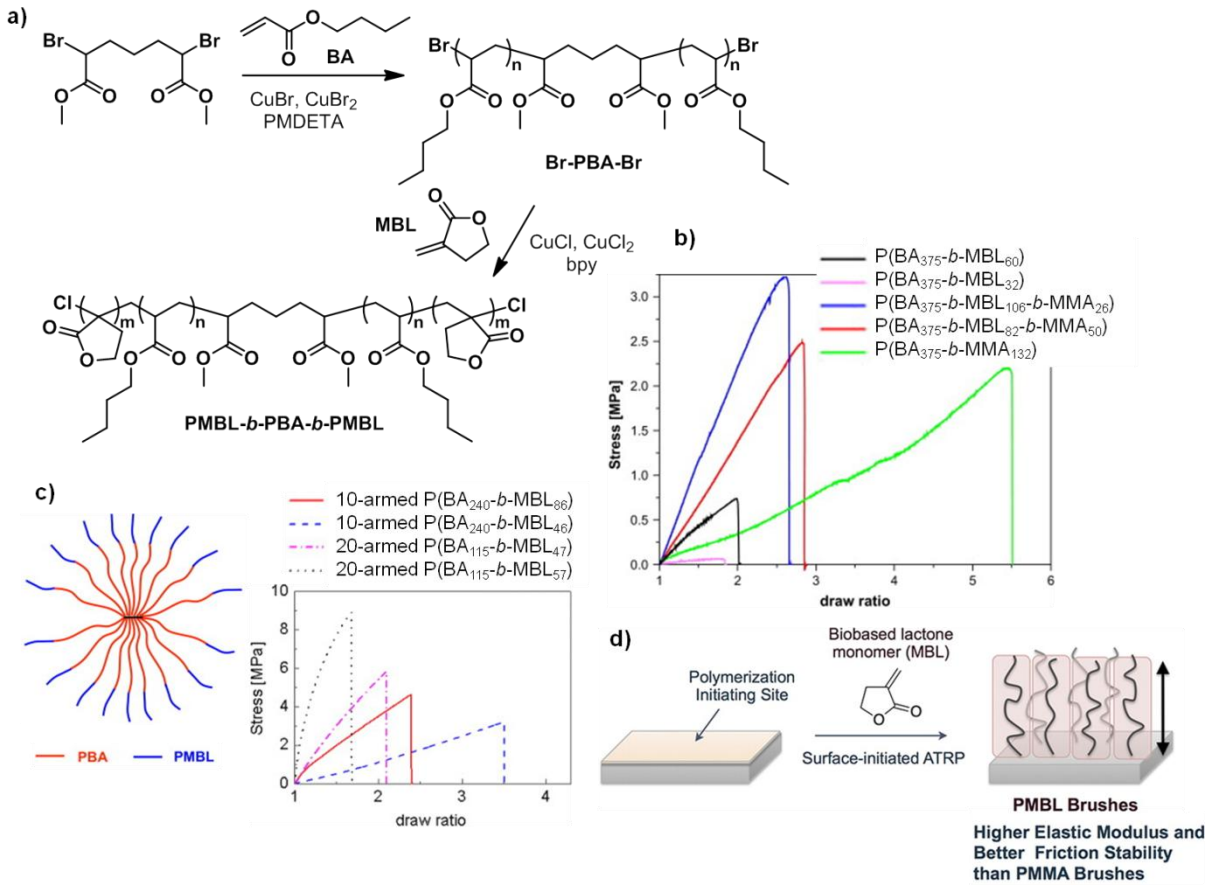

Figure 13. a) ATRP polymerisation of butyl acrylate (BA) and α-methylene-γ-butyrolactone (MBL) to form copolymers that b) have slightly improved mechanical properties (red and blue line) compared to conventional P(BA-*b*-MMA) block copolymers (green line). Reprinted with permission from *Polymer (Guildf).* **2009**, *50* (9), 2087–2094. © 2009, Elsevier Ltd. d) Multi-armed star copolymers based on the same monomers showed slightly improved mechanical properties. Adapted with permission from *Polymer (Guildf).* **2010**, *51* (21), 4806–4813. © 2010, Elsevier Ltd. e) Synthesis of a polymer film initiated from a glass substrate to synthesise MBL polymer brushes. Reprinted with permission from *ACS Macro Lett.* **2012**, *1* (9), 1124–1127 © 2012, American Chemical Society

The mechanical properties introduced by MBL to the aforementioned thermoplastic elastomers motivated the groups of Tolman and Hillmeyer to investigate a renewable ABA triblock copolymer.[88] Using sequential ROP of menthide followed by chain-end functionalisation with an ATRP initiator, and chain extension with MBL using a CuCl/bipyridine catalyst in DMF at 60 °C (Scheme 11), hard-soft block copolymers of varying block lengths were synthesised. Microphase separation into spheres of MBL in the polymenthide matrix was observed by DSC, AFM, and SAXS with no long-range ordering

and no dependence of the morphology on the copolymer composition observed. Triblock copolymers containing more than 15 wt% MBL showed comparable mechanical properties to those of commercial elastomers, *e.g.* polystyrene-*b*-polybutadiene-*b*-polystyrene, in terms of Young's modulus (>6 MPa) while the renewable triblock copolymers were superior in terms of true elasticity (recovery of shape). Additionally, the elongation at break of these renewable copolymers was remarkably high (>730%). Analogous triblock copolymers were prepared from menthide and γ-methyl-α-methylene-γ-butyrolactone (MeMBL) by the same group and further improvements of the elongation at break values to >1,600% were achieved exceeding the limits of the instrument used.[89] Their performance in adhesive blends using commercial tackifiers were determined in a preliminary test and the results demonstrated that such triblock copolymers have a fail temperature, at which the adhesive detaches, greater than those of commercial pressure sensitive adhesives (>150 °C compared to 90-125 °C for commercial duct tapes).

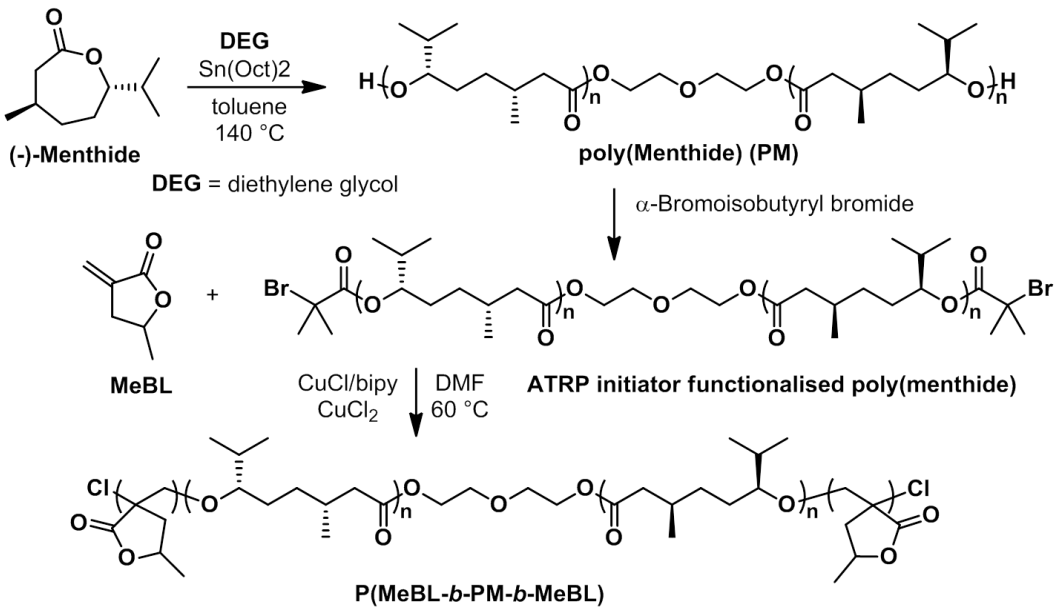

Scheme 11. Block copolymer synthesis using a combination of ROP of menthide and ATRP of α-methylene-γ-butyrolactone (MBL) or γ-methyl-α-methylene-γ-butyrolactone (MeBL). Scheme adapted from Tolman and Hillmeyer *et al.*[88,89]

In a study by Fors *et al.* Me_2BL and MBL based polymers were synthesised using a dithiobenzoate CTA (2-cyano-2-propyl benzodithioate, CPDB) for the replacement of fossil fuel-based PMMA in optical fibre applications.[81] At 80 °C in benzene well-defined high molecular weight homopolymers with T_gs above 190 °C with similar optical properties to PMMA were obtained. The above examples highlight the potential of bio-based MBL-based polymers variety of different applications. Yet no reports on the post-polymerisation

modification of the butyrolactone repeat units have been reported which could broaden the scope of properties available for such polymers.

2.2.1.2.3. Phenylpropanoids

Closely related to lignin, which will be discussed in more detail in Section 2.2.2.2, are β-methylstyrenes (Figure 14a) which can be directly extracted from a variety of different plants,[90,91] and vinylguaiacols (VG) obtained through the decarboxylation of ferulic acid (Figure 14b), a component of lignin. β-Methylstyrenes are known to not homopolymerise radically because of their bulky methyl substituent, which prevents successive β-methylstyrene additions.[23] As a result, Kamigaito *et al.* investigated the polymerisation of anethole, *o*-methyl isoeugenol, isosafrole and acetyl isoeugenol (Figure 14a) with methyl acrylate (MA) using 2,2'-(1,3-phenylene)*bis*(1,1,1,3,3,3-hexafluoropropan-2-ol) (*m*-$C_6H_4[C(CF_3)_2OH]_2$), a toluene-derived fluoroalcohol, at 60 °C (Figure 14c). A variety of different dithio- and trithio-CTAs (cumyl dithiobenzoate, *S*-2-cyano-2-propyl *S*'-ethyl trithiocarbonate (CPETC), *S*-2-cyano-4-methoxy-4-methyl-2-pentyl *S'*-ethyl trithiocarbonate (CMMETC), *S*-cumyl *S*'-ethyl trithiocarbonate (CETC), and *S*-1-isobutoxyethyl *S'*-ethyl trithiocarbonate (BEETC)) were used (Figure 14c). In all cases, slow polymerisation kinetics, <25% conversion after 24 hours, were observed. Yet, molecular weights of up to 10,000 g mol^{-1} and dispersities below 1.36 were obtained, except for CETC for which dispersities were above 1.42. No evidence for a controlled chain growth process was provided for these RAFT copolymersations.

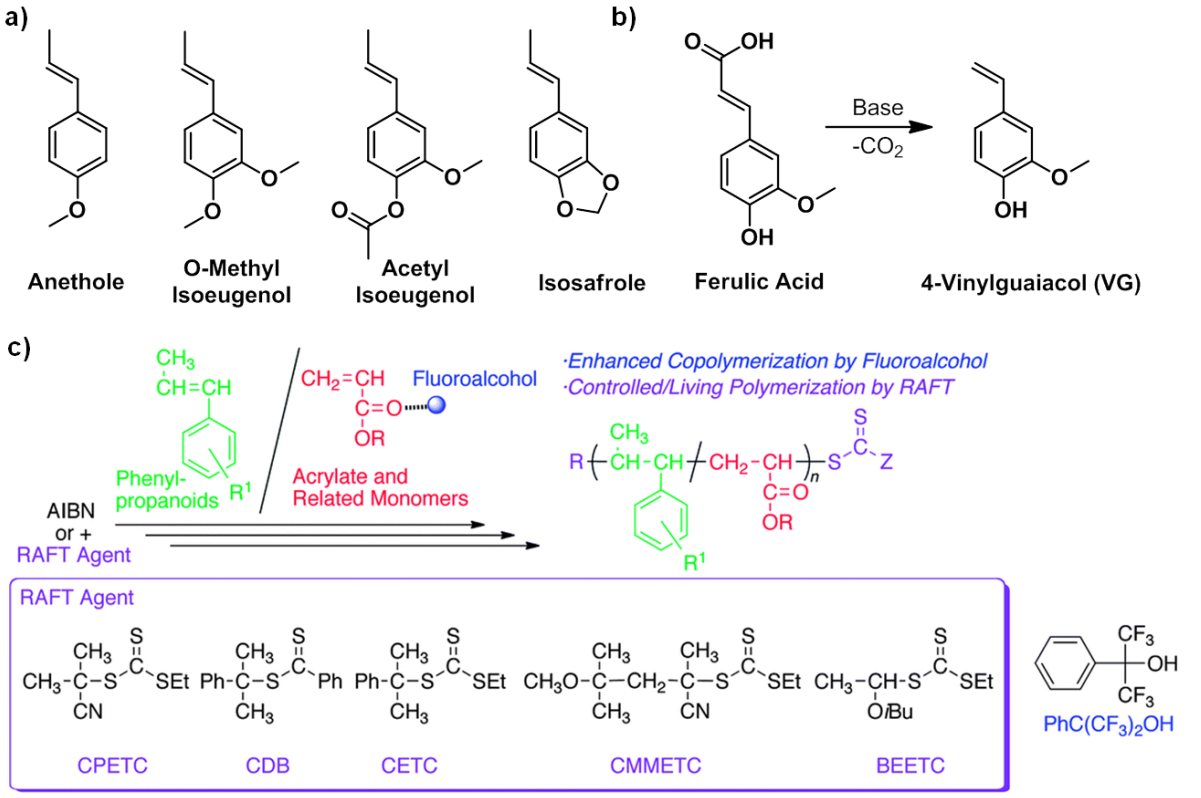

Figure 14. Structures of a) different β-methyl styrenes, b) ferulic acid and its transformation into vinylguaiacol. c) RAFT copolymerisation of β-methyl styrenes with methyl acrylate using a variety of different CTAs in a fluorinated alcohol. Adapted with permission from *Polym. Chem.* **2014**, *5* (9), 3182–3189. © 2014, Royal Society of Chemistry

Vinylguaiacol bears only one substituent on the vinyl group, thus is less sterically hindered, and can therefore be homopolymerised. However, the phenol moiety, a well-known antioxidant, quenches radical species and inhibits the homopolymerisation at low conversions.[92,93] Therefore protecting groups were found to be necessary for the phenol group prior to polymerisation. Kamigaito *et al.* investigated the RAFT polymerisation of acetyl, *tert*-butyldimethyl silyl- and triethylsilyl-protected vinylguaiacol monomers (Figure 14a) in an attempt to synthesise functional bio-based materials.[93] High conversions (>89%) and low dispersities (M_w/M_n< 1.15) were obtained for all protected VG monomers at 60 °C in toluene using CDB as CTA and AIBN as initiator, and excellent control of the polymerisation was concluded on account of the linear increase of molecular weights with conversion (Figure 14a), the complete shift of molecular weights in the SEC curves (Figure 14a), and the successful chain extension with styrene, methacrylate and methyl methacrylate. Other dithiobenzoate, dithiocarbamate and trithiocarbonate CTAs showed high molecular weight shoulders and were less suitable for such copolymerisations. Thermal initiation was also tested in the presence of CDB at 110 °C in the bulk but lower conversions (<75%) were

observed. Yet for both azo- and thermally initiated polymerisations, kinetics were very slow and required several days to reach high conversions. Even slower reaction kinetics were observed for NMP, which was also tested for this monomer at 90 and 110 °C in toluene and in bulk using *N*-tert-butyl-*N*-(2-methyl-1-phenylpropyl)-*O*-(1-phenylethyl)hydroxylamine (St-TIPNO) as the controlling agent. Nonetheless, excellent control over the polymerisations was observed. The deprotection of the silyl protected monomers was performed at room temperature in THF under acidic conditions and after 3 hours the deprotected poly(4-vinylguaiacol) and polyvinylcatechol (Figure 14b) were obtained in high yields, >90%. This strategy allowed to obtain otherwise inaccessible bio-based polymers which are promising for a variety of applications, such as adhesives and antibiofilm coatings.

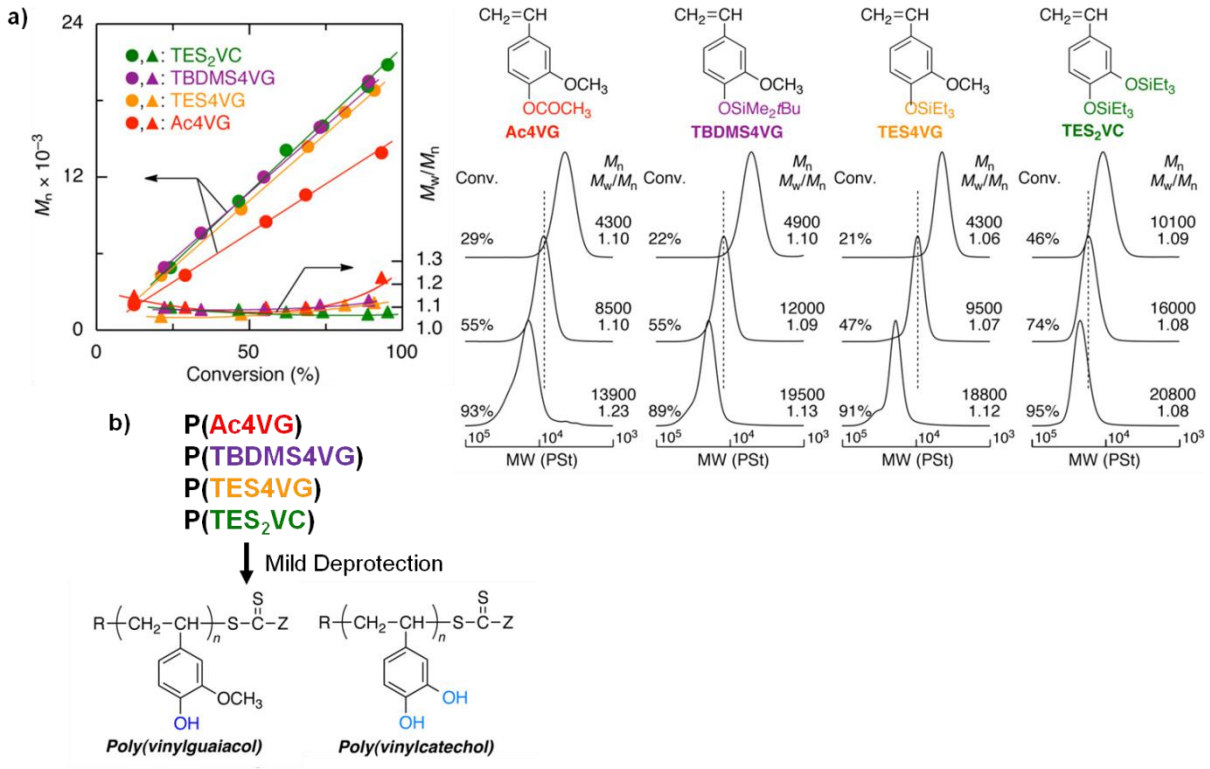

Figure 15. a) Evolution of molecular weight and dispersity with conversion and b) the size exclusion chromatography (SEC) curves for the polymerisation of protected vinylguaiacol monomers with cumyl dithiobenzoate in toluene at 60 °C. b) Structures of poly(4-vinylguaiacol) and polyvinylcatechol obtained *via* the deprotection of protected vinylguaiacol polymers. Adapted with permission from *Macromolecules* **2017**, *50* (11), 4206–4216. © 2017, American Chemical Society

2.2.2. Renewable Molecules Functionalised with Double Bonds

As discussed in the sections on terpene, itaconates and cellulose-derived monomers, the list of molecules possessing polymerisable double bonds is rather short and many efforts have been devoted to the extension of this list. Since natural molecules bear many heteroatoms, they are perfect candidates for the synthesis of functional monomers. Especially hydroxyl functions are abundant in these molecule classes and a route which has been extensively exploited is the attachment of acrylic moieties. Acrylates are versatile with respect to the polymerisation technique and the comonomer used and can be easily polymerised with good control over the radical chain growth process. Industrially acrylates are produced from non-renewable resources, such as propene or acetylene, *via* oxidations. Recent advances in the synthesis of acrylates from renewable resources, such as CO_2 or lactic acid, *via* catalytic routes hold promise for the preparation of renewably-based acrylates.[40,94–96] Yet, the synthesis of acrylate-derived monomers typically involves the use of acryloyl chloride, a toxic, flammable and hazardous to aquatic life acrylate derivative. Furthermore, these reactions require the use of stoichiometric equivalents of a base, thus generating the corresponding chloride salt as waste[97] and hence alternative catalytic routes are sought after.[40,98] This section is concerned with literature examples where natural products are functionalised with double bonds, mainly acrylates, in order to synthesise bio-derived polymers using RDRP techniques.

2.2.2.1. Sugars and Carbohydrates

Among polymers based on renewable monomers, carbohydrates are one of the most studied class of molecules as they are abundant, can be easily obtained from non-food resources and are versatile as a result of the multiple functional groups.[99] Especially glycopolymers, *i.e.* polymers bearing carbohydrate pendant moieties, have gained interest since the early 2000s in light of their potential applications as stimuli-responsive materials,[100] for cell recognition, and in drug delivery.[75,101–104] The reader is referred to reviews that have summarised the field.[101,105–109] Briefly, a large library of different glycopolymers has been prepared and RDRP has proven extremely powerful in precisely designing the polymer structures in order to target specific cell recognition and/or application. It is noteworthy that most often non-edible carbohydrates are fermented into useful platform molecules which can be transformed into monomers for RDRP *via* derivatisation with double bonds. A most recent trend in this field is the use of enzymes for the synthesis and polymerisation of glycopolymers in aqueous media

with advantageous low toxicity, sustainability, scalability and selectivity of the process.[101,110] However further details will not be herein discussed as the work described in this thesis (Chapters 2-6) is not concerned with glycopolymers.

Furfural is one example of a platform chemical derived from biomass *via* fermentation which has been recently used for classical- and photoinduced-ATRP.[111] Photoinduced ATRP was performed in the absence of a copper catalyst using α-bromophenylacetate as the initiator and 10-phenylphenothiazine as the organic photocatalyst (Figure 16) and high conversions (>73% after 12 hours) and dispersities below 1.41 were obtained for the homopolymerisation of furfural methacrylate. Block copolymers with a rosin-acid derived monomer (DAEMA) and a fatty acid-derived monomer (SBMA) were also successfully synthesised with possible applications as thermoplastic elastomers. Further investigations into other carbohydrate-derived monomers are necessary to expand the available monomers.

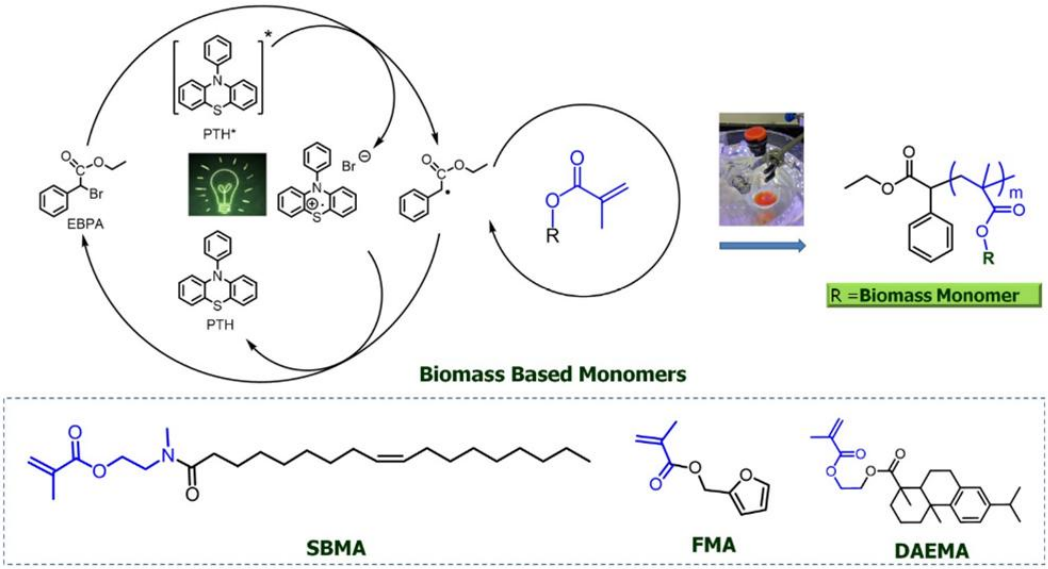

Figure 16. Photoinduced ATRP of furfural methacrylate and two other renewable monomers, soybean oil methacrylate and dehydroabietic ethyl methacrylate. Reprinted with permission from *Macromolecules* **2016**, *49* (20), 7709–7717. © 2016 American Chemical Society

2.2.2.2. Lignin

Lignin is the third main constituent of biomass after cellulose and hemicellulose and serves as the rigid and structure-giving segment of cell walls. Made up of three repeating units, paracoumaryl alcohol, coniferyl alcohol, and synapyl alcohol (Scheme 12a) connected *via* ester and carbon-carbon linkages, this polymer is obtained as a side product from the papermaking industry at a scale of ~100 Mt/year (data from 2015)[112] and is typically burned as a fuel. Recently, this insoluble, cross-linked polymer was exploited for the synthesis of a variety of different platform chemicals, [113–115] *e.g.* eugenol, vanillin, guaiacol, or syringol

(Scheme 12b), but also polymers.[61,116–118] The advantages of this feedstock are its unsuitability for food as well as its low price. However, issues related to purity, degradation of lignin during pulping, and low yields obtained by non-Kraft processes, hamper the implementation of lignin in large-scale material products, although some progress in addressing these issues has been made.[114,119,120] Indeed, several reports have been published on the RDRP of lignin-derived monomers and are herein briefly discussed.

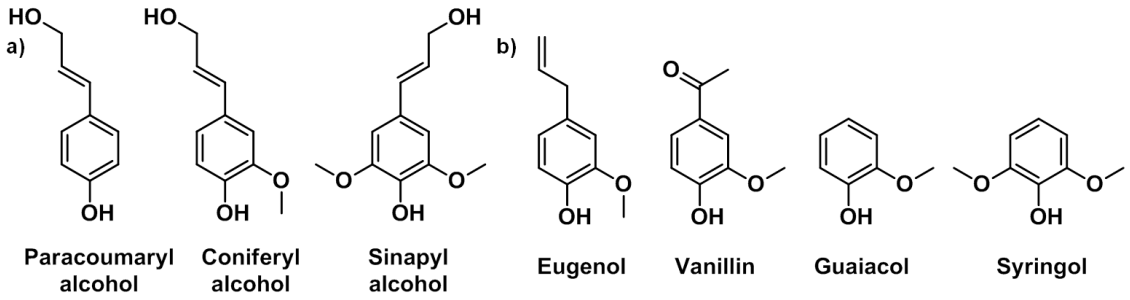

Scheme 12. Chemical structures of a) the three main repeating motifs found in the structure of lignin and b) derivatives of lignin, useful as platform chemicals and for monomer synthesis.

The groups of Wool and Epps first reported the synthesis of vanillin-based block copolymers for the replacement of petrol-based polystyrene. Using a simple base-catalysed esterification of methacrylic anhydride with the phenol of vanillin, a renewable methacylate monomer bearing substituted phenyl groups was obtained which was then successfully polymerised using RAFT polymerisation in dioxane or anisole at 72 °C using a dithiobenzoate (2-cyano-2-propyl dithiobenzoate) CTA (Figure 17).[121] Low dispersities and pseudo-first order polymerisation kinetics underline the good control over the homopolymerisation. The homopolymer showed comparable characteristics to styrene polymers in terms of thermal properties with a T_g around 100 °C and an onset of degradation (T_d) at temperatures above 300 °C (polystyrene: T_g *ca.* 100 °C , T_d = 400 °C). Additionally, different degrees of polymerisation for this lignin-derived first block were targeted and could be chain-extended using lauryl methacrylate to obtain block copolymers of up to 60,000 g mol^{-1} molecular weight at a dispersity of 1.38. These block copolymers were shown to self-assemble into nanospheres in bulk that adopted a body-centred cubic array (Figure 17), as determined by TEM and SAXS.

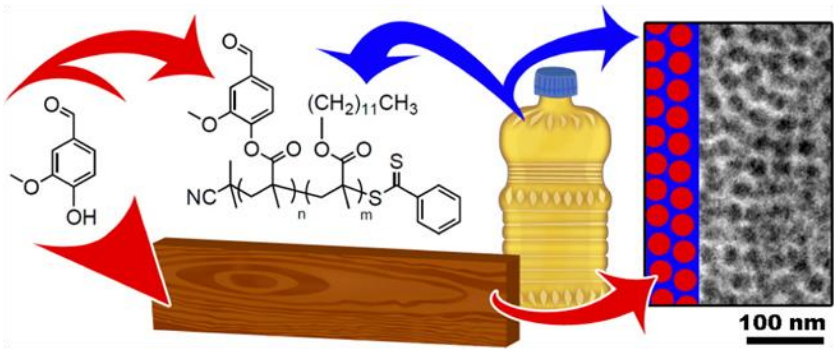

Figure 17: Lignin-based homo- and copolymers prepared by RAFT polymerisation leading to self-assembled nanospheres. Reprinted with permission from *ACS Sustain. Chem. Eng.* **2014**, *2* (4), 569–573. © 2014, American Chemical Society

Syringol methacrylate homopolymers prepared by RAFT using the same conditions as above (Figure 18a) were also shown to have very high T_gs, 190-210 °C,[122] and incorporating this monomer into copolymers with other guaiacol-derived monomers with different substituents in the *ortho*-position, namely 4-ethyl-2-methoxyphenyl methacrylate, 4-formyl-2-methoxyphenyl methacrylate and 4-methyl-2-methoxyphenyl methacrylate, allowed to tune the T_g from 120 °C to 220 °C (Figure 18b). The authors concluded that this increase in T_g was a result of the ortho-methoxy group on the phenyl ring as this bulky group restricts the rotational freedom of the side chain.

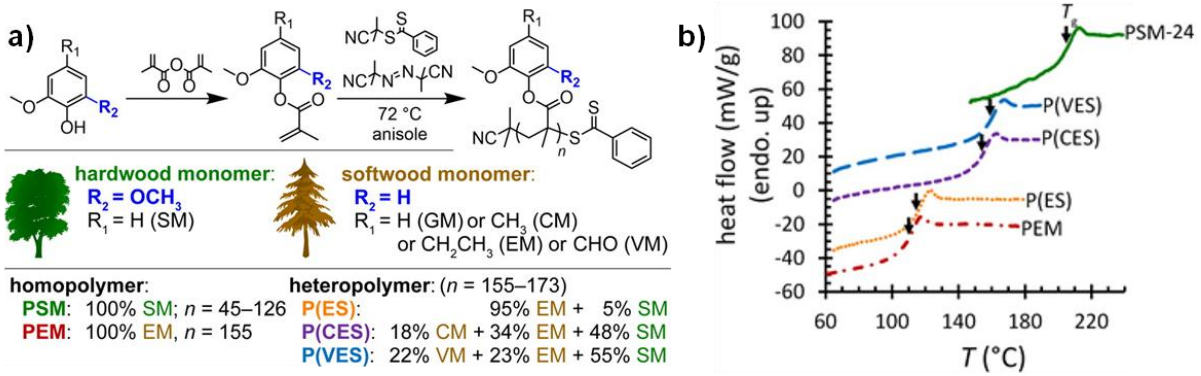

Figure 18: a) Synthesis of syringol methacrylate and its homo- and copolymerisation by RAFT with other guaiacol-derived monomers and b) the effect of the copolymer composition on the glass transition temperature (T_g) of the copolymer. Reprinted with permission from *ACS Macro Lett.* **2016**, *5* (5), 574–578. © 2016, American Chemical Society

A more detailed investigation of the role of methoxy groups on lignin-inspired monomers was provided by Epps *et al.* *Ortho-*, *meta-*, and *para*-substituted dimethoxyphenyl methacrylates were polymerised using the same CTA agent as above in anisole or DMF at 72 °C and homopolymers of varying molecular weights were obtained and compared in terms of glass

transitions and thermal stability.[123] The highest T_g at 222 °C was obtained for the two methoxy groups *ortho* to the methacrylate moiety and thus closest to the polymer backbone while the other cases had T_gs around 100 °C. Intermediate values were obtained for statistical copolymers (Figure 19). This was attributed to the higher steric hindrance of the substituents at the *ortho*-position, restricting the rotational freedom of motion of the polymer chain. Furthermore, the different positions of the methoxy group in the monomer also affected the polymer's resistance to THF and chloroform (Figure 19). As a result of these favourable properties, a similar series of guaiacol, vanillin, and syringol monomers was investigated for their suitability as polymer films for coating applications.[124] Films prepared by flow coating from solution were analysed in terms of their thermal properties, vapour swelling, contact angle and friction coefficient to determine the effect of different phenyl substituents on these properties. The authors found that changes in the polar functionalities of the polymer led to a greater effect on the solubility and friction than alterations in the aliphatic groups. Nonetheless, no comparison of the obtained properties with those of commercially available coatings was made.

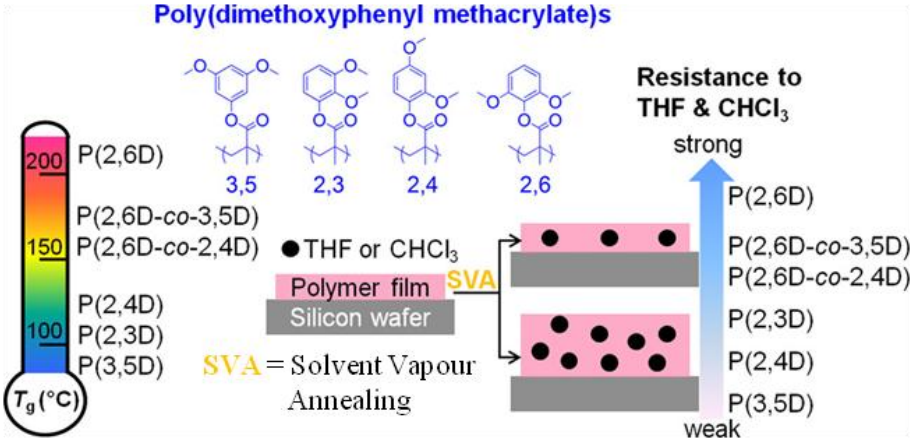

Figure 19. Structures of poly(dimethoxyphenyl methacrylate)s prepared by RAFT polymerisation and the thermal properties and resistance to solvent of the polymers. Reprinted with permission from *ACS Macro Lett.* **2017**, *6* (8), 802–807. © 2017, American Chemical Society

An interesting method for the copolymerisation of the often complex monomer mixtures originating from renewable resources was pursued by the same group.[125] A variety of different guaiacol acrylates were synthesised using a similar approach as described above,[126,127] and then used as a mixture in RAFT polymerisations under the same conditions used above. Detailed kinetic studies of the homo- and copolymerisation behaviour of these monomers and their mixtures were performed and, using the chain-transfer coefficients and

the propagation rate constants of homopolymerisations, a prediction of the molecular weights and dispersities of these random heteropolymers was possible. The authors stated that polymerisations of such complex mixtures could give access to heteropolymers with versatile properties, such as strength or stimuli-responsiveness. However, the copolymerisation of "real" monomer mixtures obtained from biomass in a controlled fashion was not discussed and therefore the incorporation of structurally diverse monomers into heteropolymers is to date unexplored.

While the aforementioned approaches utilised lignin-model molecules, such as guaiacol or syringol for the synthesis of the monomers, Epps *et al.* started from wood which they then depolymerised *via* reductive fractionation using a ruthenium catalyst on charcoal to obtain propylsyringol and propylguaiacol (Figure 20a). Triblock copolymers with a middle block consisting of BA and the outer blocks of one of the renewable monomers (Figure 20b), were synthesised using a difunctional trithiocarbonate as CTA (3,5-bis(2-dodecyl-thiocarbonothioylthio-1-oxopropoxy)benzoic acid), and excellent control was reported for molecular weights of up to 66,400 g mol^{-1}. Similar tri-block copolymers comprising a rubbery middle block and glassy end blocks are used industrially for pressure sensitive adhesives (adhesive tapes) and these lignin derived block copolymers were comparable in terms of their adhesion force to stainless steel with commercial adhesive tapes. For example in a 180° peel force test (Figure 20b), values in the range of 2-4 N cm^{-1} were obtained for the triblock copolymers which were superior to commercial Scotch Magic tape (1.7-2.0 N cm^{-1}) and slightly lower to Fisherbrand labelling tape (3.5-5 N cm^{-1}, Figure 20d). Notably these lignin-derived adhesives needed no tackifiers – additives commonly found in adhesive tapes that increase the stickiness – and are thus promising bio-based alternatives to the currently utilised poly(ethyl methacrylate-*b*-butyl acrylate) block copolymers.

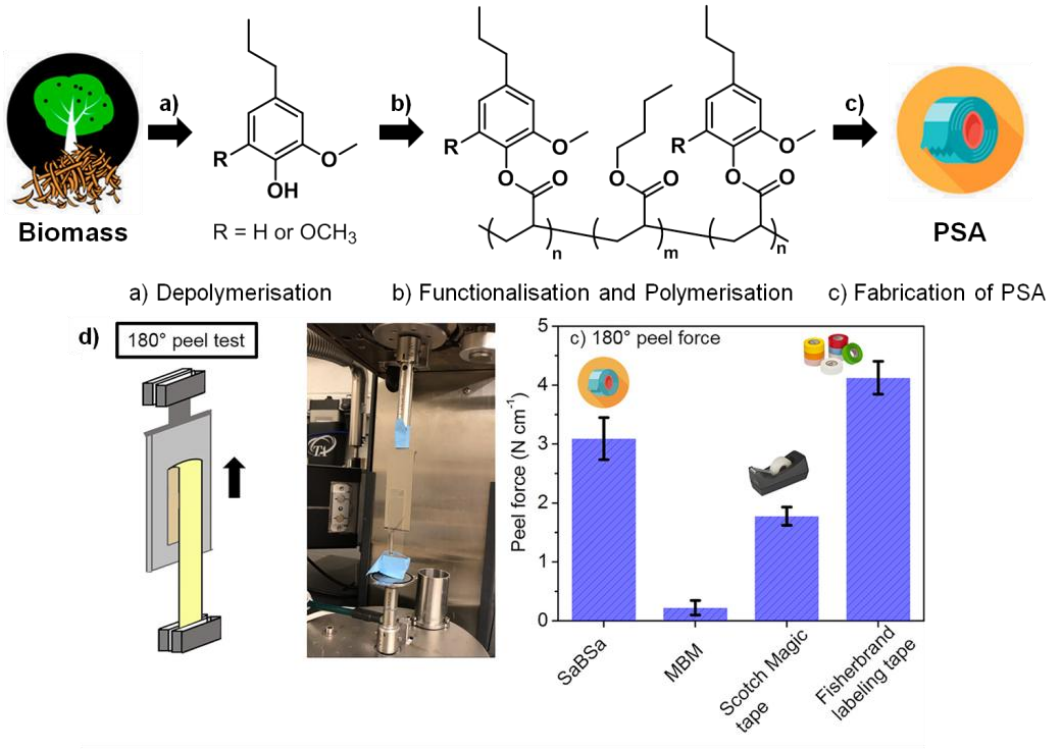

Figure 20. Lignin-derived pressure sensitive adhesives obtained from biomass *via* a) depolymerisation, b) functionalisation and RAFT polymerisation, and c) fabrication. d) Peel test of the prepared adhesives compared with commercial adhesive tapes. Adapted from *ACS Cent. Sci.* **2018**, *4* (6), 701–708. © 2018, American Chemical Society

The few examples of lignin derived polymers prepared by RDRP processes reported in the literature highlight their potential for high-value applications, such as adhesives or coatings. Yet a reliable strategy for the extraction of lignin-derived molecules from biomass which is economical (interesting for industry) is still unknown. Further research in the field of lignin extraction but also the functionalisation and RDRP of lignin-based building blocks is needed to push lignin-based copolymers towards a commercial implementation.

2.2.2.3. Terpenoids

As outlined in section 2.2.1.1, terpenes are difficult to homopolymerise using RDRP and mainly copolymerisations with acrylate monomers have been performed. (-)-Menthol (Scheme 6) is a terpene with no double bonds and hence is not directly suitable for RDRP. Yet the hydroxyl group can be easily functionalised with an acrylate moiety through the reaction with acryloyl chloride[97] and the groups of Lligadas and Percec showed that it can serve as a monomer for hydrazine-activated Cu(0)wire catalysed ATRP homopolymerisations at ambient temperatures using methyl 2-bromopropionate as initiator (Figure 21).[128] The highly hydrophobic nature of the monomer was found to be challenging, as the

polymerisation solvents need to have the right polarity to allow both the Cu(I)X disproportionation but also the dissolution of the formed polymer. As a result, only fluorinated alcohols, such as trifluoroethanol (TFE), were able to dissolve the growing polymer chain and allowed for a controlled radical chain growth process, as verified by first-order kinetic plots, low molecular weight dispersities obtained (M_w/M_n <1.2) and the complete shift of molecular weights to the high molar masses in the SEC trace. A linear increase up to10,000 g mol^{-1}, and dispersities, as low as 1.14, could only be obtained using *tris*[2-(dimethylamino)ethyl]amine (Me_6-TREN) as ligand at 25 °C. Fluorinated solvents are herein questioned with regards to its economic, environmental and toxicity aspects.[129]

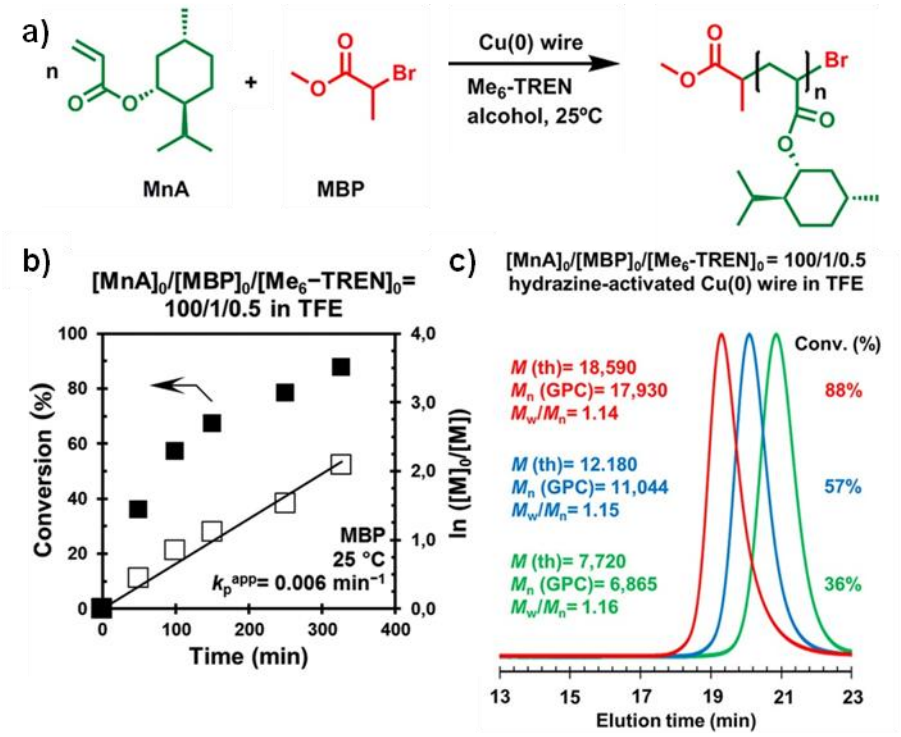

Figure 21. a) Copolymerisation of menthol acrylate in a fluorinated alcohol by ATRP, b) the increase of conversion with time and the pseudo-first order kinetic plot, and c) the size exclusion chromatograph (SEC) traces for the prepared homopolymer at different conversions. Reprinted with permission from *Biomacromolecules* **2018**, *19* (4), 1256–1268. ©2018, American Chemical Society.

Rosin acids are part of the terpene family and consist of tricyclic molecules bearing a carboxylic acid group and varying in their degree of unsaturation (Scheme 13a). Their estimated industrial production is 1 Mt per year and they can be found in soaps and tall oil.[130–132] To date, the direct RDRP of rosin derivatives has not been reported, *e.g.*: pimaric acid (Scheme 13a), nor that of vinyl-functionalised rosin-derived molecules, *e.g.* through a vinyl interchange on the acid moiety.[133] Rosin acids can be functionalised with allylic double

bonds,[134] however the polymerisation of such non-activated double bonds using RDRP is still extremely challenging and has only recently been shown to be feasible for a few examples.[98] Most literature reports use acrylate derived rosin monomers for the synthesis of renewable polymers and the different strategies are herein outlined.

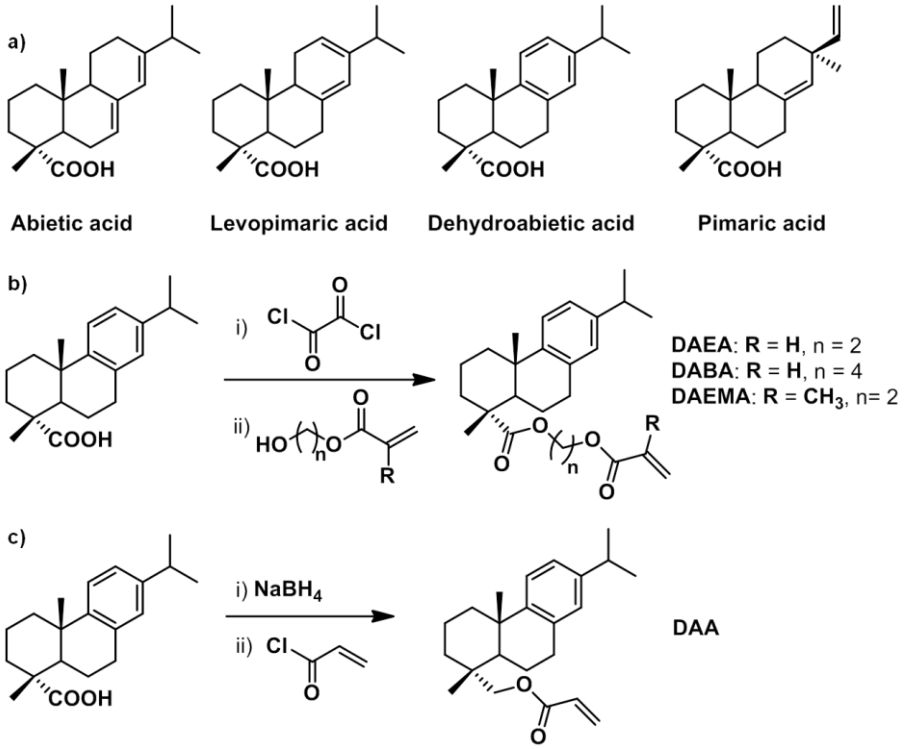

Scheme 13. a) Structures of four different acid derivatives which can be obtained from rosin gum, and the synthesis of rosin-derived monomers b) DAEA, DABA, DAEMA and c) DAA. Adapted from Tang *et al.*[135]

Tang *et al.* first reported on the preparation of four different acrylate-based rosin monomers, dehydroabietic ethyl acrylate (DAEA), dehydroabietic butyl acrylate (DABA), dehydroabietic ethyl methacrylate (DAEMA) and dehydroabietic acrylate (DAA) (Scheme 13b and c), either *via* an acyl chloride (Scheme 13b) or the reduction of the acid moiety of dehydroabietic acid into an alcohol (Scheme 13c) both followed by a subsequent attachment of the acrylate functionality.[135] Homopolymerisations of all monomers was attempted using ethyl 2-bromoisobutyrate as the initiator and tris[2-(dimethylamino)ethyl]amine (Me_6TREN) as the ligand for the Cu(I)Br-catalysed ATRP in THF at 90 °C. For both DAEA and DABA, slow reaction kinetics were observed (29% and 54% conversion after 16 hours, respectively) and no evidence on the control of the polymerisation apart from the monomodal SEC traces and the low dispersities was presented. Polymerisation of DAA was completely uncontrolled as multimodal chain distributions were obtained which was attributed to the large steric bulk of

the monomer. The methacrylate-derived dehydroabietic acid (DAEMA) was the most promising rosin-derived monomer of the four, as high conversions (>75% after 20 hours) could be obtained for polymerisations in anisole retaining low dispersities (M_w/M_n < 1.33). It was later shown that DAEMA can also be polymerised by metal-free photoinduced ATRP with good control at room temperature in THF (Figure 22a). The system used was the same as that described for the polymerisation of furfuryl methacrylate (Figure 16, Section 2.2.2.1) Furthermore, chain extension experiments of PDAEMA with other biomass-derived monomers, namely soybean oil methacrylate, were performed (Figure 22b). Although rather large dispersities were obtained (M_w/M_n *ca.* 1.78), a complete shift of the molecular weights was observed in the size exclusion chromatograms (Figure 22c).[111]

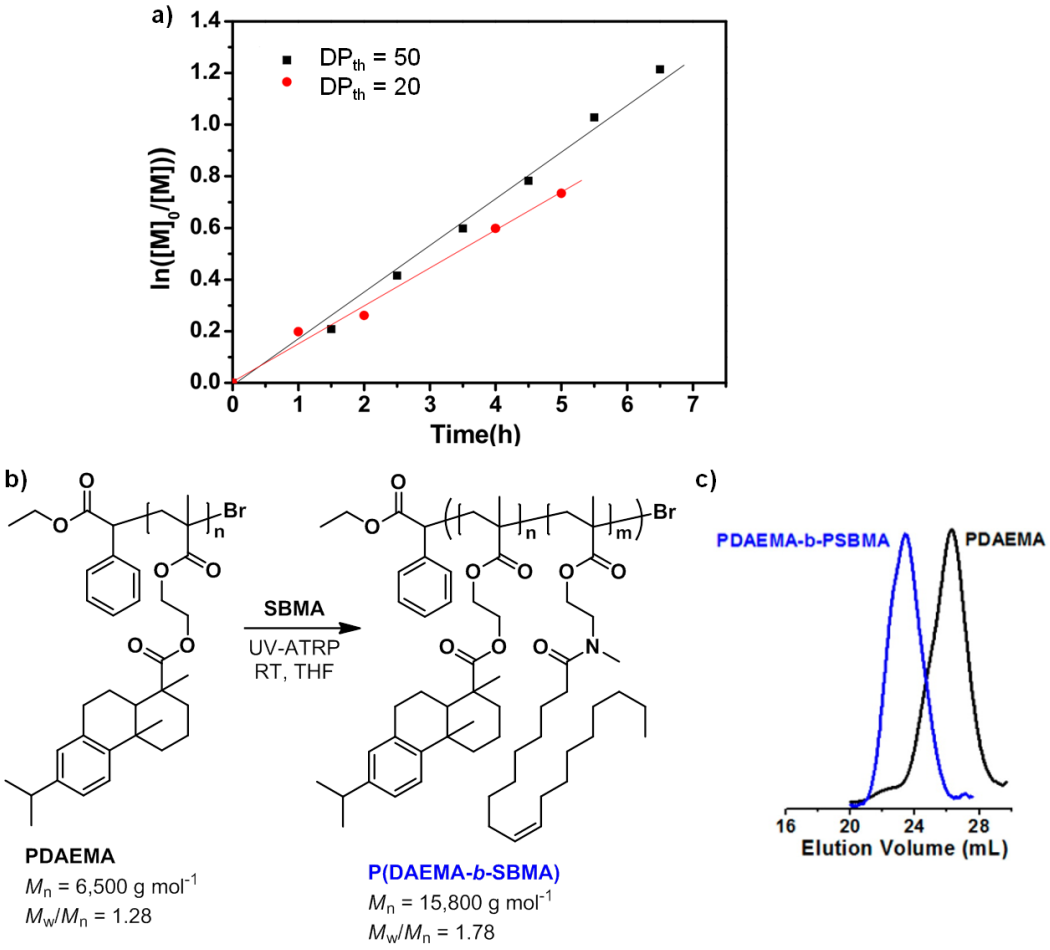

Figure 22. a) Linear first-order kinetic plot of the photo-induced ATRP polymerisations of dehydroabietic ethyl methacrylate (DAEMA), b) synthetic scheme for the block copolymer synthesis based on DAEMA and soybean-oil methacrylate (SBMA) and c) the size exclusion chromatography (SEC) curves of the macroninitiator and block copolymer. Reprinted with permission from *Macromolecules* **2016**, *49* (20), 7709–7717. © 2016, American Chemical Society

The possibility of forming block copolymers from the analogous acrylate rosin-derived monomer (DAEA) and caprolactone (CL) using a combination of ring-opening polymerisation (ROP) and ATRP was reported by Tang *et al*. (Figure 23), starting from either an ATRP initiator-terminated PCL or an alcohol-terminated PDAEA.[136] This combination of monomers was chosen because DAEA leads to a certain rigidity of the polymer chain (high T_g), PCL is biodegradable[137,138] and allows for the degradation of parts of the polymer. Indeed, the degradation of the PCL block was evidenced under acidic conditions in THF at 65 °C (Figure 23). The authors mentioned that dehydroabietic acid can be degraded by certain bacterial strains,[139,140] however such conditions were not employed in the reported work.

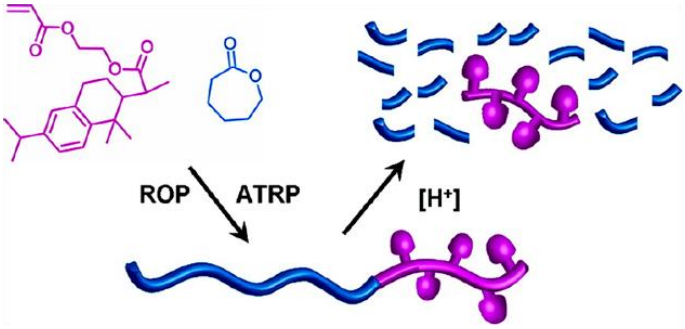

Figure 23. Block copolymers based on dehydroabietic ethyl acrylate (DAEA) and caprolactone (CL) synthesised *via* the combination of ROP and ATRP leading to partly degradable polymers. Reprinted with permission from *Macromolecules* **2010**, *43* (21), 8747–8754. © 2010, American Chemical Society

Thermoplastic elastomers based on triblock copolymers of DAEMA and BA were synthesised in a two-step procedure by the groups of Tang and Robertson using ATRP.[141] A difunctional BA macroinitiator was synthesised utilising diethyl *meso*-2,5-dibromoadipate as difunctional initiator and $NiBr_2(PPh_3)_2$ as the catalyst (Figure 24a) resulting in a PBA homopolymer with a molecular weight of 76,000 g mol^{-1} while the dispersity was not reported. This was then used to initiate the ATRP of DAEMA (employing Cu(I)Cl/PMDETA at 90 °C in DMF; Figure 24a) and the molecular characteristics of the resulting polymers were determined. The M_ns of the second PDAEMA block ranged from 10,000 to 20,000 g mol^{-1} while the dispersity was high for all block copolymers (1.45-1.66) due to the appearance of a high molecular weight shoulder for all block copolymers. This is herein attributed to a poor control over the radical chain growth process. Owing to the immiscibility of the blocks, the microphase separation of the copolymers was studied and an order-disorder transition was observed, which increased from 145 °C (12,000 g mol^{-1} second block) to 185 °C (20,000 g mol^{-1} second block) upon increasing the volume fraction of DAEMA. No order-disorder transition was observed for the

smallest second block (10,000 g mol^{-1}). Furthermore, the mechanical properties of the block copolymer with the largest second block (20,000 g mol^{-1}) were evaluated and compared to those of a conventional petrol-based acrylic thermoplastic elastomer, P(MMA-*b*-BA-*b*-MMA), synthesised under similar conditions. Although the Young's modulus and the tensile strength of the DAEMA-based copolymer were inferior (namely 0.175 MPa and 1.48 MPa versus 2.5 MPa and 4.06 MPa, respectively), the elongation at break was comparable (242% MPa versus 283%; Figure 24b). The authors argued that the molecular weight of the end block was not sufficient to allow the effective entanglement of the end block polymer chains and further improvements in the mechanical properties are to be expected for block copolymers with a second block of higher molecular weight.

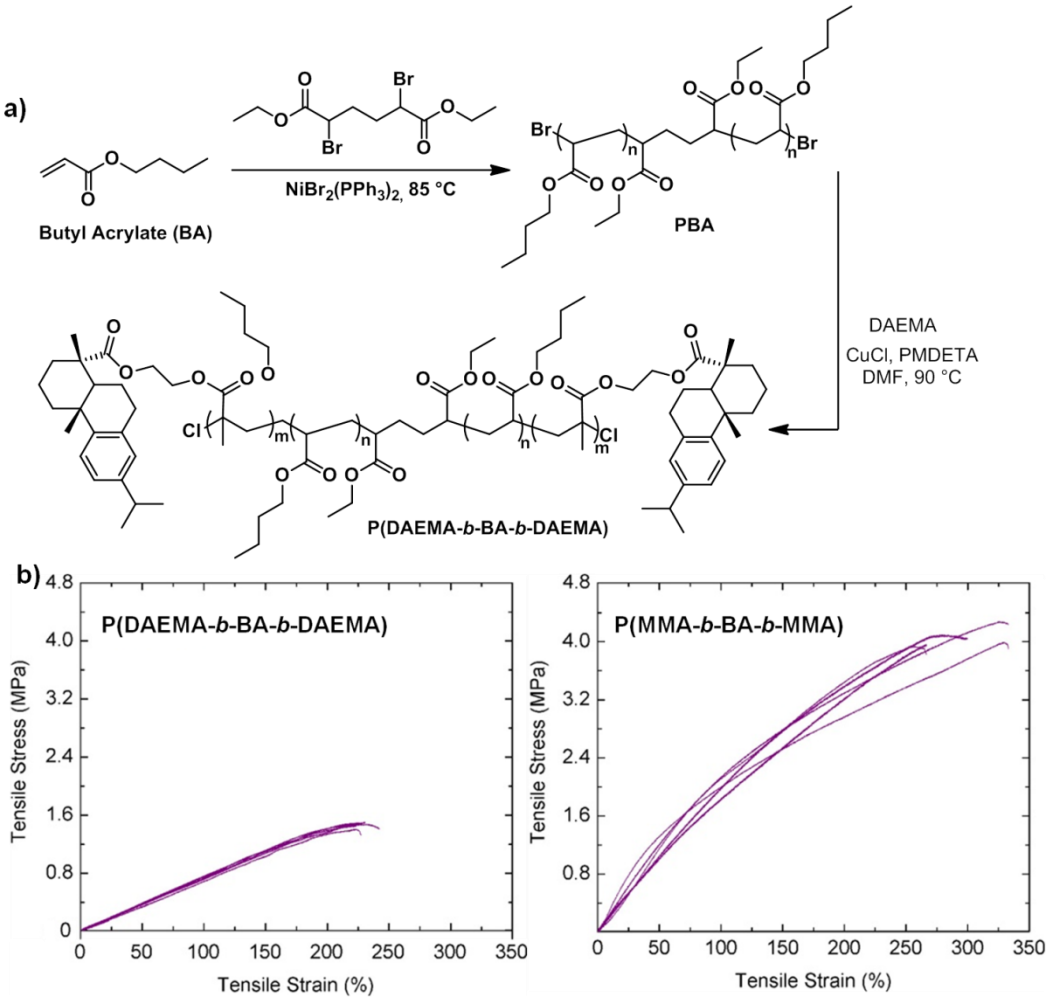

Figure 24. a) ATRP polymerisation of butyl acrylate (BA) and dehydroabietic ethyl methacrylate (DAEMA) to synthesise triblock copolymers with b) inferior mechanical properties compared to conventional methyl methacrylate (MMA)/BA triblock copolymers. Reprinted with permission from *ACS Sustain. Chem. Eng.* **2017**, *5* (12), 11470–11480. © 2017, American Chemical Society

Amphiphilic block copolymers based on poly(ethylene glycol) (PEG) and DAEMA for drug delivery applications were investigated by the groups of Tang and Jiang.[142] Starting from a PEG macroinitiator ($M_{n,\,NMR}$ = 5,100 g mol^{-1}) and using Cu(I)Br as catalyst and *N*,*N*,*N*′,*N*″,*N*″-pentamethyldiethylenetriamine **(**PMDETA) as the ligand at 90 °C in toluene, a second PDAEMA block was successfully added, leading to a block copolymer (Figure 25a) of a molecular weight of 27,600 g mol^{-1} and a dispersity of 1.26.[142] The formation of nanoparticles in the presence of a piperlongumine (PLGM), a natural anticancer product, was possible with an encapsulation efficiency of 83% while keeping a narrow nanoparticle size distribution (100 nm in diameter as determined by dynamic light scattering). *In vivo* experiments with mice demonstrated superior antitumor activity for the synthesised nanoparticles compared to the

commercial TAXOL® drug (Figure 25b), while encapsulation increased agglomeration in the tumour tissue while showing minimum adverse effects.

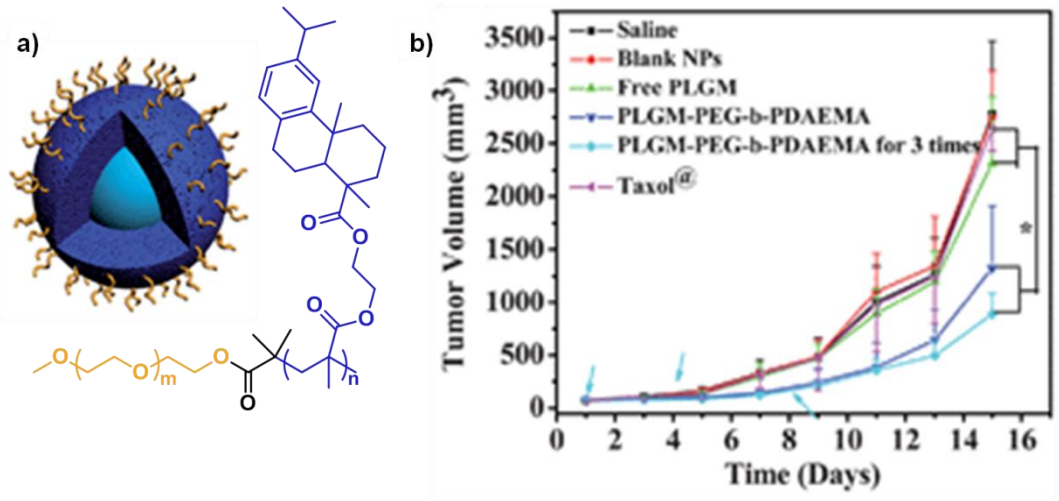

Figure 25. a) Nanoparticles of a diblock copolymer based on poly(ethylene glycol) (yellow) and dehydroabietic ethyl methacrylate (blue) able to encapsulate an antitumor drug. b) Such drug-loaded nanoparticles show a higher antitumor activity compared to a commercial antitumor drug (TAXOL®). Reprinted with permission from *J. Mater. Chem. B* **2013**, *1* (17), 2324–2332. © 2013, Royal Society of Chemistry.[142]

In another study with biomedical interest, polymer-coated glass surfaces were prepared by growing the polymer from a surface previously functionalised with an ATRP initiating moiety.[143] ATRP polymerisation under conventional conditions employing a quaternised ammonium-containing rosin acid monomer (Figure 26a) led to a change in the water contact angle of the surface and the chemical surface composition. Yet, no data on the polymer film thickness, the lengths and density of the grafts on the surface, or the efficiency of the initiating sites were presented, nor was the controlled nature of the polymerisation verified. These polymer coated glass surfaces showed antimicrobial activity against *S. aureus* and *E. coli* bacteria as a result of the cationic nature of the polymer graft. Not only did the coatings (S5; Figure 26) reduce the number of cells that attached to the surface (Figure 26b) but also reduced the number of cells surviving on the surface (Figure 26c), compared to a non-functionalised glass surface (S1) and to a surface functionalised with an analogous cationic molecule (S3). Although these coatings are based on renewably-sourced rosin acid, the monomer was prepared in a lengthy four-step synthesis in yields below 47%.[144] It is therefore difficult to call the coatings and the preparation process renewable.

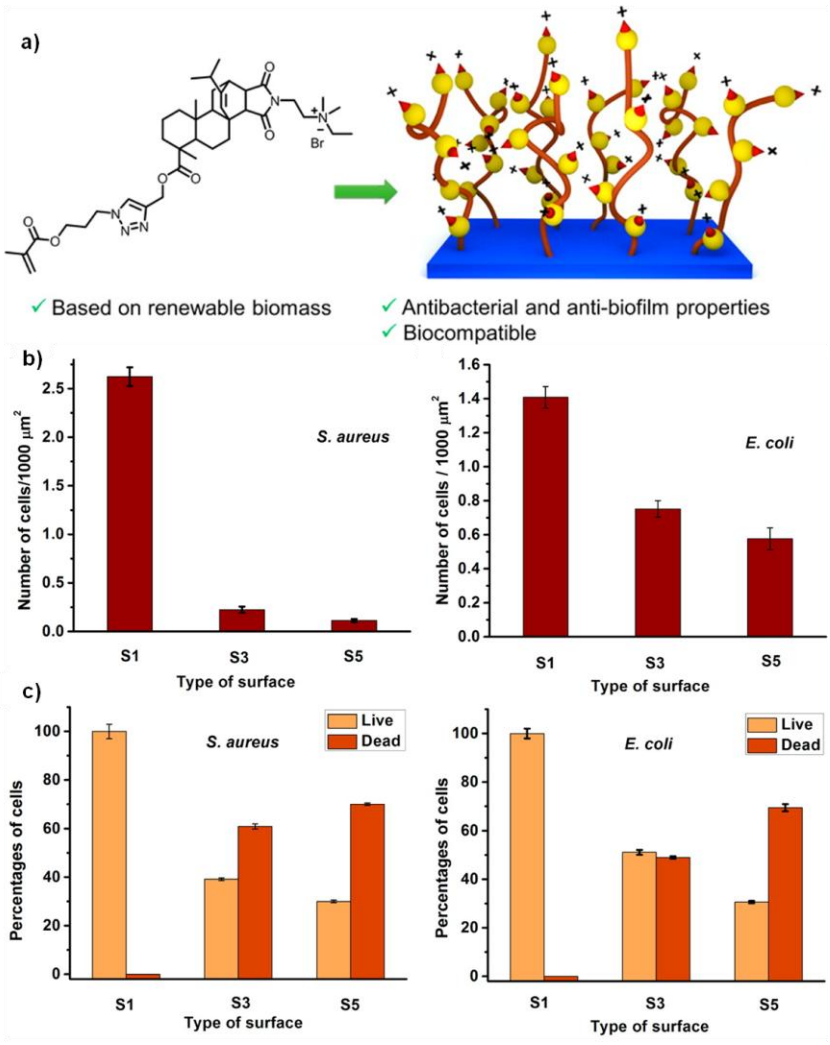

Figure 26. a) Antimicrobial coatings prepared via surface-initiated ATRP of a cationic rosin-derived monomer leading to b) a reduction in the number of cells attaching to the surface and c) a reduction of the number of cells that survive on the surface. Adapted with permission from *Biomacromolecules* **2015**, *16* (10), 3336–3344. © 2015, American Chemical Society.

Other efforts have been devoted to "grafting-from" approaches of rosin-derived monomers onto lignin and cellulose. Such natural polymers are characterised by a high heteroatom content, a poor solubility in conventional solvents (*e.g.* THF or DMSO) and a poor processability because of the absence of melting transitions.[118,145] Chemical modifications,[146] such as the attachment of polymers,[147,148] allow for an increase in solubility and the ability to obtain processable materials with a multitude of applications.[149] The first example of the grafting of rosin acid-derived monomers was reported for lignin by Tang *et al.* in search for renewable water resistant materials.[150] ATRP initiator-functionalised lignin was used as the macroinitiator for the synthesis of dehydroabietic ethyl methacrylate (DAEMA), dehydroabietic ethyl acrylate (DAEA), and dehydroabietic butyl acrylate (DABA) grafts (Figure 27a). Controlled polymerisation kinetics was confirmed by the linear increases of

molecular weight with conversion and the linear semilogarithmic plots (Figure 27b). The hydrophobicity of the obtained materials was confirmed by water contact angle and a decrease in the water uptake (from 18 wt% for lignin to 0.75 wt% for grafted lignin).

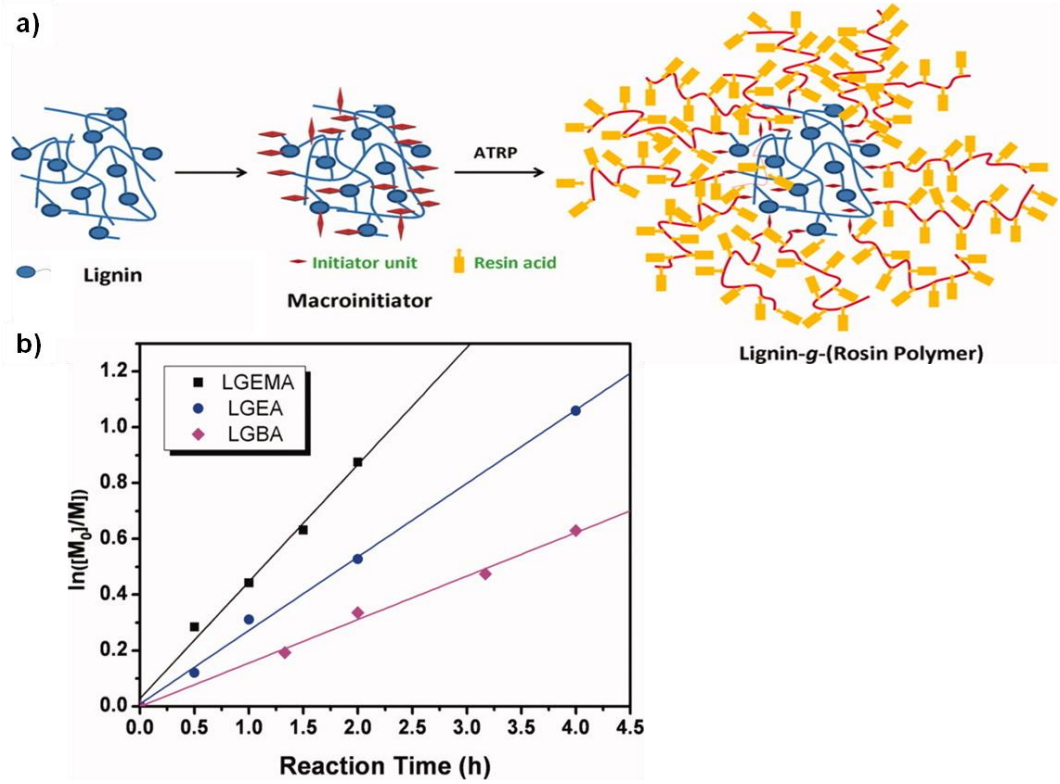

Figure 27. a) "Grafting-from" approach of rosin acid-derived monomers onto lignin using ATRP and b) the linear evolution of the first order kinetic plot. Reprinted with permission from *J. Polym. Sci. Part A Polym. Chem.* **2011**, *49* (17), 3728–3738. ©2011, John Wiley and Sons

In a similar approach by the same group, rosin acid polymer grafts were grown from ethyl cellulose using conventional ATRP conditions (Figure 28a) and controlled polymerisation kinetics were observed.[151] Solution-cast thin films of the obtained copolymers were observed to be smooth and homogeneous by AFM (Figure 28b). Furthermore, their thermal stability, hydrophobic nature and ability to absorb all the UV radiation between 200-315 nm make such films promising for UV-absorbent coating materials.

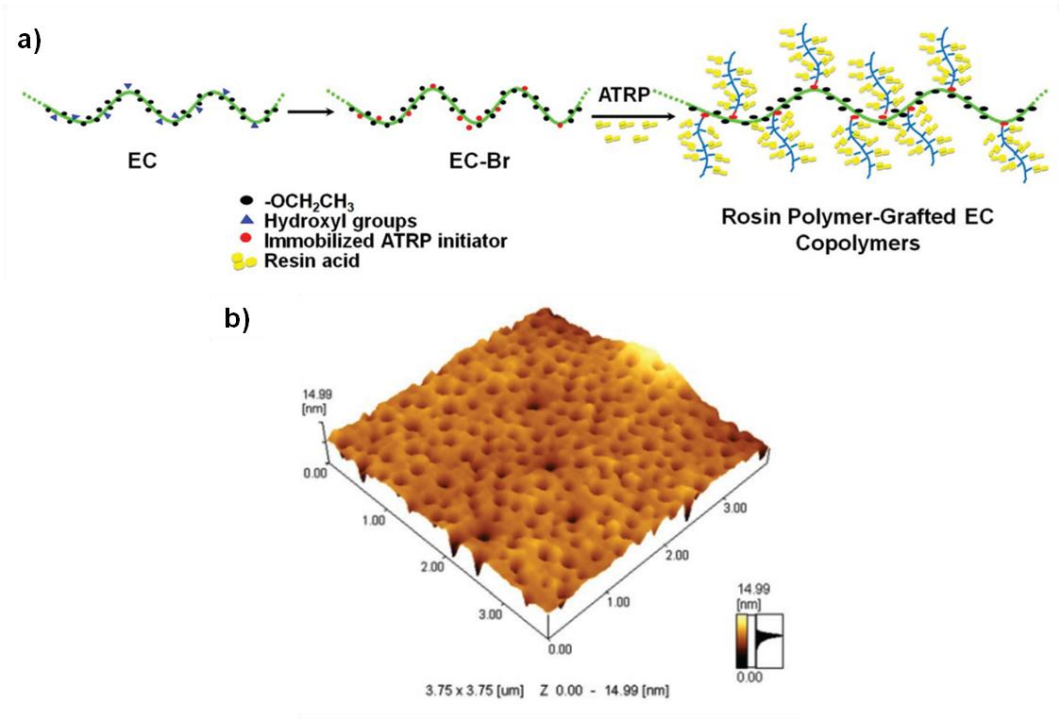

Figure 28. a) "Grafting-from" of rosin acid-derived polymers from ethyl cellulose and b) the atomic force microscopy image (AFM) of solution cast film of poly(ethyl cellulose-*g*-dehydroabietic ethyl acrylate) (P(EC-*g*-DAEA)). Reprinted with permission from *Green Chem.* **2014**, *16* (4), 1854–1864. ©2014, Royal Society of Chemistry

The potential of rosin acid-based graft copolymers grown from cellulose for thermoplastic elastomeric materials with a high elasticity were shown by Tang *et al.*[152] Similar to the approaches above, cellulose functionalised with ATRP initiating moieties was used as the macroninitiator to grow statistical dehydroabietic ethyl methacrylate (DAEMA) copolymers with butyl acrylate (BA) and lauryl methacrylate (LMA) (Figure 29a). The mechanical properties of these copolymers were found to be low in terms of maximum stress (<2.5 MPa) and linear elasticity (<1%) while both the Young's modulus (9-100 MPa) and the elasticity (>450%) were high (Figure 29b). Further improvements of these properties are needed for such renewably-based materials to replace current petrol-based thermoplastic elastomers.

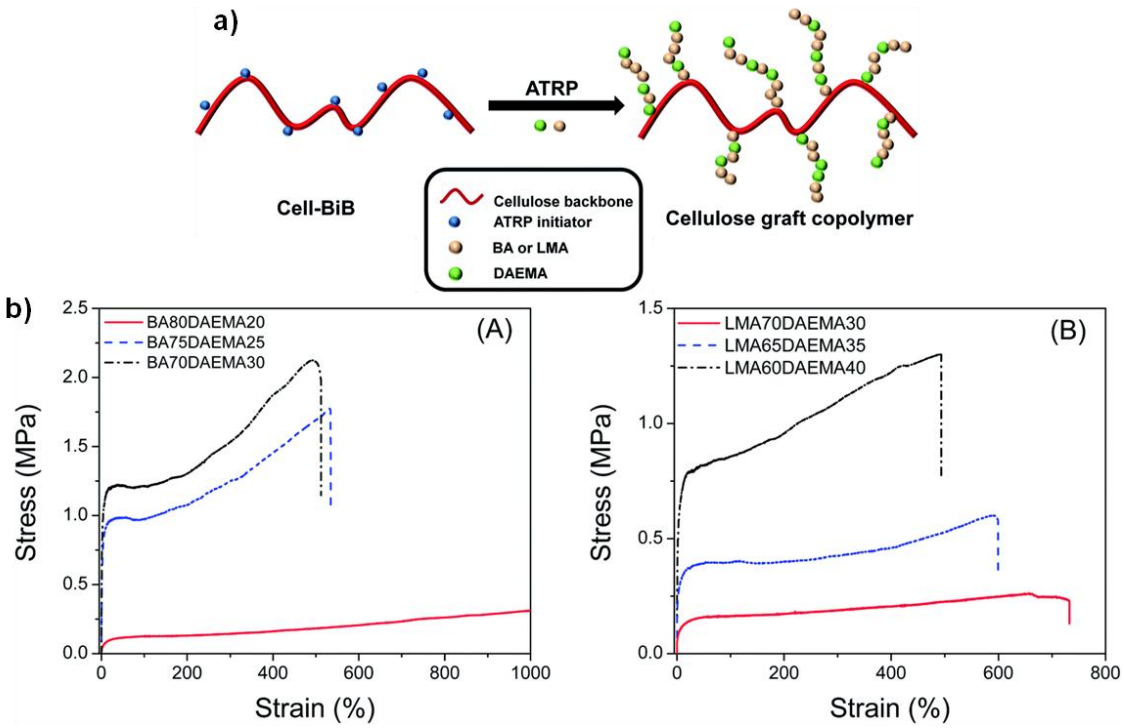

Figure 29. a) "Grafting-from" cellulose of statistical copolymers of butyl acrylate (BA), lauryl methacrylate (LMA) and dehydroabietic ethyl methacrylate (DAEMA) and b) the mechanical properties of the copolymers with different monomer feed ratios. Reprinted with permission from *Polym. Chem.* **2014**, *5* (9), 3170–3181. © 2014, Royal Society of Chemistry

The examples mentioned herein highlight the promise of renewable rosin-based materials for high-value applications as a result of their thermal stability and hydrophobic nature. Up to date only ATRP has been reported for such monomers and the use of other RDRP techniques in combination with other (bio-based) monomers leaves room for further investigations.

2.2.2.4. Triglycerides

Triglycerides, conventionally referred to as plant oils, are triesters of glycerol with fatty acid chains; the type of which is dependent on the plant the oil was extracted from (Scheme 14). For example, while rapeseed oil consists mainly of oleic acid, castor oil contains around 90 % of ricinoleic acid.[153–155] Through a simple esterification or saponification, glycerol can be split from the fatty acid chains giving rise to two very versatile molecules with different functionalities which have been exploited for the syntheses of platform chemicals and polymers,[43,153,163–168,154,156–162] some of which have already been successful in industrial settings.[169] Since then, the effective utilisation of glycerol for the synthesis of platform molecules[170–172] has been studied intensely.

In terms of RDRP of triglycerides, and their derivatives, the direct polymerisation is challenging as the double bonds of the fatty acid chains are non-activated in terms of radical stability while they are non-conjugated and/or internal. Crosslinking and termination are furthermore present and such monomers have therefore mostly been used for the preparation of thermoset resins *via* free radical polymerisation. Nonetheless, two patents stipulate that by selecting the right temperatures, controlling agents, and solvents, homopolymers of triglycerides can be obtained with no crosslinking by ATRP.[173] It is noted that by using RAFT polymerisation, hyperbranched polymers were observed.[174] Apart from these two reports, another strategy often pursued for the polymerisation of triglyceride-based monomers is the attachment of a double bond reactive towards radical polymerisations, *e.g. via* incorporation of an acrylate.[166,173,175,176] Such reactions were either performed on fatty acids or glycerol, *i.e.* the esterification products of triglycerides.

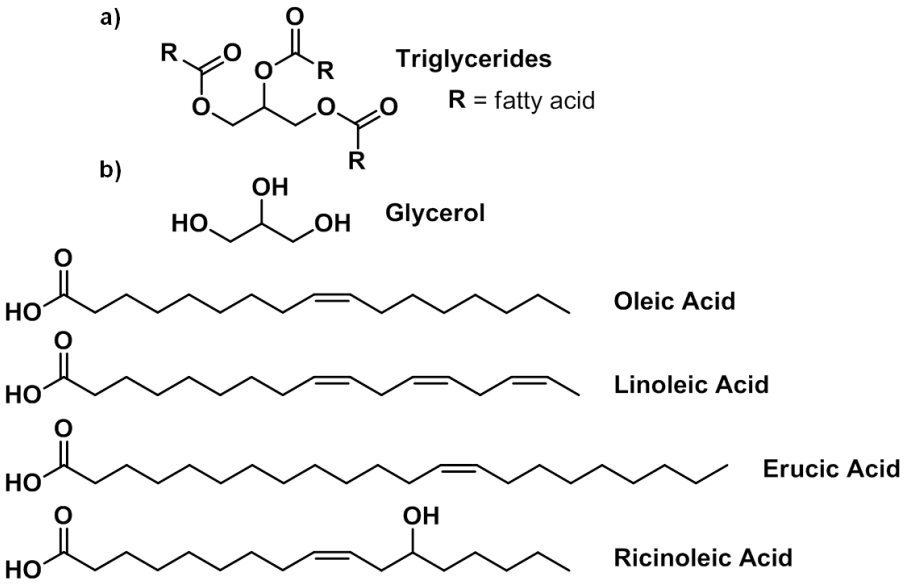

Scheme 14. Chemical structure of a) triglycerides and b) the molecules obtained after esterification of triglycerides, glycerol and a variety of different fatty acids. The type of fatty acid depends on the origin of the triglyceride.

2.2.2.4.1. Fatty Acids

Once separated from glycerol, the fatty acid chain can either be modified at the double bond (Scheme 15a) or the carboxylic acid (Scheme 15b), and several strategies have been employed for the attachment of polymerisable groups for each functional group. These polymerisable groups are usually acrylates and the synthesis and polymerisation of such acrylate-based monomers has been recently reviewed and their numerous applications highlighted.[177,178]

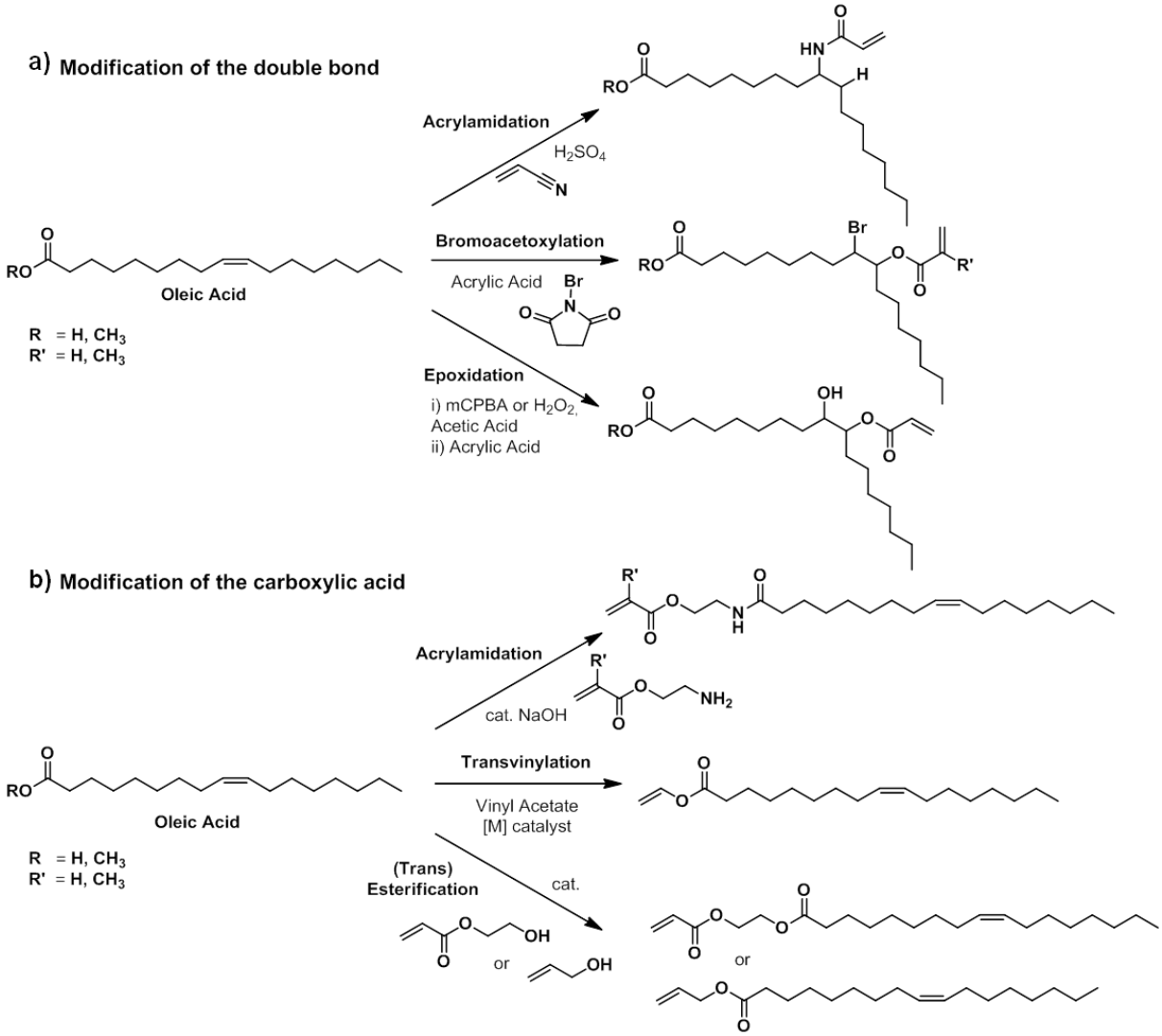

Scheme 15. Transformation of fatty acids – here with the example of oleic acid - into different monomers for RDRP by either a) modification of the double bond or b) modification of the carboxylic acid. Adapted from Calliol *et al.*[177]

Mechanically robust cellulose-based thermoplastic elastomers were also prepared by grafting two soybean oil-based methacrylate monomers from bromine-functionalised microcrystalline cellulose (Figure 30).[179] Using surface-initiated ATRP, two different monomers were

employed, namely SOM1 and SOM2 (Figure 30), and the molecular weights of the polymer grafts were between 10,000 and 63,000 g mol^{-1}. The amides present on the repeat units were stipulated to be capable of hydrogen bonding and the authors concluded, that the increase in mechanical strength was a result of this interaction. Unfortunately, no further data was shown on this aspect, whilst the grafting density of the polymer onto the cellulose was also not reported.

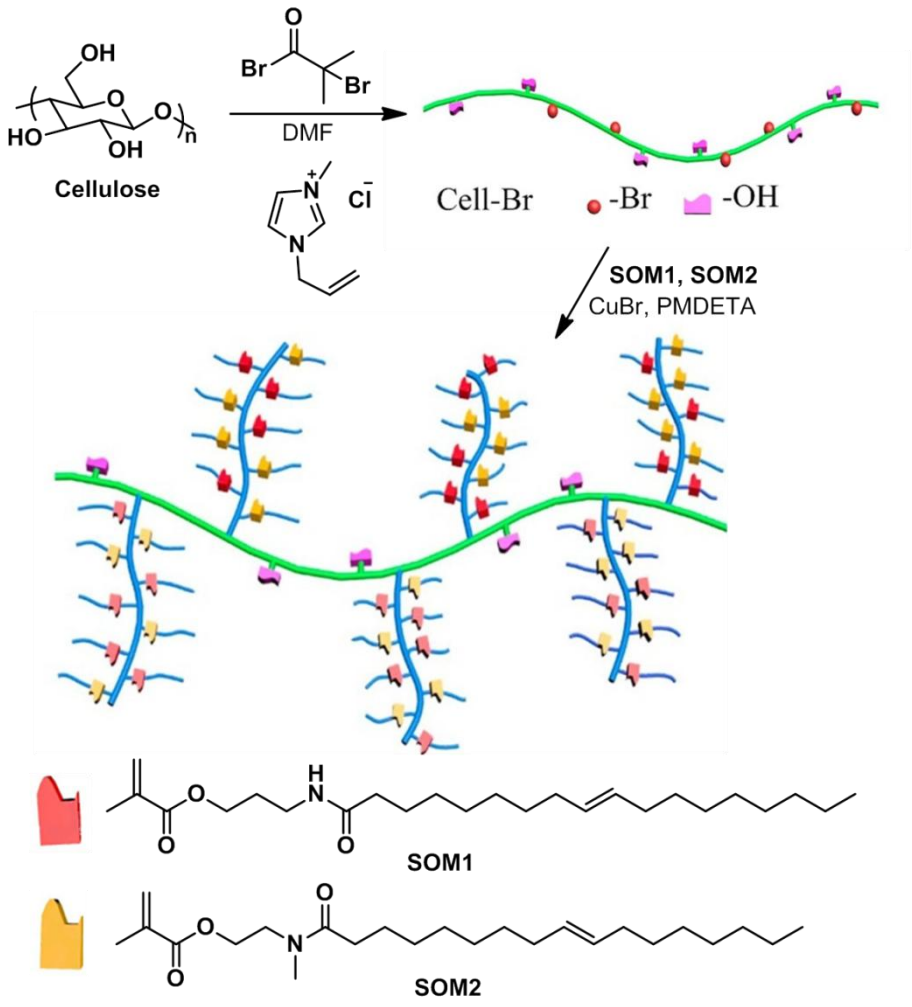

Figure 30. Synthesis of microcrystalline cellulose bearing an ATRP initiator, and the grafting of cellulose with soybean oil-based methacrylate copolymers. Reprinted with permission from *Appl. Surf. Sci.* **2018**, *458* (July), 495–502. © 2018, Elsevier Ltd.

A non-acrylate route towards fatty acid-based copolymers was only recently reported by Wang *et al.*[180] Starting from 4-vinylbenzyl chloride (VBC) a styrenic monomer with a fatty acid chain in the *para* position was synthesised using 1,1,3,3-tetramethylguanadine (TMG) as catalyst. The polymerisation of this vinylbenzyl oleate (VBO) was performed using a trithiocarbonate (*S,S′-bis*(α,α′-dimethyl-α″-acetic acid)trithiocarbonate) as bifunctional CTA at 60 °C in THF (Figure 31a). A shift of molecular weights to higher molar masses was

observed on the size exclusion chromatography traces (Figure 31b). Further evidence for the controlled nature of the polymerisation up to 30% conversion were the pseudo-first order polymerisation kinetics (Figure 31c). Moreover, two one-pot strategies for the synthesis of such copolymers by free radical polymerisations were presented, involving the polymerisation of VBC and either the attachment of the fatty acid chain during the polymerisation or by post-polymerisation modification catalysed by TMG. However, these strategies were not applied for the RAFT approach, possibly because of side reactions of TMG with the trithiocarbonate CTA.

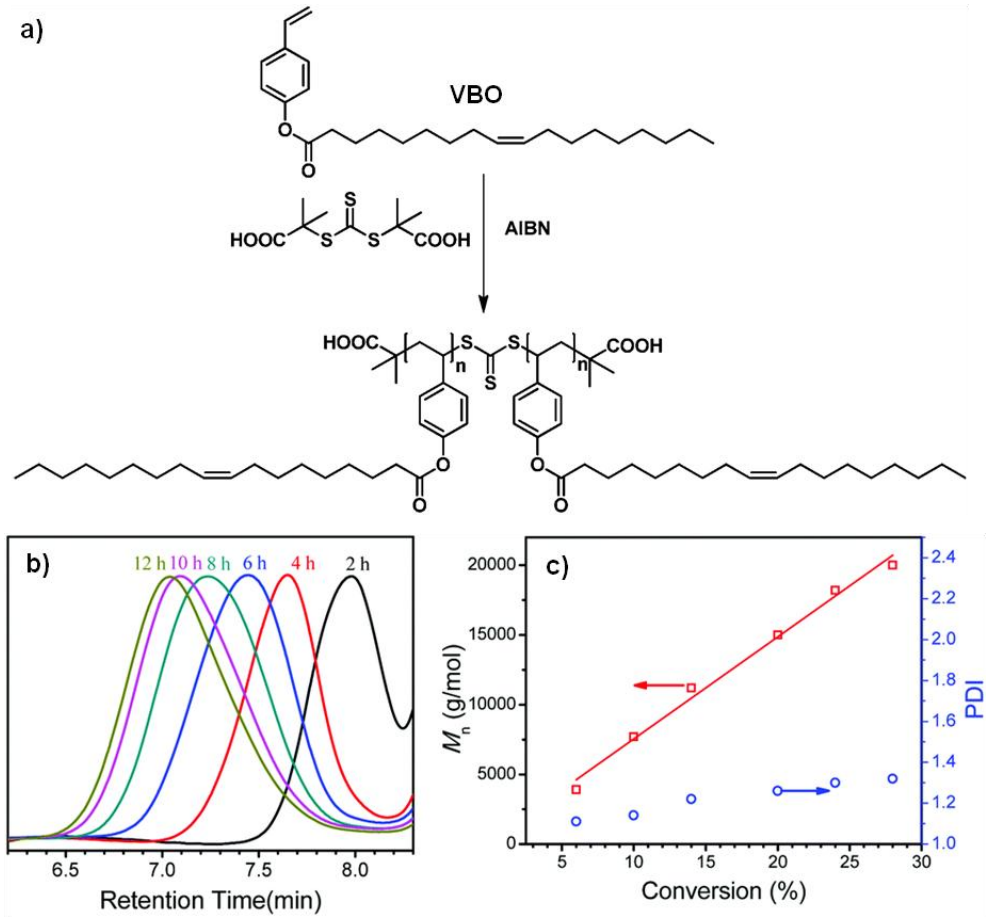

Figure 31. a) RAFT polymerisation of vinylbenzyl oleate (VBO) using a bifunctional CTA and b) the shift of molecular weights to higher molar masses during the polymerisation. c) Linear pseudo first order kinetic plot with the dispersity at different conversions. Adapted with permission from *Polym. Chem.* **2018**, *9* (21), 2880–2886. © 2018, Royal Society of Chemistry

The use of NMP for the copolymerisation of a fatty acid derived monomer, namely tridecyl methacrylate, with acrylonitrile was recently reported by Marić *et al.*[181] Although a variety of reaction conditions as well as initiators and controlling agents, such as 2-[*N*-tert-butyl-2,2-(dimethylpropyl)aminooxy]propionic acid (BlocBuilder) (Figure 32a), were tested, deviations

from linear kinetics at high conversions were observed in all cases (Figure 32b). As a result of this poor control, rather high dispersities were obtained (M_w/M_n > 1.47). Furthermore, no comment on the copolymer composition was made. The authors also describe the synthesis of block, ter-, and quadripolymers of tridecyl methacrylate, acrylonitrile, isobornyl methacrylate, and hydroxyethyl methacrylate under similar conditions. A multitude of fatty-acid derived monomers have been prepared by attaching a double bond to either the ester or the internal double bond of the fatty acid.

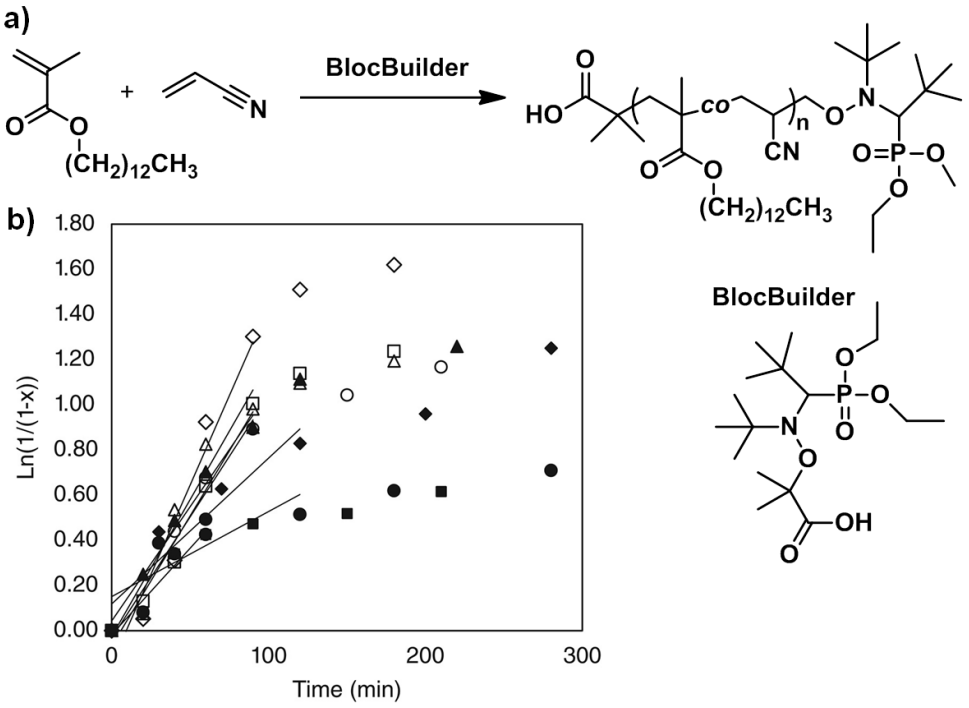

Figure 32. a) Copolymerisation of tridecyl methacrylate and acrylonitrile using NMP and b) the semilogarithmic kinetic plots for the different reaction conditions showing deviations from linearity. Reprinted with permission from *J. Polym. Sci. Part A Polym. Chem.* **2018**, *56* (21), 2422–2436. © 2018, John Wiley and Sons.

2.2.2.4.2. Glycerol-Derived Monomers

Unlike fatty acids, glycerol is highly hydrophilic with three hydroxyl groups, two primary and one secondary, and the difficulty of the selective functionalisation of just one hydroxyl group with a polymerisable function – in order to avoid crosslinking – limits the versatility of glycerol as a starting material. Enzymatic catalysis[182] has proven powerful in circumventing the laborious protection and deprotection steps necessary for the preparation of monofunctional monomers and extending the type of monomers accessible.[183,184] The polymerisation of these monomers using RDRP has already been summarised in 2012 by Lapinte *et al.*[185] The pendant hydroxyl groups of these polymers have been used for the

functionalisation of nanoparticles[186–189] or the preparation of stimuli-responsive polymers.[190,191] Solketal acrylate (SoMA), the acetal-protected derivative of glycerol methacrylate (GMA), was shown to be polymerisable by ATRP and SET-LRP.[191–193] Recently, the application of the methacrylate analogue for drug release has been shown using a biodegradable poly(ethylene glycol)-*block*-polycaprolactone copolymer (PEG-*b*-PCL) where the second block had pendant bromomethylpropanoate units that served as initiating sites for ATRP.[194] From these, a further block copolymer, poly(solketal methacrylate)-*b*-poly(2-(dimethylamino)ethyl methacrylate) (PSoMA-*b*-PDMAEMA)) was grafted to yield copolymers capable of self-assembly into uniform micelles (Figure 33a). Loaded with the anticancer drug Doxorubicine (DOX), an enhanced antitumor activity was observed for the drug-loaded micelles in *in vivo* studies on mice (Figure 33b), and a higher concentration of the micelles in the tumour compared to other vital organs was noted (Figure 33c).

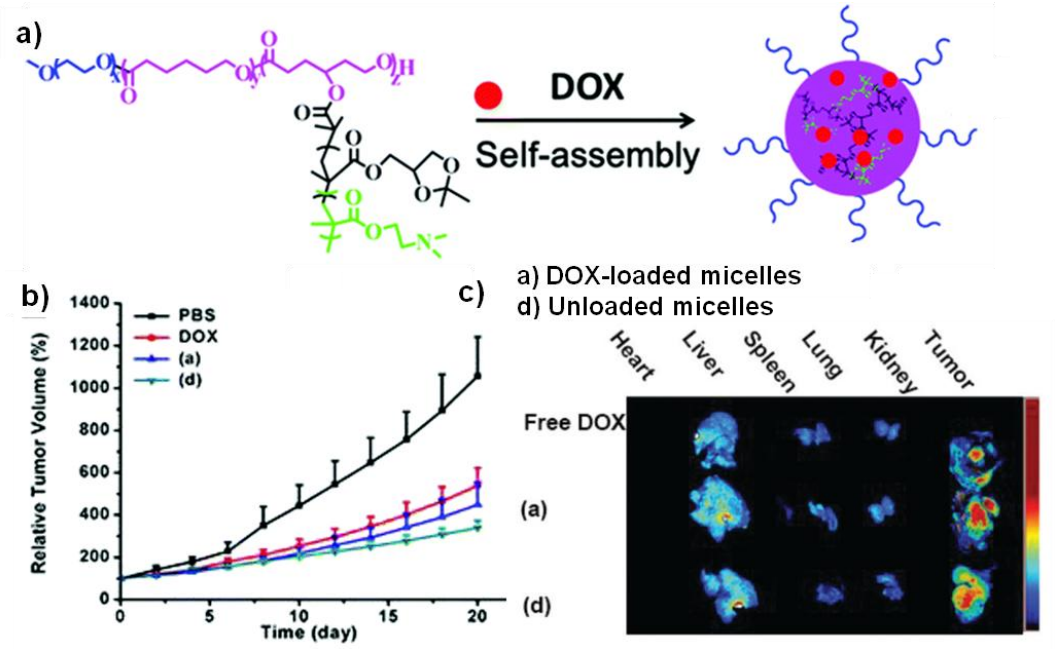

Figure 33. Block copolymer of ethylene glycol, caprolactone, solketal methacrylate and 2-(dimethylamino)ethyl methacrylate which self-assembles into micelles and is able to incorporate Doxorubicine. b) The slightly enhanced antitumor activity of the drug-loaded micelles compared to pure Doxorubicine, micelles and saline buffer solution (PBS), and c) the fluorescent images of the tissue distribution of the drug, micelles and the drug-loaded micelles. Adapted with permission from *Nanoscale* **2016**, *8* (3), 1437–1450. © 2016, Royal Society of Chemistry

Another interesting use for the dihydroxy functional groups of glycerol methacrylate (GMA) was presented by Amado *et al.*[195] Used as a complexing agent for iminophenylboronate (IPB),

the polymerisation of this IPB methacrylate allowed for the synthesis of syndiotactic poly(glycerol methacrylate) (PGMA) using ATRP which had not been discussed before (Figure 34). Different ligands, HMTETA, (+)-sparteine and dNbpy, were tested for the Cu(I)Br catalysed classical ATRP in DMF using ethyl α-bromoisobutyrate as the initiator and UV-photoinduced ATRP. Although rather high dispersities were obtained (M_w/M_n >1.51), the polymer showed a high syndiotacticity (82% of triads). The decomplexation of the IPB from the acrylate with catechols (Figure 34) was studied in detail and the quantitative recovery of the deprotected diol was observed in DMSO at 50 °C within 15 hours. This simple IPB protection strategy can be extended to other diol monomers. The copolymerisation of these monomers with hydrophobic monomers would lead to novel amphiphilic copolymers which are difficult to obtain in common organic solvents.

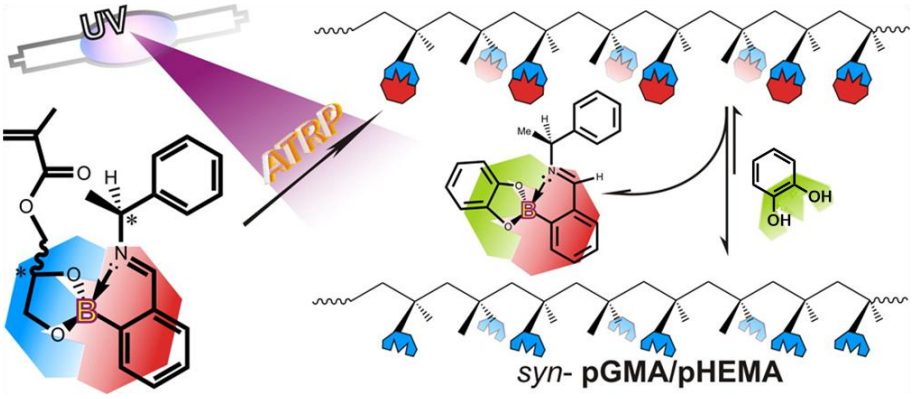

Figure 34. ATRP polymerisation of glycerol methacrylate (GMA) complexed with an iminophenylboronate ester (IPB) leading to a syndiotactic diol bearing polymer after decomplexation with catechol. Adapted with permission from *Macromolecules* **2016**, *49* (5), 1532–1544. © 2016, American Chemical Society.

A further application of boronate complexes with the pendant dihydroxy functionality of glycerol-based polymers was demonstrated with the control over the morphological transitions of amphiphilic block copolymers.[196] Using a previously reported RAFT polymerisation of GMA in ethanol with CPDB as chain transfer agent and AIBN as initiator,[197] a water-soluble macro RAFT agent with a DP_{GMA} of 45 was synthesised and successfully chain-extended using 2-hydroxypropyl methacrylate (HPMA) in an aqueous dispersion polymerisation initiated by 4,4′-azobis(4-cyanovaleric acid) (ACVA; Figure 35a). Well-defined block copolymers were obtained with molecular weights between 39,000 and 53,400 g mol^{-1} with dispersities below 1.16. Such block copolymers had previously been shown to be soft free-standing hydrogels and are promising for applications such as contact lenses or tissue engineering.[198] Vesicle formation was observed for the block copolymers by

transition electron microscopy (TEM; Figure 35b) and the morphology was changed upon the addition of aminophenylboronic acid (APBA) at pH 10.5 into a wormlike structure (Figure 35c). The salt content did not affect this transformation. This vesicle-to-worm transition was used to release silica particles at ambient temperature using the addition of APBA as a trigger and full release was observed after 12 hours at a pH of 10.5. A lowering of the pH was observed to severely retard the release of the entrapped silica nanoparticles. This proof-of-concept highlighted the promise of such temperature- and salt-independent stimulus-responsive polymer vesicles for targeted delivery and controlled release of active substances.

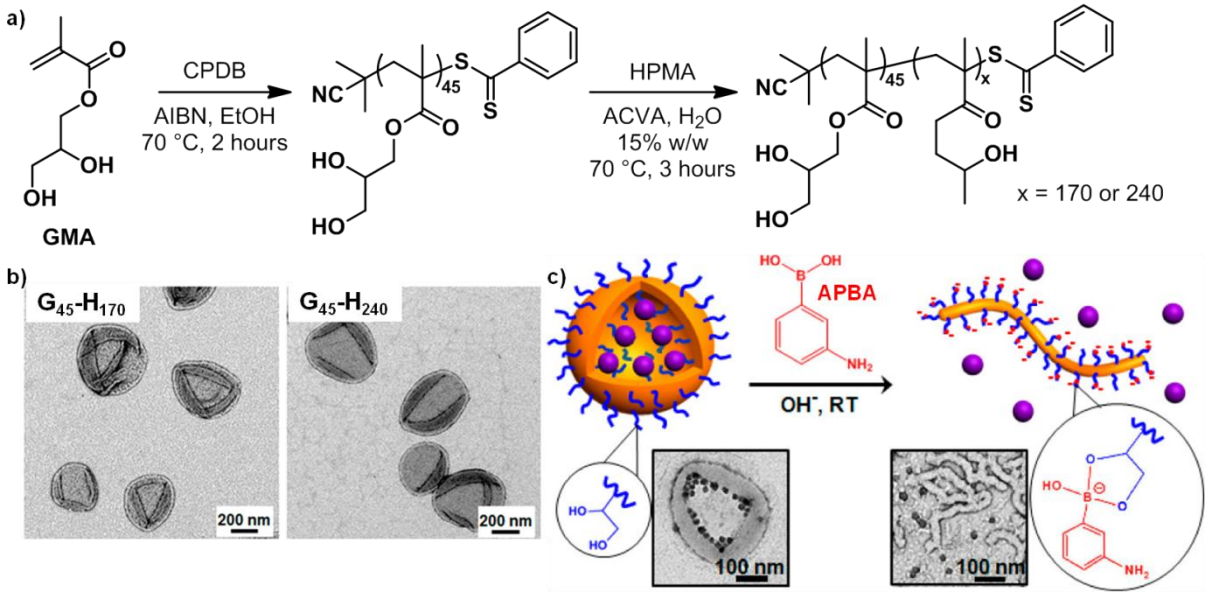

Figure 35. a) GMA macroRAFT agent used for the synthesis of diblock copolymers with 2-hydroxypropyl methacrylate (HPMA) which self-assembled into a vesicle morphology in water as observed by transition electron microscopy (TEM) which d) can be changed into worm-like structures upon the addition of aminophenylboronic acid (APBA). Adapted from Armes *et al.*[196]

A similar PGMA-*b*-HPMA block copolymer comprising a short GMA first block with a larger HPMA second block was shown to be useful as a synthetic bioinert 3D matrix for pluripotent stem cells,[199] *i.e.* cells which can still differentiate into any of the three primary cell types and are found in embryos. Similarly to the previous example, RAFT polymerisation was pursued, except that the chain extension was performed in phosphate-buffered saline solution to ensure cell compatibility. The formed worm-hydrogels were shown to allow the reversible cytostasis, *i.e.* the reversible inhibition of cell growth, of pluripotent stem cells for up to 2 weeks. Preliminary tests on human embryos showed stasis was possible for 4 days

which make these biocompatible diblock copolymers promising for the design of new biomimetic scaffolds with comparable properties to natural membranes.

Even though all the above monomers contain a glycerol moiety, their renewable content is rather low owing to the fact that the ketal and the (meth)acrylate are currently not bio-derived. Since the focus of most of these studies were novel polymer architectures or polymers targeted for specific applications, this is unsurprising. Functionality and renewability are, however, not exclusive as was recently shown through the combination of glycerol, CO_2, methanol, and methyl-10-undecenoate – a ricinoleic acid derivative – into completely bio-based cyclic carbonate monomers.[98] In a solvent-free, one-pot transesterification reaction, functional monomers bearing allylic or olefinic double bonds and a cyclic carbonate could be synthesised in a sustainable fashion (Figure 36a). The homopolymerisation of these monomers was not possible by organometallic-mediated radical polymerisation (OMRP) using an alkylcobalt initiator, which was attributed to degradative chain transfer. Nonetheless, these monomers were successfully copolymerised with vinyl acetate, a monomer which can in principle also be renewably sourced, at 40 °C with conversions of up to 50%. An incorporation of the renewable monomers of up to 50 mol% was reported (Figure 36a) and the controlled nature of the copolymerisations was established through the linear evolution of molecular weights with conversion (Figure 36b), complete shifts of the molecular weights to higher molar masses in size exclusion chromatograms and low dispersities. Yet slight deviations from pseudo-first order kinetics (Figure 36c) were noted but a detailed explanation was not provided. Nonetheless, this study opens up a plethora of possibilities for the RDRP of allylic and other non-activated monomers, as well as advocating sustainable and renewable synthetic pathways.

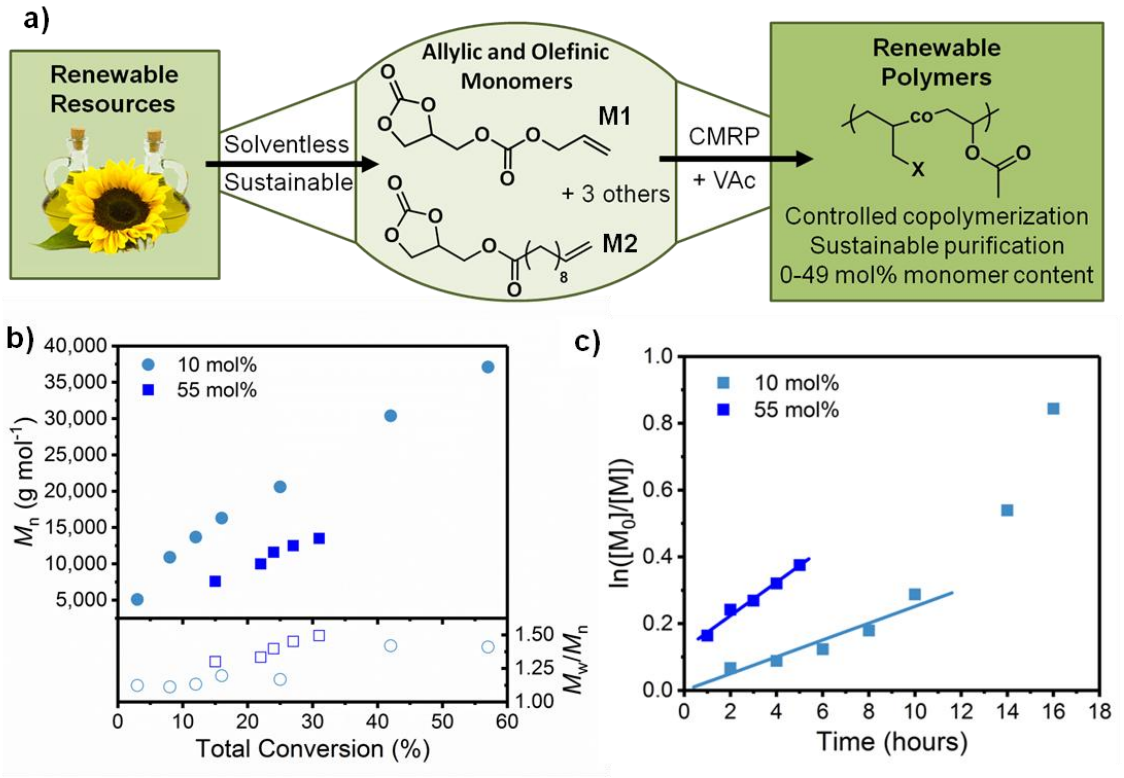

Figure 36. a) Synthesis of allylic and olefinic-based polymers from renewable resources using cobalt-mediated radical polymerisation. For copolymerisations of allyl ((2-oxo-1,3-dioxolan-4-yl)methyl) carbonate (**M1**) and vinyl acetate, b) the evolution of molecular weights and dispersity with conversion and c) the first-order kinetic plot for 10 and 55 mol% **M1** monomer feeds are shown. Reprinted with permission from *ACS Sustain. Chem. Eng.* **2019**, *7* (2), 2751–2762. © 2019, American Chemical Society

2.2.3. Conclusions

The aforementioned examples highlight the versatility of the various renewable monomers available for reversible deactivation radical polymerisations. Since the first reports in the early 2000s on simple natural molecules containing double bonds, *i.e.* terpenes, a lot of progress has been made in increasing the number of naturally-available monomers, such as itaconic acids. For renewable molecules which do not contain a double bond, their functionalisation with acrylates is still the method of choice while promising developments in other catalytic or enzymatic transformations of renewable molecules into monomers for RDRP have been reported. Nonetheless, further developments, especially in the homopolymerisation of renewable monomers bearing less activated double bonds, such as allylic monomers or fatty acids, are necessary to fully exploit the potential of renewable polymers in terms of their properties and applications.

2.3. Ethylene (Co)Polymerisations

Ethylene is one of the industrially most successful monomers of the last 100 years and is mainly obtained from the cracking of petroleum and thus non-renewable. Yet, PE can also be produced from renewable resources *via* the fermentation of sugar cane into ethanol which is then dehydrated into ethylene and subsequently polymerised.[200] This "bio-PE" is commercially available but more expensive than fossil fuel-based PE as a result of the production process and has only been implemented in Brazil. The on going research into the fermentation of non-edible biomass, such as cellulose or lignin, could allow for a shift from food-derived bio-ethylene to non-food derived bio-ethylene and thus not only solve the issue of fermenting food to make materials, but also reduce the price of this production pathway. Additionally, this type of bio-sourced ethylene is likely to gain more and more significance in light of fossil fuel depletion and the legislative requirement for a Circular Economy imposing sustainable and renewable plastic. Therefore the combination of renewable monomers, such as those mentioned in Section 2.2, with ethylene is attractive for the preparation of novel ethylene-based copolymers with pertinent applications in a variety of sectors.

Currently polymerisations of this very simple C_2H_4 monomer are industrially performed using coordination insertion or free radical polymerisations to synthesise high density polyethylene (HDPE), low density polyethylene (LDPE) and linear low density polyethylene (LLDPE), each with different applications ranging from car fuel tanks, or pipes to packaging films. In search for novel applications, the copolymerisation of ethylene with comonomers is a promising strategy as the incorporation of low amounts of comonomer can drastically affect the properties of the polymer. Up to date, the incorporation of functional, polar monomers into ethylene copolymers in the complete incorporation range, *i.e.* from ethylene-poor to ethylene-rich copolymers, has so far not been possible using either coordination insertion polymerisation or free radical polymerisations.[201,202] While coordination insertion copolymerisations of ethylene enable the incorporation of only a few mol% of comonomer (ethylene-rich) (Scheme 16),[203–205] free radical copolymerisations of ethylene incorporate above 50 mol% of the comonomer (ethylene-poor) (Scheme 16),[206] and the tuning of the comonomer content to values in between remains challenging. Furthermore, the type of polar monomers which can be incorporated by these types of polymerisations are limited to carboxylic acids, esters and ketones for varying reasons.

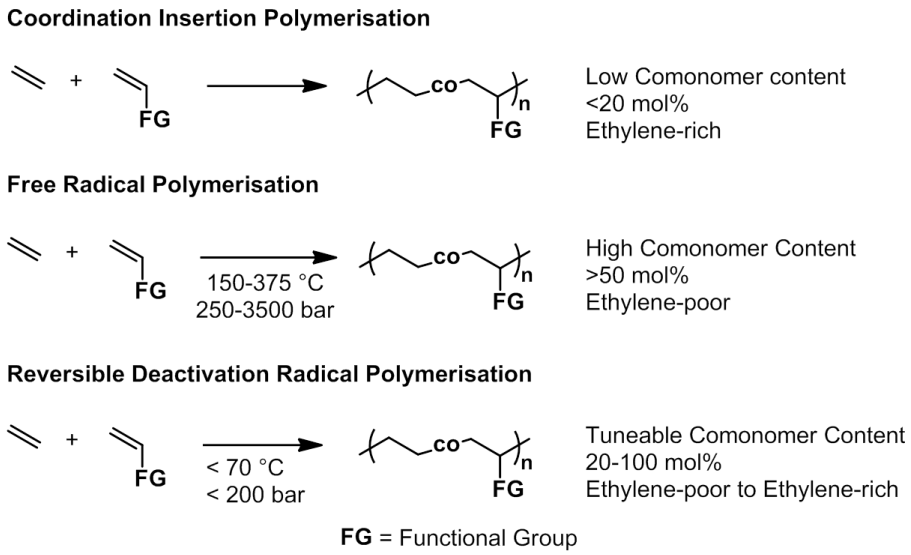

Scheme 16. Polymerisation techniques capable of copolymerising ethylene with polar monomers.

Recently, progress has been made in the field of reversible deactivation radical polymerisation (RDRP) for the copolymerisation of ethylene with polar monomers by RAFT and OMRP (Scheme 16).[5,7] At much milder conditions (below 70 °C and at pressures below 200 bar) compared to free radical polymerisations (150-375 °C and 250-3,000 bars), copolymers with a tunable comonomer content were obtained for a few homopolymerisable monomers such as vinyl esters,[5,7] vinyl amides,[9] vinyl ethers[9] and acrylonitrile.[7] As a result of the low temperature employed, very linear polymer chains were obtained with degrees of branching below 5 branches per 1000 carbon atoms. This is in sharp contrast to free radical polymerisations which produces polyethylene with more than 10 branches per 1000 carbon atoms.[207–209] The number of branches present in ethylene polymers determines some key material properties, such as mechanical strength, which directly relate to the possible applications of these polymers. For example, the low levels of branching in HDPE give it a high strength and a high impact resistance, which allows HDPE to be used as bottle caps or water pipes. LDPE on the other hand has a high amount of branching and displays lower strength and better moulding properties allowing it to be used for plastic bottles and carrier bags. The choice of initiator allows to access unprecedented ethylene copolymer architectures such as block and block-like copolymers with intriguing properties for a range of applications. Especially the preparation of ethylene block copolymers *via* one polymerisation technique is interesting because it enables the quantitative chain extension of a first block without the need for the functionalisation of the first block with another initiator, thus simplifying the current laborious synthetic strategies for PE-based block copolymers.

Nonetheless, the scope of comonomers that can be incorporated by reversible deactivation radical polymerisations remains limited and further developments in this field will allow for the synthesis of functional ethylene copolymers with drastically different properties to the currently available ones. Particularly, the introduction of reactive groups which are available for post-polymerisation modifications, are attractive for the use as compatibilisers for polyethylene composites.

2.4. Nanocomposites of Polyethylene and Cellulose

As mentioned in Section 2.3, several types of PE exist and each has unique properties as a result of the polymer chain structure. Although, HDPE presents remarkable mechanical properties in terms of strength and stress resistance, some applications require PE with superior mechanical properties to the currently available materials and reinforcing PE with fillers is one promising strategy. Particularly renewable fibres, such as cellulose, have been used as reinforcing fillers, as a result of the very high strength of these fibres.[210–212] Furthermore the addition of such fibres allows to increase the renewable and biodegradable content of PE materials.[210,212,213] The properties of cellulose strongly depend on the origin and the extraction process,[210,214–216] and different types of cellulose fibres are available. One prominent example are nanocrystalline cellulose fibres which are obtained by the removal of the amorphous regions of cellulose leaving behind highly crystalline fibres of several nanometers in size.[217] The difference in hydrophilicity between polyethylene and cellulose (Scheme 17a) makes their combination into composite materials extremely challenging as no interaction between the matrix (PE) and the filler (cellulose) is possible. As a result, aggregation of the cellulose fibres occurs leading to inferior mechanical properties. Different routes have been employed to increase the interaction between these two components, such as cellulose modification[218] and reactive compatibilisation,[219] and in the scheme of this thesis the functionalisation of polyethylene and subsequent use as compatibiliser is of particular interest. It should be noted, that an effective dispersion of such fibres within the PE matrix leads to an increase in the mechanical properties, such as Young's modulus and impact resistance, of such composites.

In terms of functional polyethylene, three main types exist (Scheme 17b): randomly functionalised polymers, chain-end functionalised polymers, and polymers bearing functionalised segments, such as block or graft copolymers.[201,202] As outlined in Section 2.3, the synthesis of randomly functionalised polyethylene copolymers over a broad polar comonomer content is currently not possible for free radical or coordination-insertion

polymerisation. Other types of polymerisations, such as acyclic diene metathesis (ADMET)[220,221] or ring-opening metathesis polymerisation (ROMP),[222,223] encounter similar difficulties in that the comonomer content is typically limited to below 25 mol%. Meanwhile, chain-end functionalisations of polyethylene are possible by most techniques, either through controlled quenching of controlled polymerisations, chain transfer reactions for transition-metal catalysed polymerisations, or the modification of unsaturated chain-ends.[201] However, these approaches are less suitable for the preparation of compatibilisers as the quantity of polar monomer introduced is small and these groups are buried within the apolar polyethylene chain, limiting their interactions with the cellulose fibres. More promising are segmented polymers, as the presence of numerous polar groups allows for the interaction with the polar fibres while the polyethylene segment can entangle with the polyethylene chains of the matrix. While several examples of block copolymers can be found using two polymerisation techniques, for example synthesis of PE *via* coordination-insertion polymerisation followed by chain-end functionalisation with a RAFT CTA and the homopolymerisation of methyl methacrylate,[224] no single polymerisation technique has given access to such highly amphiphilic block copolymers. Similarly, very few examples of "grafting from" PE chains can be found (*e.g.* Waymouth *et al.*,[225] or Matyjaszewski *et al.*[226]), while no examples of "grafting onto" the polyethylene chain exist, as the installation of randomly distributed functional moieties in the backbone is necessary for both strategies, which is up to date extremely difficult (*vide supra*).[201] An uncontrolled pathway for the installation of functional groups along the PE backbone is the reactive extrusion of PE with unsaturated polar molecules, *e.g.* maleic anhydride, to synthesise grafted PE copolymers.[227,228] While the advantages of this process are its simplicity, performed in an extruder by the simple addition of a radical initiator and the reactive molecule, and the synthesis of PE bearing randomly attached oligomeric chains of these molecules,[229–231] several disadvantages remain. The radical nature and the harsh conditions employed in this process result in poorly controlled reactions, leading to crosslinking and chain scission heavily affecting the molecular parameters.[227] Moreover, the functionalisation is typically limited to below 5% of altered ethylene repeat units.

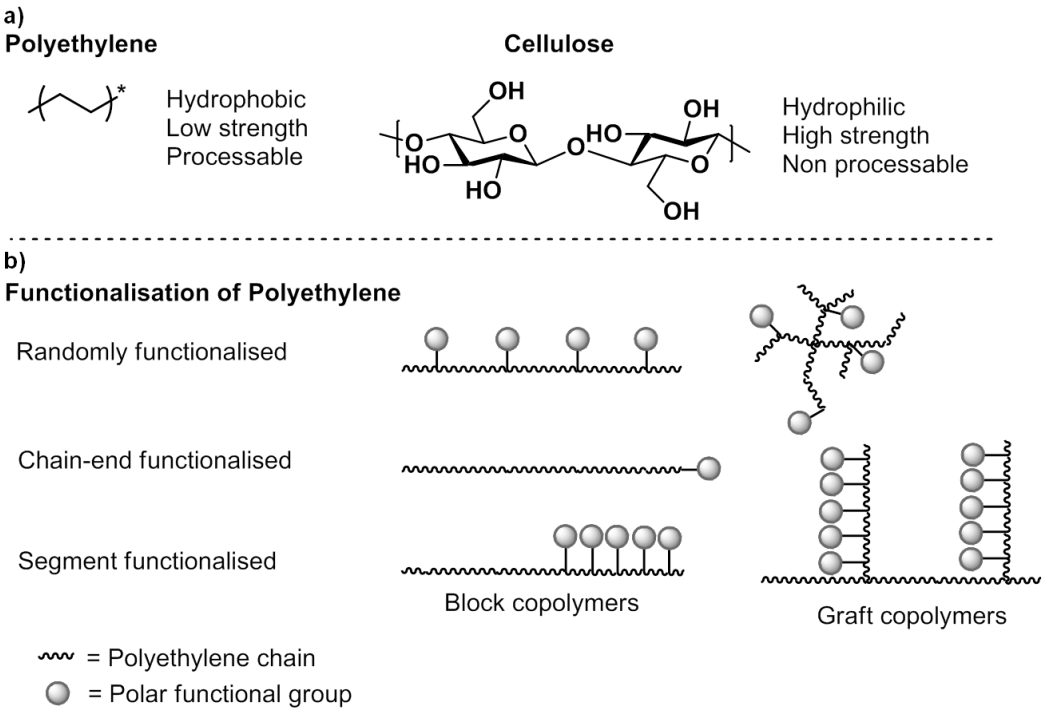

Scheme 17. a) Structures of polyethylene and cellulose and b) functionalisations of polyethylene leading to randomly, chain-end or segmented polar units in the polymer chain. Adapted from de Bruin *et al.*[201]

Recent developments in the synthesis of polyethylene copolymers by RDRP techniques (Section 2.3) now allow for the precise control over molecular weights, degree of functional monomer incorporation, and the polymer architecture. The resulting macromolecules are promising for their application in composites as they contain functional groups able to interact with cellulose through non-covalent interactions, *e.g.* hydrogen bonding of the cellulose hydroxyl groups with copolymer ketone functional groups, or through covalent bonds, *e.g.* transesterification of the cellulose hydroxyl groups with ester groups on the copolymer chain. At the same time these copolymers bear non-polar segments able to interact non-covalently with PE chains through chain entanglement and van der Waal's interactions. Moreover, unprecedented block copolymers can be synthesised as a result of the controlled chain growth process and allow for amphiphilic block copolymers to be synthesised. These are expected to show a superior compatibilisation performance compared to randomly functionalised copolymers and thus allow for the preparation of reinforced cellulose/polyethylene composites.

3 Aim of the Thesis

Renewable resources were shown to be a promising feedstock for reversible deactivation radical polymerisations (RDRP). A limited number of natural molecules bearing a double bond are available, as many other double bonds found in nature are non-activated or internal, limiting their suitability for radical polymerisations. However, the abundance of acid and alcohol moieties in natural molecules has allowed for the synthesis of a library of renewable monomers *via* the functionalisation with double bonds, namely acrylates and methacrylates. Although these monomers are renewably-based, the double bonds are obtained from fossil feedstocks reducing the renewable content of the monomer. Furthermore, these functionalisations are most often non-catalytic and non-benign, producing salts or other stoichiometric waste products. Strategies for the sustainable synthesis of novel renewable monomers using bio-derived double bonds are scarce.

In light of this, the first chaper of this thesis (Chapter 4) aims to introduce novel renewable carbonate and ester monomers derived entirely from CO_2 and plant oils using catalytic reactions. A sustainable monomer synthesis is paired with a green purification of the prepared polymers and overall this approach exemplifies the application of Green Chemistry principles and sustainability throughout the synthetic process. Moreover, this chapter presents the first polymerisation of allylic and non-activated olefinic double bonds using RDRP techniques. Organometallic-mediated radical polymerisation (OMRP) was specifically used for the above polymerisations because the *bis*(acetylacetonate)cobalt(II) complex used forms very weak carbon-cobalt bonds compared to other RDRP techniques. This weak bond is key to the reversible deactivation of the non-activated double bonds in this thesis. In a second step, the versatility of cyclic carbonate-bearing monomers for post-polymerisation modifications is presented for a CO_2-derived monomer (Chapter 5). While existing post-polymerisation modification strategies, such as hydrolysis or azide-alkyne Huisgen cycloaddition reactions, mainly allow for the preparation of one type of polymer structure from the original polymer, the presence of cyclic carbonate pendants enables both hydrolysis and aminolysis modifications to be performed leading to a large variety of structures. In this chapter (Chapter 5), copolymers with vinyl acetate are synthesised which were then effectively modified into functional poly(vinyl alcohol) with improved properties such as increased water solubility. With the advent of bio-ethylene *via* the fermentation of biomass, the incorporation of renewable building blocks into polyethylene chains is an attractive means to introduce functional and polar moieties into the hydrocarbon chain. Moreover, these polar functionalities allow to modulate its properties and are particularly interesting for the

compatibilisation of polar fillers in polyolefin matrices. The copolymerisation of ethylene and polar monomers over the whole composition range is, however, only possible for a few monomers using RAFT and OMRP techniques. Chapter 6 presents the preliminary results obtained for the copolymerisation of ethylene with the renewable monomers presented in Chapters 4 and 5 using OMRP and the copolymers obtained are the first examples of ethylene copolymers bearing cyclic carbonate units. Notably, the ethylene content of these copolymers can be tuned from ethylene-poor to ethylene-rich copolymers *via* the ethylene working pressure used during the polymerisation. These ethylene copolymers are of interest for the compatibilisation of cellulose and commercial polyethylene as the presence of both polar groups and ethylene units should enable the dispersion of the cellulose fibres within the matrix akin to classical surfactants. Unfortunately, a lack of time prevented investigations into the application of these ethylene copolymers as compatibilisers, nor were the copolymers of Chapters 4 and 5 investigated for the same reason.

One type of copolymer compatibiliser, which has already been examined for cellulose/LDPE composites, are poly(ethylene-*co*-vinyl acetate) copolymers. However up to date, no systematic study on the effect of ethylene content, molecular weight or copolymer architecture has been performed mainly because the techniques able to prepare such precisely-designed ethylene copolymers are relatively recent. Chapter 7 presents the synthesis of poly(ethylene-*co*-vinyl acetate) as well as poly(ethylene-*co*-vinyl acetate)-*b*-poly(ethylene) copolymers using OMRP. Although not all prepared copolymers were investigated, as a result of a lack of time, the preliminary results highlight the importance of ethylene content on the material properties of cellulose/LDPE composites. These compatibilisers, and in general most compatibilisers used in the literature, are based on fossil fuel-derived materials and almost no examples of fully renewable compatibilisers exist. In the last chapter of this thesis (Chapter 8) the application of a starch and plant oil-based compatibiliser to cellulose/LDPE composites is described. This compatibiliser can be easily prepared on a large scale in a sustainable process and an in-depth rheological analysis of the formed composites revealed the improvement in terms of cellulose fibre dispersion within the matrix when the compatibiliser was present. Overall, this work establishes new routes towards the synthesis of renewable and functional (co)polymers based on vinyl acetate, ethylene, and plant oils for nanocomposite applications.

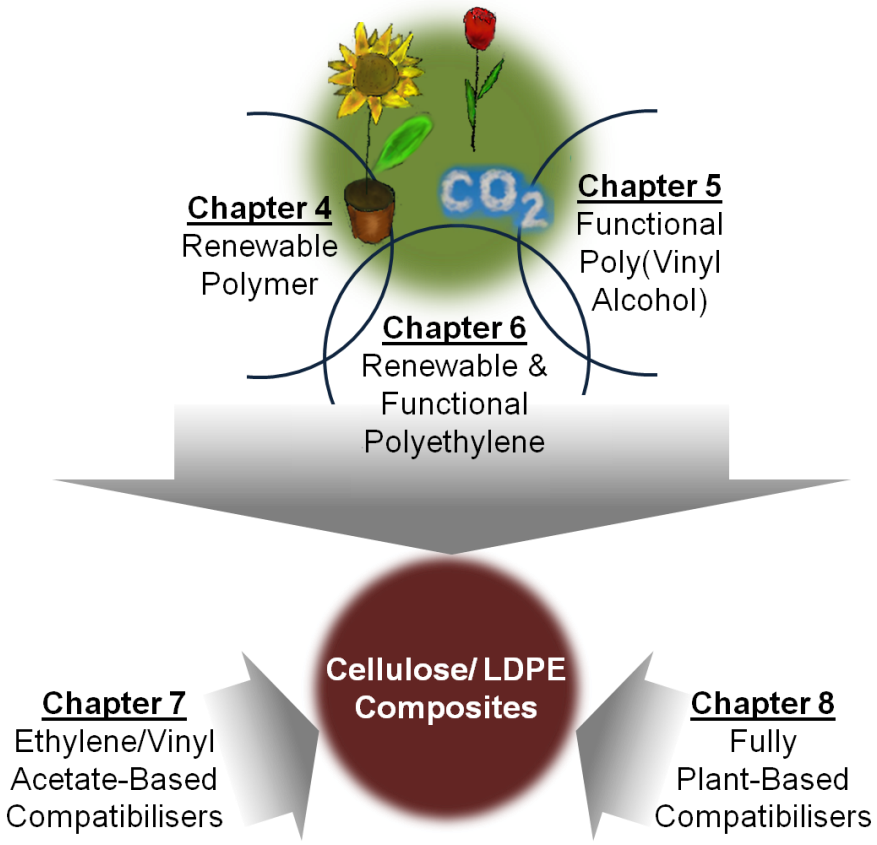

Figure 37. The preparation of a variety of polymers from renewable resources discussed in Chapters 4-6 of this thesis with possible applications as compatibilisers for cellulose/LDPE composites. Chapters 7 and 8 describe the use of other types of compatibilisers for these composites.

4 Synthesis of Plant-Based Non-Activated Olefins: A New Class of Renewable Monomers for Controlled Radical Polymerisation

This chapter and the corresponding parts in the experimental section are reprinted with permission from

Philip B. V. Scholten, Christophe Detrembleur, and Michael A. R. Meier
ACS Sustainable Chem. Eng., 2019, 7 (2), 2751–2762.
DOI 10.1021/acssuschemeng.8b05926

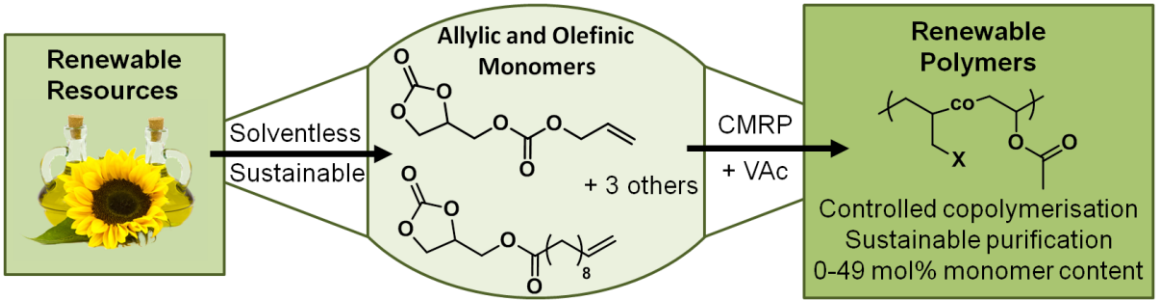

4.1. Abstract

In light of fossil fuel depletion and a general necessity for sustainable development, the synthesis of polymers from renewable resources is gaining more and more importance. Yet, industrially relevant radical polymerisations still struggle with the incorporation of renewable resources as the number of natural molecules containing suitable double bonds is limited. Herein, we present the sustainable synthesis of non-activated allylic and olefinic carbonate monomers from renewable resources in a solventless one-pot transesterification reaction. We subsequently confirm the first controlled radical copolymerisation of such challenging non-activated monomers with vinyl acetate, in which molecular weights above 10,000 g mol^{-1} were reached. The controlled nature of the copolymerisations was verified by the low dispersities obtained and the linear increase in molecular weights with conversion. The so-prepared copolymers were purified using sustainable extractions by supercritical carbon dioxide ($scCO_2$), which allowed to recover unused monomer in up to 58% yield. Using FT-IR and NMR spectroscopy, the incorporation of the renewable monomers into the copolymer in up to 49 mol% was confirmed, which is the highest reported to date. The combination of a sustainable double bond functionalisation pathway with controlled radical polymerisations highlights the potential of radical polymerisations in the quest for renewable polymers and introduces a new set of monomers for this technique.

4.2. Introduction

Renewable monomers offer the possibility to reduce the environmental impact of polymers and will contribute to the shift towards a circular economy as set-out by the European Union in 2015.[4] However, polymers made from renewable resources represent less than 1% of the plastic production worldwide,[34,232] which stems from the higher production cost and their often inferior mechanical performances. Especially ring-opening,[233,234] acyclic diene metathesis[154,163,164,235–238] and polycondensation polymerisations[232] have been used for the synthesis of a variety of different renewable polymers,[37–39,117,232,239–241] while radical polymerisations have been largely confined to naturally occurring terpenes,[41,56,239,242] methylstyrenes,[243] and itaconic acid as outlined in Section 2.2.1.[69,74] Functionalising natural molecules, for example fatty acids,[166,244] with an acrylate moiety has been one way of extending the library of monomers for radical polymerisations (Scheme 18a and Section 2.2.2),[245–247] however only a few sustainable pathways for such double bond functionalisations exist.[40]

Recently, our group reported a sustainable approach to a double bond functionalisation via the allylation of alcohols using organic carbonates.[248–250] Both reagents used herein, dimethyl carbonate and allyl alcohol, can be renewably-sourced from methanol and CO_2[251,252] and through the deoxydehydration of glycerol,[171,253] respectively. In this simple base-catalysed transesterification reaction, the allylated alcohol is obtained in excellent yield for a variety of different alcohols. Since alcohol functional groups are very abundant in natural molecules (*e.g.* glycerol and glucose as prominent examples), a large number of novel allylic molecules can be synthesised sustainably, which are then available for radical polymerisations as will be demonstrated herein. However, up to now only few examples of free radical polymerisations of such allylic monomers exist (Scheme 18b),[50,254–258] as the direct polymerisation of such non-activated double bonds is still very challenging to achieve. This difficulty has been known since the 1940s and is a result of degradative chain transfer from the polymer to the monomer during the polymerisation: A stabilised allyl radical with an extremely low propagation rate is formed, which limits the polymerisation to low conversions.[50,259–262] Equally, olefinic double bonds of fatty acids have so far not been incorporated into polymers using radical polymerisations for similar reasons. Control over the radical species during the polymerisation is necessary to suppress the observed termination reactions and reversible deactivation radical polymerisations (RDRP) have proven to be an effective tool towards this means.[22] Additionally, these techniques allow for a precise control over the molecular weight and the composition as well as microstructure of the polymers, while both α- and ω-chain-end

functionalisation are feasible. Organometallic-mediated radical polymerisation (OMRP), especially ones using $Co(acac)_2$ as the controlling agent (also known as cobalt-mediated radical polymerisation (CMRP)), has been shown capable of polymerising a large variety of non-activated monomers at low temperatures and was thus very promising for these challenging non-activated monomers.[7,8,17,263–269]

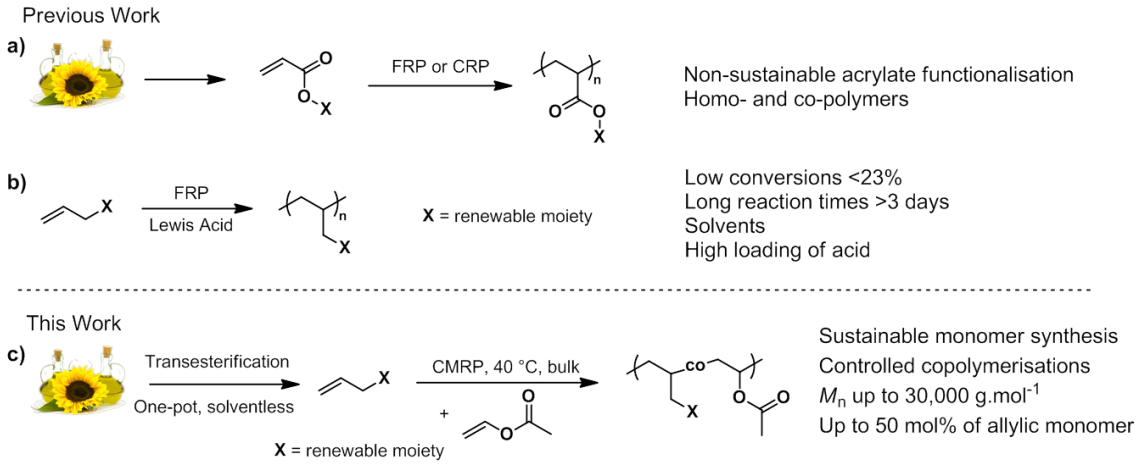

Scheme 18. a) Synthesis of acrylate monomers from renewable resources and their radical polymerisation,^{166,244}^{166,244}[166,244–246] b) polymerisation of allylic monomers using free radical polymerisation (FRP) in the presence of Lewis acids,[50,254–257] and c) the synthesis of renewable allylic monomers and their controlled copolymerisation with vinyl acetate using organometallic-mediated radical polymerisation (OMRP).

Herein, we report on the solventless, one-pot synthesis of two allylic cyclic carbonate monomers from glycerol, dimethyl carbonate and allyl alcohol and of one olefinic cyclic carbonate from glycerol, dimethyl carbonate and methyl-10-undecenoate. The inability to homopolymerise these monomers led us to investigate the copolymerisation with vinyl acetate, a very versatile monomer,[27,270–272] which can in principle also be synthesised sustainably from bioethylene and acetic acid.[273,274] For the first time, we show how such allylic and olefinic monomers can be radically copolymerised with vinyl acetate in a controlled manner using OMRP. High molecular weights were reached and an incorporation of up to 50 mol% of allylic monomers and up to 14 mol% of olefinic monomers was achieved (Scheme 18c). The ability to tune the molecular weights and also the amount of comonomer incorporated is demonstrated, while the control over the copolymer microstructure is highlighted. The controlled polymerisation of such challenging monomers in combination with their renewable synthesis is thus a powerful tool to access a whole series of novel functional and renewable polymers.

4.3. Synthesis of Plant Oil-Based Monomers

Inspired by the work of Meier *et al.*[248] and Cramail *et al.*,[159] we investigated a sustainable, solventless, atom-efficient one-pot synthesis to carbonates bearing a double bond using simple transesterification reactions catalysed by 1,5,7-triazabicyclo[4.4.0]dec-5-ene (TBD) (Scheme 19). Two synthetic routes can be employed for the synthesis of such cyclic carbonates containing a non-activated double bond: either a two-pot approach in which glycerol carbonate is isolated as an intermediate (Scheme 19b), or a one-pot approach in which glycerol is directly transformed into the desired monomers (Scheme 19a and c). In the scope of this chapter, we focused on three examples, allyl ((2-oxo-1,3-dioxolan-4-yl)methyl) carbonate (**M1**), 2-methylallyl ((2-oxo-1,3-dioxolan-4-yl)methyl) carbonate (**M2**)), and (2-oxo-1,3-dioxolan-4-yl)methyl undec-10-enoate (**M3**)). Contrary to the literature reagents, the substances used in this one-pot approach are renewable materials sourced from plant oils or CO_2.[154,171,251–253,275]

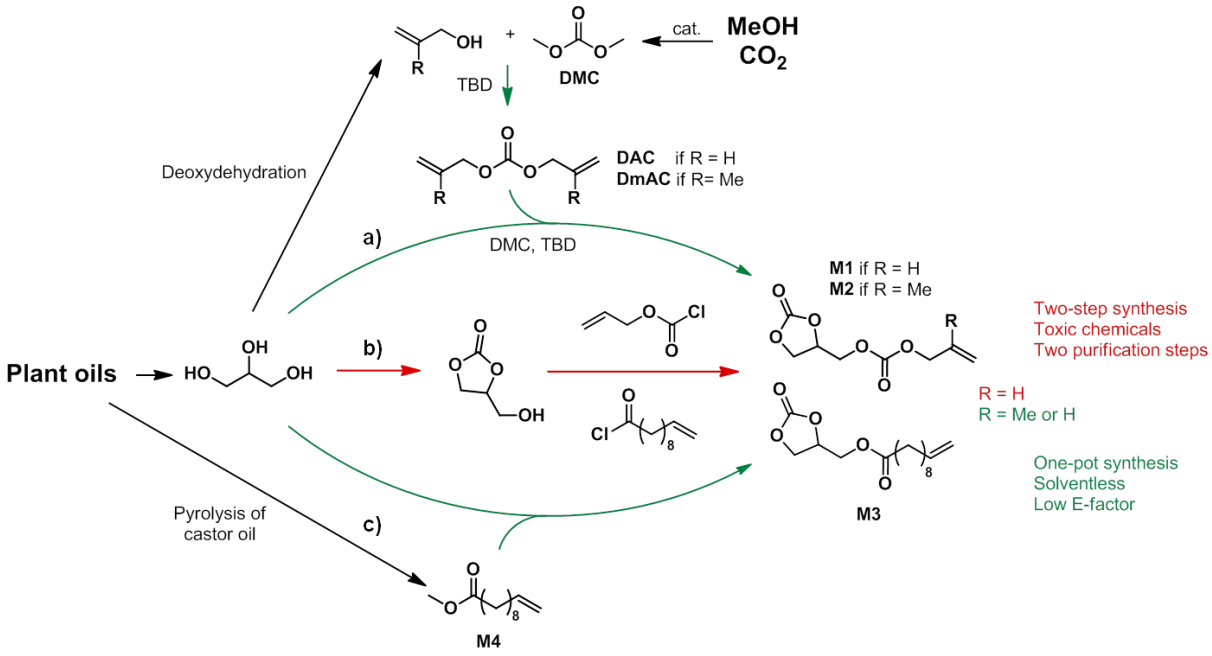

Scheme 19. a) and c) Synthesis of glycerol-based carbonate monomers (**M1**-**M3**) using a one-pot approach. b) Two-step literature procedures for the synthesis of the same monomers.[159,248,276,277]

The first one-pot synthesis we investigated involved the use of diallyl carbonate (DAC), used as an allylating agent and solvent, which was synthesised from allyl alcohol and dimethyl carbonate (DMC).[248] Using the same reaction conditions of the previously described synthesis of glycerol carbonate from glycerol and DMC as a starting point,[248] the reaction conditions

were screened in order to achieve the highest selectivity and yield of **M1**. It was found that the maximum conversion (79%) and selectivity (92%) were obtained at 80 °C and 1400 rpm stirring using 6 equivalents DAC, 1 equivalent DMC and 0.02 eq. TBD (Entry 7, Table 10). Unreacted glycerol carbonate, the intermediate formed *in-situ*, remained in the reaction mixture and had to be removed using column chromatography or extraction with water. It is worth mentioning that this side product can again be used in subsequent reactions and is, in general, a very useful intermediate.[158,278,279] The ease of synthesising different allylating carbonates allowed to attach a large number of differently substituted double bonds onto glycerol and was exemplified here using di(methylallyl) carbonate (DmAc). This particular DmAc allylating agent proved to be less efficient and **M2** could only be obtained in 40% conversion (Table 11) even at higher temperatures. The lower yield using this allylating agent was thought to originate from the higher boiling point of methylallyl alcohol compared to allyl alcohol (114 °C vs 97 °C), which led to a higher rate of evaporation for dimethyl carbonate, and thus lower yields. A similarly low yield was already observed for the preparation of di(methylallyl) alcohol (see Section 10.3).

In the second one-pot synthesis of cyclic carbonate monomers, methyl-10-undecenoate (**M4**), a fatty acid methyl ester obtained from ricinoleic acid,[153] was used. Since this plant oil derivative already contains a non-activated double bond, a slightly different approach was employed as only the formation and attachment of glycerol carbonate to the fatty acid methyl ester was necessary (Scheme 19c). Applying a vacuum ($<10^{-2}$ mbar) allowed to remove methanol liberated during the reaction and a high conversion of 72% was obtained with excellent selectivity (entry 3, Table 12). The purification of this monomer was more challenging, as a simple extraction was not possible since both **M3** and **M4** are soluble in the same solvents. Column chromatography was necessary to isolate the pure monomer which needs to be improved in order to improve the sustainability of this synthetic pathway. Yet it is worth highlighting that this transesterification approach avoids triethylamine and thionyl chloride, both toxic and harmful substances, which were used for the literature pathways.

In order to compare the synthetic approaches pursued in this chapter to existing synthetic pathways found in the literature in terms of sustainability, the environmental factor (E-factor) was calculated. The E-factor gives an appreciation of the amount of waste generated for the amount of product obtained (Equation 1).[280,281] Akin to other methods comparing the sustainability of processes, *e.g.* life cycle assessment, boundary conditions need to be chosen to allow for a fair and correct comparison. Thus the synthetic pathways from the literature and those performed in this work (Scheme 19) were compared starting from commercial

molecules, namely glycerol, allyl alcohol, dimethyl carbonate, ethylene carbonate and 10-undecenoic acid. Additionally, the use of energy, *e.g.* in the form of vacuum or heating, is not quantified for any of the pathways as its effect on waste generation strongly depends on the local electricity mix and should become an insignificant factor in the future, once all energy is sustainably sourced. In contrast to the E-Factor, such considerations are also very error prone for small scale preliminary investigations. A detailed description of the E-factor calculation for **M1** is presented hereafter while the calculations for the other monomers can be found in Chapter 10.3 (Figure 38 to Figure 83).

Equation 1 $$\mathrm{E-factor} = \frac{g\ waste}{g\ product} = \frac{g\ reagents - g\ product}{g\ product}$$

For the synthesis pathway of **M1** used in this thesis, two reactions need to be considered (Figure 38): the synthesis of the allylating agent (DAC) and the reaction transforming glycerol into **M1**. For the preparation of DAC (Figure 38a), an E-factor of 2.06 was obtained by dividing the weight of reactants and catalysts used without the weight of product (70 + 94.8 + 1.082 – 54.1) by the amount of obtained product (54.1). The purification by distillation does not make use of any additional chemicals and hence it does not have an effect on the E-factor. The E-factor could be reduced by increasing the low yield of the reaction (61%) or by recovering unreacted DMC and allyl alcohol. The E-factor for the second step of the reaction was calculated as above (Figure 38b). This one-pot preparation of **M1** from glycerol gives an E-factor of 13.74 through the simple addition of the E-factors of the first, 2.06, and second step, 11.68. However, the synthetic pathway reported in the literature (Figure 80) does not provide the exact quantities used for the purification,[277] hence only a fair comparison of the E-factors without purification can be made. This comparison clearly highlights the benefits of the synthetic pathway of **M1** presented in this work, as the E-factor (2.7) constituted a 7-fold improvement compared to the state-of-the-art synthesis (14.26, Figure 80), which is a direct reflection of the absence of any solvent and the ability to recover 60% of unreacted DAC reagent. The synthesis of **M2** had not been previously performed in the literature, so no comparison to existing values can be made. Nonetheless, the E-factor (20.77) was significantly higher compared to the synthesis of **M1** (13.74) which was a result of the much lower yield obtained during both the preparation of the allylating agent (DmAC) and **M2** from glycerol. The synthesis of **M3** suffers from the need for column chromatography, as the starting reactant **M4** and **M3** are soluble in the same solvents, which led to a very high E-factor of 27.5 (Figure 83). This constituted a three-fold increase of the E-factor compared to

the literature procedure (E-factor of 9.63; Figure 82) but the preparation of this monomer on a large scale as well as further optimisation will certainly allow for a different kind of purification to be implemented and thus lead to a reduction of the E-factor.

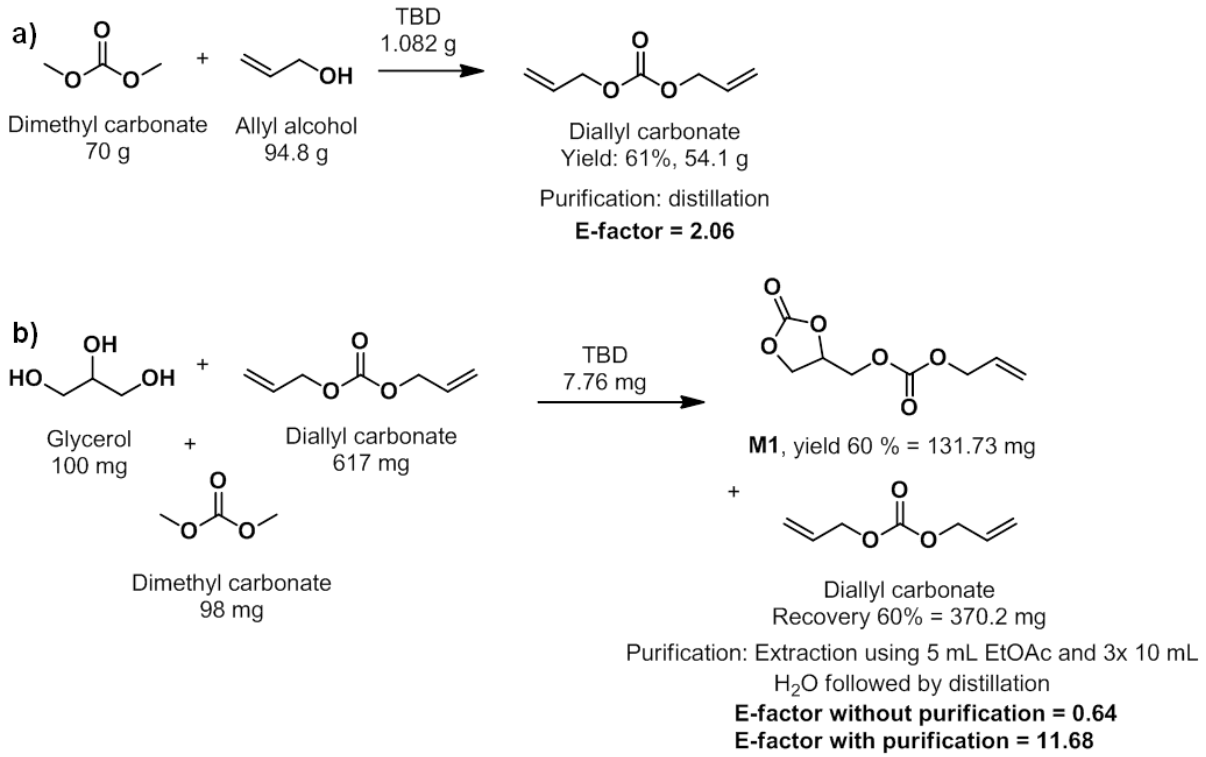

Figure 38. E-factor calculation for a) diallyl carbonate (DAC) synthesis and b) the subsequent synthesis of **M1** used in this work

In summary, three molecules bearing non-activated double bonds were synthesised from dimethyl carbonate, glycerol and allyl alcohol or a fatty acid methyl ester, in a high-yielding one-pot synthesis. Yet, the suitability of such molecules bearing non-activated double bonds for monomers in radical polymerisations needed to be investigated in detail as these double bonds remain a big challenge to polymerise.

4.4. (Co)Polymerisations of Renewable Monomers

Along with the above-mentioned monomers, two other monomers, methyl-10-undecenoate (**M4**) and allylmethyl carbonate (**M5**), were also synthesised and investigated as monomers for radical polymerisations (Scheme 20). **M4** is a reagent for the synthesis mentioned above, while **M5** can be easily synthesised from DMC and allyl alcohol.[248] As detailed in the introduction, free radical polymerisations of allylic molecules require Lewis acid additives and were inhibited at low conversions. Our first investigation was thus the

homopolymerisation of these five monomers using 2,2'-azobis(4-methoxy-2,4-dimethylvaleronitrile, V-70) as the initiator at 40 °C, at a concentration of 3 mg/mL in DMC (Table 13). In line with previous literature reports, no homopolymers were obtained.[282–284] Next, the feasibility of copolymerising the above mentioned renewable monomers with vinyl acetate was investigated using V-70 at 40 °C in the bulk and targeting a 10 mol% feed of renewable monomer (entries 6-9, Table 13). For each copolymerisation, an increase in molecular weights was observed and conversions above 23% were obtained (Table 13). In the case of **M1**, the formation of a gel after 4 hours hinted at an uncontrolled side reaction, *e.g.* hydrogen abstraction,[285] which resulted in a crosslinked polymer, as it has been reported for cyclic carbonate bearing monomers.[286,287] Using controlled radical polymerisations, in which the chains grow in a controlled fashion, would possibly allow to suppress such side reactions and thus allow for a controlled copolymer microstructure to be obtained. Encouraged by the above findings, we investigated the cobalt-mediated radical polymerisations of these monomers with vinyl acetate (Scheme 20).

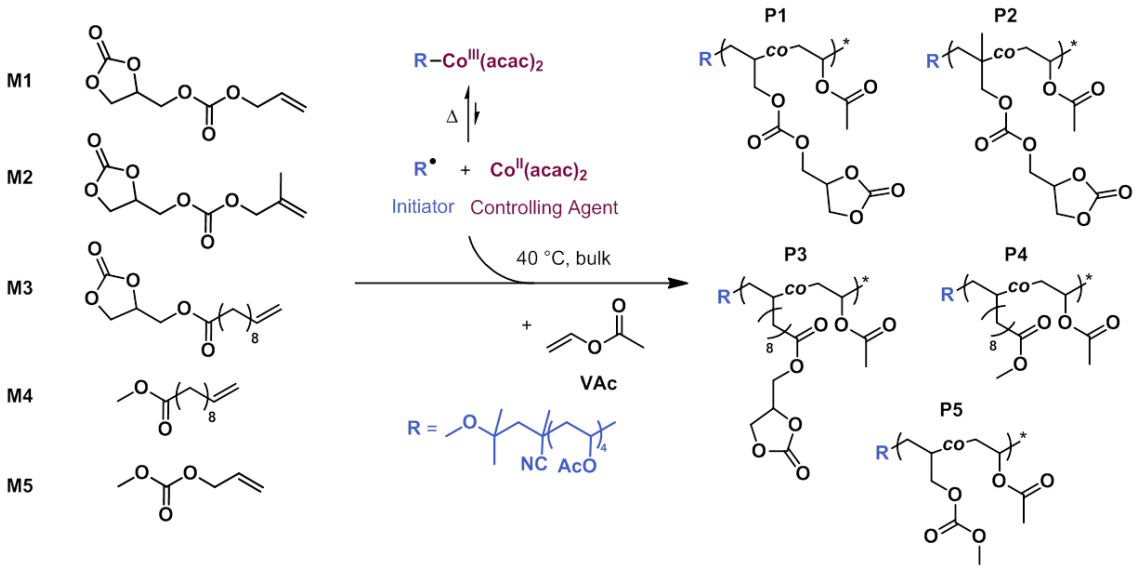

Scheme 20. Cobalt-mediated radical polymerisation of five renewable monomers (**M1**-**M5**) with vinyl acetate and the structures of the resulting statistical copolymers (**P1**-**P5**)

The copolymerisations of the renewable monomers with vinyl acetate (VAc) were investigated using a preformed alkylcobalt(III) acetylacetonate (R-Co(acac)$_2$) complex, where the alkyl group acts as a radical initiator and the Co(acac)$_2$ as the controlling agent (Scheme 20).[30] Using a feed of 10 mol% of renewable monomer, and targeting a degree of polymerisation of 400 at 40 °C in the bulk, controlled copolymerisations of all five non-activated monomers were observed, as witnessed by the linear increase of molecular weights

with conversion while maintaining low dispersities (entries 1, 3, 4, 6, and 9, Table 14 and Figure 39, Figure 84-Figure 87). As an example, the copolymerisation of **M1** with vinyl acetate attained molecular weights of 37,100 g mol^{-1} with a dispersity of 1.41 (entry 1, Table 14) and a progressive shift of molecular weights with little tailing was observed by SEC (Figure 39b). The linear pseudo-first order kinetic plot (Figure 39c) highlighted the good control over the polymerisation up until 35 % conversion, after which an increase in the rate of copolymerisation was observed as well as slightly higher dispersities, which hints at a loss of control. A similar behaviour was observed for **M5** (Figure 87). Further copolymerisations were performed at a feed of 50 mol% renewable monomer and while the molecular weights still evolved linearly with conversion for **M1** and **M5**, the rate of polymerisation decreased (entries 1 and 10, Table 14).

For **M4**, copolymerisations were inhibited at low conversions at 50 mol% feeds (entry 8, Table 14), the origin of which is still unknown. Yet, both **M3** and **M4** were successfully copolymerised at a lower feed of 27 mol% (entries 5 and 7, Table 14). For both 11 and 27 mol% feeds, slightly higher dispersities and low molecular weight tailing were observed for conversions above 35 % (Figure 85 and Figure 86). The copolymerisation results above present our initial findings and a complete understanding of the kinetic copolymerisation behaviour is not provided, as this chapter aims to introduce a new class of (renewable) monomers for radical polymerisations and to show the overall sustainability of the process. Further experiments, such as polymerisations to determine the reactivity ratios, are needed to fully understand the observed behaviour. These experiments were not performed because of a lack of time.

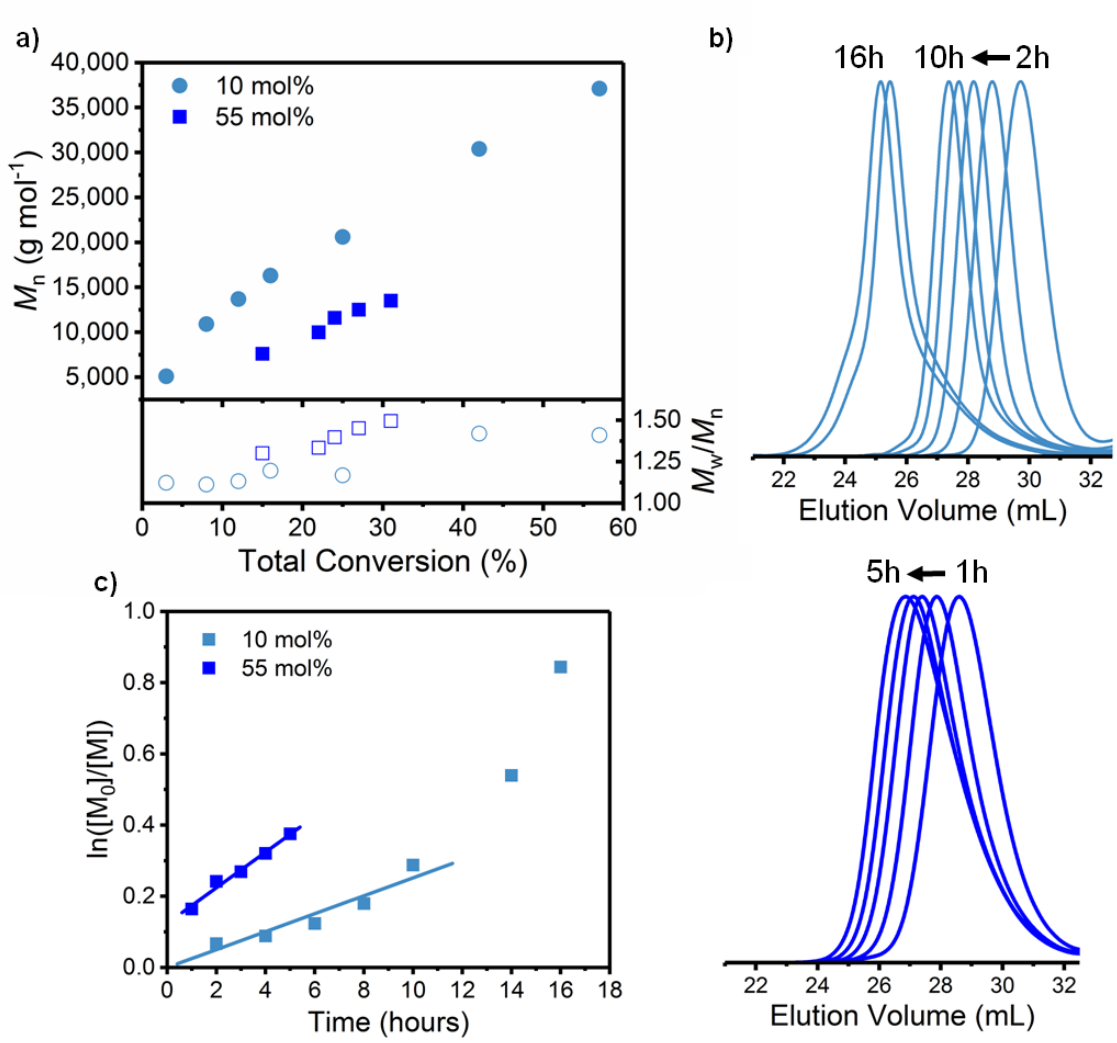

Figure 39. OMRP at 40 °C of **M1** and VAc: a) M_n and dispersity versus total monomer conversion plot, b) size-exclusion traces for **M1** feeds of 11 and 55 mol%, and c) first-order kinetic logarithm plot with linear fits.

A major challenge after the polymerisation is the efficient and sustainable purification of the obtained polymers without the use of large amounts of solvents, as is usually necessary for precipitations or dialyses. For the copolymers prepared in this study, an extraction using supercritical CO_2 ($scCO_2$) was performed (see Section 10.3). In a CO_2 reactor (Figure 88), 250-350 mL of supercritical CO_2 were used as a green and sustainable solvent to extract the unreacted monomers and obtain a white powder of pure polymer. The advantage of this procedure is that i) CO_2 is used as a benign and green solvent, which can be recycled from extraction to extraction and ii) the unreacted monomers with high boiling points, *i.e.* **M1-M4**, were recovered in up to 58 wt% (Table 15) and could be reused in subsequent polymerisations (Figure 40). Not all of the unused monomer was recovered, as some was lost during venting, which could be avoided if the process is further optimised, for example by cooling the collection cell.

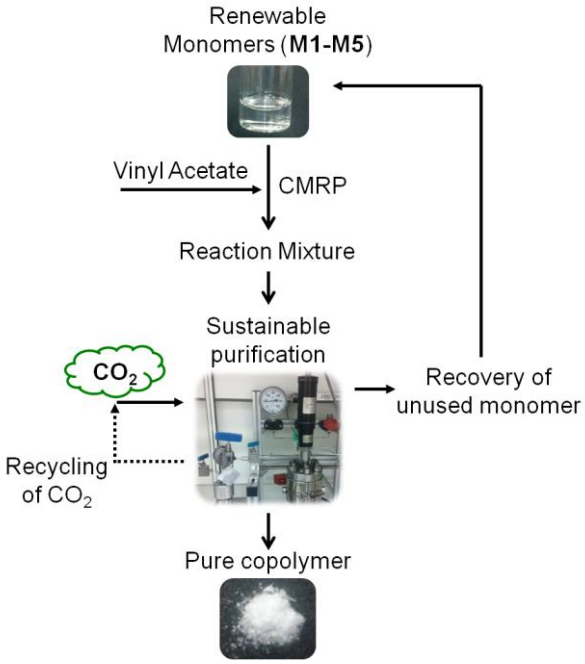

Figure 40. Flowchart of the polymerisation and $scCO_2$ extraction procedure presented in this work, including the recovery of unused monomer and the recycling of CO_2. The latter is not performed in this work.

Furthermore, it could be shown using ICP-OE measurements that up to 96% of the cobalt was removed from the copolymers after the purification procedure, for example a **P1** copolymer containing 11 mol% **M1** (entry 1, Table 14) contained 123 ppm cobalt after purification compared to an initial content of 3467 ppm. Once the copolymers were purified using this sustainable purification technique, their structure was analysed using NMR and FT-IR spectroscopy. Figure 41 shows the ^{1}H-NMR spectra of **P1** and **P4** after purification (entry 1, Table 14 and entry 7, Table 1).

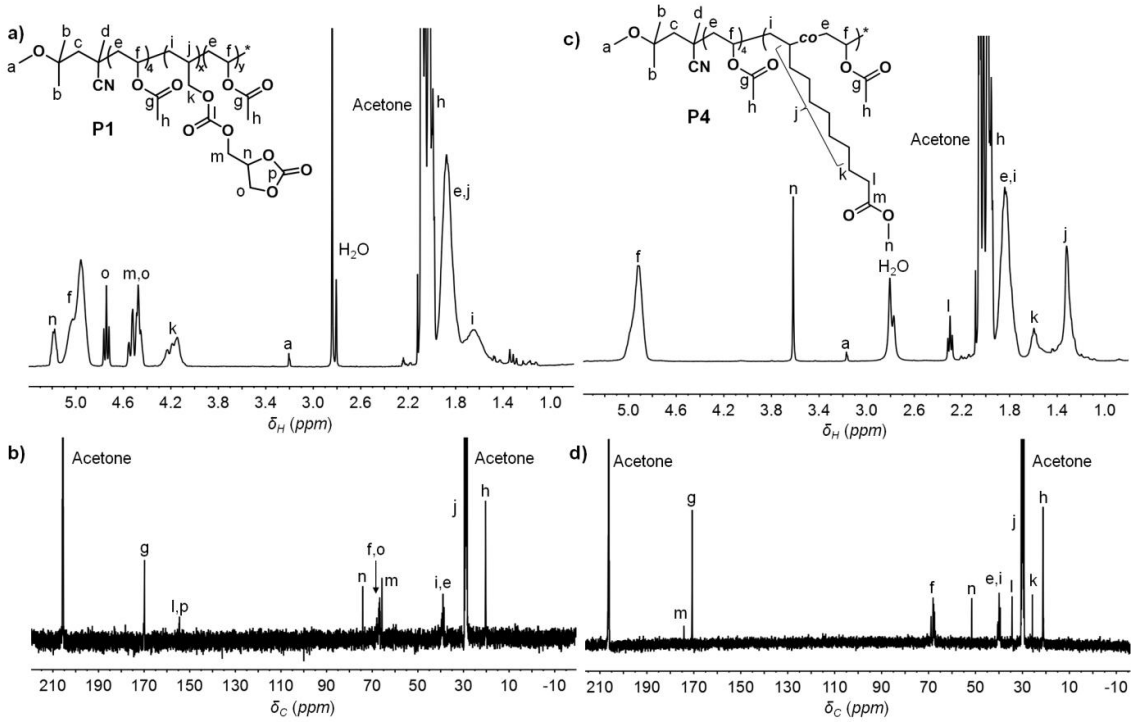

Figure 41. a) ^{1}H-NMR and b) ^{13}C-NMR spectrum of **P1** at 57% conversion containing 11 mol% **M1** (entry 1, Table 14) and c) ^{1}H-NMR and d) ^{13}C-NMR spectrum of **P4** at 47% conversion containing 5 mol% **M4** (entry 7, Table 1). NMR spectra taken in Acetone-d_6 on a 400 MHz spectrometer.

In both cases, the α-chain end of the copolymers at 3.20 ppm (**a**, $\underline{H_3}$C–O– at 3.20 ppm) and the –C$\underline{H}$–O–(C=O)– of the vinyl acetate repeat unit at 5.00 ppm (**f**, –C$\underline{H}$–O–(C=O)– at 5.00 ppm) were clearly identified (Figure 41a and c). The other two characteristic peaks of vinyl acetate corresponding to the –C$\underline{H_3}$ and –C$\underline{H_2}$– groups were observed at 2.02 ppm and 1.87 ppm, respectively (**h**, –C$\underline{H_3}$ at 2.02 ppm; **e**, –C$\underline{H_2}$– at 1.87 ppm). The incorporation of **M1** into the **P1** copolymer was confirmed by four characteristic peaks at 5.15 ppm, 4.70 ppm, 4.47 ppm and 4.15 ppm pertaining to the proton environments in or next to the carbonate ring (**n**, –O–CH$_2$–C$\underline{H}$–(CH$_2$–O(C=O)O) at 5.15 ppm; **o**, –O–CH$_2$–CH–(C$\underline{H_2}$–O(C=O)O) at 4.70 and 4.47 ppm; **m**, –O–C$\underline{H_2}$–CH–(CH$_2$–O(C=O)O) at 4.47 ppm; **k**, –O–C$\underline{H_2}$–CH–(CH$_2$–O(C=O)O) at 4.15 ppm; Figure 41a). A further broad peak at 1.60 ppm was assigned to protons **i**, while environment **j** at 1.84 ppm could only be assigned using an HSQC spectrum (**i**, –C$\underline{H_2}$–CH–CH$_2$–O– at 1.60 ppm; **j**, –CH$_2$–C$\underline{H}$–CH$_2$–O– at 1.84 ppm; Figure 90). In the ^{13}C-NMR spectrum (Figure 41b), the carbonyl peaks for vinyl acetate, **g**, and **M1**, **l** and **p**, were observed at 170.76 ppm and 155.68 ppm, respectively (**g**, –CH–O(C=O)–CH$_3$ at 170.76 ppm; **l**, –CH$_2$–O–C(C=O)O–CH$_2$– at 155.68 ppm; **p**, –O–CH$_2$–CH–(CH$_2$–O(C=O)O) at 155.68 ppm). For copolymer **P4**, an intense peak at 3.65 ppm was attributed to the **M4** repeat unit (**n**, $\underline{H_3}$C–O(C=O)CH$_2$– at 3.65 ppm), while two other characteristic peaks at 2.33 ppm and 1.35

ppm were assigned to the –C$\underline{H_2}$ adjacent to the ester group and the aliphatic –C$\underline{H}$–/–C$\underline{H_2}$– in the **M4** repeat unit, respectively (**l**, –CH_2 –C$\underline{H_2}$–C(=O)O– at 2.33 ppm; **j**, –C$\underline{H}$–/–C$\underline{H_2}$– at 1.35 ppm; Figure 41c). Two further peaks could only be assigned using COSY and HSQC analyses (**i**, –C$\underline{H_2}$– C$\underline{H}$– at 1.82 ppm; **k**, –C$\underline{H_2}$ –CH_2–C(=O)O–CH_3 at 1.59 ppm; Figure 95 and Figure 96).The ^{13}C-NMR spectrum (Figure 41d) confirmed the copolymer structure with a vinyl acetate carbonyl peak at 171.68 ppm, while the ester of the comonomer was observed at 174.21 ppm (**g**, –CH–O(C=O)–CH_3 at 171.68 ppm; **n**, –CH_2 –CH_2–C(=O)OCH_3 at 174.21 ppm). For both copolymers, several peaks were observed around 67 ppm, which belong to the VAc repeat unit (**f**, –CH_2–CH–O(C=O)–CH_3 at 67 ppm) and were a clear indication that the VAc repeat units were distributed statistically throughout the polymer chain. The same was true for the signal around 40 ppm, which belongs to the –C$\underline{H_2}$–CH–O(C=O)–CH_3 of the VAc and the –C$\underline{H_2}$–CH–CH_2– of the comonomer. In the FT-IR spectrum, an additional vibration at 1800 cm^{-1} of the cyclic carbonate carbonyl was observed for copolymer **P1**, while the ester vibration of **P4** overlapped with that of the acetate signal (Figure 99). The statistical incorporation into VAc copolymers of the other three renewable monomers, **M2**, **M3** and **M5**, was also confirmed using NMR spectroscopy and FT-IR analysis (Figure 91-Figure 94 and Figure 97-Figure 99).

Once the copolymer structures were clearly known, the copolymer compositions were determined by comparing the characteristic peaks of the vinyl acetate repeat unit with those of the renewable comonomers (see Section 10.3 for details). For **M1**, **M2** and **M5** the copolymer composition closely resembled the initial polymerisation feed (entries 2-4 and entries 10-11, Table 1). For example, increasing the **M1** feed from 10 to 50 mol% for a **M1**/VAc copolymerisation, it was observed that the final copolymer was also richer in allylic monomer, 15 versus 45 mol% respectively (entries 2 and 3, Table 1), which is the highest incorporation of allylic monomers to date. The same was not observed for **M3** and **M4**, as in both cases at 10 mol% and 25 mol% renewable comonomer feed, less comonomer was incorporated, 5 mol% and 14 mol%, respectively (entries 5-9, Table 1). It is worth pointing out that the theoretical molecular weight ($M_{n\ theo}$) and the molecular weights determined by NMR end group analysis ($M_{n\ NMR}$) were in good agreement with each other, which further highlights an excellent control over the copolymerisation of these two less-activated monomers.

Table 1. Copolymerisations of VAc and renewable monomers (**M1**-**M5**) using R-Co(acac)$_2$ at 40 °C[a]

Entry	Comon. (f^0_{Comon})[b]	t (h)	Total conv (%)[b]	Composition (F_{VAc}/ F_{Comon}) (%)[c]	$M_{n\ theo}$ (g mol^{-1})[d]	$M_{n\ NMR}$ (g mol^{-1})[c]	$M_{n\ SEC}$ (g mol^{-1})[e]	M_w/M_n[e]
1	-	10	35	1/0	12,700	8,900	16,200	1.09
2	**M1** (0.1)	10	22	85/15	9,400	14,300	12,100	1.18
3	**M1** (0.55)	5	31	51/49	18,100	13,000	13,500	1.50
4	**M2** (0.12)	10	31	86/14	13,700	10,300	14,000	1.17
5	**M3** (0.12)	10	36	93/7	13,900	9,800	12,300	1.34
6	**M3** (0.28)	10	21	87/13	9,300	10,200	10,800	1.18
7	**M4** (0.1)	10	47	94/6	18,000	21,800	20,800	1.62
8	**M4** (0.27)	8	21	89/11	8,700	11,300	10,100	1.20
9	**M4** (0.5)	10	17	76/24	9,400	11,900	7,200	1.39
10	**M5** (0.12)	10	33	87/13	12,700	9,900	12,300	1.14
11	**M5** (0.53)	10	18	52/48	7,700	9,100	6,500	1.18

[a] Conditions: bulk, M/R-Co(acac)$_2$ = 400/1, magnetic stirring at 500 rpm. Full kinetics are in Table 14. [b] Determined by ^{1}H-NMR spectroscopy in acetone-d_6 (see Section 10.3). [c] Composition of the copolymer and molecular weight determined by ^{1}H NMR spectroscopy in acetone-d_6 based on the α-chain end (see Section 10.3). [d] $M_{n\ theo} = M_{w\ init} + (Conv_{Comon} \times M_{w\ Comon} + Conv_{VAc} \times M_{w\ VAc}) + M_{w\ TEMPO}$ (for more information see Section 10.3). [e] Determined by size exclusion chromatography (SEC) in DMF/LiBr using a PS standard.

At this stage, a series of well-defined renewable copolymers with different compositions were available and were tested for their thermal properties using differential scanning calorimetry (DSC) and thermogravimetric analysis (TGA). For all copolymers, only one glass transition temperature (T_g) was observed (Figure 42a), which underlines the statistical incorporation of the two monomers. Increasing the **M1** content from 11 to 49 mol% led to the slight increase of the T_g from 51 to 60 °C (entries 2-3, Figure 42). For the fatty acid derived copolymer **P4**, the comonomer content had no effect on the T_g (entries 7-8, Figure 42), while a decrease in T_g from 24 °C to 14 °C was observed for copolymer **P3** (entries 5-6, Figure 42). A similar

decrease was observed for an increasing incorporation of **M5**, 35 °C to 20 °C for 13 mol% and 48 mol%, respectively (entries 9-10, Figure 42). All copolymers with a low renewable monomer content (6-15 mol%) displayed a thermal decomposition in two stages, which is typical of poly(vinyl acetate) (PVAc)[288] (Figure 42b) and the temperature at 5% weight loss ($T_{d\ 5\%}$) determined by TGA analysis remained relatively close to PVAc homopolymer value of 294 °C for these copolymers. Interestingly, the $T_{d\ 5\%}$ strongly decreased for an increasing incorporation of **M1** (314 °C vs. 256 °C) compared to the VAc homopolymer (entries 1-3, Figure 42), while comparing the 13 mol% **P5** copolymer with the 48 mol% one, only slight decrease by 22 °C in $T_{d\ 5\%}$ was observed (entries 9-10, Figure 42). The lower thermal stability of **P1** at a high comonomer content was clearly visible in the TGA curve (Figure 100a) and the derivative weight versus temperature plot (Figure 100b) suggested that a change in the decomposition mechanism occurred. The exact nature of this change is not known, but seems to be linked to the pendant cyclic carbonate groups. Further investigation would be required to understand this loss of thermal stability.

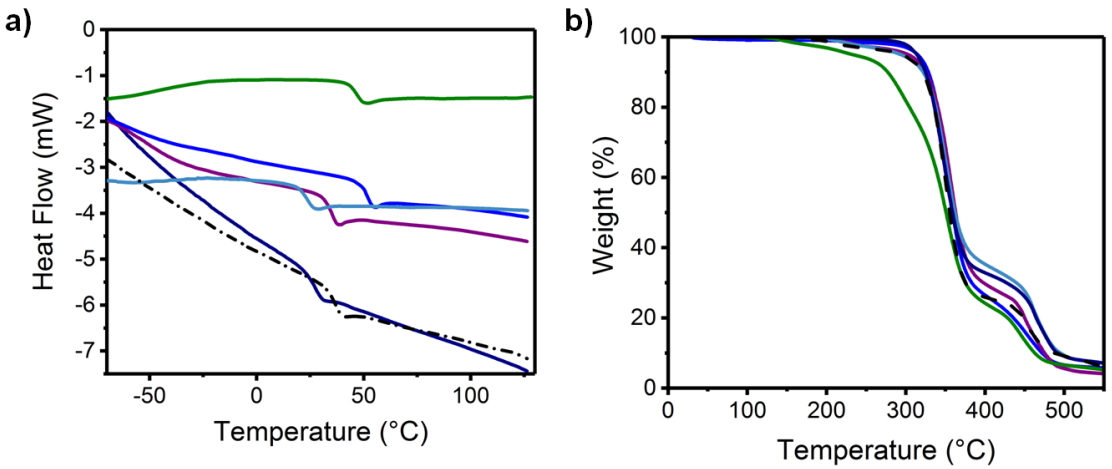

c)

Entry	Colour code	Copolymer	Comonomer content (mol%)	Conv. (%)	$M_{n,\,NMR}$ (g.mol^{-1})	T_g (°C)	$T_{d\ 5\%}$ (°C)
1	– · –	-	-	35	8,900	37	294
2	—	P1	11	57	25,300	51	314
3	-	P1	49	31	13,000	60	256
4	—	P2	14	31	10,300	32	232
5	—	P3	7	36	9,800	24	293
6	-	P3	13	21	10,200	14	284
7	—	P4	6	47	25,700	27	313
8	-	P4	15	24	10,600	27	309
9	—	P5	13	33	9,900	35	303
10	-	P5	48	18	9,100	20	281

Figure 42. a) Differential scanning calorimetry (DSC) curves and b) thermal gravimetric analysis (TGA) curves for poly(vinyl acetate) and its copolymers with different renewable monomers at low monomer content, and c) a table summarising the different thermal properties of all prepared copolymers.

4.5. Conclusion

The sustainable allylation of alcohols was exploited in a novel one-pot, solventless approach allowing to extend the current state-of-the-art synthesis pathways of monomers for radical polymerisations. We highlight the potential of such sustainable transesterification reactions with five different renewable monomers and show that these challenging non-activated monomers can be successfully copolymerised with vinyl acetate using both free radical and controlled radical polymerisations, which was up to date unknown. Using organometallic-mediated radical polymerisation at 40 °C and in bulk, a controlled increase of molecular weights with conversion and low dispersities were observed, while an incorporation of up to 49 mol% of the allylic monomer was feasible. Equally, olefinic monomers derived from a fatty acid methyl ester were successfully copolymerised and incorporated in up to 14 mol% into the copolymer. The copolymers were characterised in-depth by NMR, FT-IR and thermal measurements and a well-defined microstructure of the statistical copolymers was confirmed. The combination of a renewable synthesis pathway with the ability of copolymerising allylic and olefinic double bonds is a powerful method for the quest of functional copolymers from renewable resources and opens a completely new series of renewable monomers for radical polymerisations. Importantly, the monomers were not only prepared in a sustainable fashion, but the resulting polymers were also purified in such a way. Finally, the prepared copolymers with cyclic carbonate structure should allow applications in the sustainable synthesis of non-isocyanate polyurethanes (NIPUs),[289,290] thus also allowing applications with improved sustainability.

5 CO_2-Based Building Blocks as Monomers for the Synthesis of Functional Poly(Vinyl Alcohol)

This chapter and the corresponding parts in the experimental section are reprinted with permission from:

Philip B. V. Scholten,[1] Jérémy Demarteau, Sandro Gennen, Julien De Winter, Bruno Grignard, Antoine Debuigne, Michael A. R. Meier, and Christophe Detrembleur

Macromolecules, 2018, 51 (9), 3379–3393

DOI: 10.1021/acs.macromol.8b00492

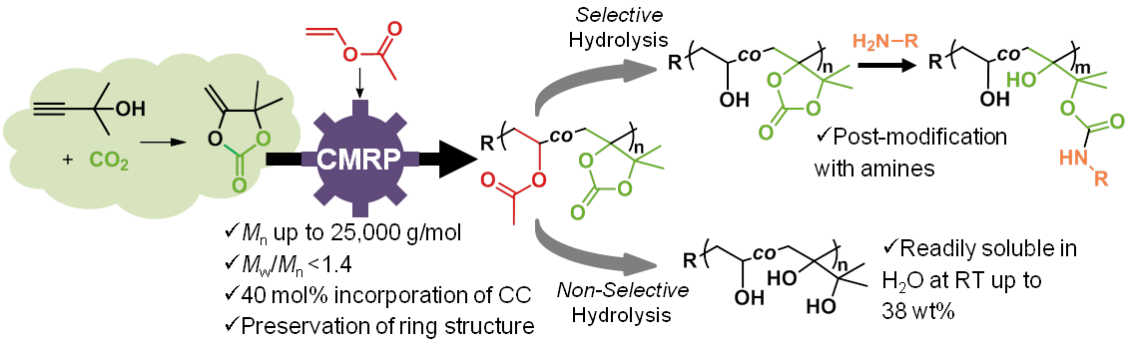

[1] P.B.V.S. performed all experiments presented in this chapter. J.D. and S.G. provided help/guidance for the synthesis of the controlling agent (R-Co(acac)$_2$) and the synthesis of the monomer, respectively. J.D.W. performed the MALDI-TOF analysis while B.G. provided help with the determination of the copolymer structure and the hydrolysis reactions. A.D. assisted P.B.V.S in the determination of the reactivity ratios.

5.1. Abstract

The use of CO_2-based α-alkylidene cyclic carbonates in controlled radical polymerisation has so far not been exploited, despite the fact that the cyclic carbonate ring offers a multitude of possible modifications. Herein, the synthesis of well-defined copolymers of vinyl acetate (VAc) and 4,4-dimethyl-5-methylene-1,3-dioxolan-2-one (**DMMDO**) using organometallic-mediated radical polymerisation (OMRP) at 40 °C is reported. Specifically the cobalt complex $Co(acac)_2$ was used as the controlling agent and this type of polymerisation is also known as cobalt-mediated radical polymerisation (CMRP). The controlled nature of the polymerisation was confirmed while molecular weights of up to 25,000 g mol^{-1} and narrow dispersities (< 1.4) were obtained. The copolymer structure was elucidated combining NMR, FT-IR and MALDI-TOF analyses and consists of a polymer backbone with pendant carbonate rings. Further insights into the copolymer structure were gained through the monomers' reactivity ratios and a homogeneous distribution of the **DMMDO** monomer along the polymer chain was observed. A highly water soluble poly(vinyl alcohol)-based copolymer was obtained by basic hydrolysis, whereas the chemo-selective acidic hydrolysis of the acetate groups left the cyclic carbonate rings untouched, which were then exploited for further post-polymerisation modification with amines. The precise copolymerisation of VAc with CO_2-sourced five-membered cyclic carbonates bearing an exomethylene moiety is therefore a powerful tool for the synthesis of new variants of poly(vinyl alcohol)-based copolymers.

5.2. Introduction

CO_2 is a very versatile and powerful C1-synthon, which has been extensively used in recent years in light of the valorisation of renewable resources. Five-membered cyclic carbonates (CCs) have emerged as one of the most widely investigated CO_2-based molecules[291–299] as they are known for their broad reactivity and have found numerous recent applications, such as precursors to chiral building blocks[300–303] and monomers for non-isocyanate polyurethanes (NIPUs)[236,304–307] to only cite a few.

Recently, the (organo)catalysed synthesis of a library of α-alkylidene cyclic carbonates (αCCs, Scheme 21) from propargylic alcohols and CO_2 was reported in several manuscripts.[308–312] These αCCs differ from conventional five-membered cyclic carbonates by the presence of an exomethylene moiety, and therefore combine two very useful functional groups: an activated cyclic carbonate and a vinyl group. The activated cyclic carbonate ring was shown to be easily opened by nucleophiles,[306] and this reactivity was recently exploited in polymer chemistry for the facile synthesis of functional regioregular polycarbonates and polyurethanes by polyaddition of *bis*(α-alkylidene cyclic carbonate)s with diols and secondary/primary diamines, respectively.[306] The vinyl group, on the other hand, is prone to radical attack and can therefore be involved in radical (co)polymerisations. Amongst all αCCs that were accessible, 4,4-dimethyl-5-methylene-1,3-dioxolan-2-one (**DMMDO**, Scheme 22) was highly attractive as it can be easily produced by organocatalysed coupling of CO_2 to 2-methyl-3-butyn-2-ol.[311] Nevertheless, the large steric hindrance induced by the two methyl groups at the 4-position rendered its homopolymerisation impossible at 60 °C.[313,314] The homopolymerisation was only possible above 120°C, however with the formation of oligomers (M_n = 2,100 g mol^{-1}) consisting of an alternating structure of cyclic carbonate and ketone units. These two structures originated from the occurrence of two different radical polymerisation pathways: a radical ring-opening (rROP) polymerisation followed by decarboxylation that provided the polyketones (route a) and a vinyl-type polymerisation that resulted in polymers bearing pendant cyclic carbonates (route b) (Scheme 21).[314] The free radical copolymerisation of **DMMDO** with vinyl acetate (VAc) was reported to be possible at lower temperature (70 °C) *via* the vinyl-type polymerisation.[313] The absence of rROP was assumed to be the result of the lower copolymerisation temperature.

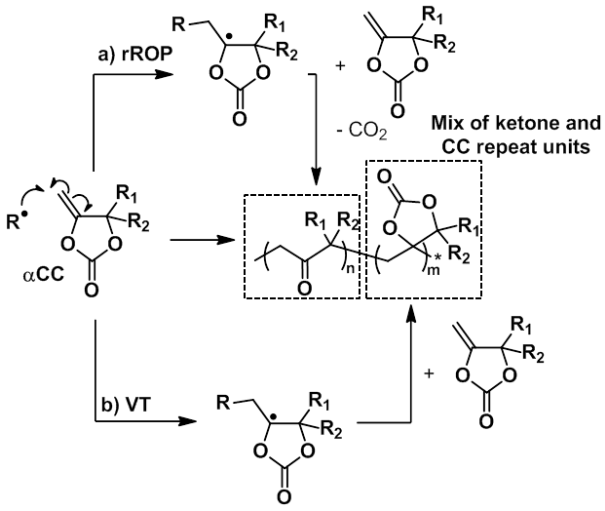

Scheme 21. Radical polymerisation of αCCs and the reported occurrence of two polymerisation mechanisms: a) radical ring-opening polymerisation (rROP) and b) vinyl-type polymerisation (VT).

Polymers bearing pendant cyclic carbonate groups, prepared by radical (co)polymerisation of αCCs, are attractive because they do not present any hydrolysable group between the polymer backbone and the CC ring, which is highly desirable for selective post-polymerisation modifications. The development of a controlled radical polymerisation technique for αCCs that would disfavour rROP is thus needed for the precise synthesis of novel functional polymers. Only a few studies reported on the controlled radical polymerisation of vinyl monomers bearing cyclic carbonates.[315,316] However, these works considered acrylate-type monomers that bear an ester function between the polymer backbone and the CC ring. Selective post-polymerisation modifications of the CC rings were therefore challenging on those polymers because side reactions (such as hydrolysis or amidification) were expected to occur on the ester groups, prohibiting the production of the desired polymer.

In this work, we considered the copolymerisation of **DMMDO** with VAc in order to provide novel well-defined poly(vinyl alcohol)-type (PVOH-type) copolymers by selective or complete hydrolysis of the P(VAc-*co*-**DMMDO**) precursor (Scheme 22). Indeed, PVOH is one of the most important industrial water-soluble synthetic polymers and the key ingredient in formulations of various products in food packaging, construction, electronics, coatings, printing, textile, cosmetics, and paper.[317–319] PVOH is commonly produced by methanolysis of poly(vinyl acetate) (PVAc) and the worldwide production capacity was estimated at 650 kT in 2015.[317] The precise localisation of CC groups along its polymer chain would bring new possibilities for further simple functionalisation and open new applications for this important polymer. This paper therefore describes the first controlled radical copolymerisation of this

CO_2-sourced monomer with VAc under experimental conditions that disfavour rROP. The reactivity ratios were determined in order to evaluate the distribution of the comonomers in the polymer, and the structure of the copolymer was thoroughly investigated. The conditions for the complete hydrolysis of the copolymer were then established to give a PVOH of high water solubility. The chemo-selective hydrolysis of the VAc units to provide PVOH bearing intact cyclic carbonate pendants was also investigated as well as its further post-polymerisation modification *via* the ring opening of the carbonate ring with butylamine. In contrast to classical PVOH-functionalisation methods relying on the transformation of the pendant hydroxyl groups,[320] our post-polymerisation modification strategy affords the advantage of preserving one hydroxyl group per repeat unit (Scheme 22).

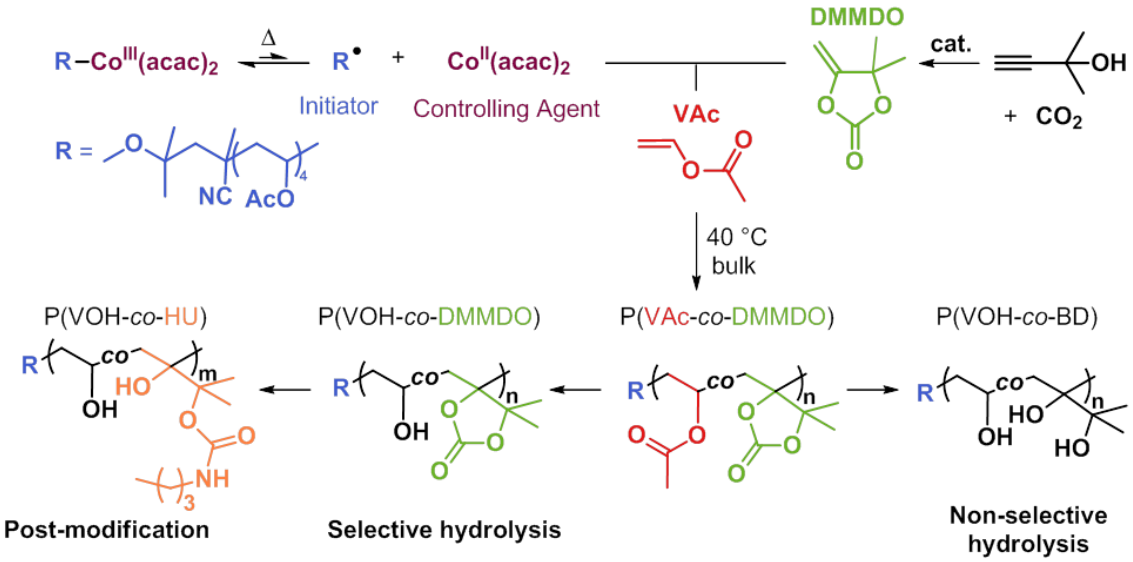

Scheme 22. OMRP of VAc and **DMMDO** using a $Co(acac)_2$ complex as the controlling agent. Subsequent hydrolysis and post-polymerisation modification routes performed in this chapter to yield functional PVOH are also indicated.

5.3. Statistical Copolymerisation of VAc and DMMDO by Cobalt-Mediated Radical Polymerisation

The choice of the polymerisation technique for the copolymerisation of **DMMDO** with VAc was of particular importance if rROP of **DMMDO** is to be avoided (see discussion in the introduction). As rROP is favoured at high temperature, mild experimental conditions had to be implemented for this copolymerisation that involves two less-activated monomers (LAMs).[27] This prompted us to use the organometallic-mediated radical polymerisation (OMRP) technique mediated by $Co(acac)_2$ as it is highly active for the VAc polymerisation and its copolymerisation with various families of monomers (acrylonitrile, acrylates, ethylene, *N*-vinyl amides, vinylidene fluoride, etc.) is feasible.[7,8,16,17,31,263,265–268] Moreover, this type of OMRP is active at low temperature, *i.e.* 0-40 °C depending on the comonomers, which is of prime importance for avoiding rROP and thus yielding copolymers with intact CC-rings (Scheme 22).

To the best of our knowledge, the copolymerisation of **DMMDO**/VAc has not been reported before using any controlled radical polymerisation technique. The **DMMDO**/VAc copolymerisation was investigated by using a preformed alkylcobalt(III) acetylacetonate (R-$Co(acac)_2$) complex, where the alkyl chain acts as the radical initiator and $Co(acac)_2$ as the controlling agent (Scheme 22).[30] First, a degree of polymerisation of 400 was targeted for various comonomer feeds ranging from 5 to 40 mol% **DMMDO** (f^0_{DMMDO} = 0.05 – 0.40) at 40 °C in the bulk. It was observed that the molar masses of the polymers increased linearly with the monomer conversion, while retaining low dispersities throughout the polymerisation (Table 2, Figure 43a). Figure 43c shows that the SEC traces of the crude product were completely shifted towards higher molecular weights with monomer conversion, with only a very small tailing at the low molar mass side for the last sample. The small peak at around 20 min in the SEC trace corresponds to some deactivated R-$Co(acac)_2$ that was removed once the polymer was precipitated. The linear pseudo-first order kinetic plot highlights a decrease in the rate of polymerisation with an increasing feed in **DMMDO** (Figure 43b). For instance, under identical polymerisation conditions, a conversion of 83% was observed for the homopolymerisation of VAc after 23 hours of reaction compared to 50% or 30% when 6 or 34 mol% **DMMDO** were present, respectively (comparison of entries 1, 3 and 6, Table 2). Copolymerisation feeds above 40 mol% **DMMDO** were also investigated, but for f^0_{DMMDO} > 0.50, the monomer conversion was limited to a few percent (entry 8, Table 16). The origin of this inhibition is not yet understood. The homopolymerisation of **DMMDO** was not observed using R-$Co(acac)_2$ (entry 2, Table 2), which is in agreement with the absence of homopolymer

under free-radical polymerisation conditions.[313,314] To accelerate the copolymerisation, 20 equivalents of water (compared to R-Co(acac)$_2$) were added and indeed the total conversion increased from 5% to 26% when about 40 mol% **DMMDO** was used in the feed (entries 7 and 8, Table 2). As previously reported,[30,31,321] water is assumed to slightly shift the active/dormant species equilibrium towards the active side by complexing the deactivating (Co(acac)$_2$) species into Co(acac)$_2$L and Co(acac)$_2$L$_2$ (where L is water).

The molar mass of the copolymer can also be adjusted by tuning the monomers M/R-Co(acac)$_2$ molar ratio. For instance, for a feed content of about 15 mol% **DMMDO** and a M/R-Co(acac)$_2$ ratio of 100, a copolymer with molecular weight of 3,900 g mol^{-1} and a dispersity of 1.10 was obtained (entry 9, Table 2). Experimental molar masses determined by ^{1}H-NMR based on the α-chain-end ($M_{n\ NMR}$, see Section 10.4 for details) were also affected in a similar way by the M/R-Co(acac)$_2$ molar ratio (comparison of entries 4 and 9, Table 2). It is worth noting that the differences in molar mass values noted in some cases between theoretical molar masses ($M_{n\ theo}$) and $M_{n\ NMR}$ notably originate from inaccuracies on both the determination of the monomer conversion and on the integration of the α-chain-end. The determination of the DMMDO conversion requires the integration of peaks in a rather crowded area of the spectrum (around 1.6 ppm, see Chapter 10.4). Thus not always completely isolated peaks were observed resulting in conversions with increased error margins. Similarly, the integration accuracy of the α-chain end peak, although well separated from any other signals, was strongly affected by the width of the peaks, *i.e.* the quality of the NMR spectrum. In some cases the spectra were characterised by broad peaks and a slight shift in the area of integration led to a significant change in the molecular weight determined by NMR.

Table 2. Copolymerisations of VAc and **DMMDO** using R-Co(acac)$_2$ at 40°C[g]

Entry	f^0_{VAc}/ f^0_{DMMDO}[a]	t (h)	Total conv. (%)[a]	Composition (F_{VAc}/ F_{DMMDO}) (%)[b]	$M_{n\ theo}$ (g mol^{-1})[c]	$M_{n\ NMR}$ (g mol^{-1})[b]	$M_{n\ SEC}$ (g mol^{-1})[d]	M_w/M_n[d]
1	1/0	23	83	100/0	29,200	29,000	29,300	1.30
2	0/1	23	0	-	-	-	-	-
3	0.94/0.06	23	50	89/11	18,100	17,500	19,300	1.26
4	0.88/0.12	23	52	87/13	20,000	25,100	24,800	1.32
5	0.75/0.25	25	45	83/17	18,000	24,900	19,800	1.37
6	0.66/0.34	25	30	78/22	11,500	14,400	13,600	1.29
7	0.60/0.40	29	5	60/40	n.d.	9,300	6,200	1.35
8[e]	0.57/0.43	29	26	67/33	10,800	17,800	15,200	1.33
9[f]	0.85/0.15	6	42	86/16	4,400	4,300	3,900	1.10

Conditions: bulk, M/R-Co(acac)$_2$ = 400/1, magnetic stirring at 500 rpm. [a] Determined by ^{1}H-NMR spectroscopy in $CDCl_3$. [b] Composition of the copolymer and molecular weight determined by ^{1}H NMR spectroscopy in $CDCl_3$ based on the α-chain end (see Section 10.4). [c] $M_{n\ theo} = M_{w\ init} + (Conv_{DMMDO} \times M_{w\ DMMDO} + Conv_{VAc} \times M_{w\ VAc}) + M_{w\ TEMPO}$ (for more information see Section 10.4). [d] Determined by size exclusion chromatography (SEC) in THF using PS standard. [e] Addition of H_2O, R-Co(acac)$_2$/H_2O = 1/20. [f] Conditions: bulk, M/R-Co = 100, magnetic stirring at 500 rpm. [g] Full kinetics are in Table 16. n.d.: not determined.

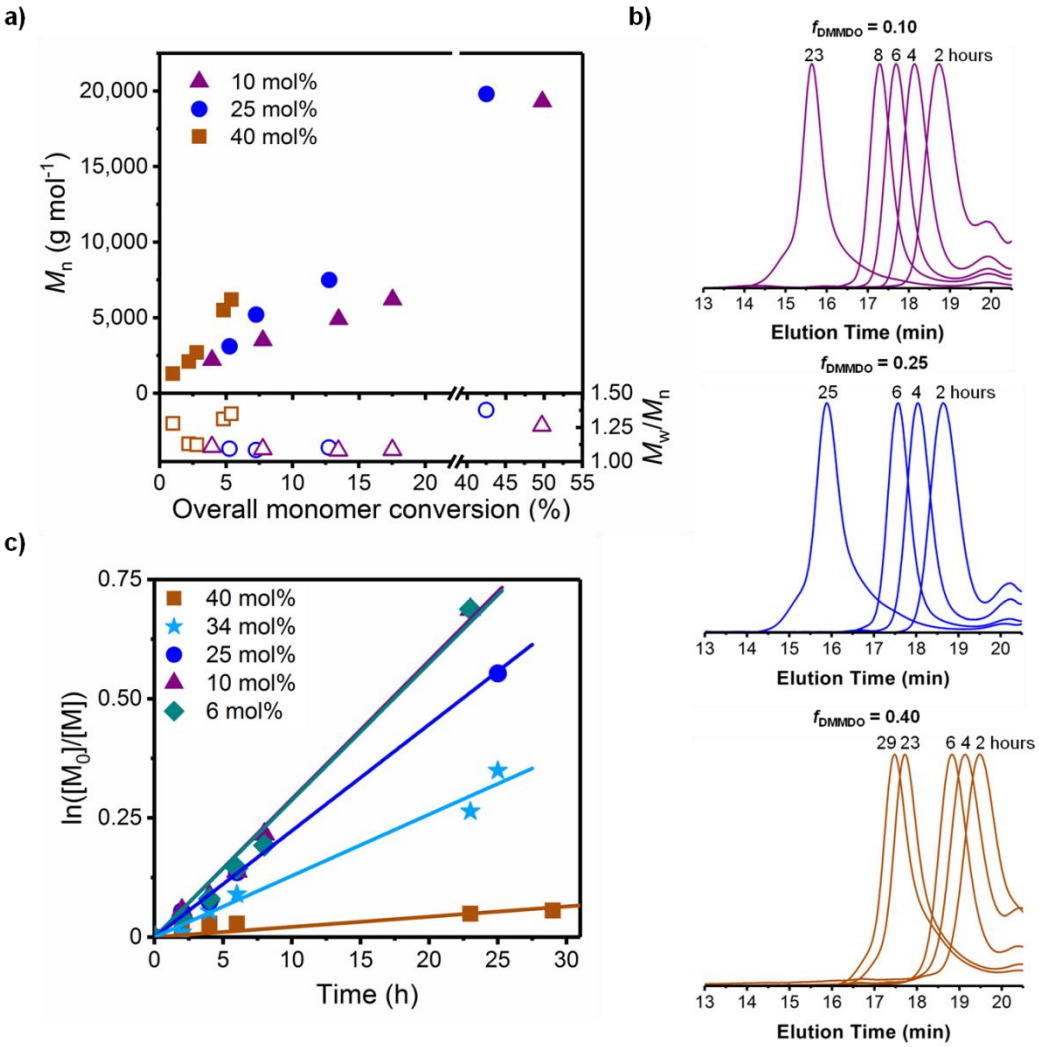

Figure 43. OMRPs at 40 °C of VAc and **DMMDO** at f^0_{DMMDO} ranging from 6 to 40 mol%: a) M_n and dispersity *vs.* total monomer conversion plot, b) first-order kinetic logarithmic plot with linear fits and c) size exclusion traces of kinetics with initial **DMMDO** feeds of 10, 25 and 40 mol%.

We then turned our attention to the copolymer structure since previously reported free radical copolymerisations of **DMMDO** yielded two possible structures: a combination of polyketones and intact cyclic carbonates when rROP, followed by decarboxylation, occurred in conjunction with a vinyl-type mechanism, and a polymer bearing exclusively intact cyclic carbonates when propagation occurred by radical addition on the double bond in the absence of rROP (Scheme 21).[313,314] ^{13}C-NMR spectroscopy strongly indicated that the polymers prepared in this study exclusively contain the intact carbonate ring with the characteristic carbonate peak at 152 ppm and the absence of a ketone signal at 210 ppm that may arise from rROP (Figure 44b). Additionally, by IR spectroscopy, two important bands were observed in the carbonyl region, one at 1730 cm^{-1} that was assigned to the ester group of the vinyl acetate repeating units, and one at 1800 cm^{-1} that was attributed to the carbonate stretching (Figure

101). The latter was unchanged in terms of wavenumber with respect to the monomer and these results reinforced the proposed structure of the copolymer.

Further evidence for the proposed structure was obtained by performing MALDI-ToF analysis on a low molar mass copolymer (entry 9, Table 2). As presented in Figure 46a, the copolymer is characterised by one narrow distribution centred around *m/z* 3650. The presence of signals separated by 128 mass units (u), characteristic of the **DMMDO** unit bearing the CC unit, and 86u, the mass of the VAc monomer unit, confirmed the incorporation of both monomers into the polymer backbone. As an illustration, theoretical models for copolymers with 36 (VAc_{33}:$\mathbf{DMMDO}_3$) and 37 (VAc_{33}:$\mathbf{DMMDO}_4$) monomer units are presented and match the experimental data (Figure 46b).

All these analyses are in line with the copolymer structure, thus with the intact cyclic carbonate. The low temperature of the OMRP used (40 °C) allowed to preserve the cyclic carbonate structure and prevent rROP. This is in line with free radical copolymerisation of **DMMDO**, favouring rROP at high temperatures (> 120 °C).[313,314] Additionally, a minimal amount of residual cobalt (147 ppm; compared to an initial content of 3,924 ppm) was determined using ICP-OE measurements on a copolymer containing 23 mol% **DMMDO** (entry 12, Table 16).

A copolymerisation was then carried out at a higher temperature, 90 °C, under otherwise identical conditions (f^0_{DMMDO} = 0.25, M/R-$Co(acac)_2$ = 400, for 4 hours) in order to evaluate the impact of the temperature on the copolymer structure. SEC analysis of the copolymer showed a $M_{n\ SEC}$ of 10,200 g mol^{-1} (for a $M_{n\ theo}$ of 8,100 g mol^{-1}) but with a high dispersity (M_w/M_n = 2.61), in line with a loss of control. Despite the expected broadening of the dispersity of the copolymer at this temperature (which was too high for an optimal control of VAc by OMRP)[17], the ^{1}H-NMR (Figure 102a) and ^{13}C-NMR (Figure 102b) spectra were similar to the copolymers formed at 40 °C. At 90°C, rROP was therefore not observed.

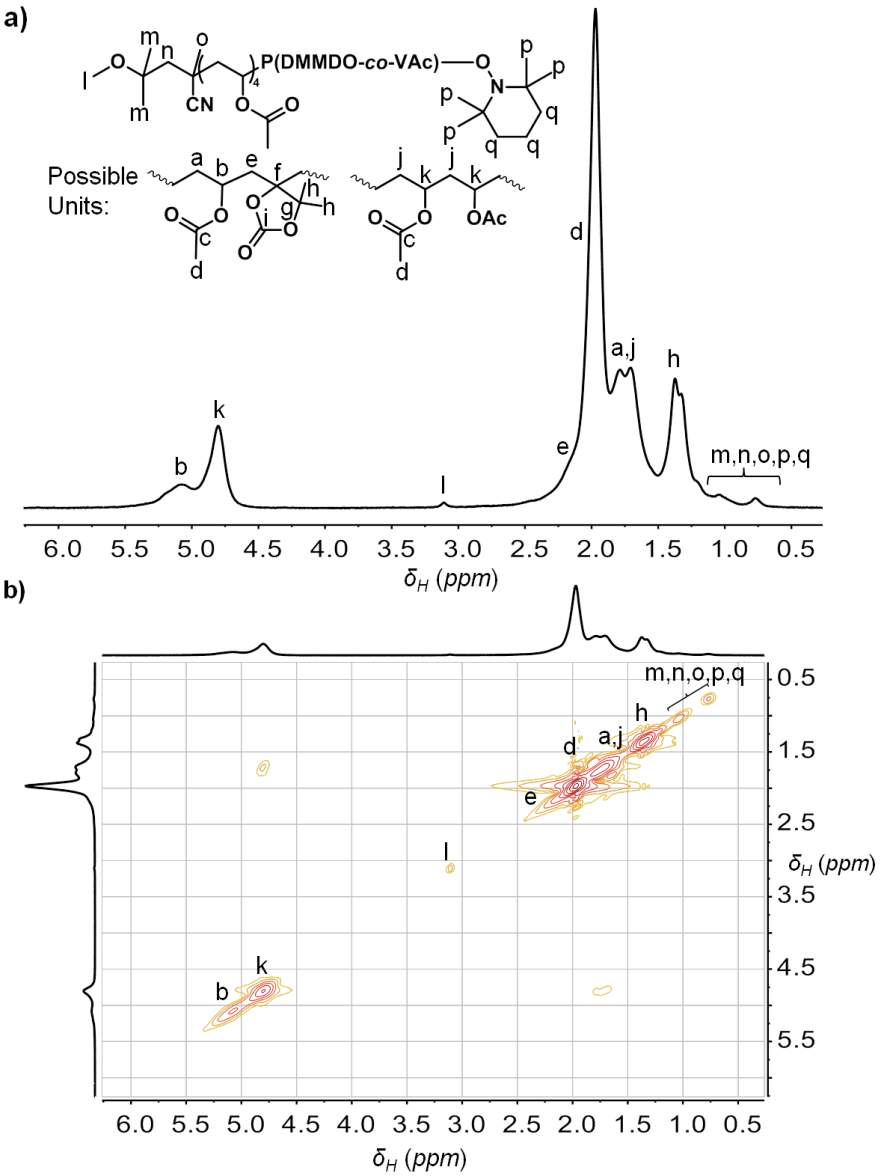

Figure 44. a) ^{1}H-NMR spectrum and b) COSY spectrum of a copolymer at 43% conversion containing 16 mol% **DMMDO** prepared by OMRP at 40 °C (entry 5, Table 2). NMR spectra taken in $CDCl_3$ on a 400 MHz spectrometer.

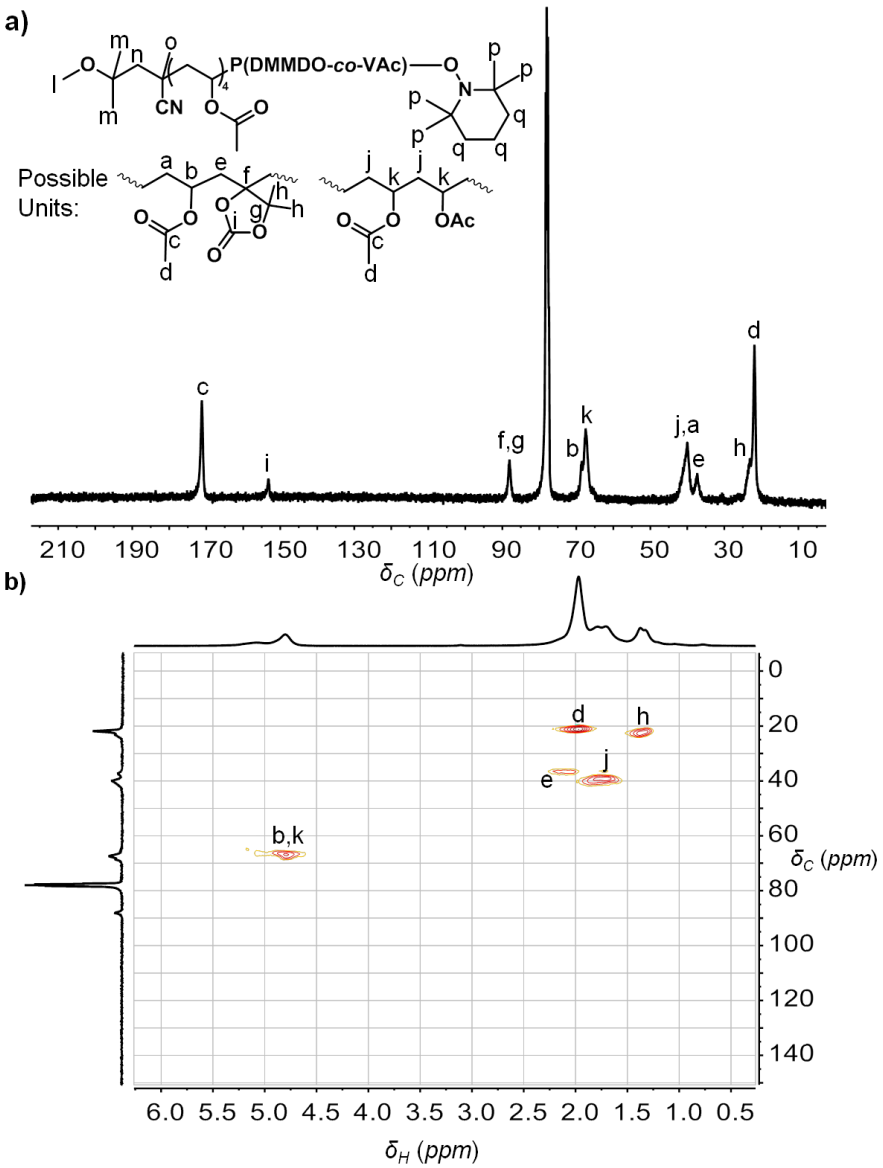

Figure 45. a) ^{13}C-NMR spectrum and b) HSQC spectrum of a copolymer at 43% conversion containing 16 mol% **DMMDO** prepared by OMRP at 40 °C (entry 5, Table 2). NMR spectra taken in $CDCl_3$ on a 400 MHz spectrometer.

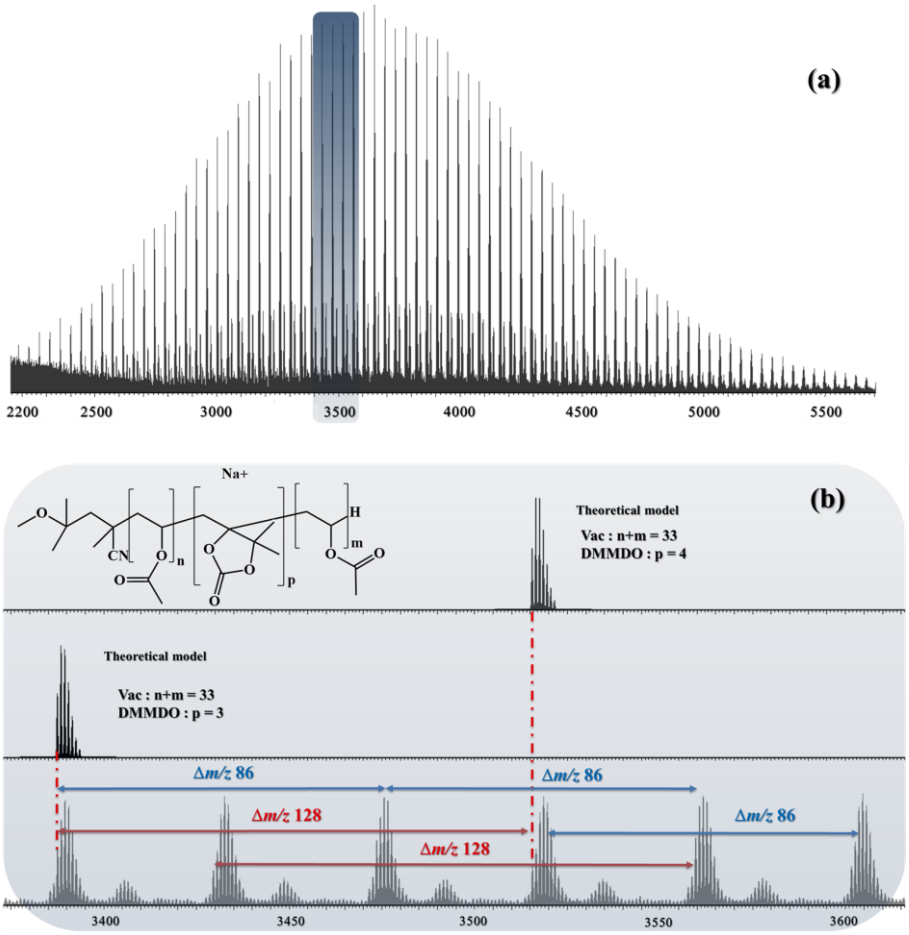

Figure 46. MALDI mass spectra recorded for a copolymer containing 16 mol% **DMMDO** (entry 9, Table 2) showing a) the global mass spectrum and b) a magnification between *m/z* 3350 and *m/z* 3600 and the comparison of the signals with a theoretical model.

Once the structure was elucidated, the composition of the final copolymers was determined by ^{1}H-NMR spectroscopy. Figure 44 and Figure 45 show the ^{1}H-, ^{13}C-NMR, COSY and HSQC spectra of the copolymer prepared using an initial VAc/**DMMDO** feed ratio of 75/25 after 25 hours of polymerisation (entry 5, Table 2). The ^{1}H-NMR spectrum clearly shows peak **l** at 3.10 ppm, which belongs to the α-chain end of the copolymers (**l**, CH_3-O at 3.10 ppm) and peaks **d**, **j**, **k** typical of the –CH_3, –CH_2– and –CH-OAc of VAc, respectively (**d**, –CH_3 at 1.97 ppm; **j**, –CH_2– at 1.74 ppm; **k**, –CH-OAc at 4.80 ppm). An additional peak at 1.35 ppm was attributed to the –CH_3 groups of the CC repeating unit (**h**, –CH_3 at 1.35 ppm), while the broad signal at 5.10 ppm originates from a deshielded –CH-OAc group of VAc next to a **DMMDO** unit, as confirmed by the HSQC spectrum (**b**, –CH-O– at 5.10 ppm). Peaks **c** and **i** in the ^{13}C-NMR spectrum were attributed to the C=O signal of the ester and carbonate of VAc and **DMMDO**, respectively (**c**, C=O at 170 ppm; **i**, C=O at 152 ppm). The remaining signals could only be attributed with reference to the HSQC spectrum (Figure 45b) and were in agreement with the proposed chemical structure. Figure 47 presents the ^{1}H-NMR spectra of

PVAc and P(VAc-*co*-**DMMDO**) copolymers prepared by OMRP with feeds ranging from 10 to 40 mol% **DMMDO**. By increasing the **DMMDO** in the feed, the integral of the characteristic broad signal, associated with the two –C$\underline{H_3}$ groups of **DMMDO** repeating units at 1.40 ppm, increased as well as the broad signal at 5.10 ppm that comes from the slightly more deshielded environment of the –C$\underline{H}$-OAc that is next to a **DMMDO** repeating unit. Using these characteristic peaks and comparing their relative intensities, the copolymer composition could be determined (see Section 10.4 for details, Figure 47 and Table 2). It should be mentioned, that the difference in **DMMDO** content of the copolymer compared to the monomer feed observed for entries 3, 4, and 9 (Table 2) is only a few mol%, reaching the limit of the accuracy of NMR spectroscopy, and hence no judgment on the deviation of these entries can be made.

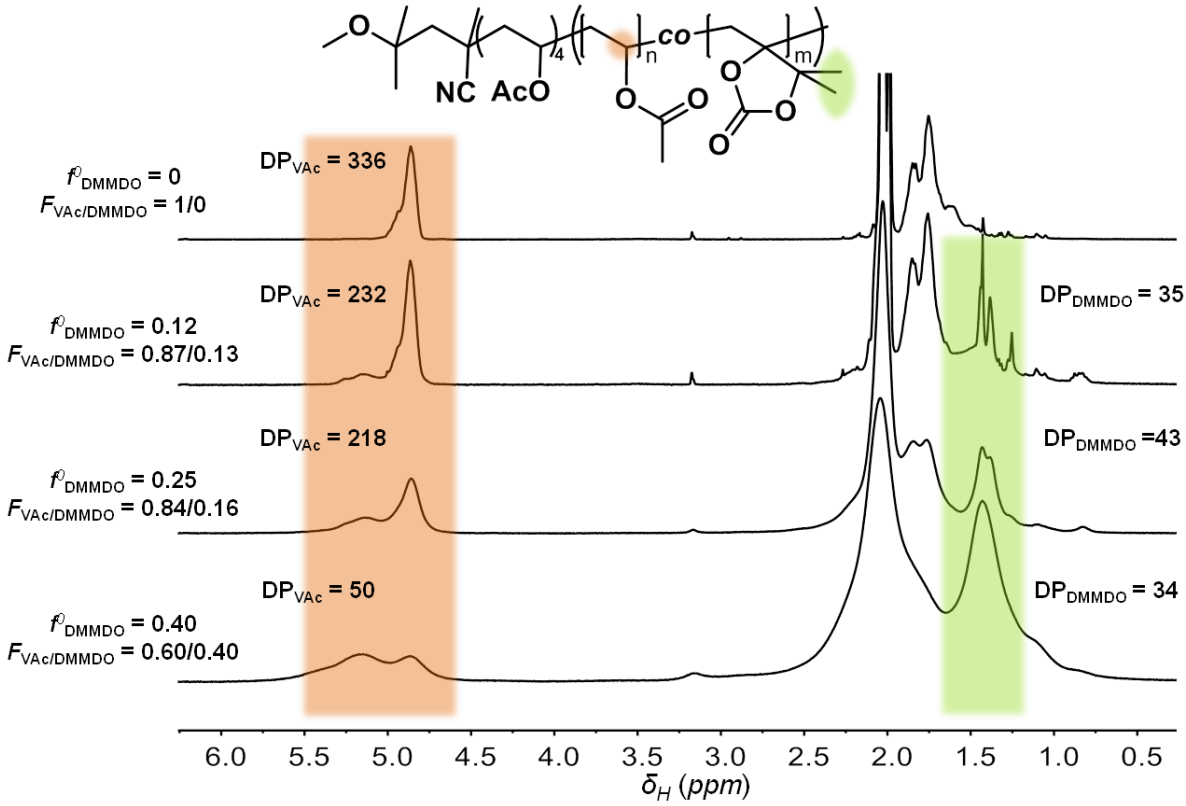

Figure 47. ^{1}H-NMR spectra of copolymers prepared by OMRP at 40 °C with f^0_{DMMDO} = 0-0.4. NMR spectra taken in $CDCl_3$ on a 400 MHz spectrometer.

Additionally, to better understand the copolymer composition and also to be able to predict the copolymer composition, the reactivity ratios of the two monomers were determined using free radical polymerisation (FRP) at 40 °C. The use of free radical polymerisations was necessary to access a larger variety in compositions, as OMRP is inhibited above 50 mol% **DMMDO** in the feed. The good agreement of the reactivity ratios values determined by FRP

with those obtained by OMRP has been demonstrated in a previous publication[267] and was verified by a few points, as discussed below.

Free radical polymerisations with feeds ranging from 11 to 92 mol% **DMMDO** were conducted and were quenched at low conversion (<15%) to avoid a composition drift. The polymers were then analysed by ^{1}H-NMR spectroscopy to evaluate their composition and the comonomers' conversion, and their macromolecular parameters were determined by SEC (Table 17). For feeds above 72 mol% **DMMDO**, extremely low polymerisation rates were noted and not enough polymer material was obtained for accurate analysis.

Three compositions (*F*) obtained at specific feeds (*f*) by FRP were verified using OMRP in order to demonstrate that compositions are similar by both processes. The discrepancies of the composition obtained by classical radical polymerisation *versus* controlled radical polymerisation were observed to be within 9 mol% of each other (comparison of entries 1, 4 and 5 for FRP with entries 12-14 for OMRP, Table 17).

The Kelen-Tüdos (KT) linearisation method was used to determine the reactivity ratios: r_{DMMDO} = 0.03, r_{VAc} = 1.11 (Figure 48a).[322–324] A reactivity ratio close to 0 for **DMMDO** highlighted the well-known inability of this monomer to homopolymerise. It also means that during the copolymerisation with VAc, a chain-end **DMMDO** radical almost always cross-propagates. On the other hand, r_{VAc} of 1.11 was obtained for VAc, meaning that such a chain-end radical can add to both monomers without inclination towards one or the other. As a result, a preferential incorporation of VAc into the copolymer was observed and the **DMMDO** repeat units are isolated within the copolymer backbone. Additionally, the final copolymer composition at different feeds was computed using the Mayo Lewis equation (Figure 48b).

In order to give further insights on the distribution of the comonomer units along the chains, the instantaneous and the cumulative copolymer compositions were predicted on the whole range of monomer conversions through the Skeist equation using the reactivity ratios determined above (see experimental part for detailed equations). Figure 49 shows the evolution of the instantaneous feed (f_{inst}), the copolymer composition (F_{inst}) and the cumulative copolymer composition (F_{cumul}) *versus* the overall comonomer conversion. As an example, we considered an initial **DMMDO** molar fraction in the feed (f^0_{DMMDO}) of 0.25 (entry 5, Table 2). The experimental cumulative copolymer composition for f^0_{DMMDO} = 0.25, determined by ^{1}H NMR spectroscopy, at different conversions are represented by black dots in Figure 49 and fitted well with the predicted cumulative composition curve (F_{cumul}, full line in Figure 49). Skeist's plot shows that the instantaneous copolymer composition does not

change during the polymerisation for conversions below 80 % and for such conversions the DMMDO monomer is homogeneously distributed throughout the polymer chain (Figure 49). As an illustration, a copolymer prepared from a feed of 25 mol% DMMDO at 43% total conversion (entry 5, Table 2) contains on average 218 repeating units of VAc and 43 repeating units of **DMMDO**. Therefore, there is an average distance of 5 VAc repeating units between two **DMMDO** ones.

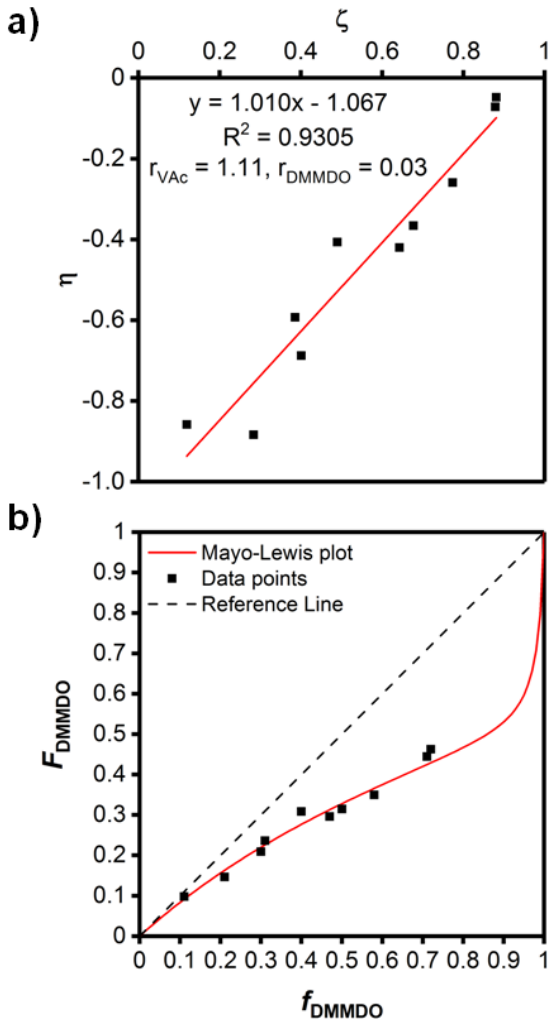

Figure 48. a) Kelen-Tüdos linearisation plot (r_{Vac} = 1.11 and r_{DMMDO} = 0.03) and b) Mayo-Lewis plot using experimental reactivity ratios.

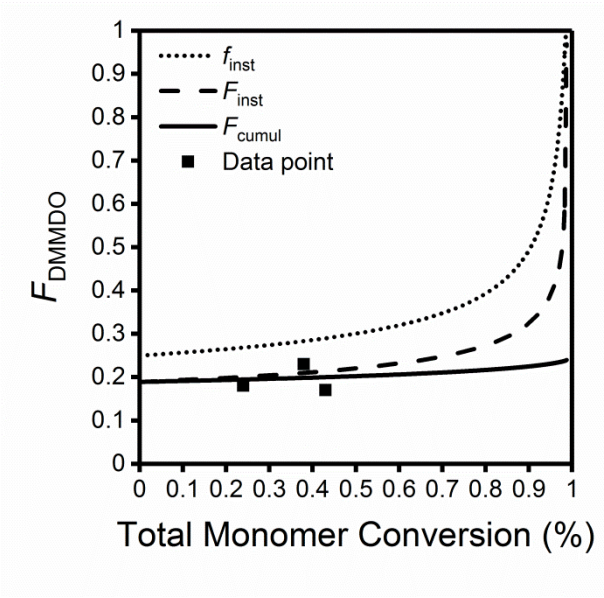

Figure 49. Skeist's plot for a feed of 25 mol% **DMMDO** of instantaneous reaction composition (f_{inst}), instantaneous copolymer composition (F_{inst}) and cumulative copolymer composition (F_{cumul}) against overall monomer conversion using r_{DMMDO} = 0.03 and r_{VAc} = 1.11. The composition of several copolymers is also plotted (entry 5, Table 2; entry 12 and 13, Table 16).

The thermal properties of the produced polymers were then investigated using thermogravimetric analysis (TGA) and differential scanning calorimetry (DSC). It was observed that the copolymers had a lower degradation temperature than PVAc with a temperature at 5% weight loss ($T_{d\ 5\%}$) of 224 to 289 °C versus 306 °C, respectively (Figure 50a). Moreover, $T_{d\ 5\%}$ strongly depends on the copolymer composition. It decreased from 281 °C to 224 °C with increasing **DMMDO** content in the copolymer. Rapid degradation of the copolymer was observed for all polymers above 300 °C.

The glass transition temperatures (T_g) of these polymers strongly increased compared to the homopolymer of PVAc, reaching a maximum of 80 °C for polymers containing 22 mol% **DMMDO** (Figure 50b), which is not unexpected due to the bulky and rigid structure of the **DMMDO** monomer. The lower T_g for the copolymer containing 40 mol% **DMMDO** was attributed to its lower molar mass compared to the copolymer containing 22 mol%. Overall, the incorporation of the cyclic carbonate in the polymer structure clearly increased the T_g while decreasing the degradation temperature.

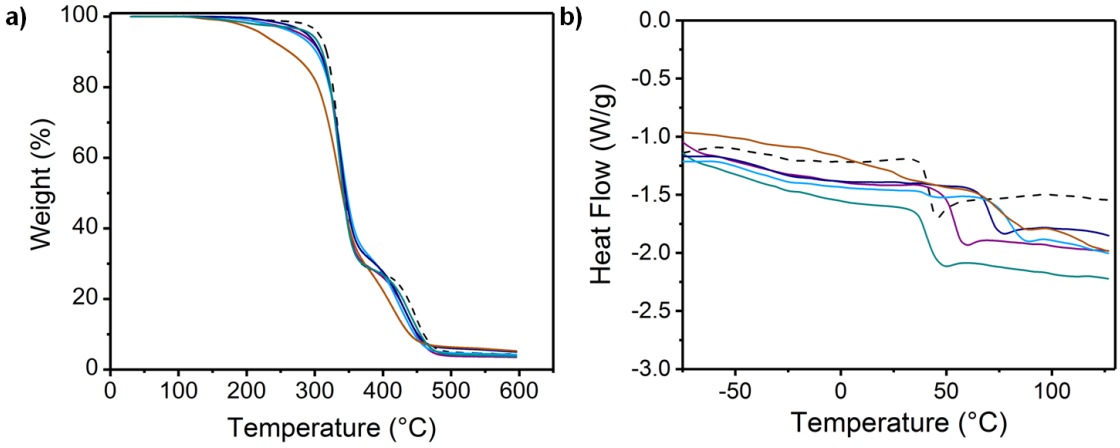

Colour code	DMMDO content (mol%)	M_n (g.mol^{-1})	T_g (°C)	$T_{d\,5\%}$ (°C)
– – –	0	29,300	42	306
	9	19,300	42	295
	13	24,800	54	281
	16	19,800	70	289
	22	13,600	80	269
	40	6,200	75	224

Figure 50. a) Thermogravimetric analysis (TGA) curves b) differential scanning calorimetry (DSC) curves of P(VAc-*co*-**DMMDO**) of various compositions (entries 1 and 3-7, Table 2).

5.4. Chemo-Selective and Complete Hydrolysis of P(VAc-*co*-DMMDO)

The hydrolysis of PVAc is the most common procedure for the synthesis of the highly hydrophilic poly(vinyl alcohol) (PVOH); both acidic[325] and basic[264,271,326] routes are used. However, PVOH presents several drawbacks, of which the main one is its poor solubility at room temperature or at high concentration as the result of its very regular hydrogen-bonding network.[317,327,328] The addition of a comonomer that is able to disrupt this network has been shown to be an effective way to increase the solubility of PVOH.[27,328–330] Hence the hydrolysis of the copolymers prepared above was very interesting as it would generate chemically modified PVOH. The chemo-selective hydrolysis of the ester groups of the VAc units would yield P(VOH-*co*-**DMMDO**), thus PVOH with pendant cyclic carbonate functionalities (Figure 51a). In contrast, full methanolysis of both ester groups of VAc units and cyclic carbonates of **DMMDO** units would provide a PVOH copolymer (P(VOH-*co*-BD)) bearing butane-2,3-diol units (BD; Figure 51a) that are expected to improve the copolymer water solubility compared to unmodified PVOH.

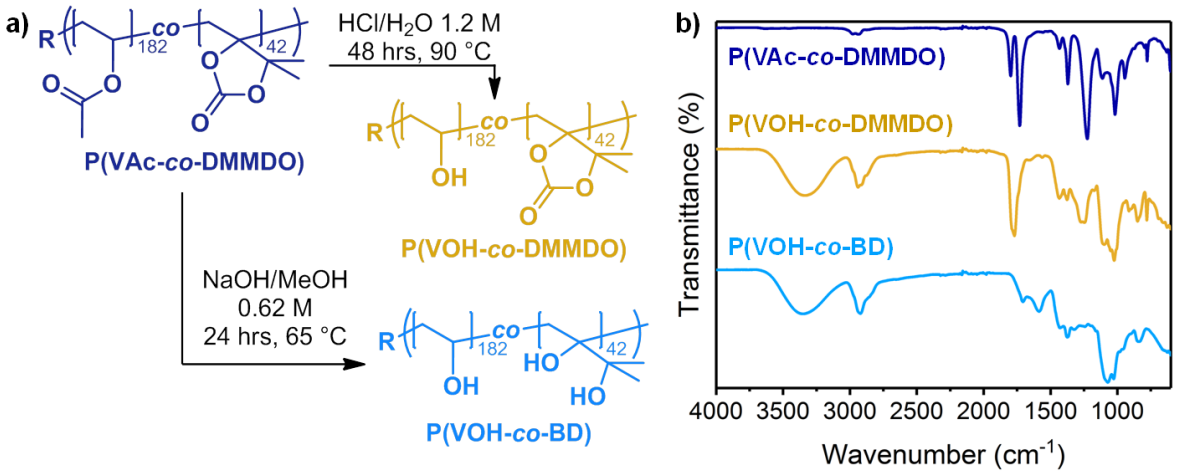

Figure 51. a) Acidic hydrolysis and methanolysis conditions of P(VAc_{182}-*co*-**$DMMDO_{42}$**) (19 mol% DMMDO; entry 10, Table 16) into the corresponding P(VOH_{182}-*co*-**$DMMDO_{42}$**) and P(VOH_{182}-*co*-BD_{42}), and b) FT-IR spectra of the various copolymers.

A P(VAc_{182}-*co*-**$DMMDO_{42}$**) copolymer containing 19 mol% **DMMDO** (entry 10, Table 16) was subjected to methanolysis and acidic hydrolysis conditions according to previous reports.[268,271,325,329] Under acidic treatment (HCl (1.2 M) in water) at 90 °C for 48h, chemo-selective hydrolysis of the ester functionality was observed. The ^{1}H-NMR and ^{13}C-NMR analyses of the starting P(VAc-*co*-**DMMDO**) copolymer before and after treatment validated

the selective hydrolysis (Figure 52 and Figure 53). In the ^{1}H-NMR spectra (Figure 52), the disappearance of signal **b** at 4.79 ppm corresponding to the –*C*<u>*H*</u>-OAc proton of PVAc (**b**, –*C*<u>*H*</u>-OAc at 4.79 ppm), and the appearance of signals typical of P(VOH) (**b**, –*C*<u>*H*</u>-OH at 3.80 ppm, and **c**, –CH-*O*<u>*H*</u> at 4.2-4.7 ppm) confirmed the hydrolysis of PVAc. The presence of signal **d** at 1.97 ppm was in line with the preserved DMMDO units (**d**, –C<u>*H*$_2$</u> at 1.97 ppm). The selective hydrolysis was also highlighted in the ^{13}C-NMR spectra (Figure 53a and b) through the complete disappearance of the characteristic signal of the ester group at 170 ppm and the preservation of the carbonate signal at 154 ppm. Additional evidence for the successful selective hydrolysis of VAc units was provided by the comparison of infrared spectra of the copolymer before and after treatment, which showed the disappearance of the absorption band of the ester groups at 1738 cm^{-1}, the appearance of the OH stretching band of PVOH at 3330 cm^{-1}, and the retention of the cyclic carbonate band at 1780 cm^{-1} (Figure 51b). Another indication that the hydrolysis was selective to the ester functionalities was obtained by comparing the DP_{DMMDO} before and after hydrolysis. The DP_{DMMDO} before hydrolysis was determined to be 42. Comparing the relative integrals of b and d (b, –C<u>*H*</u>-OH at 3.80 ppm; d, –C<u>*H*$_2$</u>– at 1.97 ppm; Figure 52b) in P(VOH$_{182}$-*co*-**DMMDO**$_{42}$), it was found that the DP_{DMMDO} after hydrolysis is 44, which was unchanged – within the accuracy that ^{1}H-NMR spectroscopy provides – compared to the initial P(VAc$_{182}$-*co*-**DMMDO**$_{42}$) (For detailed calculations see experimental part, Figure 103).

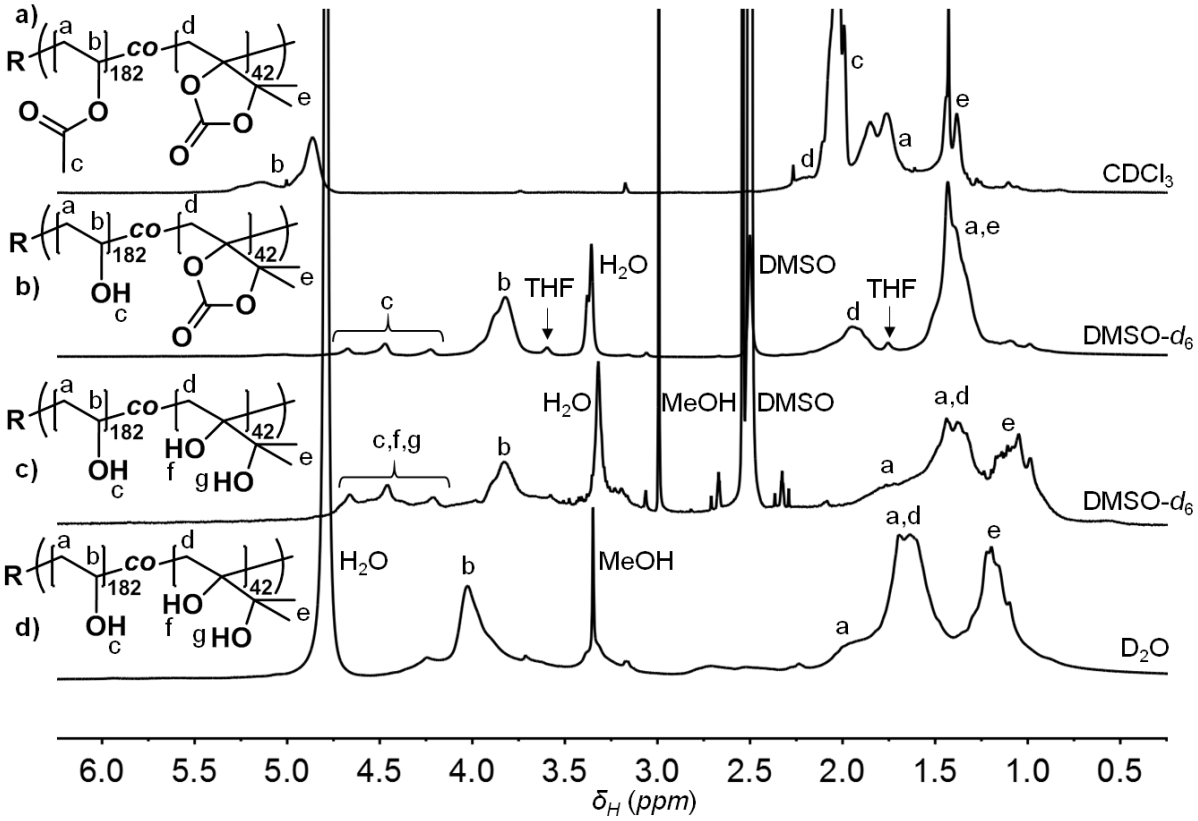

Figure 52. ^{1}H-NMR spectra of a) P(VAc$_{182}$-*co*-**DMMDO**$_{42}$) (19 mol% **DMMDO**; Table 16, Entry 10) in $CDCl_3$, b) P(VOH$_{182}$-*co*-**DMMDO**$_{42}$) in DMSO-d_6, c) P(VOH$_{182}$-*co*-BD$_{42}$) in DMSO-d_6 and d) P(VOH$_{182}$-*co*-BD$_{42}$) in D_2O. All spectra were recorded on a 400 MHz spectrometer.

On the other hand, complete methanolysis was observed under basic conditions (NaOH 0.62 M) at 65 °C for 24h, as demonstrated by the complete disappearance of the ester and carbonate vibrations in the FT-IR spectrum (Figure 51b), and of the typical ester and carbonate signals in the ^{13}C-NMR spectrum (Figure 53c). Yet, three weak peaks were observed in the ^{13}C-NMR spectrum and were attributed to the –*C*H$_2$–, –*C*HOH– and –*C*H$_3$ environments (**a** and **c**, –*C*H$_2$– at 44 ppm; **b**, –*C*HOH at 66 ppm and **f**, –*C*H$_3$ at 23 ppm), while the tertiary carbon environments **d** and **e** were not observed. In the ^{1}H-NMR spectrum (Figure 52c), peaks **d** and **e** shifted upfield, due to the methanolysis of the CC ring, while peak **a** did not change significantly from the selectively hydrolysed copolymer (**d**, –C*H*$_2$– at 1.25 ppm; **e**, –C*H*$_3$ at 23 ppm; **a**, –C*H*$_2$C*H*–*OH* at 1.4 ppm). Interestingly, the choice of solvent, in this case DMSO-d_6 or D_2O, played an important role on the chemical shift of the peaks in the ^{1}H-NMR spectra, as D_2O significantly deshielded the signals possibly because of the increased hydrogen bonding (Figure 53c and d).

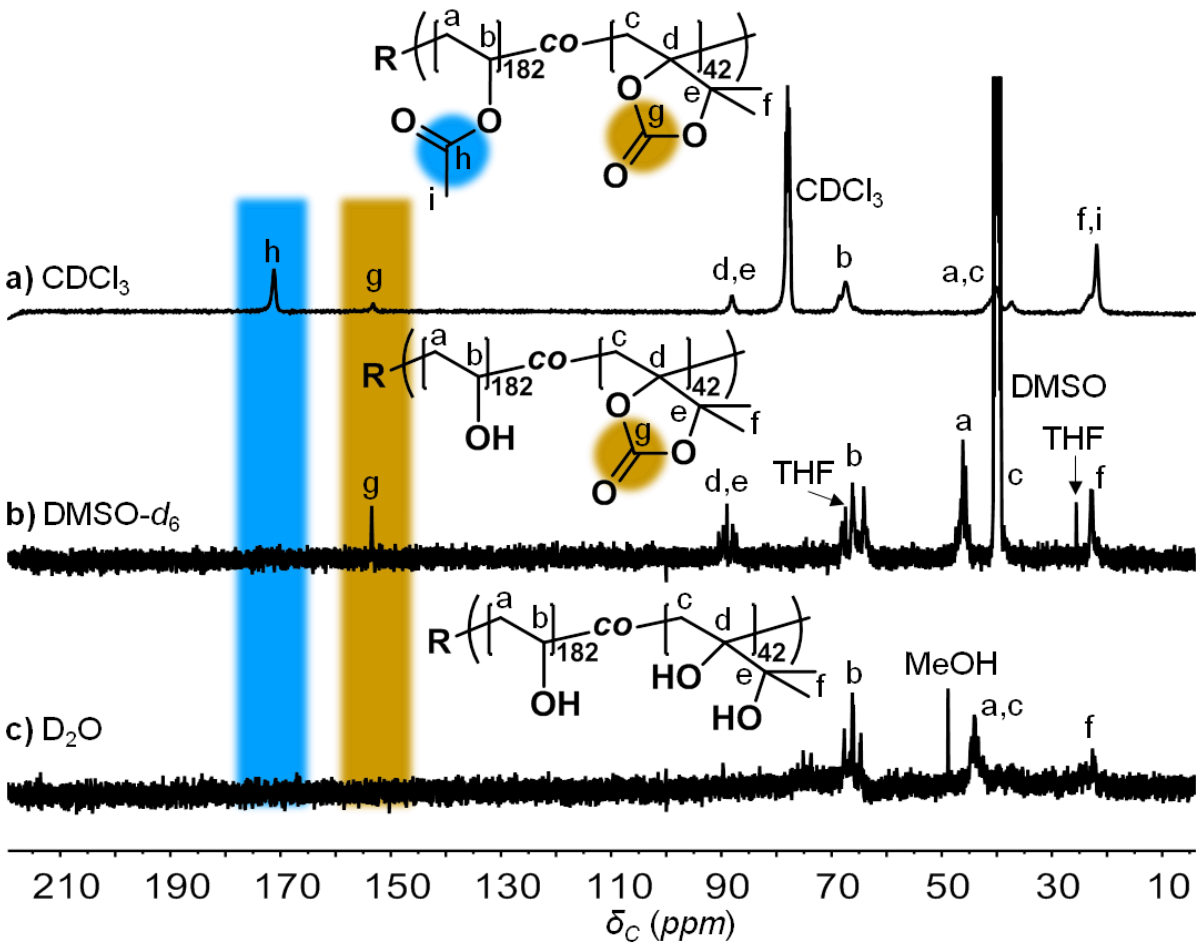

Figure 53. Overlay of ^{13}C-NMR spectra of P(VAc$_{182}$-*co*-**DMMDO**$_{42}$) (19 mol% **DMMDO**; entry 10, Table 16) in $CDCl_3$, P(VOH$_{182}$-*co*-**DMMDO**$_{42}$) in DMSO-d_6 and P(VOH$_{182}$-*co*-BD$_{42}$) in D_2O. All spectra were recorded on a 400 MHz spectrometer.

The solubility of the fully methanolysed copolymer in 0.5 mL of water was significantly improved when compared to an analogous PVOH prepared by OMRP with a similar DP_{total} (DP_{total} of both copolymers around 133; entries 1 and 2, Table 18; Figure 54). While 1 mg of PVOH$_{134}$ could only be solubilised at 50 °C, the same amount of P(VOH$_{108}$-*co*-BD$_{24}$), containing 18 mol% BD units, could be easily solubilised at room temperature. This difference in solubility was further evidenced as the concentration is increased, as the P(VOH$_{108}$-*co*-BD$_{24}$) copolymer was soluble at a concentration of 375 g/L at 30 °C, while the equivalent PVOH$_{134}$ was only partially soluble at a concentration of 150 g/L at 80°C. The selectively hydrolysed copolymer was not soluble in water.

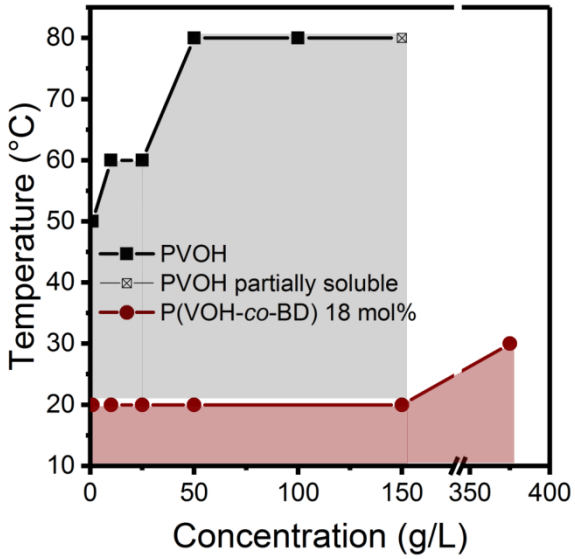

Figure 54. Temperature of solubilisation of $PVOH_{134}$ and $P(VOH_{108}$-*co*-$BD_{24})$ in water at different concentrations (Table 19)

5.5. Post-Polymerisation Modification of the Selectively Hydrolysed Copolymer P(VOH-*co*-DMMDO)

The selectively hydrolysed copolymer prepared above was of great interest for further post-polymerisation modifications on the cyclic carbonate: a nucleophilic ring opening of the carbonate allows for the functionalisation while keeping an intact backbone (Figure 55a). The functionalisation with carbamate moieties on an analogous PVOH would result in the loss of an –OH group and thus an unwanted change in the copolymer properties (Figure 55b). Furthermore, highly toxic chloroformates would be necessary for this transformation. As a proof of concept, a $P(VOH_{149}$-*co*-**DMMDO**$_{44})$ containing 23 mol% **DMMDO** (entry 12, Table 16) was treated with n-butylamine using TBD as a catalyst in DMF at 80°C under anhydrous conditions. In the FT-IR, the characteristic carbonyl absorbance at 1780 cm^{-1} decreased in intensity and two further absorbances at 1688 cm^{-1} and 1530 cm^{-1} were observed (Figure 55c). These were attributed to the C=O stretching of the newly formed urethane bond and the N-H bending, respectively. As the ring-opening can occur on either side of the ring, two possible isomers were expected to be formed (Figure 55a), but cannot be discriminated by NMR analysis (Figure 56b and c). For simplicity, only one of the two possible isomers will be shown from here on. In the ^{1}H-NMR spectrum, the appearance of peak **m** at 0.87 ppm and peak **j** at 2.97 were characteristic of the –C$\underline{H_3}$ group and the –N-C$\underline{H_2}$– of the butyl urethane functionality, respectively (**j**, –N-C$\underline{H_2}$– at 2.97 and **m**, –C$\underline{H_3}$ at 0.87 ppm). The –N$\underline{H}$– proton

was not visible (absence of peak **i**), which is likely to be a result of solvent exchange. The successful functionalisation of the copolymer was also observed in the ^{13}C-NMR spectrum (Figure 104), which resembled that of P(VOH-*co*-BD) with peaks **a**, **b**, **c** and **f**, all at the same chemical shifts as for P(VOH-*co*-BD) (**a** and **c**, –C*H*$_2$– at 46 ppm; **b**, –C*H*OH at 66 ppm; **f**, –C*H*$_3$ at 25 ppm). However, an additional peak was apparent at 14 ppm, which was attributed to the –C*H*$_3$ of the butyl urethane (**p**, –C*H*$_3$ at 14 ppm) while no trace of the urethane N-(*C*=O)-O was observed (absence of peak **l**). With the aid of the HSQC spectrum, two more peaks at 32 and 20 ppm were attributed to the –C*H*$_2$– groups of the butyl urethane group (**n**, –C*H*$_2$– at 32 ppm; **o**, –C*H*$_2$– at 20 ppm). These signals were all supported by the COSY and HSQC spectra (Figure 105). Yet the functionalisation was not complete, as the residual –C*H*$_2$– peak in the ^{1}H-NMR spectrum (d, –C*H*$_2$– at 1.90 ppm; Figure 56), and the *C*=O signal and the –*C*– signals in the ^{13}C-NMR spectrum (g, *C*=O at 154 ppm; d and e, –*C*– at 89 ppm; Figure 104) of the intact CC repeating unit were still observed and thus a terpolymer containing vinyl alcohol, **DMMDO** and hydroxy urethane repeat units (P(VOH-*co*-**DMMDO**-*co*-HU)) was formed.

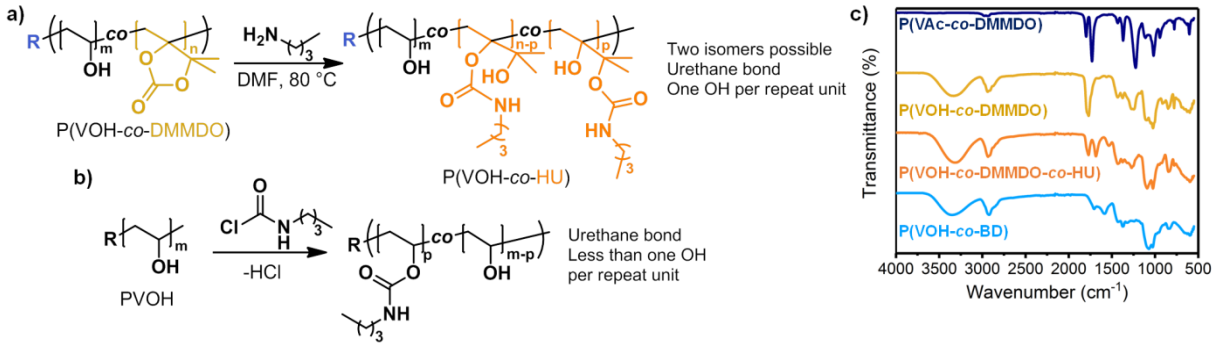

Figure 55. Post-polymerisation modification with n-butylamine of a) P(VOH-*co*-**DMMDO**) to give P(VOH-*co*-HU), a structure with one –OH unit per repeat unit which is inaccessible with b) PVOH where one less –OH unit is present after modification and c) FT-IR spectra of P(VAc$_{149}$-*co*-**DMMDO**$_{44}$), P(VOH$_{149}$-*co*-**DMMDO**$_{44}$), P(VOH$_{149}$-*co*-**DMMDO**$_{33}$-*co*-HU$_{10}$) functionalised using dry n-butylamine and P(VOH$_{182}$-*co*-BD$_{42}$)

Using MeOD-d_4 as the solvent for the ^{1}H-NMR spectroscopy analysis instead of DMSO-d_6 shifted the water signals upfield, liberating the –C*H*OH signal of the VOH (Figure 56b and c). Integrating the –NHC*H*$_2$– peak of the urethane group (3.23 – 3.01 ppm) in the ^{1}H-NMR spectra recorded in MeOD-d_4 and comparing it with the –C*H*OH integral of the VOH group (4.48 – 3.77 ppm) (see Section 10.4 for calculation details, Figure 106), the degree of functionalisation was estimated to be 23%, which corresponds to 10 urethane repeat units. The unfunctionalised DP$_{DMMDO}$ was determined to be 33, which fits with the proposed

structure. Interestingly, a slightly lower degree of functionalisation – 16% or DP_{HU} = 7 – was observed when wet (thus not pre-dried) n-butylamine was used while no difference in copolymer structure could be identified (Figure 106 and Figure 107). The structure of the selectively hydrolysed copolymer was therefore post-modified by the addition of *n*-butylamine, but further investigations are needed to optimise the reaction conditions and to determine the properties of the obtained copolymers. In summary, three different copolymer structures were thus accessed from P(VAc-*co*-**DMMDO**): P(VOH-*co*-BD), P(VOH-*co*-**DMMDO**) and P(VOH-*co*-**DMMDO**-*co*-HU) (Scheme 23).

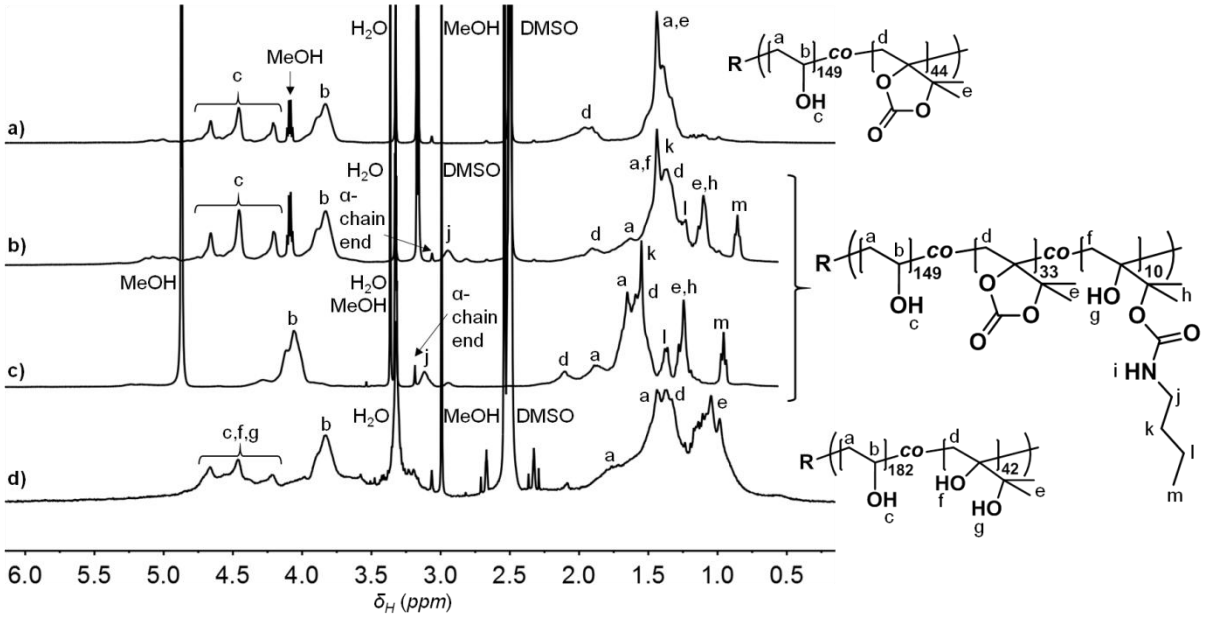

Figure 56. ^{1}H-NMR spectra of a) P(VOH_{149}-*co*-**DMMDO**$_{44}$) recorded in DMSO-d_6, b) P(VOH_{149}-*co*-**DMMDO**$_{33}$-*co*-HU_{10}) functionalised using dry n-butylamine, recorded in DMSO-d_6, c) P(VOH_{149}-*co*-**DMMDO**$_{33}$-*co*-HU_{10}) functionalised using dry n-butylamine, recorded in MeOD-d_4 and d) P(VOH_{182}-*co*-BD_{42}) recorded in DMSO-d_6. All spectra are taken on a 400 MHz spectrometer.

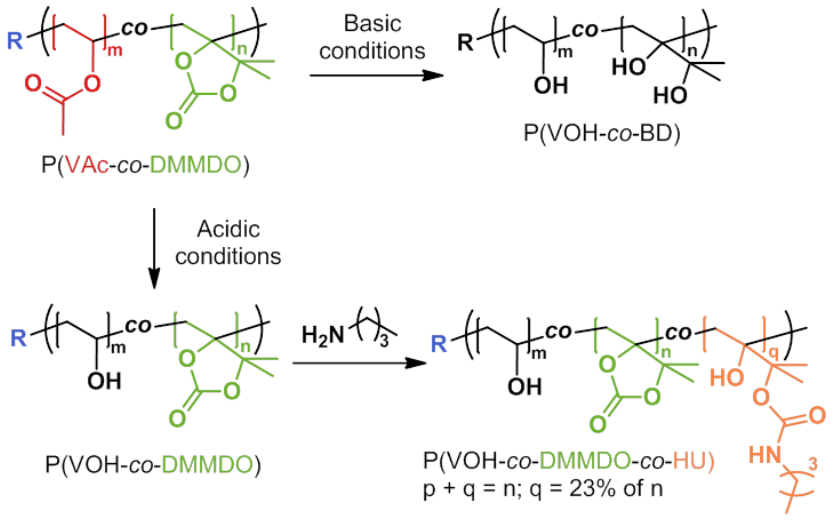

Scheme 23. Starting from a single copolymer, P(VAc-*co*-**DMMDO**), three different copolymers were accessed: P(VOH-*co*-BD), P(VOH-*co*-**DMMDO**) and P(VOH-*co*-**DMMDO**-*co*-HU).

5.6. Conclusion

For the first time, a CO_2-based α-alkylidene cyclic carbonate (**DMMDO**) was statistically copolymerised with vinyl acetate (VAc) in a controlled manner *via* OMRP using a $Co(acac)_2$ controlling agent under mild experimental conditions. Good control over the macromolecular characteristics was observed while the carbonate rings remained intact. The distribution of **DMMDO** repeat units within the copolymer chains was established using the Skeist model after the determination of the reactivity ratios of the comonomers. For a feed of 25 mol% **DMMDO** and conversions below 80%, it was observed that **DMMDO** was homogeneously distributed along the chain. Hydrolysis of both the pendant esters and carbonate groups of the P(VAc-*co*-**DMMDO**) copolymer gave PVOH-like copolymers with improved water solubility as compared to unmodified PVOH of a similar degree of polymerisation. The preparation of PVOH copolymers with pendant cyclic carbonate groups was possible by chemo-selective hydrolysis of the acetate groups. These functional copolymers were then post-modified *via* the nucleophilic ring opening of the carbonate ring with butyl amine leading to PVOH polymers with grafted side-chains. In contrast to the classical PVOH functionalisation methods relying on the transformation of pendant hydroxyl groups, the present strategy affords the advantage of preserving one hydroxyl group per repeat unit. The precise copolymerisation of VAc with CO_2-sourced five-membered cyclic carbonate bearing an exomethylene moiety is therefore a powerful tool for the synthesis of new variants of poly(vinyl alcohol)-based copolymers, whose properties have now to be investigated.

6 Functional Polyethylene by Reversible Deactivation Radical Copolymerisation of Ethylene with Renewably-Sourced Carbonate Monomers

Philip B. V. Scholten,[2] Antoine Debuigne, Michael A. R. Meier, Christophe Detrembleur

Unpublished

6.1. Abstract

Elusive ethylene copolymers bearing cyclic carbonate moieties are prepared for the first time. Two representative carbonate monomers, containing vinylic or allylic double bonds, were copolymerised with ethylene by organometallic-mediated radical polymerisation under mild experimental conditions. Notably, a $Co(acac)_2$ complex was used as the controlling agent which is also referred to as cobalt-mediated radical polymerisation (CMRP). Although additional experiments are required, preliminary investigations support the controlled nature of the polymerisation by the linear increase of the molecular weights with conversion. Molecular weights of up to 8,000 g mol^{-1} were obtained and no branching was detected as a result of the mild polymerisation temperature (40°C). The carbonate content was shown to be easily tuneable via the ethylene pressure during polymerisation ranging from 10 to 62 mol% for 500 and 10 bar, respectively, for the vinylic carbonate monomer which is the highest incorporation of such non-homopolymerisable monomers into ethylene copolymers ever reported by any polymerisation technique. Preliminary investigations for the allylic comonomer showed a less pronounced effect of the pressure on the comonomer content. Many chemoselective modification of the cyclic carbonate groups in the copolymers are expected to be possible and should give access to new functional polyethylenes.

[2] All experiments in this chapter were performed by P.B.V.S. with A.D. providing guidance during the writing of the chapter.

6.2. Introduction

Polyethylene is produced industrially *via* coordination-insertion polymerisation or free radical polymerisation (see Section 2.3), and constituted 30% of the European polymer market in 2017.[60] Modulation of its properties by introducing polar moieties into the backbone has enabled to drastically enlarge its range of applications.[331] Functional groups in commercial ethylene-based copolymers are mainly limited to carboxylic acids, ketones and esters that are introduced by free radical copolymerisation of ethylene with polar vinyl monomers,[201] eventually followed by chemical derivatisation (*e.g.* methanolysis of poly(ethylene-*co*-vinyl acetate) into poly(ethylene-*co*-vinyl alcohol)). Harsh reaction conditions are employed for their production, leading to ill-defined branched structures, and the introduction of the polar monomers over a broad composition spectrum is difficult.[332] Recent breakthroughs in reversible deactivation radical polymerisations (RDRP) have allowed to tune the comonomer incorporation over a large range (from 20 to 80 mol% for some comonomers), while at the same time controlling the polymers' molecular parameters and producing unprecedented functional ethylene-based copolymers.[5,7–9] This was made possible with less-activated polar monomers that bear an unconjugated double bond such as vinyl esters[5,7], vinyl ethers[9] or *N*-vinyl amides[7,9] (Scheme 24, previous work).[5,7–9] Expanding the monomer scope to cyclic carbonate-bearing monomers is highly attractive as the introduction of such polar functions would allow for further transformations of the cyclic carbonates into unique functional ethylene copolymers.

The versatility of such carbonate moieties is well established for the synthesis of polyurethanes and polycarbonates,[236,304–306] and has recently also been applied to polymers prepared by radical pathways.[269,315,316] Moreover, chemoselective transformations of the cyclic carbonate *via* catalysed amidations or hydrolysis are now possible for cyclic carbonate molecules[300,303] and for copolymers bearing cyclic carbonates as side groups.[269] An additional motivation is that some of these carbonate monomers bearing a double bond are easily accessible from renewable resources such as carbon dioxide[306,333] and/or plant oils.[98] Many of them are however characterized by a double bond which does not homopolymerise under radical conditions, and that is prone to transfer reactions, such as allylic monomers. Their copolymerisation with ethylene is therefore highly challenging and has never been reported.

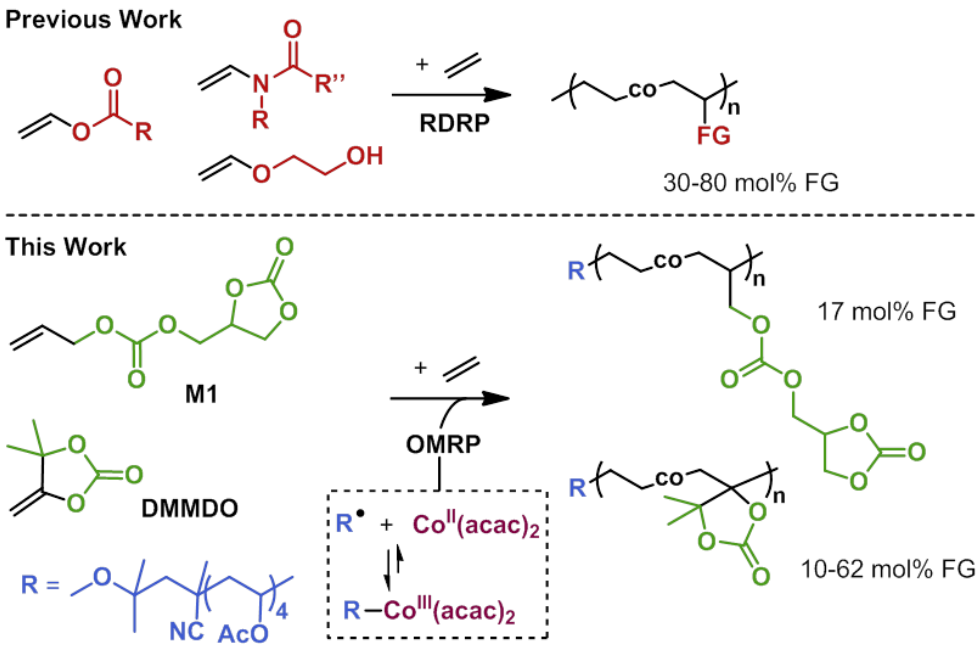

Scheme 24. Synthetic routes to functional polyethylene copolymers by reversible deactivation radical polymerisation (RDRP) previously reported[5,7–9] and the copolymerisation of ethylene with renewably-sourced carbonate monomers (**M1** and **DMMDO**) by organometallic-mediated radical polymerisation (OMRP) presented in this work.

Herein, we report the reversible deactivation radical polymerisation of ethylene (**E**) with two representative examples of these bio-sourced cyclic carbonate-bearing monomers (**M1** and **DMMDO**) over a broad comonomer content by using an organocobalt complex, R-Co(acac)$_2$, as the initiator and controlling agent (Scheme 24, this work). This organometallic-mediated radical polymerisation (OMRP) process was selected because of its activity with less-activated monomers (such as vinyl esters) under non-demanding conditions (*i.e.* 40 °C).[17] Such low temperatures are expected to disfavour side reactions, such as transfer reactions, that are commonly encountered during the polymerisation of ethylene[334] and allylic monomers.[284,335] Moreover these conditions effectively suppress the formation of defects (*i.e.* branches) which is advantageous for a controlled polymerisation. The downsides of such low temperatures are slow polymerisation kinetics and low yields. Under these conditions, monomers **M1** and **DMMDO** were previously shown to not be homopolymerisable but could be statistically copolymerized with vinyl acetate,[98,269,313,314] while only oligomers were obtained for the homopolymerisation of ethylene.[7] Copolymerisations were performed in a 30 mL autoclave and a variety of ethylene pressures, ranging from 10 to 500 bar, in dimethyl carbonate (DMC). DMC was chosen because of its low transfer to solvent constant which leads to higher molecular weights compared to other solvents.[336] This was confirmed for the copolymerisation of ethylene with DMMDO (Table 20). The materials used, the

polymerisation conditions, and the characterisations of the polymers are described in more detail in the section 10.5.

6.3. Copolymerisations of Ethylene with M1 and DMMDO using Cobalt-Mediated Radical Polymerisation

First, copolymerisations at 50 bar for 24 hours using free radical polymerisations initiated by V-70 and reversible deactivation radical polymerisation initiated by R-Co(acac)$_2$ were investigated at 40°C. The alkylcobalt complex allowed to increase the obtained yields for both **M1** and **DMMDO** (comparison of entries 1 and 2; 3 and 4, Table 21). Polymer P(**E**-*co*-**M1**) prepared by free radical polymerisation was not soluble in trichlorobenzene at 140 °C, and could suggest the occurance of radical transfer reactions during the polymerisation. Compared to previous ethylene copolymers prepared by OMRP with vinyl acetate or *N*-methyl vinyl acetamide at 50 bar and otherwise similar conditions,[7] the copolymers in this study contained a lower content of polar comonomer (17-22 mol% versus 46-50 mol%). This is a direct reflection of the incapability of homopolymerising these carbonate monomers: while an ethylene-based radical can self- and cross-propagate, **M1**- or **DMMDO**-based radical is unable to self-propagate, and leads to an overall more frequent addition of ethylene to the radical chain end and a lower comonomer content in the resulting copolymer.

Next, kinetic investigations of the copolymerisation of **M1** and **DMMDO** with ethylene at 40 °C and 50 bar of ethylene were performed. Aliquots were taken after 1, 2, 4, and 8 hours and analysed by size exclusion chromatography (SEC) in tetrahydrofuran (THF) to determine the molecular parameters of the copolymer and by ^{1}H NMR spectroscopy to determine the comonomer conversion. A linear increase of the number average molecular weights (M_n) with comonomer conversion was observed, in line with a controlled polymerisation, and the dispersities were low ($M_w/M_n < 1.50$; Figure 57a). Figure 57b shows that the SEC chromatograms are shifted towards the higher molar mass side during polymerisation. The small peak at 20 min corresponds to some deactivated R-Co(acac)$_2$ that was removed once the polymer was purified using supercritical CO_2 extraction (see Section 10.5).

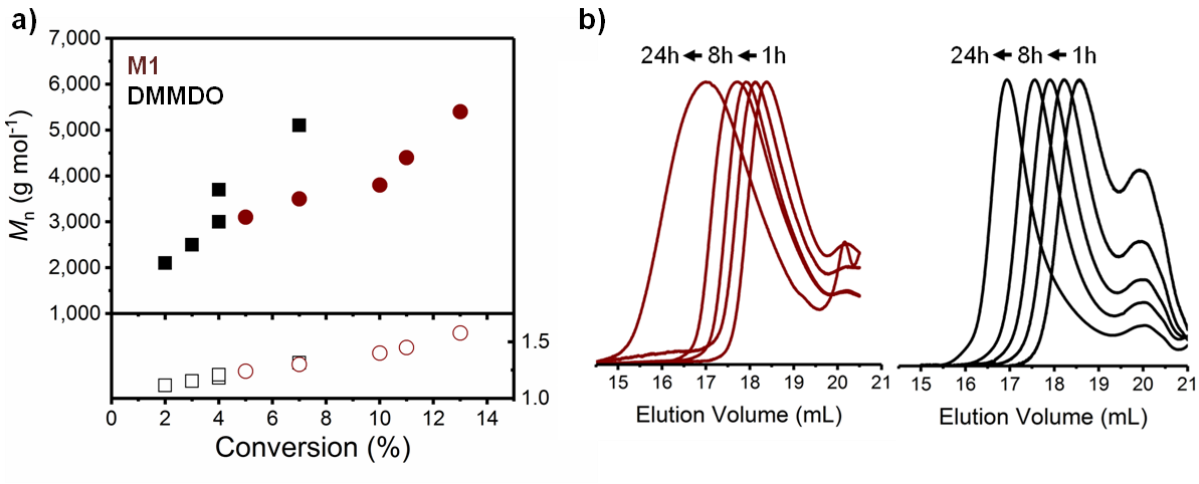

Figure 57. a) Plot of number average molecular weight (M_n) and copolymer dispersity against conversion at different times for the copolymerisation of ethylene with **M1** or **DMMDO** using R-Co(acac)$_2$ at 40 °C and 50 bar in DMC, and b) the corresponding size exclusion chromatography (SEC) curves measured at 45 °C in THF

Figure 58 depicts the ^{1}H and ^{13}C NMR spectra of P(**E**-*co*-**M1**) synthesised at 50 bar in DMC at 40 °C and quenched with TEMPO after 24 hours (entry 1, Table 3). The broad signals at 3.96 (**n**, **q, s**) and 4.4 ppm (**r**) correspond to the –CH$_2$– and –CH– groups of comonomer **M1** neighbour to the carbonate functionalities (Figure 58a). Signals characteristic of the initiator α-chain end were observed at 1.65 (**h**), 1.86 (**k**), 2.98 (**a**), and 4.84 ppm (**i**) while the intense peak at 1.18 ppm (**u**) originated from the –CH$_2$– of the ethylene repeat units. The weak signal at 0.76 ppm corresponds to the –CH$_3$ groups in the copolymer which stem from the TEMPO used to quench the reaction. In the ^{13}C NMR spectrum (Figure 58b), the signals at 37.9 (**m**), 66 (**q**, **s**), 72 (**n**), and 155 ppm (**t**, **o**) confirm the successful incorporation of the comonomer into the copolymer. Furthermore, peaks at 27 (**z**) and 31.5 ppm (**l**) highlight the ethylene-carbonate motif present in the polymer backbone. These assignments were supported by COSY and HSQC NMR analyses (Figure 111-Figure 112). Further NMR and FT-IR spectra, as well as the fully assigned spectra of P(**E**-*co*-**M2**) can be found in Figure 111-Figure 115). The structure of the ethylene copolymers were further analysed by ^{13}C NMR to probe for the presence of branches which are known to occur for free radical polymerisations as a result of the high temperatures used (150-375 °C).[334,337,338] Typical signals of the terminal carbon atoms in branches occur in the region of 5-15 ppm of a ^{13}C spectrum.[339] For the copolymers synthesised in this study, no peak was apparent in this region which indicated the absence of branches in the copolymer (Figure 58c and Figure 113) and stems from the low polymerisation temperature used, 40 °C. These findings are in line with previous literature reports on the copolymerisation of ethylene by OMRP.[7]

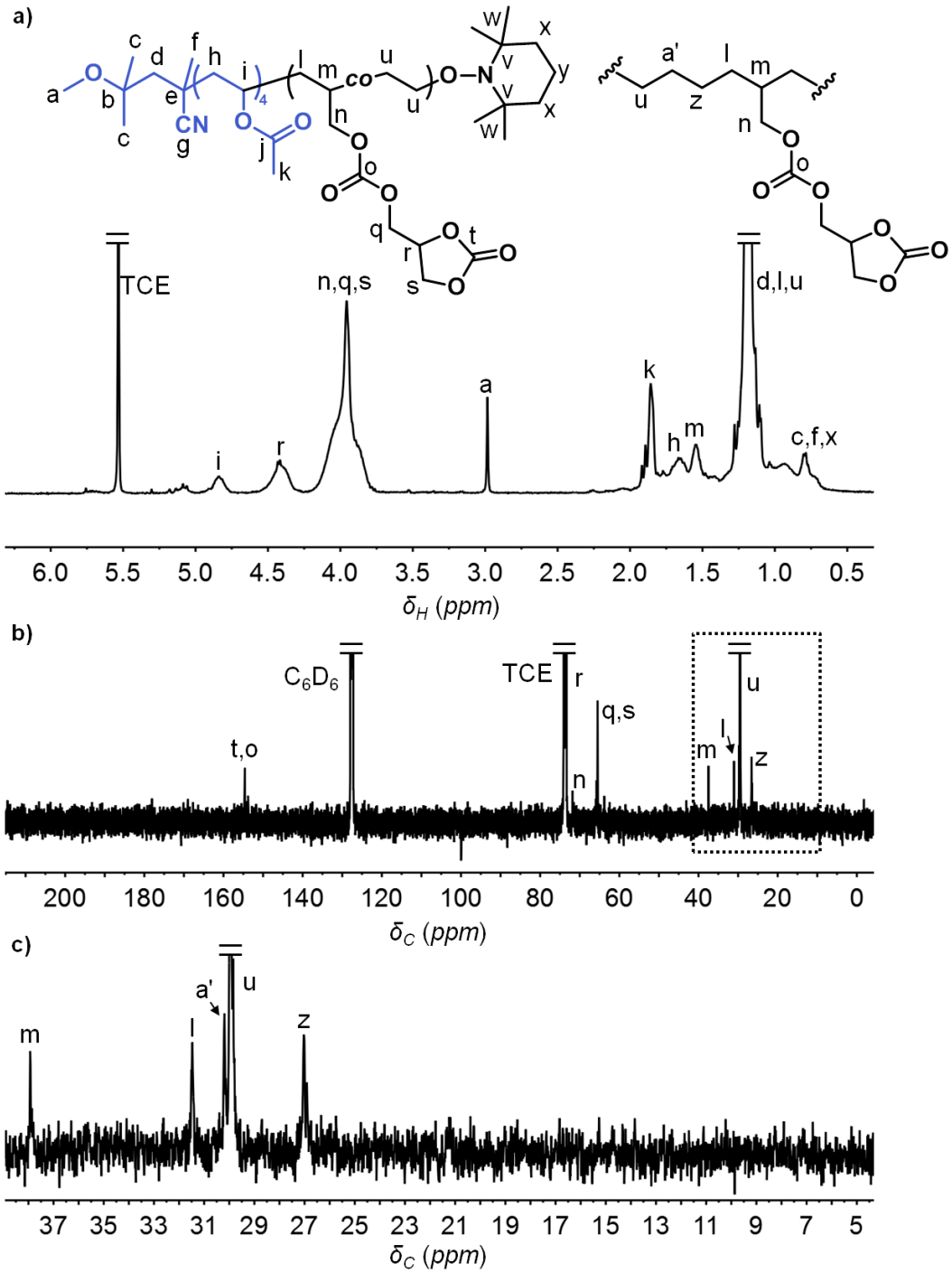

Figure 58. a) ^{1}H NMR spectrum, b) ^{13}C NMR spectrum, and c) inset of the ^{13}C NMR spectrum in the region around 20 ppm for P(**E**-*co*-**M1**) (entry 1, Table 3) taken in a 2:1 v/v mixture of tetrachloroethane (TCE):benzene (C_6D_6) on a 400 MHz spectrometer at 80 °C.

Table 3. Copolymerisations of ethylene with renewable monomers **M1** and **DMMDO** using R-Co(acac)$_2$ at 40 °C in dimethyl carbonate (DMC)

Entry	M	P [a] (bar)	Yield (mg)	X_M [b] (mol%)	M_n [c] (g mol^{-1})	M_w/M_n [c]	T_g [d] (°C)	T_m [e] (°C)	Cryst [e] (%)
1 [e]	**M1**	50	72	17 [f]	1,300	1.88	5	46	4.5
2 [e]	**M1**	500	86	16 [f]	3,900	1.50	3	108	9.6
3 [g]	**DMMDO**	10	67	62	1,000	1.46	27	-	-
4 [g]	**DMMDO**	25	163	34	1,500	1.63	17	-	-
5 [g]	**DMMDO**	50	224	22	5,400	1.66	2	47	5
6 [g]	**DMMDO**	500	162	10	8,300	1.40	n.o.	90	15

[a] Ethylene pressure (bar). [b] X_M = comonomer incorporation (mol%), determined by elemental analysis. [c] Determined using high temperature size-exclusion chromatography (HT-SEC) in trichlorobenzene (TCB) at 140 °C using a polystyrene standard. [d] T_g = glass transition temperature (°C), Cryst = copolymer crystallinity (%); determined by differential scanning calorimetry (DSC). Cryst = (ΔH_m measured/$\Delta H_{m\,\infty}$) × 100, where $\Delta H_{m\,\infty}$ = 293 J g^{-1}. [e] R-Co(acac)$_2$ = 0.025 mmol, M/R-Co(acac)$_2$ =100, 1.25 mL DMC, 40 °C, 500 rpm, 24 hours. [f] Determined by ^{1}H NMR spectroscopy in a 2:1 v/v mixture of TCE:C_6D_6 on a 400 MHz spectrometer at 80 °C using the α–chain end (see Section 10.5). [g] Conditions: R-Co(acac)$_2$ = 0.1 mmol, M/R-Co(acac)$_2$ =100, 5 mL DMC, 40 °C, 500 rpm, 24 hours. n.o. = not observable.

The influence of the ethylene pressure on the carbonate content for copolymers P(**E**-*co*-**M1**) and P(**E**-*co*-**DMMDO**) was then evaluated for pressures ranging from 10 to 500 bar (entries 1-6, Table 3). It should be noted that a 30 mL reactor was used for polymerisations at 10 to 50 bar while a 23 mL reactor was used for polymerisations at 500 bar of ethylene pressure. The comonomer content of the resulting copolymers was determined by ^{1}H NMR spectroscopy for **M1** copolymers and by elemental analysis for **DMMDO** copolymers. The composition of the latter copolymers could not be determined by ^{1}H NMR as the characteristic peaks of **DMMDO** overlapped with those of ethylene (see ^{1}H NMR spectrum Figure 113 in Section 10.5). For P(**E**-*co*-**M1**), no difference in comonomer content was observed for polymerisations performed at 50 and 500 bar of ethylene pressure (17 and 16 mol%, respectively; entries 1 and 2, Table 3). For P(**E**-*co*-**DMMDO**) on the other hand, an increase in ethylene pressure from 10 to 500 bar led to a drastic decrease in carbonate content from 62 mol% to 10 mol% (entries 3-6, Table 3). This decrease in carbonate content for P(E-*co*-M2) can be neatly followed *via* FT-IR spectroscopy, by comparing the relative intensities of the

stretching vibrations of the carbonate monomer (1,800 cm^{-1}, highlighted in green) and ethylene monomer (2,800 cm^{-1} highlighted in grey; Figure 59).

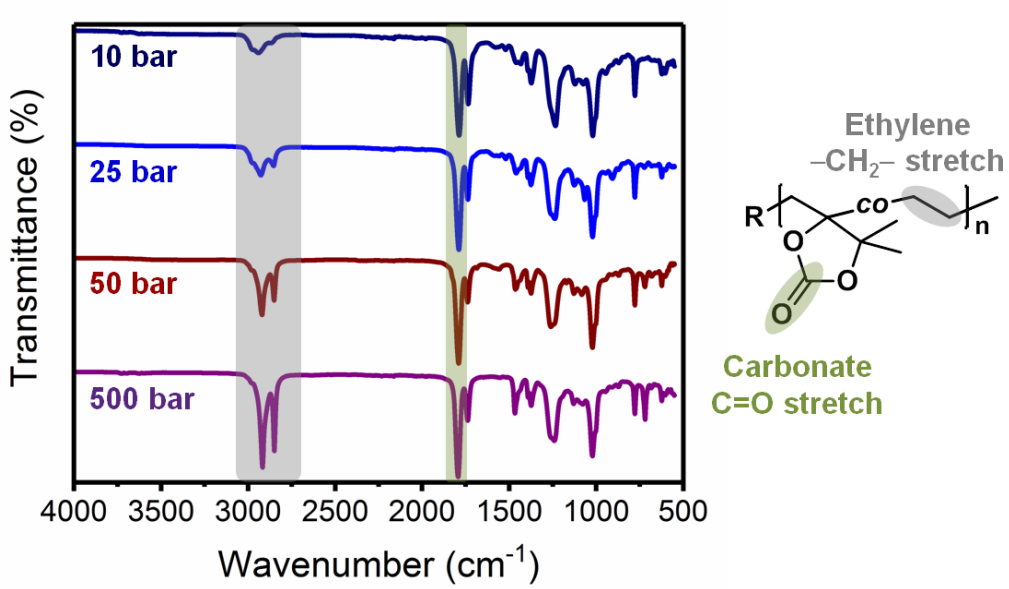

Figure 59. FT-IR spectra of P(E-*co*-**DMMDO**) synthesised at 10, 25, 50 and 500 bar using R-$Co(acac)_2$ (entries 3-6, Table 3). The characteristic C=O vibration of **DMMDO** are highlighted in green while –CH_2– vibrations characteristic of ethylene are highlighted in grey.

Increases in the polymerisation yield and the molecular weight of the copolymers with increasing ethylene pressure were also noted. A slight increase of the yield (from 72 to 86 mg) and M_n (from 1,300 to 3,000 g mol^{-1}) was noted for copolymer P(**E**-*co*-**M1**) going from 50 to 500 bar of ethylene pressure (entries 1 and 2, Table 3). For copolymer P(**E**-*co*-**DMMDO**) the yield more than doubled (from 67 to 162 mg) and the M_n increased from 1,000 to 8,300 g mol^{-1} going from 10 to 500 bar of ethylene pressure (entries 3-6, Table 3). These increases are closely related to the above discussion on chain end radical propagation for copolymers synthesised at 50 bar. For polymerisations at higher ethylene pressure, more ethylene is available in the reaction mixture and chain end radicals are more likely to add onto an ethylene monomer than at lower pressure and lead to longer ethylene segments between the non-homopolymerisable carbonate units. Conversely at low pressures, less ethylene is available during the polymerisation and the ethylene segments are shorter leading to lower molecular weight copolymers. It should be noted, that the P(**E**-*co*-**M1**) copolymer synthesised at 500 bar showed a slight shoulder at higher molecular weights (Figure 116), which hints at a loss of control over the chain growth process.

The thermal analysis of the copolymers by differential scanning calorimetry (DSC) showed a clear T_g for all copolymers synthesised below 500 bar (Table 3), confirming the statistical

incorporation of the polar monomer. The T_g was found to decrease with an increasing ethylene content for both copolymers, from 5 to 3 °C and from 27 to 2 °C for P(**E**-*co*-**M1**) and P(**E**-*co*-**DMMDO**), respectively. Copolymers synthesised at 50 and 500 bar ethylene presented a semi-crystalline behaviour as a result of their high ethylene content, above 80 mol% (entries 1-2 and 5-6, Table 3 and Figure 117). The melting temperatures of the synthesised copolymers were strongly reduced for a high incorporation of polar monomers, down to 46 °C (entries 1 and 5, Table 3), and were observed to be broad, *i.e.* over a large range of temperatures (Figure 117), which is analogous to previously reported ethylene copolymers containing polar comonomers.[340–343] As a result of this broad melting transition, a clear identification of a T_g was not possible for P(**E**-*co*-**DMMDO**) synthesised at 500 bar ethylene pressure (Figure 117b).

6.4. Conclusion

In conclusion, the successful copolymerisation of ethylene with two non-homopolymerisable carbonate-bearing vinyl monomers was achieved for the first time using cobalt-mediated radical polymerisation. The controlled chain growth process of such copolymerisations was established and by changing the pressure during the polymerisation, the incorporation of the vinylic and allylic carbonate monomers could be altered. The so-formed statistical ethylene copolymers are the first examples of ethylene copolymers containing cyclic carbonate pendants. Post-polymerisation modification of the carbonate moiety is expected to allow to synthesise a library of novel functional ethylene copolymers which are promising for a whole range of applications, such as coatings and blend compatibilisers. The preliminary investigations presented herein still need to be completed with further experiments probing the evolution of the comonomer content and the yield with time. Additionally, the chain-end fidelity of the copolymer, *i.e.* whether all chains are end-capped by the $Co(acac)_2$ complex, and thus "living", still needs to be addressed. Further copolymerisations of ethylene and **M1** still need to be performed in order to determine whether the comonomer content can be increased for lower ethylene pressure (10 and 25 bar) akin to **E**/**DMMDO** polymerisations. Moreover, the use of these ethylene copolymers, as well as the copolymers prepared in Chapters 4 and 5, for the compatibilisation of cellulose/LDPE composites is still pending.

7 Synthesis of Poly(Ethylene-*co*-Vinyl Acetate) Copolymers and Poly(Ethylene-*co*-Vinyl Acetate)-*b*-Poly(Ethylene) Block Copolymers for the Compatibilisation of Cellulose and Polyethylene

Philip B. V. Scholten,[3] Jérémy Demarteau, Antoine Debuigne, Jean-Michel Thomassin, Michael A. R. Meier, Christophe Detrembleur

Unpublished

[3] P.B.V.S. performed all experiments in this chapter. J.D and A.D guided in the polymer synthesis while J.-M.T. helped with the analysis of the data relating to the mechanical properties.

7.1. Introduction

As mentioned in Section 2.4, cellulose/LDPE composites are promising for their application as high strength materials. In order to avoid aggregation of the cellulose fibres within the matrix, the interfacial adhesion between cellulose and polyethylene needs to be ensured and many different strategies have been employed. The most versatile approach is the addition of a coupling agent or compatibiliser, which contains a hydrophilic as well as a hydrophobic segment and is thus able to interact (non-)covalently with both cellulose and the polyethylene matrix. Ideal candidates for such compatibilisers are polyethylene polymers bearing functional groups in its polymer chain. Polyethylene, or polyolefins in general, are most often functionalised by radical processes under harsh conditions, *e.g.* by grafting of maleic anhydride.[229,344–347] These modifications are often poorly controlled and cumbersome[201,230] and a direct incorporation of functional monomers during the polymerisation offers numerous advantages, especially for their use in composites.[228] Free radical polymerisations allow for the incorporation of a few polar monomers, such as acrylates and vinyl esters, as mentioned in Chapters 2.3 and 6. However, the synthesis of well-defined ethylene copolymers over a broad composition range and the synthesis of block copolymers in general is not possible by free radical means.[201] Up to date only reversible deactivation radical polymerisations (RDRP), namely reversible addition fragmentation (RAFT) polymerisation and organometallic-mediated radical polymerisation (OMRP), have at the same time allowed for a control over the radical chain growth process and a broad spectrum of comonomer incorporation (0-80 mol% of polar comonomer).[5,7–9] Particularly OMRP using a $Co(acac)_2$ complex as controlling agent enables the preparation of poly(ethylene-*co*-vinyl acetate) (EVA) copolymers and block copolymers under mild experimental conditions (40 °C, 10-50 bar of ethylene). This precise design of the copolymers allows to investigate the effect of molecular weight, comonomer content and copolymer architecture on their ability to disperse polar fillers in hydrophobic matrices.

Poly(ethylene-*co*-vinyl acetate) copolymers fulfil the role of a compatibiliser, as they combine a hydrophobic with a hydrophilic monomer. Unsurprisingly, EVA copolymers synthesised by free radical polymerisation have already been used successfully in the past for improving the mechanical properties of HDPE[348] as well as for the compatibilisation of cellulose fibres into HDPE.[349,350] Yet the samples used in these studies were limited in their vinyl acetate content, as they were synthesised by free radical polymerisation which allows a maximum of 50 mol% of vinyl acetate incorporation.

In this chapter, we report on the synthesis of a series of EVA statistical copolymers (Scheme 25a), with ethylene contents going from ethylene-rich to ethylene-poor, using a preformed alkylcobalt(III) bis(acetylacetonate) (R−Co(acac)$_2$) complex at 40 °C, where the alkyl chain acts as the radical initiator and Co(acac)$_2$ as the controlling agent (Scheme 25). Preliminary tests on the ability of such EVA copolymers to compatibilise cellulose/LDPE blends were performed and an increase in the Young modulus was observed compared to samples containing no EVA. Additionally, unprecedented P(EVA-*b*-E) block copolymers (Scheme 25b) containing more than 40 ethylene repeat units in the second block were synthesised from two EVA macroinitiators containing different amounts of ethylene. The effect of this block architecture on the dispersion of cellulose fibres is still pending, however previous block copolymers suggest that an enhancement of the mechanical properties is to be expected.[351]

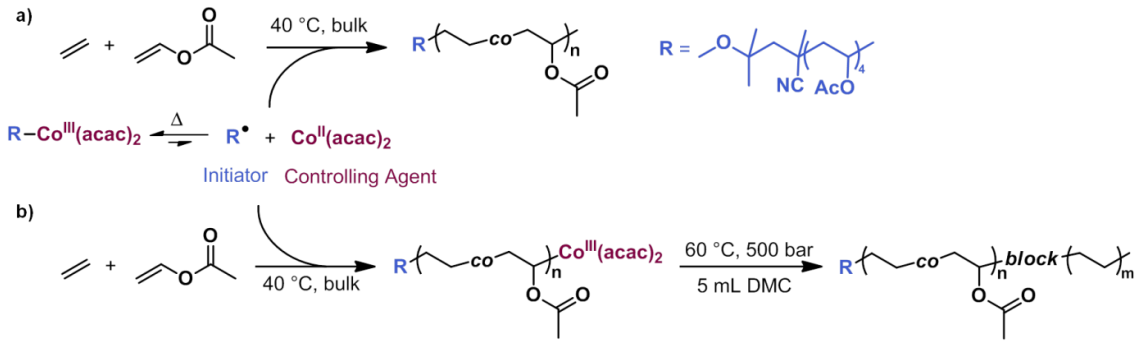

Scheme 25. Copolymerisation of ethylene and vinyl acetate to synthesise a) poly(ethylene-*co*-vinyl acetate) statistical copolymers and b) poly(ethylene-*co*-vinyl acetate)-*b*-poly(ethylene) block copolymers.

7.2. EVA Copolymer and Block Copolymer Synthesis

EVA copolymers were synthesised at 40 °C in the bulk using R-Co(acac)$_2$ as the initiator with the aim of synthesising copolymers with a degree of polymerisation (DP) of 100. To achieve this, different vinyl acetate to R-Co(acac)$_2$ ratios were used, 100 for 500 bar, 200 for 10 and 50 bar and 400 for 25 bar (Table 4), and the polymerisations stopped at VAc conversions which roughly corresponded to the wanted overall degree of polymerisation (DP ~100; entries 1-4, Table 4). Molecular weights of the obtained copolymers ranged from 5,500 to 9,400 g mol^{-1} and all showed low dispersities, < 1.43. The copolymer composition was determined by comparing the methoxy α-chain end, C$\underline{H_3}$O– at 3.15 ppm, with the characteristic signals of vinyl acetate, –C$\underline{H}$(OAc)– at 4.90 ppm, and ethylene, –C$\underline{H_2}$– at 1.16 ppm (see Section 10.6 for more details). Figure 60a shows the ^{1}H NMR spectra of copolymers obtained at 10 bar and 500 bar taken in $CDCl_3$ at room temperature and TCE:C_6D_6 at 80 °C, respectively. The copolymer synthesised at 500 bar was not soluble in $CDCl_3$ and thus high temperature NMR in high boiling solvents was performed (see Section 10.6 for more detail). The characteristic peaks of the initiator (grey), vinyl acetate (blue) and ethylene (red) are highlighted and neatly show the increasing ethylene content obtained for an increasing polymerisation pressure (Figure 60a). The increase in ethylene can also be neatly followed by the increasing absorbance at 2,800 cm^{-1} in the FT-IR spectra (Figure 60b). The variation of the pressure from 10 to 500 bar of ethylene allowed to increase the ethylene content in the copolymer from 20 mol% ethylene to 76 mol% ethylene, with intermediate compositions between these two pressures (entries 1-4, Table 4). Previous polymerisations by OMRP had only reported ethylene contents of up to 60 mol% at a pressure of 100 bar.[7,8] The thermal properties of the copolymers were analysed by differential scanning calorimetry (DSC). For an increasing ethylene content, a decrease in glass transition temperature was noted from 16 °C, for 22 mol% of ethylene, down to -23 °C, for 76 mol% of ethylene (Table 4). The difference in ethylene content has strong implications on the material properties of the copolymer, *e.g.* the glass transition temperature but also the copolymer polarity, which will most likely also influence their capability of compatibilising cellulose and polyethylene.

Table 4. Reaction conditions for the synthesis of EVA copolymers of different compositions, and their macromolecular characteristics and glass transition temperature [a]

Entry	E press. (bar)	Conv. (%)[b]	DP E/VAc[c]	% E[c]	$M_{n\ NMR}$ [c] (g mol^{-1})	$M_{n\ SEC}$ [d] (g mol^{-1})	M_w/M_n [d]	T_g [e] (°C)
1	10 [f]	30	12/47	20	4,300	5,500	1.12	16
2	25 [g]	11	79/42	35	8,000	9,400	1.25	14
3	50 [h]	16	39/36	52	4,200	7,700	1.24	-9
4	500 [i]	25	81/26	76 [j]	4,500	8,500	1.43	-23

[a] Conditions: 40 °C, 500 rpm, bulk. [b] Determined by ^{1}H-NMR spectroscopy in $CDCl_3$. [c] Composition of the copolymer and molecular weight determined by ^{1}H NMR spectroscopy in $CDCl_3$ based on the α-chain end (see section 10.6). [d] Determined by size-exclusion chromatography in THF at 45 °C using a PS standard. [e] Determined using differential scanning calorimetry. [f] VAc/R-Co(acac)$_2$ = 200, 9 hours. [g] VAc/R-Co(acac)$_2$ = 400, 5 hours. [h] VAc/R-Co(acac)$_2$ = 200, 7 hours. [i] VAc/R-Co(acac)$_2$ = 100, 24 hours. [j] Not soluble in $CDCl_3$, composition of the copolymer and molecular weight determined by ^{1}H NMR spectroscopy in a 2:1 mixture of TCE:C_6D_6 based on the α-chain end (see Section 10.6).

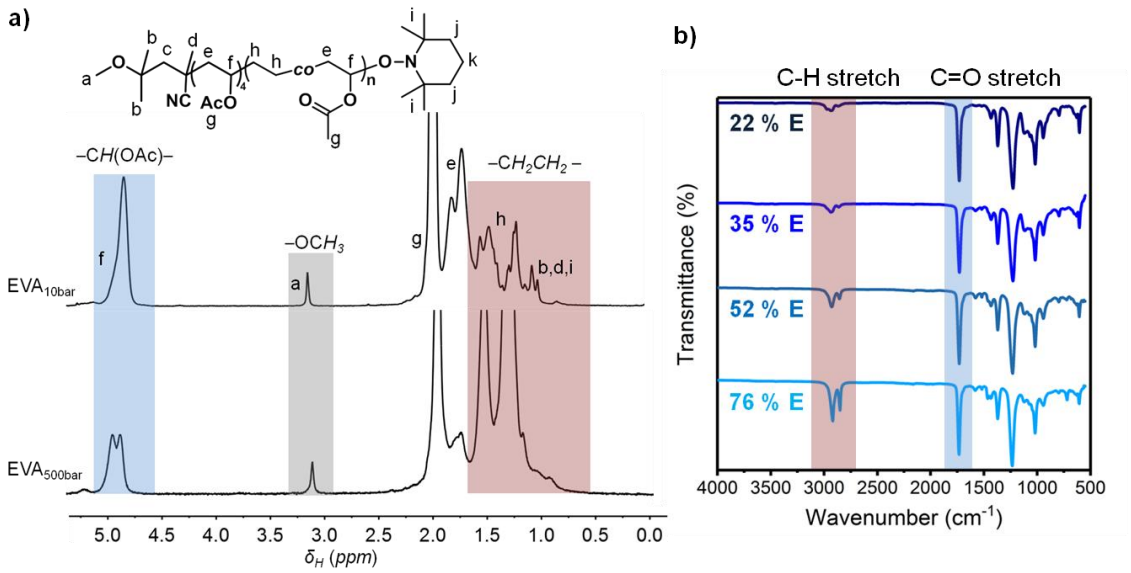

Figure 60. a) ^{1}H NMR spectra overlay of EVA synthesised at 10 and 500 bar, respectively, (entries 1 and 4, Table 4) and b) FT-IR spectra of EVA synthesised at 10, 25, 50 and 500 bar (entries 1-4, Table 4). In both images, the characteristic signals of vinyl acetate are highlighted in blue while those of ethylene are highlighted in red. The initiator fragment signal is also highlighted in grey for the NMR spectrum.

Table 5. Reaction conditions for the synthesis of EVA macroinitiators, and their macromolecular characteristics and glass transition temperature [a]

Entry	E press. (bar)	t (hrs)	Conv. (%) [b]	mol% E [c]	$M_{n\ NMR}$ [c] (g mol^{-1})	$M_{n\ SEC}$ [d] (g mol^{-1})	M_w/M_n [d]	T_g (°C) [e]
1 [f]	10	4	18	26	2,300	1,700	1.22	21
2 [g]	50	6	34	53	2,600	3,600	1.17	-3

[a] Conditions: M/R-Co(acac)$_2$ = 100, 40 °C, bulk, 500 rpm. [b] Determined by ^{1}H NMR spectroscopy in $CDCl_3$. [c] Copolymer composition and molecular weight based on the α-chain end (see experimental information) determined by ^{1}H NMR spectroscopy at 80 °C in a 2:1 mixture of TCE:C_6D_6 using a 400 MHz spectrometer. [d] Determined by size exclusion chromatograph in THF using a PS standard.[e] T_g = glass transition temperature (°C), determined by DSC. [f] R-Co(acac)$_2$ = 0.4 mmol. [g] R-Co(acac)$_2$ = 1.2 mmol.

For the synthesis of ethylene-based block copolymers (BCPs), two different EVA copolymers end-capped by Co(acac)$_2$ were synthesised using OMRP at 40 °C, one with 26 mol% of ethylene content, EVA$_{10bar}$-Co(acac)$_2$ (**1**), prepared at 10 bar, and the other with 47 mol% of ethylene content, EVA$_{50bar}$-Co(acac)$_2$ (**2;** entries 1 and 2, Table 5), prepared at 50 bar. After 4 and 6 hours, for **1** and **2** respectively, excess VAc was removed under vacuum at room temperature, and 0.9 g of the obtained sample were subsequently used as macroinitiator for the chain extension with ethylene, using conditions (60 °C, 500 bars of ethylene and 5 mL DMC as solvent) previously optimised in our group for the chain extension of PVAc-Co(acac)$_2$ with ethylene.[352] Dimethyl carbonate was the optimal solvent because it has the lowest transfer to solvent constant compared to dichloromethane or trichlorobenzene,[352] which had already been reported for free radical polymerisation of ethylene.[336] Reaction mixtures recovered from the EVA-Co(acac)$_2$ chain extensions showed signs of precipitates and the purified polymers were not soluble in regular solvents (*e.g.* THF, $CHCl_3$) at room temperature. Therefore high-temperature NMR (HT-NMR) spectroscopy in a mixture of deuterated tetrachloroethane (TCE) and deuterated benzene (C_6D_6) at 80 °C and high-temperature SEC (HT-SEC) analyses in trichlorobenzene (TCB) at 140 °C were performed to determine the molecular parameters (for further details see Section 10.6). For both macroinitiators, chain extension reactions were performed for 24 hours and a clear shift of the SEC curves to the higher molecular weight side was observed (Figure 61a). The successful block copolymer formation could also be witnessed in the FT-IR spectra, as the characteristic –CH_2– absorbance of ethylene at 2800 cm^{-1} was much more pronounced compared to the macroinitiator while the carbonyl absorbance of the vinyl acetate at 1750 cm^{-1} remained constant (Figure 61c). Furthermore, an increase in the intensity of the peak at 1.16 ppm, the ethylene –C*H*$_2$– environment, in the ^{1}H HT-NMR spectrum confirmed the successful addition

of ethylene monomers to the macroinitiator (Figure 61b). The composition of the block copolymers was analysed as for the EVA copolymers described above, and it was observed to be in the same range for both copolymers: 64 ethylene units for EVA_{10bar}-*b*-PE, and 59 ethylene units for EVA_{50bar}-*b*-PE (entries 1 and 2, Table 6). The difference in ethylene content of the two macroinitiators had almost no effect on the amount of ethylene units added to the polymer chain. By decreasing the polymerisation time from 24 to 4 hours when using EVA_{50bar}-$Co(acac)_2$ as the macroinitiator, the DP_E was decreased from 59 to 43 (comparison of entries 2 and 3, Table 6), suggesting a controlled process.

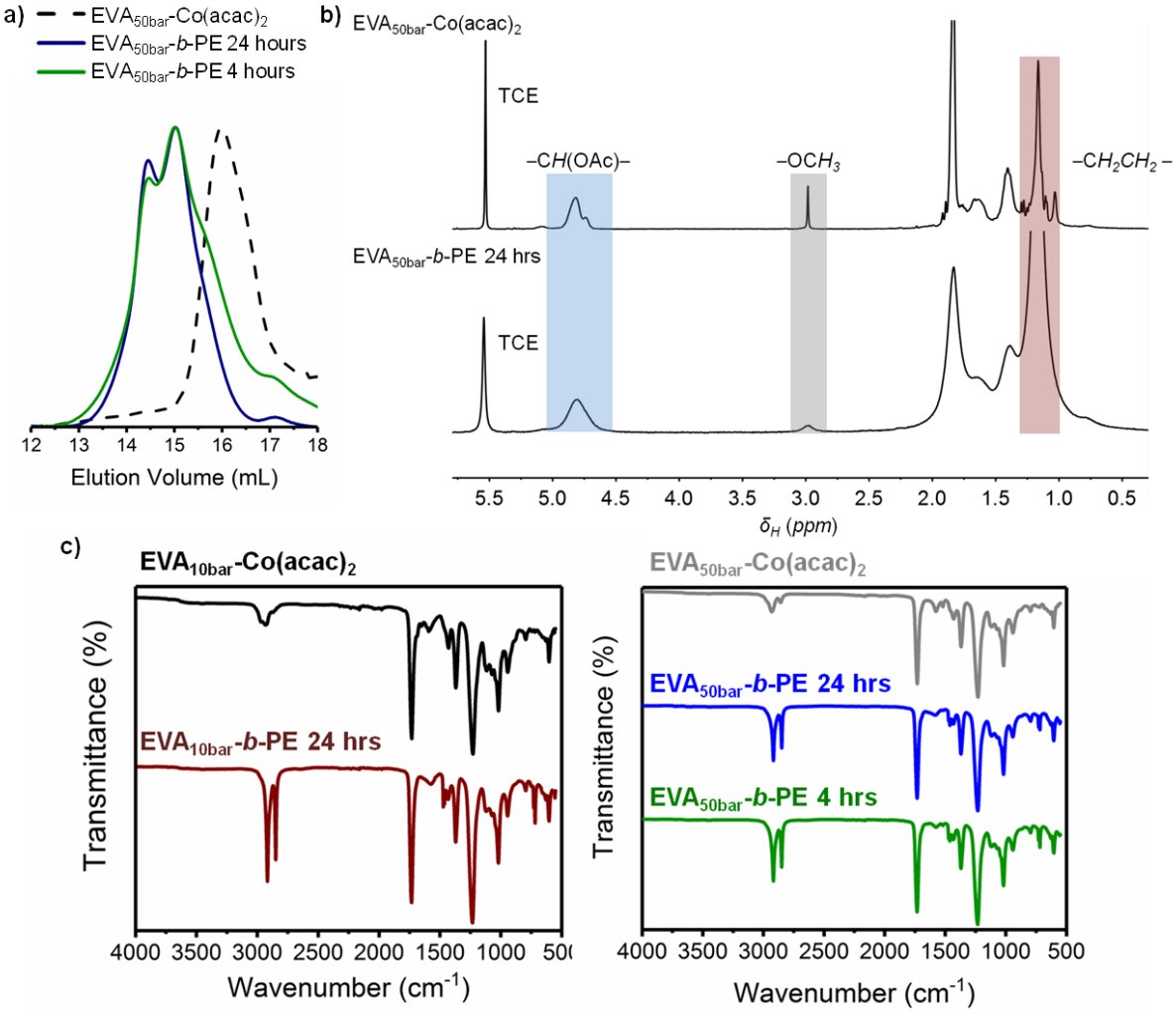

Figure 61. a) HT-SEC curves of the macroinitiator EVA-$Co(acac)_2$ and the EVA_{50bar}-*b*-PE block copolymer after 4 and 24 hours of block copolymerisation, b) ^1H HT-NMR spectra of the macroinitiator EVA_{50bar}-$Co(acac)_2$ and the block copolymer EVA_{50bar}-*b*-PE after 24 hours, and c) FT-IR spectra of the macroinitiators and different block copolymers synthesised in this study.

Table 6. Chain extension of EVA_{10bar}-$Co(acac)_2$ and EVA_{50bar}-$Co(acac)_2$ macroinitiators with ethylene at 60 °C[a]

BCP	1st block	Yield (mg)	$M_{n\ PE}$ (g mol^{-1})[b]	DP_E[b]	$M_{n\ Global}$ (g mol^{-1})[c]	$M_w/M_{n\ Global}$ (g mol^{-1})[c]	$M_{p\ 1}$ (g mol^{-1})[c] & $M_{p\ 2}$ (g mol^{-1})[c]
1	**1**	517	1,800	64	4,500	1.75	4,600 & 10,000
2	**2**	594	1,700	59	6,900	1.74	7,900 & 15,600
3[d]	**2**	493	1,200	43	4,600	1.74	8,000 & 11,200

[a] Conditions: 60 °C, 500 bar E pressure, 500 rpm, 24 hours.
1: EVA_{10bar}-$Co(acac)_2$, $M_{n,\ SEC}$ = 1,700 g mol^{-1}, M_w/M_n = 1.22, mol% E = 26;
2: EVA_{50bar}-$Co(acac)_2$, $M_{n,\ SEC}$ = 3,600 g mol^{-1}, M_w/M_n = 1.17, mol% E = 47.
[b] Molecular composition and molecular weight based on the α-chain end (see Section 10.6) determined by ^{1}H NMR spectroscopy in a 2:1 TCE/C_6D_6 solvent mixture on a 400 MHz spectrometer based. [c] Determined by high temperature size exclusion chromatography (HT-SEC) in trichlorobenzene at 90 °C using a PE standard. [d] Conditions: 60 °C, 500 bar E pressure, 500 rpm, 4 hours.

From the HT-SEC traces (Figure 61a), a bimodal distribution of the chains was observed for all block copolymers which was analogous to PVAc-*b*-PE samples previously synthesised in our group.[352] The origin of this bimodality is not yet well understood, but was most likely the result of coupling reactions occurring when the polymer becomes insoluble in the reaction medium and precipitates (Scheme 26). A similar phenomenon had already been reported for OMRP of VAc in supercritical carbon dioxide ($scCO_2$), where at a critical chain length, the polymer precipitated and coupled to give bimodal SEC curves.[353] Monomodal PVAcs were only obtained for polymers that were soluble in the reaction medium throughout the polymerisation. An estimate of the amount present in the sample was obtained by peak deconvolution of the SEC traces (Figure 61a) and a ratio of diblock EVA-*b*-PE to triblock EVA-*b*-PE-*b*-EVA of 3:1 was observed for EVA_{50bar}-*b*-PE samples. This led to a rather large overall dispersity of the copolymers, around 1.74, but by peak deconvolution, the separate peaks presented rather low dispersities, <1.35.

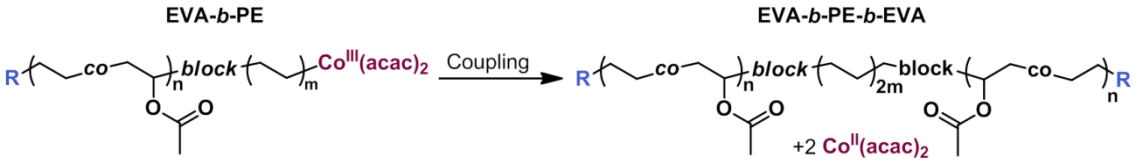

Scheme 26. Coupling reaction of EVA-*b*-PE diblock copolymers into EVA-*b*-PE-*b*-EVA triblock copolymers.

In terms of the thermal properties, all EVA-*b*-PE block copolymers clearly displayed both a glass transition temperature (T_g), originating from the first EVA block, and a melting temperature (T_m), originating from the second PE block (Figure 62), which further confirmed the block copolymer structure. Depending on the macroinitiator, the T_g was either at 19 °C or around 0 °C while the T_ms were between 101 and 111 °C, which is comparable to the T_m of commercial PE, 108-120 °C depending on the type of P(E).[338] Thus, EVA-*b*-PE block copolymers were synthesised using cobalt-mediated radical polymerisation for the first time. The use of such block copolymers for the compatibilisation of polar fillers in hydrophobic matrices appears particularly promising. Indeed, the EVA block is expected to interact with the polar filler and the PE block should favour the entanglement of the matrix with the compatibiliser and as a result improve the dispersion of the filler in the composite.

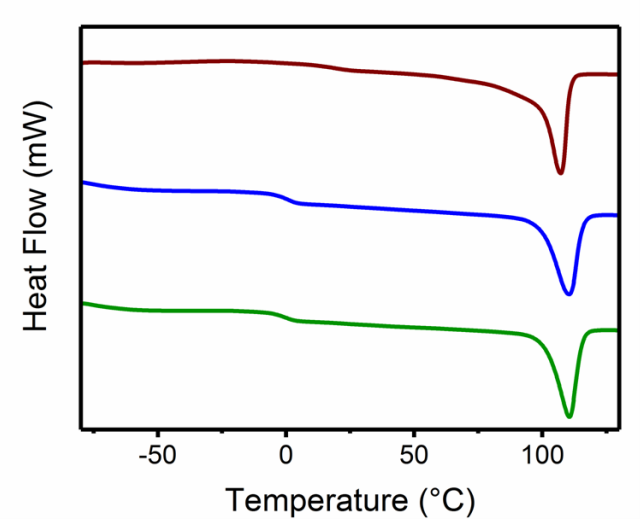

Block Copolymer	DP E	T_g (°C)	T_m (°C)	$Cryst_{PE}$ (%) [a]
EVA_{10bar}-*b*-PE 24 hrs	64	19	107	26
EVA_{50bar}-*b*-PE 24 hrs	59	1	111	14
EVA_{50bar}-*b*-PE 4 hrs	52	-1	101	17

[a] Crystallinity (%) = $\Delta H_{f\,measured}/\Delta H_{f\,\infty}) \times 100$; where $\Delta H_{f\,\infty}$ = 293 J g^{-1}; determined by DSC

Figure 62. Differential scanning calorimetry (DSC) curves and thermal properties of EVA-*b*-PE copolymers.

7.3. Compatibilisation of Cellulose and Polyethylene using EVA as Compatibiliser

In a preliminary study, the compatibilising capability of the above prepared EVA-based polymers was investigated for low density polyethylene (LDPE) and cellulose composites. The LDPE was kindly provided by INEOS Olefins & Polymers Europe while the cellulose was obtained by grinding Macherey-Nagel no. 1 filter paper. Composites were prepared using a twin screw extruder at 180 °C and 200 rpm for 10 minutes according to Table 7 and then hot pressed at 120 °C for further analysis. Two EVA samples, EVA_{50bar} synthesised at 50 bar and EVA_{500bar} synthesised at 500 bar (entries 3 and 4, Table 4), were used as compatibilisers for cellulose/LDPE composites. As outlined in the introduction, EVA copolymers enable interfacial interactions between the cellulose fibres and the LDPE matrix, leading to a higher Young's modulus.

Table 7. Composition of the composites prepared in this section

Entry	Sample Code	LDPE (wt %)	Cellulose (wt %)	EVA (wt %)
1	**C0EVA0**	100	0	0
2	**C5EVA0**	95	5	0
3	**C5EVA5**	90	5	5

Composites were analysed by stress-strain measurements and the addition of 5wt% cellulose to the LDPE matrix increased the Young's modulus by 154% relative to pure LDPE (comparison of samples C0EVA0 and C5EVA0; Figure 63). When 5 wt% EVA_{50bar} the Young's modulus of the composite (samples **$C5EVA_{50bar}$**) was similar to pure LDPE. Ethylene-poor EVA copolymer (EVA_{50bar}) had a negative effect on the composite, as its Young's modulus was lower than for when cellulose was added alone. This needs to be confirmed by control samples of just LDPE and EVA_{50bar}. In contrast, when a similar composite was formulated by using the ethylene-rich EVA_{500bar} (sample **$C5EVA_{500bar}$**), a drastic increase in the Young modulus by 247% compared to pure LDPE was observed (Figure 63). The difference between these two compatibilisers originates from their ethylene content and it appears that a higher ethylene content improved the composites Young's modulus. Pending rheological and microscopy experiments are needed in order to confirm whether this increase in Young's modulus goes hand in hand with an improved dispersion of the cellulose fibres within the matrix.

Maximum stress at break values of the composites were slightly reduced (from 9.5 to ~7.6 MPa, Table 8) while the elongation at break decreased to below 100% (Table 8), which is often observed for materials characterised by increased Young's moduli.

Table 8. Mechanical properties of pure LDPE, LDPE containing 5 wt% cellulose, and LDPE containing 5 wt% cellulose and 5 wt% EVA compatibiliser.

Sample Code	Young Modulus (MPa)	Maximum Stress (MPa)	Elongation at break (%)
C0EVA0	166 ± 2.7	9.2 ± 0.30	185 ± 35
C5EVA0	256 ± 23	9.5 ± 0.37	37 ± 1.7
C5EVA$_{50bar}$	167 ± 13	7.9 ± 0.21	77 ± 9.8
C5EVA$_{500bar}$	411 ± 70	7.4 ± 0.06	40 ± 2.9

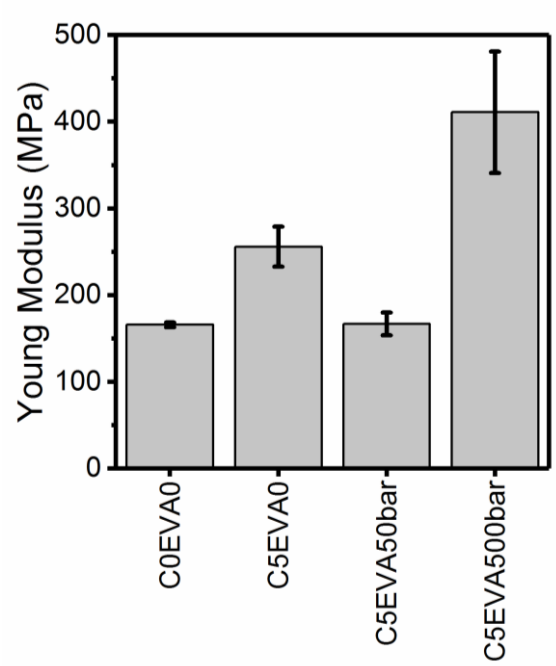

Figure 63. Young's moduli for pure LDPE (**C0EVA0**), LDPE with 5 wt% cellulose (**C5EVA0**) and samples with 5 wt% cellulose and 5 wt% EVA compatibiliser either synthesised at 50 (**C5EVA$_{50bar}$**) or 500 bar (**C0EVA$_{500bar}$**) of ethylene pressure.

7.4. Conclusion

In summary, statistical copolymers based on ethylene and vinyl acetate were successfully synthesised over a broad range of ethylene content (up to 76 mol% ethylene) using cobalt-mediated radical polymerisation. For the first time, block copolymers based on a EVA first block and a PE second block were prepared at a rather low temperature (60 °C). Bimodal molar mass distributions were however noted for these block copolymers, presumably as a result of some coupling reactions between insoluble growing EVA-*b*-PE chains. These side reactions provided mixtures of EVA-*b*-PE diblock and EVA-*b*-PE-*b*-EVA symmetrical triblock copolymers. This chain coupling is not well understood and further investigations are necessary to understand its exact mechanism. A preliminary investigation into the use of EVA copolymers as compatibilisers for cellulose/LDPE composites showed an important increase of the composites' Young's modulus for EVA copolymers that are rich in ethylene, highlighting the promise these copolymers hold for such applications. Yet further experiments are necessary to complete these results. Future investigations should vary the EVA molecular weight and test EVA-*b*-PE copolymers. Additionally, the presence of hydrolysable acetate groups in the copolymers allows for their hydrolysis into alcohol functions which are likely to alter the compatibilisers' interaction with cellulose and LDPE.

8 Rheological and Mechanical Properties of Cellulose/LDPE Composites using Sustainable and Fully Renewable Compatibilisers

Philip B. V. Scholten,[4] Begüm M. Özen, Zafer Söyler, Jean-Michel Thomassin, Manfred Wilhelm, Christophe Detrembleur, Michael A. R. Meier

Unpublished

8.1. Abstract

Cellulose composites with polyethylene permit to reinforce this commodity polymer, while at the same time introducing renewable content and thus minimizing the use of petroleum based feedstocks. The main challenge for such composites is the homogenous dispersion of cellulose fibres within the matrix. Herein, we report on two fully renewably sourced and sustainably synthesised compatibilisers based on amylose and starch, which allow for such cellulose dispersion in low-density polyethylene (LDPE). These compatibilisers advantageously combine the hydrophilicity of carbohydrates with the hydrophobicity of fatty acids. The cellulose fibres used in this study are obtained through the cheap and facile extraction of wood chips using acetic acid, improving the sustainability of these cellulose fibres compared to frequently used cellulose nanocrystals. Upon extrusion of cellulose, LDPE and the compatibilisers, a significantly improved dispersion of cellulose within LDPE was observed at loadings of 10 wt% cellulose and 5-15 wt% compatibiliser. Rheological investigations showed that the addition of 15 wt% modified amylose compatibiliser led to an 18-fold increase in the storage modulus of the composite compared to LDPE, while the addition of modified starch led to a lower improvement, a 10-fold increase. An improved interfacial adhesion was observed using scanning electron microscopy and the mechanical properties, notably the Young's modulus, improved as a result of the good stress transfer between filler and matrix material. This study highlights the potential of fully renewable compatibilisers for the preparation of composites of cellulose and the commodity plastic LDPE.

[4] All of the rheological measurements in this chapter were performed by B.M.Ö., while the preparation of the samples and the other analyses performed were performed by P.B.V.S. Guidance was provided by Z.S. during the preparation of the compatibilisers and for the mechanical analyses by J.-M.T. Prof. M.W. is the supervisor of B.M.Ö.

8.2. Introduction

As discussed in Section 2.4, cellulose fibers are an extremely attractive reinforcing filler for composite materials, as they are biodegradable, non-toxic and of extremely high strength.[210,212,213,354] The origin of cellulose and the type of its extraction from biomass play a key role in the determination of its final properties.[210,214–216] Especially crystalline nanocellulose (CNC) has been the focus of many studies in the past,[214,216,354,355] as CNCs have the highest strength possible for cellulose fibres as a result of their high crystallinity. However, the isolation of the crystals from the otherwise amorphous cellulosic material requires lengthy and expensive pre-treatments,[210,213,354–356] which make CNCs a value-added chemical with a current price of around 50€/kg.[213] Akin to the classical paper manufacturing, these nanocrystals are present as a salt and an aqueous dispersion of these CNCs is necessary to obtain isolated fibres, rendering their incorporation into hydrophobic matrices very difficult.[357,358] Thus, the extrusion of CNCs is extremely challenging, as special equipment is necessary to remove the water during the process, still hampering its industrial implementation.[212,359] A different type of cellulose fibre is therefore needed for an industrially feasible large scale production of cellulose composites and several other methods are being investigated.[213] A particularly promising example is bulk cellulose obtained as a side product from the production of lignin and other wood-derived chemicals *via* different pulping methods. For instance the acetosolv process results in cellulose fibres with a typical width below 20 μm and several hundred micrometers in length. The fibres are slightly acetylated and is in contrast to organsolv cellulose (extraction using ethanol or methanol) which mainly contains alcohol groups.[360] The acetosolv process is advantageous compared to organsolv processes, in that no high pressure equipment is needed for the extraction and that the bleeching of the cellulose can be performed directly after the end of the extraction.[360] Available as a side or waste product from an environmentally-friendly process, such fibres are more sustainable than CNCs and are thus a promising candidate for the production of reinforced composite materials.

Commodity plastics reinforced with cellulose are one of the main applications of cellulose and has been a main target for many researchers over the last decades.[210,212,213,217,354,361,362] The main objective, particularly for polyolefins (*e.g.*: polyethylene (PE)), is to increase the materials' strength with the added advantage of increasing the renewable content of the material. The major challenge for such composites of hydrophilic cellulose and hydrophobic polyolefins is the lack of compatibility between the two. The poor interfacial adhesion within the composite leads to very poor dispersion of the cellulose fibres, which tend to aggregate,

thus resulting in poor material properties. Different routes have been employed to defeat this problem, ranging from the use of grafting agents,[149,351,363,364] and reactive extrusion,[365,366] to the functionalisation of one or both components.[213,218,362,367–370] Among these, the use of compatibilisers or coupling agents is particularly attractive as these, often polymeric, molecules can be precisely synthesised and tuned in a controlled manner and the effects of the molecular structure on the dispersion of cellulose be closely investigated.

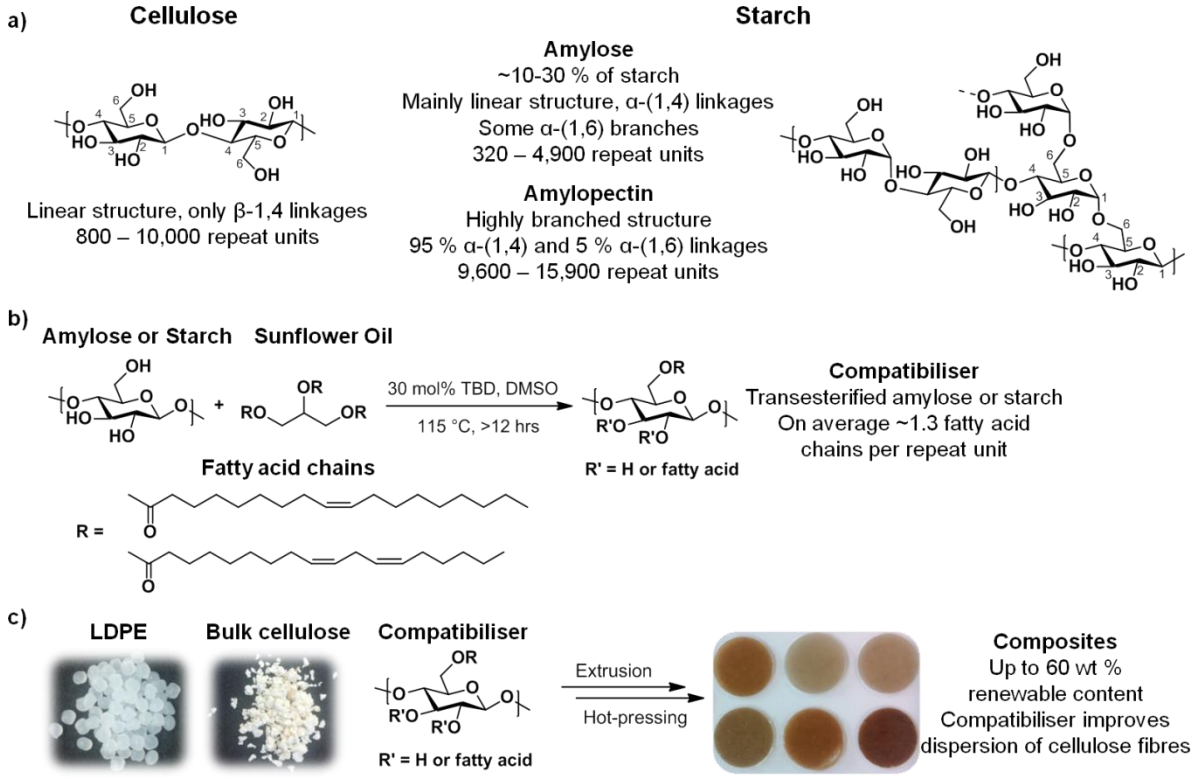

Scheme 27. a) Structures of cellulose and starch with key parameters of their structure, b) synthesis of amylose or starch based compatibiliser using high oleic sunflower oil,[371] and c) the preparation of composites using LDPE, bulk cellulose and the renewable compatibilisers prepared according to Meier *et al.*[371]

Herein we thus report on the use of new renewable compatibilisers for the preparation of cellulose-reinforced low-density polyethylene (LDPE) composites. These compatibilisers are based on starch and amylose, branched structural analogues of cellulose (Scheme 27a), which are transesterified using high oleic sunflower oil to attach fatty acid chains onto its hydroxy groups (Scheme 27b), as reported in a previous publication.[371] In this catalytic process, a processable polymeric material is obtained, combining the hydrophilicity of a glucose repeat unit with the hydrophobicity of a fatty acid chain. It is envisaged that these materials are able to interact with both cellulose and LDPE and allow for a compatibilisation of such cellulose/LDPE composites. Previous studies have shown that the acylation of cellulose with

fatty acids[372] and the use of epoxidised plant oils as compatibilisers[365] are effective strategies to improve the material properties of polyethylene. Furthermore, starch has been used to effectively reinforce polyolefin matrices in the past.[373–376] The cellulose/LDPE composites in this study were prepared using twin screw extrusion (Scheme 27c), which is industrially one of the most attractive methods of polyolefin processing. The efficacy of the compatibilisers was screened at a 10 wt% loading of cellulose using rheological analysis and microscopy, while the quest for composites containing up to 50 wt% renewable fraction was also investigated. Further insights into the dispersion of cellulose fibres within the composite and the material properties were obtained by scanning electron microscopy (SEM), stress-strain measurements and thermal analyses.

8.3. Preparation of Cellulose/LDPE Composites

In this study, the effect of two different compatibilisers, starch and amylose transesterified with high oleic sunflower oil (modified amylose (mA) and modified starch (mS), on the material properties of low-density polyethylene (LDPE) and cellulose (C; detailed analysis provided in Section 10.7) composites were investigated. As outlined in the introduction, cellulose was obtained from wood chips, while LDPE was donated from an industrial partner. Each compatibiliser was first tested at different loadings for 10 wt% cellulose (entries 2-4 and 6-7, Table 9) and then further at 45 wt% cellulose (entries 9 and 10, Table 9). The obtained results were compared to reference composites (entries 1, 5, and 8, Table 9). For the sake of clarity, the amount of LDPE is omitted in the sample names and samples are abbreviated as **C0mA/mS0** for **L90C0mA/mS0**, *etc*.

Table 9. Composition of the composites in wt % of a total of 5 g of sample

Entry	Sample code	LDPE (wt%)	Cellulose (wt%)	Compatibiliser (mA, A, mS or S)
1	**C0mA/mS0**	100	0	0
2	**C10mA/mS5**	85	10	5
3	**C10mA/mS10**	80	10	10
4	**C1mA/mS15**	75	10	15
5	**C0mA/mS10**	90	0	10
6	**C10mA/mS0**	90	10	0
7	**C10A/S10**	80	10	10
8	**C0A/S10**	90	0	10
9	**C45mA/mS10**	45	45	10
10	**C45mA/mS0**	55	45	0

LDPE: low-density polyethylene; mA: modified amylose; mS: modified starch; A: amylose; S: starch.

8.4. Rheological Properties of the Composites

The suitability of PE composite materials for various applications strongly depends on their processability.[377] Particularly the viscoelastic properties, amount of viscous (fluid-like) behaviour quantitied by $G''(\omega_1)$ versus elastic (solid-like) behaviour quantitied by $G'(\omega_1)$, and the thermal stability of the composites are important parameters and depend on the filler concentration and the extent of filler/matrix interaction. Rheology permits to measure these properties and allows to probe the microstructure of the composites giving insights into the state of cellulose dispersion within the matrix.[370,378] The viscoelastic behaviour can be investigated by measuring the storage modulus $G'(\omega_1, \gamma_0, T, t)$ (elastic contribution) and the loss modulus $G''(\omega_1, \gamma_0, T, t)$ (viscous contribution) during oscillatory shear measurements, in which the excitation frequency (ω_1), strain amplitude (γ_0), temperature (T), and time (t) are varied independently.[378] The linear viscoelastic region of the composites was determined by dynamic strain sweep measurements (Figure 120), measuring $G'(\gamma)$ as a function of strain amplitude ($\gamma_0\ (t)$) for all samples 150 °C. The samples showed a linear viscoelastic region until $\gamma_0 = 10\%$, except for the highest content of cellulose (**C45mA/mS10**), for which linear viscoelastic behaviours up to $\gamma_0 = 4\%$ were noted (Figure 120). In the linear viscoelastic

regime, G' is independent of applied strain and only depends on the microstructure at that temperature. Above this critical strain (γ), G' becomes dependent on the rate and magnitude of applied strain and is more complex.

Next, the samples were heated to 150 and 170 °C at an angular frequency of $\omega_1 = 1$ rad/s for one hour to determine their thermal stability in the linear viscoelastic regime (Figure 121-Figure 122). Samples exhibited a stable $G'(t)$ for both temperatures, indicative of the absence of degradation, except for samples with 45 wt% cellulose (**C45mA10/S10** and **C45mA0/S0**). For all samples containing 45 wt% cellulose, a decrease in $G'(t)$ was observed over the one hour period. This decrease was approximately 10% for **C45mA10** and **C45mS10**, and above 15% for C45mA0/S0 at both temperatures (Figure 121). This phenomenon is not well understood but possibly results from the loss of residual water in the cellulose fibres. Further investigations are needed to ascertain this hypothesis.

Once the thermal stability of the composites up to 170 °C was ensured for 10 wt% cellulose composites, the effect of the addition of cellulose and compatibiliser on the linear flow properties of the composites was studied by dynamic frequency sweep tests (Figure 64), in which the storage modulus ($G'(\omega_1)$) is obtained as a function of angular frequency (ω_1) at reference temperature (T_{ref}) 150 °C using the Time-Temperature-Superposition (TTS) principle. In this kind of test, an increase of $G'(\omega_1)$ at low ω_1 is an indication of the dispersion of the filler within the matrix as the $G'(\omega_1)$ only depends on the microstrucre of the composite at that temperature. Moreover, the appearance of a plateau signifies the breach of the percolation threshold. Above this threshold, the filler, in this case cellulose fibres, forms an interconnected network through a space filling dispersion of the fibres within the matrix and improves the material properties through stress transfer from the matrix (low strength) to the filler (high strength).

These tests showed that the addition of 10 wt% of cellulose to LDPE (**C10mA0** and **C10mS0**) led to no enhancement of the storage modulus compared to LDPE (comparison of violet hexagons with black triangles, Figure 64). Most likely the fibres formed agglomerates within the matrix and the addition of compatibiliser is needed to break these cellulose clusters and ensure their dispersion. The effect of the addition of 10 wt% of compatibiliser (without cellulose) on the rheological properties of the LDPE matrix was then investigated (Figure 64). While the addition of modified or unmodified amylose to the LDPE matrix showed no significant changes in G' (Figure 64), slight changes for starch were observed. For modified starch a 25% increase in G' at $\omega_1 \geq 10$ rad/s and a 90% G' increase at $\omega_1 \leq 1$ rad/s at 150 °C were observed while for non-modified starch a 10% decrease in G' at $\omega_1 \geq 10$ rad/s and 60%

increase in G' at $\omega_1 \leq 1$ rad/s at 150 °C were observed (Figure 64). These differences in G' are very minor compared to the expected improvements once both cellulose and compatibiliser are added.

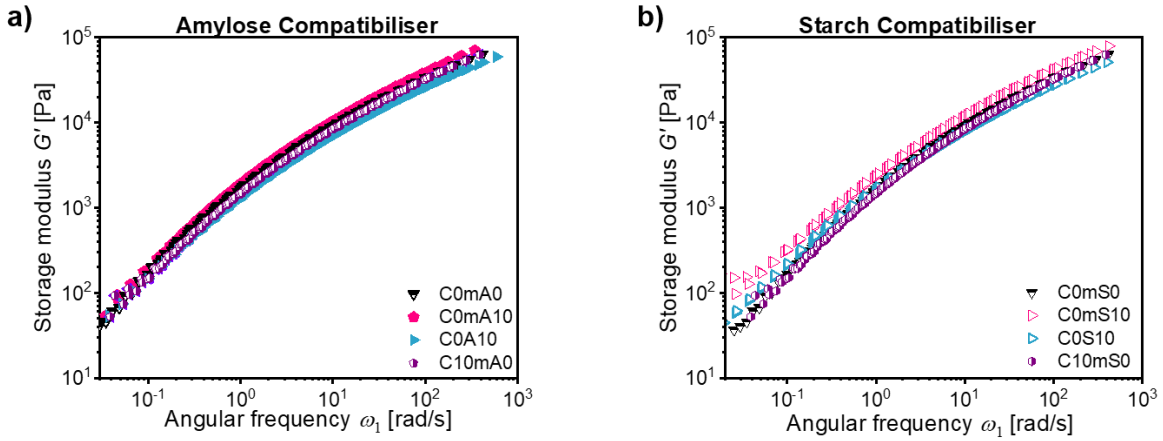

Figure 64. Storage modulus $G'(\omega_1)$ as a function of angular frequency (ω_1) at T_{ref} = 150 °C was plotted *via* TTS for pure LDPE, LDPE containing 10 wt% cellulose (**C10mA/S0**) and composites containing 10 wt% of a) modified amylose (mA) or non-modified amylose (A) and b) modified starch (mS) and non-modified starch (S).

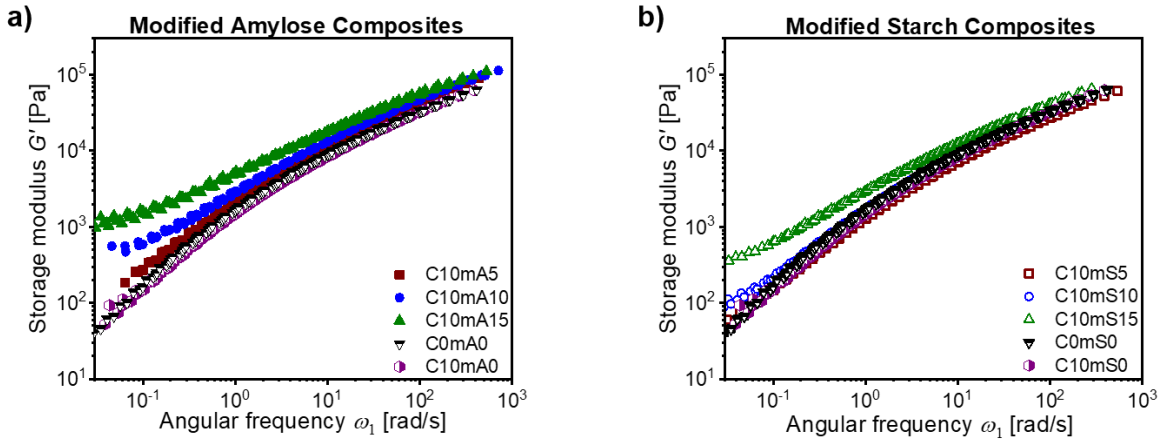

Figure 65. Storage modulus $G'(\omega_1)$ as a function of angular frequency ω_1 at T_{ref} = 150 °C as obtained *via* TTS for pure LDPE and for composites containing 10 wt% cellulose (C) with 5-15 wt% of a) modified amylose (mA) and b) modified starch (mS).

Next, the effect of the compatibiliser (5 to 15 wt%) in the presence of cellulose (10 wt%) was investigated using the same TTS principle at 150 °C. The storage modulus (G') increased successively with an increasing amount of compatibiliser (brown 5 wt%, blue 10 wt%, and green 15 wt%, Figure 65). At high frequencies (ω_1>10 rad/s), G' was almost 200% higher for **C10mA15** and 30 % higher for **C10mS15** compared to **C0mA0**. Furthermore, the appearance of a plateau of G' was noted at low frequencies (ω_1<10 rad/s) for **C10mA10**, **C10mA15** and

C10mS15 (blue and green symbols in Figure 65). The plateau indicated a space filling dispersion of the cellulose fibres within the matrix. The otherwise agglomerated cellulose fibres formed an interconnected network within the matrix,[377] able to dissipate applied stresses much better within the material, increasing the storage modulus. The formation of such a network is only possible for non-agglomerated cellulose fibres, *i.e.* fibres which have an improved interfacial adhesion with the hydrophobic matrix. This is a direct reflection of the addition of the amphiphilic compatibilisers, which are able to provide interfacial interactions between the two materials.

It is worth highlighting that the plateau was significantly more pronounced for samples containing modified amylose (**C10mA10** versus **C10mS15**), indicating a better compatibilising ability of the modified amylose compared to its modified starch analogue. This can be further emphasized by comparing in G' at $\omega_1 = 0.04$ rad/s of samples C10mA15 and **C10mS15**, which was almost two times higher for amylose and constituted a 18-fold increase compared to pure LDPE. One possible explanation for the better performance of the modified amylose compatibiliser is that the linear structure of amylose (Scheme 27a) was advantageous in the dispersion of cellulose in LDPE as it was able to enrobe the cellulose fibres more effectively, while starch, mainly composed of branched amylopectin (Scheme 27a), was not able to adhere to the fibres surface as effectively.

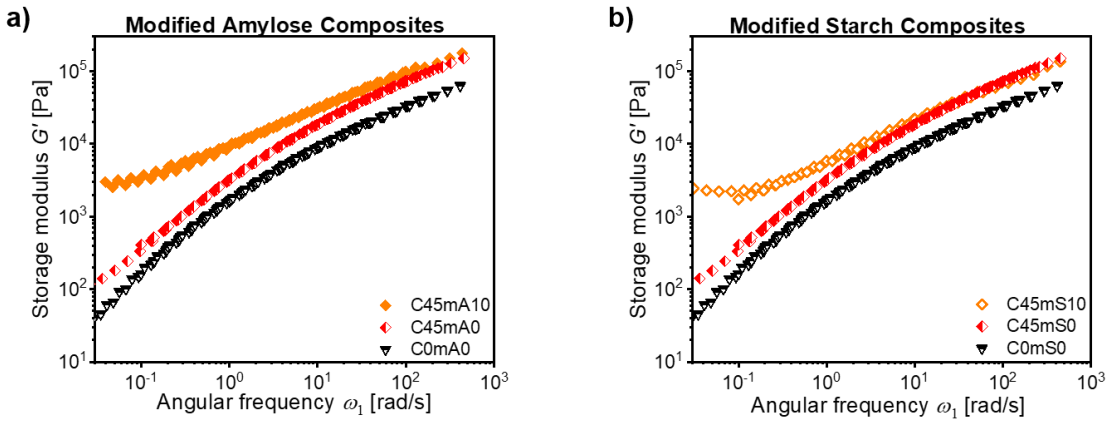

Figure 66. Storage modulus $G'(\omega_1)$ as a function of angular frequency ω_1 at T_{ref} = 150 °C as obtained *via* TTS for pure LDPE and for composites containing 45 wt% cellulose (C) and 10 wt% of a) modified amylose(mA) and b) modified starch (mS).

Moreover, increasing the amount of cellulose to 45 wt% without compatibiliser (**C45mA/mS0**) and with 10 wt% compatibiliser (**C45mA/mS10**) were investigated (Figure 3). Although a two-fold increase in $G'(\omega_1)$ was obtained in the absence of compatibiliser, no plateau was observed for these samples (red symbols, Figure 66). Upon the addition of 10

wt% compatibiliser (**C45mA/mS10**), a 49-fold increase in G' for **C45mA10** and a 38-fold increase in G' for **C45mA10** were noted at $\omega_1 = 0.04$ rad/s and a pronounced plateau at low frequencies was observed. These results confirmed that the addition of compatibiliser to the composite (**C45mA/mS10**) effectively improved the dispersion of the cellulose, compared to a simple mixture of LDPE and cellulose (**C45mA/mS10**), increasing the G' of the sample.

8.5. Scanning Electron Microscopy Analysis of the Composites

To get a different perspective of the dispersion of the cellulose fibres within the LDPE matrix, SEM images were taken. A difference in the cellulose dispersion can be seen when comparing samples with 45 wt% cellulose (**C45mA/mS10** versus **C45mA/mS0**). In the absence of compatibiliser, pull-out phenomena and large voids were observed between the fibre and the matrix (Figure 67c). Samples with compatibiliser (**C45mA/mS10**) on the other hand showed enrobed cellulose fibres as well as a better adhesion of the polymer matrix with the cellulose fibres (Figure 67d and e). This indicated that the modified amylose and modified starch successfully increased the adhesion of the cellulose fibres within the matrix, which allowed for an improved dispersion of the cellulose fibres within the LDPE matrix as observed by rheology. Unfortunately, no net difference can be observed in images for samples containing less cellulose, as no distinction between fibres, matrix and compatibiliser could be made. Further investigations using transmission electron microscopy (TEM) also led to no clarification because of the semi-crystalline nature of the matrix, which gave rise to fuzzy regions in TEM pictures and the different components could again not be clearly identified.

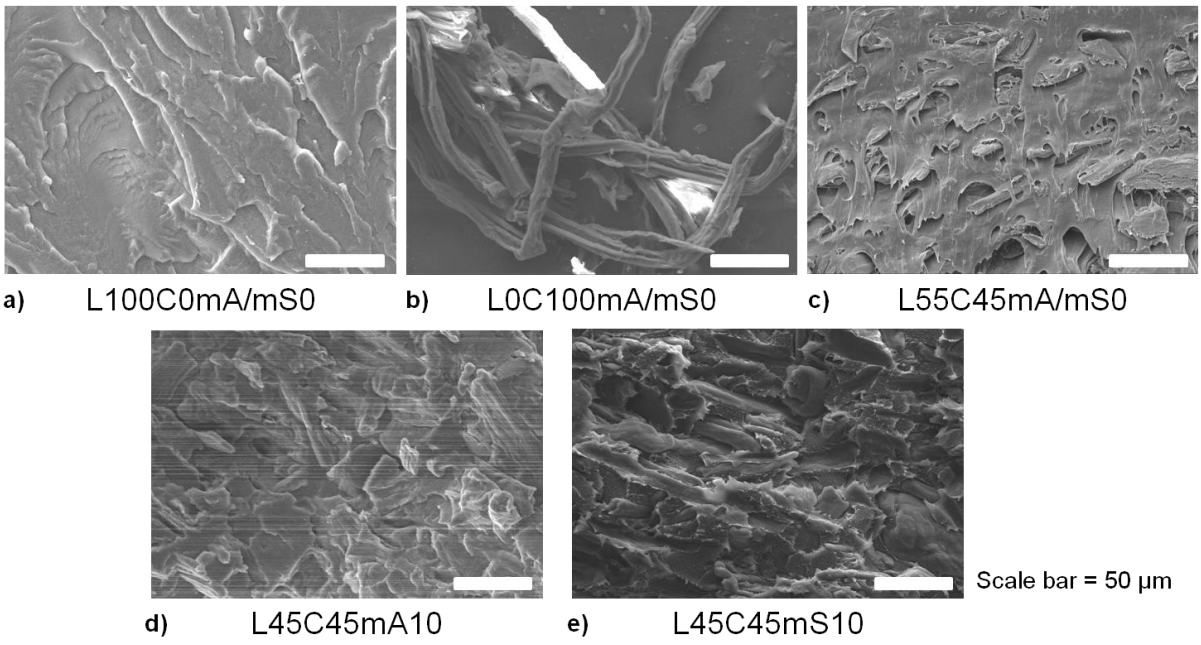

Figure 67. Scanning electron microscopy (SEM) images of a) pure LDPE (**C0mA/mS0**), b) pure cellulose (**C100mA/mS0**), c) composite **C45mA/mS0**, d) composite **C45mA10**, and e) composite **C45mS10**.

8.6. Thermal Properties of the Composites

The TGA analysis of the samples showed that the decomposition of the sample occurred in two steps. First, from 300 °C onwards, the cellulose and compatibiliser decomposed, followed by LDPE above 450 °C (Figure 68). The weight loss of the sample corresponds to the composition of the sample, for example the weight of sample **C10mA/mS5** decreased by 15 wt% up until 450 °C, which corresponds to the content in cellulose (10 wt%) and compatibiliser (5 wt%) (brown line in Figure 68). An overall decrease in thermal stability was expected due to the lower thermal stability of cellulose. In the DSC curves, no change in the T_m compared to extruded LDPE was observed, apart from the effect of dilution in the enthalpy of melting (ΔH_m) (Figure 123).

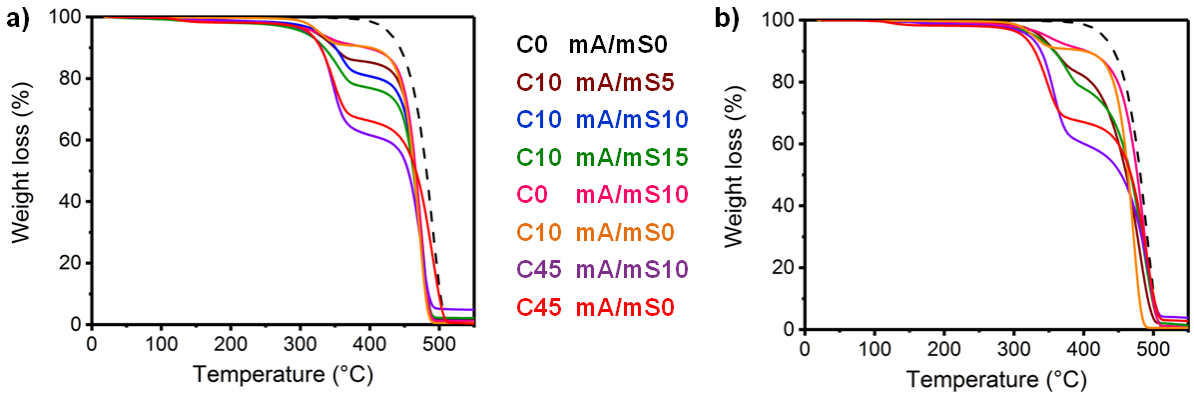

Figure 68. Thermogravimetric (TGA) curves of composites using a) modified amylose and b) modified starch compatibilisers and their respective reference samples

8.7. Mechanical Properties of the Composites

Once the successful dispersion of the cellulose fibres was demonstrated, the mechanical properties of the composites in the solid state were investigated by elongation stress-strain measurements (Table 22). The main interest in adding cellulose fibres to a polymer matrix is to increase its Young's modulus and thus increase its strength. First, the effect of the compatibiliser on the Young's modulus of LDPE was investigated. Unfortunately, they had a negative effect on the Young's moduli, decreasing their value from 166 MPa (**C0mA/mS0**) to 123 MPa and 112 MPa for modified amylose (**C0mA10**) and modified starch (**C0mS10**), respectively (entries 1, 5 and 12, Table 22; Figure 69), which is similar to a previous report on the addition of vegetable oils to HDPE.[365] The addition of cellulose to the matrix without compatibiliser slightly increased the Young's modulus to 218 MPa (entries 6 and 13, Table 22), corresponding to an increase of 31% relative to pure LDPE (166 MPa, entry 1, Table 22). Interestingly, in the presence of both cellulose and modified amylose (C10mA5-15, Figure 69) the relative increase of the Young's modulus is much larger. The largest relative increase (57%) was observed for the composite containing 10 wt% of modified amylose (261 MPa vs 123 MPa, **C10mA10**, entry 3, Table 22). Even though the rheological analyses showed that the cellulose was dispersed to an even better extent at 15 wt% compatibiliser loading (**C10mA15**), the Young's modulus dropped (202 MPa, entry 4, Table 22) as a result of the softening effect of the compatibiliser. Nonetheless, the Young's modulus was still improved for **C10mA15** compared to pure LDPE and a careful balance between the degree of cellulose dispersion and the Young's modulus needs to be found related to the type of application targeted .

Compared to the composites containing modified amylose, the addition of modified starch had a less significant impact on the Young's moduli. A maximum relative increase of 20%

was observed for 5 wt% compatibiliser (**C10mS5**) and the addition of more compatibiliser led to a decrease down to 140 MPa (**C10mS15**). This softening effect of the compatibiliser on the matrix material was more pronounced compared to modified amylose. Overall, these results support the rheological findings, which demonstrated that modified amylose led to a better cellulose dispersion compared to its starch analogues.

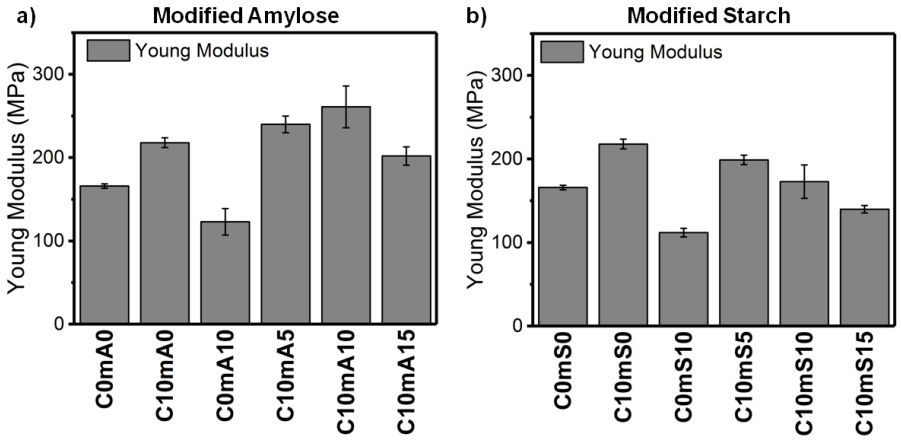

Figure 69. Young moduli for composites with a) modified amylose and b) modified starch as compatibiliser and their respective reference samples

In all samples, a severe impact of the addition of cellulose on the elongation at break was observed, as values decreased from 185 % to below 60% (Table 22). This is not unexpected, as a strengthening of the material (*i.e.* the Young's modulus) often triggers a decrease in its plastic elasticity leading to a more brittle material.

8.8. Conclusion

The preparation of LDPE composites using bulk cellulose fibres was shown to be possible using plant-oil and starch based compatibilisers synthesised in a sustainable fashion. A clear improvement in the cellulose dispersion within the polymer matrix was observed using rheology and could be confirmed by SEM. Modified amylose showed a higher capacity to compatibilise cellulose within the LDPE matrix as a plateau in the storage modulus was observed at both 10 and 15 wt% compatibiliser loading with 10 wt% cellulose (**C10mA10-15**). This was also reflected by a relative increase of 57% (**C10mA10**) in terms of the Young's modulus. Modified starch, on the other hand, gave rise to a poorer dispersion of the cellulose and as a result the composites' mechanical properties were not improved significantly, a relative increase of only 20% in the Young's modulus for **C10mS5**. In both cases, a softening effect of the compatibiliser was noted, the origin of which is not yet clearly understood. Nonetheless, this study highlights the promise of renewable compatibilisers for the preparation of reinforced polyolefin matrices using bulk cellulose fillers.

9 General Conclusions and Perspectives

Renewable feedstocks present a practicably inexhaustible source of molecules for chemistry and material science. In light of global warming and fossil fuel depletion, more and more examples of polymers based on renewable resources can be found both in academic and industrial settings. Radical polymerisations present one of the most successful polymerisation techniques for the synthesis of commodity plastics, yet relatively few polymerisations of renewable monomers can be found for this technique compared to, for example, step-growth polymerisations. A particular challenge remaining up to date is the non-activated character of the double bonds, which leads to the formation of non-stabilised radicals during the polymerisation and rapid termination or side reactions. Recent developments in the polymerisation of such less activated monomers by reversible deactivation radical polymerisation (RDRP) have given access to unprecedented copolymers and copolymer structures. The main objective of this thesis was thus the identification and sustainable synthesis of renewable monomers for RDRP, namely organometallic-mediated radical polymerisation (OMRP), to precisely design novel functional polymers (Scheme 28). Moreover, the application of such polymers and other renewable polymers as compatibilisers for composites of cellulose and low-density polyethylene was investigated (Scheme 28).

In Chapter 4 of this thesis, five entirely renewable monomers bearing allylic and olefinic double bonds were synthesised in a sustainable fashion from plant oils. These double bonds, very prone to transfer reactions, were statistically copolymerised with vinyl acetate by OMRP to yield renewable copolymers bearing polar functionalities such as esters and carbonates. This synthetic strategy, combined with the sustainable polymer purification by supercritical CO_2 extraction, provides a blueprint for the synthesis of a whole library of renewable polymers by RDRP, which were previously unattainable. Furthermore, a green and sustainable alternative to the frequently used functionalisation of renewable molecules with acrylate double bonds is established. The versatility of carbonate bearing polymers was then highlighted for a vinyl acetate copolymer containing a CO_2-based comonomer (Chapter 5). By a careful choice of hydrolysis conditions, two functional copolymer structures were obtained: either poly(vinyl alcohol)s bearing butane-diol units or poly(vinyl alcohol)s bearing cyclic carbonate units (Scheme 28). While the former led to a highly water-soluble poly(vinyl alcohol)-based copolymer, the latter copolymer was functionalised with amines to give rise to hydroxyurethane units pending off the polymer backbone with promising applications as coatings and surfactants.

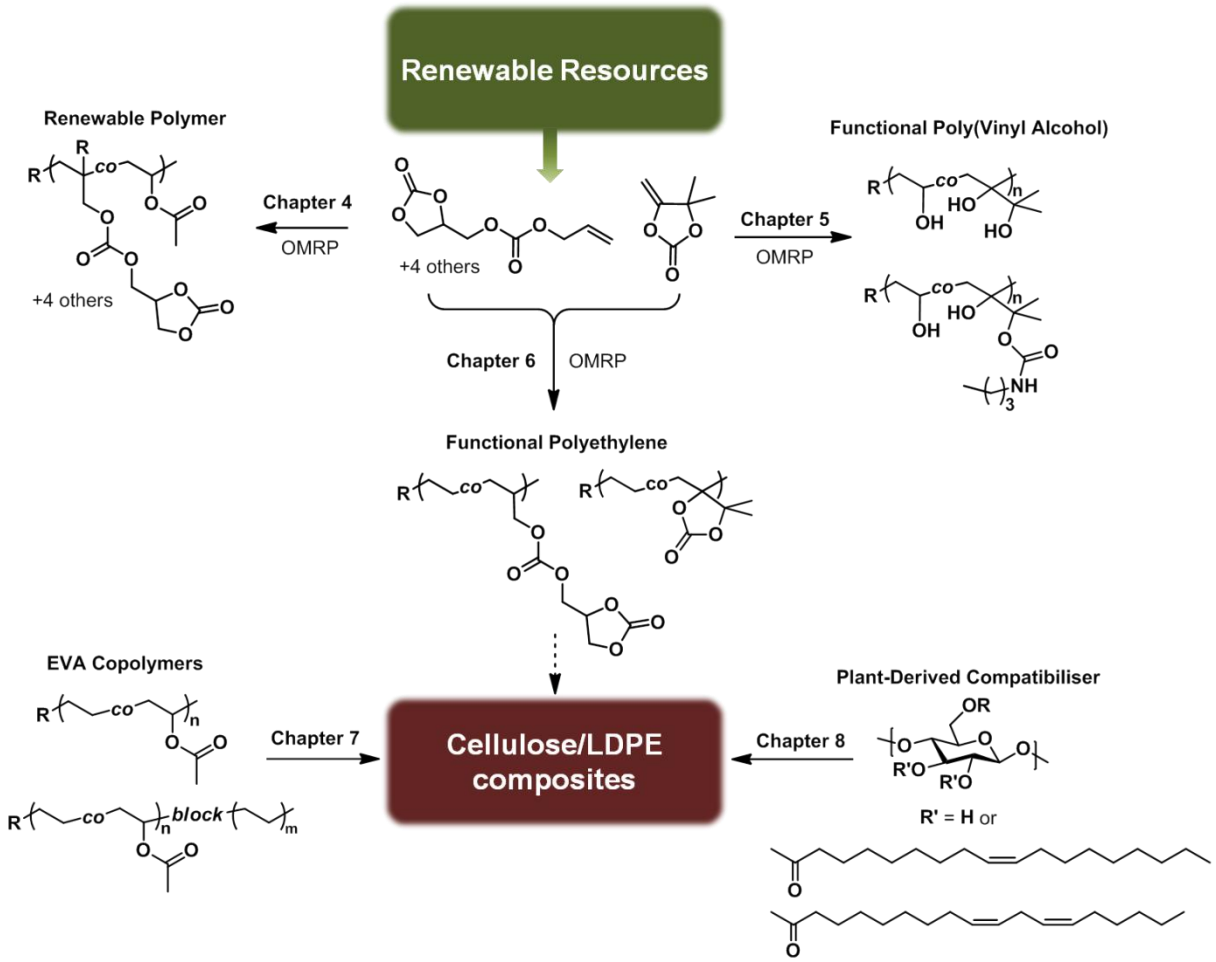

Scheme 28. Organometallic-mediated radical polymerisation of renewable monomers into renewable and functional polymers. These precisely designed copolymers and other fully renewably-sourced polymers have promising applications as compatibilisers in cellulose/low-density polyethylene composites.

Up to date, a major limitation of (reversible deactivation) radical polymerisations has been the incorporation of polar monomers into polyethylene. In Chapter 6, this shortcoming is addressed by synthesising polyethylene copolymers containing the previously addressed renewable carbonate monomers by OMRP. A range of comonomer incorporation was possible by simply changing the ethylene working pressure giving rise to copolymers containing between 10 and 62 mol% carbonate monomer with molecular weights of up to 8,300 g mol^{-1}. Although preliminary, kinetic experiments highlighted the controlled chain growth process for such copolymerisations while the highly linear nature of these polyethylene copolymers was established. Even though further studies are still needed, these amphiphilic copolymers are promising for their use as compatibilisers in cellulose/polyolefin composites.

In the last part of this thesis, the use of precisely-designed ethylene/vinyl acetate (EVA) copolymers (Chapter 7) and sustainably synthesised plant-based polymers (Chapter 8) were investigated for the dispersion of cellulose within low-density polyethylene (LDPE).

One of the main advantages of RDRP techniques, compared to classical free radical polymerisations, is the close control over the molecular parameters. This allows for the detailed examination of the performance of copolymers for a given application, here for the comptabilisation of cellulose/polymer blends. With this in mind, EVA copolymers were synthesised by OMRP at different ethylene pressures (10-500 bar), which allowed to tune the comonomer content from 80 mol% (ethylene-poor) to 20 mol% (ethylene-rich) (Chapter 7). Moreover, EVA-*b*-PE copolymers were synthesised for the first time and PE blocks of up to 64 units corresponding to a molecular weight of 1,800 g mol^{-1} were obtained. Further studies are necessary to determine the origin of the bimodal molar mass distributions noted in the size exclusion chromatography analyses. Preliminary results showed an increase in mechanical properties of cellulose/LDPE composites through the addition of EVA statistical copolymers. It appeared that the ethylene content of the copolymer is a key parameter for the successful compatibilisation. Further improvements can be expected for the EVA-*b*-PE copolymers, see perspectives below. A more in depth examination of fully renewable starch- and sunflower oil-based compatibilisers for cellulose/LDPE composites was performed in Chapter 8. By means of rheology, an improved dispersion of the cellulose fibres was observed for composites with compatibiliser while tensile stress measurements showed a slight increase of the materials strength. Yet, at high compatibiliser loadings, a softening effect on the composites was observed which is not fully understood yet. This is one of the first examples of a sustainable and fully renewably-based compatibiliser.

Overall, the synthesis of renewable monomers for RDRP guided by sustainability and principles of Green Chemistry opened up novel routes to renewable and functional polymers. In terms of polymerisation kinetics and behaviour, further investigations are necessary to fully understand the copolymerisation of allylic monomers with less-activated monomers, such as vinyl acetate and ethylene. These insights will be essential for the precision design of other novel (renewable) polymers based on non-activated allylic double bonds. Especially for ethylene copolymerisations, the chain-end fidelity, *i.e.* whether the polymer chain-ends bear the $Co(acac)_2$ complex, is of outmost importance to establish whether the complex is truly able to reversibly deactivate the chain-end radical and thus allow for a controlled radical chain growth. These tests along with copolymerisations of ethylene and the allylic carbonate monomer (**M1**) at 10 and 25 bar of ethylene are ongoing.

As demonstrated by the post-polymerisation functionalisation of the carbonate moieties, the incorporation of carbonate monomers is a unique tool to access a multitude of copolymers from one single copolymerisation. Yet improvements are necessary to attain quantitative yields *via* catalytic reactions under mild reaction conditions. Moreover, expanding the types of possible functionalisations for such carbonate moieties is extremely interesting for the synthesis of further functional copolymers.

Promising preliminary results were obtained for EVA-based compatibilisers for cellulose/LDPE composites and further improvements are expected for EVA-*b*-PE copolymers, as the PE block could allow for an entanglement with the polyethylene matrix. For this, the elucidation of the bimodality of these block copolymers is necessary to be able to differentiate between the effect of each copolymer parameter on the composites performance.

Finally, alterations of the renewable compatibiliser are needed to identify the origin of their negative effect on the mechanical properties of the composites. Additionally, hydrogenations of the fatty acid chains might lead to a better interaction of the compatibiliser with the LDPE matrix.

This work paves the way towards a sustainable exploitation of renewable resources and their polymerisation into precisely-designed functional polymers with applications in composites of cellulose and commodity plastics.

10 Experimental Part

10.1. Materials

Vinyl acetate (VAc, >99%, Aldrich) was dried over CaH_2, degassed by several freeze-pump-thaw cycles, distilled and stored at -20 °C. Dichloromethane (CH_2Cl_2), *N*-butylamine (99.5% , Aldrich), and *N*,*N*-dimethylformamide (DMF, >99%, VWR) were degassed and dried over 4 Å molecular sieves. Alkyl cobalt(III) adduct ([$Co(acac)_2$(-$CH(OCOCH_3)CH_2)_{<4}$-R_0] with R_0 being the primary radical generated by V-70) was prepared according to a previous literature report and stored at -20 °C in CH_2Cl_2.[30] Glycerol (99%, Aldrich), dimethyl carbonate (DMC, ≥99%, Merck), allyl alcohol (98+%, Alfa Aesar), 1,5,7-triazabicyclo[4.4.0]dec-5-ene (TBD, 98%, Aldrich), 10-undecenoic acid (98%, Aldrich), sodium bicarbonate (≥99.7%, Aldrich), sodium chloride (99.5%, Acros), sodium sulphate (99+%, Acros), methanol (MeOH, 99.8%, VWR), cyclohexane (100%, VWR), ethyl acetate (EtOAc, 99.8%, VWR), silica gel for column chromatography (SiO_2, 60 Å, ROCC S.A.), thin layer chromatography cards (TLC, VWR), 3 and 4 Å molecular sieves (Sigma-Aldrich), 2,2'-azobis(4-methoxy-2,4-dimethylvaleronitrile) (V-70, Wako Pure Chemicals), 2,2,6,6-Tetramethyl-1-piperidinyloxy (TEMPO, 98%, Aldrich), triethylamine (NEt_3, ≥99%, Aldrich), zinc iodide (≥98%, Sigma), carbon dioxide (CO_2, ≥99.7%, AirLiquide), Ethylene (**E**; N35, 99.95%, AirLiquide), sodium hydroxide (NaOH, ≥97%, Acros), fuming hydrochloric acid (HCl, 37% solution, Acros), 1-propanethiol (99%, Aldrich), 1 kDa pre-treated regenerated cellulose tubing (Spectrum Laboratories, Inc.), silica gel for column chromatography (60 Å, ROCC S.A.), tetrahydrofuran (THF, ≥99.9%, VWR), methanol (MeOH, ≥99.8%, VWR), *n*-pentane (>99.6%, VWR), diethyl ether (VWR, Et_2O), dimethylsulfoxide (DMSO, ≥99.9%, VWR), deuterated dimethylsulfoxide (DMSO-d_6, ≥99.8%, Euriso-top), deuterium oxide (D_2O, ≥99.9% Euriso-top), deuterated acetone (acetone-d_6, ≥99.8 %, Euriso-top), 1,1,2,2-tetra-chloroethane-d_2 (TCE; ≥99%, euriso-top), benzene-d_6 (C_6D_6; ≥99%, euriso-top), and chloroform-*d* ($CDCl_3$, >99%, Euriso-top) were used as received.

For Chapter 6, dimethylcarbonate (DMC; ≥99%, Merck), dichloromethane (DCM; 99.8%, VWR) and 1,2,4-trichlorobenzene (TCB; >99%, Aldrich) were degassed and dried over molecular sieves prior to use.

All polymerisations were performed under an inert atmosphere using Schlenk techniques.

LDPE was kindly provided by INEOS Polymers & Olefins Europe and had the following characteristics: density: 920 kg/m^3; melt index MI2.16: 8.5 g/10min; molecular weight: M_n = 17,300 g mol^{-1}, M_w = 126,000 g mol^{-1}; melting temperature (T_m): 107 °C; crystallinity: 44%. The crytallinity was calculated by using the enthalpy of melting measured

by differential scanning calorimetry (DSC): Cryst = (ΔH_m measured/$\Delta H_{m\,\infty}$) × 100, where $\Delta H_{m\,\infty}$ = 293 J g^{-1}, the enthalpy of melting for 100% crystalline PE.[379]

The cellulose pulp was obtained by pulping of European beech wood (*Fagus sylvatica L.*) using acetic acid followed by hydrogen peroxide (30 %w/w in H_2O, Aldrich) bleaching. Cellulose characterisation is provided below (Figure 118-Figure 119). The transesterified amylose or starch used in Chapter 8 were prepared according to a recent publication by Meier *et al.*[371] using high oleic sunflower oil provided by Cargill and maize starch purchased in a local supermarket. Cellulose, starch and amylose (Aldrich) were dried at 100 °C in a vacuum oven overnight prior to use. 1,5,7-Triazabicyclo[4.4.0]dec-5-ene (TBD; 98%, Aldrich) and dimethyl sulfoxide (DMSO; anhydrous, >99.9 %, Aldrich) were used as received.

10.2. Characterisation Methods

NMR spectroscopy

^{1}H- and ^{13}C NMR spectroscopy were performed on 400 MHz Bruker instrument at room temperature using deuterated acetone (acetone-d_6, $(CD_3)_2CO$), chloroform-*d* ($CDCl_3$), deuterated dimethyl sulfoxide (DMSO-d_6) or deuterated methanol (MeOD-d_4). Ethylene copolymers of Chapters 6 and 0 were measured on a 400 MHz spectrometer at 80 °C in a 2:1 mixture of tetrachloroethane (TCE):benzene (C_6D_6). For all kinetic experiments of Chapter 4 (VAc/**M1**, **M2**, **M3**, **M4**, **M5**) the conversion was determined using ^{1}H NMR spectroscopy in acetone-d_6 on a 400 MHz spectrometer. For all kinetic experiments of Chapter 5 (VAc/DMMDO) the conversion was determined using ^{1}H NMR spectroscopy in chloroform-*d* on a 250 MHz spectrometer. The determination of the monomer conversions is outlined below. The chemical shifts (δ) are reported in parts per million (ppm).

Size exclusion chromatography (SEC)

SEC analyses for copolymers synthesised in Chapter 4 (VAc/**M1**, **M2**, **M3**, **M4**, **M5)** were performed on a Waters chromatograph equipped with three columns (Waters Styragel PSS gram 1000 Å (×2), 30 Å), a dual λ absorbance detector (Waters 2487), and a refractive index detector (Waters 2414) in dimethylformamide (DMF) containing LiBr (0.025 M) at 55 °C (flow rate: 1 mL min^{-1}). A polystyrene calibration was used to evaluate the molecular parameters of the copolymers.

SEC analyses for copolymers synthesised in Chapter 5 (VAc/**DMMDO**) were carried out in THF at 45 °C at a flow rate of 1 mL min^{-1} with a Viscotek 305 TDA liquid chromatograph equipped with 2 PSS SDV linear M columns calibrated with polystyrene standards and a refractive index detector.

SEC analyses of EVA copolymers (Chapter 7) were performed in THF at 45 °C at a flow rate of 1 mL/min with a Viscotek 305 TDA liquid chromatograph equipped with 2 PSS SDV linear M columns calibrated with polystyrene standards and a refractive index detector.

SEC analyses of ethylene copolymers synthesised in Chapter 6 (P(**E-*co*-M1)**, P(**E-*co*-DMMDO**) and 7 (EVA and EVA-*b*-PE) were carried out on a PL-GPC 220 HT Agilent system equipped with 1 guard column and 2 mixed C columns calibrated with polystyrene standards, in trichlorobenzene (TCB) stabilised with BHT at 140 °C at a flow rate of 1 mL/min using refractive index detection.

Fourier-transform infrared (FT-IR) analysis

FT-IR analyses were performed on a ThermoFisher Scientific Nicolet IS5 with module ATR ID5 using a diamond crystal (650 cm^{-1} - 4000 cm^{-1}).

Differential scanning calorimetry (DSC)

DSC analyses were performed on a DSC Q100 instrument from TA Instruments by placing around 5 mg of sample in an aluminium pan. The sample was cooled to 0 °C, then heated to 140 °C, cooled to -90 °C and heated to 130 °C at a heating/cooling rate of 10 °C/min. The last heating cycle was used for the determination of the T_g. For polyethylene copolymers of Chapter 6 and 0, the sample was cooled to 0 °C, then heated to 140 °C, cooled to -90 °C and heated to 150 °C at a heating/cooling rate of 10 °C/min. The last heating cycle was used for the determination of the T_g and T_m.

Thermogravimetric analysis (TGA)

TGA was performed on a TGA Q500 instrument from TA Instruments. Around 5 mg of sample were heated to 100 °C, held there for 10 minutes to remove any remaining solvent and then heated to 600 °C at 20 °C/min.

Electron-spray ionisation mass spectrometry (ESI-MS)

ESI-MS spectra were recorded on a Q Exactive (Orbitrap) mass spectrometer (Thermo Fisher Scientific) equipped with a HESI II probe to record high resolution electrospray ionisation–MS (ESI-MS). Calibration was carried out in the m/z range 74-1.822 using premixed calibration solutions (Thermo Fisher Scientific). A constant spray voltage of 4.7 kV and a dimensionless sheath gas of 5 were employed. The S-lens RF level was set to 62.0, while the capillary temperature was set to 250 °C. All samples were dissolved at a concentration range of 0.05 – 0.01 mg mL^{-1} in a mixture of THF and MeOH (3:2) doped with 100 μmol sodium trifluoroacetate and injected with a flow of 5 μL min^{-1}.

Matrix Assisted Laser Desorption/Ionisation Time-of-Flight (MALDI-ToF)

MALDI-ToF mass spectra were recorded using a Waters QToF Premier mass spectrometer equipped with a Nd:YAG laser using the 3rd harmonic with a wavelength of 355 nm. In the context of this study, a maximum output of ~65 J was delivered to the sample in 2.2 ns pulses at 50 Hz repeating rate. Time-of-flight mass analyses were performed in reflection mode. The matrix, trans-2-[3-(4-tert-butyl-phenyl)-2-methyl-2-propenylidene]malononitrile (DCTB), was prepared as a 40 mg/mL solution in chloroform. The matrix solution (1 μL) was applied to a stainless steel MALDI target and air-dried. Polymer samples were dissolved in THF to obtain 1 mg/mL solutions and 20 μL of NaI solution (2 mg/mL in acetonitrile) are added as source of cationisation agent. Then, 1 μL aliquots of these solutions were applied onto the target area (already bearing the matrix crystals) and then air-dried.[380]

Inductively coupled plasma optical emission spectrometry (ICP-OES)

ICP-OES was performed on a Varian 720-ES. A calibration window of 1-200 mg/L was established using dilutions of a Certipur standard solution (1000 mg/L in Co, Merck).

Scanning electron microscopy (SEM)

SEM analyses were performed on a FEI Quanta 600 using a W gun at the Centre for Applied Research and Education in Microscopy (CAREM) using samples fractured in liquid nitrogen.

Material properties

Stress-strain measurements were performed on an Instron 5594 tensile machine at a speed of 10 mm/min with a load capacity of 1000 N at room temperature. Young modulus, tensile strength and elongation at break were estimated by the average values of at least 3 composite samples.

The melt rheological properties of the samples were determined using an ARES G2 strain-controlled rotational rheometer from TA Instruments. All measurements were done with 25 mm diameter parallel plate geometries under a nitrogen atmosphere. Amplitude sweep tests were performed at 150 °C with 1 rad/s for all the samples. Frequency sweep tests at small amplitude oscillatory shear (SAOS) were performed between 120 °C and 170 °C from which linear master curves of G' (ω) and G'' (ω) at a reference temperature of 150°C were constructed and used for the time-temperature super position (TTS) principle.

10.3. Experimental Section for Chapter 4

Monomer synthesis

Diallyl carbonate (DAC) was synthesised following a modified version of a previous publication:[248] 70 g dimethyl carbonate (DMC; 0.777 mol, 1 eq.) was mixed with 94.80 g allyl alcohol (1.63 mol, 2.2 eq.) and 1.082 g TBD (7.77 mmol, 0.01 eq.) was added. The reaction was heated to 85°C for 12 hrs using a distillation bridge, through which dimethyl carbonate and methanol were recovered, and the temperature was increased consecutively over the next 3 days to 115 °C. A conversion of 78% was determined using ^{1}H-NMR and yield of 61 % was obtained after distillation. ^{1}H-NMR spectroscopy (25 °C, 400 MHz, $CDCl_3$) δ (ppm): 5.93 (m, CH_2=C<u>*H*</u>-), 5.41-5.39 (m, C<u>*H*$_2$</u>=CH-), 4.64 (dt, *J* = 1.5 Hz, CH_2=CH-C<u>*H*$_2$</u>-O-). ^{13}C-NMR spectroscopy (25 °C, 400 MHz, $CDCl_3$) δ (ppm): 155.7 (O-(<u>*C*</u>=O)O-), 131.7 (CH_2=<u>*C*</u>H-), 118.1 (<u>*C*</u>H_2=CH-), 68.5 (-<u>*C*</u>H_2-O-). FT-IR (cm^{-1}): 1757 (s, C=O stretch), 1237 (s, C-O stretch). The full characterisation data of DAC can be found in the original paper by Meier *et al.* describing this synthesis.[248]

Dimethylallyl carbonate (DmAC) was synthesised using the same procedure as above except that 117.54 g methylallyl alcohol (1.63 mol, 2.2 eq.) were used in place of allyl alcohol (yield: 37 %). ^{1}H-NMR spectroscopy (25 °C, 400 MHz, $CDCl_3$) δ (ppm): 4.98 (d, J = 26.9 Hz C<u>*H*$_2$</u>=CH-), 4.56 (s, CH_2=C(CH_3)-C<u>*H*$_2$</u>-), 1.78 (s, CH_2=C(C<u>*H*$_3$</u>)-). ^{13}C-NMR spectroscopy (25 °C, 400 MHz, $CDCl_3$) δ (ppm): 155.1 (O-(<u>*C*</u>=O)O-), 139.5 (CH_2=<u>*C*</u>(CH_3)-), 113.6 (<u>*C*</u>H_2=C(CH_3)-), 71.2 (-<u>*C*</u>H_2-O-), 19.4 (CH_2=C(<u>*C*</u>H_3)-). FT-IR (cm^{-1}): 1756 (s, C=O stretch), 1252 (s, C-O stretch).

Allyl ((2-oxo-1,3-dioxolan-4-yl)methyl) carbonate (**M1**)) was synthesised in a pressure tube. 100 mg Glycerol (1.09 mmol, 1 eq.), 98 mg DMC (1.09 mmol, 1 eq.), 617 mg DAC (6.52 mmol, 6 eq.) and 3 mg TBD (0.0543 mmol, 0.02 eq.) were weighed and heated to 90 °C at 1250 rpm for 48 h. A slight yellow discolouration of the reaction mixture was observed and the product was isolated via SiO_2 column chromatography using a 4:1 mixture of cyclohexane : ethyl acetate or by diluting the reaction mixture with ethyl acetate and washing 3 times with water, to obtain a clear viscous liquid (yield: 60%). ^{1}H-NMR spectroscopy (25 °C, 400 MHz, $CDCl_3$) δ (ppm): 5.98-5.88 (m, CH_2=C<u>*H*</u>-), 5.41-5.29 (m, C<u>*H*$_2$</u>=CH-), 4.96-4.91 (m, –O–CH_2–C<u>*H*</u>–(CH_2–O(C=O)O)), 4.66 (dt, CH_2=CH-C<u>*H*$_2$</u>-), 4.59-4.29 (m, –O–C<u>*H*$_2$</u>–CH–(C<u>*H*$_2$</u>–O(C=O)O)). ^{13}C-NMR spectroscopy (25 °C, 400 MHz, $CDCl_3$) δ (ppm): 154.51 (-CH_2-O(<u>*C*</u>=O)-O-CH-), 154.29 (CH_2-O(<u>*C*</u>=O)-O-CH_2), 131.06 (-<u>*C*</u>H=CH_2), 119.77 (-CH=<u>*C*</u>H_2), 73.54 (-O-CH_2-<u>*C*</u>H-(CH_2-O-)$_2$-), 69.36 (<u>*C*</u>H_2-CH=CH_2), 66.08 (<u>*C*</u>H_2-(O-(C=O)-O-CH-), 65.89 ((-<u>*C*</u>H_2-O-(C=O)-O-CH_2). FT-IR (cm^{-1}): 2930 (w, CH_2 stretch), 1791 (m, C=O stretch), 1744

(s, C=O stretch), 1240 (s, C-O). Detailed spectra can be found below. High resolution electron spray ionisataion mass spectrometry (HR-ESI-MS) of $C_8H_{10}O_6$ $[M+Na]^+$ calc. 225.038 found 225.036.

2-Methylallyl ((2-oxo-1,3-dioxolan-4-yl)methyl) carbonate (**M2**)) was synthesised in a pressure tube. 100 mg Glycerol (1.086 mmol, 1 eq.), 98 mg DMC (1.086 mmol, 1 eq.), 1.1091 g DmAC (6.52 mmol, 6 eq.) and 3 mg TBD (0.022 mmol, 0.02 eq.) were weighed and heated to 110 °C at 1250 rpm for 48 h. A slight yellow discolouration of the reaction mixture was observed and the product was isolated via SiO_2 column chromatography using a 4:1 mixture of cyclohexane : ethyl acetate to obtain a clear viscous liquid (yield: 11%). ^{1}H-NMR spectroscopy (25 °C, 400 MHz, $CDCl_3$) δ (ppm): 5.03-4.98 (m, C$\underline{H_2}$=C(CH_3)-), 4.97-4.91 (m, –O–CH_2–C$\underline{H}$–(CH_2–O(C=O)O)), 4.58 (s, CH_2=CH(CH_3)-C$\underline{H_2}$-), 4.59-4.3 (m, –O–C$\underline{H_2}$–CH–(C$\underline{H_2}$–O(C=O)O)), 1.78 (s, C$\underline{H_2}$=C(C$\underline{H_3}$)-). ^{13}C-NMR spectroscopy (25 °C, 400 MHz, $CDCl_3$) δ (ppm): 154.62 (-CH_2-O($\underline{C}$=O)-CH-), 154.26 (-CH_2-O($\underline{C}$=O)-CH_2-), 138.93 (-$\underline{C}$=CH_2), 114.36 (-C=$\underline{C}H_2$), 73.54 (-O-CH_2-$\underline{C}$H-(CH_2-O-)$_2$), 72.11 (-$\underline{C}H_2$-C(CH_3)=CH_2), 66.07 ($\underline{C}H_2$-(O-(C=O)-O-CH-), 65.91 (-C-CH_2-O(C=O)-O-$\underline{C}H_2$-), 19.44 (CH_2=C($\underline{C}H_3$)-). FT-IR (cm^{-1}): 2960 (w, C-H), 1790 (s, C=O), 1747 (s, C=O), 1239 (s, C-O). Detailed spectra can be found below. HR-ESI-MS of $C_9H_{12}O_6$ $[M+Na]^+$ calc. 239.053 found 239.052.

(2-Oxo-1,3-dioxolan-4-yl)methyl undec-10-enoate (**M3**)) was synthesised in a Schlenk flask. 100 mg Glycerol (1.086 mmol, 1 eq.), 489 mg dimethyl carbonate (5.43 mmol, 5 eq.), 258 mg methyl 10-undecenoate (1.30 mmol, 1.2 eq.) and 3 mg TBD (0.022 mmol 0.02 eq.) were weighed and heated to 80 °C while stirring vigorously (~1400 r.p.m.). After 40 minutes of reaction time, a high vacuum (<10^{-2} mbar) was applied for 6 h. After purification using SiO_2 column chromatography in 6:1 cyclohexane : ethyl acetate and then 4:1, and a flash column over basic aluminium oxide, a waxy white solid was obtained (yield: 61%). ^{1}H-NMR spectroscopy (25 °C, 400 MHz, $CDCl_3$) δ (ppm): 5.86-5.75 (m, CH_2=C$\underline{H}$-), 4.98 (q, J = 1.8 Hz, –O–CH_2–C$\underline{H}$–(CH_2–O(C=O)O)), 4.97-4.89 (m, C$\underline{H_2}$=CH-CH_2), 4.57-4.23 (m, –O–C$\underline{H_2}$–CH–(C$\underline{H_2}$–O(C=O)O)), 2.37 (t, J = 7.6 Hz, -O(C=O)-C$\underline{H_2}$-CH_2-), 2.03 (m, CH_2=CH-C$\underline{H_2}$-), 1.62 (m, -O(C=O)-CH_2-C$\underline{H_2}$-), 1.40-1.23 (m, aliphatic -CH_2-). ^{13}C-NMR spectroscopy (25 °C, 400 MHz, $CDCl_3$) δ (ppm): 173.37 (-CH_2-O($\underline{C}$=O)-CH_2-), 157.12 ((-CH_2-O($\underline{C}$=O)-O-CH-), 139.29 (-$\underline{C}$H=CH_2), 114.28 (-CH=$\underline{C}H_2$), 73.89 ((-O-CH_2-$\underline{C}$H-(CH_2-O-)$_2$-), 66.10 ($\underline{C}H_2$-(O-(C=O)-O-CH-), 62.98 (-$\underline{C}H_2$-O-(C=O)-CH_2), 34.00 (-O(C=O)-$\underline{C}H_2$-CH_2-), 33.89 (-$\underline{C}H_2$-CH=CH_2), 29.36-28.98 (-$\underline{C}H_2$-), 24.89 (O(C=O)-CH_2-$\underline{C}H_2$). FT-IR (cm^{-1}): 2922 (m, C-H), 2854 (w, C-H), 1795 (s, C=O), 1739 (s, C=O), 1159 (s, C-O), 1051. Detailed spectra can be found below. HR-ESI-MS of $C_{15}H_{24}O_5$ $[M+Na]^+$ calc. 307.152 found 307.151.

Methyl-10-undecenoate (**M4**) was prepared by esterification of 10-undecenoic acid and methanol. 82.1 g 10-Undecenoic acid (90.0 mL, 445 mmol), 200 mL methanol and 5.80 mL concentrated sulphuric acid (109 mmol) were mixed and refluxed at 70 °C for 6 hours. After neutralisation with sodium bicarbonate and filtration of the precipitate, the mixture was concentrated *in vacuo*, dissolved in ethyl acetate (10 mL), washed three times with saturated sodium bicarbonate solution (3 times 100 mL), once with saturated sodium chloride solution (100 mL), and dried over sodium sulphate (1g). Vacuum distillation at 200 °C and 6 mbar yielded 78.22 g of a colourless liquid (yield = 88.6 %). ^{1}H-NMR spectroscopy (25 °C, 400 MHz, $CD_3C(=O)CD_3$) δ (ppm): 5.86-5.75 (m, CH_2=C$\underline{H}$-), 5.10-4.88 (m, C$\underline{H_2}$=CH-CH_2), 3.64 (s, CH_3-OC(=O)-), 2.32 (t, J = 7.3 Hz, -O(C=O)-C$\underline{H_2}$-CH_2-), 2.09 (m, CH_2=CH-C$\underline{H_2}$-), 1.62 (m, -O(C=O)-CH_2-C$\underline{H_2}$-), 1.47-1.30 (m, aliphatic -C$\underline{H_2}$-). ^{13}C-NMR spectroscopy (25 °C, 400 MHz, $CDCl_3$) δ (ppm): 173 ((CH_3-O-($\underline{C}$=O)-), 139 (CH_2=$\underline{C}$H-), 114 ($\underline{C}H_2$=CH-), 51 ($\underline{C}H_3$-O-(C=O)-), 34 (-O(C=O)-C$\underline{H_2}$-CH_2), 33 (CH_2=CH-$\underline{C}H_2$-), 29 (aliphatic -$\underline{C}H_2$-), 25 (-O(C=O)-CH_2-$\underline{C}H_2$). FT-IR (cm^{-1}): 2842 (m, CH_2 stretch), 2860 (w, CH_2 stretch), 1747 (s, C=O stretch). Detailed spectra can be found below. GC-MS of $C_{12}H_{22}O_2$ [M+] calc. 198.16 found 198.40.

Allyl methyl carbonate (**M5**) was synthesised according to a previous publication,[248] but instead of a column, fractional distillation (60 °C, 40 mbar) was performed to purify the monomer. ^{1}H-NMR spectroscopy (25 °C, 400 MHz, $CDCl_3$) δ (ppm): 5.98-5.88 (m, CH_2=C$\underline{H}$-), 5.38-5.25 (m, C$\underline{H_2}$=CH-), 4.63 (dt, J = 1.4 Hz, CH_2=CH-C$\underline{H_2}$-O-), 3.79 (s, -C(=O)-O-C$\underline{H_3}$). ^{13}C-NMR spectroscopy (25 °C, 400 MHz, $CDCl_3$) δ (ppm): 154.51 (-CH_2-O($\underline{C}$=O)-O-CH-), 154.29 (CH_2-O($\underline{C}$=O)-O-CH_2), 131.06 (-$\underline{C}$H=CH_2), 119.77 (-CH=$\underline{C}H_2$), 73.54 (-O-CH_2-$\underline{C}$H-(CH_2-O-)$_2$-), 69.36 ($\underline{C}H_2$-CH=CH_2), 66.08 ($\underline{C}H_2$-(O-(C=O)-O-CH-), 65.89 ((-$\underline{C}H_2$-O-(C=O)-O-CH_2). FT-IR (cm^{-1}): 2930 (w, CH_2 stretch), 1791 (m, C=O stretch), 1744 (s, C=O stretch), 1240 (s, C-O). Detailed spectra can be found below.

Exemplary FRP of M1

All polymerisations were performed under an inert atmosphere using Schlenk techniques. A typical bulk homopolymerisation aiming at a degree of polymerisation of 100 (Entry 1, Table 13) was carried out at 40 °C and 500 rpm. In a 30 mL Schlenk tube, 200 mg of allyl ((2-oxo-1,3-dioxolan-4-yl)methyl) carbonate (**M1**; 0.989 mmol) were weighed and freeze-pumped-thawed thrice. From a previously prepared degassed solution of 15 mg V-70 (0.0486 mmol) in 5 mL of degassed DMC, 0.5 mL were transferred to the Schlenk flask. After 24 hours, aliquots for SEC and NMR analyses were taken.

Exemplary FRP of M1 with VAc

All polymerisations were performed under an inert atmosphere using Schlenk techniques. A typical bulk VAc copolymerisation aiming at a f^0_{GAdC}= 0.10 (Entry 6,Table 13) was carried out at 40 °C and 500 rpm using a molar ratio of $[VAc]_0/[M1]_0/[V\text{-}70]_0$ = 360/40/0.5. In a 30 mL Schlenk tube, 463 mg of **M1** (2.27 mmol), 8.8 mg of V-70 (0.0284 mmol) were weighed and freeze-pumped-thawed thrice. 1.88 mL of VAc (20.4 mmol) were added using a syringe, the flask put into the preheated oil bath and an ^{1}H-NMR spectroscopy aliquot was immediately taken to determine the monomer feed ratio. After 4 hours, aliquots for SEC and NMR analyses were taken and the reaction quenched using acetone. The polymer solution was transferred into the main chamber of a $scCO_2$ high pressure reactor (Figure 88) which was heated to 50 °C, stirred at 330 rpm and a CO_2 pressure of 250 bar was applied. After 1 hour, the stirring was stopped and $scCO_2$ at 250 bar at a rate of 10 mL/min was flushed through the main chamber and released to atmospheric pressure in another cell connected to the reactor. The unused monomer was collected in this cell, however some monomer was flushed out of the collection cell by the CO_2 flow and therefore lost. Once the 250-300 mL of $scCO_2$ were passed through the main chamber, the reactor was vented and the polymer was collected using acetone. After drying under vacuum at 50 °C overnight, the resulting white powder was analysed by NMR-spectroscopy and contained no remaining monomer.

Exemplary OMRP of M1 with VAc

All polymerisations were performed under an inert atmosphere using Schlenk techniques. A typical bulk VAc copolymerisation aiming at a f^0_{GAdC}= 0.10 (entry 2, Table 1) was carried out at 40 °C using a molar ratio of $[VAc]_0/[\mathbf{M1}]_0/[R\text{-}Co(acac)_2]_0$ = 360/40/1. A solution of R-$Co(acac)_2$ (0.58 mL; 0.1136 M stock solution in CH_2Cl_2, 0.06816 mmol) was introduced under argon into a purged 30 mL Schlenk tube and evaporated to dryness under reduced pressure at room temperature. VAc (2.3 mL, 25.0 mmol) was added under argon to give solution A. In a second 30 mL Schlenk tube, M1 (0.500 g, 2.47 mmol) was freeze-pumped-thawed thrice and heated to 40 °C and stirred at 500 rpm. 1.9 mL of solution A were transferred to this second Schlenk tube using a syringe under argon atmosphere and an ^{1}H-NMR spectroscopy aliquot was immediately taken to determine the monomer feed ratio. The copolymerisation occurred at 40 °C under stirring. At regular intervals, aliquots of the reaction mixture were taken for NMR and SEC analyses to determine conversions and the molecular parameters of the polymer, respectively. The reaction mixture was quenched using a solution of TEMPO (75 mg, 0.5 mmol) in 2 mL of acetone, further diluted with a minimal amount of acetone and then passed over a micro silica column to remove the cleaved cobalt.

The polymer was extracted using supercritical CO_2 at 50 °C and 250 bar CO_2 pressure (see above) and then analysed by NMR spectroscopy, FT-IR, DSC and TGA analyses.

NMR spectra of synthesised monomers

The spectra shown in this section were taken in $CDCl_3$ on a 400 MHz spectrometer.

Allyl ((2-oxo-1,3-dioxolan-4-yl)methyl) carbonate (**M1**)

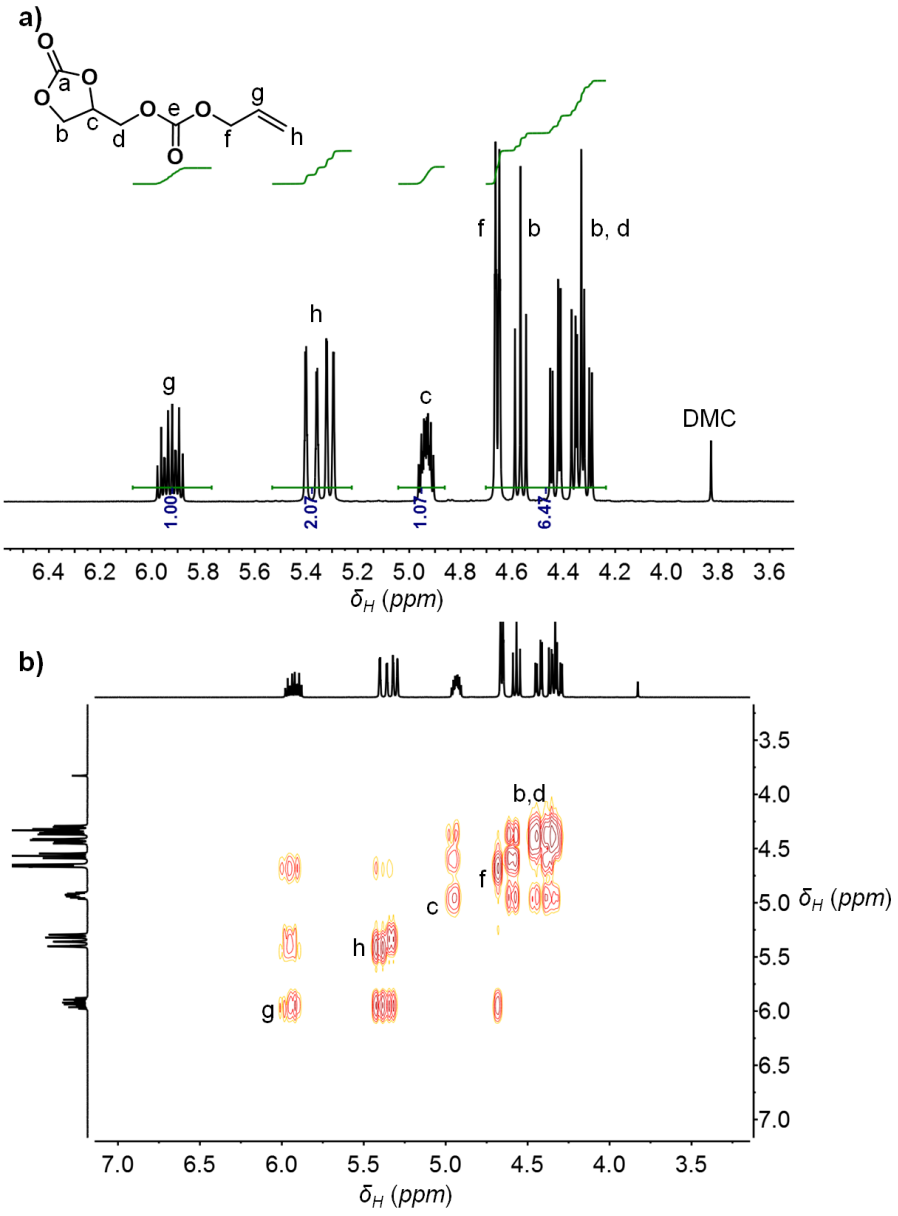

Figure 70. a) ^1H NMR spectrum and b) COSY spectrum of allyl ((2-oxo-1,3-dioxolan-4-yl)methyl) carbonate (**M1**)

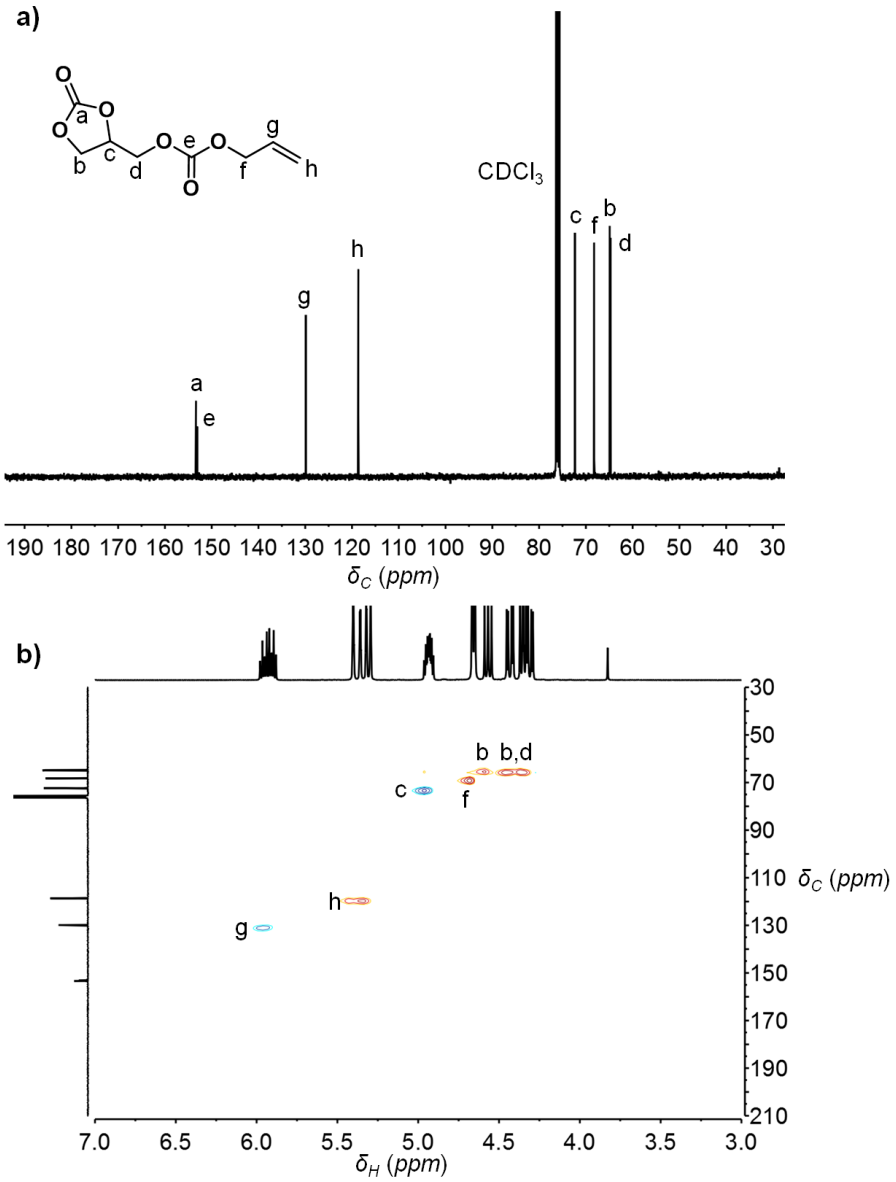

Figure 71. a) ^{13}C NMR spectrum and b) HSQC spectrum of allyl ((2-oxo-1,3-dioxolan-4-yl)methyl) carbonate (**M1**)

2-Methylallyl ((2-oxo-1,3-dioxolan-4-yl)methyl) carbonate (**M2**)

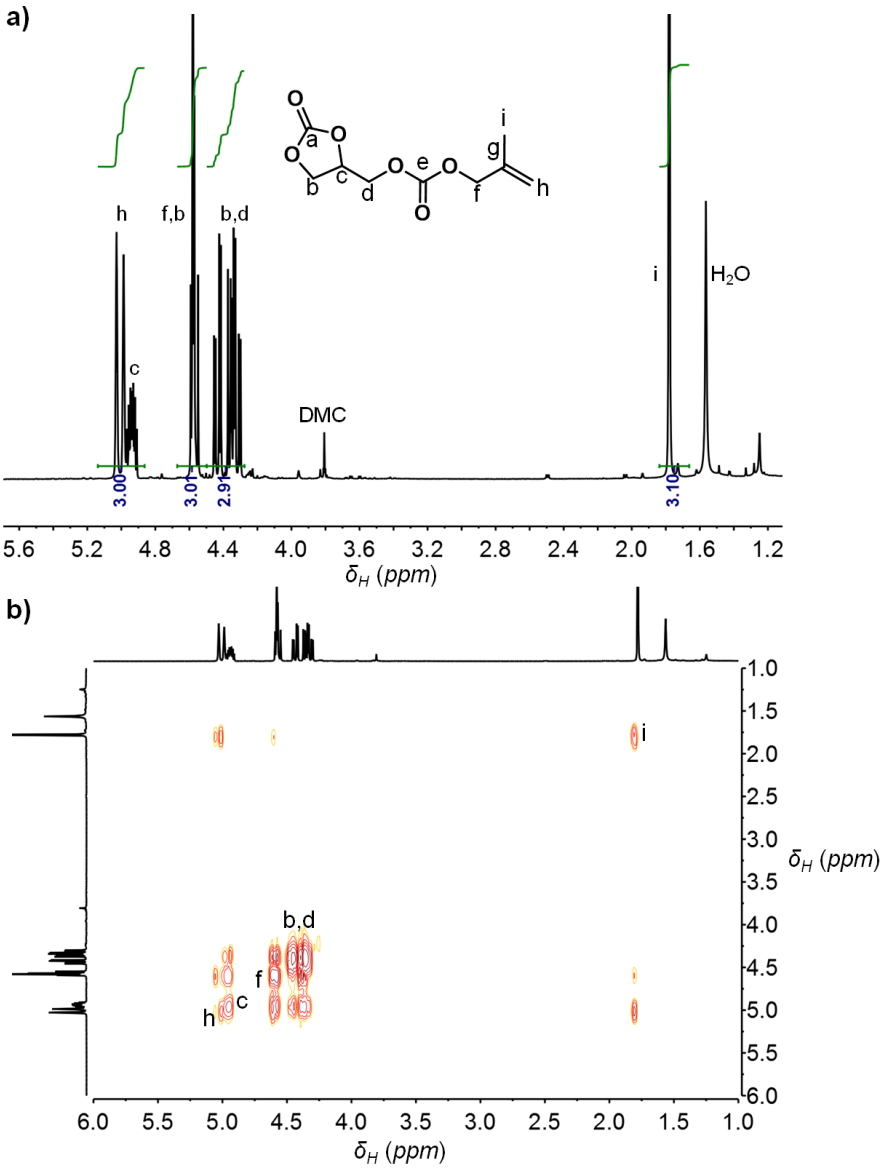

Figure 72. a) ^{1}H NMR spectrum and b) COSY spectrum of 2-methylallyl ((2-oxo-1,3-dioxolan-4-yl)methyl) carbonate (**M2**)

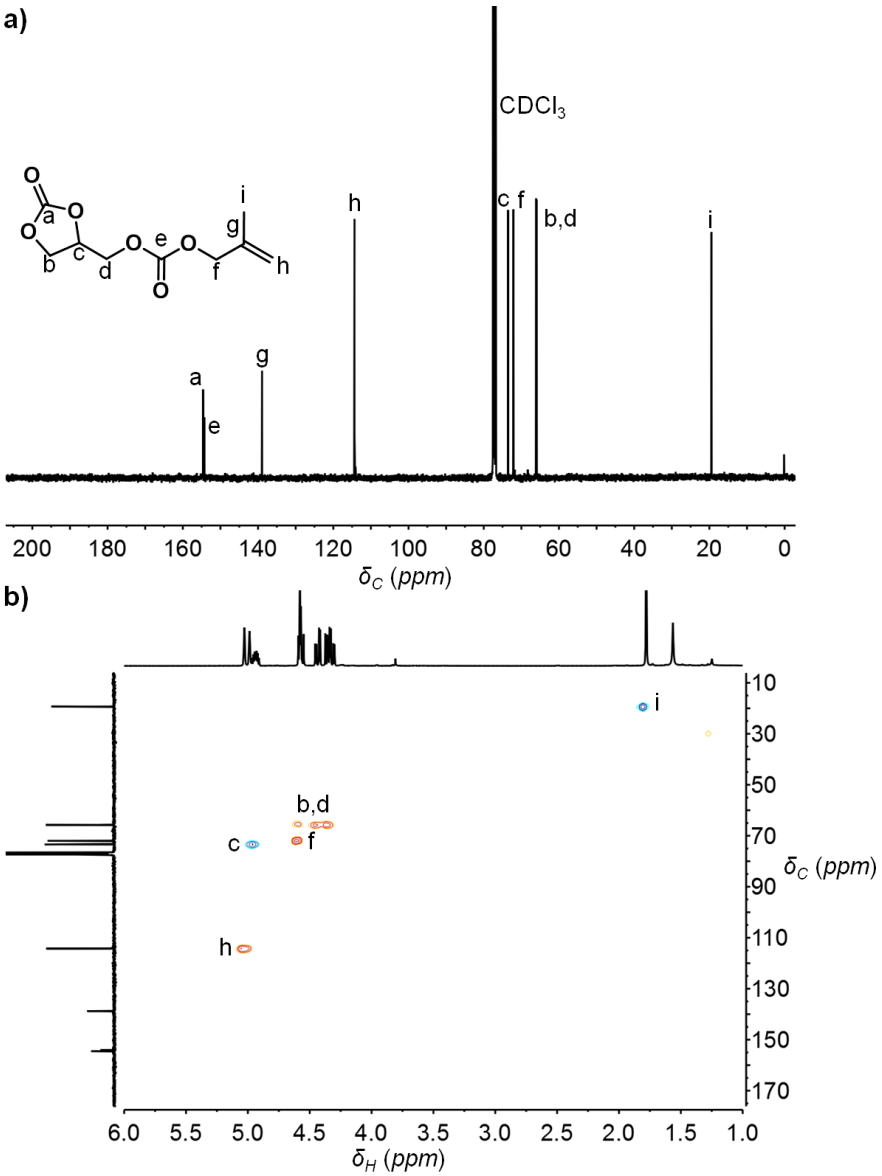

Figure 73. a) ^{13}C NMR spectrum and b) HSQC spectrum of 2-methylallyl ((2-oxo-1,3-dioxolan-4-yl)methyl) carbonate (**M2**)

(2-Oxo-1,3-dioxolan-4-yl)methyl undec-10-enoate (**M3**)

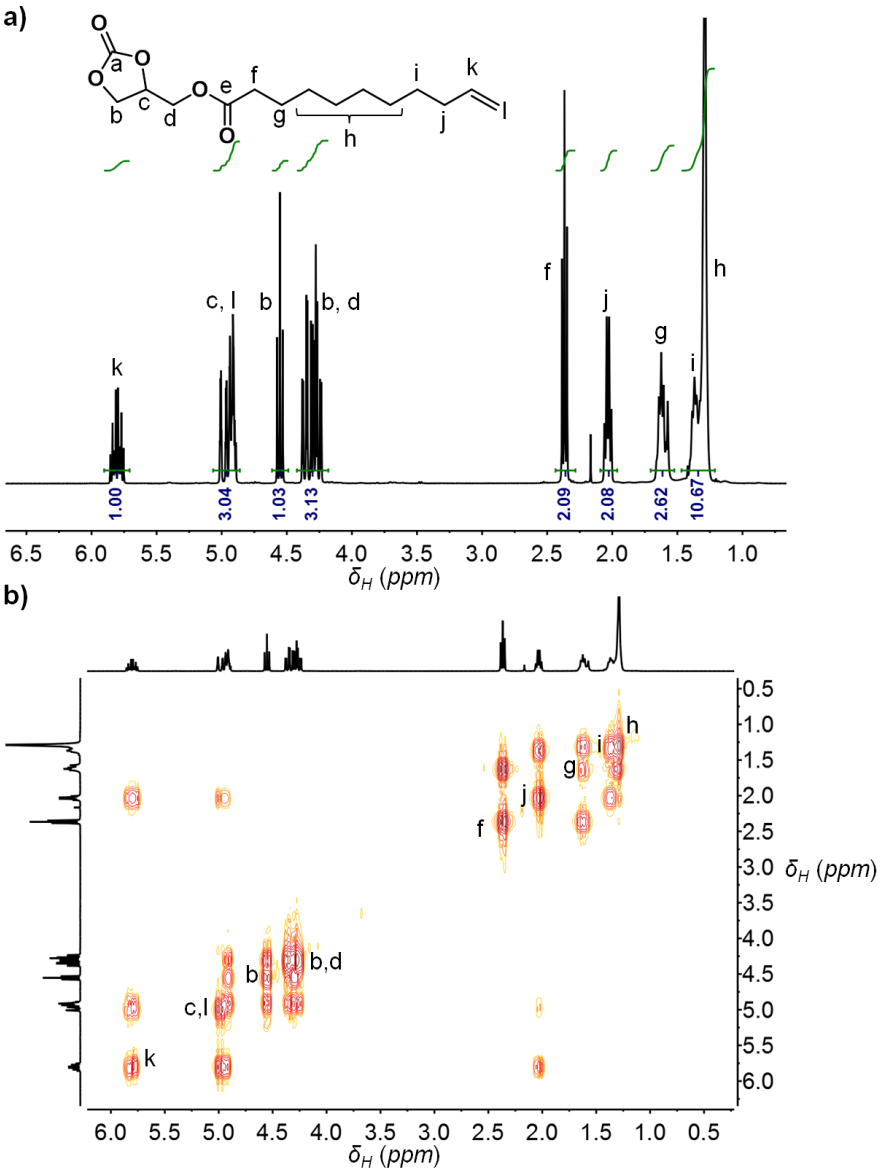

Figure 74. a) ^{1}H NMR spectrum and b) COSY spectrum of (2-oxo-1,3-dioxolan-4-yl)methyl undec-10-enoate (**M3**)

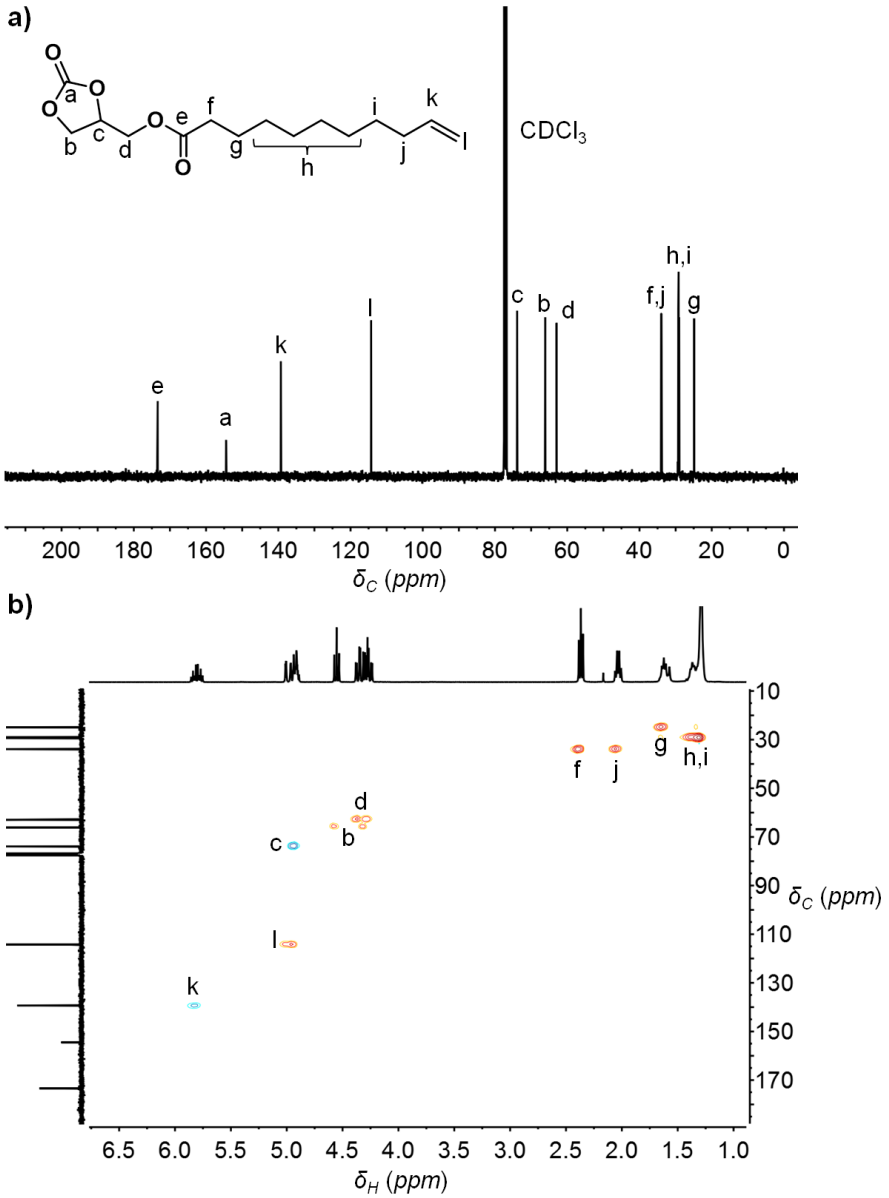

Figure 75. a) ^{13}C NMR spectrum and b) HSQC spectrum of (2-oxo-1,3-dioxolan-4-yl)methyl undec-10-enoate (**M3**)

Methyl-10-undecenoate (**M4**)

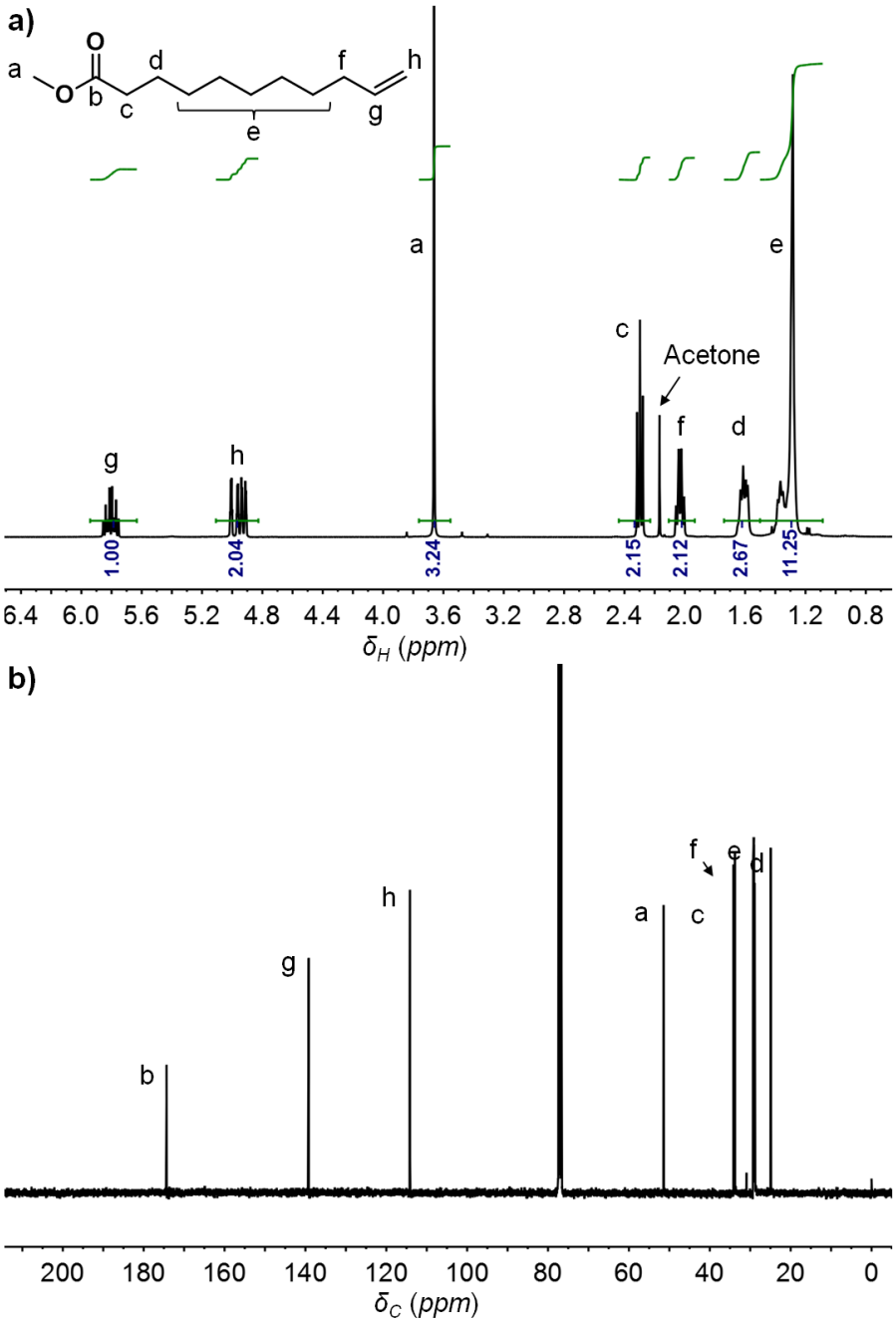

Figure 76. a) ^{1}H NMR spectrum and b) ^{13}C NMR spectrum of methyl-10-undecenoate (**M4**)

Allyl methyl carbonate (**M5**)

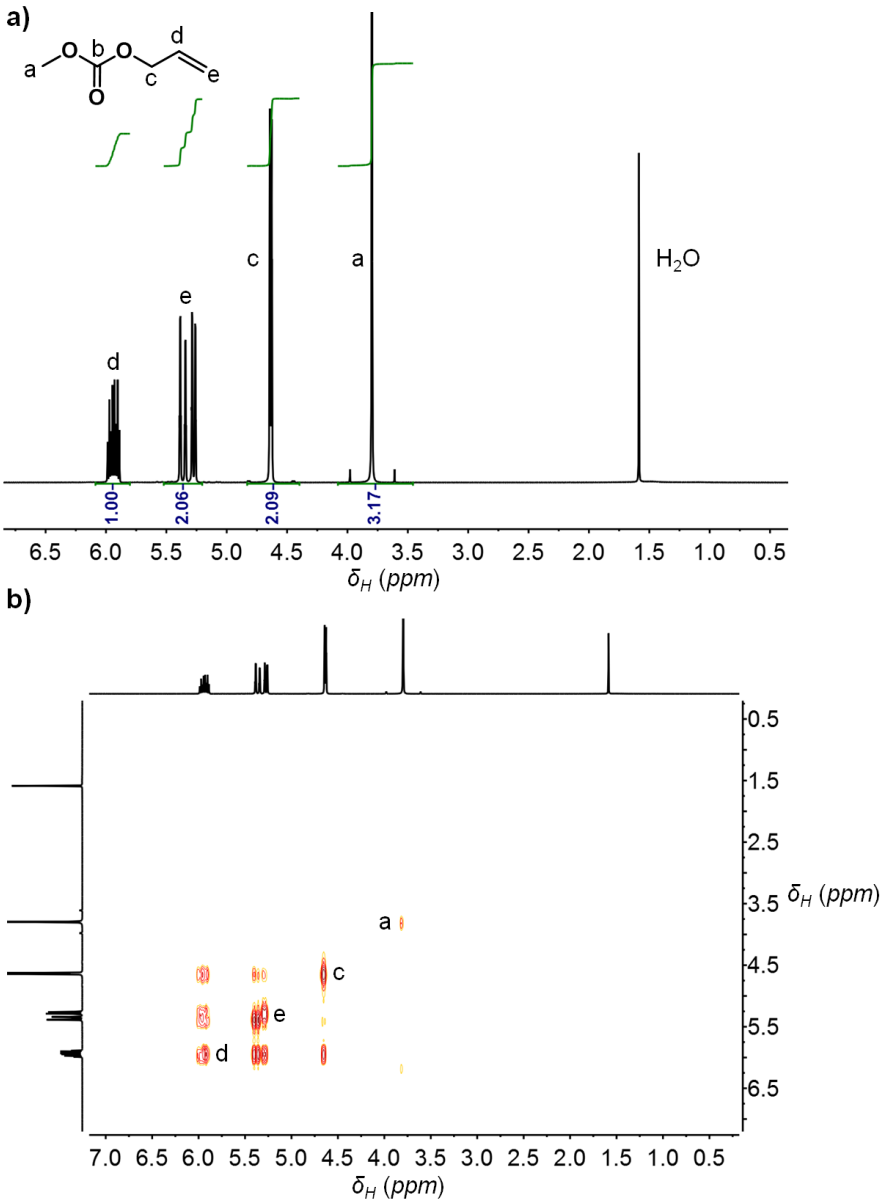

Figure 77. a) ^{1}H NMR spectrum and b) COSY spectrum of allyl methyl carbonate (**M5**)

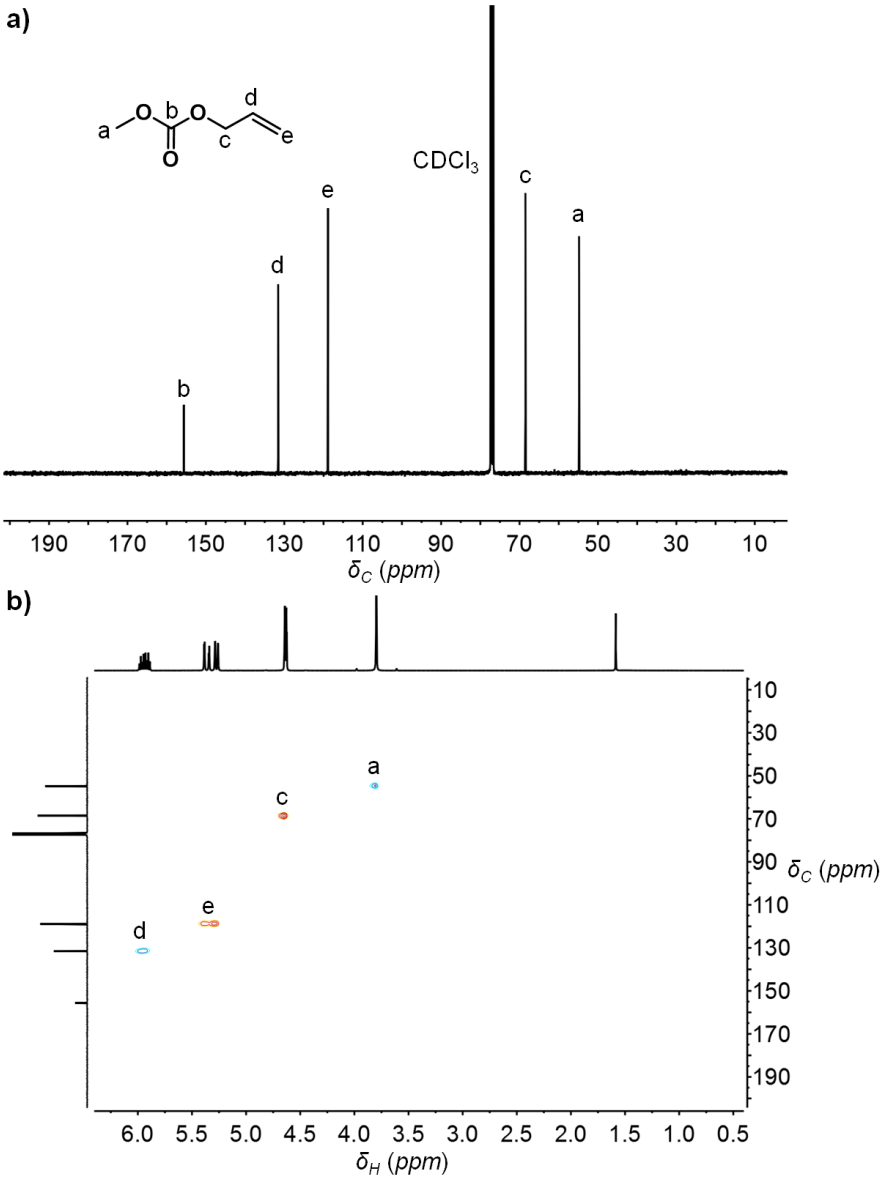

Figure 78. a) ^{13}C NMR spectrum and b) HSQC spectrum of allyl methyl carbonate (**M5**)

FT-IR overlay of renewable monomers M1-M5

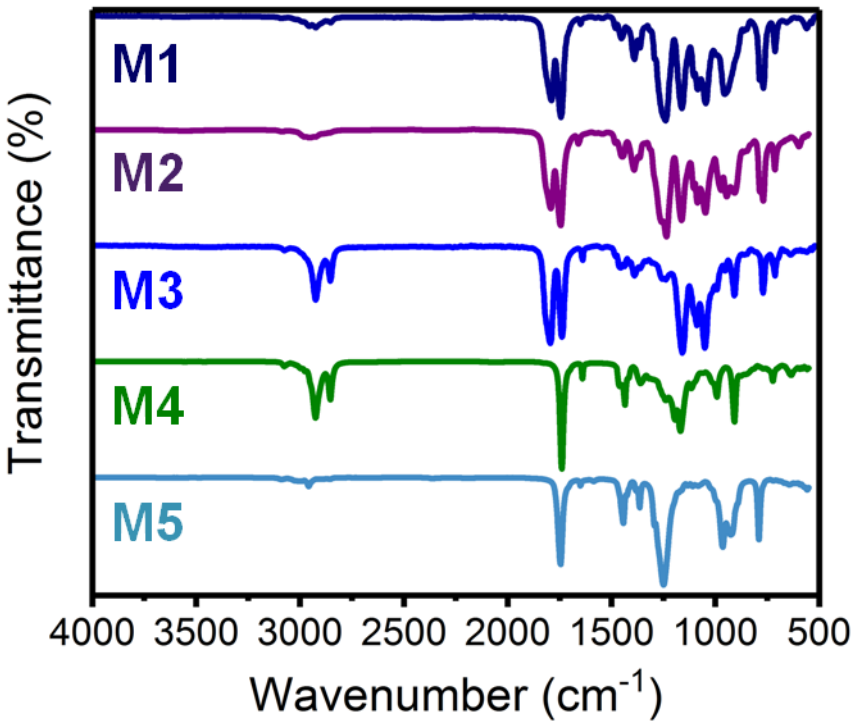

Figure 79. FT-IR spectra of **M1-M5** monomers synthesised in this publication

Optimisation of monomer synthesis

Table 10. Optimisation of the reaction conditions for the synthesis of **M1** from glycerol, dimethyl carbonate and diallyl carbonate

Entry	DAC/DMC/G	mol% TBD	Temp. (°C)	Time (hours)	Conv. (%)	Selectivity (%)
1	3:2:1	1	80	30	47	75
2	3:2:1	2	80	30	71	75
3	4:1:1	1	80	30	54	80
4	4:1:1	2	80	30	61	85
5	4:1:1	2	90	30	71	89
6	6:1:1	2	80	30	65	89
7	6:1:1	2	80	48	79	92
8	6:1:1	2	80	168	82	92
9	8:1:1	2	80	30	71	89

DAC/DMC/G = Diallyl carbonate /dimethyl carbonate/glycerol molar ratio. Reactions performed under an argon atmosphere using vigorous stirring (1250 rpm)

Table 11. Optimisation of the reaction conditions for the synthesis of **M2** from glycerol, dimethyl carbonate and dimethylallyl carbonate

Entry	DAC/DMC/G	mol% TBD	Temp. (°C)	Time (hours)	Conv. (%)	Selectivity (%)
1	6:1:1	2	110	48	31	95
2	6:1:1	5	110	48	40	93
3	6:1:1	2	120	48	48	83

DmAC/DMC/G = Dimethylallyl carbonate /dimethyl carbonate/glycerol molar ratio. Reactions performed under an argon atmosphere using vigorous stirring (1250 rpm)

Table 12. Optimisation of the reaction conditions for the synthesis of M3 from glycerol, dimethyl carbonate and methyl-10-undecenoate

Entry	**M10U /DMC/G**	**mol% TBD**	**Temp. (°C)**	**Time (hours)**	**Vac. (<10^{-3} mbar)**	**Conv. (%)**	**Selectivity (%)**
1	1:5:1	1	80	20	No	44	71
2	1.5:5:1	1	80	6	Yes	11	79
3	1.5:5:1	2	80	6	Yes	72	100
4	1.5:5:1	2	80	20	Yes	86	70
5	1.2:5:1	2	80	6	Yes	75	90
6	1.2:2:1	2	80	6	Yes	35	95

M10U/DMC/G = methyl-10-undecenoate/dimethyl carbonate/glycerol. Reactions performed under an argon atmosphere using vigorous stirring (1250 rpm) and if indicated, a vacuum was applied after 40 minutes of reaction time

E-Factor calculations

M1 synthesis pathway according to Tale *et al.*[277]

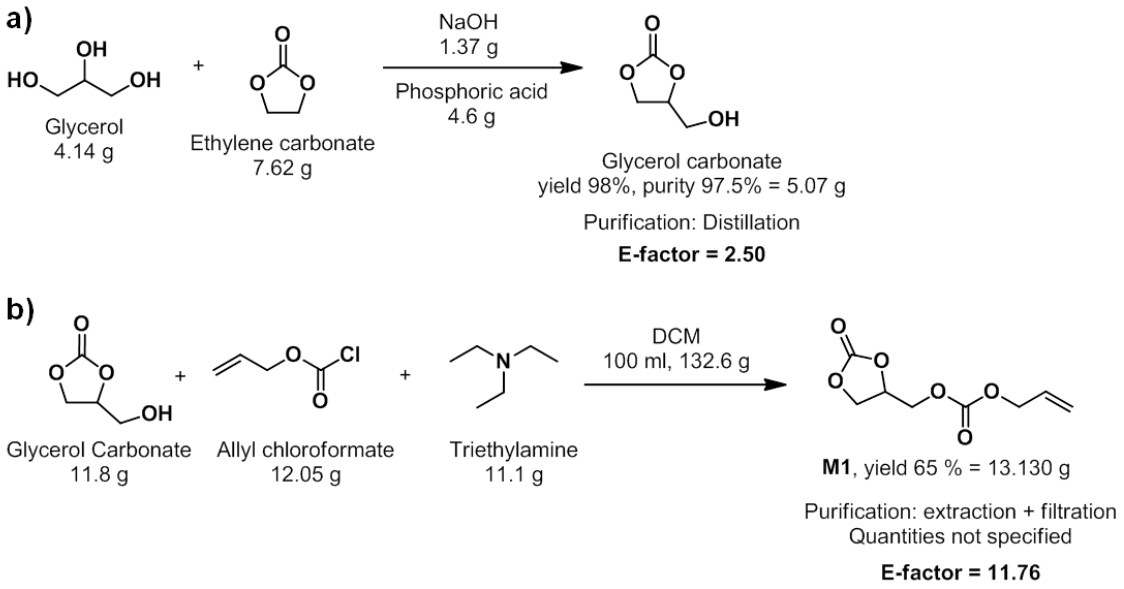

Figure 80. E-factor calculation for a) glycerol carbonate synthesis according to Bell *et al.*[276] and b) the subsequent synthesis of **M1** according to Tale *et al.*[277]

Overall E-Factor of synthetic pathway: $2.50 + 11.76 = 14.26$

M2 synthesis pathway in this work

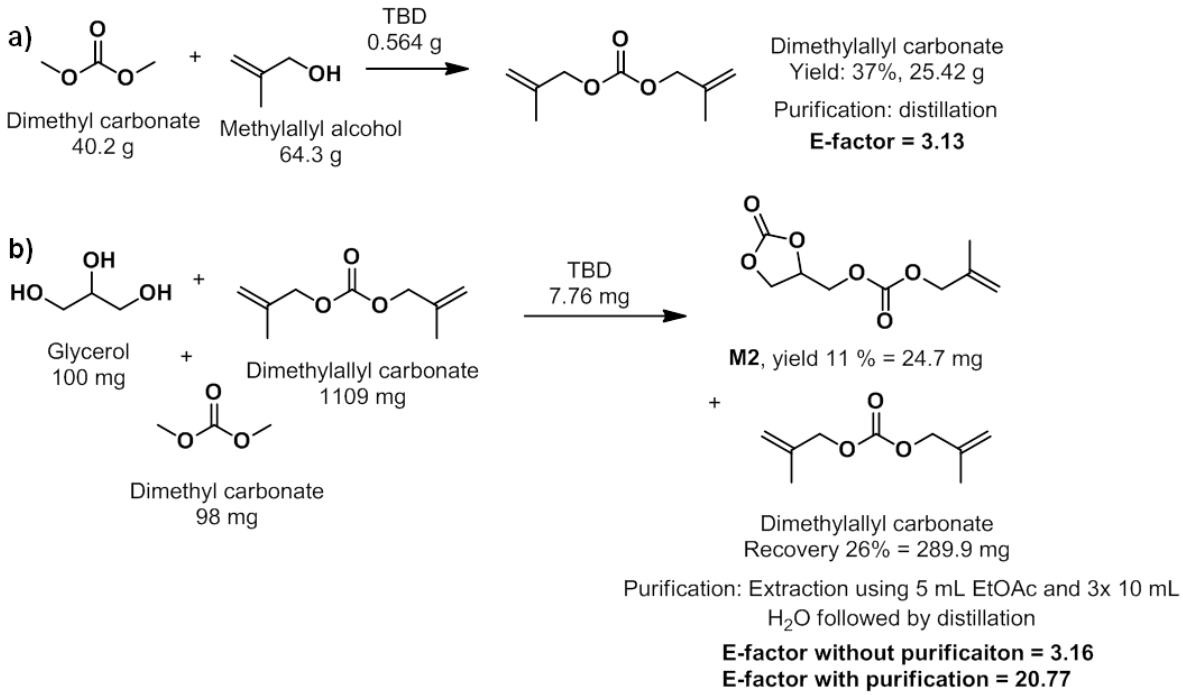

Figure 81. E-factor calculation for a) dimethylallyl carbonate (DmAC) synthesis and b) the subsequent synthesis of **M2** used in this work

Overall E-Factor of synthetic pathway: $3.13 + 3.16 = 6.29$

M3 synthesis pathway according to Cramail *et al.*[159]

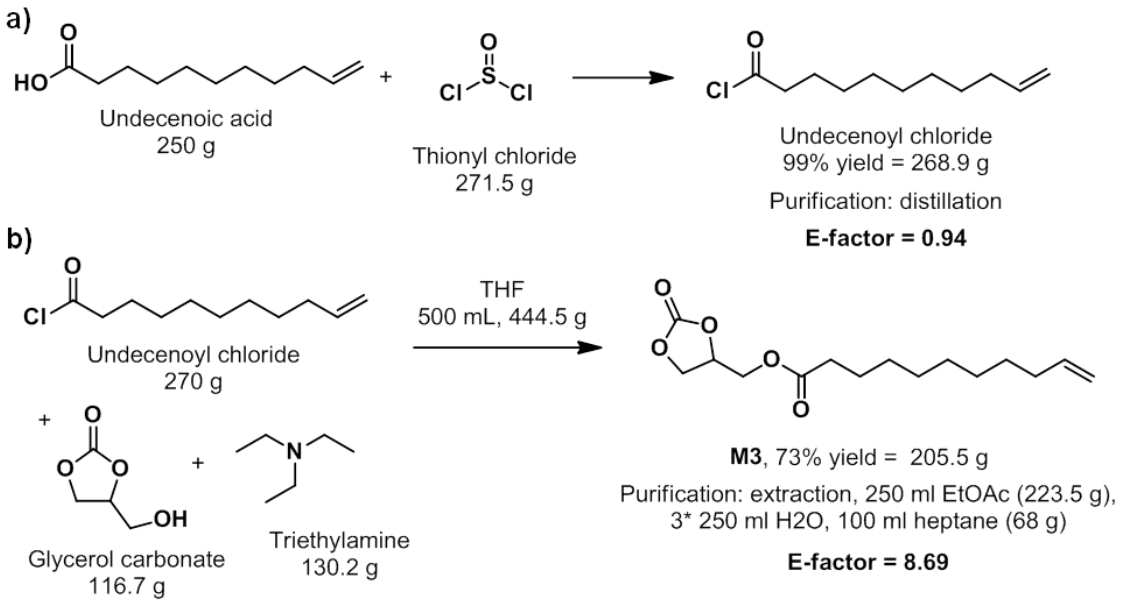

Figure 82. E-factor calculation for a) undecenoyl chloride synthesis and b) the subsequent synthesis of **M3** according to Cramail *et al.*[159] Commercial glycerol carbonate was used in this synthesis.

Overall E-Factor of synthetic pathway: $0.94 + 8.69 = 9.63$

M3 synthesis pathway in this work

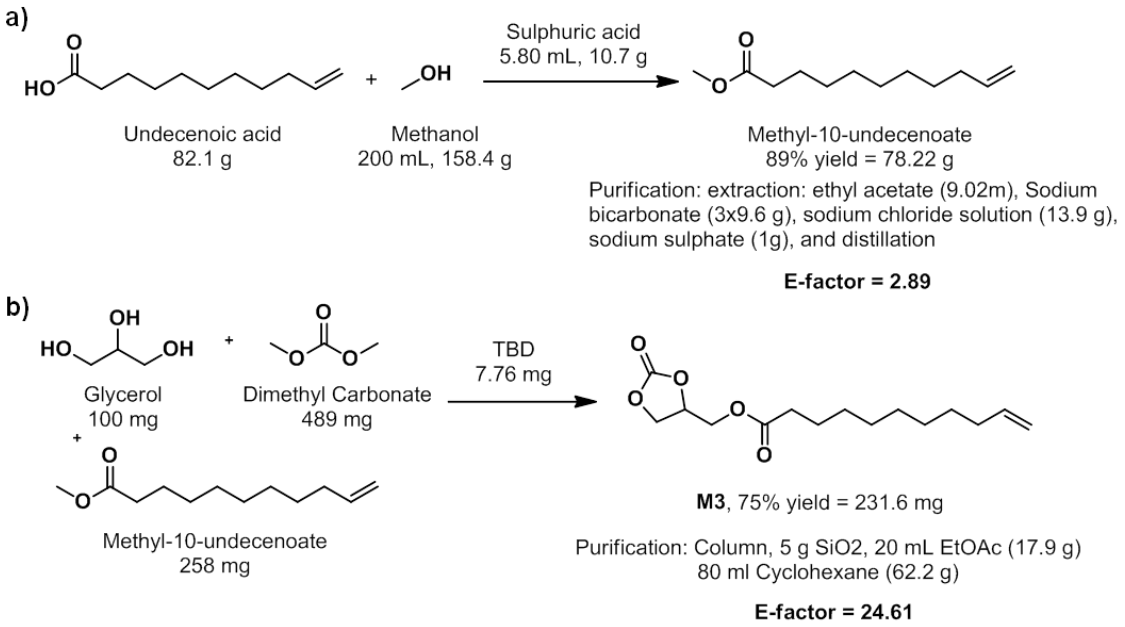

Figure 83. E-factor calculation for a) **M4** and b) the subsequent synthesis of **M3** used in this work

Overall E-Factor of synthetic pathway: $2.89 + 24.61 = 27.5$

Determination of monomer conversions using ^{1}H NMR spectroscopy

All spectra were taken in acetone-d_6 using a 400 MHz spectrometer.

The conversion in **M1** was determined by comparing the peak centred at 6.00 ppm corresponding to the –C=C$\underline{H}$ of the monomer ($\int_{5.80}^{6.07} Mon(CH)$) with the peak centred at 4.15 ppm corresponding to the –C$\underline{H_2}$ of the polymer ($\int_{3.95}^{4.33} Pol(CH_2)$) (Equation 2). The conversion in VAc was determined by comparing the peak at 7.31 corresponding to the –C=C$\underline{H}$ of the monomer ($\int_{6.90}^{7.6} Mon(CH)$) with the peak centred at 4.90 ppm corresponding to one proton of the –C$\underline{H_2}$– of the monomer VAc and to the –C$\underline{H}$-OAc in the copolymer ($\int_{4.78}^{5.10} Pol(CH) + Mon(CH)$) (Equation 3).

Equation 2: $$\text{conversion M1} = \frac{\int_{3.95}^{4.33} Pol(CH_2)}{2\times\int_{5.80}^{6.07} Mon(CH)+\int_{3.95}^{4.33} Pol(CH_2)}$$

Equation 3: $$\text{conversion VAc} = 1 - \frac{\int_{7.05}^{7.34} Mon(CH)}{\int_{4.71}^{5.03} Pol(CH_2)}$$

The conversion in **M2** was determined by comparing the peaks centred around 4.71 ppm corresponding to one of the two –CH_2–CH–C$\underline{H_2}$– protons in the monomer environment ($\int_{4.65}^{4.78} Mon(CH_2)$) with the peak centred at 3.92 ppm corresponding to the –C$\underline{H_2}$– of the polymer ($\int_{3.87}^{4.05} Pol(CH_2)$) (Equation 4). The conversion in VAc was determined by comparing the peak at 7.28 ppm ($\int_{6.95}^{7.55} Mon(CH)$) corresponding to the –C$\underline{H}$=CH_2 of VAc with the group of peaks at 5.00 ppm ($\int_{4.78}^{5.35} H$) (1H of the VAc monomer (–C=C$\underline{H_2}$), 1H of the copolymer –C$\underline{H}$-OAc, 1H of the –CH_2–C$\underline{H}$–CH_2–environment in both polymer and monomer and 2H of the –C$\underline{H_2}$–C(CH_3)=CH_2 **M2** environment) (Equation 5).

Equation 4: $$\text{conversion M2} = \frac{\int_{3.87}^{4.05} Pol(CH_2)}{2\times\int_{4.65}^{4.78} Mon(CH)}$$

Equation 5:

$$\text{conversion VAc} = \frac{\int_{4.78}^{5.35} H-\int_{4.65}^{4.78} Mon(CH_2)-\frac{1}{2}\int_{3.87}^{4.05} Pol(CH_2)-2(\int_{4.65}^{4.78} Mon(CH_2))-\int_{6.95}^{7.55} Mon(CH)}{\int_{4.78}^{5.35} H-\int_{4.65}^{4.78} Mon(CH_2)-\frac{1}{2}\int_{3.87}^{4.05} Pol(CH_2))-2(\int_{4.65}^{4.78} Mon(CH_2)}$$

The conversion in **M3** was determined by comparing the peak centred at 5.83 ppm corresponding to the –C=C$\underline{H}$ of the monomer ($\int_{5.73}^{6.00} Mon(CH)$) with the peak centred at 2.39 ppm corresponding to a –C$\underline{H_2}$– environment of both monomer and polymer ($\int_{2.31}^{2.45} Mon + Pol(CH_2)$) (Equation 6). The conversion in VAc was determined by comparing the peak at

7.26 ppm corresponding to the –C=C$\underline{H}$ of the monomer ($\int_{6.90}^{7.60} Mon(CH)$) with all protons centred at 4.96 ppm ($\int_{4.75}^{5.21} H$; 1H of the monomer VAc (–C$\underline{H_2}$–), 1H of the –C$\underline{H}$-OAc in the copolymer, 1H of both monomer and polymer **M3** (–C$\underline{H}$–) and 2H of monomer **M3** (HC=C$\underline{H_2}$–) (Equation 7).

Equation 6:
$$\text{conversion M3} = 1 - \frac{2 \times \int_{5.73}^{6.00} Mon(CH)}{\int_{2.31}^{2.45} Mon+Pol(CH_2)}$$

Equation 7:
$$\text{conversion VAc} = 1 - \frac{\int_{4.75}^{5.21} H - \int_{6.90}^{7.60} Mon(CH) - \int_{2.31}^{2.45} Mon+Pol(CH_2) - 2\int_{5.73}^{6.00} Mon(CH)}{\int_{4.75}^{5.21} H - \frac{1}{2}\int_{2.31}^{2.45} Mon+Pol(CH_2) - 2\int_{5.73}^{6.00} Mon(CH)}$$

Conversion in **M4** was determined by comparing the peak at 5.86 ppm corresponding to the –C=C$\underline{H}$ of the monomer ($\int_{5.77}^{6.00} Mon(CH)$) with the peak centred at 3.66 ppm corresponding to the –C$\underline{H_3}$ of the **M4** repeat unit in both the monomer and copolymer ($\int_{3.56}^{3.71} Mon + Pol(CH_3)$) (Equation 8). The conversion in VAc was determined by comparing the peak at 7.31 corresponding to the –C=C$\underline{H}$ of VAc ($\int_{6.90}^{7.6} VAc(CH)$) with all protons centred at 4.90 ppm ($\int_{4.75}^{5.22} H$; corresponding to 2H of the monomer VAc (–C$\underline{H_2}$–), 1H of the VAc in the copolymer (–C$\underline{H}$-OAc) and 2H of **M4** (-CH=C$\underline{H_2}$)). Since 2 protons from **M4** overlap, the integral corresponding to 2 **M4** protons, centred at 5.86 ppm, is subtracted ($2 \times \int_{5.77}^{6.00} M4(CH)$; –C=C$\underline{H}$)) (Equation 9).

Equation 8:
$$\text{conversion M4} = \frac{3 \times \int_{5.77}^{6.00} Mon(CH)}{\int_{3.56}^{3.71} Mon+Pol(CH_3)}$$

Equation 9:
$$\text{conversion VAc} = 1 - \frac{\int_{4.75}^{5.22} H - 2 \times \int_{5.77}^{6.00} M4(CH) - \int_{6.90}^{7.6} VAc(CH)}{\int_{4.75}^{5.22} H - 2 \times \int_{5.77}^{6.00} M4(CH)}$$

The conversion in **M5** was determined by comparing the peak at 6.00 ppm corresponding to the –C=C$\underline{H}$ of the monomer ($\int_{5.90}^{6.15} Mon(CH)$) with the peak centred at 4.15 ppm corresponding to the –C$\underline{H_2}$ of the polymer ($\int_{4.00}^{4.33} Pol(CH_2)$) (Equation 10). The conversion in VAc was determined by comparing the peak at 7.31 corresponding to the –C=C$\underline{H}$ of the monomer ($\int_{6.90}^{7.6} Mon(CH)$) with the peak centred at 4.90 ppm corresponding to one proton of the –C$\underline{H_2}$– of the monomer VAc and to the –C$\underline{H}$-OAc in the copolymer ($\int_{4.78}^{5.20} Pol(CH) + Mon(CH)$) (Equation 11).

Equation 10:
$$\text{conversion M5} = \frac{\int_{4.00}^{4.33} Pol(CH_2)}{2 \times \int_{5.90}^{6.15} Mon(CH) + \int_{4.00}^{4.33} Pol(CH_2)}$$

Equation 11: $$\text{conversion VAc} = 1 - \frac{\int_{6.90}^{7.6} Mon(CH)}{\int_{4.78}^{5.20} Pol(CH) + Mon(CH) - 2 \times \int_{5.90}^{6.15} Mon(CH))}$$

Kinetic data for the copolymerisation of the renewable monomers with VAc

Table 13. Free radical homopolymerisation of the renewable monomers (**M1**-**M5**) using V-70 at 40 °C in DMC (entries 1-5)[a] and their free radical copolymerisations with VAc in bulk (entries 6-9)[b]

Entry	Comonomer (f^0_{Comon})[c]	t (h)	VAc conv.[c] (%)	Comon conv.[c] (%)	Total conv.[c] (%)	Comp. (F_{VAc}/ F_{Comon})[d]	$M_{n\,SEC}$[e] (g mol^{-1})	M_w/M_n[e]
1	**M1** (1)[a]	24	-	0	0	-	-	-
2	**M2** (1)[a]	24	-	0	0	-	-	-
3	**M3** (1)[a]	24	-	0	0	-	-	-
4	**M4** (1)[a]	24	-	0	0	-	-	-
5	**M5** (1)[a]	24	-	0	0	-	-	-
6	**M1** (0.1)[b]	4	33	33	33	ins. gel	-	-
7	**M3** (0.1)[b]	4	28	15	27		83,100	2.15
		8	53	26	51	0.97/0.03	112,400	2.16
8	**M4** (0.1)[b]	4	10	10	10		33,600	1.75
		8	18	15	18		41,500	1.68
		12	24	17	23	0.95/0.05	42,300	1.88
9	**M5** (0.1)[b]	4	27	28	27		87,400	2.29
		8	57	58	58	0.88/0.12	125,500	5.46

[a] Conditions: 0.5 ml DMC, M/V-70 = 100/0.5, magnetic stirring at 500 rpm. [b] Conditions: bulk, M/V-70 = 400/1, magnetic stirring at 500 rpm. [c] Determined by ^{1}H-NMR spectroscopy in acetone-d_6. [d] Composition of the copolymer determined by ^{1}H NMR spectroscopy in acetone-d_6 based on the α-chain end (see above). [e] Determined by size exclusion chromatography (SEC) in DMF/LiBr using a PS standard.

Table 14. Full kinetics of the copolymerisations of VAc and renewable monomers (**M1**-**M5**) using R-Co(acac)$_2$ at 40°C[a]

Entry	Comonomer (f^0_{Comon})[b]	t (h)	VAc conv.[b] (%)	Comon conv.[b] (%)	Total conv.[b] (%)	Comp. (F_{VAc}/ F_{Comon})[c]	$M_{n,theo}$[d] (g mol^{-1})	$M_{n\,SEC}$[e] (g mol^{-1})	M_w/ M_n[e]
1	**M1** (0.1)	2	2	9	3		2,000	5,100	1.12
		6	12	21	13		6,100	10,400	1.12
		8	18	25	19		8,200	12,900	1.13
		10	20	28	21	0.85/0.15	9,100	14,300	1.18
		14	39	66	42		18,100	30,400	1.42
		16	55	75	57	0.89/0.11	23,800	37,100	1.41
2	**M1** (0.5)	1	19	12	15		9,200	7,600	1.30
		2	27	17	22		12,700	10,000	1.33
		4	34	22	27		16,000	12,500	1.45
		5	39	25	31	0.51/0.49	18,100	13,500	1.50
3	**M2** (0.1)	2	10	10	10		4,700	4,700	1.12
		4	16	17	16		7,300	7,000	1.11
		6	20	23	20		9,100	9,400	1.11
		8	24	29	25		10,900	12,200	1.11
		10	31	35	31	0.86/0.14	13,700	14,000	1.17
4	**M3** (0.13)	2	14	6	13		5,800	7,200	1.21
		4	24	11	22		9,200	10,700	1.23
		6	27	14	25		10,500	13,100	1.32
		10	38	13	36	0.87/0.13	13,900	12,300	1.34
		16	41	26	39		16,600	20,300	1.37
		18	45	28	43	0.95/0.05	18,100	22,700	1.50
5	**M3** (0.28)	4	13	3	10		4,800	6,800	1.11
		6	16	5	13		6,200	8,200	1.16
		8	23	6	18		8,300	10,000	1.16
		10	26	7	21	0.93/0.07	9,300	10,800	1.18
6	**M4** (0.1)	2	14	3	13		5,200	9,900	1.11
		4	24	6	22		8,500	12,500	1.12
		8	33	13	30		11,900	15,500	1.20
		10	36	20	34	0.95/0.05	13,400	18,100	1.20
		15	47	21	44		16,900	19,300	1.55
		19	50	23	47	0.95/0.05	18,000	20,800	1.62

7	**M4** (0.27)	2	12	4	10		4,500	6,500	1.12
		4	18	7	15		6,700	8,600	1.13
		6	20	8	17		7,400	9,600	1.15
		8	26	7	21		8,700	10,100	1.20
		14	37	9	29		11,900	12,100	1.35
		16	41	10	33		13,100	12,300	1.38
		18	41	10	33		13,100	12,500	1.35
		20	43	13	25	0.86/0.14	14,200	13,900	1.40
8	**M4** (0.52)	2	15	10	12		7,200	5,700	1.22
		4	19	12	15		8,700	6,100	1.36
		6	23	13	18		9,800	6,600	1.37
		8	22	12	17		9,200	6,900	1.39
		10	23	13	17	0.76/0.24	9,400	7,200	1.39
		20	24	13	18		10,000	7,700	1.44
9	**M5** (0.12)	2	10	9	10		4,200	3,600	1.10
		4	16	18	16		6,500	6,000	1.09
		6	21	28	22		8,600	8,600	1.09
		8	27	38	28		10,900	10,400	1.12
		10	31	48	33	0.88/0.12	12,800	12,300	1.14
		14	69	67	69		25,300	n.d.	n.d.
		16	75	88	77	ins. gel	28,300	n.d.	n.d.
10	**M5** (0.53)	2	9	5	7		3,300	2,700	1.16
		4	13	9	11		5,000	4,000	1.14
		6	17	10	13		5,900	5,000	1.15
		8	19	11	15		6,400	5,700	1.16
		10	22	14	18	0.52/0.48	7,700	6,500	1.18

[a] Conditions: bulk, M/R-Co(acac)$_2$ = 400/1, magnetic stirring at 500 rpm. [b] Determined by ^{1}H-NMR spectroscopy in acetone-d_6. [c] Composition of the copolymer determined by ^{1}H NMR spectroscopy in acetone-d_6 based on the α-chain end (see above). [d] $M_{n\ theo} = M_{w\ init} + (Conv_{\ Comon} \times M_{w\ Comon} + Conv_{\ VAc} \times M_{w\ VAc}) + M_{w\ TEMPO}$ (for more information see above). [e] Determined by size exclusion chromatography (SEC) in DMF/LiBr using a PS standard.

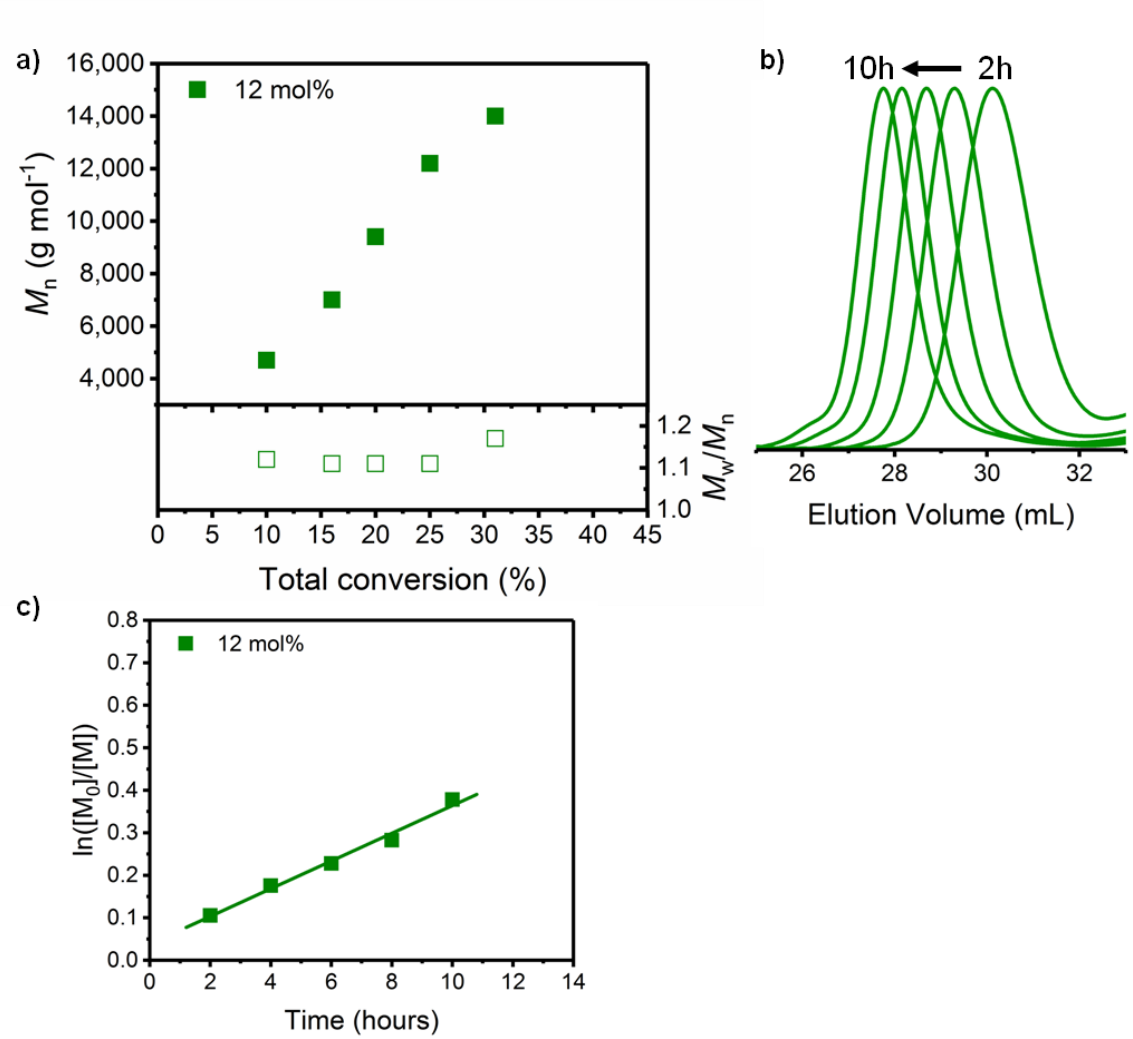

Figure 84. OMRP at 40 °C of **M2** with VAc at 12 mol% **M2** feed: a) M_n and dispersity versus total monomer conversion plot, b) size-exclusion traces and c) first-order kinetic logarithm plot with linear fits.

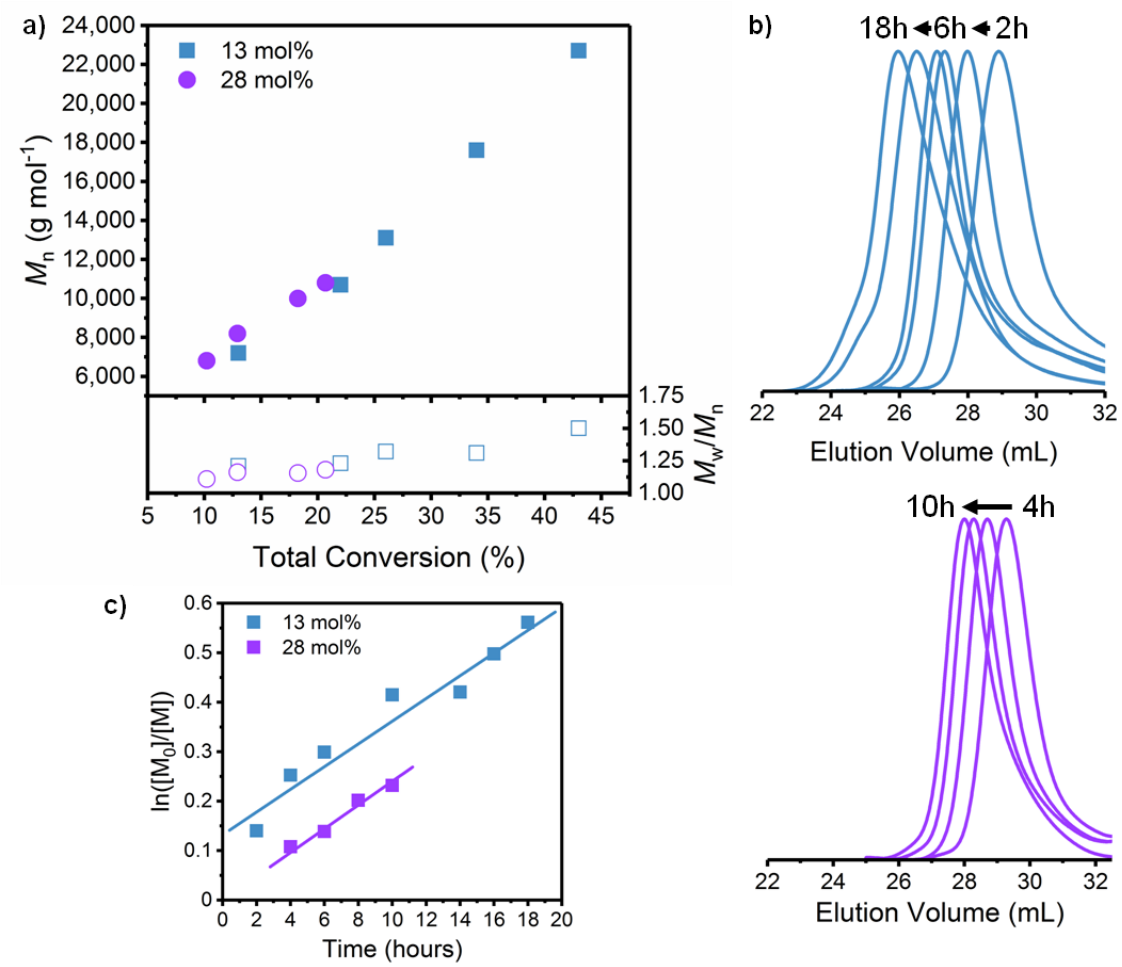

Figure 85. OMRP at 40 °C of **M3** with VAc at 13 and 28 mol% **M3** feed: a) M_n and dispersity versus total monomer conversion plot, b) size-exclusion traces and c) first-order kinetic logarithm plot with linear fits.

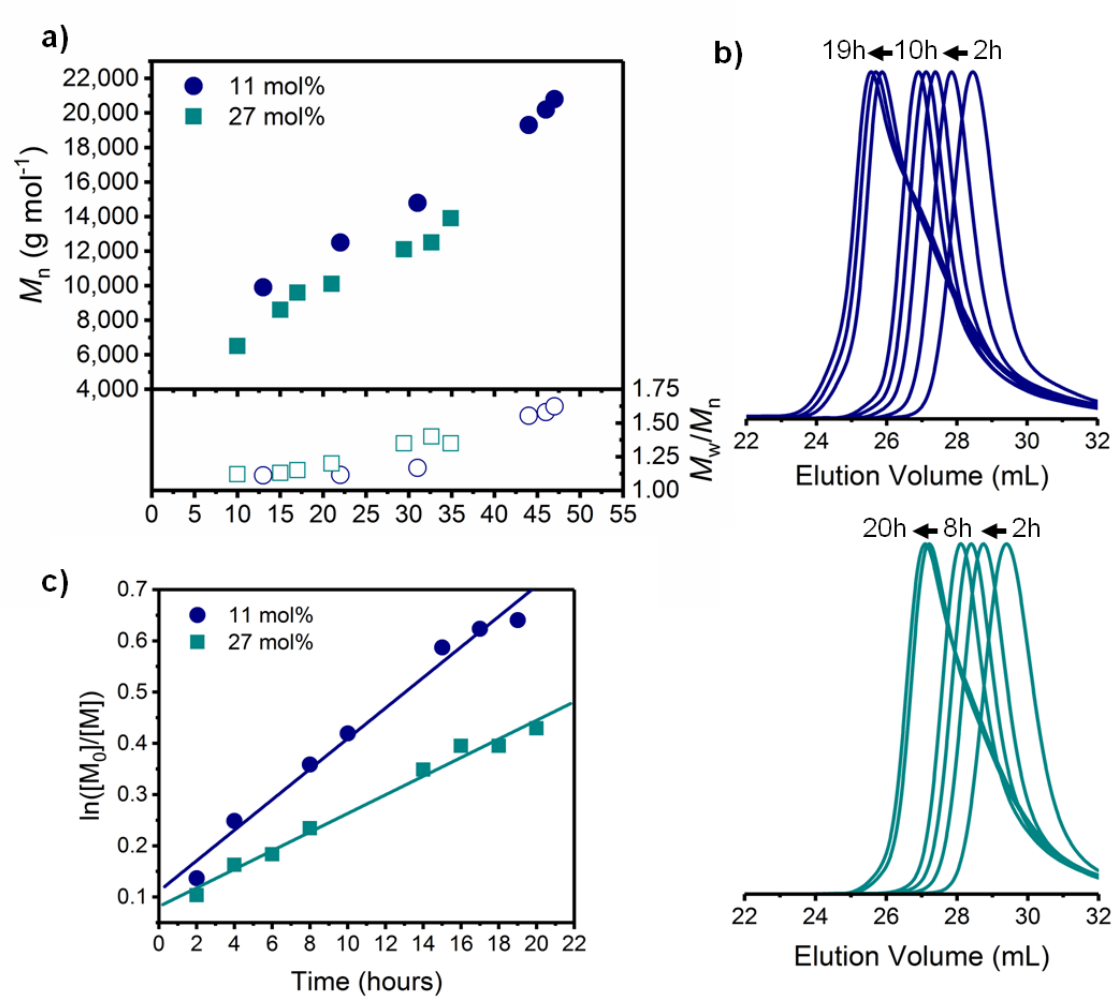

Figure 86. OMRP at 40 °C of **M4** and VAc at 11 and 27 mol% **M4** feed: a) M_n and dispersity versus total monomer conversion plot, b) size-exclusion traces and c) first-order kinetic logarithm plot with linear fits.

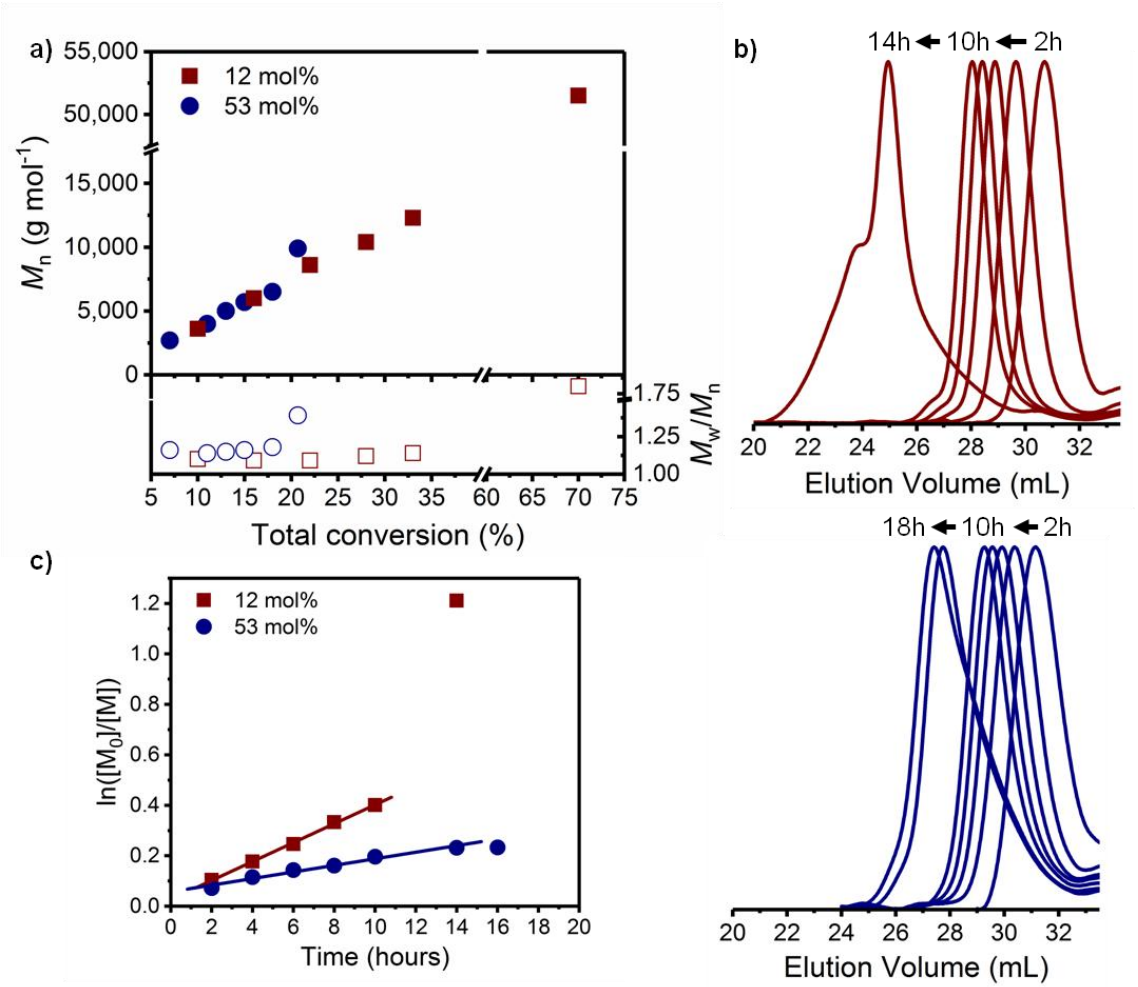

Figure 87. OMRP at 40 °C of **M5** with VAc at 12 and 53 mol% feed **M5**: a) M_n and dispersity versus total monomer conversion plot, b) size-exclusion traces and c) first-order kinetic logarithm plot with linear fits.

Supercritical CO_2 extraction

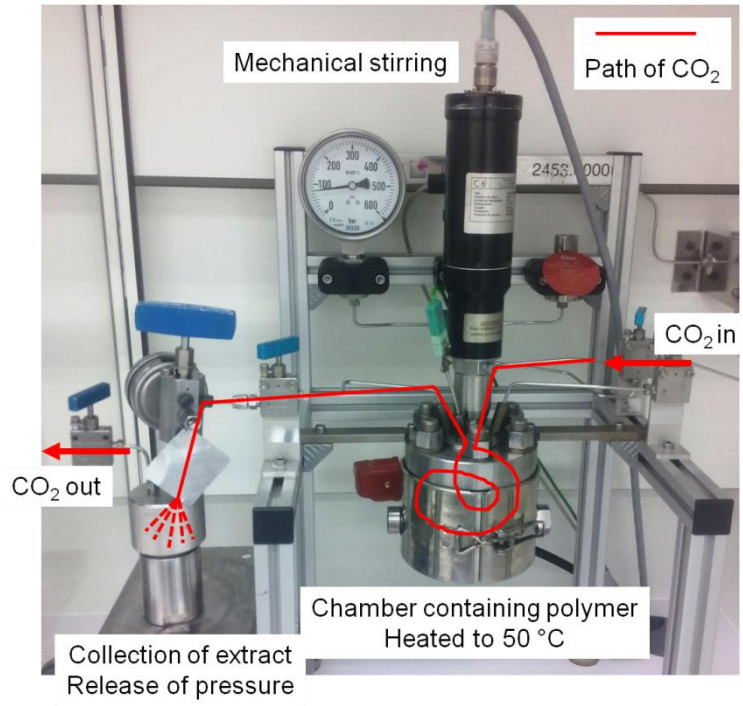

Figure 88. Reactor set-up for the $scCO_2$ extraction of the prepared polymers

Table 15. Representative examples of recovered monomer after $scCO_2$ purification

Entry	Comonomer	Conversion in Comonomer (%)	Unreacted Comonomer (mg)	Comonomer recovered (mg)	% recovered
1	**M1**	25	346.1	116.5	34
2	**M2**	35	317.5	100.8	32
3	**M3**	43	366.2	211.6	58
4	**M4**	18	855.0	384.6	45

NMR spectra of synthesised polymers

Unless otherwise stated, the NMR spectra were recorded in Acetone-d_6 on a 400 MHz instrument

P1

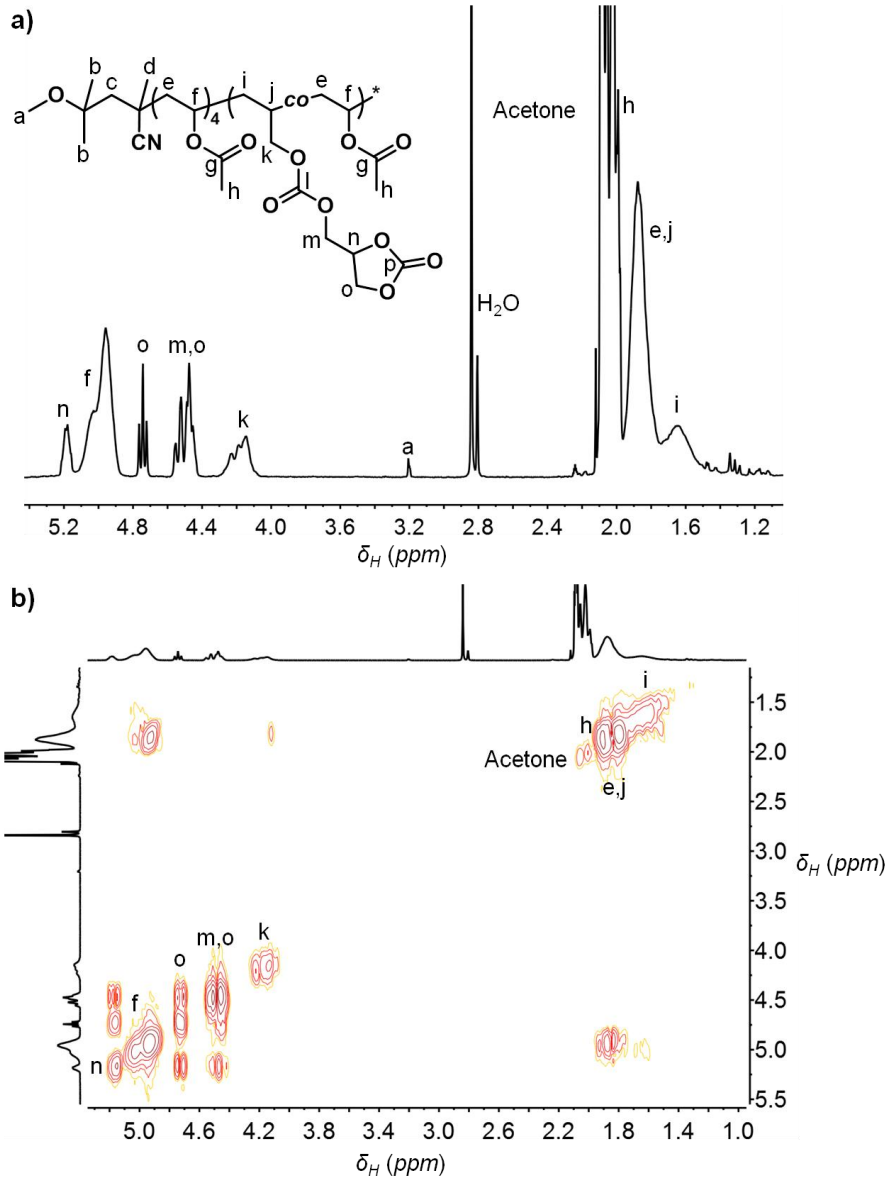

Figure 89. a) ^{1}H-NMR spectrum and b) COSY spectrum of a **P1** copolymer at 57% conversion containing 11 mol% **M1** (entry 1, Table 14)

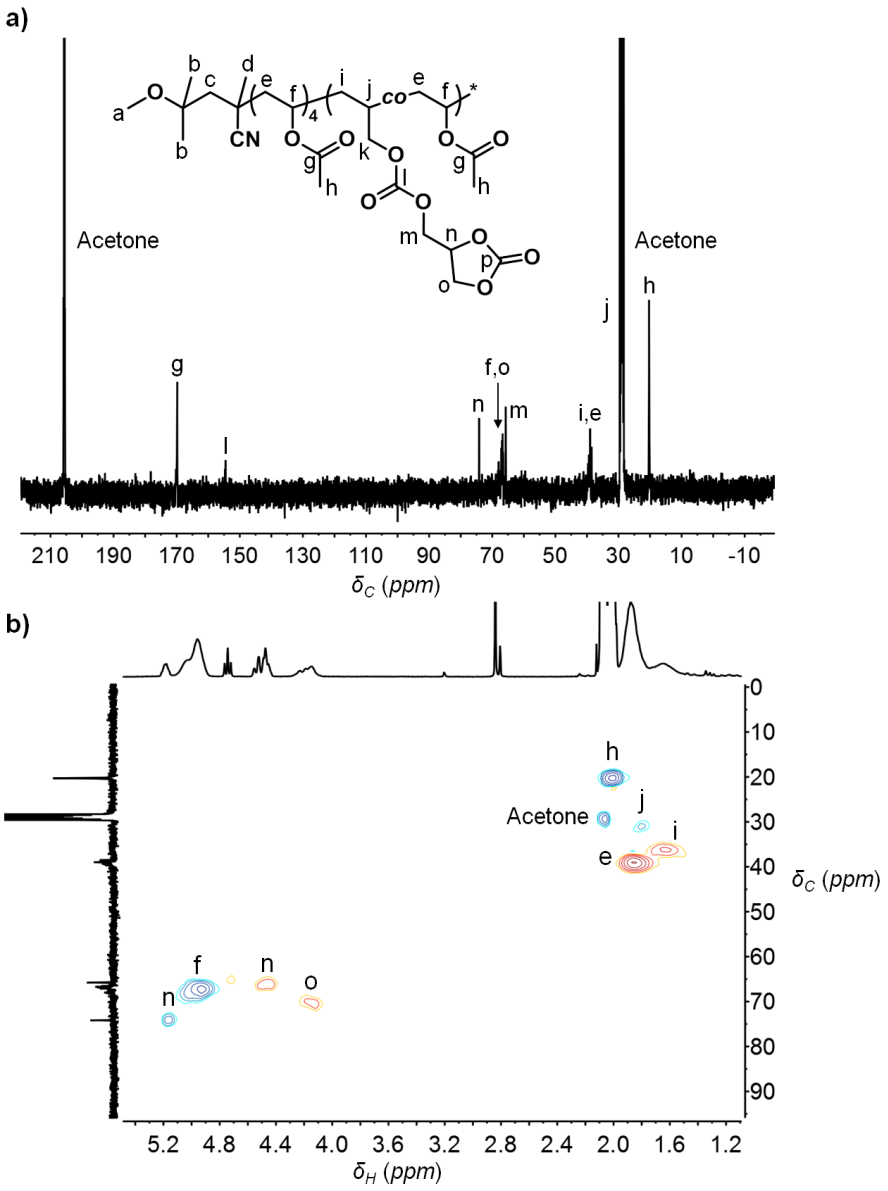

Figure 90. a) ^{13}C-NMR spectrum and b) HSQC spectrum of a **P1** copolymer at 57% conversion containing 11 mol% **M1** (entry 1, Table 14)

P2

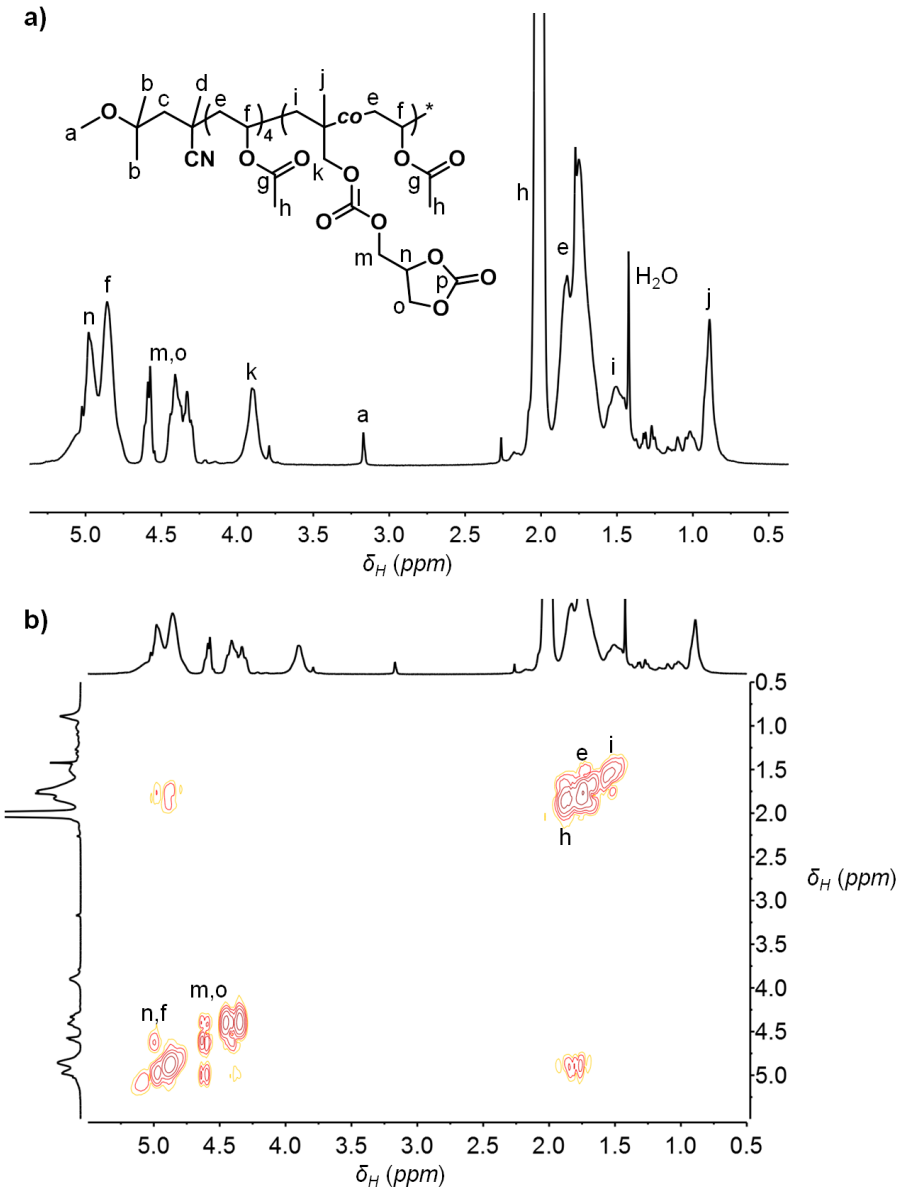

Figure 91. a) ^{1}H-NMR spectrum and b) COSY spectrum of a **P2** copolymer at 31% conversion and containing 14 mol% **M2** (entry 4, Table 1) taken on a 400 MHz spectrometer in $CDCl_3$

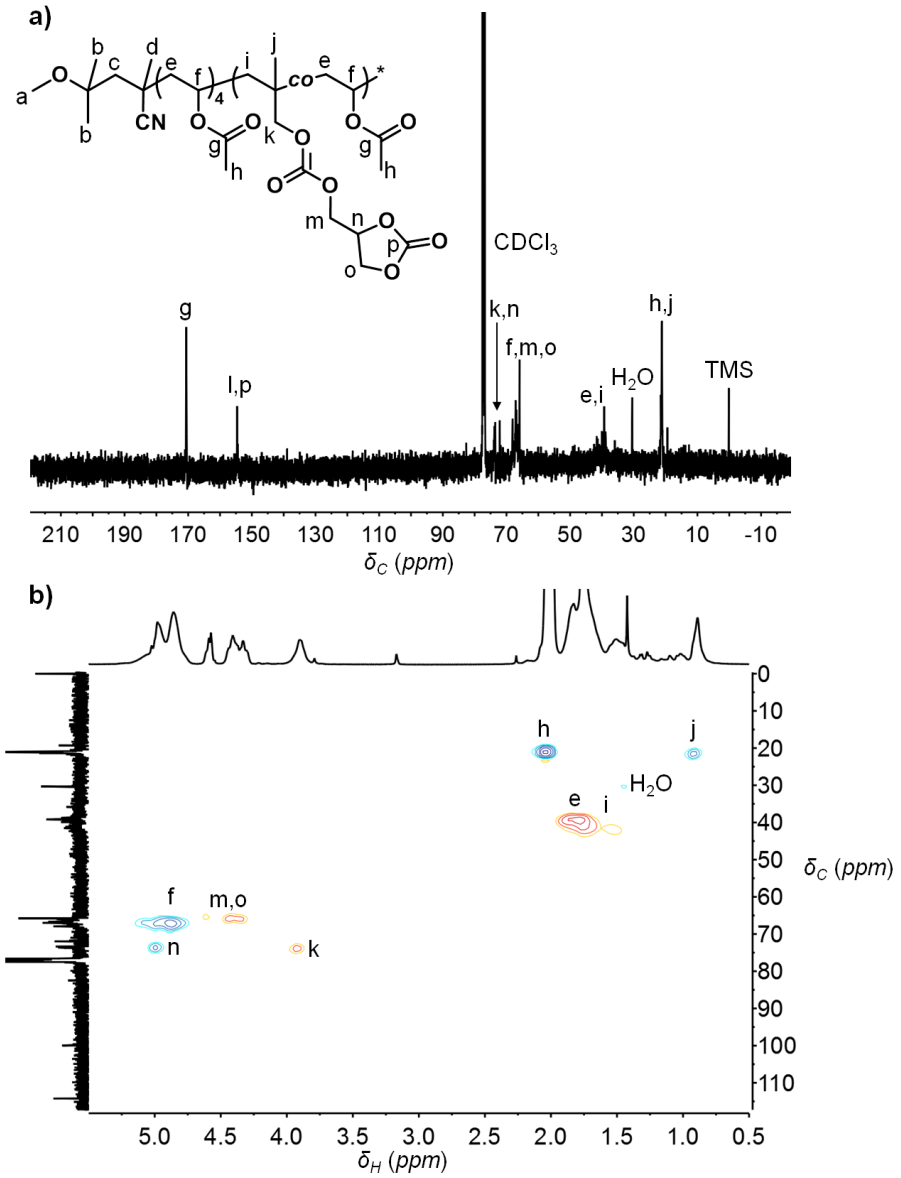

Figure 92. a) ^{13}C-NMR spectrum and b) HSQC spectrum of a **P2** copolymer at 31% conversion and containing 14 mol% **M2** (entry 4, Table 1) taken on a 400 MHz spectrometer in $CDCl_3$

P3

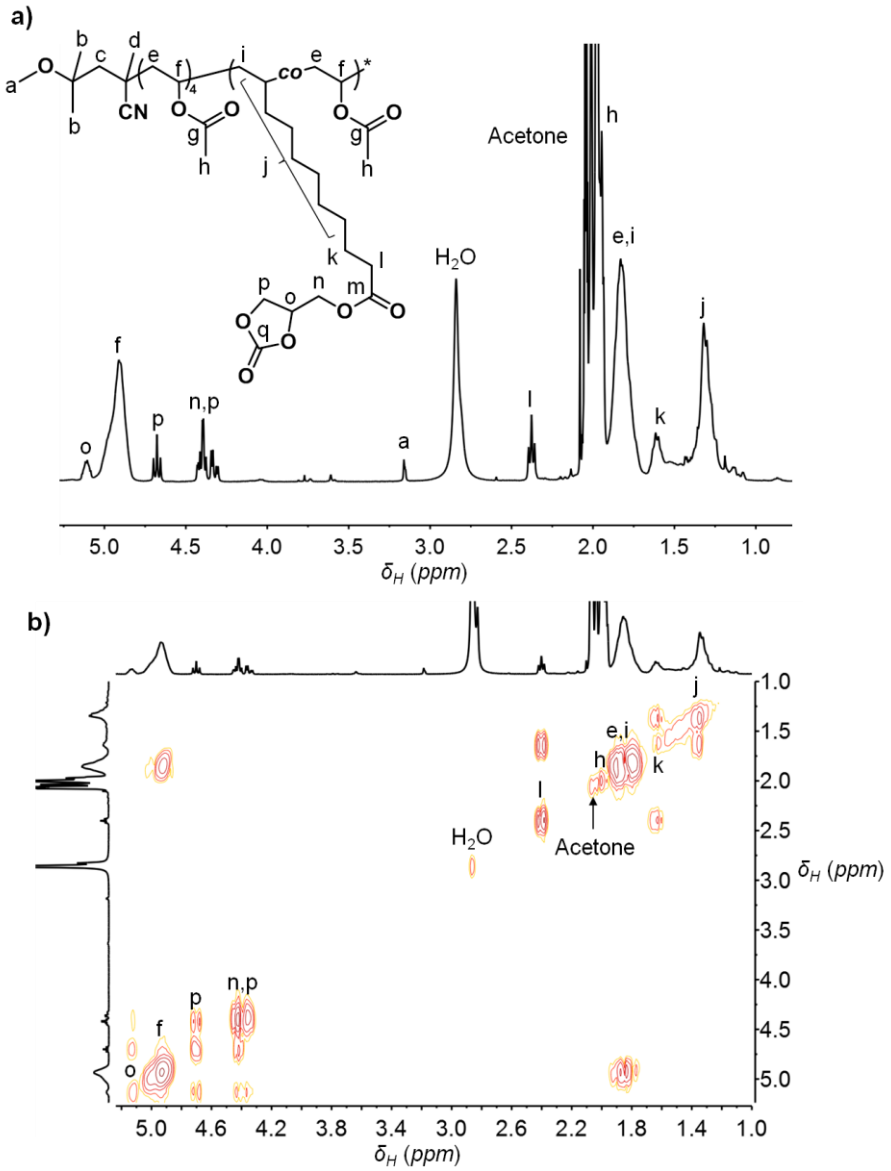

Figure 93. a) ^{1}H-NMR spectrum and b) COSY spectrum of a **P3** copolymer at 36% conversion containing 7 mol% **M3** (entry 5, Table 1)

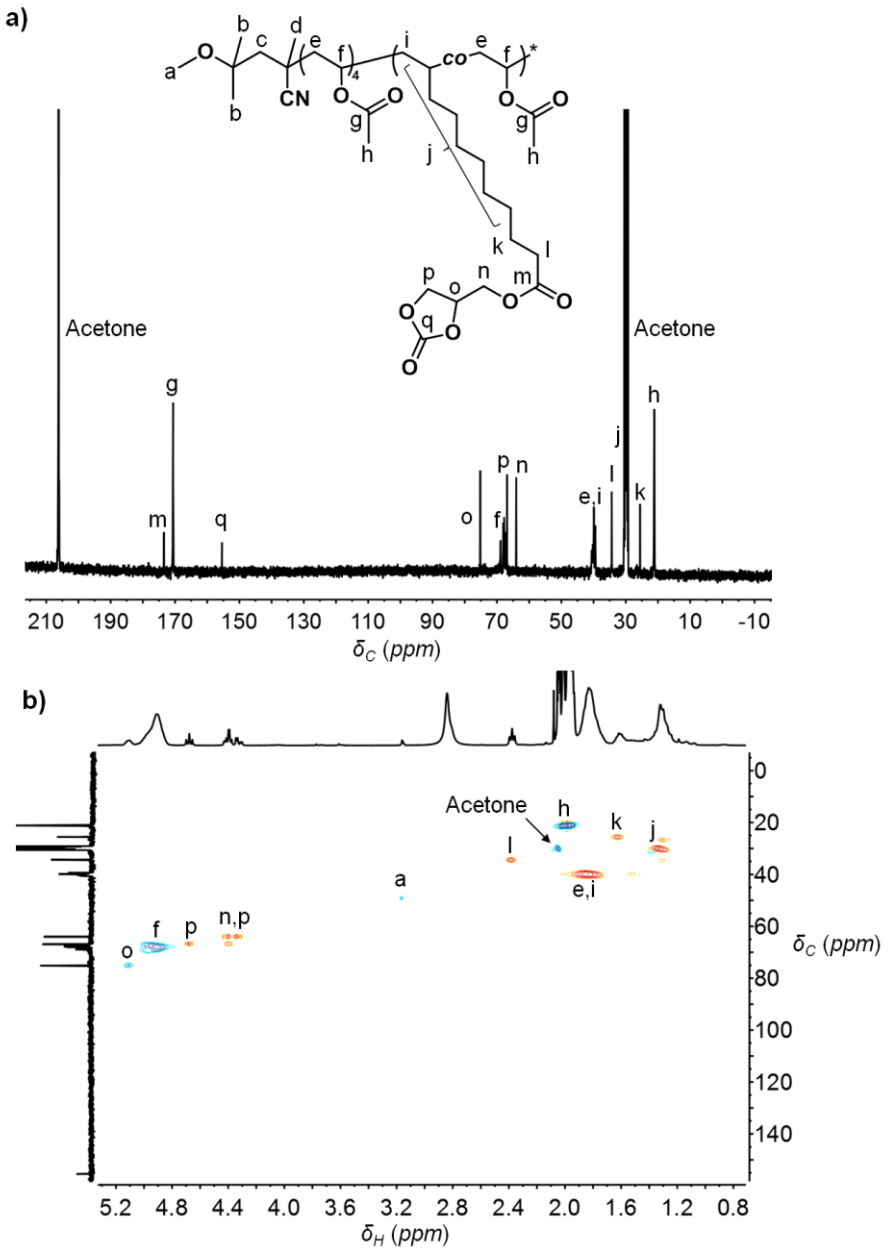

Figure 94. a) ^{13}C-NMR spectrum and b) HSQC spectrum of a **P3** copolymer at 36% conversion containing 7 mol% **M3** (entry 5, Table 1)

P4

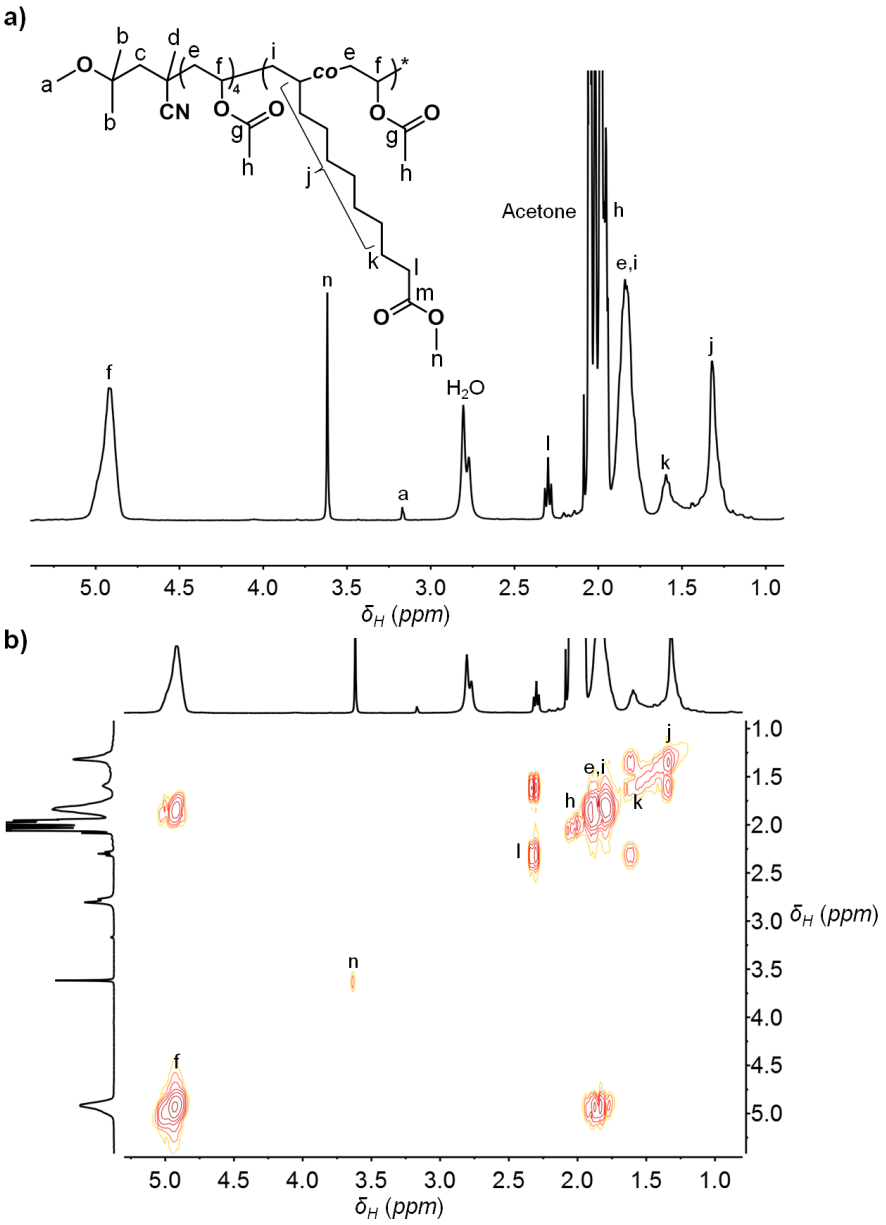

Figure 95. a) ^{1}H-NMR spectrum and b) COSY spectrum of a **P4** copolymer at 47% conversion containing 5 mol% **M4** (entry 7, Table 1)

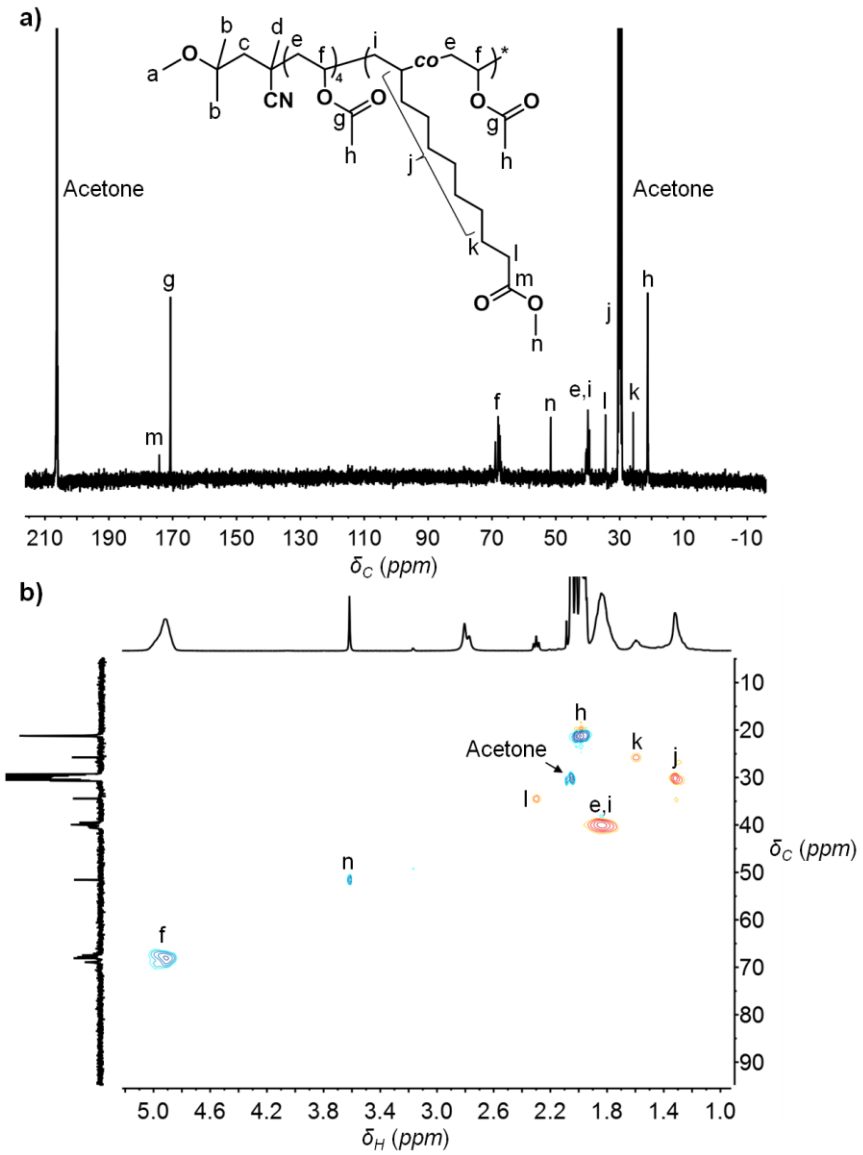

Figure 96. a) ^{13}C-NMR spectrum and b) HSQC spectrum of a **P4** copolymer at 47% conversion containing 5 mol% **M4** (entry 7, Table 1)

P5

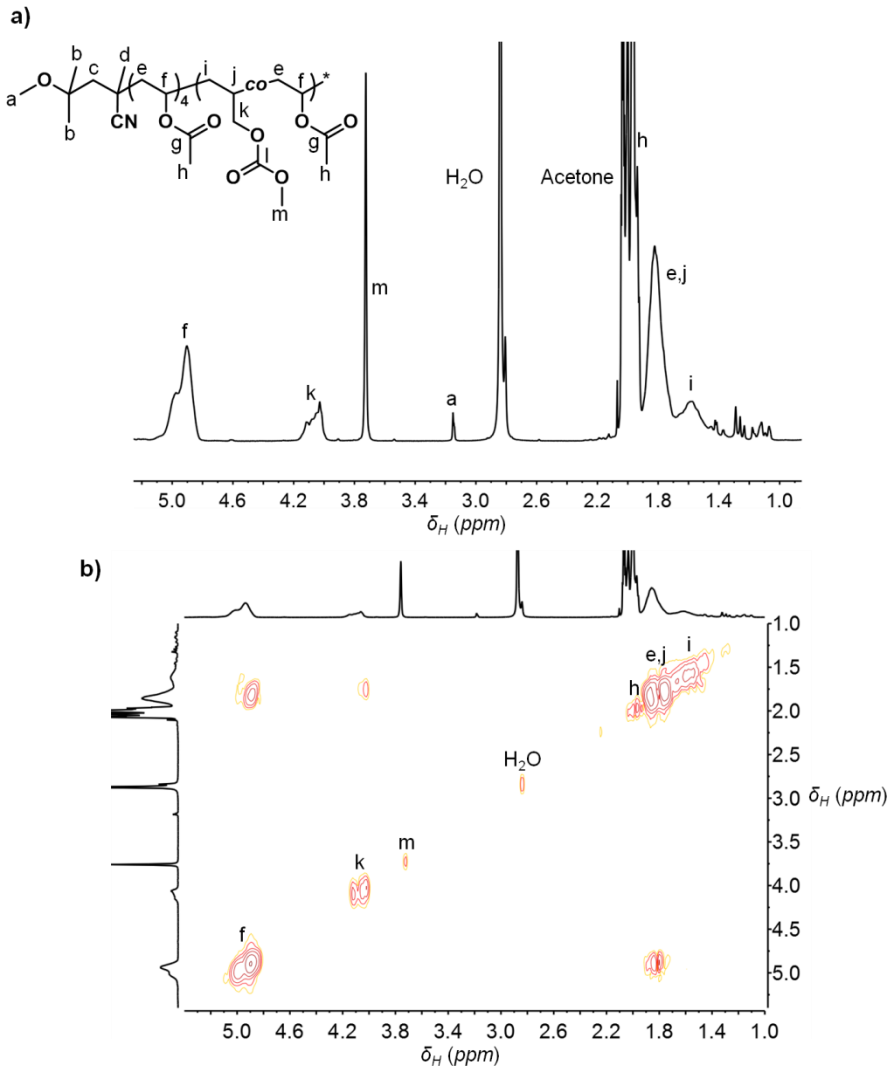

Figure 97. a) ^{1}H-NMR spectrum and b) COSY spectrum of a **P5** copolymer at 33% conversion containing 13 mol% of **M5** (entry 10, Table 1)

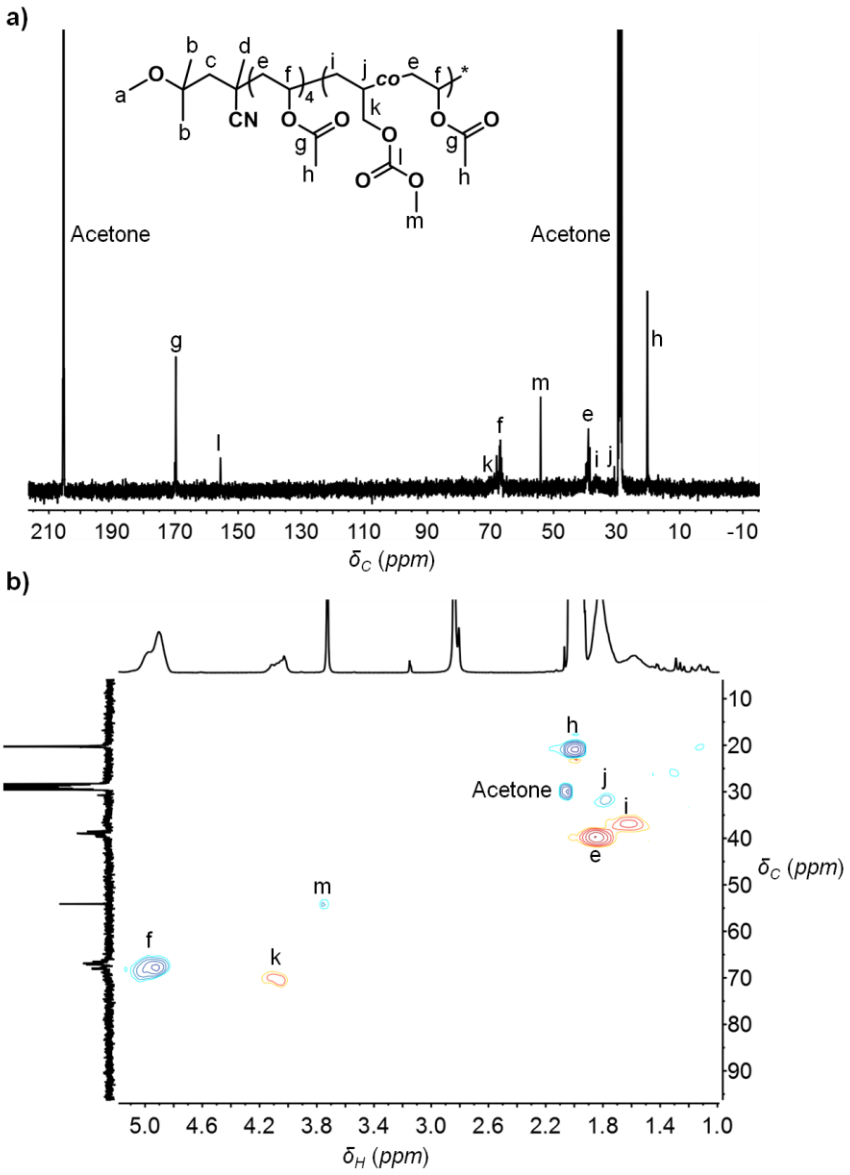

Figure 98. a) ^{13}C-NMR spectrum and b) HSQC spectrum of a **P5** copolymer at 33% conversion containing 13 mol% of **M5** (entry 10, Table 1)

FT-IR spectra of synthesised copolymers P1-P5

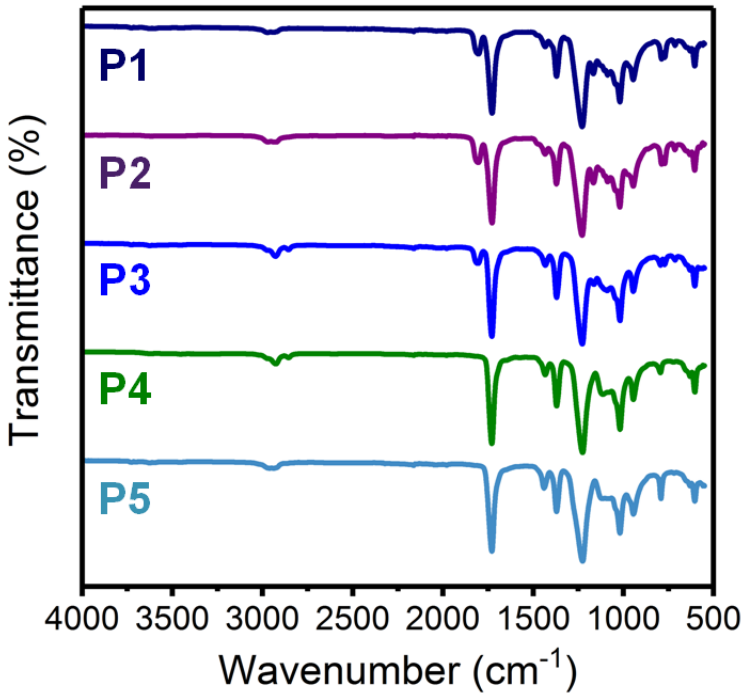

Figure 99. Overlay of the FT-IR spectra of copolymers synthesised using OMRP at 40 °C at a feed of 0.9/0.1 VAc/Comonomer (entries 1, 3, 4, 6, and 9, Table 1)

TGA curves for VAc copolymers with high comonomer content

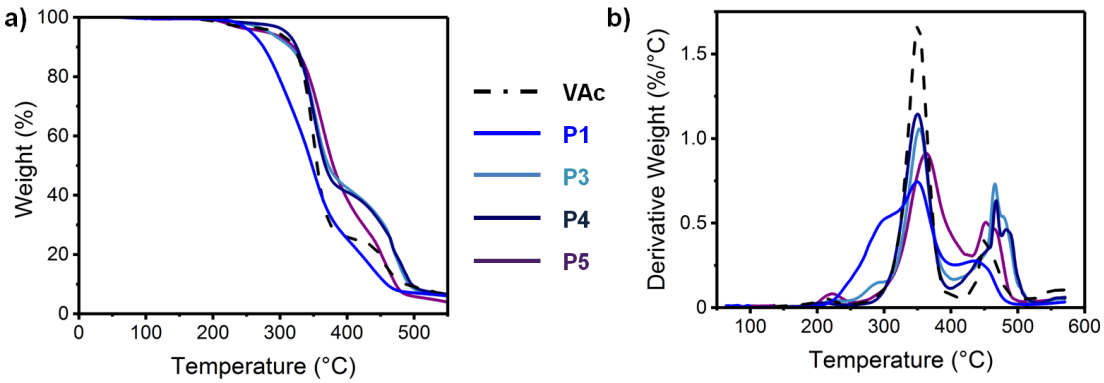

Figure 100. Thermal gravimetric analysis (TGA) for poly(vinyl acetate) and its copolymers with different renewable monomers at high comonomer content. a) Weight versus temperature curve and b) the derivative weight against temperature curve.

10.4. Experimental Section for Chapter 5

Monomer synthesis

A previous literature procedure[308] for the synthesis of 4,4-dimethyl-5-methylene-1,3-dioxolan-2-one (**DMMDO**) was slightly modified: After the removal of triethylamine, the remaining zinc was removed by a silica oxide filter column and the product was purified by sublimation. Prior to use, the solid was degassed using 3 cycles of freeze-pump-thawing.

Copolymerisation of DMMDO with VAc.

A typical bulk VAc copolymerisation aiming at a f_{DMMDO}= 0.10 (Entry 4, Table 2) was carried out at 40 °C using a molar ratio of $[VAc]_0/[\mathbf{DMMDO}]_0/[R\text{-}Co(acac)_2]_0$ = 360/40/1. A solution of R-Co(acac)$_2$ (0.6 mL; 0.1136 M stock solution in CH_2Cl_2, 0.06816 mmol) was introduced under argon into a purged 30 mL Schlenk tube and evaporated to dryness under reduced pressure at room temperature. VAc (2.3 mL, 25.0 mmol) was added under argon to give solution **A**. In a second 30 mL Schlenk tube, 4,4-dimethyl-5-methylene-1,3-dioxolan-2-one (**DMMDO**; 0.2911 g, 2.27 mmol) was added and heated to 40 °C and stirred at 500 rpm. 1.9 mL of solution **A** were transferred to this second Schlenk tube using a syringe under argon atmosphere and an ^{1}H-NMR spectroscopy aliquot was immediately taken to determine the monomer feed ratio. The copolymerisation occurred at 40°C under stirring. At regular intervals, aliquots of the reaction mixture were taken for NMR and SEC analyses to determine conversions and the molecular parameters of the polymer, respectively. The M_n of these non-precipitated reaction mixtures was determined by integrating the copolymer peak while excluding the small peak originating from deactivated R-Co(acac)$_2$. When the polymers were precipitated, this small peak was not present. After 25 hours, the reaction mixture was quenched using a degassed solution of TEMPO (150 mg, 1 mmol) in 2 mL of THF and was passed over a micro silica column to remove the cleaved cobalt. The polymer was then precipitated three times in n-pentane (~200 mL) from THF and dried overnight under vacuum at 50 °C.

For the polymer to be analysed by MALDI-TOF, a molar ratio of $[VAc]_0/[\mathbf{DMMDO}]_0/[R\text{-}Co(acac)_2]_0$ = 90/10/1 was used and a solution of R-Co(acac)$_2$ (1.33 mL; 0.1710 M stock solution in CH_2Cl_2, 0.2272 mmol) was introduced under argon into a purged 30 mL Schlenk tube and evaporated to dryness under reduced pressure at room temperature. VAc (1.9 mL, 20.6 mmol) was added under argon and the solution was added to a second 30 mL Schlenk tube, in which 4,4-dimethyl-5-methylene-1,3-dioxolan-2-one (**DMMDO**; 0.2911 g, 2.27 mmol) had been added. The reaction mixture was heated to 40 °C at 500 rpm stirring. A ^{1}H-NMR spectroscopy aliquot was immediately taken to determine the monomer feed ratio. The

copolymerisation occurred at 40 °C under stirring and after 6 hours of polymerisation at 42% overall conversion, ~1 mL of the reaction mixture was transferred to a purged Schlenk containing propanethiol (1mL, 11 mmol) and allowed to react for 1 hour, dried under vacuum, then dissolved in THF and passed over 0.45 µm filter to remove the thiol-cobalt complex and finally dried under vacuum at 50 °C. The remaining reaction solution was purified as previously described and analysed using NMR spectroscopy, FT-IR and SEC.

100 mg of the copolymer (entry 12, Table 16) to be analysed by the ICP-OE spectrometer were added to 2 mL of HNO_3 and allowed to react for 2 hours at 65 °C. After dilution with 10 mL of distilled water, the solution was filtered, filled into a 25 mL volumetric flask and made up to 25 mL.

Determination of reactivity ratios

Reactivity ratios were determined by using both V-70 and R-Co(acac)$_2$ as the initiator and molar ratios of monomer to initiator of 400:0.5 and 400:1 were used respectively. Using OMRP, the same protocol as above was used, while for free radical polymerisations using V-70, reaction feeds ranged from 10 to 80 mol% of DMMDO. A typical reaction with a molar ratio of 10 : 90 of **DMMDO**:VAc was performed as follows: In a 15 mL Schlenk flask, V-70 (8.8 mg, 0.0284 mmol) and **DMMDO** (0.2911 g, 2.27 mmol) were weighed out and degassed three times using freeze-pump-thaw cycles. The Schlenk flask was heated to 40 °C at 500 rpm stirring and VAc (2.3 mL, 2.5 mmol) was added. A ^{1}H-NMR sample was immediately taken to determine the feed of the reaction. In order to stop the reactions at conversions below 15%, the reaction was monitored by taking aliquots and precipitating these in a small amount of n-pentane (20 mL). Once a precipitate was observed, a ^{1}H-NMR sample was taken of the reaction mixture to determine the conversion and the reaction was quenched using TEMPO/THF (150 mg, 1 mmol; in 2 mL). The polymer was precipitated three times into n-pentane (200 mL) from THF for feeds below 50 mol% **DMMDO** and 5 times above 50 mol%. The polymer was then dried in vacuum overnight at 50 °C. SEC and ^{1}H-NMR spectroscopy analysis were performed to determine the molecular parameters and the composition of the polymer. The reaction time, feed of the polymerisation medium, conversion and composition of the copolymer were used to create different plots according to Kelen-Tüdos and the Mayo-Lewis equation (Equation 12-Equation 13).[322–324]

The Kelen-Tüdos linearisation can be obtained from the Mayo-Lewis equation (Equation 12). Using the mole ratios of the monomers in the feed (f) and in the copolymer (F) along with parameter α (f^2/F) two mathematical functions ζ and η (Equation 13) were created. A linear

plot of η as a function of ζ leads to r_1 and ($-r_2/\alpha$) *via* the intercepts at ζ = 1 and ζ = 0, respectively.

Equation 12 $F_1 = (r_1 f_1^2 + f_1 f_2) / (r_1 f_1^2 + 2 f_1 f_2 + r_2 f_2^2)$

Equation 13 $\eta = (r_1 + (r_2/\alpha)) \zeta - (r_2/\alpha)$

where $f = f_1/f_2$ and $F = F_1/F_2$

$\eta = (f(F\text{-}1)) / (F(\alpha + (f^2/F))$

$\zeta = (f^2/F) / (\alpha + (f^2/F))$

$\alpha = ((f^2/F)_{max} \times (f^2/F)_{min})^{0.5}$

Using the above determined reactivity ratios, the Skeist model[381] was applied, which allows to predict the instantaneous and cumulative copolymer composition as well as the instantaneous feed (Equation 14).

Equation 14

$$Conversion = 1 - (M/M_0) = 1 - (f_1/f_1^0)^{\propto} (f_2/f_2^0)^{\beta} [(f_1^0 - \delta)/(f_1 - \delta)]^{\gamma}$$

where M_0 and M are the initial and instantaneous monomer concentrations and f^0 and f correspond to the initial and instantaneous molar fractions of the monomers in the feed, respectively. α, β, δ and γ are defined as $\alpha = r_2/(1-r_2)$, $\beta = r_1/(1-r_1)$, $\gamma = (1-r_1 r_2)/(1-r_1)(1-r_2)$, and $\delta = (1-r_2)/(2-r_1-r_2)$.

The cumulative copolymer composition was calculated using: $F_{1\ cumul} = [f_1^{\ 0} - f_1 (1-$ conversion)]/ conversion

Hydrolysis and methanolysis of P(VAc-*co*-DMMDO)

Both acidic and basic hydrolysis were performed on a copolymer containing 19 mol% **DMMDO** (M_n = 18,400 g mol^{-1}, M_w/M_n = 1.29; entry 10, Table 16).

Acidic hydrolysis. 500 mg of the copolymer were dissolved in 5 mL of THF and added to a 25 mL round bottom flask. 5 mL of deionised water and 0.5 mL of concentrated, fuming HCl (37% solution, 6.038 mmol) were added and the solution was refluxed at 90 °C for 48 hours at 500 rpm. An orange-yellow solution was obtained. The reaction mixture was neutralised using a 1M NaOH solution and transferred to a 1 kDa regenerated cellulose dialysis tubing, which was dialysed in a water/MeOH mixture starting with 30 vol% of water, then 20 vol%, 5% and pure methanol. The solution was lyophilised to obtain 192.1 mg of a bright yellow solid. FT-IR: ν_{max}: 3330 cm^{-1} (b, OH stretch); 2900 cm^{-1} (b, C-H stretch); 1780 cm^{-1} (s, -O-(*C*=O)-O- stretch). ^{13}C-NMR (400 MHz, DMSO-d_6): 170 ppm (-O-(C=O)-O-); 90 ppm (CH_2-

$\underline{C}$-$\underline{C}$-(CH_3)$_2$-); 65 ppm (-$\underline{C}$H-OH); 47 ppm (-$\underline{C}$H$_2$-CH-OH); 40 ppm (-$\underline{C}$H$_2$-C-O-); 22 ppm (-C-$\underline{C}$H$_3$). The ^{1}H-NMR peaks are assigned in Figure 9.

Methanolysis. 3.7 g NaOH (0.093 mol) were dissolved in 150 mL MeOH in a 250 mL round-bottom flask, to which 500 mg of the copolymer dissolved in 5 mL of THF were added. The mixture was refluxed at 65 °C for 24 hours at 500 rpm. The resulting solution was neutralised using a 1M HCl solution, stripped of its solvent until around 15 mL remained and dialysed using 1kDa regenerated cellulose tubing in a water/MeOH mixture starting with 30 vol% of water, then 20 vol%, 5% and pure methanol. The solution was lyophilised to obtain 123.6 mg of a brick-red powder. FT-IR: 3330 cm^{-1} (b, OH stretch); 2900 cm^{-1} (b, C-H stretch). ^{13}C-NMR (400 MHz, DMSO-d_6): 65 ppm (-$\underline{C}$H-OH); 45 ppm (-$\underline{C}$H$_2$-CH-OH and -$\underline{C}$H$_2$-C-O-); 22 ppm (-C-$\underline{C}$H$_3$). The ^{1}H-NMR peaks are assigned in Figure 51.

To compare the influence of the comonomer on the polymer characteristics, a copolymer and a PVAc homopolymer of equivalent DP were synthesised (entries 1 and 2, Table 18). The copolymer was hydrolysed as outlined above, while 1 g of the PVAc homopolymer was methanolysed using 0.25 g KOH in 60 mL MeOH at room temperature for 24 hours, as previously described.[326] After filtration and dialysis in water using 1kDa tubing and subsequent lyophilisation, 446 mg of a white solid were obtained. The methanolysed copolymer (P(VOH-*co*-BD)) and PVOH were dissolved in 0.5 mL water at different concentrations (1, 10, 25, 50, 150, 375 g/L) and the temperature increased from 20 °C to 80 °C, noting the temperature at which the polymer solubilised (Table 19).

Post-polymerisation modification of selectively hydrolysed copolymer

A P(VAc-*co*-**DMMDO**) copolymer (entry 12, Table 16) subjected to acidic/selective hydrolysis was post-modified using butylamine. 100 mg of P(VOH-*co*-**DMMDO**) and 2 mg of TBD (0.01 mmol) were dissolved in 0.5 mL of dry butylamine (0.37 g, 5.059 mmol) and 0.5 mL dry DMF and heated to 80 °C for 24 hours in a Schlenk flask. The reaction mixture was precipitated into 100 mL cold diethyl ether, dialysed in MeOH using a 1 kDa cellulose tubing and then lyophilised to remove residual solvent. The obtained 85 mg of modified copolymer were analysed by NMR spectroscopy and FT-IR.

Determination of monomer conversion

For all the kinetic experiments, the consumption of VAc during the reaction was determined by comparing the integrals of the ^{1}H-NMR spectroscopy peak centred at 4.89 ppm corresponding to one proton of the C$\underline{H_2}$= of the monomer VAc and the –C$\underline{H}$-OAc in the copolymer ($\int_{4.62}^{5.40} Mon(CH_2) + Pol(CH)$) with the peak centred at 4.58 ppm corresponding to the –C$\underline{H}$-OAc of only the monomer VAc ($\int_{4.44}^{4.62} Mon(CH)$, Equation 15). Since one of the

symmetric vinyl –C<u>*H*</u> peaks of **DMMDO** overlaps with the peak centred at 4.89 ppm, the integral of the other –C<u>*H*</u> peak of **DMMDO** at 4.32 ppm ($\int_{4.20}^{4.44} DMMDO(CH)$) is subtracted (Equation 15). For the conversion of **DMMDO**, the monomer –C<u>H_3</u> peak at 1.50 - 1.70 ppm ($\int_{1.50}^{1.70} Mon(CH_3)$) was integrated with respect to a broad doublet at 1.50-1.34 ppm corresponding to the two –C<u>H_3</u> environments in the polymer ($\int_{1.34}^{1.50} Pol(CH_3)$); Equation 16).

Equation 15

$$\%\ VAc\ conversion = \left(1 - \frac{\int_{4.44}^{4.62} Mon(CH)}{\int_{4.62}^{5.40} Pol(CH) + Mon(CH) - \int_{4.20}^{4.44} DMMDO(CH)}\right) \times 100$$

Equation 16

$$\%\ DMMDO\ conversion = \frac{\int_{1.34}^{1.50} Pol(CH_3)}{\int_{1.50}^{1.70} Mon(CH_3)} \times 100$$

where $\int_m^n CH_x$ is the integral of the CH_x environment from *m* ppm to *n* ppm.

Calculation of the theoretical molecular weight ($M_{n\ theo}$)

The theoretical molecular weight ($M_{n\ theo}$) was calculated by adding the molecular weight of the initiator fragment ($M_{w\ init}$ = 485.57 g mol^{-1}) and the TEMPO chain-end ($M_{w\ TEMPO}$ = 156.25 g mol^{-1}) to the molecular weight of the copolymer chain ($M_{n\ chain}$) which was calculated using the conversion of VAc and **DMMDO** according to the equation below:

Equation 17

$$M_{n\ chain} = M_{w\ VAc} \times Conv_{VAc} \times f^0_{VAc} + M_{w\ DMMDO} \times Conv_{DMMDO} \times f^0_{DMMDO}$$

Where $M_{w\ Mon}$ is the molecular weight of the monomer in g mol^{-1}, $Conv_{Mon}$ is the conversion of the monomer and f^0_{Mon} is the initial feed of the monomer in the reaction mixture.

Equation 18

$$M_{n\ theo} = M_{w\ init} + M_{w\ TEMPO} + M_{n\ chain}$$

Determination of the copolymer composition

The copolymer composition of P(VAc-*co*-**DMMDO**) was determined by ^{1}H-NMR spectroscopy of the purified polymers in $CDCl_3$ (Figure 102). The degree of polymerisation of VAc (DP_{VAc}) was determined by ^{1}H-NMR spectroscopy by comparing the integrals of the methoxy groups (O-*CH*$_3$) ($\int_{3.05}^{3.25} OCH_3$) at the α-chain end at 3.15 ppm with the integral of –*CH*- of the VAc repeating unit (-CH$_2$-*CH*OAc) ($\int_{4.5}^{5.6} CH$) at 4.8 ppm. The equation to determine DP_{VAc} is:

Equation 19

$$\text{DP of VAc} = \int_{4.5}^{5.6} CH \,/ \left(\frac{\int_{3.05}^{3.25} OCH_3}{3}\right)$$

The DP of **DMMDO** (DP_{DMMDO}) was determined by comparing the integrals of the methoxy groups (-O*CH*$_3$) ($\int_{3.05}^{3.25} OCH_3$) at the α-chain end at 3.15 ppm with the integral of all protons from 2.6 - 1.2 ppm ($\int_{1.2}^{2.6} H$; corresponding to 5H of VAc unit (-<u>*CH*$_2$</u>-CHOC(=O)<u>*CH*$_3$</u>) + 8H of **DMMDO** unit (-<u>*CH*$_2$</u>-C-C(<u>*CH*$_3$</u>)$_2$-O-C=O)-O-) + 11H of the initiating fragment (CH$_3$O-C(<u>*CH*$_3$</u>)$_2$-<u>*CH*$_2$</u>-C(*CH*$_3$)(CN)-). The equation to determine DP_{DMMDO} is:

Equation 20

$$\text{DP of DMMDO} = \left(\frac{\int_{1.2}^{2.6} H - 5 \times \int_{4.5}^{5.6} CH - 11 \times \left(\frac{\int_{3.05}^{3.25} OCH_3}{3}\right)}{8}\right) / \left(\frac{\int_{3.05}^{3.25} OCH_3}{3}\right)$$

The copolymer composition of P(VOH-*co*-**DMMDO**) was determined by ^{1}H-NMR spectroscopy of the purified polymers in DMSO-d_6 (Figure 103). The DP of VOH (DP_{VOH}) was identical to DP_{VAc} of the starting P(VAc-*co*-**DMMDO**). The DP of **DMMDO** (DP_{DMMDO}) was determined by comparing the integrals of the VOH unit (-CH_2-*CH*(OH)-) at 3.8 ppm ($\int_{3.5}^{4.1} CH(OH)$ $\int_{3.5}^{4.1}$ CH(OH)) with the integral of the **DMMDO** unit (2H; -*CH*$_2$-C-C(CH_3)$_2$-O-C(=O)-O-) ($\int_{1.80}^{2.28} CH_2$))$\int_{1.80}^{2.28}$ CH2) by the following equation:

Equation 21

$$\text{DP of DMMDO} = (DP_{VOH} \times \left(\frac{\int_{1.80}^{2.28} CH_2}{2}\right) / \int_{3.5}^{4.1} CH(OH)$$

The copolymer composition of P(VOH-*co*-**DMMDO**-*co*-HU) was determined by ^{1}H-NMR spectroscopy of the purified polymers in MeOD-d_4 (Figure 106). The DP of VOH (DP_{VOH}) was identical to DP_{VAc} of the starting P(VAc-*co*-**DMMDO**). The DP of HU units (DP_{HU}) was determined by comparing the integrals of the VOH unit (-CH_2-*CH*(OH)-) at 4 ppm () with the integral of HU unit ($\int_{3.02}^{3.24} NHCH_2$) which includes the three protons of the methoxy groups of the α-chain end (3H, -O*CH*$_3$) and the two protons next to the amine function (2H; -CH_2-C(OH)-C(CH_3)$_2$-O-C(=O)-NH-*CH*$_2$-(CH_2)$_2$-CH_3) by the following equation:

Equation 22

$$\text{DP of HU } = (DP_{VOH} \times \frac{\int_{3.02}^{3.24} NHCH_2 - 3H(OCH_3)}{2}) / \int_{3.68}^{4.48} CH(OH)$$

The DP of **DMMDO** (DP_{DMMDO}) in P(VOH-*co*-DMMDO-*co*-HU) was determined by comparing the integrals of the VOH unit (-CH_2-<u>*CH*</u>(OH)-) at 4 ppm with the integral of HU unit ($\int_{3.02}^{3.24} NHCH_2$) which includes the three protons of the methoxy groups of the α-chain end (3H, -O<u>*CH*$_3$</u>) and the two protons next to the amine function (2H; -CH_2-C(OH)-C$(CH_3)_2$-O-C(=O)-NH-<u>*CH*$_2$</u>-$(CH_2)_2$-CH_3), and the integral of all protons between 0.9 and 2.4 ppm ($\int_{0.9}^{2.4} H$; corresponding to 2H of VOH unit (-<u>*CH*$_2$</u>-CH(OH)) + 8H of DMMDO unit (-<u>*CH*$_2$</u>-C-C<u>*(CH*$_3$*)*$_2$</u>-O-C=O)-O-) + 15H of HU unit (-<u>*CH*$_2$</u>-C(OH)-C<u>*(CH*$_3$*)*$_2$</u>-O-C(=O)-NH-CH_2-<u>*(CH*$_2$*)*$_2$</u>-<u>*CH*$_3$</u>) + 11H of the initiating fragment (CH_3O-C(<u>*CH*$_3$*)*$_2$</u>-<u>*CH*$_2$</u>-C<u>*(CH*$_3$*)*</u>(CN)-) by the following equation:

Equation 23

$$\text{DP of DMMDO} = (DP_{VOH} \times \frac{(\int_{0.9}^{2.4} H - (\int_{3.68}^{4.48} CH(OH) \times 2 - (\frac{\int_{3.02}^{3.24} NHCH_2 - 3H(OCH_3)}{2} \times 15)}{8}) / \int_{3.68}^{4.48} CH(OH)$$

Kinetic data for the copolymerisation of VAc with DMMDO

Table 16. Copolymerisations of VAc and DMMDO at 40 °C using R-Co(acac)$_2$

Entry	f^0_{VAc}/ f^0_{DMMDO} [a]	Time (h)	VAc conv.[a] (%)	DMMDO conv.[a] (%)	Total conv.[a] (%)	Comp. (F_{VAc}/ F_{DMMDO})[b]	$M_{n,theo}$[c] (g mol^{-1})	$M_{n\ SEC}$[d] (g mol^{-1})	M_w/M_n[d]
1	1/0	23	83	-	83	1/0	29,200	29,300	1.30
2	0/1	23	-	0	0	-	-	-	-
3	0.94/0.06	2	4	3	4		2,000	2,200	1.11
		4	8	4	8		3,400	3,500	1.09
		6	14	5	13		5,300	4,900	1.08
		8	18	10	18		6,800	6,200	1.09
		23	51	30	50	0.89/0.11	18,100	19,300	1.36
4	0.88/0.12	2	6	1	6		2,500	2,700	1.11
		4	9	2	8		3,500	4,500	1.09
		6	14	3	13		5,100	6,500	1.08
		8	21	5	19		7,300	8,700	1.09
		23	51	56	52	0.87/0.13	19,500	24,800	1.32
5	0.75/0.25	2	6	3	5		2,600	3,100	1.09
		4	9	2	7		3,200	5,200	1.08
		6	15	6	13		5,300	7,500	1.10
		25	46	43	45	0.83/0.16	18,000	19,800	1.37
6	0.66/0.34	2	1	1	1		1,000	2,700	1.11
		4	7	2	5		2,600	4,000	1.10
		6	12	2	9		3,800	5,300	1.10
		23	31	8	23		9,100	11,900	1.28
		25	38	13	30	0.78/0.22	11,500	13,600	1.29
7	0.60/0.40	2	2	1	2		n.d.	1,300	1.28
		4	4	1	3		n.d.	2,100	1.13
		6	4	1	3		n.d.	2,700	1.12
		23	6	3	5		n.d.	5,500	1.31
		29	7	3	5	0.60/0.40	n.d.	6,200	1.35
8	0.26/0.74	24	3	0	2		n.d.	5,700	1.54
		48	3	0	2	-	n.d.	6,200	1.66
9[e]	0.57/0.43	29	16	34	26	0.69/0.31	10,800	15,200	1.33
10	0.78/0.22	25	25	48	43	0.81/0.19	17,000	18,400	1.29
11[f]	0.85/0.15	6	45	26	42	0.86/0.16	4,400	3,900	1.10

12	0.78/0.22	25	41	26	38	0.77/0.23	14,600	15,700	1.36
13	0.72/0.28	21	27	17	24	0.82/0.18	9,800	11,800	1.25

Conditions: bulk, M/R-Co(acac)$_2$ = 400/1, magnetic stirring at 500 r.p.m. [a]Determined by ^{1}H-NMR spectroscopy. [b]Composition of the copolymer determined by ^{1}H-NMR spectroscopy. [c]$M_{n,\,theo} = M_{w\,init} + (Conv_{DMMDO} \times M_{w\,DMMDO} + Conv_{VAc} \times M_{w\,VAc}) + M_{w\,TEMPO}$ [d]Determined by size exclusion chromatography (SEC) in THF using PS standard. [e]Addition of H_2O, R-Co(acac)$_2$/H_2O = 1/20. [f]Conditions: bulk, M/R-Co = 100, magnetic stirring at 500 r.p.m. n.d. = not determined

Characterisation of P(VAc-*co*-DMMDO) copolymers

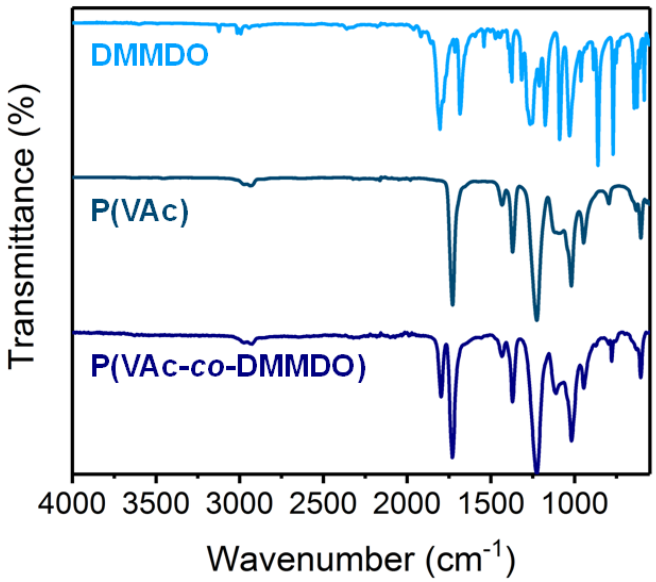

Figure 101. FT-IR spectra of **DMMDO**, PVAc (Entry 1, Table 2), P(VAc-*co*-**DMMDO**) at 43% conversion containing 16 mol% **DMMDO** (Entry 5, Table 2).

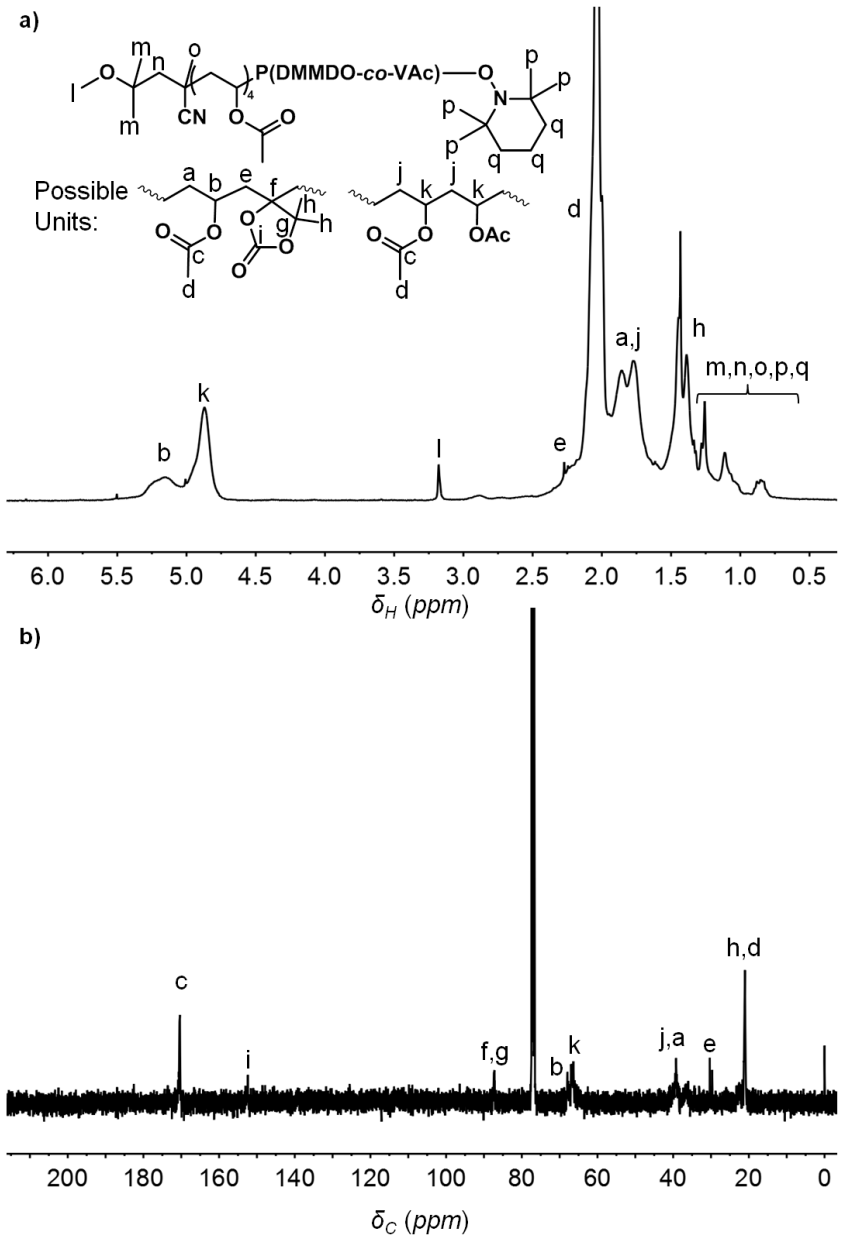

Figure 102. a) ^{1}H-NMR spectrum and b) ^{13}C-NMR spectrum of a copolymer at 21% conversion containing 23 mol% **DMMDO** prepared by OMRP at 90 °C. NMR spectra taken in $CDCl_3$ on a 400 MHz spectrometer.

Data used for the determination of the reactivity ratios

Table 17. Polymerisations of VAc and **DMMDO** by free radical polymerisation (Entries 1-11) and by cobalt-mediated radical polymerisation (Entries 11-14) at 40 °C to determine the reactivity ratios of the monomers.

Entry	f^0_{VAc}/f^0_{DMMDO} [a]	Time (h)	VAc conv.[a] (%)	DMMDO conv. (%)	Total conv.[a] (%)	Comp. (F_{VAc}/F_{DMMDO})[b]	$M_{n\,SEC}$[c] (g mol^{-1})	M_w/M_n[c]
1	0.89/0.11	1	3	2	3	0.90/0.10	25,300	2.70
2	0.79/0.21	4	5	2	4	0.85/0.15	21,100	1.75
3	0.70/0.30	4	5	1	4	0.79/0.21	18,500	1.62
4	0.69/0.31	6	2	2	2	0.76/0.24	16,800	1.93
5	0.60/0.40	9.5	2	2	2	0.69/0.31	11,200	1.76
6	0.53/0.47	30	3	2	3	0.70/0.30	12,100	1.92
7	0.50/0.50	20	4	0	2	0.68/0.32	10,200	1.97
8	0.42/0.58	42	1	1	1	0.66/0.34	10,400	1.71
9	0.29/0.71	62	0	1	1	0.56/0.44	5,500	1.74
10	0.28/0.72	62	1	0	0	0.54/0.46	6,300	1.73
11[d]	0.08/0.92	-	-	-	-	-	-	-
12	0.89/0.11	2	11	3	11	0.87/0.13	4,800	1.08
13	0.68/0.32	8	17	4	13	0.76/0.24	8,100	1.13
14	0.60/0.40	29	7	3	5	0.60/0.40	6,200	1.35

Conditions: Entries 1-11: 40°C, bulk, M/V-70 = 200 (as two radicals are formed from one molecule of V-70), magnetic stirring at 500 r.p.m. Entries 12-14: 40°C, bulk, M/R-Co(acac)$_2$ = 400, magnetic stirring at 500 r.p.m. [a]Determined using ^{1}H-NMR spectroscopy [b]Composition of the copolymer determined by ^{1}H-NMR spectroscopy. [c]Determined using size exclusion chromatography in THF using PS standard. [d]No precipitate/polymer observable after >250 hours.

Characterisation of functionalised P(VAc-*co*-DMMDO) copolymers

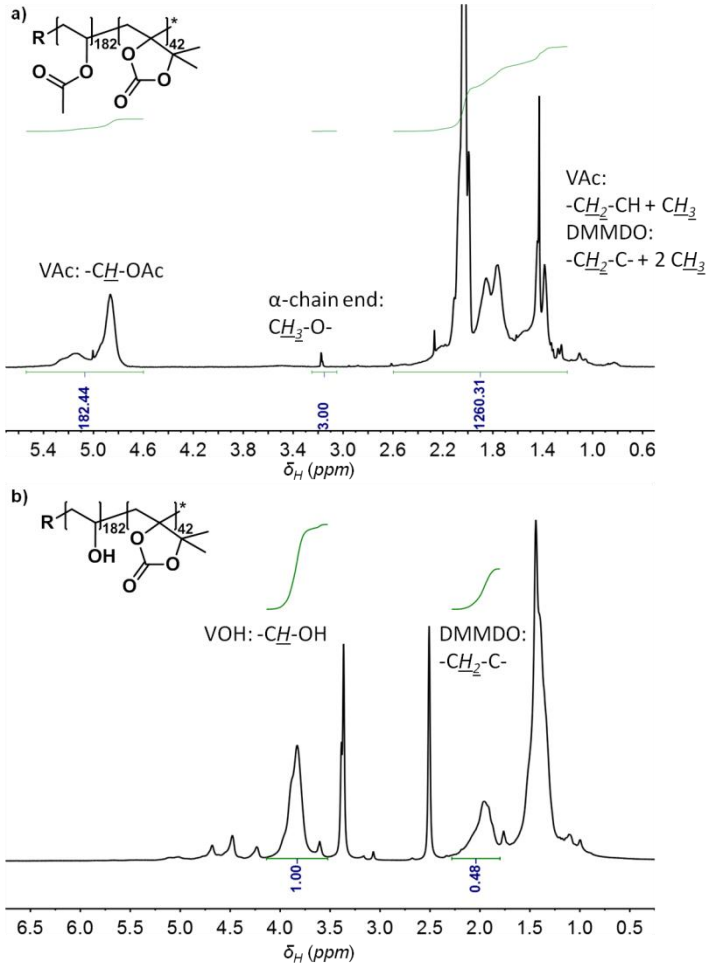

Figure 103. ^{1}H-NMR spectra of a) P(VAc$_{182}$-*co*-**DMMDO**$_{42}$) (Entry 10, Table 16) and b) P(VOH$_{182}$-*co*-**DMMDO**$_{42}$) recorded in $CDCl_3$ and DMSO-d_6, respectively, on a 400 MHz spectrometer..

Table 18. PVAc and P(VAc-*co*-**DMMDO**) prepared by OMRP with similar DPs for the comparison of solubility.

Entry	f^0_{VAc}/ f^0_{DMMDO} [a]	Time (h)	Total conv.[a] (%)	Comp. (F_{VAc}/F_{DMMDO})[b]	DP (VAc/ DMMDO)[a]	$M_{n,theo}$ [c] (g mol^{-1})	$M_{n\ SEC}$ [d] (g mol^{-1})	M_w/M_n [d]
1	1/0	8	31	1/0	134/0	11,500	12,800	1.10
2	0.72/0.28	21	24	0.82/0.18	108/24	9,800	11,800	1.25

Conditions: bulk, M/R-Co(acac)$_2$ = 400/1, magnetic stirring at 500 r.p.m. [a] Determined by ^{1}H-NMR spectroscopy. [b] Composition of the copolymer determined by ^{1}H-NMR spectroscopy. [c] $^{c}M_{n,\ theo} = M_{w\ init} + (Conv_{DMMDO} \times M_{w\ DMMDO} + Conv_{VAc} \times M_{w\ VAc}) + M_{w\ TEMPO}$ [d] Determined by size exclusion chromatography (SEC) in THF using PS standard.

Table 19. Solubility of $PVOH_{134}$ compared with $P(VOH_{108}\text{-}co\text{-}BD_{24})$ at different concentrations (Entries 1 and 2, Table 18)

	Concentration (g/L)					
	1	10	25	50	150	375
PVOH soluble at (°C)	50	60	60	80	80 (only partially soluble)	-
P(VOH-*co*-BD) soluble at (°C)	20	20	20	20	20	30

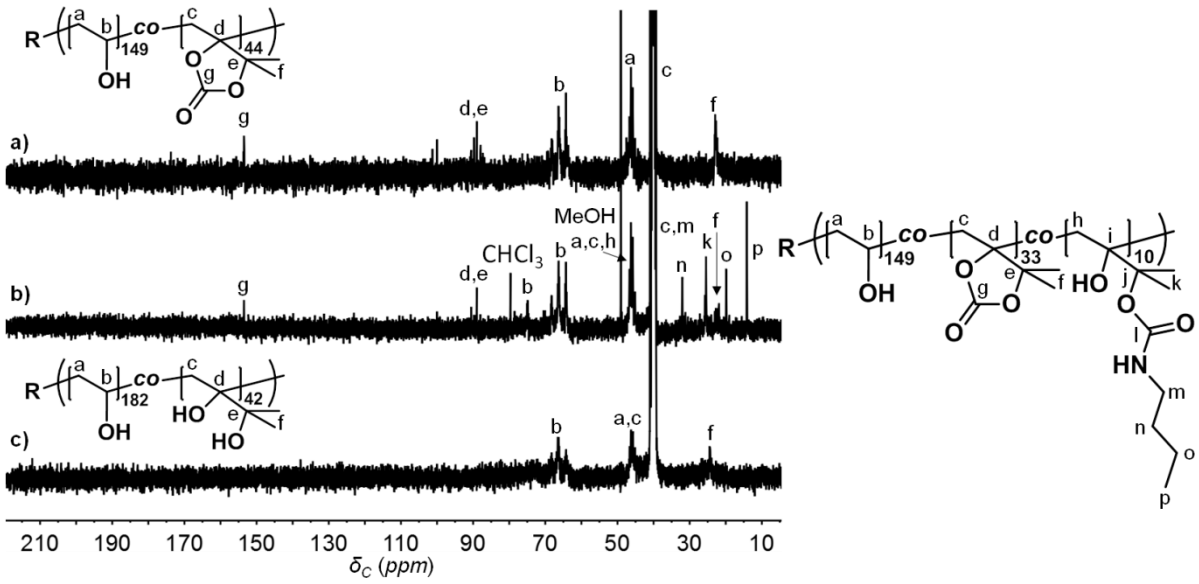

Figure 104. ^{13}C-NMR spectra of a) $P(VOH_{149}\text{-}co\text{-}\mathbf{DMMDO}_{44})$, b) $P(VOH_{149}\text{-}co\text{-}\mathbf{DMMDO}_{33}\text{-}co\text{-}HU_{10})$ functionalised using dry *n*-butylamine and c) $P(VOH_{182}\text{-}co\text{-}BD_{42})$; all spectra are recorded in DMSO-d_6 on a 400 MHz spectrometer.

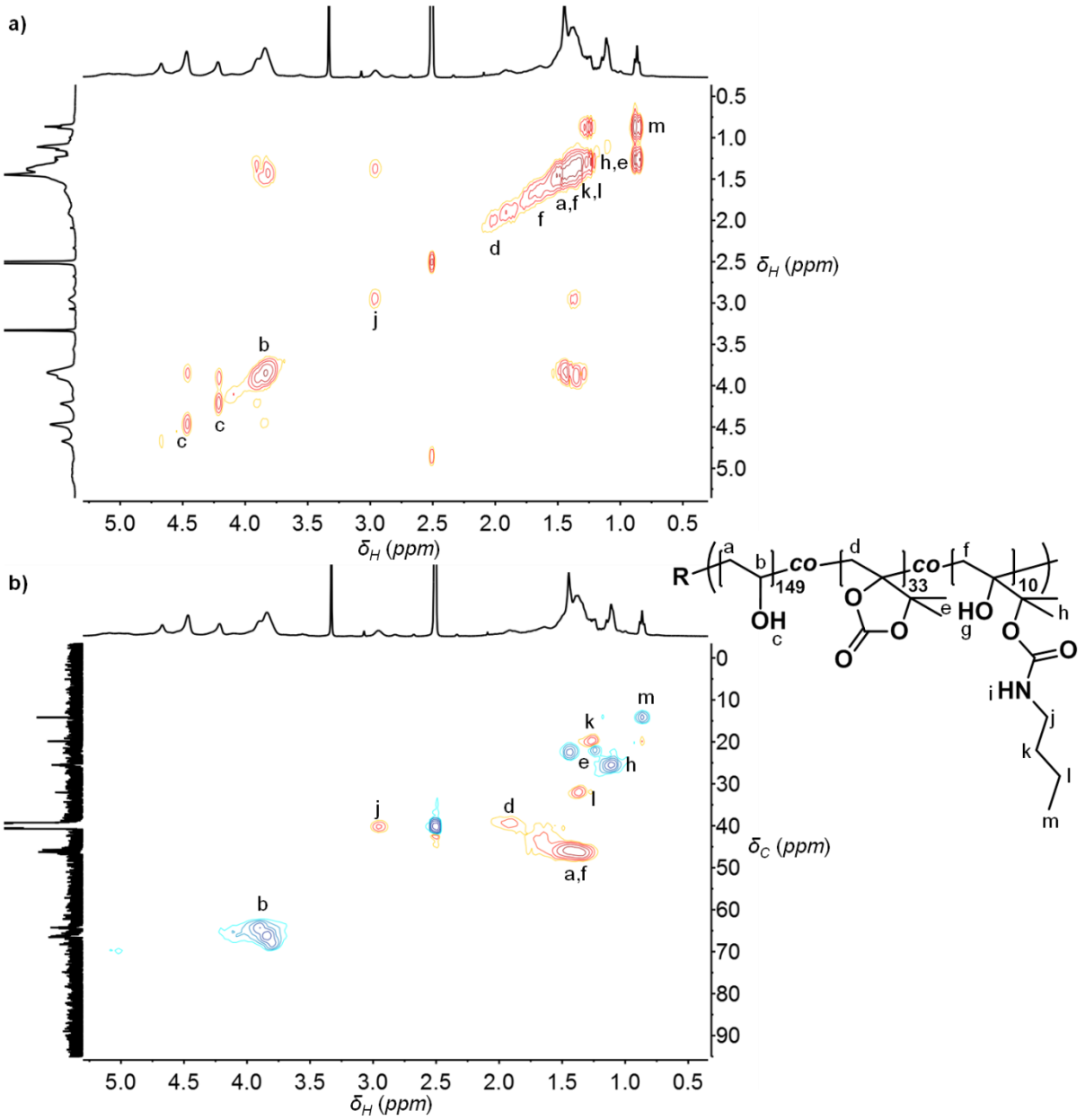

Figure 105. a) COSY and b) HSQC spectra of P(VOH$_{149}$-*co*-**DMMDO**$_{33}$-*co*-HU$_{10}$) functionalised using dry *n*-butylamine; recorded in DMSO-d_6 on a 400 MHz spectrometer.

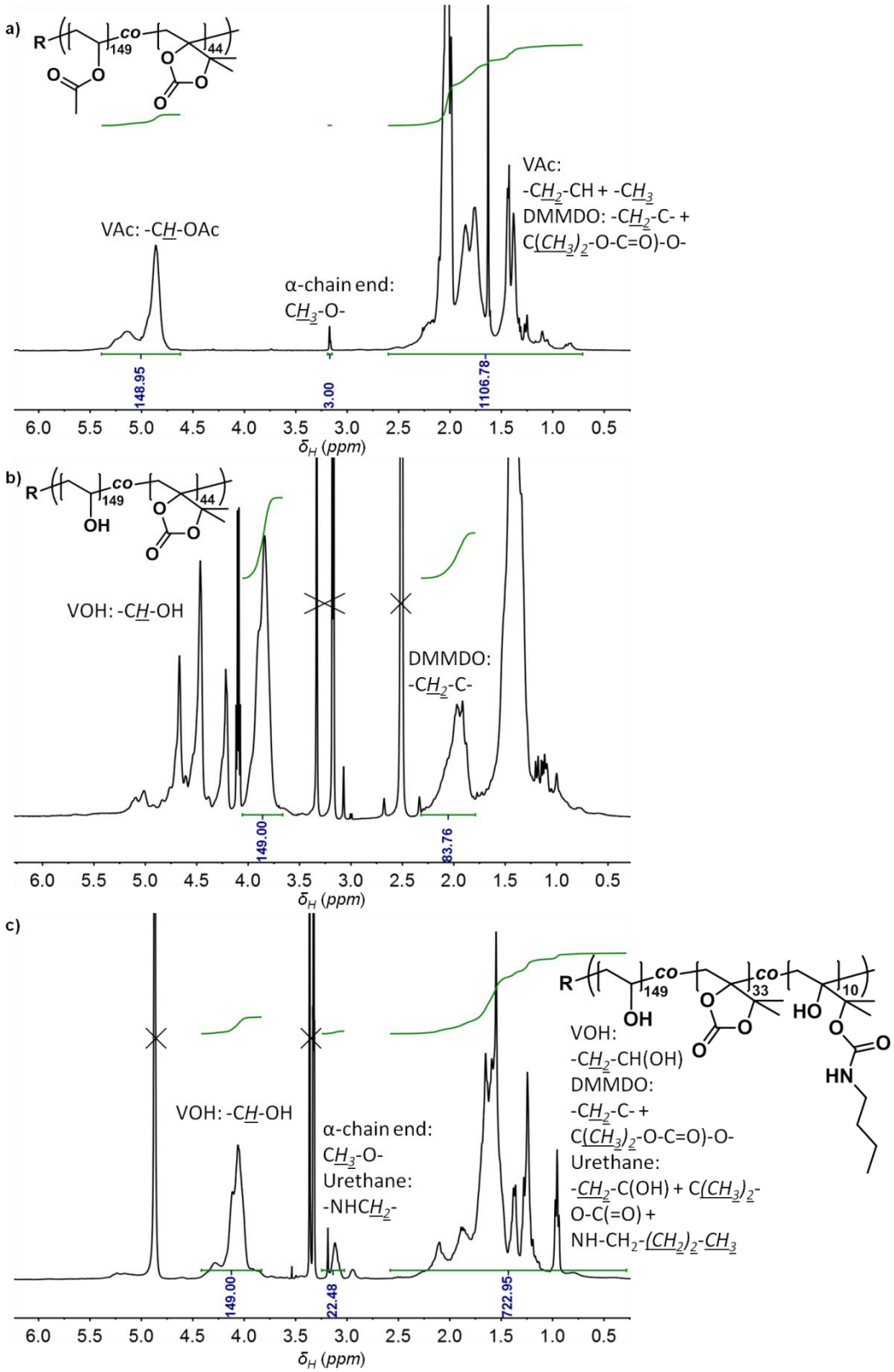

Figure 106. ^{1}H-NMR spectra of a) P(VAc$_{149}$-*co*-**DMMDO**$_{44}$) recorded in $CDCl_3$ b) P(VOH$_{149}$-*co*-**DMMDO**$_{44}$) recorded in DMSO-d_6 and c) P(VOH$_{149}$-*co*-**DMMDO**$_{33}$-*co*-HU$_{10}$) functionalised using dry *n*-butylamine, recorded in MeOD-d_4. All spectra recorded on a 400 MHz spectrometer.

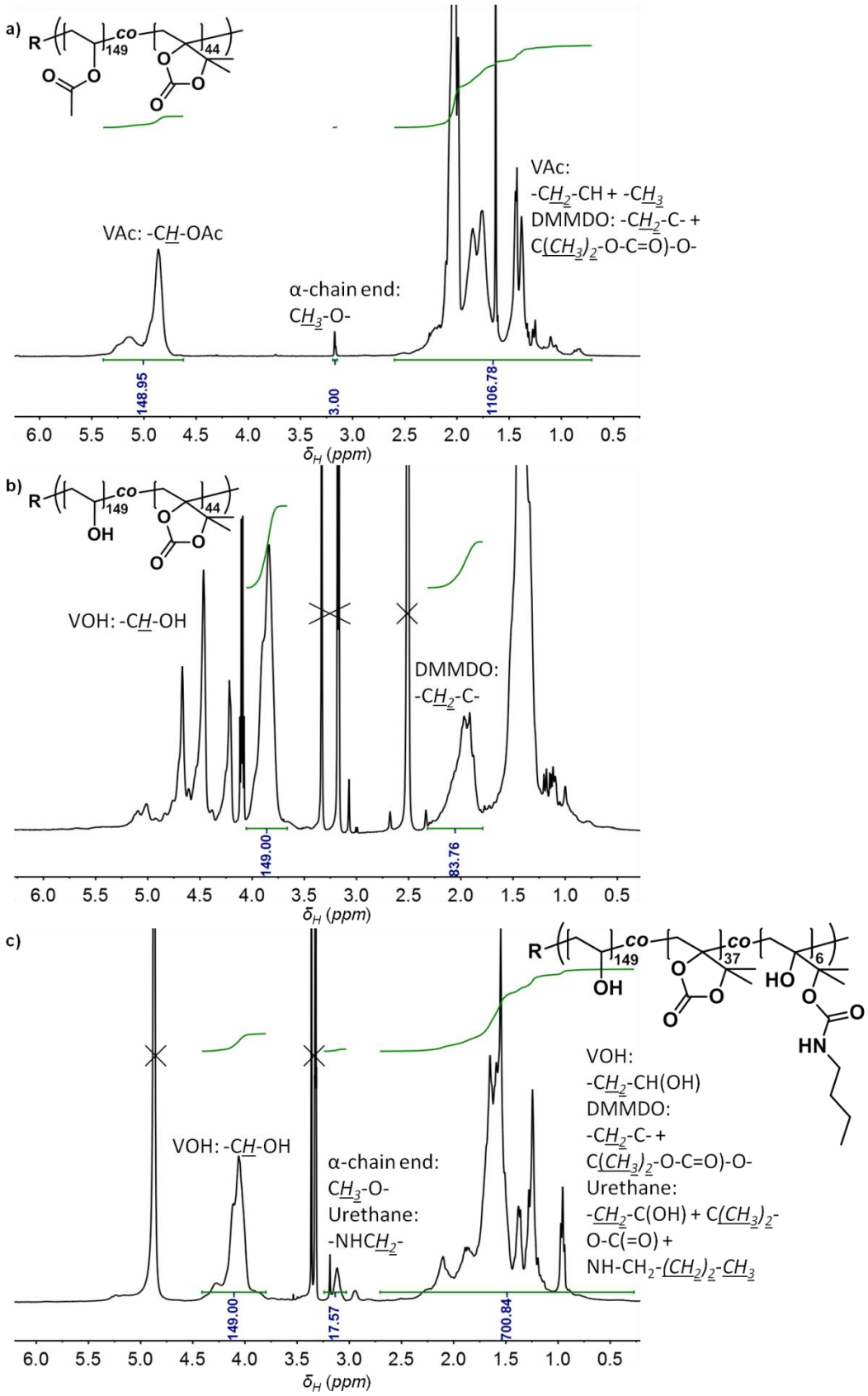

Figure 107. ^{1}H-NMR spectra of a) P(VAc$_{149}$-*co*-**DMMDO**$_{44}$) recorded in $CDCl_3$, b) P(VOH$_{149}$-*co*-**DMMDO**$_{44}$) recorded in DMSO-d_6 and c) P(VOH$_{149}$-*co*-**DMMDO**$_{36}$-*co*-HU$_7$) functionalised using wet *n*-butylamine recorded in MeOD-d_4. All spectra are recorded on a 400 MHz spectrometer.

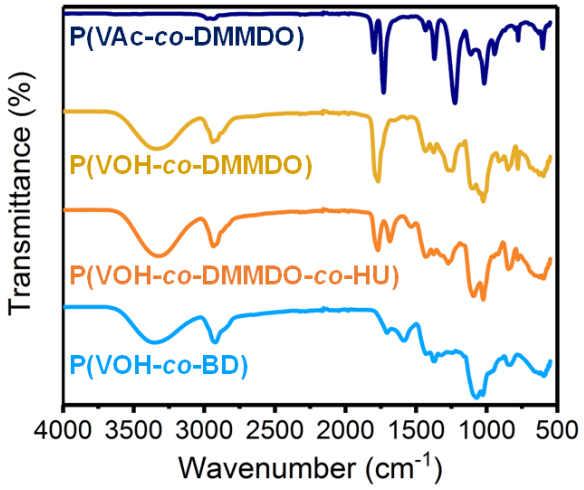

Figure 108. FT-IR spectra of P(VAc_{149}-*co*-**DMMDO**$_{44}$), P(VOH_{149}-*co*-**DMMDO**$_{44}$), P(VOH_{149}-*co*-**DMMDO**$_{36}$-*co*-HU_7) functionalised using wet *n*-butylamine and P(VOH_{182}-*co*-BD_{42})

10.5. Experimental Section for Chapter 6

Characterisation

^{1}H- and ^{13}C NMR spectroscopy were performed on a 400 MHz Bruker instrument at 80 °C using a 2:1 mixture of deuterated TCE:C_6D_6. The composition of copolymers P(**E**-*co*-**M1**) were determined by comparing the $\underline{H_3}$C–O– signal of the α-chain ($\int_{2.9}^{3.1} CH_3O$) with the comonomer peaks at 3.96 and 4.4 ppm ($\int_{3.5}^{5.3} CH \,\&\, CH_2$) corresponding to the –CH–C$\underline{H_2}$–O(C=O)O–CH_2–, –O–C$\underline{H_2}$–CH–CH_2(O(C=O)O), –O–CH_2–CH–C$\underline{H_2}$(O(C=O)O) and –O–CH_2–C$\underline{H}$–CH_2(O(C=O)O), respectively, as well as four protons from the oligo-VAc of the initiator ($\int_{4.75}^{5} CH$).

Equation 24

$$DP\ \boldsymbol{M1} = \frac{\int_{3.5}^{5.3} CH \,\&\, CH_2 - \int_{4.75}^{5} CH}{\int_{2.9}^{3.1} CH_3O}$$

The DP of ethylene was determined by integrating all the protons from 2.0 to 0.5 ppm ($\int_{0.5}^{2.0} H$; corresponding to 4H of the **E** repeat unit (−C$\underline{H_2}$−) + 39H of the initiating fragment and TEMPO (CH$_3$O−C(C$\underline{H_3}$)$_2$−C$\underline{H_2}$−C(C$\underline{H_3}$)-(CN)−(C$\underline{H_2}$−CH−O−CO−C$\underline{H_3}$)−) and −N−(C(C$\underline{H_3}$)$_2$−(C$\underline{H_2}$)$_3$−C(C$\underline{H_3}$)$_2$) + 3H of the –CH– and –CH_2– of **M1** (–C$\underline{H_2}$–C$\underline{H}$–CH_2–O–CO–O–).

Equation 25

$$DP\ \boldsymbol{E} = \frac{\int_{0.5}^{2.0} H - \frac{39}{3}\int_{2.9}^{3.1} CH_3O - 3\frac{\int_{3.5}^{5.3} CH \,\&\, CH_2 - \int_{4.75}^{5} CH}{\int_{2.9}^{3.1} CH_3O}}{\frac{4}{3}\int_{2.9}^{3.1} CH_3O}$$

Copolymerisation procedure

All polymerisations were performed under an inert atmosphere using Schlenk techniques. A typical ethylene copolymerisation aimed at a [**M1**]$_0$/[R-Co(acac)$_2$]$_0$ = 100/1. A solution of R-Co(acac)$_2$ (0.95 mL; 0.1182 M stock solution in CH_2Cl_2, 0.112 mmol) was introduced under argon into a purged 30 mL Schlenk tube and evaporated to dryness under reduced pressure at room temperature and 5.6 mL of degassed DMC were added to give solution **A**. In a second 30 mL Schlenk tube, **M1** was freeze-pumped-thawed thrice to which 5 mL of solution **A** were added using a syringe. This reaction mixture of R-Co(acac)$_2$, **M1** and DMC was then transferred to a previously purged 30 mL autoclave under ethylene atmosphere. The pressure was increased to 50 bar of ethylene and the polymerisation took place at 40°C and 500 rpm. After 24 hrs, aliquots of the reaction mixture were taken for NMR and SEC analyses to

determine conversions and the molecular parameters of the polymer, respectively. The reaction mixture was quenched using a degassed solution of TEMPO (150 mg, 1 mmol) in 2 mL of DMC, left to stir for at least 1 hour and then passed over a microsilica column to remove the cobalt using THF. Copolymers which were not soluble in THF were dissolved in hot toluene (65 °C) and the microcolumn was heated as well to keep the polymer soluble. The polymer was then purified by supercritical CO_2 ($scCO_2$) extraction, (see below) according to a previous publication.[98] The resulting pure polymer was then analysed by NMR spectroscopy, FT-IR, DSC, TGA and elemental analyses.

Copolymerisations performed at 500 bar ethylene pressure were performed in a 23 mL autoclave reactor.

Supercritical CO_2 extraction

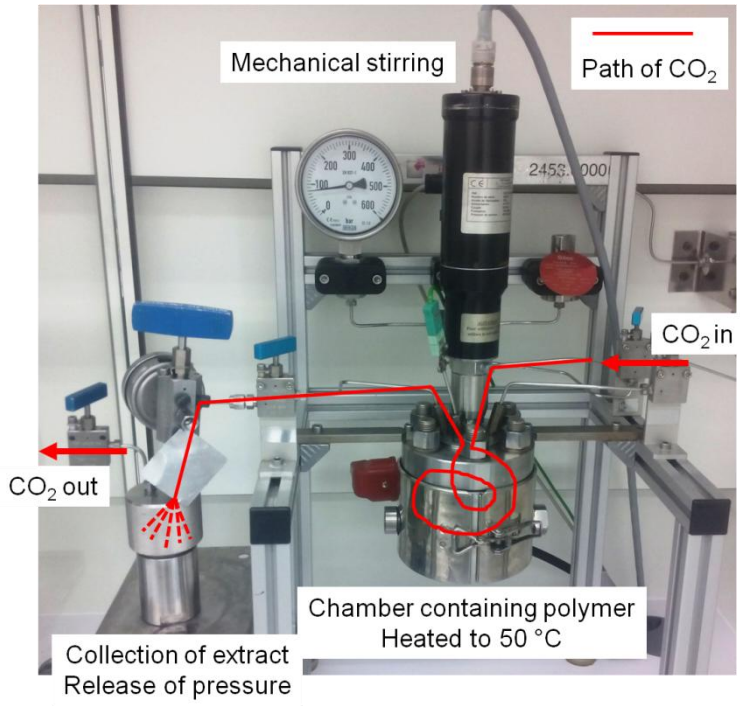

Figure 109. Reactor set-up for the $scCO_2$ extraction of the ethylene copolymers

The polymer solution was then transferred into the main chamber of a $scCO_2$ high pressure reactor (Figure 109) which was heated to 50 °C, stirred at 330 rpm and a CO_2 pressure of 250 bar was applied. After 1 hour, the stirring was stopped and $scCO_2$ at 250 bar at a rate of 10 mL/min was flushed through the main chamber and released to atmospheric pressure in another cell connected to the reactor. The unreacted monomers and excess TEMPO were collected in this cell. Once the 250-300 mL of $scCO_2$ were passed through the main chamber, the reactor was vented and the polymer was collected using THF or hot toluene and then dried at 50 °C under vacuum overnight.

Copolymerisation data

Table 20. Copolymerisations of ethylene with **DMMDO** at 40 °C and 50 bar in different solvents initiated by R-Co(acac)$_2$[a]

Entry	Solvent	Yield (mg)	X_M [b] (mol%)	$M_{n\ SEC}$ [c] (g mol^{-1})	M_w/M_n [c]
1	DCM	209	13	1,600	1.41
2	DMC	224	17	6,400	1.49
3	TCB	37.8	n.d.	1,400	1.45

[a] Conditions: R-Co(acac)$_2$ = 0.1 mmol, 5 mL of solvent, 24 hours, 500 rpm. [b] X_M = comonomer incorporation (mol%), determined by elemental analysis. [c] Size exclusion chromatography (SEC) in THF at 45 °C using a PS calibration. n.d. = not determined.

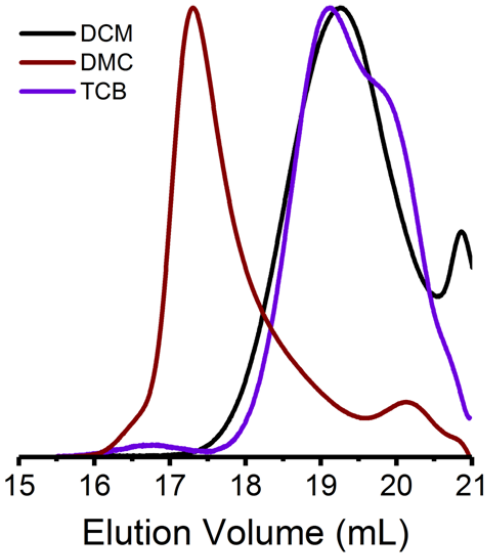

Figure 110. Size exclusion chromatography (SEC) curves for the copolymerisation of ethylene with **DMMDO** in dichloromethane (DCM), dimethylcarbonate (DCM), and trichlorobenzene (TCB) using R-Co(acac)$_2$ at 40 °C.

Table 21. Copolymerisations of ethylene with **M1** and **DMMDO** for 24 hours at 40 °C, 50 bar, and 500 rpm using either free radical polymerisation (V-70) or controlled radical polymerisation (R-Co(acac)$_2$)

Entry	**Initiator**	**Comonomer**	**Yield (mg)**	X_M [a] **(mol%)**	$M_{n\ SEC}$ [b] **(g mol^{-1})**	M_w/M_n [b]
1 [c]	V-70	**M1**	56	35	ins.	ins.
2 [d]	R-Co	**M1**	72	17[e]	1,300	1.88
3 [f]	V-70	**DMMDO**	67	20	8,400	1.70
4 [g]	R-Co	**DMMDO**	224	22	5,400	1.66

[a] X_M = comonomer incorporation (mol%), determined by elemental analysis. [b] High temperature size exclusion chromatography (HT-SEC) in trichlorobenzene at 140 °C using a PS standard. [c] Conditions: 5 mL DMC, V-70 = 0.05 mmol. [d] Conditions: 5 mL DMC, R-Co(acac)$_2$ = 0.1 mmol. [e] Determined by ^{1}H NMR spectroscopy using the α-chain end. [f] Conditions: 2.5 mL DMC, V-70 = 0.012 mmol. [g] Conditions: 2.5 mL DMC, R-Co = 0.025 mmol. ins. = insoluble in TCB at 140 °C.

Characterisation of the copolymers

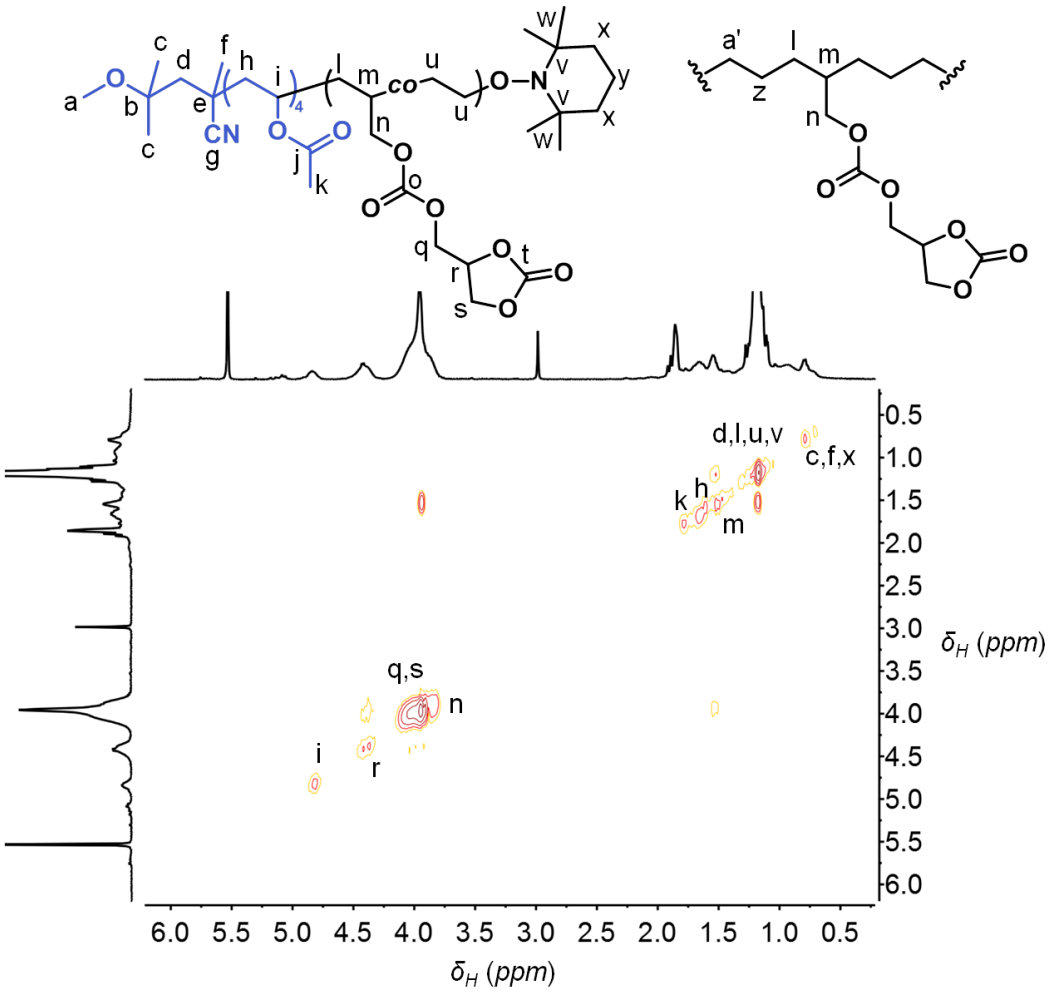

Figure 111. COSY NMR spectrum of P(**E**-*co*-**M1**) (entry 3, Table 3).

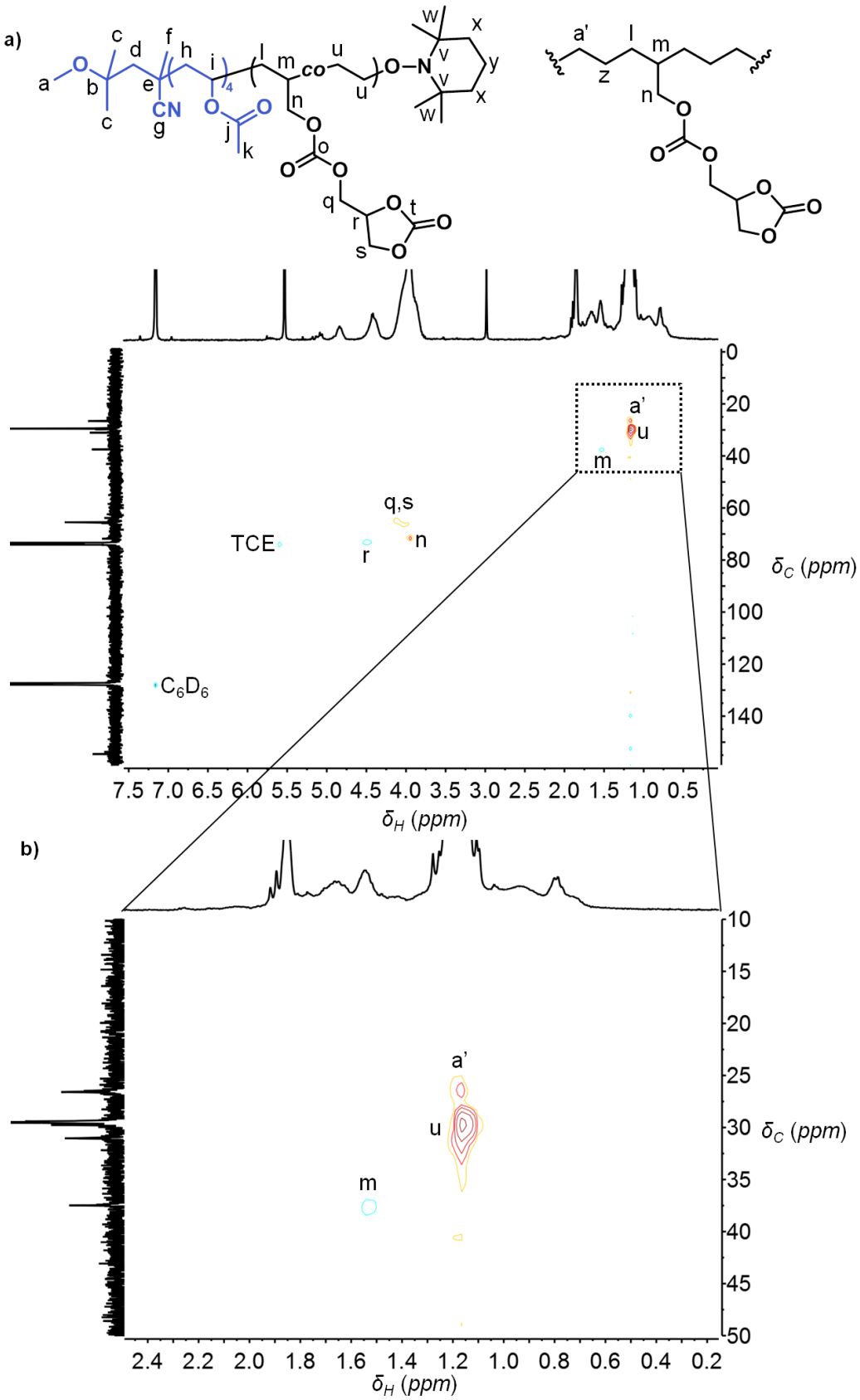

Figure 112. HSQC NMR spectra of P(**E**-*co*-**M1**) (entry 3, Table 3).

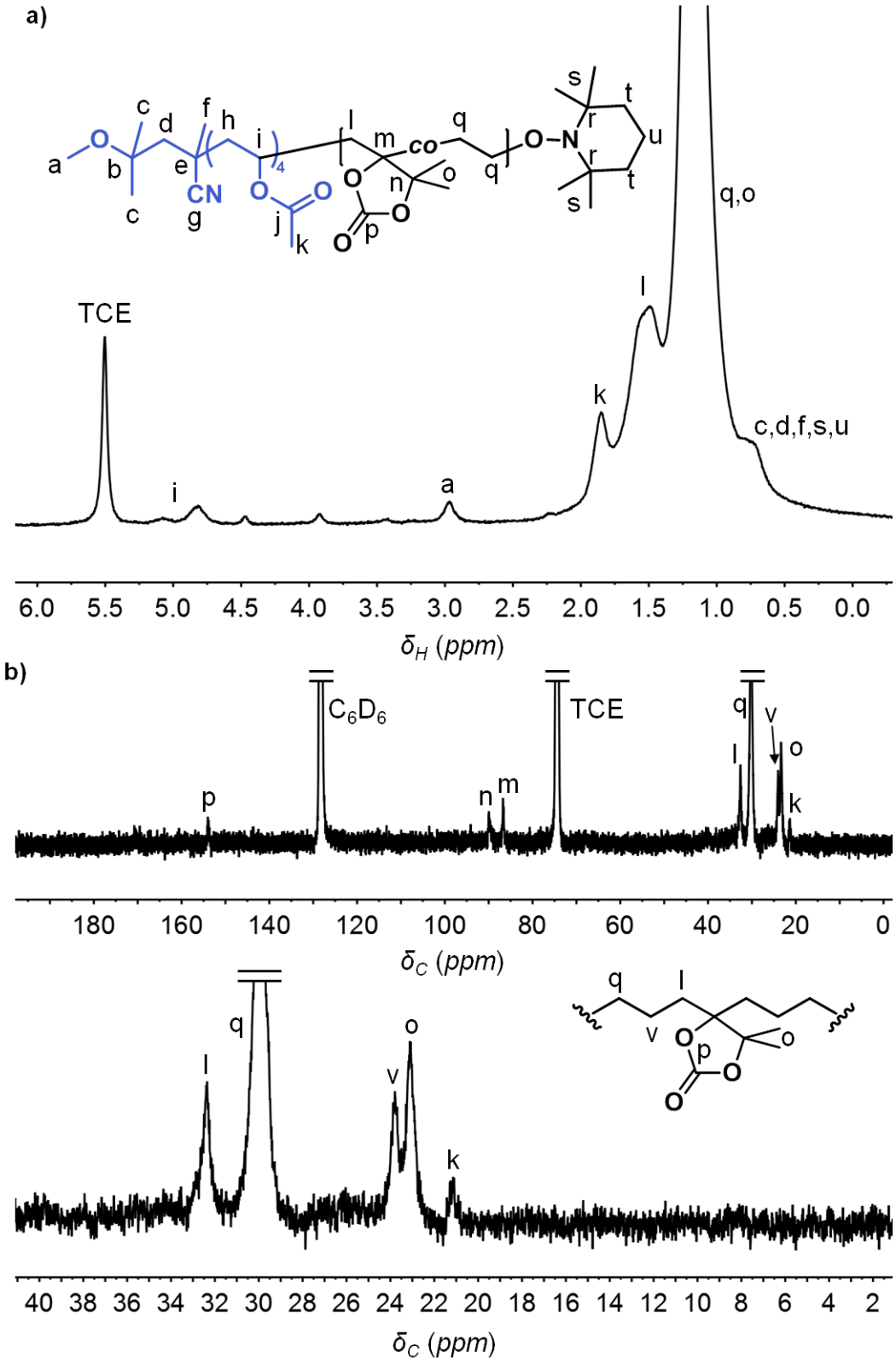

Figure 113. a) ^{1}H NMR spectrum and b) ^{13}C NMR spectrum of P(**E**-*co*-**DMMDO**) (entry 5, Table 3). An inset of the region around 20 ppm where signals from branching would occur is also shown.

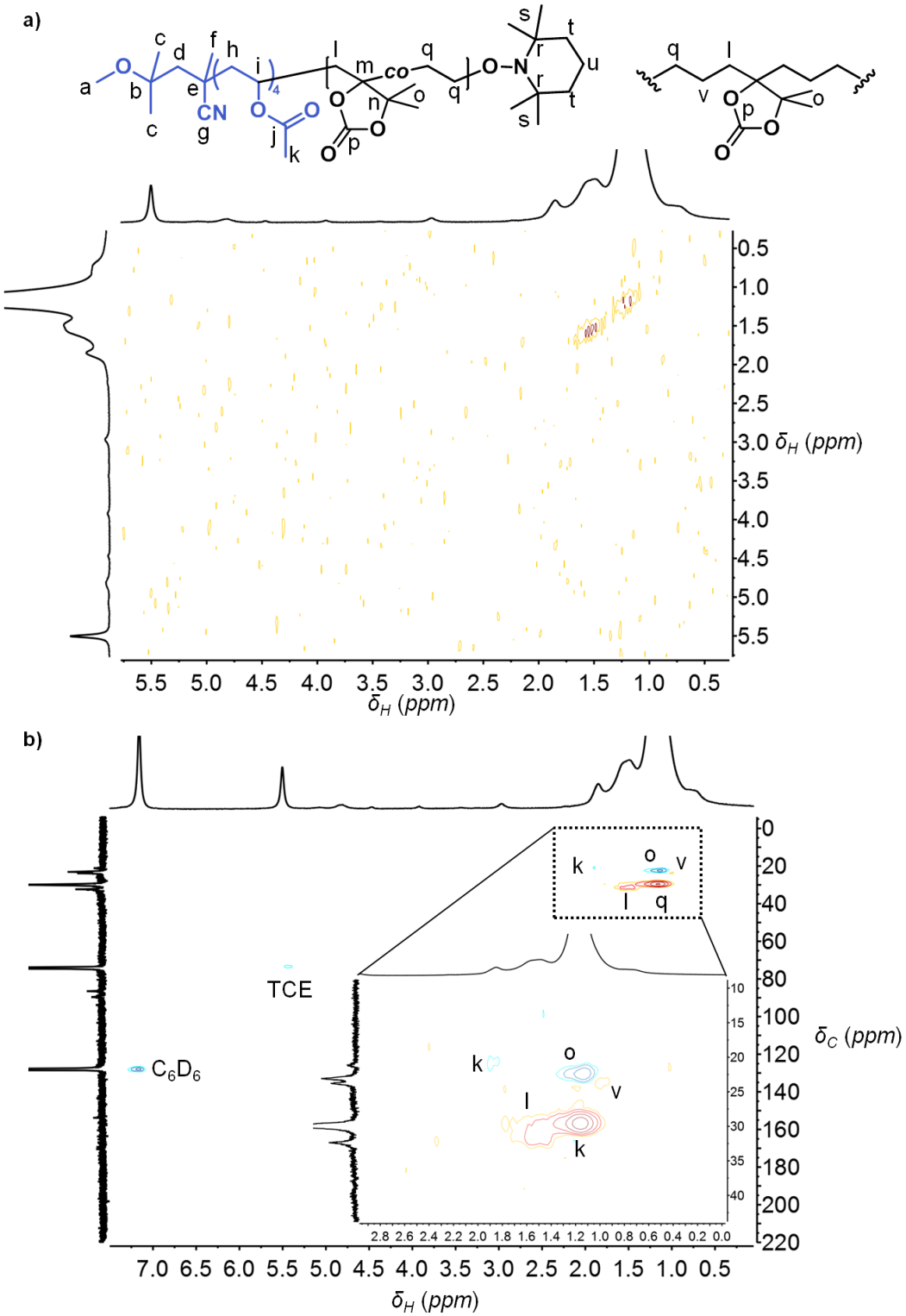

Figure 114. a) COSY NMR spectrum and b) HSQC NMR spectrum of P(**E**-*co*-**DMMDO**) (entry 5, Table 3). An inset of the HSQC spectrum is also shown.

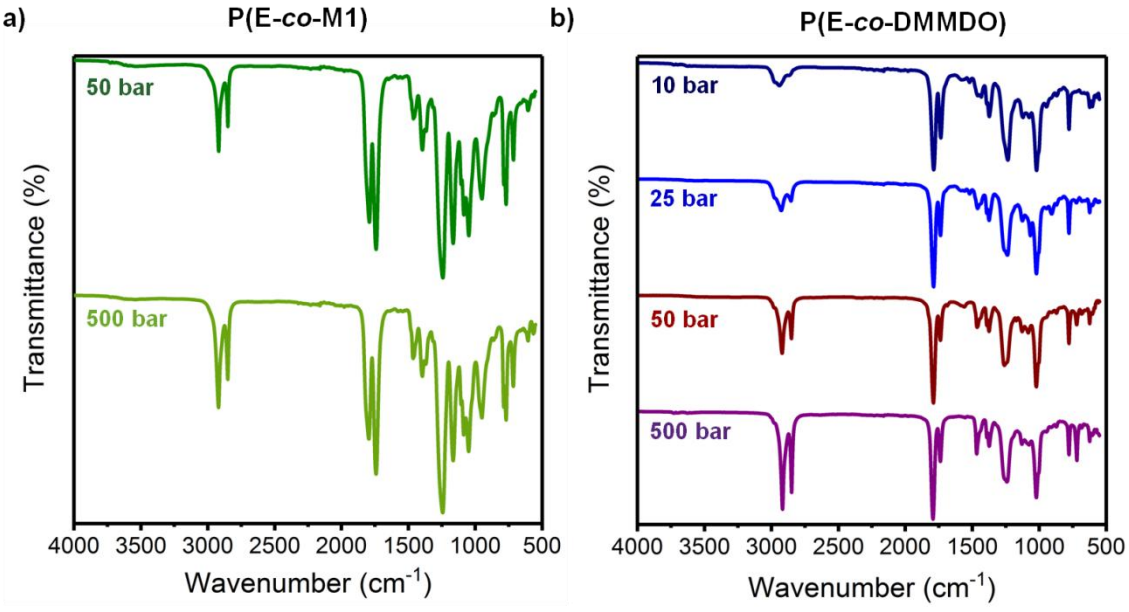

Figure 115. FT-IR spectra of a) P(**E**-*co*-**M1**) copolymers both synthesised at 40 °C in 1.25 mL DMC using R-Co(acac)$_2$, and b) P(**E**-*co*-**DMMDO**) synthesised at 40 °C in 5 mL DMC using R-Co(acac)$_2$.

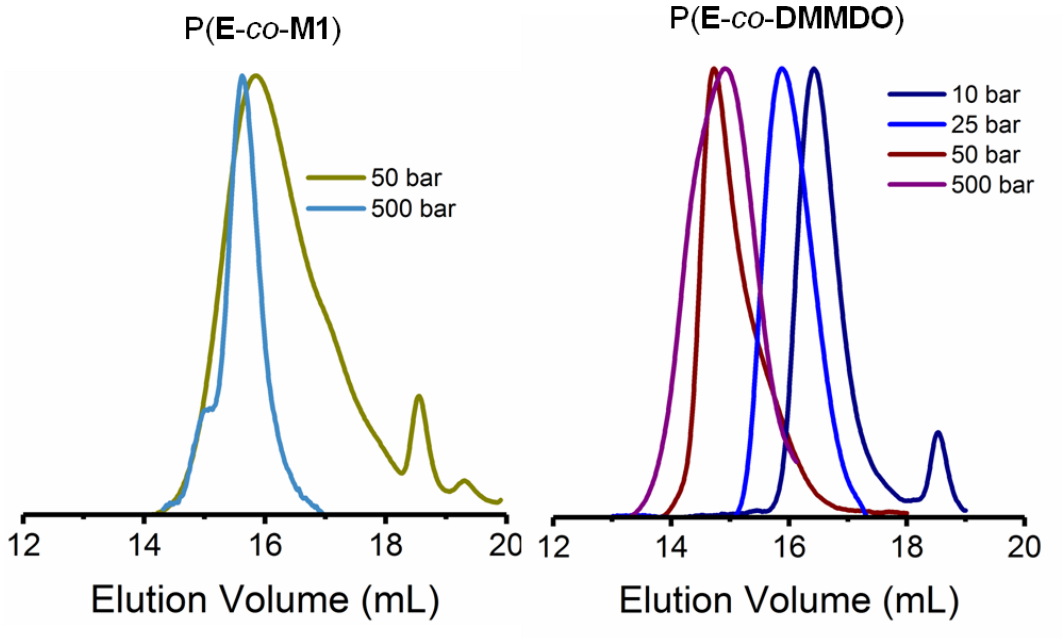

Figure 116. High temperature size-exclusion chromatography (HT-SEC) curves for P(**E**-*co*-**M1**) and P(**E**-*co*-**DMMDO**) copolymers synthesised at 40 °C in DMC (Table 3). HT-SEC analyses were performed in TCB at 140 °C using a polystyrene standard.

Differential scanning calirometry (DSC) characterisation of the copolymers

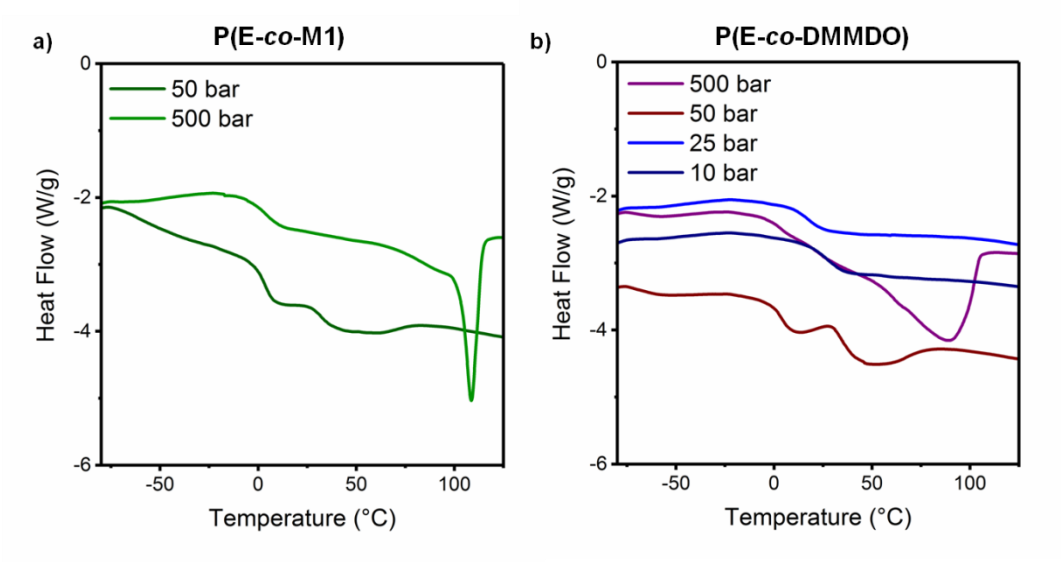

Figure 117. Differential scanning calorimetry (DSC) curves of a) P(**E**-*co*-**M1**) and b) P(**E**-*co*-**DMMDO**) synthesised using R-Co(acac)$_2$ at 40 °C at different ethylene pressures (Table 3).

10.6. Experimental Section for Chapter 7

Exemplary synthesis of an EVA copolymer

All reactions were performed under inert atmosphere using Schlenk techniques. EVA copolymers were synthesised according to a previous report.[7] The copolymerisation at 25 bar used a VAc/R-Co(acac)$_2$ molar ratio of 400/1. A solution of organocobalt initiator (3.5 mL, 0.1136 M stock solution in CH_2Cl_2, 0.4 mmol) was introduced under argon in a purged 30 mL Schlenk tube and evaporated to dryness under reduced pressure at room temperature. A volume of VAc (14.7 mL, 0.16 mol) was added and the solution transferred via a cannula to a purged 30 ml stainless-steel autoclave. An ethylene pressure of 25 bar was applied and the reactor heated to 40 °C using an oil bath at 500 rpm. After 5 hours an aliquot for SEC and NMR analysis was taken and the solution was quenched using a TEMPO/THF solution (180 mg in 2 mL). The copolymer was precipitated in cold n-hexane twice and dried under vacuum at 50 °C and analysed by FT-IR, NMR, and DSC.

For Co(acac)$_2$ end-capped EVA that will be used for the preparation of EVA-*b*-PE (see below), the reaction mixture was transferred into a Schlenk flask from the reactor and the remaining VAc monomer removed under vacuum at room temperature. The pink solid (EVA-Co(acac)$_2$) was stored at -20 °C.

Exemplary EVA$_{500bar}$-*b*-PE block copolymer synthesis:

The first block (3.67 g), synthesised according to the procedure described above, was dissolved in 8 mL CH_2Cl_2. Of this solution, 2 mL (corresponding to 0.9 g of EVA-Co(acac)$_2$) were transferred to a Schlenk tube and dried under vacuum at room temperature. 5 mL of DMC were added and the reaction mixture was transferred into a purged 24 mL stainless-steel high pressure autoclave. An ethylene pressure of 500 bar was applied and the reaction heated to 60 °C at 500 rpm, maintaining a constant ethylene pressure of 500 bar. After 24 hours, the reactor was allowed to cool to room temperature and was slowly depressurised, before a degassed solution of TEMPO (150 mg, 1 mmol; in 2 mL DMC) was introduced. A light brown inhomogeneous solution was obtained and was then dialysed against acetone (3.5 kDa regenerated cellulose tubing, Spectrum Labs) to remove DMC, excess TEMPO and the released cobalt complex. The polymer was finally dried at 40 °C under vacuum overnight. The block copolymer was subsequently analysed using FT-IR, SEC, NMR, and DSC analyses.

Determination of VAc conversion and the comonomer composition

The consumption of VAc during the reaction was determined by comparing the integrals of the peak centred at 4.89 ppm, corresponding to one proton of C$\underline{H_2}$=CH(OAc)– of the

monomer VAc and the –C<u>H</u>-OAc in the copolymer ($\int_{4.62}^{5.40} Pol(CH) + Mon(CH)$), with the peak centred at 4.58 ppm, corresponding to the other proton of the C<u>H₂</u>=CH(OAc)– environment of the monomer VAc ($\int_{4.44}^{4.62} Mon(CH)$.

Equation 26 $$\%\, VAc\ conversion = \left(1 - \frac{\int_{4.44}^{4.62} Mon(CH)}{\int_{4.62}^{5.40} Pol(CH) + Mon(CH)}\right) \times 100$$

The copolymer composition was determined by ^{1}H-NMR spectroscopy of the purified polymers in $CDCl_3$ or TCE:C_6D_6 for copolymers prepared at 500 bar ethylene pressure. The degree of polymerisation of VAc (DP_{VAc}) was determined by comparing the integral of the methoxy group (O-*C*<u>*H*₃</u>) ($\int_{3.05}^{3.25} OCH_3$) at the α-chain end at 3.15 ppm with the integral of –*CH*- of the VAc repeating unit (-CH_2-*C*<u>*H*</u>OAc) ($\int_{4.5}^{5.6} CH$) at 4.8 ppm.

Equation 27 $$\text{DP of VAc} = \int_{4.5}^{5.6} CH \,/ \left(\frac{\int_{3.05}^{3.25} OCH_3}{3}\right)$$

The degree of polymerisation of E (DP_E) was determined by comparing the integral of the methoxy group (O-*C*<u>*H*₃</u>) ($\int_{3.05}^{3.25} OCH_3$) at the α-chain end at 3.15 ppm with the integral of all protons from 0.5-2.5 ppm ($\int_{0.5}^{2.5} H$, corresponding to 29H of the initiating fragment + TEMPO chain-end, 5H of the VAc repeat unit ($\int_{4.5}^{5.6} CH$) and 4H of the ethylene repeat units. The DP_E was determined using the following equation:

Equation 28 $$\text{DP of E} = \frac{\int_{0.5}^{2.5} H - 5 \times \int_{4.5}^{5.6} CH - 29\left(\frac{\int_{3.05}^{3.25} OCH_3}{3}\right)}{4 \times \frac{\int_{3.05}^{3.25} OCH_3}{3}}$$

10.7. Experimental Section for Chapter 8

Preparation of composites

The different composites were prepared according to Table 7. The cellulose, modified amylose, and modified starch were cut into small pieces, premixed with a spatula and, along with LDPE, inserted into a Haake Mini 5g twin-screw extruder at 180 °C and 30 rpm. Once the sample was inserted, the rpm was increased to 80. The pure LDPE was also extruded under the same conditions to have the same thermal and shear history as LDPE composites samples. Subsequently, the samples were compression-moulded under vacuum at 120 °C and 10 kN pressure for 10 min in a laboratory press to make 1.1 mm thick disks that were 25 mm in diameter. The cooled films were then analysed by TGA, DSC, SEM, rheology and stress-strain measurements.

Cellulose characterisation

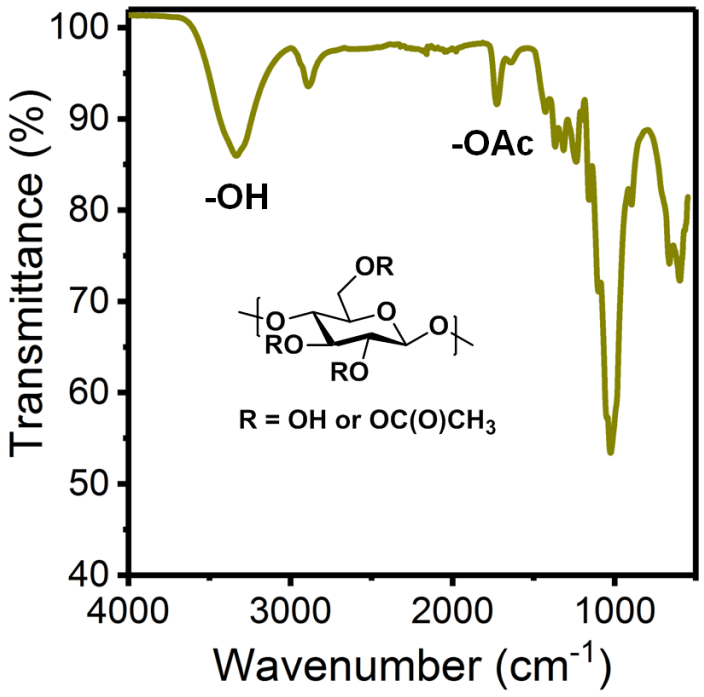

Figure 118. FT-IR spectrum of cellulose obtained by the acetic acid extraction of wood chips clearly showing an absorption in the carbonyl region as a result of acetylation during extraction

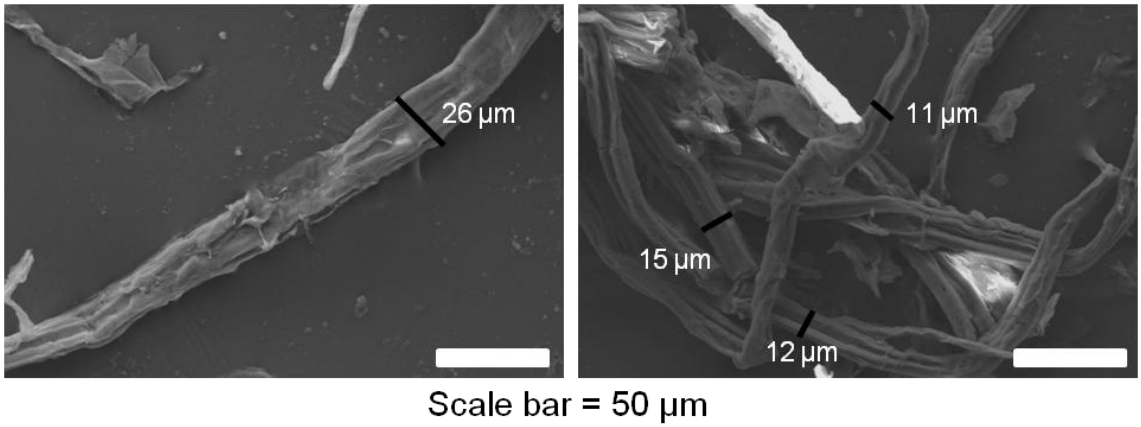

Figure 119. SEM image of the obtained bulk cellulose showing fibres of length and width

Rheological properties

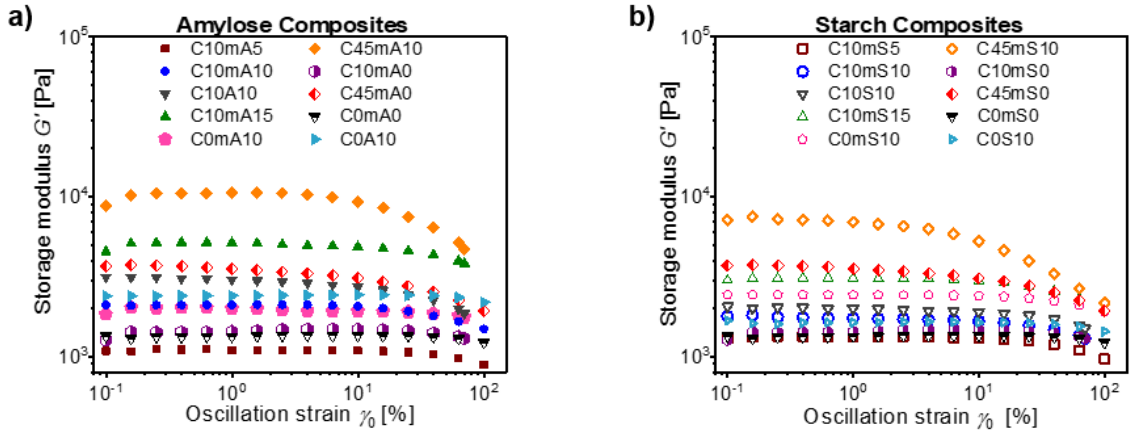

Figure 120. Storage modulus G' as a function of the strain amplitude γ at 150 °C and ω_1 = 1 rad/s for the neat LDPE and the composite materials with cellulose (C), a) modified (mA) and non-modified amylose (A) compatibiliser and b) modified (mA) and non-modified starch (S) compatibiliser.

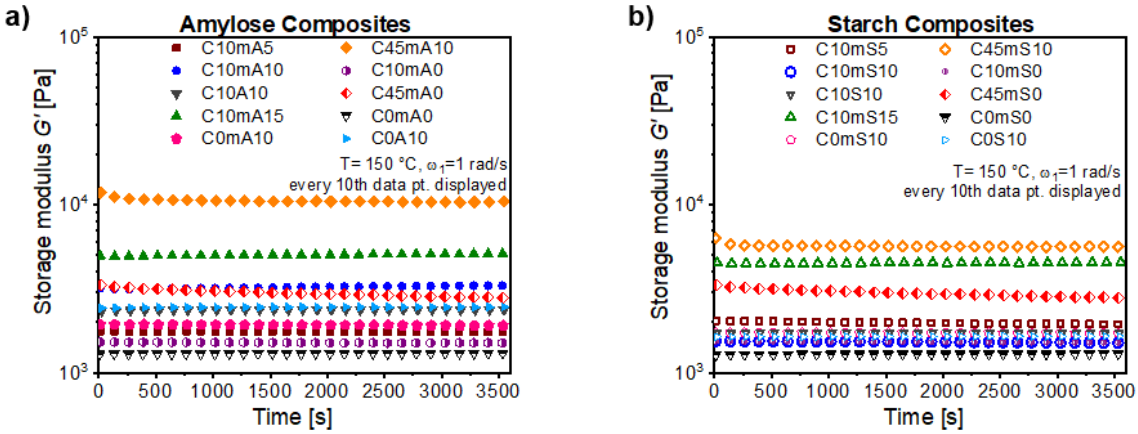

Figure 121. Time dependency of storage modulus G' at 150 °C and ω_1 = 1 rad/s in the linear viscoelastic regime for the neat LDPE and the composite materials.

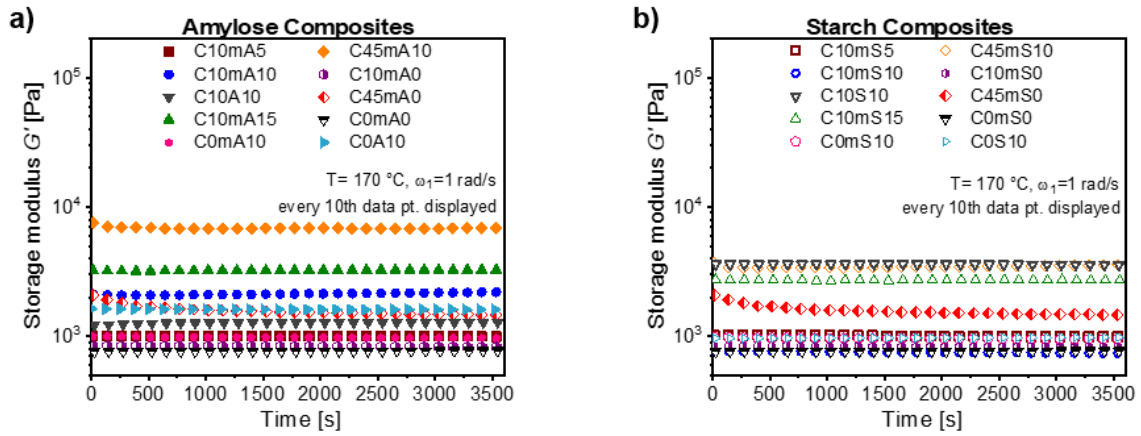

Figure 122. Time dependency of storage modulus G' at 170 °C and ω_1 = 1 rad/s in the linear viscoelastic regime for the neat LDPE and the composite materials.

Differential scanning calorimetry (DSC)

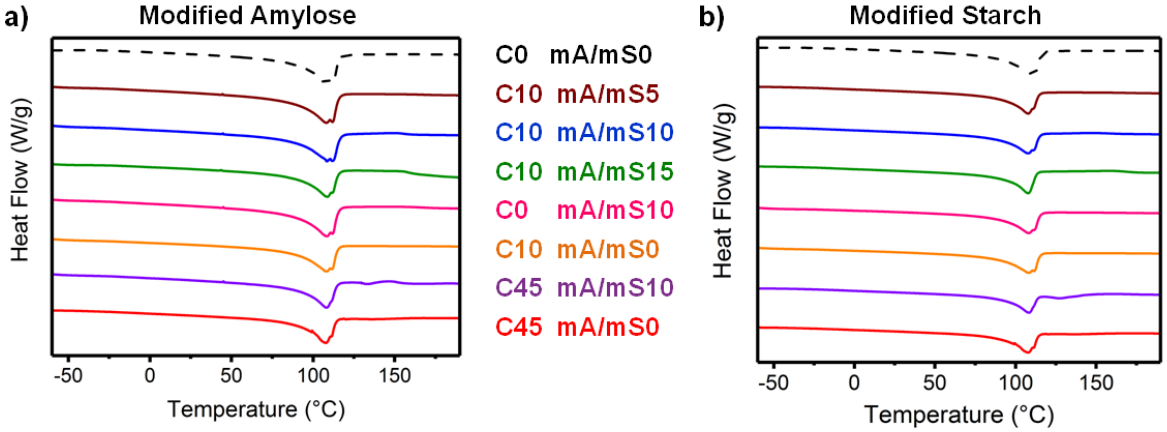

Figure 123. Differential scanning calorimetry of samples containing a) modified amylose and b) modified starch compatibiliser and their respective reference samples.

Mechanical properties in the solid state

Table 22. Mechanical properties determined by stress-strain measurements

Entry	Sample	Young Modulus (MPa)	Maximum Stress (MPa)	Elongation at break (%)
1	**C0mA/mS0**	166 ± 2.7	9.2 ± 0.30	185 ± 35
		Amylose Compatibiliser		
2	**C10mA5**	240 ± 10	9.4 ± 0.19	42 ± 5.6
3	**C10mA10**	261 ± 25	8.7 ± 0.36	37 ± 3.4
4	**C10mA15**	202 ± 11	9.1 ± 0.38	38 ± 2.6
5	**C0mA10**	123 ± 16	9.5 ± 0.13	142 ± 16
6	**C10mA0**	218 ± 5.8	9.4 ± 0.16	58 ± 11
		Starch Compatibiliser		
7	**C10mS5**	199 ± 5.6	7.9 ± 0.52	40 ± 1.8
8	**C10mS10**	173 ± 20	9.8 ± 0.16	33 ± 0.32
9	**C10mS15**	140 ± 4.4	9.5 ± 0.10	28 ± 3.0
10	**C0mS10**	112 ± 5.1	9.2 ± 0.25	143 ± 4.1
11	**C10mS0**	218 ± 5.8	9.4 ± 0.16	58 ± 11

11 Bibliography

(1) Destarac, M. Controlled Radical Polymerization: Industrial Stakes, Obstacles and Achievements. *Macromol. React. Eng.* **2010**, *4* (3–4), 165–179.

(2) Destarac, M. Industrial Developments of Reversible-Deactivation Radical Polymerizations: Is the Induction Period Over? *Polym. Chem.* **2018**, *9* (40), 4947–4967.

(3) Anastas, P. T.; Warner, J. C. *Green Chemistry: Theory and Practice*; Oxford University Press, 1998.

(4) European Commision. *An EU Action Plan for the Circular Economy*; 2015.

(5) Dommanget, C.; D'Agosto, F.; Monteil, V. Polymerization of Ethylene through Reversible Addition-Fragmentation Chain Transfer (RAFT). *Angew. Chemie - Int. Ed.* **2014**, *53* (26), 6683–6686.

(6) Nakamura, Y.; Ebeling, B.; Wolpers, A.; Monteil, V.; D'Agosto, F.; Yamago, S. Controlled Radical Polymerization of Ethylene Using Organotellurium Compounds. *Angew. Chemie - Int. Ed.* **2018**, *57* (1), 305–309.

(7) Kermagoret, A.; Debuigne, A.; Jérôme, C.; Detrembleur, C. Precision Design of Ethylene- and Polar-Monomer-Based Copolymers by Organometallic-Mediated Radical Polymerization. *Nat. Chem.* **2014**, *6* (3), 179–187.

(8) Demarteau, J.; Kermagoret, A.; Jérôme, C.; Detrembleur, C.; Debuigne, A. Controlled Synthesis of Ethylene-Vinyl Acetate Based Copolymers by Organometallic Mediated Radical Polymerization. *ACS Symp. Ser.* **2015**, 47–61.

(9) Chen, Q. B.; Zeng, T. Y.; Xia, L.; Zhang, Z.; Hong, C. Y.; Zou, G.; You, Y. Z. A RAFT/MADIX Method Finely Regulating the Copolymerization of Ethylene and Polar Vinyl Monomers under Mild Conditions. *Chem. Commun.* **2017**, *53* (78), 10780–10783.

(10) Tatemoto, M.; Nakagawa, T. Segemented Polymers Containing Fluroine and Iodine and Their Production. US 4,158,678, 1979.

(11) Otsu, T.; Yoshida, M. Role of Initiator-Transfer Agent-Terminator (Iniferter) in Radical Polymerizations: Polymer Design by Organic Disulfides as Iniferters. *Die Makromol. Chemie, Rapid Commun.* **1982**, *3* (2), 127–132.

(12) Matyjaszewski, K.; Xia, J. Atom Transfer Radical Polymerization. *Chem. Rev.* **2001**, *101* (9), 2921–2990.

(13) Moad, G.; Rizzardo, E.; Thang, S. H. RAFT Polymerization and Some of Its Applications. *Chem. - An Asian J.* **2013**, *8* (8), 1634–1644.

(14) Nicolas, J.; Guillaneuf, Y.; Lefay, C.; Bertin, D.; Gigmes, D.; Charleux, B. Nitroxide-Mediated Polymerization. *Prog. Polym. Sci.* **2013**, *38* (1), 63–235.

(15) Sciannamea, V.; Jérôme, R.; Detrembleur, C. In-Situ Nitroxide-Mediated Radical Polymerization (NMP) Processes: Their Understanding and Optimization. *Chem. Rev.* **2008**, *108* (3), 1104–1126.

(16) Hurtgen, M.; Detrembleur, C.; Jerome, C.; Debuigne, A. Insight into Organometallic-Mediated Radical Polymerization. *Polym. Rev.* **2011**, *51* (2), 188–213.

(17) Debuigne, A.; Jérôme, C.; Detrembleur, C. Organometallic-Mediated Radical Polymerization of 'Less Activated Monomers': Fundamentals, Challenges and Opportunities. *Polym. (United Kingdom)* **2017**, *115*, 285–307.

(18) Allan, L. E. N.; Perry, M. R.; Shaver, M. P. Organometallic Mediated Radical Polymerization. *Prog. Polym. Sci.* **2012**, *37* (1), 127–156.

(19) Poli, R. Relationship between One-Electron Transition-Metal Reactivity and Radical Polymerization Processes. *Angew. Chemie Int. Ed.* **2006**, *45* (31), 5058–5070.

(20) Yamago, S. Precision Polymer Synthesis by Degenerative Transfer Controlled/Living Radical Polymerization Using Organotellurium, Organostibine, and Organobismuthine Chain-Transfer Agents. *Chem. Rev.* **2009**, *109* (11), 5051–5068.

(21) Ouchi, M.; Terashima, T.; Sawamoto, M. Transition Metal-Catalyzed Living Radical Polymerization: Toward Perfection in Catalysis and Precision Polymer Synthesis. *Chem. Rev.* **2009**, *109* (11), 4963–5050.

(22) Matyjaszewski, K.; Gnanou, Y.; Leibler, L. *Macromolecular Engineering: Precise Synthesis, Materials Properties, Applications*; Wiley, 2011.

(23) Odian, G. *Principles of Polymerization*, 4th ed.; Wiley, 2004.

(24) Morin, A.; Detrembleur, C.; Jérôme, C.; Tullio, P. De; Poli, R.; Debuigne, A. Effect of Head-to-Head Addition in Vinyl Acetate Controlled Radical Polymerization: Why Is Co(Acac)2‑Mediated Polymerization so Much Better? *Macromolecules* **2013**, *46* (11), 4303–4312.

(25) Stenzel, M. H.; Cummins, L.; Roberts, G. E.; Davis, T. P.; Vana, P.; Barner-Kowollik, C. Xanthate Mediated Living Polymerization of Vinyl Acetate: A Systematic Variation in MADIX/RAFT Agent Structure. *Macromol. Chem. Phys.* **2003**, *204* (9), 1160–1168.

(26) Venkatesh, R.; Staal, B. B. P.; Klumperman, B. Olefin Copolymerization via Reversible Addition-Fragmentation Chain Transfer. *Chem. Commun.* **2004**, *4* (13), 1554–1555.

(27) Harrisson, S.; Liu, X.; Ollagnier, J.-N.; Coutelier, O.; Marty, J.-D.; Destarac, M. RAFT

Polymerization of Vinyl Esters: Synthesis and Applications. *Polymers (Basel).* **2014**, *6* (5), 1437–1488.

(28) Wayland, B. B.; Poszmik, G.; Mukerjee, S. L.; Fryd, M. Living Radical Polymerization of Acrylates by Organocobalt Porphyrin Complexes. *J. Am. Chem. Soc.* **1994**, *116* (17), 7943–7944.

(29) Clayden, J.; Greeves, N.; Warren, S.; Wothers, P. *Organic Chemistry*; OUP Oxford, 2000.

(30) Debuigne, A.; Champouret, Y.; Jérôme, R.; Poli, R.; Detrembleur, C. Mechanistic Insights into the Cobalt-Mediated Radical Polymerization (CMRP) of Vinyl Acetate with Cobalt(III) Adducts as Initiators. *Chem. - A Eur. J.* **2008**, *14* (13), 4046–4059.

(31) Debuigne, A.; Morin, A. N.; Kermagoret, A.; Piette, Y.; Detrembleur, C.; Jérôme, C.; Poli, R. Key Role of Intramolecular Metal Chelation and Hydrogen Bonding in the Cobalt-Mediated Radical Polymerization of N-Vinyl Amides. *Chem. - A Eur. J.* **2012**, *18* (40), 12834–12844.

(32) Kwak, Y.; Goto, A.; Fukuda, T.; Kobayashi, Y.; Yamago, S. A Systematic Study on Activation Processes in Organotellurium-Mediated Living Radical Polymerizations of Styrene, Methyl Methacrylate, Methyl Acrylate, and Vinyl Acetate. *Macromolecules* **2006**, *39* (14), 4671–4679.

(33) Stahel, Walter, R.; Reday-Mulvey, G. *Jobs for Tomorrow, the Potential for Substituting Manpower for Energy*; Vantage Press, 1981.

(34) European-Bioplastics; nova-Institute. *Bioplastics Market Data 2017*; 2017.

(35) Gandini, A.; Belgacem, M. N. The State of the Art. In *Monomers, Polymers and Composites from Renewable Resources*; 2008; pp 1–16.

(36) Röper, H. Renewable Raw Materials in Europe — Industrial Utilisation of Starch and Sugar [1]. *Starch - Stärke* **2002**, *54* (3–4), 89–99.

(37) Yao, K.; Tang, C. Controlled Polymerization of Next-Generation Renewable Monomers and Beyond. *Macromolecules* **2013**, *46* (5), 1689–1712.

(38) Satoh, K. Controlled / Living Polymerization of Renewable Vinyl Monomers into Bio-Based Polymers. *Polym. J.* **2015**, *47*, 527–536.

(39) Tang, C.; Ryu, C. Y. *Sustainable Polymers from Biomass*; 2017.

(40) Yee, G. M.; Hillmyer, M. A.; Tonks, I. A. Bioderived Acrylates from Alkyl Lactates via Pd-Catalyzed Hydroesterification. *ACS Sustain. Chem. Eng.* **2018**, *6* (8), 9579–9584.

(41) Kamigaito, M.; Satoh, K. Sustainable Vinyl Polymers via Controlled Polymerization of

Terpenes. In *Sustainable Polymers from Biomass*; Tang, C., Ryu, C. Y., Eds.; Wiley, 2017; pp 55–81.

(42) Winnacker, M. Pinenes: Abundant and Renewable Building Blocks for a Variety of Sustainable Polymers. *Angew. Chemie Int. Ed.* **2018**, *57* (44), 14362–14371.

(43) Bergman, J. A.; Kessler, M. R. Monomers and Resulting Polymers from Biomass. *Introd. to Chem. from Biomass Second Ed.* **2015**, *9781118714*, 157–204.

(44) Molina-Gutierrez, S.; Ladmiral, V.; Bongiovanni, R. M.; Caillol, S.; Lacroix-Desmazes, P. Radical Polymerization of Biobased Monomers in Aqueous Dispersed Media. *Green Chem.* **2019**, *21* (1), 36–53.

(45) Buckingham, J. *Dictionary of Natural Products*, 1st ed.; Chapman & Hall: London, 1993.

(46) Singh, A.; Kamal, M. Synthesis and Characterization of Polylimonene: Polymer of an Optically Active Terpene. *J. Appl. Polym. Sci.* **2012**, *125* (2), 1456–1459.

(47) Kamigaito, M.; Satoh, K. Sustainable Vinyl Polymers via Controlled Polymerization of Terpenes. In *Sustainable Polymers from Biomass*; Tang, C., Ryu, C. Y., Eds.; Wiley, 2017; pp 55–81.

(48) Li, A.-L.; Wang, L.; Liang, H.; Lu, J. Controlled Radical Copolymerization of β-Pinene and Acrylonitrile. *J. Polym. Sci. Part A Polym. Chem.* **2006**, *44* (8), 2376–2387.

(49) Wang, Y.; Li, A. L.; Liang, H.; Lu, J. Reversible Addition-Fragmentation Chain Transfer Radical Copolymerization of β-Pinene and Methyl Acrylate. *Eur. Polym. J.* **2006**, *42* (10), 2695–2702.

(50) Laible, R. C. Allyl Polymerizations. *Chem. Rev.* **1958**, *58* (5), 807–843.

(51) Wang, Y.; Chen, Q.; Liang, H.; Lu, J. Conventional and RAFT Radical Copolymerizations of β-Pinene with N-Substituted Maleimides. *Polym. Int.* **2007**, *56* (12), 1514–1520.

(52) Wang, Y.; Ai, Q.; Lu, J. RAFT Radical Copolymerization of Beta-Pinene with Maleic Anhydride and Aggregation Behaviors of Their Copolymer in Aqueous Solution. *J. Polym. Sci. Part A Polym. Chem.* **2015**, *53* (12), 1422–1429.

(53) Satoh, K.; Matsuda, M.; Nagai, K.; Kamigaito, M. AAB-Sequence Living Radical Chain Copolymerization of Naturally Occurring Limonene with Maleimide: An End-to-End Sequence-Regulated Copolymer. *J. Am. Chem. Soc.* **2010**, *132* (29), 10003–10005.

(54) Matsuda, M.; Satoh, K.; Kamigaito, M. 1:2-Sequence-Regulated Radical Copolymerization of Naturally Occurring Terpenes With Maleimide Derivatives in

Fluorinated Alcohol. *J. Polym. Sci. Part A Polym. Chem.* **2013**, *51* (8), 1774–1785.

(55) Hilschmann, J.; Kali, G. Bio-Based Polymyrcene with Highly Ordered Structure via Solvent Free Controlled Radical Polymerization. *Eur. Polym. J.* **2015**, *73*, 363–373.

(56) Bauer, N.; Brunke, J.; Kali, G. Controlled Radical Polymerization of Myrcene in Bulk: Mapping the Effect of Conditions on the System. *ACS Sustain. Chem. Eng.* **2017**, *5* (11), 10084–10092.

(57) Métafiot, A.; Kanawati, Y.; Gérard, J. F.; Defoort, B.; Marić, M. Synthesis of β-Myrcene-Based Polymers and Styrene Block and Statistical Copolymers by SG1 Nitroxide-Mediated Controlled Radical Polymerization. *Macromolecules* **2017**, *50* (8), 3101–3120.

(58) Miyaji, H.; Satoh, K.; Kamigaito, M. Bio-Based Polyketones by Selective Ring-Opening Radical Polymerization of α-Pinene-Derived Pinocarvone. *Angew. Chemie - Int. Ed.* **2016**, *55* (4), 1372–1376.

(59) Phun, L.; Snead, D.; Hurd, P.; Jing, F. Industrial Applications of Pine-Chemical-Based Materials. In *Sustainable Polymers from Biomass*; Tang, C., Ryu, C. Y., Eds.; Wiley, 2017; pp 151–179.

(60) Plastics Europe. *Plastics – The Facts 2018*; 2018.

(61) Delidovich, I.; Hausoul, P. J. C.; Deng, L.; Pfützenreuter, R.; Rose, M.; Palkovits, R. Alternative Monomers Based on Lignocellulose and Their Use for Polymer Production. *Chem. Rev.* **2016**, *116* (3), 1540–1599.

(62) Sheldon, R. A. The Road to Biorenewables: Carbohydrates to Commodity Chemicals. *ACS Sustain. Chem. Eng.* **2018**, *6* (4), 4464–4480.

(63) Tomaszewska, J.; Bieliński, D.; Binczarski, M.; Berlowska, J.; Dziugan, P.; Piotrowski, J.; Stanishevsky, A.; Witońska, I. A. Products of Sugar Beet Processing as Raw Materials for Chemicals and Biodegradable Polymers. *RSC Adv.* **2018**, *8* (6), 3161–3177.

(64) Okabe, M.; Lies, D.; Kanamasa, S.; Park, E. Y. Biotechnological Production of Itaconic Acid and Its Biosynthesis in Aspergillus Terreus. *Appl. Microbiol. Biotechnol.* **2009**, *84* (4), 597–606.

(65) Steiger, M. G.; Blumhoff, M. L.; Mattanovich, D.; Sauer, M. Biochemistry of Microbial Itaconic Acid Production. *Front. Microbiol.* **2013**, *4*, 1–5.

(66) Hartford, S. L.; Subramanian, S.; Parker, J. A. Synthesis of N-Substituted Bisitaconimide Monomers for Use As Thermosetting Polyimide Resins. *J Polym Sci Polym Chem Ed* **1978**, *16* (1), 137–153.

(67) Anand, V.; Agarwal, S.; Greiner, A.; Choudhary, V. Synthesis of Methyl Methacrylate and N-Aryl Itaconimide Block Copolymers via Atom-Transfer Radical Polymerization. *Polym. Int.* **2005**, *54* (5), 823–828.

(68) Velickovic, J.; Coseva, S.; Fort, R. J. Solution Properties of Poly(Dicyclohexyl Itaconate). *Eur. Polym. J.* **1975**, *11* (5–6), 377–380.

(69) Okada, S.; Matyjaszewski, K. Synthesis of Bio-Based Poly(N-Phenylitaconimide) by Atom Transfer Radical Polymerization. *J. Polym. Sci. Part A Polym. Chem.* **2015**, *53* (6), 822–827.

(70) Fernandez-Garcia, M.; Fernandez-Sanz, M.; De la Fuente, J. L.; Madruga, E. L. Atom-Transfer Radical Polymerization of Dimethyl Itaconate. *Macromol. Chem. Phys.* **2001**, *202* (7), 1213–1218.

(71) Deoghare, C.; Baby, C.; Nadkarni, V. S.; Behera, R. N.; Chauhan, R. Synthesis, Characterization, and Computational Study of Potential Itaconimide-Based Initiators for Atom Transfer Radical Polymerization. *RSC Adv.* **2014**, *4* (89), 48163–48176.

(72) Liu, S.; Zhang, X.; Li, M.; Ren, X.; Tao, Y. Precision Synthesis of Sustainable Thermoplastic Elastomers from Lysine-Derived Monomers. *J. Polym. Sci. Part A Polym. Chem.* **2016**, *55* (2), 349–355.

(73) Szablan, Z.; Toy, A. A.; Davis, T. P.; Hao, X.; Stenzel, M. H.; Barner-Kowollik, C. Reversible Addition Fragmentation Chain Transfer Polymerization of Sterically Hindered Monomers: Toward Well-Defined Rod/Coil Architectures. *J. Polym. Sci. Part A Polym. Chem.* **2004**, *42* (10), 2432–2443.

(74) Satoh, K.; Lee, D. H.; Nagai, K.; Kamigaito, M. Precision Synthesis of Bio-Based Acrylic Thermoplastic Elastomer by RAFT Polymerization of Itaconic Acid Derivatives. *Macromol. Rapid Commun.* **2014**, *35* (2), 161–167.

(75) Moad, G. RAFT Polymerization to Form Stimuli-Responsive Polymers. *Polym. Chem.* **2017**, *8* (1), 177–219.

(76) Javakhishvili, I.; Kasama, T.; Jankova, K.; Hvilsted, S. RAFT Copolymerization of Itaconic Anhydride and 2-Methoxyethyl Acrylate: A Multifunctional Scaffold for Preparation of "Clickable" Gold Nanoparticles. *Chem. Commun.* **2013**, *49* (42), 4803–4805.

(77) Wong, H.; Brown, G. D. β-Methoxy-γ-Methylene-α,β-Unsaturated-γ-Butyrolactones from Artabotrys Hexapetalus. *Phytochemistry* **2002**, *59* (1), 99–104.

(78) Fetizon, M.; Golfier, M.; Louis, J.-M. Oxydations Par Le Carbonate d'argent Sur Celite-Xiii. *Tetrahedron* **1975**, *31*, 171–176.

(79) Gowda, R. R.; Chen, E. Y.-X. Synthesis of β-Methyl-α-Methylene-γ-Butyrolactone from Biorenewable Itaconic Acid. *Org. Chem. Front.* **2014**, *1* (3), 230.

(80) Manzer, L. E. Catalytic Synthesis of α-Methylene-γ-Valerolactone: A Biomass-Derived Acrylic Monomer. *Appl. Catal. A Gen.* **2004**, *272* (1–2), 249–256.

(81) Trotta, J. T.; Jin, M.; Stawiasz, K. J.; Michaudel, Q.; Chen, W. L.; Fors, B. P. Synthesis of Methylene Butyrolactone Polymers from Itaconic Acid. *J. Polym. Sci. Part A Polym. Chem.* **2017**, *55* (17), 2730–2737.

(82) Mosnáček, J.; Matyjaszewski, K. Atom Transfer Radical Polymerization of Tulipalin A: A Naturally Renewable Monomer. *Macromolecules* **2008**, *41* (15), 5509–5511.

(83) Qi, G.; Nolan, M.; Schork, F. J.; Jones, C. W. Emulsion and Controlled Miniemulsion Polymerization of the Renewable Monomer γ-Methyl-α-Methylene-γ-Butyrolactone. *J. Polym. Sci. Part A Polym. Chem.* **2008**, *46* (17), 5929–5944.

(84) Xu, S.; Huang, J.; Xu, S.; Luo, Y. RAFT Ab Initio Emulsion Copolymerization of γ-Methyl-α- Methylene-γ-Butyrolactone and Styrene. *Polym. (United Kingdom)* **2013**, *54* (7), 1779–1785.

(85) Mosnáček, J.; Yoon, J. A.; Juhari, A.; Koynov, K.; Matyjaszewski, K. Synthesis, Morphology and Mechanical Properties of Linear Triblock Copolymers Based on Poly(α-Methylene-γ-Butyrolactone). *Polymer (Guildf).* **2009**, *50* (9), 2087–2094.

(86) Juhari, A.; Mosnáček, J.; Yoon, J. A.; Nese, A.; Koynov, K.; Kowalewski, T.; Matyjaszewski, K. Star-like Poly(n-Butyl Acrylate)-b-Poly(α-Methylene-γ-Butyrolactone) Block Copolymers for High Temperature Thermoplastic Elastomers Applications. *Polymer (Guildf).* **2010**, *51* (21), 4806–4813.

(87) Higaki, Y.; Okazaki, R.; Takahara, A. Semirigid Biobased Polymer Brush: Poly(α-Methylene-γ- Butyrolactone) Brushes. *ACS Macro Lett.* **2012**, *1* (9), 1124–1127.

(88) Shin, J.; Lee, Y.; Tolman, W. B.; Hillmyer, M. A. Thermoplastic Elastomers Derived from Menthide and Tulipalin A. *Biomacromolecules* **2012**, *13* (11), 3833–3840.

(89) Ding, K.; John, A.; Shin, J.; Lee, Y.; Quinn, T.; Tolman, W. B.; Hillmyer, M. A. High-Performance Pressure-Sensitive Adhesives from Renewable Triblock Copolymers. *Biomacromolecules* **2015**, *16* (8), 2537–2539.

(90) Ou, S.; Kwok, K. C. Ferulic Acid: Pharmaceutical Functions, Preparation and Applications in Foods. *J. Sci. Food Agric.* **2004**, *84* (11), 1261–1269.

(91) Kumar, N.; Pruthi, V. Potential Applications of Ferulic Acid from Natural Sources. *Biotechnol. Reports* **2014**, *4* (1), 86–93.

(92) Kodaira, K.; Onishi, Y.; Ito, K. An Oligomerization of 2-Methoxy-4-Vinylphenol.

Makromol. Chem. Rapid Commun. **1980**, *1* (7), 427–431.

(93) Takeshima, H.; Satoh, K.; Kamigaito, M. Bio-Based Functional Styrene Monomers Derived from Naturally Occurring Ferulic Acid for Poly(Vinylcatechol) and Poly(Vinylguaiacol) via Controlled Radical Polymerization. *Macromolecules* **2017**, *50* (11), 4206–4216.

(94) Lejkowski, M. L.; Lindner, R.; Kageyama, T.; Bódizs, G. É.; Plessow, P. N.; Müller, I. B.; Schäfer, A.; Rominger, F.; Hofmann, P.; Futter, C.; Schunk, S. A.; Limbach, M. The First Catalytic Synthesis of an Acrylate from CO2 and an Alkene-A Rational Approach. *Chem. - A Eur. J.* **2012**, *18* (44), 14017–14025.

(95) Dabral, S.; Schaub, T. The Use of Carbon Dioxide (CO2) as a Building Block in Organic Synthesis from an Industrial Perspective. *Adv. Synth. Catal.* **2019**, *361* (2), 223–246.

(96) Xu, X.; Lin, J.; Cen, P. Advances in the Research and Development of Acrylic Acid Production from Biomass. *Chinese J. Chem. Eng.* **2006**, *14* (4), 419–427.

(97) Baek, S. S.; Jang, S. J.; Hwang, S. H. Preparation and Adhesion Performance of Transparent Acrylic Pressure Sensitive Adhesives: Effects of Substituent Structure of Acrylate Monomer. *Int. J. Adhes. Adhes.* **2016**, *64* (3), 72–77.

(98) Scholten, P. B. V.; Detrembleur, C.; Meier, M. A. R. Plant-Based Non-Activated Olefins: A New Class of Renewable Monomers for Controlled Radical Polymerisation. *ACS Sustain. Chem. Eng.* **2019**, *7* (2), 2751–2762.

(99) El Khadem, H. S. 1 - Carbohydrates. In *Carbohydrate Chemistry*; El Khadem, H. S. B. T.-C. C., Ed.; Academic Press, 1988; pp 1–8.

(100) Özyürek, Z.; Komber, H.; Gramm, S.; Schmaljohann, D.; Müller, A. H. E.; Voit, B. Thermoresponsive Glycopolymers via Controlled Radical Polymerization. *Macromol. Chem. Phys.* **2007**, *208* (10), 1035–1049.

(101) Miura, Y.; Hoshino, Y.; Seto, H. Glycopolymer Nanobiotechnology. *Chem. Rev.* **2016**, *116* (4), 1673–1692.

(102) Rieger, J.; Jérôme, C.; Jérôme, R.; Auzély-Velty, R. Polymeric Nanoparticles - Synthesis, Functionalization and Applications in Diagnosis and Therapy. In *Volume 10: Nanomaterials for Medicinal Diagnosis and Therapy*; Kumar, C., Ed.; 2007; pp 342–407.

(103) Boyer, C.; Corrigan, N. A.; Jung, K.; Nguyen, D.; Nguyen, T. K.; Adnan, N. N. M.; Oliver, S.; Shanmugam, S.; Yeow, J. Copper-Mediated Living Radical Polymerization (Atom Transfer Radical Polymerization and Copper(0) Mediated Polymerization):

From Fundamentals to Bioapplications. *Chem. Rev.* **2016**, *116* (4), 1803–1949.

(104) Von Der Ehe, C.; Weber, C.; Gottschaldt, M.; Schubert, U. S. Immobilized Glycopolymers: Synthesis, Methods and Applications. *Prog. Polym. Sci.* **2016**, *57*, 64–102.

(105) Bernard, J.; Hao, X.; Davis, T. P.; Barner-Kowollik, C.; Stenzel, M. H. Synthesis of Various Glycopolymer Architectures via RAFT Polymerization : From Block Copolymers to Stars. *Biomacromolecules* **2006**, *7* (1), 232–238.

(106) Ghadban, A.; Albertin, L. Synthesis of Glycopolymer Architectures by Reversible-Deactivation Radical Polymerization. *Polymers (Basel).* **2013**, *5* (2), 431–526.

(107) Abdounni, Y.; Yilmaz, G.; Becer, R. C. Sequence and Architectural Control in Glycopolymer Synthesis. In *Sequence-Controlled Polymers*; Lutz, J.-F., Ed.; 2017.

(108) Vázquez-Dorbatt, V.; Lee, J.; Lin, E. W.; Maynard, H. D. Synthesis of Glycopolymers by Controlled Radical Polymerization Techniques and Their Applications. *ChemBioChem* **2012**, *13* (17), 2478–2487.

(109) Kristufek, S. L.; Wacker, K. T.; Tsao, Y. Y. T.; Su, L.; Wooley, K. L. Monomer Design Strategies to Create Natural Product-Based Polymer Materials. *Nat. Prod. Rep.* **2017**, *34* (4), 433–459.

(110) Adharis, A.; Vesper, D.; Koning, N.; Loos, K. Synthesis of (Meth)Acrylamide-Based Glycomonomers Using Renewable Resources and Their Polymerization in Aqueous Systems. *Green Chem.* **2018**, *20* (2), 476–484.

(111) Wang, J.; Yuan, L.; Wang, Z.; Rahman, M. A.; Huang, Y.; Zhu, T.; Wang, R.; Cheng, J.; Wang, C.; Chu, F.; Tang, C. Photoinduced Metal-Free Atom Transfer Radical Polymerization of Biomass-Based Monomers. *Macromolecules* **2016**, *49* (20), 7709–7717.

(112) Reportlinker. *Global Lignin Products Market - Segmented by Porduct Type, Source, Application, And Geography - Trends and Forecasts (2015-2020)*; 2015.

(113) Gillet, S.; Aguedo, M.; Petitjean, L.; Morais, A. R. C.; Da Costa Lopes, A. M.; Łukasik, R. M.; Anastas, P. T. Lignin Transformations for High Value Applications: Towards Targeted Modifications Using Green Chemistry. *Green Chem.* **2017**, *19* (18), 4200–4233.

(114) Schutyser, W.; Renders, T.; Van Den Bosch, S.; Koelewijn, S. F.; Beckham, G. T.; Sels, B. F. Chemicals from Lignin: An Interplay of Lignocellulose Fractionation, Depolymerisation, and Upgrading. *Chem. Soc. Rev.* **2018**, *47* (3), 852–908.

(115) Sun, Z.; Fridrich, B.; De Santi, A.; Elangovan, S.; Barta, K. Bright Side of Lignin

Depolymerization: Toward New Platform Chemicals. *Chem. Rev.* **2018**, *118* (2), 614–678.

(116) Upton, B. M.; Kasko, A. M. Strategies for the Conversion of Lignin to High-Value Polymeric Materials: Review and Perspective. *Chem. Rev.* **2016**, *116* (4), 2275–2306.

(117) Llevot, A.; Grau, E.; Carlotti, S.; Grelier, S.; Cramail, H. From Lignin-Derived Aromatic Compounds to Novel Biobased Polymers. *Macromol. Rapid Commun.* **2016**, *37* (1), 9–28.

(118) Laurichesse, S.; Avérous, L. Chemical Modification of Lignins: Towards Biobased Polymers. *Prog. Polym. Sci.* **2014**, *39* (7), 1266–1290.

(119) Shuai, L.; Saha, B. Towards High-Yield Lignin Monomer Production. *Green Chem.* **2017**, *19* (16), 3752–3758.

(120) Fache, M.; Boutevin, B.; Caillol, S. Vanillin Production from Lignin and Its Use as a Renewable Chemical. *ACS Sustain. Chem. Eng.* **2016**, *4* (1), 35–46.

(121) Holmberg, A. L.; Stanzione, J. F.; Wool, R. P.; Epps, T. H. A Facile Method for Generating Designer Block Copolymers from Functionalized Lignin Model Compounds. *ACS Sustain. Chem. Eng.* **2014**, *2* (4), 569–573.

(122) Holmberg, A. L.; Reno, K. H.; Nguyen, N. A.; Wool, R. P.; Epps, T. H. Syringyl Methacrylate, a Hardwood Lignin-Based Monomer for High-Tg Polymeric Materials. *ACS Macro Lett.* **2016**, *5* (5), 574–578.

(123) Wang, S.; Bassett, A. W.; Wieber, G. V.; Stanzione, J. F.; Epps, T. H. Effect of Methoxy Substituent Position on Thermal Properties and Solvent Resistance of Lignin-Inspired Poly(Dimethoxyphenyl Methacrylate)S. *ACS Macro Lett.* **2017**, *6* (8), 802–807.

(124) Emerson, J. A.; Garabedian, N. T.; Burris, D. L.; Furst, E. M.; Epps, T. H. Exploiting Feedstock Diversity to Tune the Chemical and Tribological Properties of Lignin-Inspired Polymer Coatings. *ACS Sustain. Chem. Eng.* **2018**, *6* (5), 6856–6866.

(125) Holmberg, A. L.; Karavolias, M. G.; Epps, T. H. RAFT Polymerization and Associated Reactivity Ratios of Methacrylate-Functionalized Mixed Bio-Oil Constituents. *Polym. Chem.* **2015**, *6* (31), 5728–5739.

(126) Stanzione, J. F.; Sadler, J. M.; La Scala, J. J.; Wool, R. P. Lignin Model Compounds as Bio-Based Reactive Diluents for Liquid Molding Resins. *ChemSusChem* **2012**, *5* (7), 1291–1297.

(127) Stanzione, J. F.; Giangiulio, P. A.; Sadler, J. M.; La Scala, J. J.; Wool, R. P. Lignin-Based Bio-Oil Mimic as Biobased Resin for Composite Applications. *ACS Sustain.*

Chem. Eng. **2013**, *1* (4), 419–426.

(128) Bensabeh, N.; Ronda, J. C.; Galià, M.; Cádiz, V.; Lligadas, G.; Percec, V. SET-LRP of the Hydrophobic Biobased Menthyl Acrylate. *Biomacromolecules* **2018**, *19* (4), 1256–1268.

(129) Pattison, F. L. M.; Howell, W. C.; McNamara, A. J.; Schneider, J. C.; Walker, J. F. Toxic Fluorine Compounds. III. ω-Fluoroalcohols. *J. Org. Chem.* **1956**, *21* (7), 739–747.

(130) Wilbon, P. A.; Chu, F.; Tang, C. Progress in Renewable Polymers from Natural Terpenes, Terpenoids, and Rosin. *Macromol. Rapid Commun.* **2013**, *34* (1), 8–37.

(131) Zhang, M.; Zhou, Y.; Zhang, J. Use of Rosin and Turpentine as Feedstocks for the Preparation of Polyurethane Polymers. In *Sustainable Polymers from Biomass*; 2017; pp 91–101.

(132) Wang, J.; Liu, S.; Yu, J.; Lu, C.; Wang, C.; Chu, F. Rosin-Derived Monomers and Their Progress in Polymer Application. In *Sustainable Polymers from Biomass*; Tang, C., Ryu, C. Y., Eds.; Wiley, 2017; pp 103–141.

(133) Adelman, R. L. The Interchange Reaction of Vinyl Acetate with Organic Acids. *J. Org. Chem.* **1949**, *14* (6), 1057–1077.

(134) Ma, Q.; Liu, X.; Zhang, R.; Zhu, J.; Jiang, Y. Synthesis and Properties of Full Bio-Based Thermosetting Resins from Rosin Acid and Soybean Oil: The Role of Rosin Acid Derivatives. *Green Chem.* **2013**, *15* (5), 1300–1310.

(135) Zheng, Y.; Yao, K.; Lee, J.; Chandler, D.; Wang, J.; Wang, C.; Chu, F.; Tang, C. Well-Defined Renewable Polymers Derived from Gum Rosin. *Macromolecules* **2010**, *43* (14), 5922–5924.

(136) Wilbon, P. A.; Zheng, Y.; Yao, K.; Tang, C. Renewable Rosin Acid-Degradable Caprolactone Block Copolymers by Atom Transfer Radical Polymerization and Ring-Opening Polymerization. *Macromolecules* **2010**, *43* (21), 8747–8754.

(137) Huang, S. Biodegradable Polymers. In *Encyclopedia of Polymer Science and Engineering*; Wiley: New York, 1985; pp 220–243.

(138) Woodruff, M. A.; Hutmacher, D. W. The Return of a Forgotten Polymer - Polycaprolactone in the 21st Century. *Prog. Polym. Sci.* **2010**, *35* (10), 1217–1256.

(139) Liss, S. N.; Bicho, P. A.; Saddler, J. N. Microbiology and Biodegradation of Resin Acids in Pulp Mill Effluents: A Minireview. *Can. J. Microbiol.* **1997**, *43* (7), 599–611.

(140) Cheremnykh, K. M.; Grishko, V. V.; Ivshin, I. B. Bacterial Degradation of Ecotoxic Dehydroabietic Acid. *Catal. Ind.* **2017**, *9* (4), 331–338.

(141) Ding, W.; Wang, S.; Yao, K.; Ganewatta, M. S.; Tang, C.; Robertson, M. L. Physical Behavior of Triblock Copolymer Thermoplastic Elastomers Containing Sustainable Rosin-Derived Polymethacrylate End Blocks. *ACS Sustain. Chem. Eng.* **2017**, *5* (12), 11470–11480.

(142) Wang, J.; Yao, K.; Wang, C.; Tang, C.; Jiang, X. Synthesis and Drug Delivery of Novel Amphiphilic Block Copolymers Containing Hydrophobic Dehydroabietic Moiety. *J. Mater. Chem. B* **2013**, *1* (17), 2324–2332.

(143) Ganewatta, M. S.; Miller, K. P.; Singleton, S. P.; Mehrpouya-Bahrami, P.; Chen, Y. P.; Yan, Y.; Nagarkatti, M.; Nagarkatti, P.; Decho, A. W.; Tang, C. Antibacterial and Biofilm-Disrupting Coatings from Resin Acid-Derived Materials. *Biomacromolecules* **2015**, *16* (10), 3336–3344.

(144) Ganewatta, M. S.; Chen, Y. P.; Wang, J.; Zhou, J.; Ebalunode, J.; Nagarkatti, M.; Decho, A. W.; Tang, C. Bio-Inspired Resin Acid-Derived Materials as Anti-Bacterial Resistance Agents with Unexpected Activities. *Chem. Sci.* **2014**, *5* (5), 2011–2016.

(145) Hon, D. N. S. Cellulose: A Random Walk along Its Historical Path. *Cellulose* **1994**, *1* (1), 1–25.

(146) Onwukamike, K. N.; Grelier, S.; Grau, E.; Cramail, H.; Meier, M. A. R. A Critical Review on Sustainable Homogeneous Cellulose Modification: Why Renewability Is Not Enough. *ACS Sustain. Chem. Eng.* **2019**, *7* (2), 1826–1840.

(147) Hansson, S.; Trouillet, V.; Tischer, T.; Goldmann, A. S.; Carlmark, A.; Barner-Kowollik, C.; Malmström, E. Comparative Study of Grafting-from versus Grafting-To. *Biomacromolecules* **2013**, *14* (1), 64−74.

(148) Malmström, E.; Carlmark, A. Controlled Grafting of Cellulose Fibres - An Outlook beyond Paper and Cardboard. *Polym. Chem.* **2012**, *3* (7), 1702–1713.

(149) Wohlhauser, S.; Delepierre, G.; Labet, M.; Morandi, G.; Thielemans, W.; Weder, C.; Zoppe, J. O. Grafting Polymers from Cellulose Nanocrystals: Synthesis, Properties, and Applications. *Macromolecules* **2018**, *51* (16), 6157–6189.

(150) Wang, J.; Yao, K.; Korich, A. L.; Li, S.; Ma, S.; Ploehn, H. J.; Iovine, P. M.; Wang, C.; Chu, F.; Tang, C. Combining Renewable Gum Rosin and Lignin: Towards Hydrophobic Polymer Composites by Controlled Polymerization. *J. Polym. Sci. Part A Polym. Chem.* **2011**, *49* (17), 3728–3738.

(151) Yu, J.; Liu, Y.; Liu, X.; Wang, C.; Wang, J.; Chu, F.; Tang, C. Integration of Renewable Cellulose and Rosin towards Sustainable Copolymers by “Grafting from” ATRP. *Green Chem.* **2014**, *16* (4), 1854–1864.

(152) Liu, Y.; Yao, K.; Chen, X.; Wang, J.; Wang, Z.; Ploehn, H. J.; Wang, C.; Chu, F.; Tang, C. Sustainable Thermoplastic Elastomers Derived from Renewable Cellulose, Rosin and Fatty Acids. *Polym. Chem.* **2014**, *5* (9), 3170–3181.

(153) Mutlu, H.; Meier, M. A. R. Castor Oil as a Renewable Resource for the Chemical Industry. *Eur. J. Lipid Sci. Technol.* **2010**, *112* (1), 10–30.

(154) Biermann, U.; Bornscheuer, U.; Meier, M. A. R.; Metzger, J. O.; Schäfer, H. J. Oils and Fats as Renewable Raw Materials in Chemistry. *Angew. Chemie Int. Ed.* **2011**, *50* (17), 3854–3871.

(155) Kenar, J. A.; Moser, B. R.; List, G. R. Naturally Occurring Fatty Acids: Source, Chemistry, and Uses. In *Fatty Acids Chemistry, Synthesis, and Applications*; Ahmand, M. U., Ed.; Elsevier Inc., 2017; pp 23–82.

(156) Ishak, Z. I.; Sairi, N. A.; Alias, Y.; Aroua, M. K. T.; Yusoff, R. Production of Glycerol Carbonate from Glycerol with Aid of Ionic Liquid as Catalyst. *Chem. Eng. J.* **2016**, *297*, 128–138.

(157) Gade, S. M.; Munshi, M. K.; Chherawalla, B. M.; Rane, V. H.; Kelkar, A. A. Synthesis of Glycidol from Glycerol and Dimethyl Carbonate Using Ionic Liquid as a Catalyst. *Catal. Commun.* **2012**, *27*, 184–188.

(158) Simão, A.-C.; Lynikaite-Pukleviciene, B.; Rousseau, C.; Tatibouët, A.; Cassel, S.; Sackus, A.; Rauter, A. P.; Rollin, P. 1,2-Glycerol Carbonate: A Versatile Renewable Synthon. *Lett. Org. Chem.* **2006**, *3* (10), 744–748.

(159) Lamarzelle, O.; Durand, P. L.; Wirotius, A. L.; Chollet, G.; Grau, E.; Cramail, H. Activated Lipidic Cyclic Carbonates for Non-Isocyanate Polyurethane Synthesis. *Polym. Chem.* **2016**, *7* (7), 1439–1451.

(160) Yuan, L.; Wang, Z.; Trenor, N. M.; Tang, C. Robust Amidation Transformation of Plant Oils into Fatty Derivatives for Sustainable Monomers and Polymers. *Macromolecules* **2015**, *48* (5), 1320–1328.

(161) Gale, C. B.; Brook, M. A. Deoxygenation of Triglycerides by Silylation under Exceptionally Mild Conditions. *Green Chem.* **2018**, *20* (16), 3717–3721.

(162) Fieser, M. E.; Schimler, S. D.; Mitchell, L. A.; Wilborn, E. G.; John, A.; Hogan, L. T.; Benson, B.; LaPointe, A. M.; Tolman, W. B. Dual-Catalytic Decarbonylation of Fatty Acid Methyl Esters to Form Olefins. *Chem. Commun.* **2018**, *54* (55), 7669–7672.

(163) Montero De Espinosa, L.; Meier, M. A. R. Plant Oils: The Perfect Renewable Resource for Polymer Science?! *Eur. Polym. J.* **2011**, *47* (5), 837–852.

(164) Meier, M. A. R.; Metzger, J. O.; Schubert, U. S. Plant Oil Renewable Resources as

Green Alternatives in Polymer Science. *Chem. Soc. Rev.* **2007**, *36* (11), 1788–1802.

(165) Xia, Y.; Larock, R. C. Vegetable Oil-Based Polymeric Materials: Synthesis, Properties, and Applications. *Green Chem.* **2010**, *12* (11), 1893–1909.

(166) Khot, S. N.; Lascala, J. J.; Can, E.; Morye, S. S.; Williams, G. I.; Palmese, G. R.; Kusefoglu, S. H.; Wool, R. P. Development and Application of Triglyceride-Based Polymers and Composites. *J. Appl. Polym. Sci.* **2001**, *82* (3), 703–723.

(167) Lligadas, G.; Ronda, J. C.; Galià, M.; Cádiz, V. Renewable Polymeric Materials from Vegetable Oils: A Perspective. *Mater. Today* **2013**, *16* (9), 337–343.

(168) Axelsson, A.; Antoine-Michard, A.; Sundén, H. Organocatalytic Valorisation of Glycerol: Via a Dual NHC-Catalysed Telescoped Reaction. *Green Chem.* **2017**, *19* (11), 2477–2481.

(169) Hill, K. Industrial Development and Application of Biobased Oleochemicals. *Pure Appl. Chem.* **2007**, *79* (11), 1999–2011.

(170) Kenar, J. A.; Knothe, G. 1,2-Isopropylidene Glycerol Carbonate: Preparation, Characterization, and Hydrolysis. *J. Am. Oil Chem. Soc.* **2008**, *85* (4), 365–372.

(171) Arceo, E.; Marsden, P.; Bergman, R. G.; Ellman, J. A. An Efficient Didehydroxylation Method for the Biomass-Derived Polyols Glycerol and Erythritol. Mechanistic Studies of a Formic Acid-Mediated Deoxygenation. *Chem. Commun.* **2009**, *0* (23), 3357–3359.

(172) Remón, J.; Zhu, G.; Budarin, V. L.; Clark, J. H. Analysis and Optimisation of a Microwave-Assisted Hydrothermal Process for the Production of Value-Added Chemicals from Glycerol. *Green Chem.* **2018**, *20* (11), 2624–2636.

(173) Cochran, E. W.; Williams, R. C.; Hernandez, N.; Cascione, A. Thermoplastic Elastomers via Atom Transfer Radical Polymerization of Plant Oil. WO 2013/109878 Al, 2013.

(174) Cochran, E. W.; Williams, R. C.; Hernandez, N.; Cascione, A. Thermoplastic Elastomers via Reversible Addition-Fragmentation Chain Transfer Polymerization of Triglycerides. WO 2014/189939 A2, 2014.

(175) Maiti, B.; De, P. RAFT Polymerization of Fatty Acid Containing Monomers: Controlled Synthesis of Polymers from Renewable Resources. *RSC Adv.* **2013**, *3* (47), 24983–24990.

(176) Montero De Espinosa, L.; Ronda, J. C.; Galià, M.; Cádiz, V. A Straightforward Strategy for the Efficient Synthesis of Acrylate and Phosphine Oxide-Containing Vegetable Oils and Their Crosslinked Materials. *J. Polym. Sci. Part A Polym. Chem.* **2009**, *47* (16), 4051–4063.

(177) Lomège, J.; Lapinte, V.; Negrell, C.; Robin, J.-J.; Caillol, S. Fatty Acid-Based Radically Polymerizable Monomers: From Novel Poly(Meth)Acrylates to Cutting-Edge Properties. *Biomacromolecules* **2019**, *20* (1), 4–26.

(178) Vendamme, R.; Schüwer, N.; Eevers, W. Recent Synthetic Approaches and Emerging Bio-Inspired Strategies for the Development of Sustainable Pressure-Sensitive Adhesives Derived from Renewable Building Blocks. *J. Appl. Polym. Sci.* **2014**, *131* (17), 8379–8394.

(179) Wu, M.; Zhang, Y.; Peng, Q.; Song, L.; Hu, Z.; Li, Z.; Wang, Z. Mechanically Strong Plant Oil-Derived Thermoplastic Polymers Prepared via Cellulose Graft Strategy. *Appl. Surf. Sci.* **2018**, *458* (July), 495–502.

(180) Zhou, J.; Wu, M.; Peng, Q.; Jiang, F.; Pan, H.; Wang, B.; Liu, S.; Wang, Z. Highly Efficient Strategies toward Sustainable Monomers and Polymers Derived from Fatty Acids: Via Tetramethylguanidine Promoted Esterification. *Polym. Chem.* **2018**, *9* (21), 2880–2886.

(181) Hajiali, F.; Métafiot, A.; Benitez-Ek, L.; Alloune, L.; Marić, M. Nitroxide Mediated Polymerization of Sustainably Sourced Isobornyl Methacrylate and Tridecyl Methacrylate with Acrylonitrile Co-Monomer. *J. Polym. Sci. Part A Polym. Chem.* **2018**, *56* (21), 2422–2436.

(182) Popescu, D.; Hoogenboom, R.; Keul, H.; Moeller, M. Hydroxy Functional Acrylate and Methacrylate Monomers Prepared via Lipase-Catalyzed Transacylation Reactions. *J. Mol. Catal. B Enzym.* **2010**, *62* (1), 80–89.

(183) Save, M.; Weaver, J. V. M.; Armes, S. P.; McKenna, P. Atom Transfer Radical Polymerization of Hydroxy-Functional Methacrylates at Ambient Temperature: Comparison of Glycerol Monomethacrylate with 2-Hydroxypropyl Methacrylate. *Macromolecules* **2002**, *35* (4), 1152–1159.

(184) Wolf, F. K.; Hofmann, A. M.; Frey, H. Poly(Isoglycerol Methacrylate)-b-Poly(D or L-Lactide) Copolymers: A Novel Hydrophilic Methacrylate as Building Block for Supramolecular Aggregates. *Macromolecules* **2010**, *43* (7), 3314–3324.

(185) Pham, P. D.; Monge, S.; Lapinte, V.; Raoul, Y.; Robin, J. J. Various Radical Polymerizations of Glycerol-Based Monomers. *Eur. J. Lipid Sci. Technol.* **2013**, *115* (1), 28–40.

(186) Wan, S.; Zheng, Y.; Liu, Y.; Yan, H.; Liu, K. Fe3O4 Nanoparticles Coated with Homopolymers of Glycerol Mono(Meth)Acrylate and Their Block Copolymers. *J. Mater. Chem.* **2005**, *15* (33), 3424–3430.

(187) Guo, M.; Yan, Y.; Zhang, H.; Yan, H.; Cao, Y.; Liu, K.; Wan, S.; Huang, J.; Yue, W. Magnetic and PH-Responsive Nanocarriers with Multilayer Core-Shell Architecture for Anticancer Drug Delivery. *J. Mater. Chem.* **2008**, *18* (42), 5104–5112.

(188) Zhang, Q.; Luan, L.; Feng, S.; Yan, H.; Liu, K. Using a Bifunctional Polymer for the Functionalization of Fe3O4 Nanoparticles. *React. Funct. Polym.* **2012**, *72* (3), 198–205.

(189) Ragupathy, L.; Millar, D. G.; Tirelli, N.; Cellesi, F. An Orthogonal Click-Chemistry Approach to Design Poly(Glycerol Monomethacrylate)-Based Nanomaterials for Controlled Immunostimulation. *Macromol. Biosci.* **2014**, *14* (11), 1528–1538.

(190) Yang, J.; Zhang, D.; Jiang, S.; Yang, J.; Nie, J. Synthesis of Y-Shaped Poly(Solketal Acrylate)-Containing Block Copolymers and Study on the Thermoresponsive Behavior for Micellar Aggregates. *J. Colloid Interface Sci.* **2010**, *352* (2), 405–414.

(191) Kipping, M.; Krahl, F.; Döring, A.; Adler, H. J. P.; Kuckling, D. Synthesis and Characterization of Particles Consisting of a Biodegradable Poly(l-Lactide) Core and a Functional Hydrophilic Shell. *Eur. Polym. J.* **2010**, *46* (2), 313–323.

(192) Batt-Coutrot, D.; Haddleton, D. M.; Jarvis, A. P.; Kelly, R. L. Synthesis and Properties of Amphiphilic Vinyl Acetate Triblock Copolymers Prepared by Copper Mediated Living Radical Polymerisation. *Eur. Polym. J.* **2003**, *39* (12), 2243–2252.

(193) Whittaker, M. R.; Urbani, C. N.; Monteiro, M. J. Synthesis of Linear and 4-Arm Star Block Copolymers of Poly(Methyl Acrylate-b-Solketal Acrylate) by SET-LRP at 25 °C. *J. Polym. Sci. Part A Polym. Chem.* **2008**, *46* (18), 6346–6357.

(194) Deng, H.; Zhao, X.; Liu, J.; Zhang, J.; Deng, L.; Liu, J.; Dong, A. Synergistic Dual-PH Responsive Copolymer Micelles for PH-Dependent Drug Release. *Nanoscale* **2016**, *8* (3), 1437–1450.

(195) Amado, E.; Kressler, J. Reversible Complexation of Iminophenylboronates with Mono- and Dihydroxy Methacrylate Monomers and Their Polymerization at Low Temperature by Photoinduced ATRP in One Pot. *Macromolecules* **2016**, *49* (5), 1532–1544.

(196) Deng, R.; Derry, M. J.; Mable, C. J.; Ning, Y.; Armes, S. P. Using Dynamic Covalent Chemistry to Drive Morphological Transitions: Controlled Release of Encapsulated Nanoparticles from Block Copolymer Vesicles. *J. Am. Chem. Soc.* **2017**, *139* (22), 7616–7623.

(197) Blanazs, A.; Madsen, J.; Battaglia, G.; Ryan, A. J.; Armes, S. P. Mechanistic Insights for Block Copolymer Morphologies: How Do Worms Form Vesicles? *J. Am. Chem. Soc.* **2011**, *133* (41), 16581–16587.

(198) Blanazs, A.; Verber, R.; Mykhaylyk, O. O.; Ryan, A. J.; Heath, J. Z.; Douglas, C. W. I.; Armes, S. P. Sterilizable Gels from Thermoresponsive Block Copolymer Worms. *J. Am. Chem. Soc.* **2012**, *134* (23), 9741–9748.

(199) Canton, I.; Warren, N. J.; Chahal, A.; Amps, K.; Wood, A.; Weightman, R.; Wang, E.; Moore, H.; Armes, S. P. Mucin-Inspired Thermoresponsive Synthetic Hydrogels Induce Stasis in Human Pluripotent Stem Cells and Human Embryos. *ACS Cent. Sci.* **2016**, *2* (2), 65–74.

(200) Braskem. I'M GREEN™ POLYETHYLENE http://plasticoverde.braskem.com.br/site.aspx/Im-greenTM-Polyethylene (accessed Feb 5, 2019).

(201) Franssen, N. M. G.; Reek, J. N. H.; de Bruin, B. Synthesis of Functional 'Polyolefins': State of the Art and Remaining Challenges. *Chem. Soc. Rev.* **2013**, *42* (13), 5809–5832.

(202) Chung, T. C. (Mike). General Approaches in Functionalization of Polyolefins. In *Functionalization of Polyolefins*; Chung, T. C. (Mike), Ed.; Academic Press: London, 2002; pp 9–17.

(203) Nakamura, A.; Ito, S.; Nozaki, K. Coordination – Insertion Copolymerization of Fundamental Polar Vinyl Monomers. *Chem. Rev.* **2009**, *109* (11), 5215–5244.

(204) Chen, E. Y.-X. Coordination Polymerization of Polar Vinyl Monomers by Single-Site Metal Catalysts. *Chem. Rev.* **2009**, *109* (11), 5157–5214.

(205) Guo, L.; Liu, W.; Chen, C. Late Transition Metal Catalyzed α-Olefin Polymerization and Copolymerization with Polar Monomers. *Mater. Chem. Front.* **2017**, *1* (12), 2487–2494.

(206) Grau, E. Polymerization of Ethylene: From Free Radical Homopolymerization to Hybrid Radical / Catalytic Copolymerization, Université Claude Bernard - Lyon, 2010.

(207) Axelson, D. E.; Levy, G. C.; Mandelkern, L. A Quantitative Analysis of Low-Density (Branched) Polyethylenes by Carbon-13 Fourier Transform Nuclear Magnetic Resonance at 67.9 MHz. *Macromolecules* **1979**, *12* (1), 41–52.

(208) Moad, G.; Solomon, D. H. *The Chemistry of Free Radical Polymerization*, 1st ed.; Elsevier, 1995.

(209) Spalding, M. A.; Chatterjee, A. M. *Handbook of Industrial Polyethylene Technology*; 2016.

(210) Miao, C.; Hamad, W. Y. Cellulose Reinforced Polymer Composites and Nanocomposites: A Critical Review. *Cellulose* **2013**, *20* (5), 2221–2262.

(211) Gallos, A.; Paës, G.; Allais, F.; Beaugrand, J. Lignocellulosic Fibers: A Critical

Review of the Extrusion Process for Enhancement of the Properties of Natural Fiber Composites. *RSC Adv.* **2017**, *7* (55), 34638–34654.

(212) Dufresne, A. Cellulose Nanomaterial Reinforced Polymer Nanocomposites. *Curr. Opin. Colloid Interface Sci.* **2017**, *29*, 1–8.

(213) Abdul Khalil, H. P. S.; Bhat, A. H.; Ireana Yusra, A. F. Green Composites from Sustainable Cellulose Nanofibrils: A Review. *Carbohydr. Polym.* **2012**, *87* (2), 963–979.

(214) Rajinipriya, M.; Nagalakshmaiah, M.; Robert, M.; Elkoun, S. Importance of Agricultural and Industrial Waste in the Field of Nanocellulose and Recent Industrial Developments of Wood Based Nanocellulose: A Review. *ACS Sustain. Chem. Eng.* **2018**, *6* (3), 2807–2828.

(215) Prakash Menon, M.; Selvakumar, R.; Suresh Kumar, P.; Ramakrishna, S. Extraction and Modification of Cellulose Nanofibers Derived from Biomass for Environmental Application. *RSC Adv.* **2017**, *7* (68), 42750–42773.

(216) Jonoobi, M.; Oladi, R.; Davoudpour, Y.; Oksman, K.; Dufresne, A.; Hamzeh, Y.; Davoodi, R. Different Preparation Methods and Properties of Nanostructured Cellulose from Various Natural Resources and Residues: A Review. *Cellulose* **2015**, *22* (2), 935–969.

(217) Oksman, K.; Aitomäki, Y.; Mathew, A. P.; Siqueira, G.; Zhou, Q.; Butylina, S.; Tanpichai, S.; Zhou, X.; Hooshmand, S. Review of the Recent Developments in Cellulose Nanocomposite Processing. *Compos. Part A Appl. Sci. Manuf.* **2016**, *83*, 2–18.

(218) Li, X.; Tabil, L. G.; Panigrahi, S. Chemical Treatments of Natural Fiber for Use in Natural Fiber-Reinforced Composites: A Review. *J. Polym. Environ.* **2007**, *15* (1), 25–33.

(219) Bledzki, A. K.; Gassan, J. Composites Reinforced with Cellulose Based Fibres. *Prog. Polym. Sci.* **1999**, *24* (2), 221–274.

(220) Mutlu, H.; De Espinosa, L. M.; Meier, M. A. R. Acyclic Diene Metathesis: A Versatile Tool for the Construction of Defined Polymer Architectures. *Chem. Soc. Rev.* **2011**, *40* (3), 1404–1445.

(221) Opper, K. L.; Wagener, K. B. ADMET: Metathesis Polycondensation. *J. Polym. Sci. Part A Polym. Chem.* **2011**, *49* (4), 821–831.

(222) Buchmeiser, M. R. Ring-Opening Metathesis Polymerization. *Handbook of Ring-Opening Polymerization*. August 6, 2009.

(223) Leitgeb, A.; Wappel, J.; Slugovc, C. The ROMP Toolbox Upgraded. *Polymer (Guildf).* **2010**, *51* (14), 2927–2946.

(224) Kawahara, N.; Kojoh, S. I.; Matsuo, S.; Kaneko, H.; Matsugi, T.; Saito, J.; Kashiwa, N. Synthetic Method of Polyethylene-Poly(Methylmethacrylate) (PE-PMMA) Polymer Hybrid via Reversible Addition-Fragmentation Chain Transfer (RAFT) Polymerization with Functionalized Polyethylene. *Polym. Bull.* **2006**, *57* (6), 805–812.

(225) Bowden, N. B.; Dankova, M.; Wiyatno, W.; Hawker, C. J.; Waymouth, R. M. Synthesis of Polyethylene Graft Block Copolymers from Styrene, Butyl Acrylate, and Butadiene. *Macromolecules* **2002**, *35* (25), 9246–9248.

(226) Inoue, Y.; Matsugi, T.; Kashiwa, N.; Matyjaszewski, K. Graft Copolymers from Linear Polyethylene via Atom Transfer Radical Polymerization. *Macromolecules* **2004**, *37* (10), 3651–3658.

(227) Passaglia, E.; Coiai, S.; Augier, S. Control of Macromolecular Architecture during the Reactive Functionalization in the Melt of Olefin Polymers. *Prog. Polym. Sci.* **2009**, *34* (9), 911–947.

(228) Xanthos, M. Interfacial Agents for Multiphase Polymer Systems: Recent Advances. *Polym. Eng. Sci.* **1988**, *28* (21), 1392–1400.

(229) Priola, A.; Bongiovanni, R.; Gozzelino, G. Solvent Influence on the Radical Grafting of Maleic Anhydride on Low Density Polyethylene. *Eur. Polym. J.* **1994**, *30* (9), 1047–1050.

(230) Heinen, W.; Rosenmöller, C. H.; Wenzel, C. B.; de Groot, H. J. M.; Lugtenburg, J. 13C NMR Study of the Grafting of Maleic Anhydride onto Polyethene, Polypropene, and Ethene-Propene Copolymers. *Macromolecules* **1996**, *29* (4), 1151–1157.

(231) Yang, L.; Zhang, F.; Endo, T.; Hirotsu, T. Microstructure of Maleic Anhydride Grafted Polyethylene by High-Resolution Solution-State NMR and FTIR Spectroscopy. *Macromolecules* **2003**, *36* (13), 4709–4718.

(232) Rabnawaz, M.; Wyman, I.; Auras, R.; Cheng, S. A Roadmap towards Green Packaging: The Current Status and Future Outlook for Polyesters in the Packaging Industry. *Green Chem.* **2017**, *19* (20), 4737–4753.

(233) Poland, S. J.; Darensbourg, D. J. A Quest for Polycarbonates Provided: Via Sustainable Epoxide/CO2 Copolymerization Processes. *Green Chem.* **2017**, *19* (21), 4990–5011.

(234) Jin, L.; Zeng, H.; Ullah, A. Rapid Copolymerization of Canola Oil Derived Epoxide Monomers with Anhydrides and Carbon Dioxide (CO2). *Polym. Chem.* **2017**, *8* (41), 6431–6442.

(235) Seniha Güner, F.; Yağci, Y.; Tuncer Erciyes, A. Polymers from Triglyceride Oils. *Prog. Polym. Sci.* **2006**, *31* (7), 633–670.

(236) Blattmann, H.; Fleischer, M.; Bähr, M.; Mülhaupt, R. Isocyanate- and Phosgene-Free Routes to Polyfunctional Cyclic Carbonates and Green Polyurethanes by Fixation of Carbon Dioxide. *Macromol. Rapid Commun.* **2014**, *35* (14), 1238–1254.

(237) Ortmann, P.; Heckler, I.; Mecking, S. Physical Properties and Hydrolytic Degradability of Polyethylene-like Polyacetals and Polycarbonates. *Green Chem.* **2014**, *16* (4), 1816–1827.

(238) Dannecker, P. K.; Biermann, U.; von Czapiewski, M.; Metzger, J. O.; Meier, M. A. R. Renewable Polyethers via GaBr3-Catalyzed Reduction of Polyesters. *Angew. Chemie - Int. Ed.* **2018**, *57* (28), 8775–8779.

(239) Gandini, A.; Lacerda, T. M. Progress in Polymer Science From Monomers to Polymers from Renewable Resources : Recent Advances. *Prog. Polym. Sci.* **2015**, *48*, 1–39.

(240) Stößer, T.; Li, C.; Unruangsri, J.; Saini, P. K.; Sablong, R. J.; Meier, M. A. R.; Williams, C. K.; Koning, C. Bio-Derived Polymers for Coating Applications: Comparing Poly(Limonene Carbonate) and Poly(Cyclohexadiene Carbonate). *Polym. Chem.* **2017**, *8* (39), 6099–6105.

(241) Mathers, R. T. How Well Can Renewable Resources Mimic Commodity Monomers and Polymers? *J. Polym. Sci. Part A Polym. Chem.* **2012**, *50* (1), 1–15.

(242) Silvestre, A. J. D.; Gandini, A. Terpenes: Majors Sources, Properties and Applications. In *Monomers, Polymers and Composites from Renewable Resources*; Belgacem, M. N., Gandini, A., Eds.; Elsevier Ltd, 2008; pp 17–38.

(243) Nonoyama, Y.; Satoh, K.; Kamigaito, M. Renewable β-Methylstyrenes for Bio-Based Heat-Resistant Styrenic Copolymers: Radical Copolymerization Enhanced by Fluoroalcohol and Controlled/Living Copolymerization by RAFT. *Polym. Chem.* **2014**, *5* (9), 3182–3189.

(244) Yuan, L.; Wang, Z.; Trenor, N. M.; Tang, C. Preparation and Applications of Polymers with Pendant Fatty Chains from Plant Oils. In *Sustainable Polymers from Biomass*; Tang, C., Ryu, C. Y., Eds.; Wiley, 2017; pp 181–204.

(245) Holmberg, A. L.; Nguyen, N. A.; Karavolias, M. G.; Reno, K. H.; Wool, R. P.; Epps, T. H. Softwood Lignin-Based Methacrylate Polymers with Tunable Thermal and Viscoelastic Properties. *Macromolecules* **2016**, *49* (4), 1286–1295.

(246) Sarkar, P.; Bhowmick, A. K. Terpene Based Sustainable Methacrylate Copolymer Series by Emulsion Polymerization: Synthesis and Structure-Property Relationship. *J.*

Polym. Sci. Part A Polym. Chem. **2017**, *55* (16), 2639–2649.

(247) Obata, M.; Otobuchi, R.; Kuroyanagi, T.; Takahashi, M.; Hirohara, S. Synthesis of Amphiphilic Block Copolymer Consisting of Glycopolymer and Poly(l-Lactide) and Preparation of Sugar-Coated Polymer Aggregates. *J. Polym. Sci. Part A Polym. Chem.* **2017**, *55* (3), 395–403.

(248) Mutlu, H.; Ruiz, J.; Solleder, S. C.; Meier, M. A. R. TBD Catalysis with Dimethyl Carbonate: A Fruitful and Sustainable Alliance. *Green Chem.* **2012**, *14* (6), 1728–1735.

(249) Kreye, O.; Over, L. C.; Nitsche, T.; Lange, R. Z.; Meier, M. A. R. Organic Carbonates: Sustainable and Environmentally-Friendly Ethylation, Allylation, and Benzylation Reagents. *Tetrahedron* **2015**, *71* (2), 293–300.

(250) Over, L. C.; Meier, M. A. R. Sustainable Allylation of Organosolv Lignin with Diallyl Carbonate and Detailed Structural Characterization of Modified Lignin. *Green Chem.* **2015**, *18* (1), 197–207.

(251) Honda, M.; Tamura, M.; Nakagawa, Y.; Tomishige, K. Catalytic CO2 Conversion to Organic Carbonates with Alcohols in Combination with Dehydration System. *Catal. Sci. Technol.* **2014**, *4* (9), 2830–2845.

(252) Zhang, Z.; Liu, S.; Zhang, L.; Yin, S.; Yang, G.; Han, B. Driving Dimethyl Carbonate Synthesis from CO2 and Methanol and Production of Acetylene Simultaneously Using CaC2. *Chem. Commun.* **2018**, *54* (35), 4410–4412.

(253) Tshibalonza, N. N.; Monbaliu, J.-C. M. Revisiting the Deoxydehydration of Glycerol towards Allyl Alcohol under Continuous-Flow Conditions. *Green Chem.* **2017**, *19* (13), 3006–3013.

(254) Gorbunova, M. N. Copolymerization of N-Vinylpyrrolidone with New Allyl Monomers. *Russ. J. Appl. Chem.* **2010**, *83* (8), 1429–1434.

(255) Inoue, S.; Kumagai, T.; Tamezawa, H.; Aota, H.; Matsumoto, A.; Yokoyama, K.; Matoba, Y.; Shibano, M. Predominant Methyl Radical Initiation Preceded by B-Scission of Alkoxy Radicals in Allyl Polymerization with Organic Peroxide Initiators at Elevated Temperatures. *Polym. J.* **2010**, *42* (9), 716–721.

(256) Inoue, S.; Kumagai, T.; Tamezawa, H.; Aota, H.; Matsumoto, A.; Yokoyama, K.; Matoba, Y.; Shibano, M. Pursuit of Reinitiation Efficiency of Resonance-Stabilized Monomeric Allyl Radical Generated via “Degradative Monomer Chain Transfer” in Allyl Polymerization. *J. Polym. Sci. Part A Polym. Chem.* **2011**, *49* (1), 156–163.

(257) Alaaeddine, A.; Boschet, F.; Ameduri, B. Synthesis of Methallylic Monomers Bearing Ammonium Side-Groups and Their Radical Copolymerization with

Chlorotrifluoroethylene. *J. Polym. Sci. Part A Polym. Chem.* **2014**, *52* (12), 1721–1729.

(258) Yildirim, Y.; Balcan, M. Radiation Induced Copolymerization Reactivity of Different Allyl Monomers with Styrene. *Radiat. Phys. Chem.* **2012**, *81* (7), 840–845.

(259) Bartlett, P. D.; Altschul, R. The Polymerization of Allyl Compounds. I. Factors Governing the Acyl Peroxide-Induced Polymerization of Allyl Acetate, and the Fate of the Peroxide. *J. Am. Chem. Soc.* **1945**, *67* (5), 812–816.

(260) Bartlett, P. D.; Altschul, R. The Polymerization of Allyl Compounds. II. Preliminary Kinetic Study of the Peroxide-Induced Polymerization of Allyl Acetate. *J. Am. Chem. Soc.* **1951**, *67* (4), 816–822.

(261) Bartlett, P. D.; Nozaki, K. The Polymerization of Allyl Compounds. III. The Peroxide-Induced Copolymerization of Allyl Acetate with Maleic Anhydride. *J. Am. Chem. Soc.* **1946**, *68* (8), 1495–1504.

(262) Bartlett, P. D.; Tate, F. A. The Polymerization of Allyl Compounds. VI. The Polymerization of Allyl-1-D2 Acetate and the Mechanism of Its Chain Termination. *J. Am. Chem. Soc.* **1953**, *75* (1), 91–95.

(263) Bryaskova, R.; Willet, N.; Degée, P.; Dubois, P.; Jérôme, R.; Detrembleur, C. Copolymerization of Vinyl Acetate with 1-Octene and Ethylene by Cobalt-Mediated Radical Polymerization. *J. Polym. Sci. Part A Polym. Chem.* **2007**, *45* (1), 2532–2342.

(264) Bryaskova, R.; Willet, N.; Debuigne, A.; Jérôme, R.; Detrembleur, C. Synthesis of Poly(Vinyl Acetate)-b-Polystyrene and Poly(Vinyl Alcohol)-b-Polystyrene Copolymers by Cobalt-Mediated Radical Polymerization. *J. Polym. Sci. Part A-Polymer Chem.* **2007**, *45* (1), 81–89.

(265) Debuigne, A.; Michaux, C.; Jérôme, C.; Jérôme, R.; Poli, R.; Detrembleur, C. Cobalt-Mediated Radical Polymerization of Acrylonitrile: Kinetics Investigations and DFT Calculations. *Chem. - A Eur. J.* **2008**, *14* (25), 7623–7637.

(266) Banerjee, S.; Ladmiral, V.; Debuigne, A.; Detrembleur, C.; Poli, R.; Ameduri, B. M. Organometallic Mediated Radical Polymerization of Vinylidene Fluoride. *Angew. Chemie Int. Ed.* **2018**, *57* (11), 2934–2937.

(267) Dréan, M.; Guégan, P.; Detrembleur, C.; Jérôme, C.; Rieger, J.; Debuigne, A. Controlled Synthesis of Poly(Vinylamine)-Based Copolymers by Organometallic-Mediated Radical Polymerization. *Macromolecules* **2016**, *49* (13), 4817–4827.

(268) Demarteau, J.; Améduri, B.; Ladmiral, V.; Mees, M. A.; Hoogenboom, R.; Debuigne, A.; Detrembleur, C. Controlled Synthesis of Fluorinated Copolymers via Cobalt-

Mediated Radical Copolymerization of Perfluorohexylethylene and Vinyl Acetate. *Macromolecules* **2017**, *50* (10), 3750–3760.

(269) Scholten, P. B. V.; Demarteau, J.; Gennen, S.; De Winter, J.; Grignard, B.; Debuigne, A.; Meier, M. A. R.; Detrembleur, C. Merging CO2-Based Building Blocks with Cobalt-Mediated Radical Polymerization for the Synthesis of Functional Poly(Vinyl Alcohol)S. *Macromolecules* **2018**, *51* (9), 3379–3393.

(270) Cordeiro, C.; Petrocelli, F. P. Vinyl Acetate Polymers. *Kirk-Othmer Encyclopedia of Chemical Technology*; 2005.

(271) Detrembleur, C.; Stoilova, O.; Bryaskova, R.; Debuigne, A.; Mouithy-Mickalad, A.; Jérôme, R. Preparation of Well-Defined PVOH/C60 Nanohybrids by Cobalt-Mediated Radical Polymerization of Vinyl Acetate. *Macromol. Rapid Commun.* **2006**, *27* (7), 498–504.

(272) Ding, D.; Pan, X.; Zhang, Z.; Li, N.; Zhu, J.; Zhu, X. A Degradable Copolymer of 2-Methylene-1,3-Dioxepane and Vinyl Acetate by Photo-Induced Cobalt-Mediated Radical Polymerisation. *Polym. Chem.* **2016**, *7* (33), 5258–5264.

(273) Mohsenzadeh, A.; Zamani, A.; Taherzadeh, M. J. Bioethylene Production from Ethanol: A Review and Techno-Economical Evaluation. *ChemBioEng Rev.* **2017**, *4* (2), 75–91.

(274) Samanos, B.; Boutry, P.; Montarnal, R. The Mechanism of Vinyl Acetate Formation by Gas-Phase Catalytic Ethylene Acetoxidation. *J. Catal.* **1971**, *23* (1), 19–30.

(275) Sakakura, T.; Choi, J. C.; Yasuda, H. Transformation of Carbon Dioxide. *Chem. Rev.* **2007**, *107* (6), 2365–2387.

(276) Bell Jr., J. B.; Silver, L. N. J.; Currier, V. A.; Malkemus, J. D. Method for Preparing Glycerin Carbonate. US 2,915,529, 1959.

(277) Tale, N. V.; Jagtap, R. N.; Tathe, D. S. An Efficient Approach for the Synthesis of Thermoset Polyurethane Acrylate Polymer and Its Film Properties. *Des. Monomers Polym.* **2014**, *17* (2), 147–155.

(278) Sonnati, M. O.; Amigoni, S.; Taffin de Givenchy, E. P.; Darmanin, T.; Choulet, O.; Guittard, F. Glycerol Carbonate as a Versatile Building Block for Tomorrow: Synthesis, Reactivity, Properties and Applications. *Green Chem.* **2013**, *15* (2), 283–306.

(279) Rousseau, J.; Rousseau, C.; Lynikaite, B.; Šačkus, A.; de Leon, C.; Rollin, P.; Tatibouët, A. Tosylated Glycerol Carbonate, a Versatile Bis-Electrophile to Access New Functionalized Glycidol Derivatives. *Tetrahedron* **2009**, *65* (41), 8571–8581.

(280) Sheldon, R. A. Organic Synthesis; Past, Present and Future. *Chem. Ind.* **1992**, 903–906.

(281) Sheldon, R. A. The: E Factor 25 Years on: The Rise of Green Chemistry and Sustainability. *Green Chem.* **2017**, *19* (1), 18–43.

(282) Hill, D. J. T.; O'Donnell, H. J.; Perera, M. C. S.; Pomery, P. J. Polymerisation Kinetics of Allyl Monomers at Low Conversions. *Eur. Polym. J.* **1997**, *33* (8), 1353–1364.

(283) Tamezawa, H.; Kumagai, T.; Aota, H.; Matsumoto, A.; Totsuka, T.; Fujie, H. Peculiar Initiation Behavior of Azo-Initiators in Allyl Polymerization. *J. Polym. Sci. Part A Polym. Chem.* **2012**, *50* (13), 2732–2737.

(284) Inoue, S.; Tamezawa, H.; Aota, H.; Matsumoto, A.; Yokoyama, K.; Matoba, Y.; Shibano, M. Addition-Fragmentation Chain Transfer in Allyl Polymerization at Elevated Temperatures. *Macromolecules* **2011**, *44* (8), 3169–3173.

(285) Junkers, T.; Barner-Kowollik, C. The Role of Mid-Chain Radicals in Acrylate Free Radical Polymerization: Branching and Scission. *J. Polym. Sci. Part A Polym. Chem.* **2008**, *46* (23), 7585–7605.

(286) Brosse, J.-C.; Couvret, D. Monomères Acryliques à Fonction Carbonate Cyclique. *Makromol. Chem., Rapid Commun.* **1990**, *28* (11), 123–128.

(287) Kihara Takeshi, N. E. Synthesis and Reaction of Polymethacrylate Bearing Cyclic Carbonate Moieties in the Side Chain. *Makromol. Chemie* **1992**, *193* (6), 1481–1492.

(288) Holland, B. J.; Hay, J. N. The Thermal Degradation of Poly(Vinyl Acetate) Measured by Thermal Analysis-Fourier Transform Infrared Spectroscopy. *Polymer (Guildf).* **2002**, *43* (8), 2207–2211.

(289) Kreye, O.; Mutlu, H.; Meier, M. A. R. Sustainable Routes to Polyurethane Precursors. *Green Chem.* **2013**, *15* (6), 1431–1455.

(290) Poussard, L.; Mariage, J.; Grignard, B.; Detrembleur, C.; Jérôme, C.; Calberg, C.; Heinrichs, B.; Winter, J. De; Gerbaux, P.; Raquez, J.-M.; Bonnaud, L.; Dubois, P. Non-Isocyanate Polyurethanes from Carbonated Soybean Oil Using Monomeric or Oligomeric Diamines To Achieve Thermosets or Thermoplastics. *Macromolecules* **2016**, *49* (6), 2162–2171.

(291) Rokicki, G. Aliphatic Cyclic Carbonates and Spiroorthocarbonates as Monomers. *Prog. Polym. Sci.* **2000**, *25* (2), 259–342.

(292) Clements, J. H. Reactive Applications of Cyclic Alkylene Carbonates. *Ind. Eng. Chem. Res.* **2003**, *42* (4), 663–674.

(293) Alves, M.; Grignard, B.; Gennen, S.; Mereau, R.; Detrembleur, C.; Jerome, C.; Tassaing, T. Organocatalytic Promoted Coupling of Carbon Dioxide with Epoxides: A

Rational Investigation of the Cocatalytic Activity of Various Hydrogen Bond Donors. *Catal. Sci. Technol.* **2015**, *5* (9), 4636–4643.

(294) Martín, C.; Fiorani, G.; Kleij, A. W. Recent Advances in the Catalytic Preparation of Cyclic Organic Carbonates. *ACS Catal.* **2015**, *5* (2), 1353–1370.

(295) Büttner, H.; Longwitz, L.; Steinbauer, J.; Wulf, C.; Werner, T. Recent Developments in the Synthesis of Cyclic Carbonates from Epoxides and CO2. *Top. Curr. Chem.* **2017**, *375* (50), 1–56.

(296) Alves, M.; Grignard, B.; Mereau, R.; Jerome, C.; Tassaing, T.; Detrembleur, C. Organocatalyzed Coupling of Carbon Dioxide with Epoxides for the Synthesis of Cyclic Carbonates: Catalyst Design and Mechanistic Studies. *Catal. Sci. Technol.* **2017**, *7* (13), 2651–2684.

(297) Fiorani, G.; Guo, W.; Kleij, A. W. Sustainable Conversion of Carbon Dioxide: The Advent of Organocatalysis. *Green Chem.* **2015**, *17* (3), 1375–1389.

(298) Comerford, J. W.; Ingram, I. D. V.; North, M.; Wu, X. Sustainable Metal-Based Catalysts for the Synthesis of Cyclic Carbonates Containing Five-Membered Rings. *Green Chem.* **2015**, *17* (4), 1966–1987.

(299) North, M.; Pasquale, R.; Young, C. Synthesis of Cyclic Carbonates from Epoxides and CO2. *Green Chem.* **2010**, *12* (9), 1514.

(300) Cai, A.; Guo, W.; Martínez-Rodríguez, L.; Kleij, A. W. Palladium-Catalyzed Regio- and Enantioselective Synthesis of Allylic Amines Featuring Tetrasubstituted Tertiary Carbons. *J. Am. Chem. Soc.* **2016**, *138* (43), 14194–14197.

(301) Guo, W.; Martínez-Rodríguez, L.; Martin, E.; Escudero-Adán, E. C.; Kleij, A. W. Homogeneous Catalysis Highly Efficient Catalytic Formation of (Z)-1,4-But-2-Ene Diols Using Water as a Nucleophile. *Angew. Chemie - Int. Ed.* **2016**, *55* (37), 11037–11040.

(302) Guo, W.; Mart, L.; Kuniyil, R.; Martin, E.; Escudero-Adán, E. C.; Maseras, F.; Kleij, A. W. Stereoselective and Versatile Preparation of Tri- and Tetrasubstituted Allylic Amine Scaffolds under Mild Conditions. *J. Am. Chem. Soc.* **2016**, *138* (36), 11970–11978.

(303) Sopeña, S.; Laserna, V.; Guo, W.; Martin, E.; Escudero-Adán, E. C.; Kleij, A. W. Regioselective Organocatalytic Formation of Carbamates from Substituted Cyclic Carbonates. *Adv. Synth. Catal.* **2016**, *358* (14), 2172–2178.

(304) Besse, V.; Camara, F.; Voirin, C.; Auvergne, R.; Caillol, S.; Boutevin, B. Synthesis and Applications of Unsaturated Cyclocarbonates. *Polym. Chem.* **2013**, *4* (17), 4545–4561.

(305) Maisonneuve, L.; Lamarzelle, O.; Rix, E.; Grau, E.; Cramail, H. Isocyanate-Free Routes to Polyurethanes and Poly(Hydroxy Urethane)S. *Chem. Rev.* **2015**, *115* (22), 12407–12439.

(306) Gennen, S.; Grignard, B.; Tassaing, T.; Jerome, C.; Detrembleur, C. CO2-Sourced α-Alkylidene Cyclic Carbonates: A Step Forward in the Quest for Functional Regioregular Poly(Urethane)s and Poly(Carbonate)S. *Angew. Chemie Int. Ed.* **2017**, *56* (35), 10394 –10398.

(307) Grignard, B.; Thomassin, J.-M.; Gennen, S.; Poussard, L.; Bonnaud, L.; Raquez, J.-M.; Dubois, P.; Tran, M.-P.; Park, C. B.; Jerome, C.; Detrembleur, C. CO2 -Blown Microcellular Non-Isocyanate Polyurethane (NIPU) Foams: From Bio- and CO2 -Sourced Monomers to Potentially Thermal Insulating Materials. *Green Chem.* **2016**, *18* (7), 2206–2215.

(308) Hu, J.; Ma, J.; Zhu, Q.; Qian, Q.; Han, H.; Mei, Q.; Han, B. Zinc(II)-Catalyzed Reactions of Carbon Dioxide and Propargylic Alcohols to Carbonates at Room Temperature. *Green Chem.* **2015**, *18* (2), 382–385.

(309) Li, W.; Yang, N.; Lyu, Y. Theoretical Insights into the Catalytic Mechanism of N-Heterocyclic Olefins in Carboxylative Cyclization of Propargyl Alcohol with CO2. *J. Org. Chem.* **2016**, *81* (13), 5303–5313.

(310) Yuan, Y.; Xie, Y.; Zeng, C.; Song, D.; Chaemchuen, S.; Chen, C.; Verpoort, F. A Recyclable AgI/OAc $^{-}$ Catalytic System for the Efficient Synthesis of α-Alkylidene Cyclic Carbonates: Carbon Dioxide Conversion at Atmospheric Pressure. *Green Chem.* **2017**, *19* (13), 2936–2940.

(311) Boyaval, A.; Méreau, R.; Grignard, B.; Detrembleur, C.; Jerome, C.; Tassaing, T. Organocatalytic Coupling of CO2 with a Propargylic Alcohol: A Comprehensive Mechanistic Study. *ChemSusChem* **2017**, *10* (6), 1241–1248.

(312) Méreau, R.; Grignard, B.; Boyaval, A.; Detrembleur, C.; Jerome, C.; Tassaing, T. Tetrabutyl Ammonium Salts: Cheap Catalysts for the Facile and Selective Synthesis of α-Alkylidene Cyclic Carbonates from CO2 and Alkynol. *ChemCatChem* **2018**, *10*, 956–960.

(313) Cho, I.; Lee, T. Radical Polymerization of 4-Methylene-l,3-Dioxolan-2-One and Its Hydrolyzed Water-Soluble Polymer. *Macromol. Rapid Commun.* **1989**, *10*, 453–456.

(314) Ochiai, B.; Sano, Y.; Endo, T. Synthesis and Crosslinking of Oligo(Carbonate-Ketone) Obtained by Radical Polymerization of 4-Methylene-5,5-Dimethyl-1,3-Dioxolan-2-One. *J. Netw. Polym. Japan* **2005**, *26* (3), 132–137.

(315) Jana, S.; Yu, H.; Parthiban, A.; Chai, C. L. L. Controlled Synthesis and Functionalization of PEGylated Methacrylates Bearing Cyclic Carbonate Pendant Groups. *J. Polym. Sci. Part A Polym. Chem.* **2010**, *48* (7), 1622–1632.

(316) Palaskar, D. V.; Sane, P. S.; Wadgaonkar, P. P. A New ATRP Initiator for Synthesis of Cyclic Carbonate-Terminated Poly(Methyl Methacrylate). *React. Funct. Polym.* **2010**, *70* (12), 931–937.

(317) Hallensleben, M. L.; Fuss, R.; Mummy, F. Polyvinyl Compounds, Others. *Ullmann's Encyclopedia of Industrial Chemistry*; 2015; pp 1–23.

(318) Fink, J. K. Poly(Vinyl Alcohol). In *Handbook of Engineering and Specialty Thermoplastics: Water Soluble Polymers*; 2011; Vol. 2, pp 39–68.

(319) Ben Halima, N. Poly(Vinyl Alcohol): Review of Its Promising Applications and Insights into Biodegradation. *RSC Adv.* **2016**, *6* (46), 39823–39832.

(320) Moulay, S. Review: Poly(Vinyl Alcohol) Functionalizations and Applications. *Polym. - Plast. Technol. Eng.* **2015**, *54* (12), 1289–1319.

(321) Maria, S.; Kaneyoshi, H.; Matyjaszewski, K.; Poli, R. Effect of Electron Donors on the Radical Polymerization of Vinyl Acetate Mediated by [Co(Acac)2]: Degenerative Transfer versus Reversible Homolytic Cleavage of an Organocobalt(III) Complex. *Chem. - A Eur. J.* **2007**, *13* (9), 2480–2492.

(322) Ting, J. M.; Navale, T. S.; Bates, F. S.; Reineke, T. M. Precise Compositional Control and Systematic Preparation of Multimonomeric Statistical Copolymers. *ACS Macro Lett.* **2013**, *2* (9), 770–774.

(323) Wamsley, A.; Jasti, B.; Phiasivongsa, P.; Li, X. Synthesis of Random Terpolymers and Determination of Reactivity Ratios of N-Carboxyanhydrides of Leucine , β-Benzyl Aspartate , and Valine. *J. Polym. Sci. Part A Polym. Chem.* **2004**, *42* (2), 317–325.

(324) Kelen, T.; Tüdos, F. Analysis of the Linear Methods for Determining Copolymerization Reactivity Ratios . I . A New Improved Linear Graphic Method. *J. Macromol. Sci. Part A - Chem.* **1957**, *9* (1), 1–27.

(325) Park, S.; Yoon, H. Acid-Catalyzed Hydrolysis Reaction of Poly(Vinyl Acetate). *Polym.* **2005**, *29* (3), 304–307.

(326) Debuigne, A.; Caille, J. R.; Willet, N.; Jérôme, R. Synthesis of Poly(Vinyl Acetate) and Poly(Vinyl Alcohol) Containing Block Copolymers by Combination of Cobalt-Mediated Radical Polymerization and ATRP. *Macromolecules* **2005**, *38* (23), 9488–9496.

(327) Hassan, C. M.; Peppas, N. a. Structure and Applications of Poly (Vinyl Alcohol)

Hydrogels Produced by Conventional Crosslinking or by Freezing/Thawing Methods. *Adv. Polym. Sci.* **2000**, *153*, 37–65.

(328) Arai, K.; Okuzono, M.; Shikata, T. Reason for the High Solubility of Chemically Modified Poly(Vinyl Alcohol)s in Aqueous Solution. *Macromolecules* **2015**, *48* (5), 1573–1578.

(329) Debuigne, A.; Willet, N.; Jérôme, R.; Detrembleur, C. Amphiphilic Poly (Vinyl Acetate)-b-Poly(N-Vinylpyrrolidone) and Novel Double Hydrophilic Poly(Vinyl Alcohol)-b-Poly(N-Vinylpyrrolidone) Block Copolymers Prepared by Cobalt-Mediated Radical Polymerization. *Macromolecules* **2007**, *40* (20), 7111–7118.

(330) Bernard, J.; Favier, A.; Zhang, L.; Nilasaroya, A.; Davis, T. P.; Barner-Kowollik, C.; Stenzel, M. H. Poly(Vinyl Ester) Star Polymers via Xanthate-Mediated Living Radical Polymerization : From Poly(Vinyl Alcohol) to Glycopolymer Stars. *Macromolecules* **2005**, *38* (13), 5475–5484.

(331) Boffa, L. S.; Novak, B. M. Copolymerization of Polar Monomers with Olefins Using Transition-Metal Complexes. *Chem. Rev.* **2000**, *100* (4), 1479–1493.

(332) Sen, A.; Borkar, S. Perspective on Metal-Mediated Polar Monomer/Alkene Copolymerization. *J. Organomet. Chem.* **2007**, *692* (15), 3291–3299.

(333) Hu, J.; Ma, J.; Zhu, Q.; Qian, Q.; Han, H.; Mei, Q.; Han, B. Zinc(II)-Catalyzed Reactions of Carbon Dioxide and Propargylic Alcohols to Carbonates at Room Temperature. *Green Chem.* **2016**, *18* (2), 382–385.

(334) Roedel, J. M. The Molecular Structure of Polyethylene. I. Chain Branching in Polyethylene during Polymerization. *J. Am. Chem. Soc.* **1953**, *75* (24), 6110–6112.

(335) Matsumoto, A. Polymerization of Multiallyl Monomers. *Prog. Polym. Sci.* **2001**, *26* (2), 189–257.

(336) Grau, E.; Broyer, J. P.; Boisson, C.; Spitz, R.; Monteil, V. Unusual Activation by Solvent of the Ethylene Free Radical Polymerization. *Polym. Chem.* **2011**, *2* (10), 2328–2333.

(337) Randall, J. C.; Ruff, C. J.; Kelchtermans, M. 13C NMR Microstructure Determinations of Low-Density Polyethylene Homopolymers and Copolymers. *Recl. des Trav. Chim. des Pays-Bas* **1991**, *110* (12), 543–552.

(338) Aggarwal, S. L.; Sweeting, O. J. Polyethylene: Preparation, Structure, and Properties. *Chem. Rev.* **1957**, *57* (4), 665–742.

(339) Usami, T.; Takayama, S. Fine-Branching Structure in High-Pressure, Low-Density Polyethylenes by 50.10-MHz 13C NMR Analysis. *Macromolecules* **1984**, *17* (9),

1756–1761.

(340) Na, Y.; Dai, S.; Chen, C. Direct Synthesis of Polar-Functionalized Linear Low-Density Polyethylene (LLDPE) and Low-Density Polyethylene (LDPE). *Macromolecules* **2018**, *51* (11), 4040–4048.

(341) Yasuda, H.; Nakano, R.; Ito, S.; Nozaki, K. Palladium/IzQO-Catalyzed Coordination − Insertion Copolymerization of Ethylene and 1,1-Disubstituted Ethylenes Bearing a Polar Functional Group. *J. Am. Chem. Soc.* **2018**, *140* (5), 1876–1883.

(342) Takeuchi, D.; Iwasawa, T.; Osakada, K. Double-Decker-Type Dipalladium Catalysts for Copolymerization of Ethylene with Acrylic Anhydride. *Macromolecules* **2018**, *51* (14), 5048–5054.

(343) Jian, Z.; Mecking, S. Insertion Homo- and Copolymerization of Diallyl Ether. *Angew. Chemie - Int. Ed.* **2015**, *54* (52), 15845–15849.

(344) Minoura, Y.; Ueda, M.; Mizunuma, S.; Oba, M. The Reaction of Polypropylene with Maleic Anhydride. *J. Appl. Polym. Sci.* **1969**, *13* (8), 1625–1640.

(345) Ho, R. M.; Su, A. C.; Chen, S. I. Functionalization of Polypropylene via Melt Mixing. *Polymer (Guildf).* **1993**, *34* (15), 3264–3269.

(346) Coutinho, F. M. B.; Ferreira, M. I. P. Optimization of Reaction Conditions of Bulk Functionalization of EPDM Rubbers with Maleic Anhydride. **1994**, *30* (8), 911–918.

(347) Li, C.; Zhang, Y.; Zhang, Y. Melt Grafting of Maleic Anhydride onto Low-Density Polyethylene/Polypropylene Blends. *Polym. Test.* **2003**, *22* (2), 191–195.

(348) Na, B.; Zhang, Q.; Fu, Q.; Zhang, G.; Shen, K. Super Polyolefin Blends Achieved via Dynamic Packing Injection Molding: The Morphology and Mechanial Properties of HDPE/EVA Blends. *Polymer (Guildf).* **2002**, *43* (26), 7367–7376.

(349) Haque, M. M. U.; Pracella, M. Reactive Compatibilization of Composites of Ethylene-Vinyl Acetate Copolymers with Cellulose Fibres. *Compos. Part A Appl. Sci. Manuf.* **2010**, *41* (10), 1545–1550.

(350) Morais, J. A. De; Gadioli, R.; De Paoli, M.-A.; Paoli, M. De. Curaua Fiber Reinforced High-Density Polyethylene Composites: Effect of Impact Modifier and Fiber Loading. *Polímeros* **2016**, *26* (2), 115–122.

(351) Sakakibara, K.; Moriki, Y.; Yano, H.; Tsujii, Y. Strategy for the Improvement of the Mechanical Properties of Cellulose Nanofiber-Reinforced High-Density Polyethylene Nanocomposites Using Diblock Copolymer Dispersants. *ACS Appl. Mater. Interfaces* **2017**, *9* (50), 44079–44087.

(352) Demarteau, J. Organocobalt Complexes as Sources of Radicals for Macromolecular

Engineering Based on Ethylene or α-Olefins, Université de Liège, 2018.

(353) Kermagoret, A.; Chau, N. D. Q.; Grignard, B.; Cordella, D.; Debuigne, A.; Jérôme, C.; Detrembleur, C. Cobalt-Mediated Radical Polymerization of Vinyl Acetate and Acrylonitrile in Supercritical Carbon Dioxide. *Macromol. Rapid Commun.* **2016**, *37* (6), 539–544.

(354) Kontturi, E.; Laaksonen, P.; Linder, M. B.; Nonappa; Gröschel, A. H.; Rojas, O. J.; Ikkala, O. Advanced Materials through Assembly of Nanocelluloses. *Advanced Materials*. 2018.

(355) Lee, K. Y.; Aitomäki, Y.; Berglund, L. A.; Oksman, K.; Bismarck, A. On the Use of Nanocellulose as Reinforcement in Polymer Matrix Composites. *Composites Science and Technology*. Elsevier Ltd 2014, pp 15–27.

(356) Azouz, K. Ben; Ramires, E. C.; Van Den Fonteyne, W.; El Kissi, N.; Dufresne, A. Simple Method for the Melt Extrusion of a Cellulose Nanocrystal Reinforced Hydrophobic Polymer. *ACS Macro Lett.* **2012**, *1* (1), 236–240.

(357) Khoshkava, V.; Kamal, M. R. Effect of Drying Conditions on Cellulose Nanocrystal (CNC) Agglomerate Porosity and Dispersibility in Polymer Nanocomposites. *Powder Technol.* **2014**, *261*, 288–298.

(358) Peng, Y.; Nair, S. S.; Chen, H.; Yan, N.; Cao, J. Effects of Lignin Content on Mechanical and Thermal Properties of Polypropylene Composites Reinforced with Micro Particles of Spray Dried Cellulose Nanofibrils. *ACS Sustain. Chem. Eng.* **2018**, *6* (8), 11078–11086.

(359) Oksman, K.; Mathew, A. P.; Bondeson, D.; Kvien, I. Manufacturing Process of Cellulose Whiskers/Polylactic Acid Nanocomposites. *Compos. Sci. Technol.* **2006**, *66* (15), 2776–2784.

(360) Nimz, H. H.; Casten, R. Chemical Processing of Lignocellulosics. *Holz als Roh- und Werkst.* **1986**, *44* (6), 207–212.

(361) Eichhorn, S. J.; Dufresne, A.; Aranguren, M.; Marcovich, N. E.; Capadona, J. R.; Rowan, S. J.; Weder, C.; Thielemans, W.; Roman, M.; Renneckar, S.; Gindl, W.; Veigel, S.; Keckes, J.; Yano, H.; Abe, K.; Nogi, M.; Nakagaito, A. N.; Mangalam, A.; Simonsen, J.; Benight, A. S.; Bismarck, A.; Berglund, L. A.; Peijs, T. *Review: Current International Research into Cellulose Nanofibres and Nanocomposites*; 2010; Vol. 45.

(362) Faruk, O.; Bledzki, A. K.; Fink, H. P.; Sain, M. Biocomposites Reinforced with Natural Fibers: 2000-2010. *Prog. Polym. Sci.* **2012**, *37* (11), 1552–1596.

(363) Yano, H.; Omura, H.; Honma, Y.; Okumura, H.; Sano, H.; Nakatsubo, F. Designing

Cellulose Nanofiber Surface for High Density Polyethylene Reinforcement. *Cellulose* **2018**, *25* (6), 3351–3362.

(364) Kaynak, B.; Spoerk, M.; Shirole, A.; Ziegler, W.; Sapkota, J. Polypropylene/Cellulose Composites for Material Extrusion Additive Manufacturing. *Macromol. Mater. Eng.* **2018**, *303* (5), 1–8.

(365) Oliveira De Castro, D.; Frollini, E.; Ruvolo-Filho, A.; Dufresne, A. "Green Polyethylene" and Curauá Cellulose Nanocrystal Based Nanocomposites: Effect of Vegetable Oils as Coupling Agent and Processing Technique. *J. Polym. Sci. Part B Polym. Phys.* **2015**, *53* (14), 1010–1019.

(366) Pracella, M.; Haque, M. M. U.; Alvarez, V. Functionalization, Compatibilization and Properties of Polyolefin Composites with Natural Fibers. *Polymers (Basel).* **2010**, *2* (4), 554–574.

(367) Singh, A. A.; Palsule, S. Coconut Fiber Reinforced Chemically Functionalized High-Density Polyethylene (CNF/CF-HDPE) Composites by Palsule Process. *J. Compos. Mater.* **2014**, *48* (29), 3673–3684.

(368) Prasad, N.; Agarwal, V. K.; Sinha, S. Banana Fiber Reinforced Low-Density Polyethylene Composites: Effect of Chemical Treatment and Compatibilizer Addition. *Iran. Polym. J.* **2016**, *25* (3), 229–241.

(369) Alidadi-Shamsabadi, M.; Behzad, T.; Bagheri, R.; Nari-Nasrabadi, B. Preparation and Characterization of Low-Density Polyethylene Thermoplastic Starch Composites Reinforced by Cellulose Nanofibers. *Polym. Compos.* **2015**, *36* (12), 2309–2316.

(370) Sdrobi, A.; Darie, R. N.; Totolin, M.; Cazacu, G.; Vasile, C. Low Density Polyethylene Composites Containing Cellulose Pulp Fibers. *Compos. Part B Eng.* **2012**, *43* (4), 1873–1880.

(371) Söyler, Z.; Meier, M. A. R. Catalytic Transesterification of Starch with Plant Oils : A Sustainable and Efficient Route to Fatty Acid Starch Esters. *ChemSusChem* **2016**, *10* (1), 182–188.

(372) Freire, C. S. R.; Silvestre, A. J. D.; Neto, C. P.; Gandini, A.; Martin, L.; Mondragon, I. Composites Based on Acylated Cellulose Fibers and Low-Density Polyethylene: Effect of the Fiber Content, Degree of Substitution and Fatty Acid Chain Length on Final Properties. *Compos. Sci. Technol.* **2008**, *68* (15–16), 3358–3364.

(373) Prinos, J.; Bikiaris, D.; Theologidis, S.; Panayiotou, C. Preparation and Characterization of LDPE/Starch Blends Containing Ethylene/Vinyl Acetate Copolymer as Compatibilizer. *Polym. Eng. Sci.* **1998**, *38* (6), 954–964.

(374) Basu, D.; Datta, C.; Banerjee, A. Biodegradability, Mechanical Properties, Melt Flow Index, and Morphology of Polypropylene/Amylose/Amylose-Ester Blends. *J. Appl. Polym. Sci.* **2002**, *85* (7), 1434–1442.

(375) Tanrattanakul, V.; Panwiriyarat, W. Compatibilization of Low-Density Polyethylene/Cassava Starch Blends by Potassium Persulfate and Benzoyl Peroxide. *J. Appl. Polym. Sci.* **2009**, *114* (2), 742–753.

(376) Sailaja, R. R. N. Mechanical Properties of Esterified Tapioca Starch-LDPE Blends Using LDPE-Co-Glycidyl Methacrylate as Compatibilizer. *Polym. Int.* **2005**, *54* (2), 286–296.

(377) Kontopoulou, M. *Applied Polymer Rheology: Polymeric Fluids with Industrial Applications*; Kontopoulou, M., Ed.; 2012.

(378) Goodwin, J. W.; Hughes, R. W. *Rheology for Chemists An Introduction*; The Royal Society of Chemistry: Cambridge, UK, 2000.

(379) Wunderlich, B. *Thermal Analysis*; Elsevier Ltd, 1990.

(380) Meier, M. A. R.; Schubert, U. S. Evaluation of a New Multiple-Layer Spotting Technique for Matrix-Assisted Laser Desorption / Ionization Time-of-Flight Mass Spectrometry of Synthetic Polymers. *Rapid Commun. Mass Spectrom.* **2003**, *17* (7), 713–716.

(381) Skeist, I. Copolymerization: The Composition Distribution Curve. *J. Am. Chem. Soc.* **1946**, *68* (9), 1781–1784.

12 Appendix

12.1. Abbreviations

^{13}C NMR - ^{13}Carbon Nuclear Magnetic Resonance

^{1}H NMR - ^{1}Hydrogen Nuclear Magnetic Resonance

Å - Ångström

ACVA - 4,4′-Azobis(4-cyanovaleric acid)

ADMET - Acyclic Diene Metathesis

AFM - Atomic Force Microscopy

AIBN - Azobisisobutyronitrile

APBA - Aminophenylboronic Acid

ATRP - Atom Transfer Radical Polymerisation

b - block

BA - Butyl Acrylate

BB - (2-[*N*-Tert-Butyl-2,2-(Dimethylpropyl)aminooxy]propionic Acid, BlocBuilder

NHS-BB - 2-Methyl-2-[*N*-Tert-Butyl-*N*-(1-Diethoxyphosphoryl-2,2-Dimethylpropyl)-Aminoxy]-*N*-Propionyloxysuccinimide, NHS-BlocBuilder

BCP - Block Copolymer

BDAT - *S,S*'-*Bis*(α,α'-Dimethyl-α''-Acetic acid) Trithiocarbonate

BEETC - *S*-1-Isobutoxyethyl *S'*-Ethyl Trithiocarbonate

Bipy - Bipyridine

C_6D_6 - Deuterated Benzene

CBTC - *n*-Butyl Cumyl Trithiocarbonate

CDB - Cumyl Dithiobenzoate

$CDCl_3$ - Deuterated Chloroform

CED - 2-Cyanoethyl Dithiobenzoate

CETC - *S*-Cumyl *S*'-Ethyl Trithiocarbonate

CH_2Cl_2 - Dichloromethane

$CHCl_3$ - Chloroform

CMMETC - *S*-2-Cyano-4-Methoxy-4-Methyl-2-Pentyl *S'*-Ethyl Trithiocarbonate

CMRP - Cobalt-Mediated Radical Polymerisation

co - costatistical

CO_2 - Carbon Dioxide

COSY - ^{1}Hydrogen Correlation Spectroscopy

CPADB - 4-Cyanopentanoic Acid Dithiobenzoate

CPBTC - *n*-Butyl 2-Cyano-2-Propyl Trithiocarbonate

CPDA - Cumyl Phenyl Dithioacetate

CPDB - 2-Cyano-2-Propyl Dithiobenzoate

CPETC - *S*-2-Cyano-2-Propyl-*S*'-Ethyl Trithiocarbonate

CTA - Chain Transfer Agent

DAA - Dehydroabietic Acrylate

DABA - Dehydroabietic Butyl Acrylate

DAC - Diallyl Carbonate

DAEA - Dehydroabietic Ethyl Acrylate

DFT - Density Functional Theory

DLS - Dynamic Light Scattering

DmAC - Dimethylallyl Carbonate

DMAEMA - 2-(Dimethylamino)ethyl Methacrylate

DMC - Dimethylcarbonate

DMF - Dimethylformamide

DMMDO - 4,4-Dimethyl-5-Methylene-1,3-Dioxolan-2-One

DMSO - Dimethylsulfoxide

DP - Degree of Polymerisation

DP_{total} - Degree of Polymerisation of All Monomers

DP_{DMMDO} - Degree of Polymerisation of the DMMDO Monomer

DP_{HU} - Degree of Polymerisation of the Hydroxy Urethane Monomer

DP_{VAc} - Degree of Polymerissation of the Vinyl Acetate Monomer

DP_{VOH} - Degree of Polymerisation of the Vinyl Alcohol Monomer

DSC - Differential Scanning Calorimetry

DT - Degenerative Transfer

E - Ethylene

EC - Ethyl Cellulose

EETP - Ethyl 2-[(Ethylthio)thiocarbonylthio]propionate

ESI-MS - Electron-Spray Ionisation Mass Spectrometry

EVA - Poly(Ethylene-*co*-Vinyl Acetate)

EVA-b-PE - Poly(Ethylene-*co*-Vinyl Acetate)-*b*-poly(Ethylene)

$FeBr_3$(IDipp) - Iron Bromide 1,3-Bis(2,6-Diisopropylphenyl)imidazol-2-Ylidene

FT-IR - Fourrier-Transfrom Infrared Spectroscopy

g	- graft
G'	- Storage Modulus
G"	- Loss Modulus
GC	- Gas Chromatography
GMA	- Glycerol Methacrylate
HDPE	- High-Density Polyethylene
HH	- Head-To-Head Addition
HSQC	- Heteronuclear Single-Quantum Correlation Spectroscopy
HT	- Head-To-Tail Addition
HU	- Hydroxy Urethane
ICP-OES	- Inductively Coupled Plasma Optical Emission Spectrometry
LDPE	- Low-Density Polyethylene
LLDPE	- Linear Low Density Polyethylene
LMA	- Lauryl Methacrylate
M1	- Allyl ((2-Oxo-1,3-Dioxolan-4-Yl)Methyl) Carbonate
M2	- 2-Methylallyl ((2-Oxo-1,3-Dioxolan-4-Yl)Methyl) Carbonate
M3	- 2-Oxo-1,3-Dioxolan-4-Yl)methyl Undec-10-Enoate
M4	- Methyl-10-Undecenoate
M5	- Allylmethyl Carbonate
mA	- Modified Amylose
MA	- Methyl Acrylate
MADIX	- Macromolecular Design by Interchange of Xanthate
MALDI-TOF	- Matrix-Assisted Laser Desorption/Ionisation Time of Flight Mass Spectroscopy
MBL	- α-Methylene-γ-Butyrolactone
Me_2BL	- γ,γ-Dimethyl-α-Methylene-γ-Butyrolactone
Me_6-TREN	- *Tris*[2-(Dimethylamino)ethyl]amine
MeBL	- γ-Methyl-α-Methylene-γ-Butyrolactone
MEDB	- 1-(Methoxycarbonyl)ethyl Dithiobenzoate
MeOH	- Methanol
MeOD	- Deuterated Methanol
MEPD	- 1-(Methoxycarbonyl)ethyl Phenyl Dithioacetate
MMA	- Methyl Methacrylate
mS	- Modified Starch

NMP - Nitroxide Mediated Radical Polymerisation

OMRP - Organometallic Mediated Radical Polymerisation

PCL - Polycaprolactone

PE - Polyethylene

PEG - poly(Ethylene Glycol)

PMDETA - N,N,N′,N″,N″-Pentamethyldiethylenetriamine

PMMA - Poly(Methyl Methacrylate)

PS - Polystyrene

RAFT - Reversible Addition Fragmentation

R-Co(acac)$_2$ - Preformed Alkylcobalt(III) Acetylacetonate Complex where the Alkyl is the Initiating Fragment of V-70

RDRP - Reversible Deactivation Radical Polymerisation

ROP - Ring-Opening Polymerisation

ROMP - Ring-Opening Metathesis Polymerisation

rROP - Radical Ring-Opening Polymerisation

RT - Reversible Termination

S - Starch

SAXS - Small Angle X-Ray Scattering

SBMA - Soybean-Oil Methacrylate

SEC - Size-Exclusion Chromatography

SEM - Scanning Electron Microscopy

SET-LRP - Single Electron Transfer-Living Radical Polymerisation

SOM1 - Soybean Oil Monomer 1

SOM2 - Soybean Oil Monomer 2

SoMA - Solketal Methacrylate

St-TIPNO - *N*-Tert-Butyl-*N*-(2-Methyl-1-Phenylpropyl)-*O*-(1-Phenylethyl)hydroxylamine

T - Temperature (°C)

t - Time

TAXOL® - Paclitaxel

TBD - 1,5,7-Triazabicyclo[4.4.0]dec-5-ene

TCB - Trichlorobenzene

TCE - Tetrachloroethane

$T_{d\,5\%}$ - Temperature at 5% Weight Loss

TEM - Transition Electron Microscopy

TEMPO - 2,2,6,6-Tetramethylpiperidin-1-yl)oxyl

TERP - Tellurium Radical Polymerisation

TFE - Trifluoroethanol

T_g - Glass Transition Temperature

TGA - Thermogravimetric Analysis

THF - Tetrahydrofuran

T_m - Melting Temperature

TTS - Time-Temperature Superposition

UV - Ultra-Violet Radiation

V-70 - 2,2'-Azobis(4-methoxy-2,4-dimethylvaleronitrile)

VAc - Vinyl Acetate

VBC - 4-Vinylbenzyl Chloride

VBO - Vinylbenzyl Oleate

VG - Vinyl Guaiacol

VOH - Vinyl Alcohol

γ - Strain Amplitude

ω - Excitation Frequency

12.2. List of Figures

Figure 1. The different steps of reversible deactivation radical polymerisations: a) initiation, and b) propagation, while the different termination modes which are suppressed during RDRP through the controlling agent are shown in c). 5

Figure 2. RDRP allows to control the molecular weight, functionality, and architecture of the polymers as well as the copolymer composition. 6

Figure 3. a) Polymerisation mechanism of β-pinene, b) homopolymerisable comonomers bearing activated double bonds used for the copolymerisation of β-pinene, c) various CTA agents tested for the copolymerisation of β-pinene with acrylonitrile and methyl acrylate. d) first-order kinetic plot and d) molecular weights and dispersity versus conversion plot for 10 mol% β-pinene feeds for its copolymerisation with acrylonitrile. e) Degradatative transfer of allylic hydrogen bearing monomers. Adapted with permission from *J. Polym. Sci. Part A Polym. Chem.* **2006**, *44* (8), 2376–2387. © 2006, John Wiley and Sons 18

Figure 4. a) Copolymerisation of β-pinene and maleic anhydride into a macroRAFT agent and subsequent chain extension using styrene to form poly(maleic anhydride-*co*-β-pinene-*block*-styrene) copolymers which were b) hydrolysed into poly(maleic acid- *co*-β-pinene-*block*-styrene) copolymers showing self-assembly in aqueous solution. Adapted with permission from *J. Polym. Sci. Part A Polym. Chem.*, **2015**, *53*, 1422-1429. © 2015, John Wiley and Sons 19

Figure 5. a) Copolymerisation of limonene and maleimide as performed by Satoh *et al.* The presence of a fluoroalcohol favours a sequenced addition of the monomers as verified by b) MALDI-TOF analyses. Adapted with permission from *J. Am. Chem. Soc.*, **2010**, *132*, 10003-10005. © 2010, American Chemical Society 20

Figure 6. a) Copolymerisation of myrcene into polymyrcene in the bulk with different monomer repeat units identified,[55] b) plot of molecular weight and dispersity versus conversion, and c) plot of conversion and pseudo first order monomer consumption versus time. Reprinted with permission from *Eur. Polym. J.*, **2015**, 73, 363-373. © 2015, Elsevier Ltd. 21

Figure 7. a) Nitroxide-mediated homopolymerisation of myrcene and copolymerisation of myrcene with styrene using BlocBuilder (BB) and NHS-functionalised BlocBuilder and b) a plot of T_g against poly(myrcene-*co*-styrene) composition for copolymers obtained by Marić *et al*.[57] Adapted with permission from *Macromolecules*, **2017**, *50*, 3101-3120. © 2017, American Chemical Society 23

Figure 8. a) Structure of pinocarvone and its synthesis from α-pinene, b) RAFT polymerisation of pinocarvone yielding a polymer with two possible repeating units, c) plot of molecular weight and dispersity versus conversion for different types of CTA tested as well the SEC curves for the obtained polymers, and d) the synthesis of thermoplastic elastomers from butylacrylate and pinocarvone using a difunctional RAFT agent with different phase transitions observed in AFM phase images depending on the block copolymer composition. Reprinted with permission from *Angew. Chemie - Int. Ed.* **2016**, *55* (4), 1372–1376. © 2015, John Wiley and Sons 25

Figure 9. a) Structures of the protected lysine-derived monomer, *N*-phenyl itaconimide, ROP initiator, and acyl halide used to functionalise the lysine block with ATRP initiators, and b) stress-strain curves of triblock copolymers containing different amount of *N*-phenyl itaconimide. Adapted with permission from *J. Polym. Sci. Part A Polym. Chem.* **2016**, *55* (2), 349–355. © 2016, John Wiley and Sons 29

Figure 10. a) Homopolymerisation of dibutyl and diphenyl itaconate using different CTAs and the evolution of molecular weights and dispersities as a function of time for of a) dibutyl itaconate, and b) diphenyl itaconate. Adapted with permission from *J. Polym. Sci. Part A Polym. Chem.* **2004**, *42* (10), 2432–2443. © 2004, John Wiley and Sons. c) Initialisation mechanism for RAFT polymerisations, adapted from Moad.[75] 31

Figure 11. RAFT polymerisations of a) *N*-phenyl and *N*-*p*-tolyl itaconimide at 50 °C in 1,4-dioxane using CDB, and b) dibutyl- and di-2-ethylhexyl itaconate at 20 °C in bulk using a bifunctional CPADB-derivative. c) Block copolymer architectures possible for either CTA and the microphase pattern of the block copolymers as observed by AFM. Adapted with permission from *Macromol. Rapid Commun.* **2014**, *35* (2), 161–167. © 2013, John Wiley and Sons 32

Figure 12. Miniemulsion polymerisation of styrene and MeMBL using a macroCTA agent.[84] a) Plot of molecular weight (M_n) and dispersity versus conversion and b) size exclusion chromatography (SEC) curves of emulsion copolymersiations of styrene and MeMBL at a styrene:MeMBL feed of 1:1. Adapted with permission from *Polym. (United Kingdom)* **2013**, *54* (7), 1779–1785. © 2013 Elsevier Ltd. 35

Figure 13. a) ATRP polymerisation of butyl acrylate (BA) and α-methylene-γ-butyrolactone (MBL) to form copolymers that b) have slightly improved mechanical properties (red and blue line) compared to conventional P(BA-*b*-MMA) block copolymers (green line). Reprinted with permission from *Polymer (Guildf).* **2009**, *50* (9), 2087–2094. © 2009, Elsevier Ltd. d) Multi-armed star copolymers based on the same monomers showed slightly improved

mechanical properties. Adapted with permission from *Polymer (Guildf).* **2010**, *51* (21), 4806–4813. © 2010, Elsevier Ltd. e) Synthesis of a polymer film initiated from a glass substrate to synthesise MBL polymer brushes. Reprinted with permission from *ACS Macro Lett.* **2012**, *1* (9), 1124–1127 © 2012, American Chemical Society 36

Figure 14. Structures of a) different β-methyl styrenes, b) ferulic acid and its transformation into vinylguaiacol. c) RAFT copolymerisation of β-methyl styrenes with methyl acrylate using a variety of different CTAs in a fluorinated alcohol. Adapted with permission from *Polym. Chem.* **2014**, *5* (9), 3182–3189. © 2014, Royal Society of Chemistry 39

Figure 15. a) Evolution of molecular weight and dispersity with conversion and b) the size exclusion chromatography (SEC) curves for the polymerisation of protected vinylguaiacol monomers with cumyl dithiobenzoate in toluene at 60 °C. b) Structures of poly(4-vinylguaiacol) and polyvinylcatechol obtained *via* the deprotection of protected vinylguaiacol polymers. Adapted with permission from *Macromolecules* **2017**, *50* (11), 4206–4216. © 2017, American Chemical Society 40

Figure 16. Photoinduced ATRP of furfural methacrylate and two other renewable monomers, soybean oil methacrylate and dehydroabietic ethyl methacrylate. Reprinted with permission from *Macromolecules* **2016**, *49* (20), 7709–7717. © 2016 American Chemical Society..... 42

Figure 17: Lignin-based homo- and copolymers prepared by RAFT polymerisation leading to self-assembled nanospheres. Reprinted with permission from *ACS Sustain. Chem. Eng.* **2014**, *2* (4), 569–573. © 2014, American Chemical Society 44

Figure 18: a) Synthesis of syringol methacrylate and its homo- and copolymerisation by RAFT with other guaiacol-derived monomers and b) the effect of the copolymer composition on the glass transition temperature (T_g) of the copolymer. Reprinted with permission from *ACS Macro Lett.* **2016**, *5* (5), 574–578. © 2016, American Chemical Society 44

Figure 19. Structures of poly(dimethoxyphenyl methacrylate)s prepared by RAFT polymerisation and the thermal properties and resistance to solvent of the polymers. Reprinted with permission from *ACS Macro Lett.* **2017**, *6* (8), 802–807. © 2017, American Chemical Society 45

Figure 20. Lignin-derived pressure sensitive adhesives obtained from biomass *via* a) depolymerisation, b) functionalisation and RAFT polymerisation, and c) fabrication. d) Peel test of the prepared adhesives compared with commercial adhesive tapes. Adapted from *ACS Cent. Sci.* **2018**, *4* (6), 701–708. © 2018, American Chemical Society..... 47

Figure 21. a) Copolymerisation of menthol acrylate in a fluorinated alcohol by ATRP, b) the increase of conversion with time and the pseudo-first order kinetic plot, and c) the size

exclusion chromatograph (SEC) traces for the prepared homopolymer at different conversions. Reprinted with permission from *Biomacromolecules* **2018**, *19* (4), 1256–1268. ©2018, American Chemical Society. 48
Figure 22. a) Linear first-order kinetic plot of the photo-induced ATRP polymerisations of dehydroabietic ethyl methacrylate (DAEMA), b) synthetic scheme for the block copolymer synthesis based on DAEMA and soybean-oil methacrylate (SBMA) and c) the size exclusion chromatography (SEC) curves of the macroninitiator and block copolymer. Reprinted with permission from *Macromolecules* **2016**, *49* (20), 7709–7717. © 2016, American Chemical Society 50
Figure 23. Block copolymers based on dehydroabietic ethyl acrylate (DAEA) and caprolactone (CL) synthesised *via* the combination of ROP and ATRP leading to partly degradable polymers. Reprinted with permission from *Macromolecules* **2010**, *43* (21), 8747–8754. © 2010, American Chemical Society 51
Figure 24. a) ATRP polymerisation of butyl acrylate (BA) and dehydroabietic ethyl methacrylate (DAEMA) to synthesise triblock copolymers with b) inferior mechanical properties compared to conventional methyl methacrylate (MMA)/BA triblock copolymers. Reprinted with permission from *ACS Sustain. Chem. Eng.* **2017**, *5* (12), 11470–11480. © 2017, American Chemical Society 53
Figure 25. a) Nanoparticles of a diblock copolymer based on poly(ethylene glycol) (yellow) and dehydroabietic ethyl methacrylate (blue) able to encapsulate an antitumor drug. b) Such drug-loaded nanoparticles show a higher antitumor activity compared to a commercial antitumor drug (TAXOL®). Reprinted with permission from *J. Mater. Chem. B* **2013**, *1* (17), 2324–2332. © 2013, Royal Society of Chemistry.[142] 54
Figure 26. a) Antimicrobial coatings prepared via surface-initiated ATRP of a cationic rosin-derived monomer leading to b) a reduction in the number of cells attaching to the surface and c) a reduction of the number of cells that survive on the surface. Adapted with permission from *Biomacromolecules* **2015**, *16* (10), 3336–3344. © 2015, American Chemical Society.. 55
Figure 27. a) "Grafting-from" approach of rosin acid-derived monomers onto lignin using ATRP and b) the linear evolution of the first order kinetic plot. Reprinted with permission from *J. Polym. Sci. Part A Polym. Chem.* **2011**, *49* (17), 3728–3738. ©2011, John Wiley and Sons 56
Figure 28. a) "Grafting-from" of rosin acid-derived polymers from ethyl cellulose and b) the atomic force microscopy image (AFM) of solution cast film of poly(ethyl cellulose-*g*-dehydroabietic ethyl acrylate) (P(EC-*g*-DAEA)). Reprinted with

permission from *Green Chem.* **2014**, *16* (4), 1854–1864. ©2014, Royal Society of Chemistry 57
Figure 29. a) "Grafting-from" cellulose of statistical copolymers of butyl acrylate (BA), lauryl methacrylate (LMA) and dehydroabietic ethyl methacrylate (DAEMA) and b) the mechanical properties of the copolymers with different monomer feed ratios. Reprinted with permission from *Polym. Chem.* **2014**, *5* (9), 3170–3181. © 2014, Royal Society of Chemistry 58
Figure 30. Synthesis of microcrystalline cellulose bearing an ATRP initiator, and the grafting of cellulose with soybean oil-based methacrylate copolymers. Reprinted with permission from *Appl. Surf. Sci.* **2018**, *458* (July), 495–502. © 2018, Elsevier Ltd. 61
Figure 31. a) RAFT polymerisation of vinylbenzyl oleate (VBO) using a bifunctional CTA and b) the shift of molecular weights to higher molar masses during the polymerisation. c) Linear pseudo first order kinetic plot with the dispersity at different conversions. Adapted with permission from *Polym. Chem.* **2018**, *9* (21), 2880–2886. © 2018, Royal Society of Chemistry 62
Figure 32. a) Copolymerisation of tridecyl methacrylate and acrylonitrile using NMP and b) the semilogarithmic kinetic plots for the different reaction conditions showing deviations from linearity. Reprinted with permission from *J. Polym. Sci. Part A Polym. Chem.* **2018**, *56* (21), 2422–2436. © 2018, John Wiley and Sons. 63
Figure 33. Block copolymer of ethylene glycol, caprolactone, solketal methacrylate and 2-(dimethylamino)ethyl methacrylate which self-assembles into micelles and is able to incorporate Doxorubicine. b) The slightly enhanced antitumor activity of the drug-loaded micelles compared to pure Doxorubicine, micelles and saline buffer solution (PBS), and c) the fluorescent images of the tissue distribution of the drug, micelles and the drug-loaded micelles. Adapted with permission from *Nanoscale* **2016**, *8* (3), 1437–1450. © 2016, Royal Society of Chemistry 64
Figure 34. ATRP polymerisation of glycerol methacrylate (GMA) complexed with an iminophenylboronate ester (IPB) leading to a syndiotactic diol bearing polymer after decomplexation with catechol. Adapted with permission from *Macromolecules* **2016**, *49* (5), 1532–1544. © 2016, American Chemical Society. 65
Figure 35. a) GMA macroRAFT agent used for the synthesis of diblock copolymers with 2-hydroxypropyl methacrylate (HPMA) which self-assembled into a vesicle morphology in water as observed by transition electron microscopy (TEM) which d) can be changed into

worm-like structures upon the addition of aminophenylboronic acid (APBA). Adapted from Armes *et al.*[196] 66
Figure 36. a) Synthesis of allylic and olefinic-based polymers from renewable resources using cobalt-mediated radical polymerisation. For copolymerisations of allyl ((2-oxo-1,3-dioxolan-4-yl)methyl) carbonate (**M1**) and vinyl acetate, b) the evolution of molecular weights and dispersity with conversion and c) the first-order kinetic plot for 10 and 55 mol% **M1** monomer feeds are shown. Reprinted with permission from *ACS Sustain. Chem. Eng.* **2019**, *7* (2), 2751–2762. © 2019, American Chemical Society 68
Figure 37. The preparation of a variety of polymers from renewable resources discussed in Chapters 4-6 of this thesis with possible applications as compatibilisers for cellulose/LDPE composites. Chapters 7 and 8 describe the use of other types of compatibilisers for these composites. 78
Figure 38. E-factor calculation for a) diallyl carbonate (DAC) synthesis and b) the subsequent synthesis of **M1** used in this work 87
Figure 39. OMRP at 40 °C of **M1** and VAc: a) M_n and dispersity versus total monomer conversion plot, b) size-exclusion traces for **M1** feeds of 11 and 55 mol%, and c) first-order kinetic logarithm plot with linear fits. 90
Figure 40. Flowchart of the polymerisation and $scCO_2$ extraction procedure presented in this work, including the recovery of unused monomer and the recycling of CO_2. The latter is not performed in this work. 91
Figure 41. a) ^{1}H-NMR and b) ^{13}C-NMR spectrum of **P1** at 57% conversion containing 11 mol% **M1** (entry 1, Table 14) and c) ^{1}H-NMR and d) ^{13}C-NMR spectrum of **P4** at 47% conversion containing 5 mol% **M4** (entry 7, Table 1). NMR spectra taken in Acetone-d_6 on a 400 MHz spectrometer. 92
Figure 42. a) Differential scanning calorimetry (DSC) curves and b) thermal gravimetric analysis (TGA) curves for poly(vinyl acetate) and its copolymers with different renewable monomers at low monomer content, and c) a table summarising the different thermal properties of all prepared copolymers. 96
Figure 43. OMRPs at 40 °C of VAc and **DMMDO** at f^0_{DMMDO} ranging from 6 to 40 mol%: a) M_n and dispersity *vs.* total monomer conversion plot, b) first-order kinetic logarithmic plot with linear fits and c) size exclusion traces of kinetics with initial **DMMDO** feeds of 10, 25 and 40 mol% 106

Figure 44. a) ^{1}H-NMR spectrum and b) COSY spectrum of a copolymer at 43% conversion containing 16 mol% **DMMDO** prepared by OMRP at 40 °C (entry 5, Table 2). NMR spectra taken in $CDCl_3$ on a 400 MHz spectrometer. 108
Figure 45. a) ^{13}C-NMR spectrum and b) HSQC spectrum of a copolymer at 43% conversion containing 16 mol% **DMMDO** prepared by OMRP at 40 °C (entry 5, Table 2). NMR spectra taken in $CDCl_3$ on a 400 MHz spectrometer. 109
Figure 46. MALDI mass spectra recorded for a copolymer containing 16 mol% **DMMDO** (entry 9, Table 2) showing a) the global mass spectrum and b) a magnification between *m/z* 3350 and *m/z* 3600 and the comparison of the signals with a theoretical model. 110
Figure 47. ^{1}H-NMR spectra of copolymers prepared by OMRP at 40 °C with f^{0}_{DMMDO} = 0-0.4. NMR spectra taken in $CDCl_3$ on a 400 MHz spectrometer. 111
Figure 48. a) Kelen-Tüdos linearisation plot (r_{Vac} = 1.11 and r_{DMMDO} = 0.03) and b) Mayo-Lewis plot using experimental reactivity ratios. 113
Figure 49. Skeist's plot for a feed of 25 mol% **DMMDO** of instantaneous reaction composition (f_{inst}), instantaneous copolymer composition (F_{inst}) and cumulative copolymer composition (F_{cumul}) against overall monomer conversion using r_{DMMDO} = 0.03 and r_{VAc} = 1.11. The composition of several copolymers is also plotted (entry 5, Table 2; entry 12 and 13, Table 16). 114
Figure 50. a) Thermogravimetric analysis (TGA) curves b) differential scanning calorimetry (DSC) curves of P(VAc-*co*-**DMMDO**) of various compositions (entries 1 and 3-7, Table 2). 115
Figure 51. a) Acidic hydrolysis and methanolysis conditions of P(VAc_{182}-*co*-**DMMDO**$_{42}$) (19 mol% DMMDO; entry 10, Table 16) into the corresponding P(VOH_{182}-*co*-**DMMDO**$_{42}$) and P(VOH_{182}-*co*-BD_{42}), and b) FT-IR spectra of the various copolymers. 116
Figure 52. ^{1}H-NMR spectra of a) P(VAc_{182}-*co*-**DMMDO**$_{42}$) (19 mol% **DMMDO**; Table 16, Entry 10) in $CDCl_3$, b) P(VOH_{182}-*co*-**DMMDO**$_{42}$) in DMSO-d_6, c) P(VOH_{182}-*co*-BD_{42}) in DMSO-d_6 and d) P(VOH_{182}-*co*-BD_{42}) in D_2O. All spectra were recorded on a 400 MHz spectrometer. 118
Figure 53. Overlay of ^{13}C-NMR spectra of P(VAc_{182}-*co*-**DMMDO**$_{42}$) (19 mol% **DMMDO**; entry 10, Table 16) in $CDCl_3$, P(VOH_{182}-*co*-**DMMDO**$_{42}$) in DMSO-d_6 and P(VOH_{182}-*co*-BD_{42}) in D_2O. All spectra were recorded on a 400 MHz spectrometer. 119
Figure 54. Temperature of solubilisation of $PVOH_{134}$ and P(VOH_{108}-*co*-BD_{24}) in water at different concentrations (Table 19) 120

Figure 55. Post-polymerisation modification with n-butylamine of a) P(VOH-*co*-**DMMDO**) to give P(VOH-*co*-HU), a structure with one –OH unit per repeat unit which is inaccessible with b) PVOH where one less –OH unit is present after modification and c) FT-IR spectra of P(VAc_{149}-*co*-**DMMDO**$_{44}$), P(VOH_{149}-*co*-**DMMDO**$_{44}$), P(VOH_{149}-*co*-**DMMDO**$_{33}$-*co*-HU_{10}) functionalised using dry n-butylamine and P(VOH_{182}-*co*-BD_{42}) 121

Figure 56. ^{1}H-NMR spectra of a) P(VOH_{149}-*co*-**DMMDO**$_{44}$) recorded in DMSO-d_6, b) P(VOH_{149}-*co*-**DMMDO**$_{33}$-*co*-HU_{10}) functionalised using dry n-butylamine, recorded in DMSO-d_6, c) P(VOH_{149}-*co*-**DMMDO**$_{33}$-*co*-HU_{10}) functionalised using dry n-butylamine, recorded in MeOD-d_4 and d) P(VOH_{182}-*co*-BD_{42}) recorded in DMSO-d_6. All spectra are taken on a 400 MHz spectrometer. 122

Figure 57. a) Plot of number average molecular weight (M_n) and copolymer dispersity against conversion at different times for the copolymerisation of ethylene with **M1** or **DMMDO** using R-$Co(acac)_2$ at 40 °C and 50 bar in DMC, and b) the corresponding size exclusion chromatography (SEC) curves measured at 45 °C in THF 128

Figure 58. a) ^{1}H NMR spectrum, b) ^{13}C NMR spectrum, and c) inset of the ^{13}C NMR spectrum in the region around 20 ppm for P(**E**-*co*-**M1**) (entry 1, Table 3) taken in a 2:1 v/v mixture of tetrachloroethane (TCE):benzene (C_6D_6) on a 400 MHz spectrometer at 80 °C. 129

Figure 59. FT-IR spectra of P(E-*co*-**DMMDO**) synthesised at 10, 25, 50 and 500 bar using R-$Co(acac)_2$ (entries 3-6, Table 3). The characteristic C=O vibration of **DMMDO** are highlighted in green while –CH_2– vibrations characteristic of ethylene are highlighted in grey. 131

Figure 60. a) ^{1}H NMR spectra overlay of EVA synthesised at 10 and 500 bar, respectively, (entries 1 and 4, Table 4) and b) FT-IR spectra of EVA synthesised at 10, 25, 50 and 500 bar (entries 1-4, Table 4). In both images, the characteristic signals of vinyl acetate are highlighted in blue while those of ethylene are highlighted in red. The initiator fragment signal is also highlighted in grey for the NMR spectrum..... 138

Figure 61. a) HT-SEC curves of the macroinitiator EVA-$Co(acac)_2$ and the EVA_{50bar}-*b*-PE block copolymer after 4 and 24 hours of block copolymerisation, b) ^{1}H HT-NMR spectra of the macroinitiator EVA_{50bar}-$Co(acac)_2$ and the block copolymer EVA_{50bar}-*b*-PE after 24 hours, and c) FT-IR spectra of the macroinitiators and different block copolymers synthesised in this study. 140

Figure 62. Differential scanning calorimetry (DSC) curves and thermal properties of EVA-*b*-PE copolymers. 143

Figure 63. Young's moduli for pure LDPE (**C0EVA0**), LDPE with 5 wt% cellulose (**C5EVA0**) and samples with 5 wt% cellulose and 5 wt% EVA compatibiliser either synthesised at 50 (**C5EVA$_{50bar}$**) or 500 bar (**C0EVA$_{500bar}$**) of ethylene pressure. 145
Figure 64. Storage modulus $G'(\omega 1)$ as a function of angular frequency ($\omega 1$) at T_{ref} = 150 °C was plotted *via* TTS for pure LDPE, LDPE containing 10 wt% cellulose (**C10mA/S0**) and composites containing 10 wt% of a) modified amylose (mA) or non-modified amylose (A) and b) modified starch (mS) and non-modified starch (S). 154
Figure 65. Storage modulus $G'(\omega 1)$ as a function of angular frequency $\omega 1$ at T_{ref} = 150 °C as obtained *via* TTS for pure LDPE and for composites containing 10 wt% cellulose (C) with 5-15 wt% of a) modified amylose (mA) and b) modified starch (mS). 154
Figure 66. Storage modulus $G'(\omega 1)$ as a function of angular frequency $\omega 1$ at T_{ref} = 150 °C as obtained *via* TTS for pure LDPE and for composites containing 45 wt% cellulose (C) and 10 wt% of a) modified amylose(mA) and b) modified starch (mS). 155
Figure 67. Scanning electron microscopy (SEM) images of a) pure LDPE (**C0mA/mS0**), b) pure cellulose (**C100mA/mS0**), c) composite **C45mA/mS0**, d) composite **C45mA10**, and e) composite **C45mS10**. 157
Figure 68. Thermogravimetric (TGA) curves of composites using a) modified amylose and b) modified starch compatibilisers and their respective reference samples 158
Figure 69. Young moduli for composites with a) modified amylose and b) modified starch as compatibiliser and their respective reference samples 159
Figure 70. a) ^{1}H NMR spectrum and b) COSY spectrum of allyl ((2-oxo-1,3-dioxolan-4-yl)methyl) carbonate (**M1**) 175
Figure 71. a) ^{13}C NMR spectrum and b) HSQC spectrum of allyl ((2-oxo-1,3-dioxolan-4-yl)methyl) carbonate (**M1**) 176
Figure 72. a) ^{1}H NMR spectrum and b) COSY spectrum of 2-methylallyl ((2-oxo-1,3-dioxolan-4-yl)methyl) carbonate (**M2**) 177
Figure 73. a) ^{13}C NMR spectrum and b) HSQC spectrum of 2-methylallyl ((2-oxo-1,3-dioxolan-4-yl)methyl) carbonate (**M2**) 178
Figure 74. a) ^{1}H NMR spectrum and b) COSY spectrum of (2-oxo-1,3-dioxolan-4-yl)methyl undec-10-enoate (**M3**) 179
Figure 75. a) ^{13}C NMR spectrum and b) HSQC spectrum of (2-oxo-1,3-dioxolan-4-yl)methyl undec-10-enoate (**M3**) 180
Figure 76. a) ^{1}H NMR spectrum and b) ^{13}C NMR spectrum of methyl-10-undecenoate (**M4**) 181

Figure 77. a) ^{1}H NMR spectrum and b) COSY spectrum of allyl methyl carbonate (**M5**)... 182
Figure 78. a) ^{13}C NMR spectrum and b) HSQC spectrum of allyl methyl carbonate (**M5**) . 183
Figure 79. FT-IR spectra of **M1**-**M5** monomers synthesised in this publication..... 184
Figure 80. E-factor calculation for a) glycerol carbonate synthesis according to Bell *et al.*[276] and b) the subsequent synthesis of **M1** according to Tale *et al.*[277] 187
Figure 81. E-factor calculation for a) dimethylallyl carbonate (DmAC) synthesis and b) the subsequent synthesis of **M2** used in this work..... 188
Figure 82. E-factor calculation for a) undecenoyl chloride synthesis and b) the subsequent synthesis of **M3** according to Cramail *et al.*[165] Commercial glycerol carbonate was used in this synthesis. 189
Figure 83. E-factor calculation for a) **M4** and b) the subsequent synthesis of **M3** used in this work..... 190
Figure 84. OMRP at 40 °C of **M2** with VAc at 12 mol% **M2** feed: a) M_n and dispersity versus total monomer conversion plot, b) size-exclusion traces and c) first-order kinetic logarithm plot with linear fits. 197
Figure 85. OMRP at 40 °C of **M3** with VAc at 13 and 28 mol% **M3** feed: a) M_n and dispersity versus total monomer conversion plot, b) size-exclusion traces and c) first-order kinetic logarithm plot with linear fits. 198
Figure 86. OMRP at 40 °C of **M4** and VAc at 11 and 27 mol% **M4** feed: a) M_n and dispersity versus total monomer conversion plot, b) size-exclusion traces and c) first-order kinetic logarithm plot with linear fits. 199
Figure 87. OMRP at 40 °C of **M5** with VAc at 12 and 53 mol% feed **M5**: a) M_n and dispersity versus total monomer conversion plot, b) size-exclusion traces and c) first-order kinetic logarithm plot with linear fits. 200
Figure 88. Reactor set-up for the $scCO_2$ extraction of the prepared polymers..... 201
Figure 89. a) ^{1}H-NMR spectrum and b) COSY spectrum of a **P1** copolymer at 57% conversion containing 11 mol% **M1** (entry 1, Table 14) 202
Figure 90. a) ^{13}C-NMR spectrum and b) HSQC spectrum of a **P1** copolymer at 57% conversion containing 11 mol% **M1** (entry 1, Table 14) 203
Figure 91. a) ^{1}H-NMR spectrum and b) COSY spectrum of a **P2** copolymer at 31% conversion and containing 14 mol% **M2** (entry 4, Table 1) taken on a 400 MHz spectrometer in $CDCl_3$ 204

Figure 92. a) ^{13}C-NMR spectrum and b) HSQC spectrum of a **P2** copolymer at 31% conversion and containing 14 mol% **M2** (entry 4, Table 1) taken on a 400 MHz spectrometer in $CDCl_3$ 205
Figure 93. a) ^{1}H-NMR spectrum and b) COSY spectrum of a **P3** copolymer at 36% conversion containing 7 mol% **M3** (entry 5, Table 1) 206
Figure 94. a) ^{13}C-NMR spectrum and b) HSQC spectrum of a **P3** copolymer at 36% conversion containing 7 mol% **M3** (entry 5, Table 1) 207
Figure 95. a) ^{1}H-NMR spectrum and b) COSY spectrum of a **P4** copolymer at 47% conversion containing 5 mol% **M4** (entry 7, Table 1) 208
Figure 96. a) ^{13}C-NMR spectrum and b) HSQC spectrum of a **P4** copolymer at 47% conversion containing 5 mol% **M4** (entry 7, Table 1) 209
Figure 97. a) ^{1}H-NMR spectrum and b) COSY spectrum of a **P5** copolymer at 33% conversion containing 13 mol% of **M5** (entry 10, Table 1) 210
Figure 98. a) ^{13}C-NMR spectrum and b) HSQC spectrum of a **P5** copolymer at 33% conversion containing 13 mol% of **M5** (entry 10, Table 1) 211
Figure 99. Overlay of the FT-IR spectra of copolymers synthesised using OMRP at 40 °C at a feed of 0.9/0.1 VAc/Comonomer (entries 1, 3, 4, 6, and 9, Table 1) 212
Figure 100. Thermal gravimetric analysis (TGA) for poly(vinyl acetate) and its copolymers with different renewable monomers at high comonomer content. a) Weight versus temperature curve and b) the derivative weight against temperature curve. 212
Figure 101. FT-IR spectra of **DMMDO**, PVAc (Entry 1, Table 2), P(VAc-*co*-**DMMDO**) at 43% conversion containing 16 mol% **DMMDO** (Entry 5, Table 2) 222
Figure 102. a) ^{1}H-NMR spectrum and b) ^{13}C-NMR spectrum of a copolymer at 21% conversion containing 23 mol% **DMMDO** prepared by OMRP at 90 °C. NMR spectra taken in $CDCl_3$ on a 400 MHz spectrometer. 223
Figure 103. ^{1}H-NMR spectra of a) P(VAc_{182}-*co*-**DMMDO**$_{42}$) (Entry 10, Table 16) and b) P(VOH_{182}-*co*-**DMMDO**$_{42}$) recorded in $CDCl_3$ and DMSO-d_6, respectively, on a 400 MHz spectrometer.. 225
Figure 104. ^{13}C-NMR spectra of a) P(VOH_{149}-*co*-**DMMDO**$_{44}$), b) P(VOH_{149}-*co*-**DMMDO**$_{33}$-*co*-HU_{10}) functionalised using dry *n*-butylamine and c) P(VOH_{182}-*co*-BD_{42}); all spectra are recorded in DMSO-d_6 on a 400 MHz spectrometer. 226
Figure 105. a) COSY and b) HSQC spectra of P(VOH_{149}-*co*-**DMMDO**$_{33}$-*co*-HU_{10}) functionalised using dry *n*-butylamine; recorded in DMSO-d_6 on a 400 MHz spectrometer. 227

Figure 106. ^{1}H-NMR spectra of a) P(VAc$_{149}$-*co*-**DMMDO**$_{44}$) recorded in $CDCl_3$ b) P(VOH$_{149}$-*co*-**DMMDO**$_{44}$) recorded in DMSO-d_6 and c) P(VOH$_{149}$-*co*-**DMMDO**$_{33}$-*co*-HU$_{10}$) functionalised using dry *n*-butylamine, recorded in MeOD-d_4. All spectra recorded on a 400 MHz spectrometer. 228

Figure 107. ^{1}H-NMR spectra of a) P(VAc$_{149}$-*co*-**DMMDO**$_{44}$) recorded in $CDCl_3$, b) P(VOH$_{149}$-*co*-**DMMDO**$_{44}$) recorded in DMSO-d_6 and c) P(VOH$_{149}$-*co*-**DMMDO**$_{36}$-*co*-HU$_7$) functionalised using wet *n*-butylamine recorded in MeOD-d_4. All spectra are recorded on a 400 MHz spectrometer. 229

Figure 108. FT-IR spectra of P(VAc$_{149}$-*co*-**DMMDO**$_{44}$), P(VOH$_{149}$-*co*-**DMMDO**$_{44}$), P(VOH$_{149}$-*co*-**DMMDO**$_{36}$-*co*-HU$_7$) functionalised using wet *n*-butylamine and P(VOH$_{182}$-*co*-BD$_{42}$) 230

Figure 109. Reactor set-up for the $scCO_2$ extraction of the ethylene copolymers 232

Figure 110. Size exclusion chromatography (SEC) curves for the copolymerisation of ethylene with **DMMDO** in dichloromethane (DCM), dimethylcarbonate (DCM), and trichlorobenzene (TCB) using R-Co(acac)$_2$ at 40 °C. 233

Figure 111. COSY NMR spectrum of P(**E**-*co*-**M1**) (entry 3, Table 3). 235

Figure 112. HSQC NMR spectra of P(**E**-*co*-**M1**) (entry 3, Table 3). 236

Figure 113. a) ^{1}H NMR spectrum and b) ^{13}C NMR spectrum of P(**E**-*co*-**DMMDO**) (entry 5, Table 3). An inset of the region around 20 ppm where signals from branching would occur is also shown. 237

Figure 114. a) COSY NMR spectrum and b) HSQC NMR spectrum of P(**E**-*co*-**DMMDO**) (entry 5, Table 3). An inset of the HSQC spectrum is also shown. 238

Figure 115. FT-IR spectra of a) P(**E**-*co*-**M1**) copolymers both synthesised at 40 °C in 1.25 mL DMC using R-Co(acac)$_2$, and b) P(**E**-*co*-**DMMDO**) synthesised at 40 °C in 5 mL DMC using R-Co(acac)$_2$. 239

Figure 116. High temperature size-exclusion chromatography (HT-SEC) curves for P(**E**-*co*-**M1**) and P(**E**-*co*-**DMMDO**) copolymers synthesised at 40 °C in DMC (Table 3). HT-SEC analyses were performed in TCB at 140 °C using a polystyrene standard. 239

Figure 117. Differential scanning calorimetry (DSC) curves of a) P(**E**-*co*-**M1**) and b) P(**E**-*co*-**DMMDO**) synthesised using R-Co(acac)$_2$ at 40 °C at different ethylene pressures (Table 3). 240

Figure 118. FT-IR spectrum of cellulose obtained by the acetic acid extraction of wood chips clearly showing an absorption in the carbonyl region as a result of acetylation during extraction 243

Figure 119. SEM image of the obtained bulk cellulose showing fibres of length and width 244
Figure 120. Storage modulus G' as a function of the strain amplitude γ at 150 °C and ω_1 = 1 rad/s for the neat LDPE and the composite materials with cellulose (C), a) modified (mA) and non-modified amylose (A) compatibiliser and b) modified (mA) and non-modified starch (S) compatibiliser. 244
Figure 121. Time dependency of storage modulus G' at 150 °C and ω_1 = 1 rad/s in the linear viscoelastic regime for the neat LDPE and the composite materials. 244
Figure 122. Time dependency of storage modulus G' at 170 °C and ω_1 = 1 rad/s in the linear viscoelastic regime for the neat LDPE and the composite materials. 245
Figure 123. Differential scanning calorimetry of samples containing a) modified amylose and b) modified starch compatibiliser and their respective reference samples. 245

12.3. List of Schemes

Scheme 1. Different RDRP methods and their equilibrium between dormant and active species: a) atom transfer polymerisation (ATRP), b) reversible addition fragmentation (RAFT) polymerisation or macromolecular design by interchange of xanthate (MADIX), c) nitroxide-mediated radical polymerisation (NMP), d) organometallic-mediated radical polymerisation (OMRP), and e) organotellurium-, organostibine-, and organobismuthine-mediated radical polymerisation. 7
Scheme 2. Examples of a) more activated monomers (MAMs), b) less activated monomers (LAMs),[17,27] and c) the resonance stabilisation of the formed radical species as observed for MAMs while for LAMs no stabilisation is possible. d) Displays the two types of additions which can take place during radical polymerisations, Head-to-Tail and Head-to-Head. 9
Scheme 3. a) Preparation of the alkylcobalt complex R-Co(acac)$_2$ used in the experiments performed in this thesis, with b) reversible termination (RT) and c) degenerative transfer mechanisms that can occur for this complex. 11
Scheme 4. Active/dormant equilibria for the head-to-head (HH) and head-to-tail addition (HT) of vinyl acetate to a growing polymer chain using Co(acac)$_2$ as the controlling agent. The intramolecular chelation observed for the HT and HH dormant species stabilising these species is also shown. 12
Scheme 5. Active/dormant species equilibria for OMRP in the presence of ligands such as water, dimethyl sulfoxide (DMSO), and dimethylformamide (DMF). 13
Scheme 6. A selection of naturally occurring terpenoids with different degrees of unsaturation and number of oxygen atoms. 16

Scheme 7. a) Structure of itaconic acid and its transformation into b) disubstituted itaconates *via* esterifications[68] and c) into itaconic anhydride *via* dehydration[66] and d) subsequent aminolysis leading to itaconimides.[67] e) Structure of iron bromide 1,3-bis(2,6-diisopropylphenyl)imidazol-2-ylidene ($FeBr_3$(IDipp) catalyst for ATRP of phenylitaconimides.[69] 27

Scheme 8. a) Copolymerisation of *N*-phenyl itaconimide and methyl methacrylate using ATRP as reported by Deoghare *et al.*,[71] and b) a *N*-heterocyclic carbene-based iron catalyst used for the homopolymerisation of *N*-phenyl itaconimide.[69] 28

Scheme 9. Structures of a) poly(methoxyethyl acrylate-*co*-itaconic anhydride) prepared by RAFT polymerisation using CPDB and its aminolysed form, and b) the copolymer attached to a gold nanoparticle via its thiol chain end, bearing a protected amino acid residue on some of its itaconic anhydride repeat units. Adapted from Hvilsted *et al.*[76] 33

Scheme 10. Transformation of a) itaconic acid and b) levulinic acid into c) methylene butyrolactones, and d) the controlled radical polymerisation of these monomers into poly(α-methylene-γ-butyrolactone)s 34

Scheme 11. Block copolymer synthesis using a combination of ROP of menthide and ATRP of α-methylene-γ-butyrolactone (MBL) or γ-methyl-α-methylene-γ-butyrolactone (MeBL). Scheme adapted from Tolman and Hillmeyer *et al.*[88,89] 37

Scheme 12. Chemical structures of a) the three main repeating motifs found in the structure of lignin and b) derivatives of lignin, useful as platform chemicals and for monomer synthesis.43

Scheme 13. a) Structures of four different acid derivatives which can be obtained from rosin gum, and the synthesis of rosin-derived monomers b) DAEA, DABA, DAEMA and c) DAA. Adapted from Tang *et al.*[135] 49

Scheme 14. Chemical structure of a) triglycerides and b) the molecules obtained after esterification of triglycerides, glycerol and a variety of different fatty acids. The type of fatty acid depends on the origin of the triglyceride. 59

Scheme 15. Transformation of fatty acids – here with the example of oleic acid - into different monomers for RDRP by either a) modification of the double bond or b) modification of the carboxylic acid. Adapted from Calliol *et al.*[177] 60

Scheme 16. Polymerisation techniques capable of copolymerising ethylene with polar monomers. 71

Scheme 17. a) Structures of polyethylene and cellulose and b) functionalisations of polyethylene leading to randomly, chain-end or segmented polar units in the polymer chain. Adapted from de Bruin *et al.*[201] 74

Scheme 18. a) Synthesis of acrylate monomers from renewable resources and their radical polymerisation,[159,244–246] b) polymerisation of allylic monomers using free radical polymerisation (FRP) in the presence of Lewis acids,[50,254–257] and c) the synthesis of renewable allylic monomers and their controlled copolymerisation with vinyl acetate using organometallic-mediated radical polymerisation (OMRP). 83
Scheme 19. a) and c) Synthesis of glycerol-based carbonate monomers (**M1**-**M3**) using a one-pot approach. b) Two-step literature procedures for the synthesis of the same monomers.[165,248,276,277] 84
Scheme 20. Cobalt-mediated radical polymerisation of five renewable monomers (**M1**-**M5**) with vinyl acetate and the structures of the resulting statistical copolymers (**P1**-**P5**) 88
Scheme 21. Radical polymerisation of αCCs and the reported occurrence of two polymerisation mechanisms: a) radical ring-opening polymerisation (rROP) and b) vinyl-type polymerisation (VT). 101
Scheme 22. OMRP of VAc and **DMMDO** using a $Co(acac)_2$ complex as the controlling agent. Subsequent hydrolysis and post-polymerisation modification routes performed in this chapter to yield functional PVOH are also indicated. 102
Scheme 23. Starting from a single copolymer, P(VAc-*co*-**DMMDO**), three different copolymers were accessed: P(VOH-*co*-BD), P(VOH-*co*-**DMMDO**) and P(VOH-*co*-**DMMDO**-*co*-HU). 123
Scheme 24. Synthetic routes to functional polyethylene copolymers by reversible deactivation radical polymerisation (RDRP) previously reported[5,7–9] and the copolymerisation of ethylene with renewably-sourced carbonate monomers (**M1** and **DMMDO**) by organometallic-mediated radical polymerisation (OMRP) presented in this work. 126
Scheme 25. Copolymerisation of ethylene and vinyl acetate to synthesise a) poly(ethylene-*co*-vinyl acetate) statistical copolymers and b) poly(ethylene-*co*-vinyl acetate)-*b*-poly(ethylene) block copolymers. 136
Scheme 26. Coupling reaction of EVA-*b*-PE diblock copolymers into EVA-*b*-PE-*b*-EVA triblock copolymers. 142
Scheme 27. a) Structures of cellulose and starch with key parameters of their structure, b) synthesis of amylose or starch based compatibiliser using high oleic sunflower oil,[371] and c) the preparation of composites using LDPE, bulk cellulose and the renewable compatibilisers prepared according to Meier *et al.*[371] 150
Scheme 28. Organometallic-mediated radical polymerisation of renewable monomers into renewable and functional polymers. These precisely designed copolymers and other fully

renewably-sourced polymers have promising applications as compatibilisers in cellulose/low-density polyethylene composites. 163

12.4. List of Tables

Table 1. Copolymerisations of VAc and renewable monomers (**M1**-**M5**) using R-Co(acac)$_2$ at 40 °C[a] 94

Table 2. Copolymerisations of VAc and **DMMDO** using R-Co(acac)$_2$ at 40°C[g] 105

Table 3. Copolymerisations of ethylene with renewable monomers **M1** and **DMMDO** using R-Co(acac)$_2$ at 40 °C in dimethyl carbonate (DMC) 130

Table 4. Reaction conditions for the synthesis of EVA copolymers of different compositions, and their macromolecular characteristics and glass transition temperature [a] 138

Table 5. Reaction conditions for the synthesis of EVA macroinitiators, and their macromolecular characteristics and glass transition temperature [a] 138

Table 6. Chain extension of EVA$_{10bar}$-Co(acac)$_2$ and EVA$_{50bar}$-Co(acac)$_2$ macroinitiators with ethylene at 60 °C[a] 141

Table 7. Composition of the composites prepared in this section 144

Table 8. Mechanical properties of pure LDPE, LDPE containing 5 wt% cellulose, and LDPE containing 5 wt% cellulose and 5 wt% EVA compatibiliser. 145

Table 9. Composition of the composites in wt % of a total of 5 g of sample 152

Table 10. Optimisation of the reaction conditions for the synthesis of **M1** from glycerol, dimethyl carbonate and diallyl carbonate 185

Table 11. Optimisation of the reaction conditions for the synthesis of **M2** from glycerol, dimethyl carbonate and dimethylallyl carbonate 185

Table 12. Optimisation of the reaction conditions for the synthesis of M3 from glycerol, dimethyl carbonate and methyl-10-undecenoate 186

Table 13. Free radical homopolymerisation of the renewable monomers (**M1**-**M5**) using V-70 at 40 °C in DMC (entries 1-5)[a] and their free radical copolymerisations with VAc in bulk (entries 6-9)[b] 194

Table 14. Full kinetics of the copolymerisations of VAc and renewable monomers (**M1**-**M5**) using R-Co(acac)$_2$ at 40°C[a] 195

Table 15. Representative examples of recovered monomer after scCO$_2$ purification 201

Table 16. Copolymerisations of VAc and DMMDO at 40 °C using R-Co(acac)$_2$ 221

Table 17. Polymerisations of VAc and **DMMDO** by free radical polymerisation (Entries 1-11) and by cobalt-mediated radical polymerisation (Entries 11-14) at 40 °C to determine the reactivity ratios of the monomers. 224
Table 18. PVAc and P(VAc-*co*-**DMMDO**) prepared by OMRP with similar DPs for the comparison of solubility. 225
Table 19. Solubility of $PVOH_{134}$ compared with $P(VOH_{108}$-*co*-$BD_{24})$ at different concentrations (Entries 1 and 2, Table 18) 226
Table 20. Copolymerisations of ethylene with **DMMDO** at 40 °C and 50 bar in different solvents initiated by R-$Co(acac)_2$[a] 233
Table 21. Copolymerisations of ethylene with **M1** and **DMMDO** for 24 hours at 40 °C, 50 bar, and 500 rpm using either free radical polymerisation (V-70) or controlled radical polymerisation (R-$Co(acac)_2$) 234
Table 22. Mechanical properties determined by stress-strain measurements 246